SEAKEEPING: Ship behaviour in rough weather

By

A R J M LLOYD BSc PhD FEng FRINA

Published by A R J M Lloyd, 26 Spithead Avenue, Gosport, Hampshire, United Kingdom

First published 1989 by Ellis Horwood, Chichester, Sussex, United Kingdom.

Printed and bound in Great Britain by RPM Reprographics, Chichester, Sussex, United Kingdom.

British Library Cataloguing-in-Publication Data
A catalogue record for this book is available from the British Library.

ISBN 0 9532634 0 1 (Revised edition)
First published by
Ellis Horwood Ltd (ISBN 0 7458 0230 3)
Halstead Press (ISBN 0 470 21232 2)
International Book Distributors Ltd (ISBN 0 13798562 2)

Cover photograph: The view from the bridge of HMS Hermione as she takes a green sea over the fo'c's'le during the Comparative Seakeeping Trial (Andrew and Lloyd (1981)). Photo Paul Wilson.

Dedicated to the memory of No 1 Ship Tank

at the Admiralty Experiment Works, Haslar, Gosport

1886 - 1993

CONTENTS

FOREWARD

Seakeeping

There are three things which are too wonderful for me, yea, four which I know not:
the way of an eagle in the air;
the way of a serpent on a rock;
the way of a ship in the midst of the sea;
and the way of a man with a maid.

Proverbs Chapter 30 verses 18-19

In the days of sail ships were very much more dependent on the weather than they are today. Square rigged sailing vessels could not sail directly into the wind and were strictly limited in their ability to go where the master wanted. In severe conditions it was necessary to shorten sail and even to ride out a storm under bare poles. Many a ship was lost because she was driven ashore under such circumstances.

Economic pressures often demanded that the ship's master spread as much canvas as he dared in order to make the best speed. This is nowhere more graphically illustrated than in the stories of the clipper "races" from China to Europe in the nineteenth century. The first ship home with the newly harvested tea crop could demand a premium price for her cargo. Speed was of the essence and these ships sprouted all sorts of additional sails to make the most of every breath of wind available.

A heavily laden over canvassed ship was an unpleasant home for the sailors and passengers in rough weather. With the lee gunwale submerged, the decks continually awash, deckhouses damp and cold, life must have been miserable. Yet even in these circumstances the crew would be expected to continue to navigate and steer the ship and to go aloft in order to shorten sail or spread additional canvas as the master demanded.

However, the real problems of seakeeping only came to be recognised with the demise of sail and the advent of steam as the prime motive power. Now, for the first time, ships could steam directly into the wind and sea with a consequent increase of pitch and heave motions. The damaging effects of shipping heavy seas over the bow began to be experienced. The punishing consequences of high speed in rough weather were not fully understood and at least one ship (HMS *Cobra* in 1901) is believed to have been lost after her hull broke in two after slamming in rough weather.

At the same time the steadying effects of tall masts and a good spread of canvas were lost and the new steam ships were found to roll heavily. It is ironic that this beneficial effect of sails has only recently been rediscovered with the emerging technology of wind assisted propulsion for low powered merchant ships.

At about this time William Froude, an eminent Victorian engineer, proposed to build the world's first purpose built model towing tank at Torquay in the United Kingdom. He had recently developed scaling laws for predicting the resistance of ships from tests on models and he

intended to use the tank for the required scale model experiments. The British Admiralty accepted Froude's proposal on the condition that he also used the tank to investigate ways of reducing the rolling motion of ships.

In due course Froude's Admiralty Experiment Works was moved to Haslar in Gosport and similar towing tanks were built in many different countries. These were often fitted with wave makers which allowed the behaviour of model ships in waves to be studied at leisure providing for the first time, a rudimentary technique for refining a full scale design to ensure adequate performance in rough weather. These model experiments were usually confined to tests in regular head or following waves with occasional tests at zero speed in beam waves. Tests at other headings or in more realistic irregular waves were impossible because of the long narrow shape of the towing tanks and the simplicity of the wave makers.

These early model experiments allowed some limited developments in the study of seakeeping but they could not be used to predict the actual performance of ships at sea because no technique for relating the behaviour of the model in the tank's regular waves to the behaviour of the ship in the chaotic environment of the real ocean was available. Graphic evidence for this may be found in contrasting the performance of many of the Royal Navy's destroyers of the Second World War with that of their successors in the postwar period. The specifications for the wartime ships often called for speeds as high as 35 knots and the shipbuilder was required to demonstrate that this could be achieved before the Navy would accept the ship. . Invariably the trials were done in calm water and service experience soon demonstrated that these "trial" speeds could hardly ever be achieved in practice despite engines capable of developing as much as 70,000 horse power (50 MW). Commonly occurring moderate wave conditions were usually enough to limit the speed in one way or another and it became obvious that the powerful engines were not cost effective.

The early postwar designs had half the installed power of their war time predecessors but much more attention was devoted to their performance in rough weather so that their reduced speed potential of perhaps 30 knots was achievable most of the time. The relationship between hull form and good seakeeping performance was not well understood and the classic design of the period, the Type 12 frigate (which evolved into the ***Leander*** class), had a superb rough weather performance as a result of the designer's intuition rather than any precise science.

This situation prevailed for many years and the study of seakeeping remained in effective limbo until the publication of a landmark paper by St Denis and Pierson in 1953[1]. This showed, for the first time, how the motions experienced in the random waves of the ocean could be calculated using the techniques of spectral analysis borrowed from the field of electromagnetic communications.

At about the same time theoretical methods of predicting the behaviour of ships in regular waves were being developed. The breakthrough came with Ursell's (1949a,b) theory for predicting the characteristics of the flow around a circular cylinder oscillating in a free surface. Classical transformation techniques allowed these results to be applied to a wide range of shapes of ship

[1] References are listed in the Bibliography in Appendix 3

like cross-section and the fundamentals of modern ship motion theory were born.

These developments some fifty years ago provided the basic tools required to develop routine techniques for the prediction of ship motions in something approaching the real irregular wave environment of the ocean. It was now possible for the first time to predict the rough weather performance of a ship at the design stage and to allow seakeeping to take its rightful place in the design process.

Since that time seakeeping has remained an active field of research, but developments have been in the nature of progressive refinements rather than spectacular advances. Techniques for designing roll stabilisers, criteria determination, prediction of long term motion statistics and operational effectiveness have all been added to the naval architect's tool box: seakeeping performance prediction should now be a routine in any ship design office.

Unfortunately these developments have not been accompanied by much readily obtainable literature on the subject outside the specialist papers and publications of the learned societies and research institutions. Although the underlying physical principles of seakeeping theory are not generally difficult to understand, the intimate details are mathematically complicated. It follows that calculations of ship motions and related phenomena require access to suitable computer programs and computers. No real progress can be made without them. Fortunately many suitable programs are available in educational, research and design establishments as well as computer bureaux throughout the world. The PAT-86 suite of seakeeping computer programs (available at the Defence Evaluation and Research Agency at Haslar in the United Kingdom) was used for the examples of ship motion calculations presented in this book.

The first edition of this book (Lloyd, 1989) covered all aspects of the subject in detail, resulting in a comprehensive, if rather long and expensive text. This edition is shorter and private publication by the author has allowed the book to be marketed at a realistic price within the range of the average student of naval architecture. This has been achieved by revising the entire text and omitting material which can be readily found elsewhere such as the chapter on basic fluid mechanics and the detailed derivation of the dynamics of the spring mass system.. The opportunity has been taken to include some new material on the growth of wave heights in the ocean, the effect of ship motions on crew task performance and the influence of hull form on seakeeping.

I was privileged to lead the Seakeeping Research Group at the Defence Evaluation and Research Agency (formerly the Admiralty Experiment Works) at Haslar in the United Kingdom for the best part of 25 years and this book represents the accumulated knowledge of that period. During that time I have been helped by many colleagues both within the DERA and outside. In particular I would like to acknowledge the contributions of Mrs P R Loader, Dr R N Andrew, Dr D Fryer, the late Mr W B Marshfield, Mr P Crossland, Mr M Johnson and Mr D K Brown as well as fellow members of the ITTC Seakeeping Committee and colleagues at the United States Naval Academy. I am also indebted to Mr R E Small and Mrs W E Ball, whose painstaking proof reading of the manuscript was invaluable. Without their constant support, advice and inspiration this book would probably have never been written.

A R J M Lloyd
Gosport 1998

1

REGULAR WAVES

1.1 INTRODUCTION

The waves which influence the behaviour of ships at sea are generally irregular and more or less random in nature. No two waves have exactly the same height and they travel across the surface at different speeds and in different directions. Techniques for coping with the chaotic nature of these waves on the real sea surface are described in Chapter 2 but it is first necessary to discuss the characteristics of ideal regular waves. Such waves never occur in the real ocean environment although they can be produced in laboratory towing tanks and form the basis of many seakeeping model experiments. Of equal importance is the fact that the theory of irregular waves is based on the assumption that they can be represented by ***superposing*** or adding together a suitable assembly of regular waves. So it is clear that the characteristics of regular waves have a profound influence on the behaviour of ships in rough weather even though they are never actually encountered at sea: an understanding of their nature is one of the vital tools in the study of seakeeping.

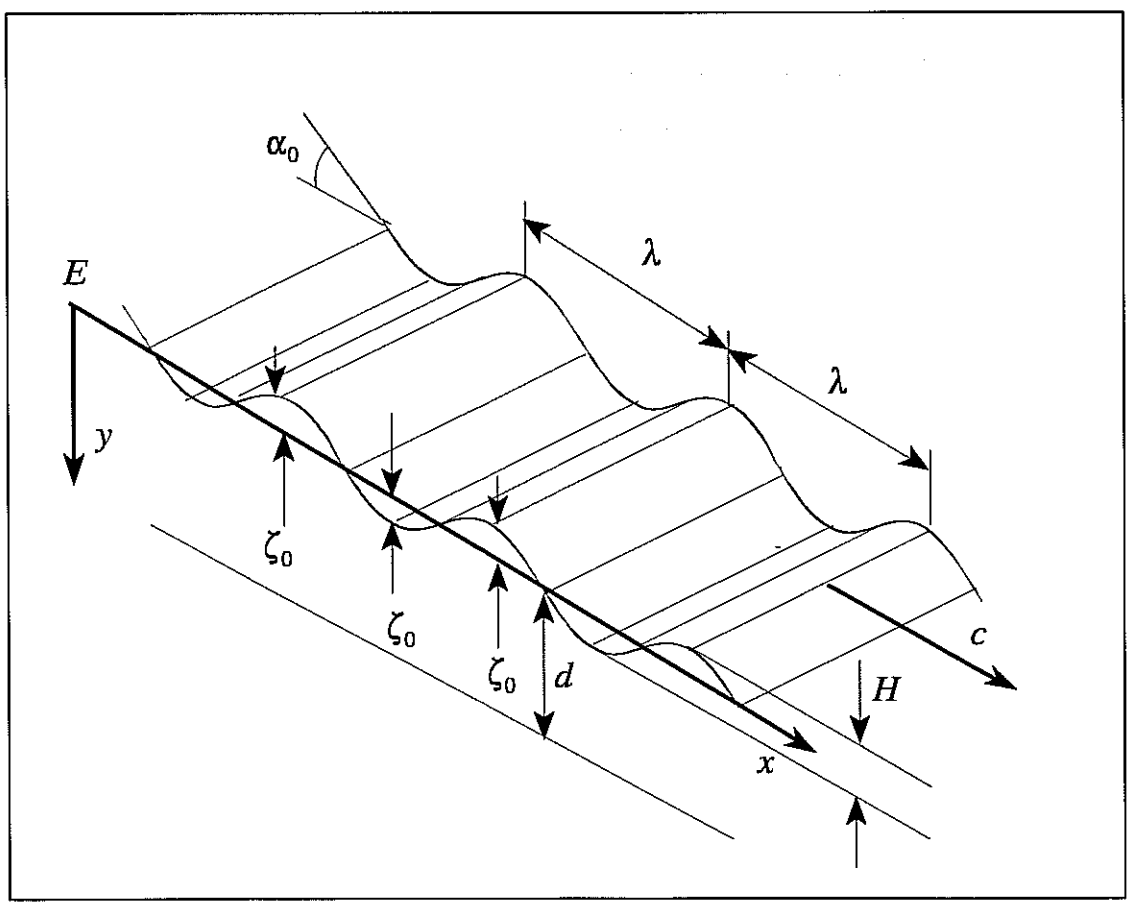

Fig 1.1 - Regular waves

Figure 1.1 shows a train of regular waves advancing across the surface of a body of water of constant depth d. The waves are two dimensional: that is, they advance in the x direction and the crests are perpendicular to the x axis. The crests may be considered as extending to infinity on either side of the x axis; alternatively the waves may be imagined to be advancing down a long narrow tank bounded by vertical walls parallel to the x axis.

The salient characteristics of the waves are:

ζ	The instantaneous depression of the water surface below the mean level $(y=0)$	metres
ζ_0	The wave amplitude or vertical distance from the mean level $(y=0)$ to a crest or a trough; ζ_0 is always positive.	metres
H	The wave height: twice the wave amplitude	metres
λ	The wave length: the horizontal distance between one crest (or trough) and the next	metres
c	The wave celerity: the velocity of an individual crest in the x direction	metres/second
T	The wave period: the time interval between successive crests (or troughs) passing a fixed point.	seconds
α	The instantaneous wave slope: the gradient of the surface profile	radians
α_0	The maximum wave slope or wave slope amplitude. α_0 is always positive.	radians
H/λ	The wave steepness	-

These waves progress across the surface in a regular orderly fashion. Each wave crest advances at the same steady velocity c so that the waves never overtake each other and the wave length λ and period T remain constant. The shape of each wave remains the same and the whole wave train appears to advance like a rigid corrugated sheet.

1.2 THE VELOCITY POTENTIAL

We shall use the potential flow techniques of classical fluid dynamics[1] to predict the characteristics and structure of regular waves.

The velocity potential ϕ is defined by the equations

$$\frac{\partial \phi}{\partial x} = u \quad ; \quad \frac{\partial \phi}{\partial y} = v \quad m/sec \tag{1.1}$$

where u and v are the horizontal and vertical velocities and ϕ must satisfy Laplace's equation

$$\Delta^2 \phi = 0 \quad sec^{-1} \tag{1.2}$$

if it is to represent a valid fluid flow.

[1] It is assumed that the reader has a working knowledge of classical fluid dynamics

It is necessary to find a velocity potential ϕ which describes the fluid flow associated with a regular wave. Lamb (1932) showed that the velocity potential

$$\phi = \frac{g\,\zeta_0}{\omega}\,\frac{\cosh\,[\,k\,(\,d\,-\,y\,)\,]}{\cosh\,(k\,d)} \qquad m^2/sec$$

is appropriate to the case of the two dimensional regular (sine) wave of small amplitude ζ_o advancing across the surface of a body of fluid of any constant depth d as illustrated in Figure 1.1; k and ω are constants whose physical meaning will be derived in Section 1.3.

Almost all calculations of seakeeping performance assume that the water is deep compared to the wave length. If we assume that the depth of water is infinite[2] then

$$\frac{\cosh\,[\,k\,(\,d\,-\,y\,)\,]}{\cosh\,(\,k\,d\,)} \approx \exp\,(-k\,y\,)$$

and the velocity potential becomes

$$\phi = \frac{g\,\zeta_0}{\omega}\,\exp\,(-\,k\,y\,) \qquad m^2/sec \tag{1.3}$$

1.3 PRESSURE CONTOURS AND THE SURFACE PROFILE

Bernoulli's equation for the unsteady motion of an ideal fluid is

$$\frac{q^2}{2} + \frac{\partial\phi}{\partial t} - \Omega + \frac{P}{\rho} = 0 \qquad m^2/sec^2 \tag{1.4}$$

where

$$q^2 = u^2 + v^2 \qquad m^2/sec^2 \tag{1.5}$$

and Ω is the force potential defined by

$$\frac{\partial\Omega}{\partial x} = X; \qquad \frac{\partial\Omega}{\partial y} = Y \qquad m^2/sec^2$$

Bernoulli's equation must apply everywhere and can be used to find the surface profile associated

---

[2] In practice $d > \frac{\lambda}{2}$ is an adequate restriction.

with the velocity potential given by Equation (1.3). The only force applied externally to any fluid particle is gravity. Hence

$$X = \frac{\partial \Omega}{\partial x} = 0; \quad Y = \frac{\partial \Omega}{\partial y} = g \qquad m/sec^2$$

so that

$$\Omega = g\ y \quad m^2/sec^2$$

and Equation (1.4) becomes

$$\frac{q^2}{2} + \frac{\partial \phi}{\partial t} - g\ y + \frac{P}{\rho} = 0 \quad m^2/sec^2 \tag{1.6}$$

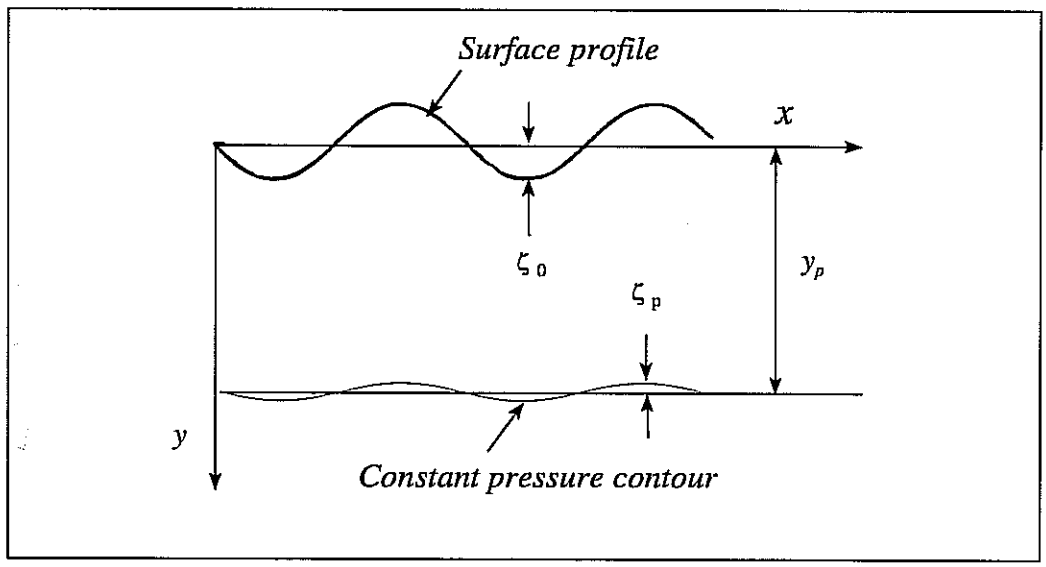

Fig 1.2 - Constant pressure contour beneath a regular wave

In calm water the pressure at depth y_p is

$$P = \rho\ g\ y_p \quad kN/m^2$$

and a constant pressure contour is a horizontal straight line. Under regular waves this contour is distorted as shown in Figure 1.2. The depth of a point on this contour is

$$y = y_p + \zeta_p \quad m$$

where ζ_p is the depression of the contour below the depth y_p.

Since the pressure everywhere along the contour and the depth y_p are both constant the quantity

$$\int_0^t \left(\frac{P}{\rho} - g\, y_p \right) dt \quad m^2/sec$$

will be a constant on the contour at any given time t. It may be added to the potential without affecting the velocities in any way (since they are functions of the potential gradients and not of the potential itself). So we may define a new velocity potential

$$\phi' = \phi + \int_0^t \left(\frac{P}{\rho} - g\, y_p \right) dt \quad m^2/sec$$

so that

$$\frac{\partial \phi'}{\partial t} = \frac{\partial \phi}{\partial t} + \frac{P}{\rho} - g\, y_p \quad m^2/sec^2$$

and Equation (1.6) becomes

$$\frac{q^2}{2} + \frac{\partial \phi'}{\partial t} - g\, \zeta_p = 0 \quad m^2/sec^2$$

and the prime may now of course be omitted.

If we now assume that the velocity is small (tantamount to assuming that the wave amplitude ζ_0 is small compared with the wave length) we may neglect q^2 so that the depression of the constant pressure surface is

$$\zeta_p = \frac{1}{g} \left(\frac{\partial \phi}{\partial t} \right)_{y\, =\, y_p + \zeta_p} \quad m$$

or, since ζ_p is small,

$$\zeta_p \approx \frac{1}{g} \left(\frac{\partial \phi}{\partial t} \right)_{y\, =\, y_p} \quad m \qquad (1.7)$$

Substituting the expression for the velocity potential (Equation (1.3)) yields the equation for the constant pressure contour at depth y_p

$$\zeta_p = \zeta_0\, exp\, (-k\, y_p)\, sin\, (k\, x - \omega\, t) \quad m \qquad (1.8)$$

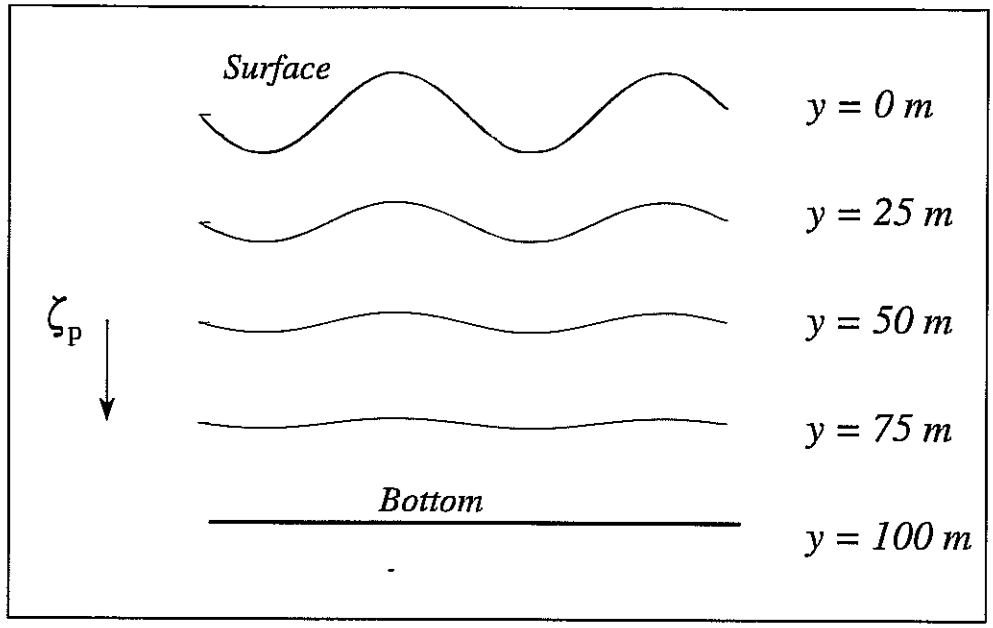

Fig 1.3 - Constant pressure contours beneath a 100 m wave: depth 100m

As an illustration of this equation Figure 1.3 shows typical pressure contours beneath a regular wave of length 100 metres in water 100 metres deep. These results have been obtained by setting $t = 0$ in Equation (1.8).

The surface profile is one of these constant pressure contours (with the pressure equal to the atmospheric pressure). It is obtained by setting $y_P = 0$ in Equation (1.8) to give

$$\zeta = \zeta_0 \sin (k x - \omega t) \quad m \tag{1.9}$$

which is the equation of a regular wave of small amplitude ζ_o advancing across the fluid surface.

Equation (1.9) is illustrated in Figure 1.4. Consider first the wave shape in the geographical or spatial sense. This is tantamount to fixing time at some instant t as, for example, when taking a photograph. If for simplicity we choose $t = 0$, Equation (1.9) is reduced to

$$\zeta = \zeta_0 \sin (k x) \quad m$$

which represents a simple sine wave starting at the x origin. The wave length is λ and the ***wave number*** k is now seen to be

$$k = \frac{2 \pi}{\lambda} \quad m^{-1} \tag{1.10}$$

A second photograph taken a short while later at $t = t_1$ would reveal exactly the same wave profile with the same amplitude and wave length moved along the x axis a distance ($\omega t_1 / k$)

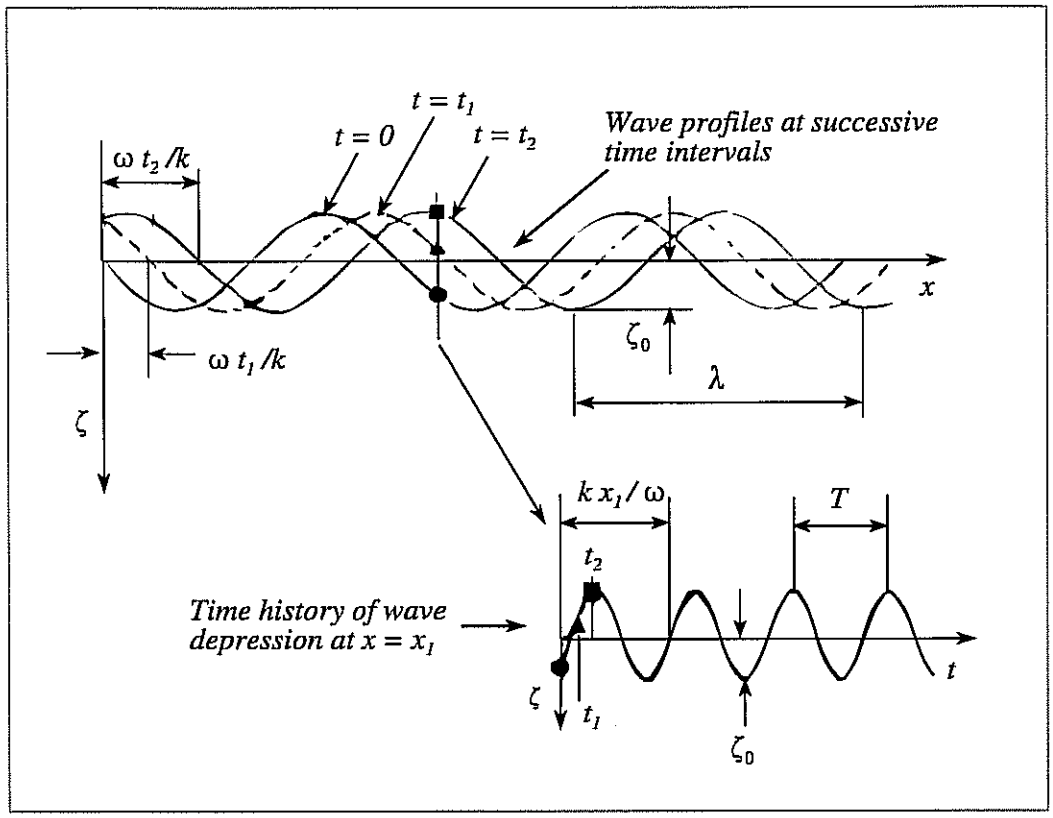

Fig 1.4 - Regular waves pictured in space and time

metres. This can be seen by recasting Equation (1.9) as

$$\zeta = \zeta_0 \sin\left[k\left(x - \frac{\omega\ t_1}{k} \right) \right] \quad m$$

and the term $\omega t_1/k$ can be recognised as a phase `lag' which governs the location of the wave along the x axis. As time passes, the lag increases and the wave advances steadily away from the origin with velocity

$$c = \frac{\omega}{k} \quad m/sec \qquad (1.11)$$

c is the ***wave celerity.***

An alternative view of events can be obtained by fixing the distance x and allowing time to pass.

Physically this can be considered as recording the time history of the rise and fall of the water surface at some fixed point $x = x_1$. The resulting sine wave of amplitude ζ_o and period T is also illustrated in Figure 1.4 and the frequency ω is related to the period by

$$\omega = \frac{2\pi}{T} \quad rad/sec \tag{1.12}$$

The time history is given by recasting Equation (1.9) as

$$\zeta = -\zeta_0 \sin\left[\omega\left(t - \frac{k x_1}{\omega}\right)\right] \quad m \tag{1.13}$$

and the term ($k x_1 / \omega$ seconds) may now be recognised as a phase 'lag' which governs the temporal location of the sine wave along the t axis.

1.4 WAVE SLOPE

It is sometimes convenient to quantify the severity of the waves in terms of their slope rather than their height or amplitude. The slope of the pressure contours may be obtained by differentiating Equation (1.8) with respect to x:

$$\alpha_{yp} = k\,\zeta_0\,exp\,(-k\,y_p)\,cos\,(k\,x - \omega\,t) \tag{1.14}$$

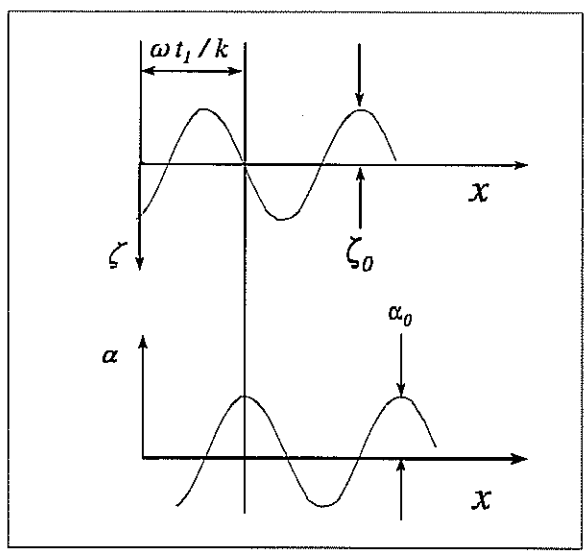

Fig 1.5 - Wave depression and wave slope profiles at $t = t_1$

The wave slope at the surface is obtained by setting $y_p = 0$ to give

$$\alpha = \alpha_0 \cos(k x - \omega t) \quad rad \tag{1.15}$$

where the wave slope amplitude is

$$\alpha_0 = k\,\zeta_0 \quad rad \tag{1.16}$$

So the wave slope varies sinusoidally in both time and space in much the same way as the surface depression. Figure 1.5 shows the surface profile and the corresponding wave slope at time $t = t_1$. The wave slope is a maximum when the surface depression is zero and vice versa.

The time history of the wave slope at a certain location $x = x_1$ is obtained by recasting Equation (1.15) as

$$\alpha = \alpha_0 \cos\left[\omega\left(t - \frac{k\,x_1}{\omega}\right)\right] \quad rad$$

and this is compared with the corresponding surface depression time history (Equation (1.13)) in Figure 1.6. The wave slope lags the surface depression by a quarter of a wave period.

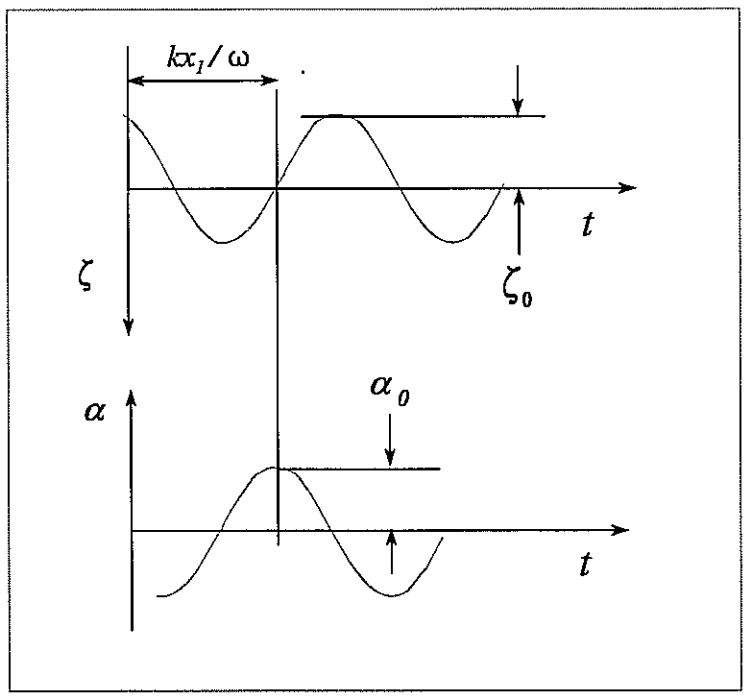

Fig 1.6 - Wave slope time history at $x = x_1$

1.5 PARTICLE ORBITS

According to Equation (1.1) the velocities at any point under the wave can be found by differentiating the velocity potential given by Equation (1.3). This gives

$$u = \frac{\partial \phi}{\partial x} = -\,u_0 \sin(k\,x - \omega\,t) \quad m/sec \tag{1.17}$$

$$v = \frac{\partial \phi}{\partial y} = - v_0 \cos (k x - \omega t) \quad m/sec \tag{1.18}$$

where the velocity amplitudes are

$$u_0 = v_0 = \frac{g k \zeta_0}{\omega} exp (- k y) \quad m/sec \tag{1.19}$$

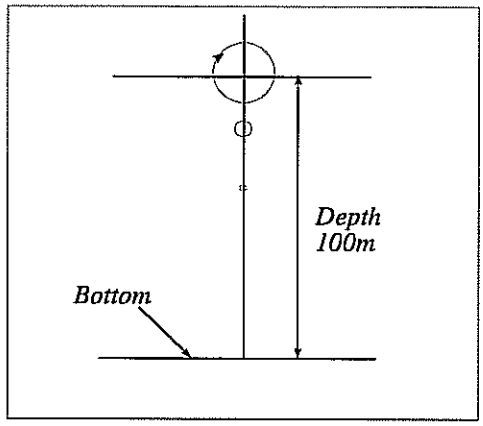

Fig 1.7 - Particle orbits under a 100 m wave

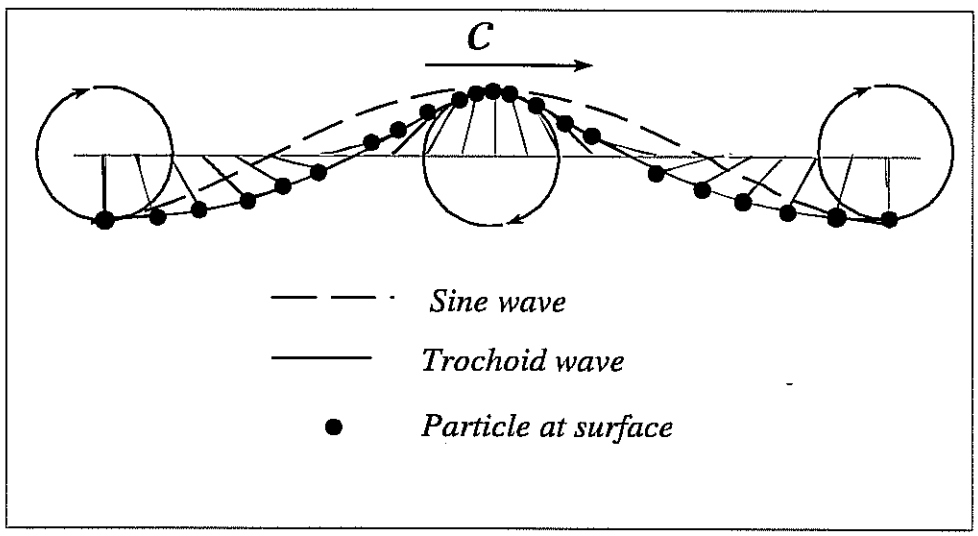

Fig. 1.8 - Orbits of particles at the water surface

Since the wave amplitude is assumed to be small the velocity amplitudes given by Equation (1.19) must also be small and it follows that a particle of water oscillating about some point (x, y) will never stray very far from that point. The path of the particle can therefore be calculated approximately by assuming that it is always subject to the velocities calculated for the point (x, y). With this assumption the particle's trajectory is obtained by integrating Equations (1.17) and (1.18) to give

$$\Delta x = - x_0 \cos (k x - \omega t) \quad m \tag{1.20}$$

$$\Delta y = y_0 \sin (k x - \omega t) \quad m \tag{1.21}$$

where Δx and Δy are the deviations of the particle from its datum position (x, y) and the amplitudes of its displacements are

$$x_0 = y_0 = \zeta_o \exp (- k y) \quad m \tag{1.22}$$

Figure 1.7 illustrates these formulae and we see that the water particles follow circular orbits and that the amplitude decays very rapidly with depth. Figure 1.8 shows how the circular orbit of a particle at the surface results in the wave profile[3].

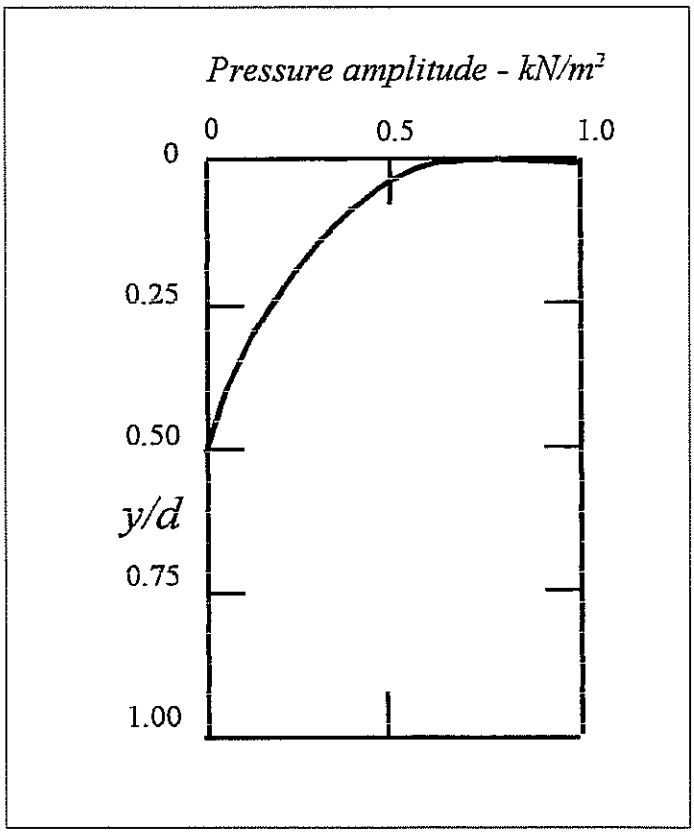

Fig 1.9 - Pressure amplitude under a wave: wave length 100 m; wave amplitude 1.0 m

[3] Figure 1.8 shows that the wave profile generated by particles following circular orbits at the surface is a trochoid with sharper crests and flatter troughs compared to a sine wave. However, the trochoid wave approaches a sine wave as the amplitude becomes infinitesimal and the assumption of sinusoidal waves is adequate for the linear treatment used in this book.

1.6 PRESSURE FLUCTUATIONS UNDER A WAVE

The pressure at any point under a regular wave may be found from Bernoulli's equation (1.6). If we assume that the velocity is small we obtain

$$P \approx \rho\, g\, y + \tilde{P} \quad kN/m^2$$

so the pressure at any depth y oscillates around the steady hydrostatic pressure $\rho\, g\, y$. The fluctuating part of the pressure is

$$\tilde{P} = -\rho\, g\, \zeta_0\, exp\,(-\,k\, y\,)\ \ sin\,(\,k\, x\, -\, \omega\, t) \quad kN/m^2 \qquad (1.23)$$

Figure 1.9 shows the variation of the pressure amplitude $\rho\, g\, \zeta_0\, exp\,(\,-k\, y\,)$ beneath a 100 metre long wave. The pressure amplitude decreases with depth and becomes negligible for depths greater than about half the water depth.

1.7 ENERGY IN A REGULAR WAVE

The energy associated with a train of regular waves includes contributions from both potential and kinetic energy. Consider a small element of length δx metres and width Δ metres (perpendicular to the page) of the regular wave shown in Figure. 1.10. The surface depression ζ is given by Equation (1.9) and the mass of water over the element is approximately $-\rho\ \zeta\ \delta x\ \Delta$

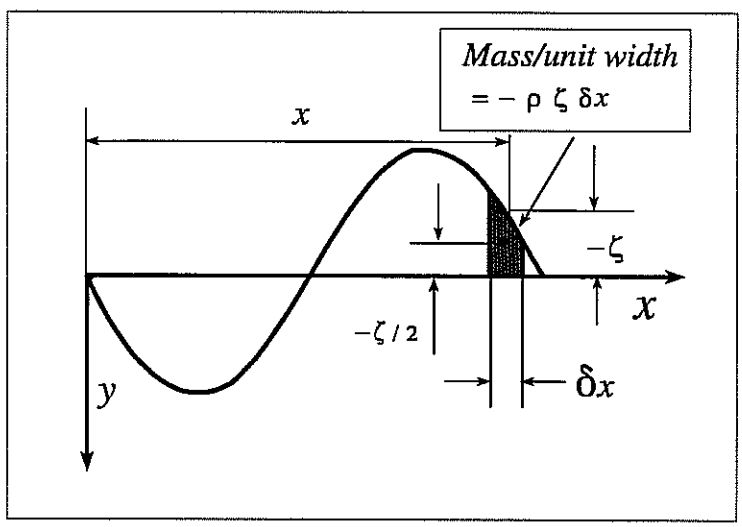

Fig 1.10 - Potential energy in a regular wave

tonnes. The centre of gravity of this mass is approximately $-\zeta/2$ metres above the undisturbed surface level and its potential energy relative to the undisturbed (calm water) state is $(\,\rho\, g\, \zeta^2\, \delta x\, \Delta\,)\ /\ 2$ kJ. If we now allow δx to become infinitesimally small we may integrate to obtain the total potential energy in a single wave length:

$$E_P = \int_0^{\lambda} \frac{\rho\, g\, \zeta^2\, \Delta}{2}\, dx$$

$$= \frac{\rho\, g\, \zeta_0^2\, \Delta}{2} \int_0^{\lambda} \sin^2 (k\, x - \omega\, t)\, dx \qquad (1.24)$$

$$= \frac{\rho\, g\, \lambda\, \zeta_0^2\, \Delta}{4} \quad kJ$$

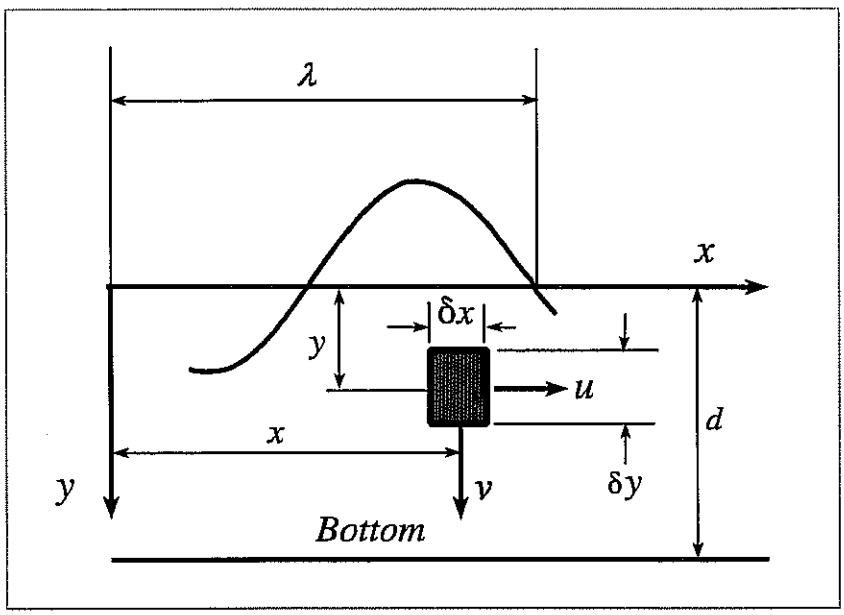

Fig 1.11 - Kinetic energy in a regular wave

Consider now a small element of fluid of width Δ metres beneath a wave as shown in Figure 1.11. The mass of the element is $\rho\ \delta x\ \delta y\ \Delta$ tonnes and it has a total velocity q given by Equation (1.5). So the kinetic energy of the element is $(\rho\ q^2\ \delta x\ \delta y\ \Delta)\ /\ 2$ kJ. If we now allow δx and δy to become infinitesimally small we may integrate to obtain the total kinetic energy of the fluid in one wave length between the surface and the bottom:

$$E_K = \frac{\rho\, \Delta}{2} \int_0^{\lambda} \int_0^{\infty} q^2\, dx\, dy \quad kJ$$

Substituting Equations (1.17) - (1.19) in Equation (1.5) gives

$$q^2 = \frac{g^2\, k^2\, \zeta_0^2\, exp\ (-\ 2\ k\ y\ )}{\omega^2} \qquad m^2/sec^2 \qquad (1.25)$$

and the kinetic energy in one wave length is found to be

$$E_K = \frac{\rho\, g\, \lambda\, \zeta_0^2\, \Delta}{4} \quad kJ \tag{1.26}$$

So the potential and kinetic energies are equal and the total energy in one wave length is

$$E = E_P + E_K = \frac{\rho\, g\, \lambda\, \zeta_0^2\, \Delta}{2} \quad kJ \tag{1.27}$$

which leads to the remarkable result that the average energy per square metre of sea surface is independent of the wave frequency and depends only on the wave amplitude:

$$\bar{E} = \frac{\rho\, g\, \zeta_0^2}{2} \quad kJ/m^2 \tag{1.28}$$

1.8 ENERGY TRANSMISSION AND GROUP VELOCITY

The energy associated with a sequence of regular waves is transmitted in the direction of their propagation. The rate of energy transmission can be found by considering the energy flux across the plane AA in Figure 1.12. We begin by calculating the rate at which the fluid on the left of a small element of height δy and width Δ is doing work on the fluid on the right of the element.

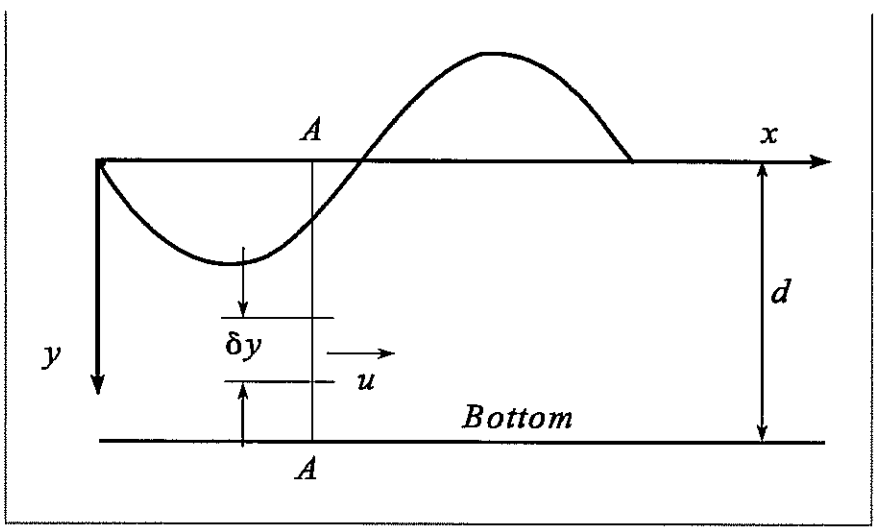

Fig 1.12 - Energy transmission in a regular wave

Since the element is small the pressure and velocity acting on its face may be regarded as constant (at a given time) and the force exerted by the fluid on the left is $P\ \delta y\ \Delta$ kN. The work done by the fluid on the left is $u\ P\ \delta y\ \Delta$ kJ /sec. If we now allow δy to become infinitesimal the total rate of transmission of energy across the plane AA is obtained by integrating over the depth of the fluid.

Neglecting the small contribution due to the portion of fluid above the undisturbed surface level ($y = 0$), the rate of transmission of energy is

$$\dot{E} = \Delta \int_0^d u\ P\ dy \quad kJ/sec \tag{1.29}$$

Using Equations (1.17) and (1.23) we find that for very deep water the energy is transmitted at a rate

$$\dot{E} = \frac{\rho\ g\ c\ \zeta_0^2\ \Delta\ sin^2\ (k\ x - \omega\ t)}{2} \quad kJ/sec$$

The rate of transmission of energy evidently fluctuates with time but we are concerned with its mean value. Over a long period of time (or an integral number of wave periods) the mean value of $\sin^2\ (k\ x - \omega\ t)$ is 0.5. So the mean rate of energy transmission is

$$\bar{\dot{E}} = \frac{\rho\ g\ c\ \zeta_0^2\ \Delta}{4} \quad kJ/sec \tag{1.30}$$

Now the total energy is given by Equation (1.27) and this energy is transmitted at a mean velocity given by

$$u_G = \frac{\bar{\dot{E}}}{\bar{E}} = \frac{c}{2} \quad m/sec \tag{1.31}$$

We may interpret this result by considering the progression of a group of regular waves down a laboratory tank. If the mean energy associated with each wave length is $\bar{E}$ kJ per square metre the amplitude of the waves is, from Equation (1.28),

$$\zeta_0 = \sqrt{\frac{2\ \bar{E}}{\rho\ g}} \quad m \tag{1.32}$$

Each individual wave within the group is propagating forward at the celerity c (Equation (1.11)) but the energy is only propagating at $c/2$ m/sec (Equation (1.31)). So after one wave period each wave will have moved forward one wave length, taking half of its associated energy with it. The other half of the energy is left behind to be added to the energy brought forward by the next wave. In this way the total energy per square metre within the group is kept constant.

At the leading edge of the group the first wave will be propagating into calm water. So the orderly exchange of energy from wave to wave does not happen and after one wave period the

TABLE 1.1

REGULAR WAVE FORMULAE FOR DEEP WATER

$(d > \frac{\lambda}{2})$

	ω	T	k	λ	c	u_G
ω		$T=\frac{2\pi}{\omega}$	$k=\frac{\omega^2}{g}$	$\lambda=\frac{2\pi g}{\omega^2}$	$c=\frac{g}{\omega}$	$u_G=\frac{g}{2\omega}$
T	$\omega=\frac{2\pi}{T}$		$k=\frac{4\pi^2}{gT^2}$	$\lambda=\frac{gT^2}{2\pi}$	$c=\frac{gT}{2\pi}$	$u_G=\frac{gT}{4\pi}$
k	$\omega=\sqrt{gk}$	$T=\frac{2\pi}{\sqrt{gk}}$		$\lambda=\frac{2\pi}{k}$	$c=\sqrt{\frac{g}{k}}$	$u_G=\sqrt{\frac{g}{4k}}$
λ	$\omega=\sqrt{\frac{2\pi g}{\lambda}}$	$T=\sqrt{\frac{2\pi\lambda}{g}}$	$k=\frac{2\pi}{\lambda}$		$c=\sqrt{\frac{g\lambda}{2\pi}}$	$u_G=\sqrt{\frac{g\lambda}{8\pi}}$
c	$\omega=\frac{g}{c}$	$T=\frac{2\pi c}{g}$	$k=\frac{g}{c^2}$	$\lambda=\frac{2\pi c^2}{g}$		$u_G=\frac{c}{2}$
u_G	$\omega=\frac{g}{2u_G}$	$T=\frac{4\pi u_G}{g}$	$k=\frac{g}{4u_G^2}$	$\lambda=\frac{8\pi u_G^2}{g}$	$c=2u_G$	

energy of the leading wave is halved. The wave amplitude is reduced and this process continues as the leading edge of the wave train propagates down the tank at the wave celerity.

The leading edge of the group proper (defined as the position of the first wave of full amplitude given by Equation (1.32)) propagates down the tank at velocity u_G and this is called the ***group velocity***. Individual waves within the group propagate at the wave celerity c, which is twice the group velocity (see Equation (1.31)).

TABLE 1.1 (continued)

REGULAR WAVE FORMULAE FOR DEEP WATER

$(d > \frac{\lambda}{2})$

	α_0	u_0 , v_0	x_0 , y_0
ω	$\alpha_0=\frac{\omega^2\zeta_0}{g}$	$u_0=v_0=\zeta_0\omega\ exp\left(-\frac{\omega^2 y}{g}\right)$	$x_0=y_0=\zeta_0\ exp\left(\frac{-\omega^2 y}{g}\right)$
T	$\alpha_0=\frac{4\pi^2\zeta_0}{gT^2}$	$u_0=v_0=\frac{2\pi\zeta_0}{T}\ exp\left(\frac{-4\pi^2 y}{gT^2}\right)$	$x_0=y_0=\zeta_0\ exp\left(\frac{-4\pi^2 y}{gT^2}\right)$
k	$\alpha_0=k\zeta_0$	$u_0=v_0=\zeta_0\ \sqrt{gk}\ exp(-ky)$	$x_0=y_0=\zeta_0\ exp(-ky)$
λ	$\alpha_0=\frac{2\pi\zeta_0}{\lambda}$	$u_0=v_0=\zeta_0\sqrt{\frac{2\pi g}{\lambda}}\ exp\left(\frac{-2\pi y}{\lambda}\right)$	
c	$\alpha_0=\frac{g\zeta_0}{c^2}$	$u_0=v_0=\frac{g\zeta_0}{c}\ exp\left(\frac{-gy}{c^2}\right)$	$x_0=y_0=\zeta_0\ exp\left(\frac{-gy}{c^2}\right)$

1.9 SUMMARY OF THE CHARACTERISTICS OF REGULAR WAVES

The equations derived above may be combined in various ways to produce a multitude of different formulae which are listed for easy reference in Table 1.1. Figure 1.13 shows how wave frequency and celerity depend on wave length. As might have been expected long waves have very low frequencies and vice versa. As if to compensate, the celerity increases with wave length. For example the celerity of a 1000 metre wave is almost 40 metres/second (over 75 knots) compared with only about 4 metres/second (about 8 knots) for a 10 metre wave. This dependency

of celerity on wave length distinguishes surface waves from most other types of wave motion (notably electromagnetic radiation) and we shall see that it is responsible for some peculiar effects when the waves are encountered by a moving ship.

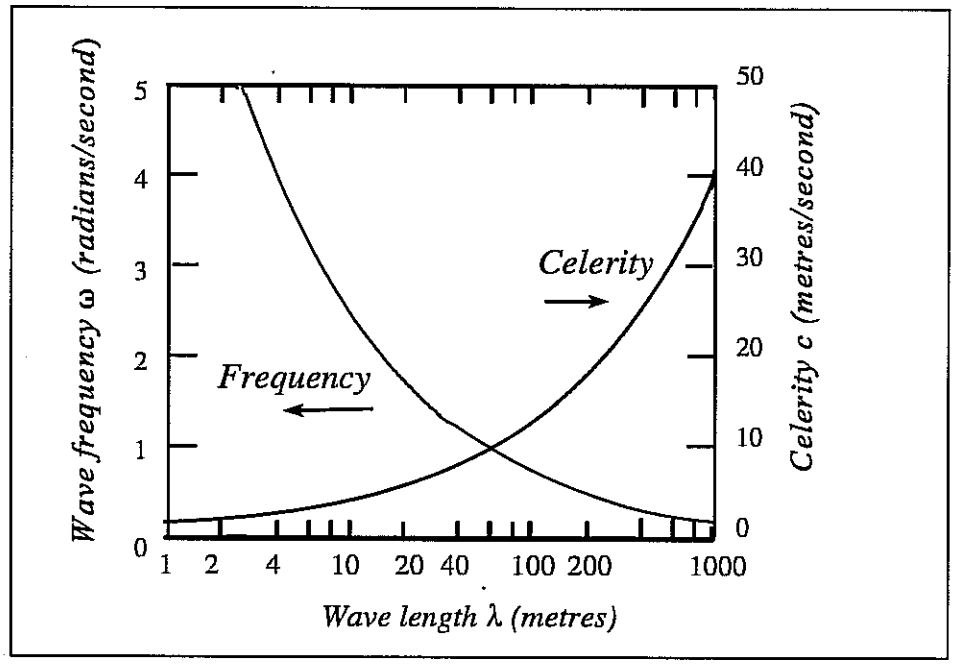

Fig 1.13 - Wave frequency, length and celerity in deep water

1.10 ENCOUNTER FREQUENCY AND HEADING

Although the wave frequency ω has some influence on ship motions in regular waves, the motions are more closely dependent on the frequency with which the moving ship encounters the waves.

Before deriving expressions for the encounter frequency we must adopt the convention for defining the ship's heading μ shown in Figure 1.14 and Table 1.2. The ship is assumed to be attempting to maintain a straight line track at a constant speed U (metres/second) across the sea surface. The waves will cause deviations from the intended course and track, but a directionally stable ship in the hands of an experienced helmsman (or an autopilot) will usually be able to follow a sensibly straight mean course so that the heading angle μ can be readily defined as the angle between the intended track of the ship and the direction of wave propagation.

Since the wave crests are λ metres apart, a crest will meet the ship every T_e seconds, where the encounter period is given by

$$T_e = \frac{\lambda}{c - U \cos \mu} \quad sec \tag{1.33}$$

The component velocity of the ship in the direction of wave propagation is $U \cos \mu$ and the

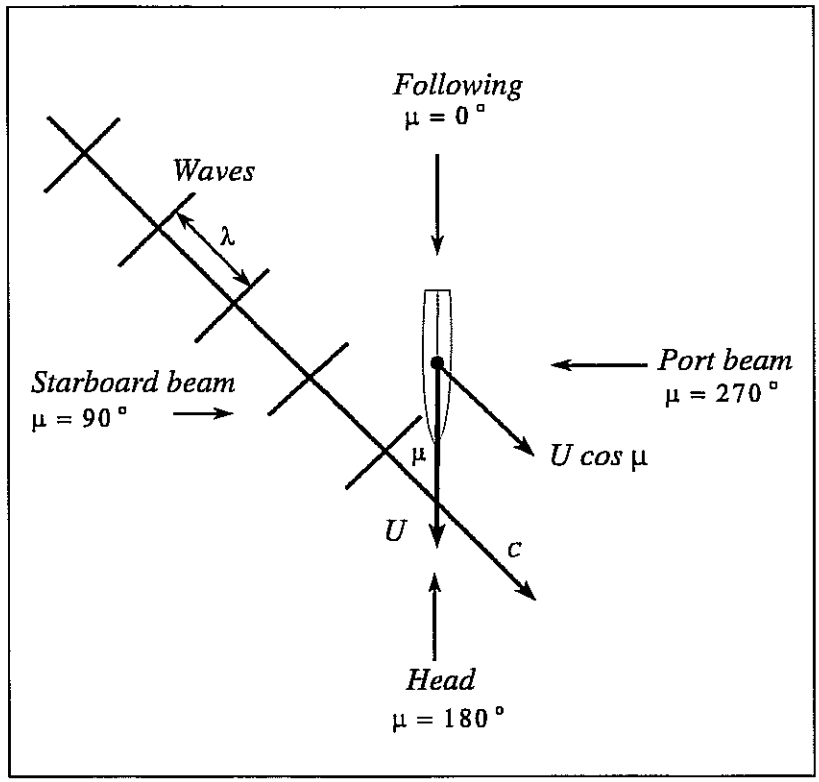

Fig 1.14 - Heading definitions

waves will overtake the ship with a relative velocity $c - U \cos \mu$ metres/second. The corresponding encounter frequency ω_e is defined as

$$\omega_e = \frac{2\pi}{T_e} = \frac{2\pi}{\lambda} (c - U \cos \mu) \quad rad/sec \tag{1.34}$$

or

$$\begin{aligned} \omega_e &= \omega - k\, U \cos \mu \\ &= \omega - \frac{\omega^2\, U}{g} \cos \mu \quad rad/sec \end{aligned} \tag{1.35}$$

and this is illustrated in Figure 1.15.

In head and bow waves ($90° < \mu < 270°$) the ship is heading into the waves and the encounter frequency is always greater than the wave frequency. In beam waves ($\mu = 90°$ or $270°$) the encounter frequency is equal to the wave frequency and is unaffected by ship speed.

On headings abaft the beam ($0° < \mu < 90°$ or $270° < \mu < 360°$) the encounter frequency is reduced and high values are never experienced, whatever the wave frequency. The encounter frequency is negative for higher values of ω. These high frequency waves advance only slowly and ***the negative encounter frequency means that the ship is overtaking the waves. A positive***

encounter frequency means that the waves are overtaking the ship.

When $U \cos \mu = c$ the ship remains stationary relative to the waves and the encounter frequency is zero.

These definitions and observations are summarised in Table 1.2.

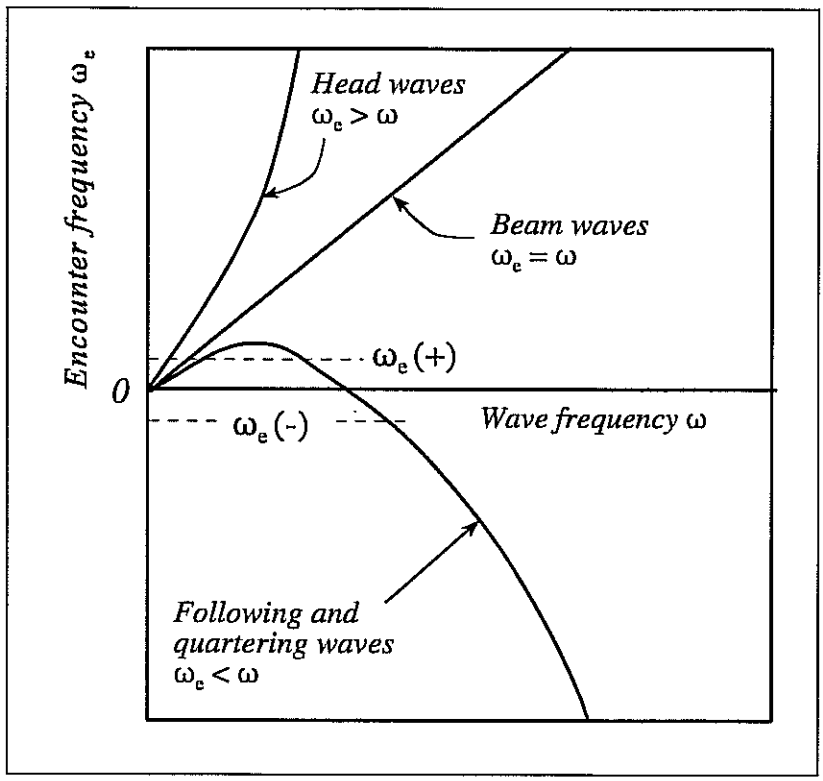

Fig 1.15 - Encounter frequency and heading

In following and quartering waves a given (absolute) value of encounter frequency may be experienced in three different wave systems. Two of these wave systems will give positive encounter frequencies and the third will give a negative encounter frequency. The corresponding wave frequencies can be obtained by rearranging Equation (1.34) to give

$$\omega = \frac{g}{2U \cos \mu}\left(1 \pm \sqrt{1 - \frac{4\,\omega_e}{g} U \cos \mu}\right) \quad \textit{rad/sec} \qquad (1.36)$$

The physical interpretation of this phenomenon is best illustrated with a numerical example. Consider a ship steaming at 20 knots (U= 10.3 m/sec) in regular following waves. Suppose that the ship encounters the wave system at a frequency $|\omega_e|$ = 0.2 rad/sec. It is required to find the wave systems which could be responsible. Possible results, obtained from Equation (1.36), are given in Table 1.3 together with corresponding celerities and wave lengths.

TABLE 1.2

HEADING AND ENCOUNTER FREQUENCY

Heading μ (degrees)	Wave direction	Encounter frequency
0	Following waves. The waves travel in the same direction as the ship. Long waves with high celerity overtake the ship. The ship overtakes short waves with low celerity.	$\omega_e < \omega$. ω_e can be negative. The same ω_e can occur in three different wave lengths.
0 - 90	Quartering waves encountering the ship on the starboard side.	$\omega_e < \omega$. ω_e can be negative. The same ω_e can occur in three different wave lengths.
90	Beam waves encountering the ship on the starboard side	$\omega_e = \omega$ ω_e corresponds to a single wave length
90 - 180	Bow waves encountering the ship on the starboard side.	$\omega_e > \omega$ ω_e corresponds to a single wave length
180	Head waves. The waves travel in the opposite direction to the ship	$\omega_e > \omega$ ω_e corresponds to a single wave length
180 - 270	Bow waves encountering the ship on the port side.	$\omega_e > \omega$ ω_e corresponds to a single wave length
270	Beam waves encountering the ship on the port side.	$\omega_e = \omega$ ω_e corresponds to a single wave length
270 - 360	Quartering waves encountering the ship on the port side.	$\omega_e < \omega$. ω_e can be negative. The same ω_e can occur in three different wave lengths.

Wave A has crests about 0.75 kilometres apart, but its celerity is very high and it overtakes the ship with a relative velocity of nearly 47 knots. So the high celerity compensates for the distant crests and results in the required encounter frequency. Wave B is much shorter and slower and overtakes the ship with a relative velocity of only about 8.5 knots. However, the closer crests compensate for the lower relative velocity and the wave again gives the required encounter frequency. Wave C is very short and the celerity is only 8.8 m/sec. The ship overtakes this wave with a relative velocity of about 3 knots, giving the required encounter frequency. Again the very low relative velocity compensates for the short wave length. Wave D is a trivial result: negative wave frequencies have no physical meaning.

TABLE 1.3

REGULAR WAVE SYSTEMS GIVING $|\omega_e| = 0.2$ RAD/SEC
SHIP SPEED 20 KNOTS: FOLLOWING WAVES.

Wave	ω_e (rad/sec)	ω (rad/sec)	c (m/sec)	$U-c$ (knots)	λ (m)
A	0.2	0.285	34.4	-46.8	759
B	0.2	0.667	14.7	-8.5	139
C	- 0.2	1.12	8.8	+2.9	49
D	(- 0.2)	(-0.17)	-	-	-

Using the identity

$$\lambda = \frac{2\pi g}{\omega^2} \quad m$$

(see Table 1.1), Equation (1.36) is plotted in Figure 1.16. The diagram may be used to find the wave length corresponding to any given encounter frequency for a particular speed and heading. As already demonstrated, a particular encounter frequency is experienced at only one wave length (or wave frequency) in head or bow waves; but in following and quartering waves up to three different wave systems will yield the same absolute encounter frequency. Figure 1.16 also demonstrates another peculiar property of regular waves. In following and quartering waves a wide range of wave lengths may produce virtually the same encounter frequency. For example, a ship steaming at 20 knots in quartering waves ($\mu = 45°$) has a component velocity $U \cos \mu$ of about 7.0 metres/second. In this condition all the wave lengths from about 50 metres to about 400 metres yield an encounter frequency close to about 0.3 radians/second. Heavy rolling will occur if the ship's natural roll frequency is close to this common encounter frequency.

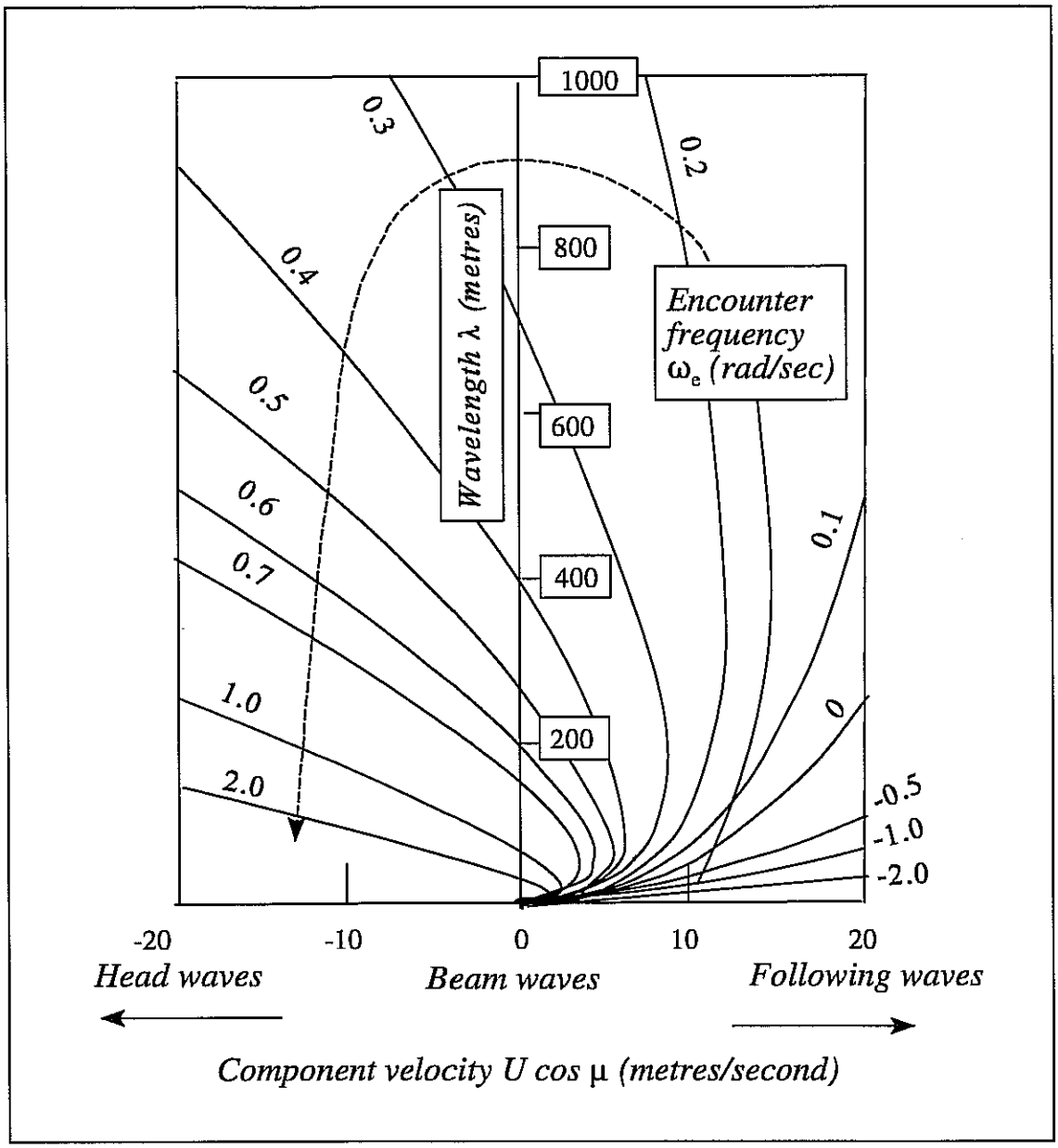

Fig 1.16 - Encounter frequency and wave length.

2

OCEAN WAVE SPECTRA AND STATISTICS

"Great fleas have littler fleas
upon their backs to bite 'em.
And little fleas have lesser fleas
and so on ad infinitum"

Augustus de Morgan: "A budget of paradoxes" c 1850.

2.1 WAVE GENERATION

As explained in Chapter 1, a knowledge of the characteristics of regular waves is an important asset to the naval architect. However, such waves do not occur in the real ocean environment and this chapter is concerned with the characteristics of naturally occurring "real" waves. The waves which are of the most concern are those which arise in the ocean through the action of the natural wind. Other wave generation mechanisms exist but are of little practical importance except in special circumstances.

The average reader of this book need not concern himself with the detailed study of the way wind driven waves are formed. Suffice it to say that a steady wind blowing over an open stretch of calm water will create ripples which will travel across the surface in more or less the same direction as the wind (see Figure 2.1).

If the wind continues to blow for long enough and sufficient length of water or ***fetch*** is available, the ripples will advance and grow in length and height until they can more properly be called waves. At the same time, the wind generates new ripples on the surface of the growing waves and these ripples will eventually grow into waves themselves. The process is of course continuous and the observed waves at any particular place and time will consist of a mixture of wave lengths and heights superimposed on each other.

It is assumed that the individual (regular) wave components still behave in the same way as they would in ideal conditions, uncontaminated by waves of other lengths. Thus the fast moving long waves continually overtake the slow moving short waves and the shape of the surface is changing all the time as the waves progress through each other.

Clearly the waves are absorbing energy from the wind. This energy absorption is countered by two principal decay mechanisms: wave breaking and viscosity. If the wind continues to blow at constant velocity for long enough and sufficient fetch is available, the rate at which energy is absorbed by the waves will eventually be exactly balanced by the rate of energy dissipation and a steady state ***fully developed*** wave system will exist. Such wave systems are rare because the required steady conditions do not often persist for long enough and the fetch may be limited by

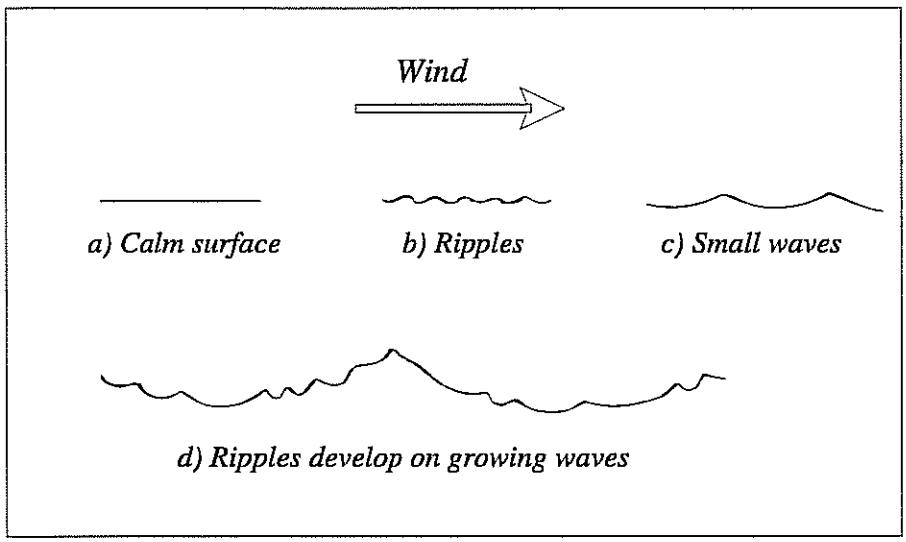

Fig 2.1 - Wind generated waves

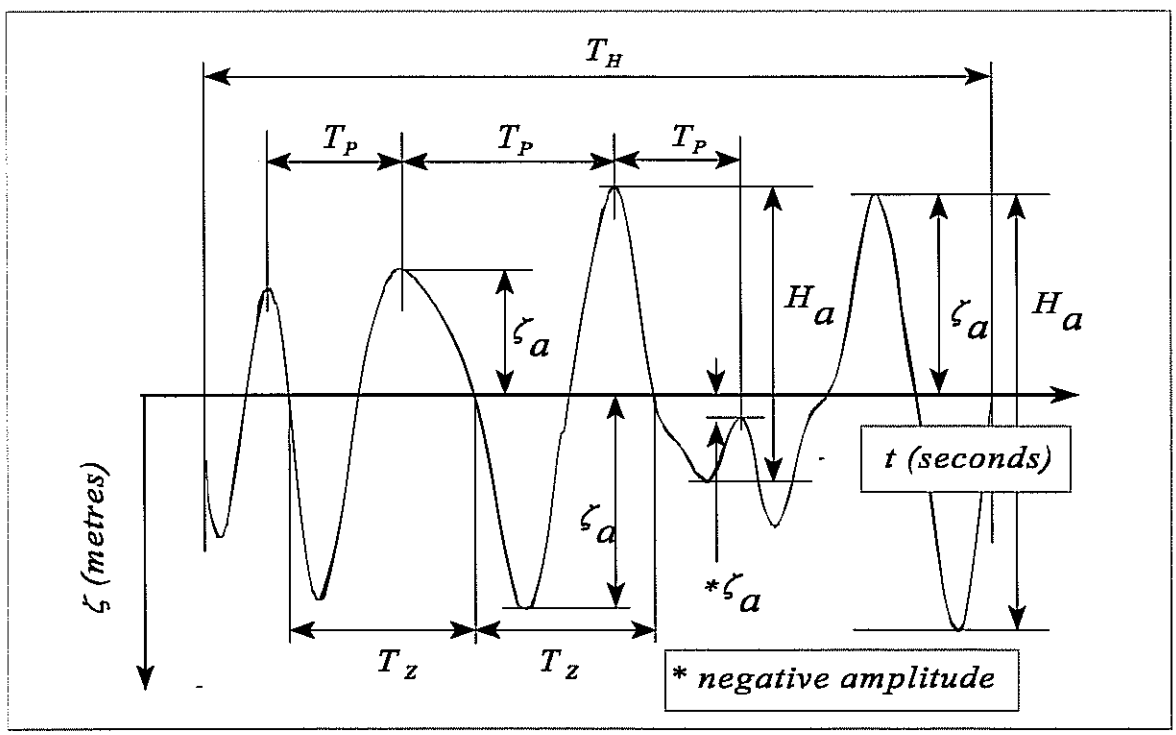

Fig 2.2 - Typical wave record: analysis of peaks and troughs

the local geography. If the wind ceases to blow, the wave system it has created will decay as the energy in the waves is dissipated. Wave breaking is a powerful decay mechanism and the short, steep waves, which are more likely to break, decay first leaving the longer waves to be dissipated by the relatively weak forces of viscosity. This decay process may last several days, during which these fast moving long waves may travel several thousand kilometres and be recognised at some distant location as a swell. Swells are generally of long period and comparatively regular. Locally generated wave systems may therefore be contaminated by swells generated elsewhere. These swells will, of course, bear no relationship to the local wind.

2.2 STATISTICAL ANALYSIS OF TIME HISTORIES OF IRREGULAR WAVES[1]

Whatever the complexities of local geography and the vagaries of the wind, an observer at sea will see a confused (and confusing) pattern of ever changing wave crests and troughs travelling in different directions. For many years this apparent chaos (and the resulting unpredictable nature of ship motions) provided an insurmountable obstacle to progress in the field of seakeeping. However, considerable progress has now been made in the application of statistical methods to quantify the characteristics of the waves on the sea surface, and these methods form one of the foundations of the modern theory of seakeeping.

Figure 2.2 shows part of a typical record of wave elevation obtained from a wave sensing device in the ocean. The record lasts for T_H seconds. As expected, the record is irregular in nature and no coherent pattern is obvious. The mean values (averaged over many samples) of four basic measurements are used to quantify the characteristics of the wave record:

Mean wave amplitude	$\bar{\zeta}_a$	metres	The mean value of many measurements of the vertical distance from the mean water level to a peak or a trough (a peak below the mean level or a trough above the mean level gives a negative amplitude; otherwise amplitudes are always positive).
Mean wave height	$\bar{H}_a$	metres	The mean value of many measurements of the vertical distance from a trough to a preceding or succeeding peak (always positive).
Mean period of the peaks	$\bar{T}_P$	seconds	The mean value of many measurements of the time between two successive peaks (or troughs).
Mean zero crossing period	$\bar{T}_z$	seconds	The mean value of many measurements of the time between two successive upward or downward zero crossings.

[1] The spectral analysis techniques and the derivation of the spectral moments in this chapter are written in the context of waves on the sea surface. However with appropriate changes of units these techniques can be equally well applied to any continuous irregular time history such as pitch, heave, roll, vertical acceleration, lateral velocity etc.

Two additional quantities are also used:

$\bar{\zeta}_{1/3}$	Significant single amplitude	The mean value of the highest third[2] of many measurements of ζ_a
$\bar{H}_{1/3}$	Significant wave height	The mean value of the highest third of many measurements of H_a

They are related as follows:

$$\bar{H}_{1/3} = 2.0\ \bar{\zeta}_{1/3} \quad m$$

In addition to the statistical measures associated with peaks, troughs and zero crossings, another class of measurements is used to quantify the characteristics of an irregular wave record. Here the time history is sampled at discrete (short) intervals of time to obtain successive measurements of the surface depression ζ_n relative to some arbitrary datum as shown in Figure 2.3. For a typical irregular wave record an appropriate time interval would be of the order of 0.5 or 1.0 second.

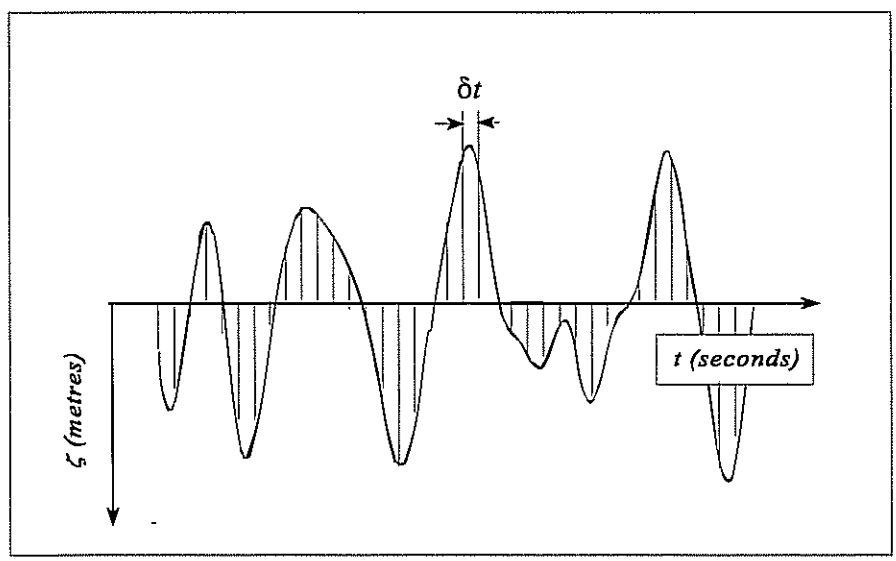

Fig 2.3 - Typical wave record: analysis at successive time intervals

[2] The "highest third" is defined as follows: Suppose that there are N measurements of wave amplitude. They are arranged in order of magnitude from the highest to the lowest. Then the significant amplitude is the mean value of the highest $N/3$ measurements.

These measurements enable three important quantities to be defined:

The mean surface depression:

$$\bar{\zeta} = \sum_{n=1}^{N} \frac{\zeta_n}{N} \quad m \tag{2.1}$$

(where N is the number of observations of surface depression)

The variance of the surface depression relative to the mean:

$$m_o = \sum_{n=1}^{N} \frac{(\zeta_n - \bar{\zeta})^2}{N} \quad m^2 \tag{2.2}$$

The standard deviation or root mean square (rms) of the surface depression relative to the mean:

$$\sigma_0 = \sqrt{m_0} \quad m \tag{2.3}$$

In passing it should be noted that a sensible analysis using either of these techniques requires a wave record containing at least 100 pairs of peaks and troughs. Such a record will be typically of about 20-30 minutes duration. Shorter records run the risk of yielding unreliable results because they may, by chance, be unusually severe or unusually moderate. The record illustrated in Figures 2.2 and 2.3 would therefore not be of adequate length for analysis. Very long records of, say, several hours should also be avoided. This is because it is quite likely that real changes in the wave statistics would occur in this time due to changes in the wind speed or the arrival of swells from distant storms.

2.3 FOURIER ANALYSIS

The continuous process of wave generation (and the typical form of an irregular wave record) suggests that any given time history of length T_H seconds might reasonably be represented by the Fourier series

$$\zeta(t) = \bar{\zeta} + \sum_{n=1}^{\infty} A_n \cos(\omega_n t) + B_n \sin(\omega_n t) \quad m \tag{2.4}$$

where the equally spaced frequencies are given by

$$\omega_n = \frac{2\pi n}{T_H} \quad rad/sec \tag{2.5}$$

with n=1, 2, 3.....∞

The coefficients are given by

$$A_n = \frac{2}{T_H} \int_0^{T_H} \zeta(t) \cos (\omega_n t) \, dt \quad m \tag{2.6}$$

$$B_n = \frac{2}{T_H} \int_0^{T_H} \zeta(t) \sin (\omega_n t) \, dt \quad m \tag{2.7}$$

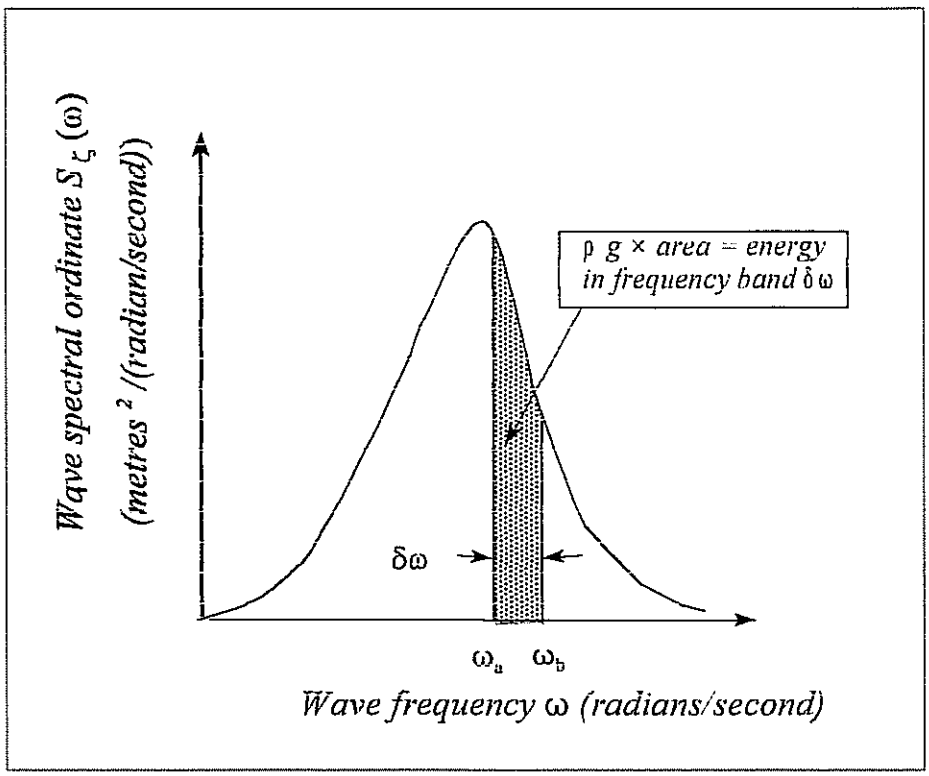

Fig 2.4 - Definition of wave energy spectrum

Equation (2.4) may be written as

$$\zeta(t) = \bar{\zeta} + \sum_{n=1}^{\infty} \zeta_{n0} \cos (\omega_n t + \epsilon_n) \quad m \tag{2.8}$$

where the coefficients are

$$\zeta_{n0} = \sqrt{A_n^2 + B_n^2} \quad m \tag{2.9}$$

and the phase angles are given by

$$\tan \epsilon_n = -\frac{B_n}{A_n} \tag{2.10}$$

In physical terms Equation (2.8) may be interpreted as representing the irregular record by the

sum of an infinite number of sine waves of amplitude ζ_{n0} and frequency ω_n. These frequencies have been chosen (using Equation (2.5)) so that one period of the lowest frequency ω_1 corresponds to the length T_H seconds of the record. Similarly the record length corresponds to two cycles of the second sine wave, three of the third and so on. The fixed interval between the frequencies is

$$\delta\omega = \omega_1 = \frac{2\pi}{T_H} \quad rad/sec \tag{2.11}$$

and $\delta\omega$ becomes very small as T_H becomes very large.

The individual sine waves are staggered with respect to each other. The phase angles ϵ_n which define the stagger are related to the time origin. $\bar{\zeta}$, the mean value of the record, is often made zero by judicious choice of the datum level of the measurements.

2.4 THE WAVE ENERGY SPECTRUM

The relative importance of the component sine waves making up an irregular wave time history (Equation (2.8)) may be quantified in terms of a ***wave amplitude energy density spectrum*** (usually abbreviated to the more easily managed ***wave energy spectrum***). The energy per square metre of the sea surface of the nth wave component is $(\rho g \zeta_{n0}^2) / 2 \quad kJ/m^2$ (Equation (1.28)). The wave energy spectrum is defined so that the area bounded by a frequency range (say ω_a to ω_b, as shown in Figure 2.4) is proportional to the total energy (per square metre of sea surface) of all the wave components within that range of frequencies. It follows that the total area enclosed by the spectrum is proportional to the total energy per square metre of the complete wave system.

We set

$$\omega_a = \omega_n - \frac{\delta\omega}{2} \quad rad/sec$$

and

$$\omega_b = \omega_n + \frac{\delta\omega}{2} \quad rad/sec$$

where $\delta\omega$ is the frequency interval.

There will be only one component frequency ω_n in the range ω_a - ω_b and the wave amplitude spectral ordinate $S_\zeta(\omega_n)$ corresponding to the frequency ω_n is defined by

$$\rho g S_\zeta(\omega_n)\, \delta\omega = \frac{\rho g \zeta_{n0}^2}{2} \quad kJ/m^2$$

so that the ***spectral ordinate*** is

$$S_\zeta(\omega_n) = \frac{\zeta_{n0}^2}{2\,\delta\omega} \quad m^2/(rad/sec) \tag{2.12}$$

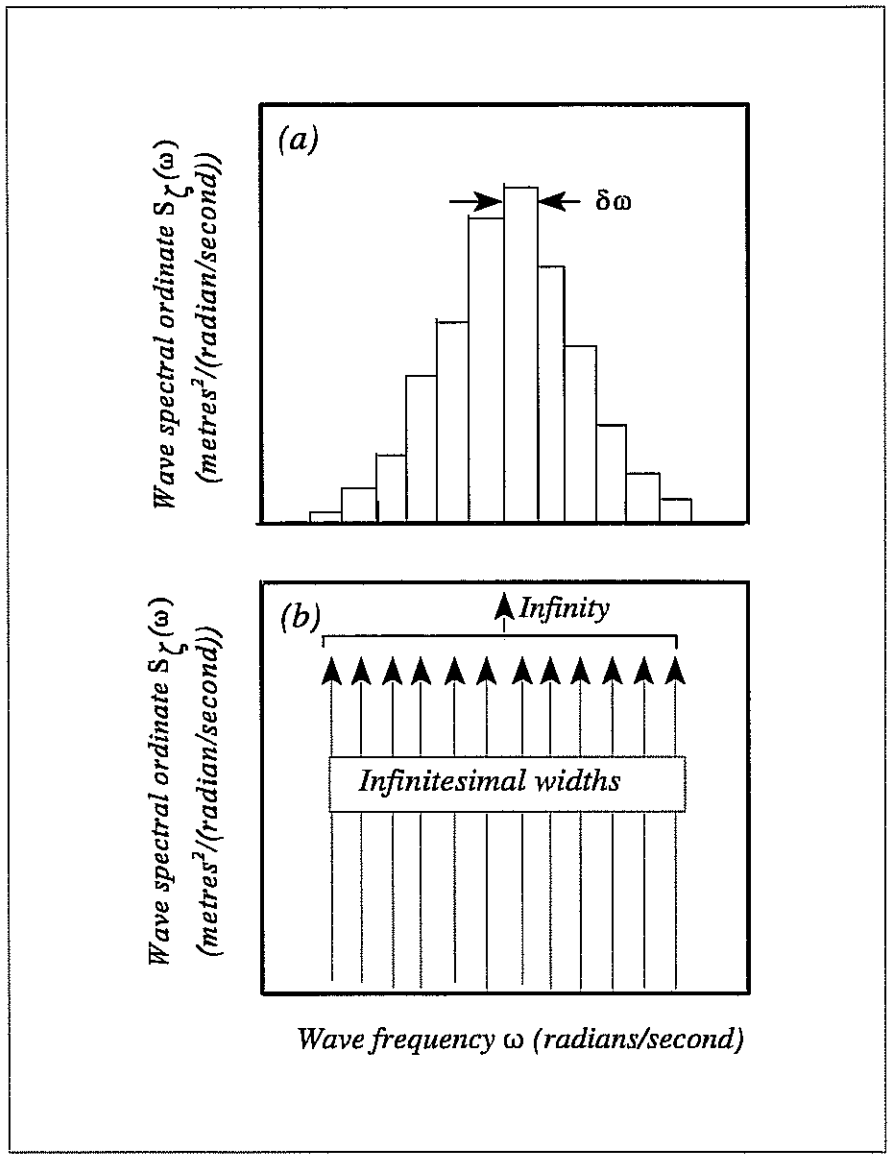

Fig 2.5 - Wave energy spectra: (a) Typical spectrum from Fourier analysis of an irregular wave time history and (b) Typical line spectrum for a time history synthesised by summing sine waves.

An energy spectrum corresponding to any irregular time history can be derived in this way and a typical example is shown in Figure 2.5(a). The spectrum is discontinuous and consists of a series of rectangles of width $\delta\omega$. The area of each rectangle is proportional to the energy attributed to that frequency band and represented by the corresponding single sine wave component.

2.5 GENERATING A TIME HISTORY FROM A SPECTRUM

If the energy spectrum is known it is possible to reverse the spectral analysis process and generate a corresponding time history by adding a large number of component sine waves according to Equation (2.8). In principle an infinite number of sine wave components is required but acceptable results can be obtained with a limited number (say 50). The form of the wave energy spectrum can be used as a guide to choosing an appropriate range of frequencies. Clearly

components corresponding to large spectral ordinates must be included but little will be lost by omitting very high and very low frequencies if their contributions to the spectrum are small.

The use of a limited number of component sine waves may give an apparently acceptable time history but it should be remembered that the energy spectrum actually being realised is not the original spectrum but a series of infinitely high spikes of infinitesimal width at each of the chosen frequencies as shown in Figure 2.5(b). The synthesised time history contains ***no*** energy at frequencies between those chosen for the synthesis.

The amplitude of each component sine wave is given by recasting Equation (2.12) as

$$\zeta_{n0} = \sqrt{2\, S_\zeta(\omega_n)\, \delta\omega} \quad m \tag{2.13a}$$

It is also necessary to specify the phase angles ϵ_n. One possible choice is the set derived from the original wave time history using Equation (2.10) and this will recreate the original time history. Other (randomly chosen) phases will give different time histories but all will have the original energy spectrum.

This classic procedure has a major flaw: the resulting synthesised time history repeats itself at intervals of T_H seconds [3] and its statistical characteristics will be unrealistic: in particular there will be one maximum wave amplitude which will be repeated at intervals of T_H seconds and the probability of the wave amplitude exceeding this value will be zero. Real ocean waves never repeat themselves and there is a finite probability of greater wave amplitudes being exceeded (see Chapter 11).

This can be avoided by synthesising the time history using ***randomly chosen frequencies***. The frequencies are selected as follows. Let us suppose that there are to be N frequencies in the range from ω_1 to ω_N. Excluding the highest and lowest frequencies we choose $N-2$ frequencies using the equation

$$\omega = \omega_1 + R(\omega_N - \omega_1) \quad rad/sec$$

where R is a random number in the range from 0 to 1. The frequencies (including ω_1 and ω_N) are then arranged in ascending order and the $N-1$ (random) frequency intervals calculated:

---

[3] Rearrange Equation (2.5) to give

$$T_H = \frac{2\,\pi\,n}{\omega_n} \quad sec$$

and substitute in Equation (2.8) to show that

$$\zeta(t) = \zeta(t + T_H) = \zeta(t + 2\,T_H) \quad ,$$

etc

$$\delta\omega_n = \omega_{n+1} - \omega_n \quad rad/sec \quad (n=1,\ N-1)$$

The random frequencies ω_n are then recalculated as the centre frequency of each frequency interval:

$$\omega_n = \sum_{m=1}^{n-1} \delta\omega_m + \frac{\delta\omega_n}{2} \quad rad/sec; \quad (n=2,\ N-1)$$

Finally the associated sine wave amplitudes are calculated using a version of Equation (2.13a)[4]:

$$\zeta_{n0} = \sqrt{2\ S_\zeta(\omega_n)\ \delta\omega_n} \quad m \qquad (2.13b)$$

where $\delta\omega_n$ is the frequency interval associated with the *n*th frequency ω_n.

2.6 SPECTRAL MOMENTS

The definition of variance given in Equation (2.2) can be written as

$$m_0 = \frac{1}{T_H} \int_0^{T_H} \zeta(t)^2\ dt \quad m^2 \qquad (2.14)$$

if the time history has a zero mean and the number of observations is very large. A time history represented by Equation (2.8) therefore has a variance

$$m_0 = \frac{1}{T_H} \int_0^{T_H} \left(\sum_{n=1}^{\infty} \zeta_{n0}\ cos\ (\ \omega_n\ t + \epsilon_n\ ) \right)^2 dt \quad m^2 \qquad (2.15)$$

Since the frequencies are chosen in accordance with Equation (2.5) this reduces to

---

[4] If the spectrum is defined at equally spaced frequencies it will be necessary to interpolate the spectral ordinates at the randomly spaced frequencies.

$$m_0 = \frac{1}{2} \sum_{n=1}^{\infty} \zeta_{n0}^2 \quad m^2 \tag{2.16}$$

and, from Equation (2.13a),

$$m_o = \sum_{n=1}^{\infty} S_\zeta(\omega)\ \delta\omega = \int_0^{\infty} S_\zeta(\omega)\ d\omega \quad m^2 \tag{2.17}$$

So the variance of the irregular wave time history is equal to the area under the wave energy spectrum.

The time history given by Equation (2.8) can be differentiated to obtain the vertical velocity and acceleration of the sea surface:

$$\dot{\zeta}(t) = \sum_{n=1}^{\infty} - \zeta_{n0}\ \omega_n\ sin\ (\ \omega_n\ t + \epsilon_n\ ) \quad m/sec \tag{2.18}$$

$$\ddot{\zeta}(t) = \sum_{n=1}^{\infty} - \zeta_{n0}\ \omega_n^2\ cos\ (\ \omega_n\ t + \epsilon_n\ ) \quad m/sec^2 \tag{2.19}$$

These can be regarded as irregular wave time histories in their own right and can be analysed to obtain statistics of velocity and acceleration in exactly the same way as for the surface depression. The amplitudes of the component sine waves for velocity and acceleration are now $(\zeta_{n0}\ \omega_n)$ and $(\zeta_{n0}\ \omega_n^2)$ respectively.

These velocity and acceleration time histories can be analysed to produce corresponding velocity and acceleration spectra. By analogy with Equation (2.12) the spectral ordinates are respectively

$$S_{\dot{\zeta}}(\omega_n) = \frac{\omega_n^2\ \zeta_{n0}}{2\ \delta\omega} = \omega_n^2\ S_\zeta(\omega_n) \quad m^2/sec^2\ per\ rad/sec \tag{2.20}$$

$$S_{\ddot{\zeta}}(\omega_n) = \frac{\omega_n^4\ \zeta_{n0}}{2\ \delta\omega} = \omega_n^4\ S_\zeta(\omega_n) \quad m^2/sec^4\ per\ rad/sec \tag{2.21}$$

So the velocity and acceleration spectral ordinates can be obtained by multiplying the displacement spectral ordinates by the second and fourth powers of the frequency.

By analogy with Equation (2.17) it is clear that the area under the velocity and acceleration spectra must be equivalent to the variances of velocity and acceleration respectively. The

variance of velocity is

$$m_2 = \int_0^\infty S_{\dot{\zeta}}(\omega)\, d\omega = \int_0^\infty \omega^2\, S_\zeta(\omega)\, d\omega \quad m^2/sec^2 \tag{2.22}$$

and the variance of acceleration is

$$m_4 = \int_0^\infty S_{\ddot{\zeta}}(\omega)\, d\omega = \int_0^\infty \omega^4\, S_\zeta(\omega)\, d\omega \quad m^2/sec^4 \tag{2.23}$$

m_2 and m_4 are called ***spectral moments*** since they can be considered as moments of area of the energy spectrum about the vertical axis. In general

$$m_n = \int_0^\infty \omega^n\, S_\zeta(\omega)\, d\omega \quad m^2/sec^n \tag{2.24}$$

and n may take any positive integer value ($n = 0, 1, 2, ...$).

2.7 MEAN PERIODS

The mean frequency can be found by taking moments about the spectral ordinate axis and determining the centre of area of the spectrum from

$$\bar{\omega} = \frac{m_1}{m_0} \quad rad/sec \tag{2.25}$$

and the corresponding mean period is

$$\bar{T} = \frac{2\,\pi\, m_0}{m_1} \quad sec \tag{2.26}$$

(The spectral moment m_1 in these formulae may be obtained by setting $n = 1$ in Equation (2.24)).

Ochi and Bolton (1973) showed that the mean period of the peaks is

$$\bar{T}_P = 2\,\pi \sqrt{\frac{m_2}{m_4}} \quad sec \tag{2.27}$$

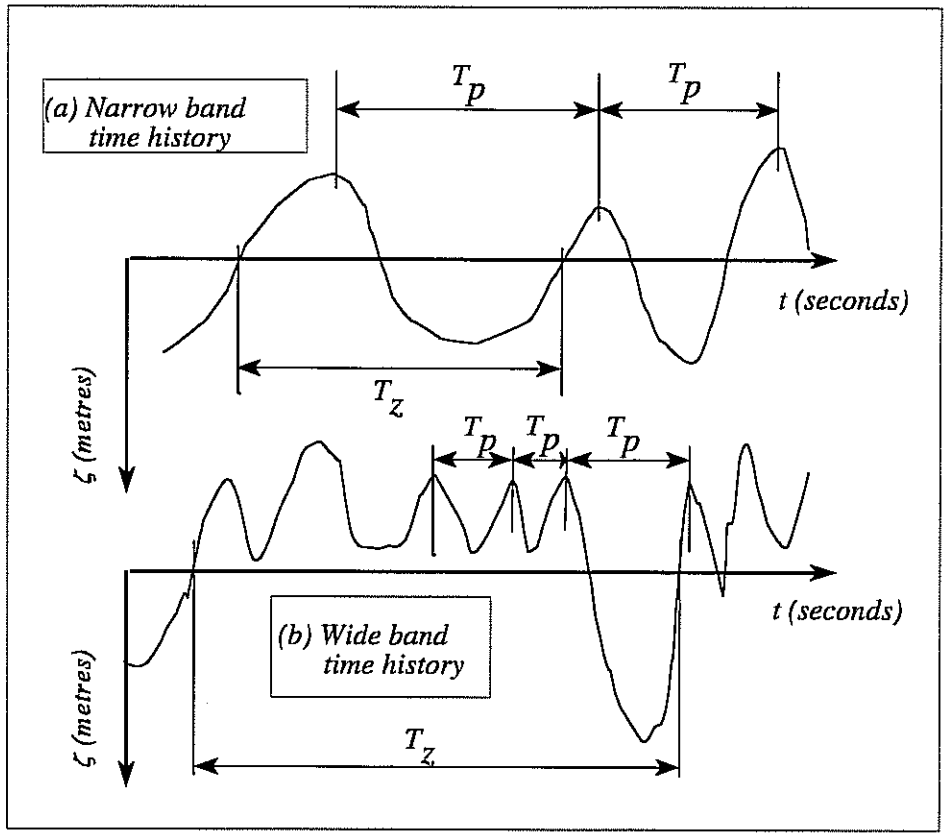

Fig 2.6 - (a) Narrow band and (b) wide band time histories

and the mean zero crossing period is

$$\bar{T}_z = 2\,\pi\,\sqrt{\frac{m_0}{m_2}} \quad sec \qquad (2.28)$$

Strictly speaking Equations (2.27) and (2.28) are valid only if the surface depression measured at equal intervals of time is normally distributed (see Chapter 11). In practice this assumption is invariably true for real ocean waves.

2.8 SPECTRUM BANDWIDTH

Figure 2.6 shows two irregular wave time histories, and sketches of the corresponding wave energy spectra are shown in Figure. 2.7. The ***narrow band*** time history of Figure 2.6(a) could loosely be described as a sine wave of varying amplitude, and the origin of the terminology is clear from the appearance of the spectrum: the wave energy is concentrated in a narrow band of frequencies and little or no energy is present at other frequencies. A peak is nearly always followed in orderly succession by a downward zero crossing, a trough, an upward zero crossing

and another peak. Peaks below the datum level are rare and it follows that the average period of the peaks is almost the same as the average zero crossing period.

The ***wide band*** time history contains energy over a wider band of frequencies as shown in Figure 2.7. In this case there are many peaks and troughs which are not immediately followed by zero crossings and the average period of the peaks is much less than the average zero crossing period. There are many peaks below the datum level and many troughs above the datum level.

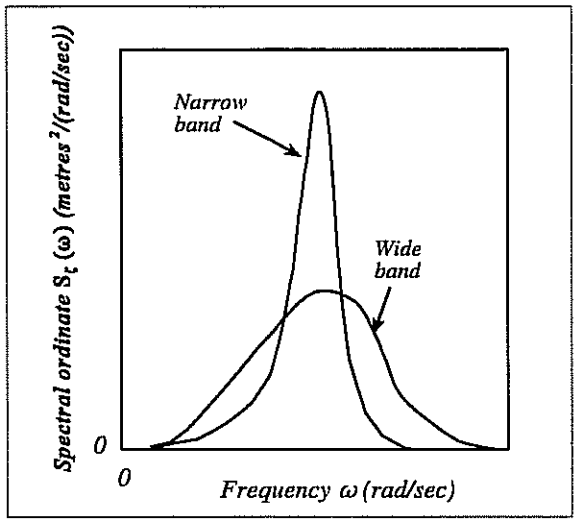

Fig 2.7 - Narrow and wide band spectra

The ratio between the average period of the peaks and the average zero crossing period can be regarded as a measure of the "narrow bandedness" of the time history and its wave energy spectrum. The ***bandwidth parameter*** is defined as

$$\epsilon = \sqrt{1 - \frac{\bar{T}_p^{\,2}}{\bar{T}_z^{\,2}}} = \sqrt{1 - \frac{m_2^2}{m_0\, m_4}} \qquad (2.29)$$

and values of ϵ lie in the range 0 to 1: $\epsilon = 0$ corresponds to a very narrow banded spectrum with

$$\overline{T_p} \approx \overline{T_z} \quad sec$$

and $\epsilon = 1$ corresponds to a very wide banded spectrum with

$$\overline{T_p} \approx 0 \quad sec$$

It is customary to assume that the spectra associated with waves and ship motions are narrow banded with $\epsilon = 0$.

Cartwright and Longuet-Higgins (1956) showed that the significant wave height can be related to the area under the wave energy spectrum by the equation

$$\bar{H}_{1/3} = 4.00 \sqrt{m_0} \sqrt{1-\frac{\epsilon^2}{2}} \quad m \tag{2.30}$$

if $\epsilon = 0$ this reduces to

$$\bar{H}_{1/3} = 4.00 \sqrt{m_0} = 4.00 \sqrt{\int_0^\infty S_\zeta(\omega)\, d\omega} \quad m \tag{2.31}$$

(see Equation (2.17))

So the significant wave height can be estimated by integrating the wave energy spectrum.

2.9 IDEALISED WAVE SPECTRA

2.9.1 Introduction

In general the wave energy spectrum derived from an analysis of an irregular wave record obtained at a particular place and time in the ocean will be a unique result that will never be exactly repeated. Although it may be a useful guide to likely wave conditions, its use for ship design purposes is strictly limited and it is customary to rely instead on families of idealised wave spectra. Current practice is to use different formulae for open ocean and coastal (limited fetch) conditions.

2.9.2 Open ocean conditions

The International Towing Tank Conference (ITTC) has adopted the Bretschneider spectrum (1952, 1957) as the standard wave energy spectrum to represent the conditions which occur in the open ocean. It is often called the ***ITTC two-parameter spectrum*** to distinguish it from an earlier standard spectrum. It is given by

$$S_{B\zeta}(\omega) = \frac{A}{\omega^5} exp\left(\frac{-B}{\omega^4}\right) \quad m^2/(rad/sec) \tag{2.32}$$

where

$$A = 172.75 \frac{\bar{H}_{1/3}^2}{\bar{T}^4} \quad m^2/sec^4 \tag{2.33}$$

and

$$B = \frac{691}{\bar{T}^4} \quad sec^{-4} \tag{2.34}$$

The "two parameters" are the significant wave height $\bar{H}_{1/3}$ and the average period $\bar{T}$ (Equation (2.26)).

The area under the Bretschneider spectrum is

$$m_0 = \int_0^\infty \frac{A}{\omega^5} exp\left(\frac{-B}{\omega^4}\right) d\omega$$

$$= \frac{A}{4B} = 0.0625\ \bar{H}_{1/3}^2 \quad m^2 \tag{2.35}$$

which confirms Equation (2.31). The moments are

$$m_2 = \int_0^\infty \frac{A}{\omega^3} exp\left(\frac{-B}{\omega^4}\right) d\omega$$

$$= \frac{A}{4}\sqrt{\frac{\pi}{B}} = 2.916\ \frac{\bar{H}_{1/3}^2}{\bar{T}^2} \quad m^2/sec^2 \tag{2.36}$$

and

$$m_4 = \int_0^\infty \frac{A}{\omega} exp\left(\frac{-B}{\omega^4}\right) d\omega$$

$$= \frac{A}{4}\Gamma(0) = \infty \quad m^2/sec^4 \tag{2.37}$$

where Γ is the gamma function.

The mean zero crossing period (Equation (2.28)) is

$$\bar{T}_z = 2\,\pi\sqrt{\frac{m_0}{m_2}} = \frac{2\,\pi}{\sqrt[4]{\pi\,B}} = 0.92\,\bar{T} \quad sec \tag{2.38}$$

and the mean period of the peaks (Equation (2.27)) is

$$\bar{T}_P = 2\,\pi\sqrt{\frac{m_2}{m_4}} = 0 \quad sec \tag{2.39}$$

The modal period T_0 of the spectrum corresponds to the frequency ω_0 of the peak, which may be obtained by differentiating Equation (2.32) and setting the result to zero. It is found that

$$\omega_0 = \sqrt[4]{\frac{4\,B}{5}} = \frac{4.849}{\bar{T}} \quad rad/sec \tag{2.40}$$

and the modal period is

$$T_0 = \frac{2\,\pi}{\omega_0} = 1.296\,\bar{T} = 1.41\,\bar{T}_z \quad sec \tag{2.41}$$

(see Equation (2.38)).

Equations (2.38) and (2.41) may now be used to define the constants A and B more fully:

$$A = 487\,\frac{\bar{H}_{1/3}^2}{T_0^4} = 173\,\frac{\bar{H}_{1/3}^2}{\bar{T}^4} = 123\,\frac{\bar{H}_{1/3}^2}{\bar{T}_z^4} \quad m^2/sec^4 \tag{2.42}$$

$$B = \frac{1949}{T_0^4} = \frac{691}{\bar{T}^4} = \frac{495}{\bar{T}_z^4} \quad sec^{-1} \tag{2.43}$$

It should be emphasised that the relationships between the periods (Equation (2.41)) are not general and apply only to the special case of the Bretschneider spectrum. Figure 2.8 shows some specimen Bretschneider wave energy spectra for a significant wave height of 4 metres and various modal periods. As expected from Equation (2.35), the area under each spectrum is the same since the significant wave height is the same in each case. The position and height of the peaks depend on the modal period.

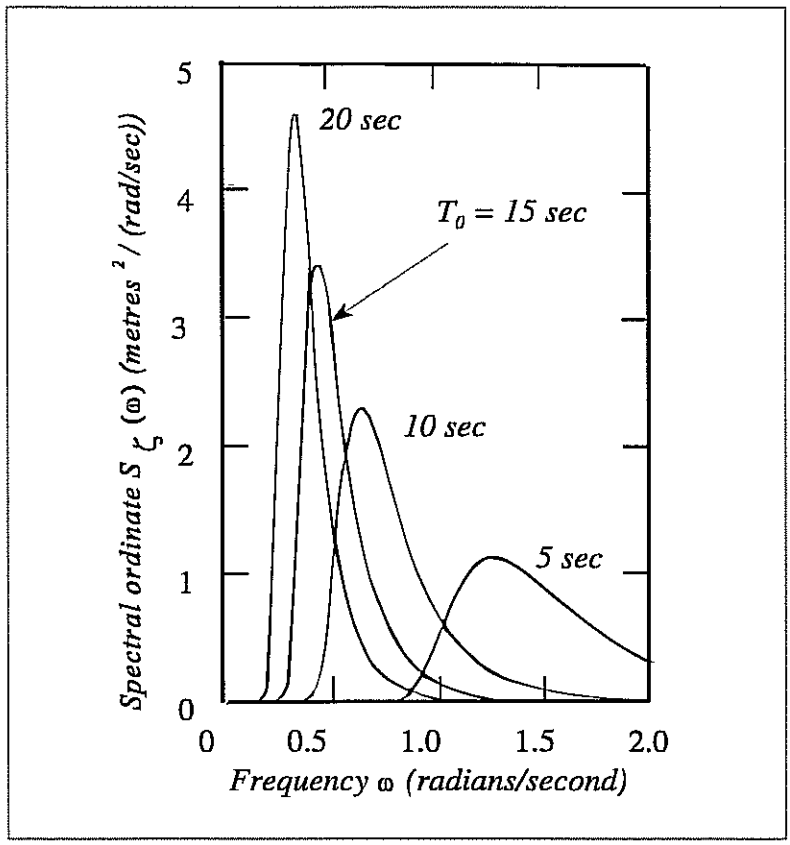

Fig 2.8 - Bretschneider wave energy spectra: Significant wave height 4.0 metres

2.9.3 Coastal waters

In coastal waters with limited fetch the Joint North Sea Wave Project spectrum is used [1] (Ewing(1975)). In the form accepted by the ITTC the spectral ordinates are defined by

$$S_{J\zeta}(\omega) = 0.658\ C\ S_{B\zeta}(\omega) \quad m^2/(rad/sec) \tag{2.44}$$

where $S_{B\zeta}(\omega)$ is the Bretschneider wave spectral density ordinate (Equation (2.32)). The factor C is given by

$$C = 3.3^J$$

where

$$J = exp\left[\frac{-1}{2\ \gamma^2}\left(\frac{\omega\ T_0}{2\ \pi} - 1\right)^2\right]$$

where $\gamma = 0.07$ for $\omega < \frac{2\pi}{T_0}$ and $\gamma = 0.09$ for $\omega > \frac{2\pi}{T_0}$

[1] Commonly known as the JONSWAP spectrum

Figure 2.9 shows a comparison between the two spectra for a significant wave height of 4 metres and modal period of 10 seconds.

2.10 WAVE SLOPE SPECTRA

An irregular record of wave slope can be analysed to produce an energy spectrum in the same way as an irregular record of wave depression. There are now an infinite number of component sine waves of the form given in Equation (1.15) and the wave number of the *n*th sine wave component is

$$k_n = \frac{\omega_n^2}{g} \quad m^{-1}$$

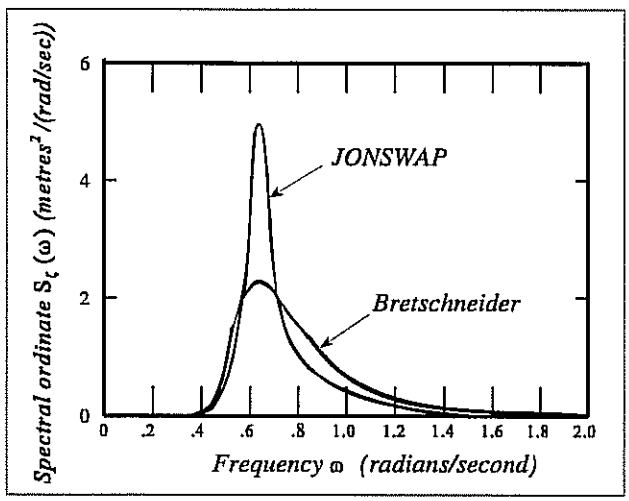

Fig 2.9 - JONSWAP and Bretschneider wave energy spectra: significant wave height 4.0 metres; modal period 10 seconds.

The wave slope amplitude of the *n*th sine wave is given by Equation (1.16):

$$\alpha_{n0} = k_n \zeta_{n0} = \frac{\omega_n^2 \zeta_{n0}}{g} \quad rad \qquad (2.45)$$

and the wave slope spectral ordinates are given by

$$S_\alpha(\omega_n) = \frac{\alpha_{n0}^2}{2\,\delta\omega} = \frac{\zeta_{n0}^2\,\omega_n^4}{2\,g^2\,\delta\omega} = \frac{\omega_n^4}{g^2} S_\zeta(\omega_n) \quad rad^2/(rad/sec) \qquad (2.46)$$

(see Equation (2.12)).

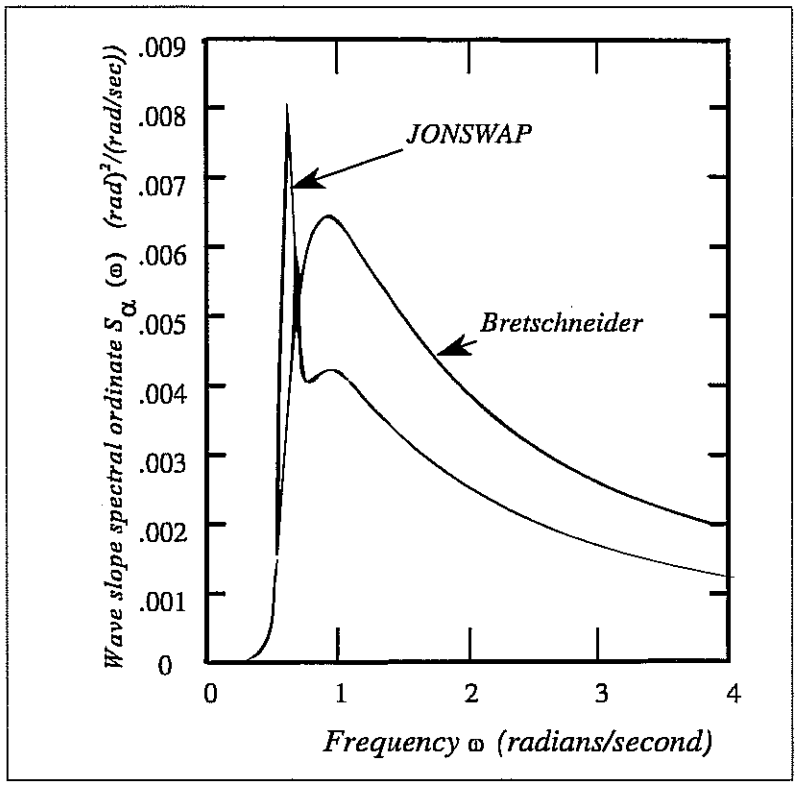

Fig 2.10 - Wave slope spectra: significant wave height 4.0 metres; modal period 10 seconds

So the wave slope energy spectrum can be obtained by multiplying the wave amplitude spectral ordinates by ω_n^4 / g^2.

The Bretschneider and JONSWAP wave slope spectra are then

$$S_{B\alpha}(\omega) = \frac{A}{\omega\, g^2} \exp\left(\frac{-B}{\omega^4}\right) \quad rad^2/(rad/sec) \qquad (2.47)$$

and

$$S_{J\alpha}(\omega) = 0.658\ C\ S_{B\alpha}(\omega) \quad rad^2/(rad/sec) \qquad (2.48)$$

Figure 2.10 shows examples of these wave slope spectra. The JONSWAP spectrum is very sharply peaked but the most striking comparison with the shapes of the corresponding wave amplitude spectra (Figure 2.9) is the much greater comparative importance of high wave frequencies. This corresponds with practical observations: short high frequency waves are often very steep even though their amplitudes are very small.

All the relationships derived for wave amplitude spectra (Equations (2.12)-(2.30)) have

analogous relationships for wave slope spectra. Thus, for example, the variance of wave slope can be obtained by integrating the wave slope spectrum.

2.11 WAVE SPREADING AND SHORT CRESTED WAVES

In ideal conditions in the open ocean all the waves might be expected to travel in the same direction. However, these ***long crested*** waves in which the wave crests remain straight and parallel are never experienced outside the artificial confines of the laboratory towing tank, although approximations may occasionally be found at sea. It is much more likely that the real waves in the ocean will be travelling in many different directions, although an easily recognised "primary" direction, often more or less aligned with the local wind, may be discernible. Changes in wind direction, the influence of coastlines and bottom topography and the presence of wave systems originally generated elsewhere will all conspire to ensure that the true long crested wave system is at least a rarity and probably a myth.

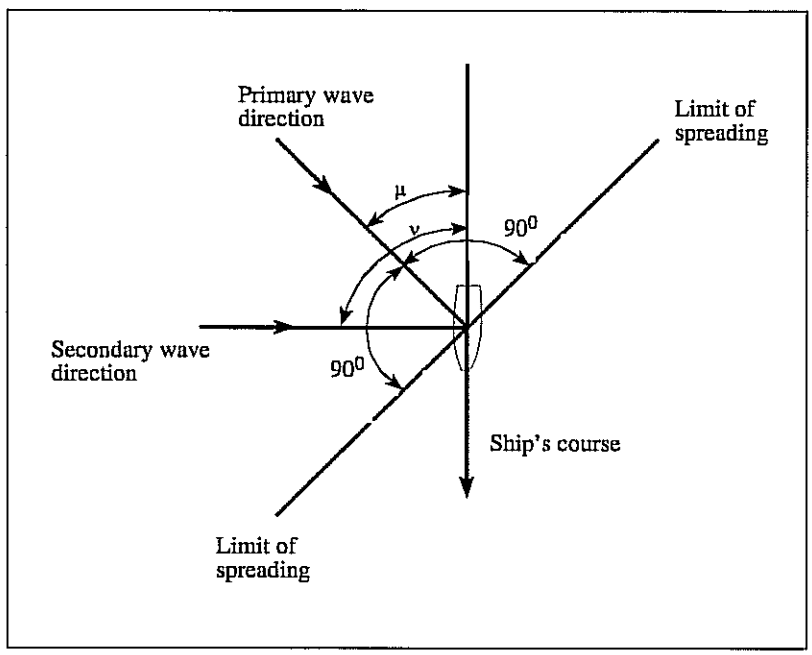

Fig 2.11 - Primary and secondary wave directions.

The presence of more than one long crested wave system results in alternate enhancement and cancellation of wave crests and troughs, and this phenomenon gives rise to the term ***short crested*** to describe the appearance of a wave system with a spread of wave directions.

The wave energy spectrum derived from a record of surface elevations obtained at a particular point in the ocean will invariably contain contributions from several different wave directions. It is often convenient to ignore this fact and assume that the wave system is long crested, and for many purposes this may give acceptable results. However, the degree of wave spreading does have a profound influence on some ship motions (particularly roll) and its effect cannot always be ignored (see Chapter 8).

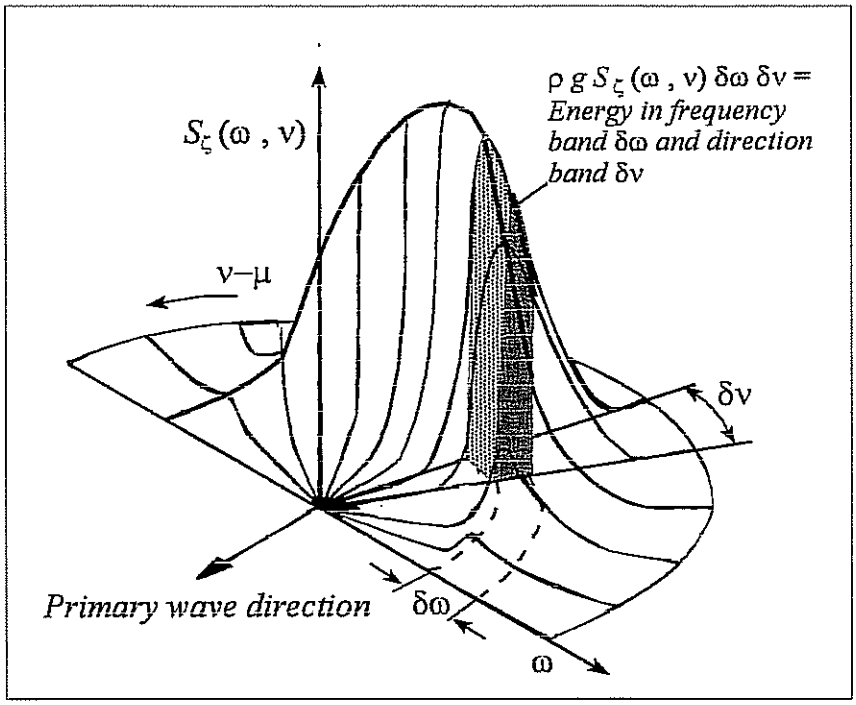

Fig 2.12 - Directional wave spectrum

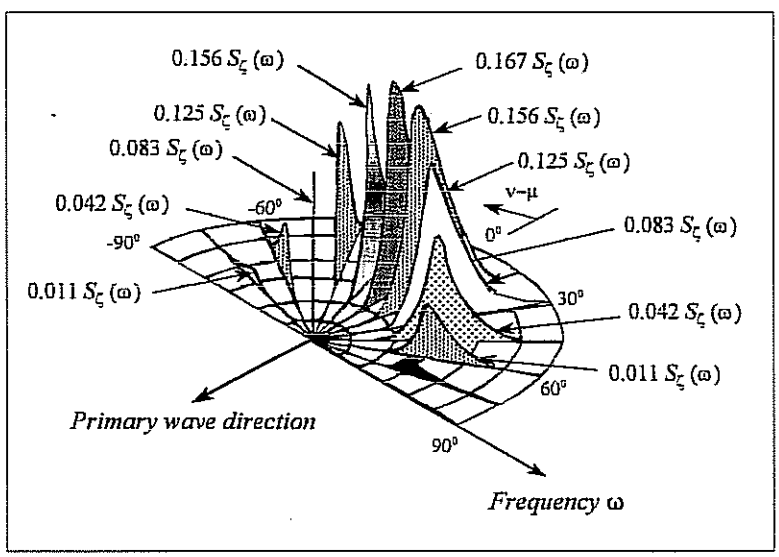

Fig 2.13 - Representation of a directional wave spectrum by thirteen long crested spectra at discrete heading intervals of 15^0 : cosine squared spreading over $\pm 90^0$.

An infinite number of possibilities exist, but for design purposes it is usual to assume that if the primary wave direction is μ relative to some fixed datum (usually the ship's course: see Figure 2.11), the secondary wave directions ν are distributed in the range $-\pi/2 < (\nu - \mu) < \pi/2$. The directional wave spectrum is defined such that the quantity $\rho\, g\, S_\zeta(\omega,\nu)\, \delta\omega\, \delta\nu$ is equivalent to the wave energy contained in the frequency band $\delta\omega$ and the direction band $\delta\nu$ as shown in Figure 2.12. Hence the directional spectral density ordinate, by analogy with Equation

(2.12), is given by

$$S_\zeta(\omega,\nu) = \frac{\zeta_{nj0}^2}{2\ \delta\omega\ \delta\nu} \quad m^2/(rad/sec)\ per\ rad \tag{2.49}$$

where ζ_{nj0} is now the amplitude of the component sine wave appropriate to the nth frequency and the jth direction. For ship design purposes it is assumed that the directional wave spectral ordinates are related to the ordinates of the equivalent total wave energy spectrum $S_\zeta(\omega)$ by

$$S_\zeta(\omega,\nu) = \frac{2}{\pi}\ cos^2(\ \nu - \mu\ )\ S_\zeta(\omega) \quad m^2/(rad/sec)\ per\ rad \tag{2.50}$$

Trials evidence (Cummins and Bales (1980)) suggests that this ***cosine squared*** spreading is appropriate for typically occurring conditions in the open ocean.

TABLE 2.1

WEIGHTING FACTORS FOR CALCULATIONS OF SHIP MOTIONS IN SHORT CRESTED WAVES.
Cosine squared spreading over $\pm\ 90^0$

$\delta\nu = 15^0$

$\nu - \mu$	W
$\pm\ 90^0$	0.000
$\pm\ 75^0$	0.011
$\pm\ 60^0$	0.042
$\pm\ 45^0$	0.083
$\pm\ 30^0$	0.125
$\pm\ 15^0$	0.156
0	0.167

Equation (2.50) is of little direct use in practical computations of ship motions in short crested seas. These calculations (see Chapter 8) require the spread wave spectrum to be represented by a discrete (long crested) contribution from each of a finite number of secondary wave directions within the range of the spreading. Each contribution is essentially a scaled down version of the total wave energy spectrum as shown in Figure 2.13. If the secondary wave directions are spaced at intervals of $\delta\nu$ the appropriate wave energy spectrum at each secondary direction is given by

$$W\ S_\zeta(\omega) \quad m^2/(rad/sec)$$

where the weighting factor W is

$$W = \frac{2}{\pi} \cos^2 (\nu - \mu) \delta\nu \qquad (2.51)$$

Table 2.1 lists the weighting factors for intervals of $\delta\nu = 15°$.

2.12 OCEAN WAVE STATISTICS

2.12.1 Introduction

We have seen how an idealised wave energy spectrum may be defined in terms of the significant wave height and various measures of the average wave period. This allows representative spectra to be constructed for any point in the ocean provided these quantities are known. Of course many different combinations of significant wave height and average period may occur at any particular location. For practical ship design purposes we need to choose appropriate values for the sea areas and seasons in which the ship is expected to operate.

2.12.2 Visual Observations of Wave Height and Period

The description of the mechanism of wave generation given at the start of this chapter shows that there can be no unique correlation between wind speed and wave height. Nevertheless mariners have traditionally used the visual appearance or "state" of the sea as an indication of the local wind speed. This led to the concept of a numerical scale of ***sea state*** as a measure of the severity of the waves and different scales were evolved by different national authorities. These scales have often been used to report sea conditions in preference to more precise estimates of wave height and period.

TABLE 2.2
WORLD METEOROLOGICAL ORGANISATION (WMO)
SEA STATE CODES

Sea state code	Significant wave height range (m)	Mean significant wave height (m)	Description
0	0	0	Calm (glassy)
1	0 - 0.1	0.05	Calm (rippled)
2	0.1 - 0.5	0.3	Smooth (wavelets)
3	0.5 - 1.25	0.875	Slight
4	1.25 - 2.5	1.875	Moderate
5	2.5 - 4.0	3.25	Rough
6	4.0 - 6.0	5.0	Very rough
7	6.0 - 9.0	7.5	High
8	9.0 - 14.0	11.5	Very high
9	Over 14.0	Over 14.0	Phenomenal

In 1970 the World Meteorological Organisation (WMO) agreed the standard sea state code given in Table 2.2. Each sea state number corresponds to a range of significant wave heights but there is no indication of period.

As such the sea state can be regarded, at best, as a rather vague and indeterminate indication of wave conditions which is of only limited use in reporting sea conditions. Nevertheless its use is so well established and wide spread in the seafaring community that naval architects and oceanographers must sometimes tolerate its deficiencies.

With encouragement from oceanographers sailors now often report sea conditions in more detail by estimating the "average" wave height and period. Hogben and Lumb (1967) compared these visual observations with values measured by wave buoys and other suitable instruments and obtained the following approximate relationships:

$$\bar{H}_{1/3} \approx 1.06\ \bar{H}_{obs} \quad m \tag{2.52}$$

$$\bar{T}_z \approx 0.73\ \bar{T}_{obs} \quad sec \tag{2.53}$$

$$T_0 \approx 1.12\ \bar{T}_{obs} \quad sec \tag{2.54}$$

Nordenström (1969) derived alternative expressions:

$$\bar{H}_{1/3} \approx 1.68\ \bar{H}_{obs}^{0.75} \quad m \tag{2.55}$$

$$\bar{T}_z \approx 0.82\ \bar{T}_{obs}^{0.96} \quad sec \tag{2.56}$$

If we assume the Bretschneider spectrum period relationships (Equations (2.41)), Nordenström's period relationship can also be written as

$$T_0 \approx 1.16\ \bar{T}_{obs}^{0.96} \quad sec \tag{2.57}$$

These relationships are illustrated in Figures 2.14 and 2.15. It may be concluded that observer's estimates of average wave height correspond reasonably closely to the significant wave height[2]. Average visual estimates of wave period apparently agree quite well with the modal period but Hogben and Lumb (1967) found that individual estimates were often widely scattered and could not be regarded as reliable.

2.12.3 Wave Atlases

A very comprehensive atlas based on over 55 million visual observations from ships on passage between 1854 and 1984 was published as "***Global Wave Statistics***" by Hogben, Dacunha and Olliver (1986). This superseded the earlier work by Hogben and Lumb (1967).

---

[2] Since the true mean wave height must, by definition, be less than the significant wave height this implies that observers ignore the smaller waves when making their estimates.

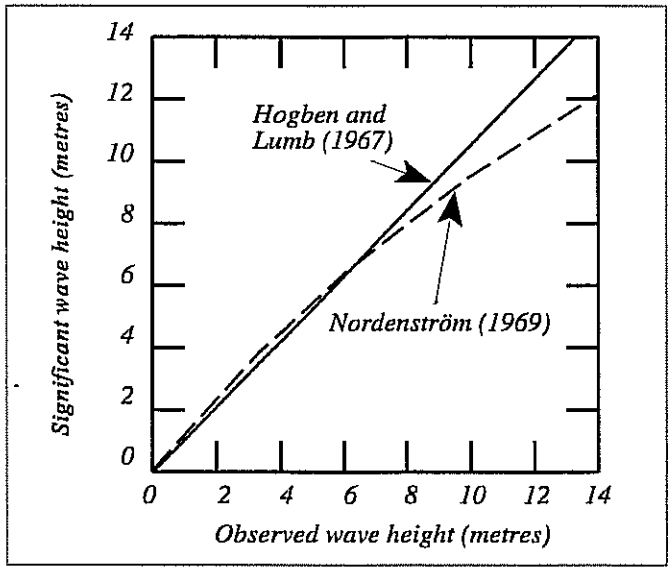

Fig 2.14 - Observed and significant wave heights.

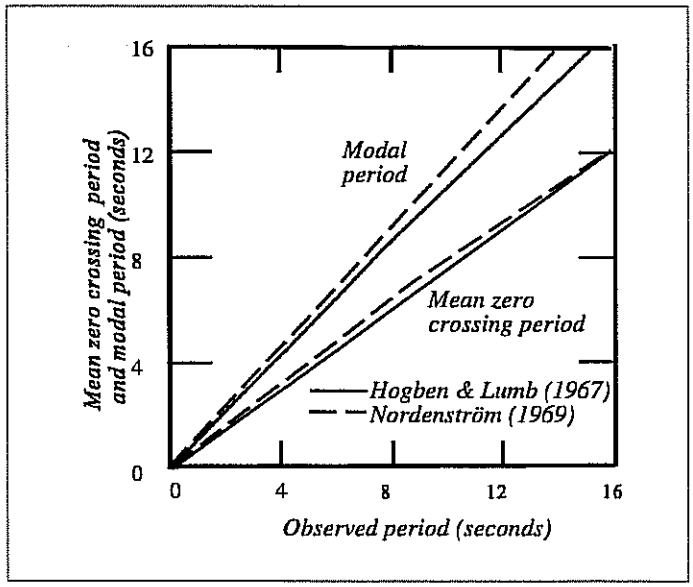

Fig 2.15 - Observed, modal and mean zero crossing periods

The reliability of the raw visual observations of wave height was enhanced by correlating them with simultaneous observations of wind speed. This allowed obviously unrealistic estimates of wave height to be eliminated from the data base. The unreliable visual estimates of the wave period were not used at all. Instead, wave period statistics were constructed from correlations with measured data.

Data were collected for the sea areas shown in Figure 2.16. Table 2.3 shows a typical set of data for Area 9 (west of the British Isles) in winter. The data are subdivided into different wave directions and are presented in the form of scatter diagrams, giving the joint frequency of occurrence (in parts per thousand) of particular combinations of significant wave height and zero crossing period occurring simultaneously.

For example the probability of occurrence of wave heights from all directions in the range 4 - 5 metres with periods in the range 9 - 10 seconds is 58/1000 = 0.058.

The frequency of occurrence of waves from each of the specified directions is given as "percentage of observations" at the top of each scatter diagram. Also shown at the right hand side of each diagram is the frequency of occurrence of each significant wave height range for all periods. The frequency of occurrence of each period range for all wave heights is shown at the top of each diagram. For example the probability of waves of any period from the West having a significant wave height falling in the range 4 - 5 metres is 149/1000 = 0.149.

We shall see in Chapter 17 that a proper assessment of seakeeping performance should take account of all the wave conditions the ship might experience during its service life. Data sources like those presented in Table 2.3 provide a basis for such an assessment. However a less comprehensive evaluation is sometimes more appropriate (say in the early stages of a new design) and the calculations may then be restricted to a range of significant wave heights and their associated most probable modal periods. Figure 2.17 gives data in the required form, taken from Table 2.3.[4]

Figure 2.18 shows the probability of exceeding specified significant wave heights for four different sea areas. Clearly Area 9 has one of the most severe wave environments in the world, closely followed by the North Sea. The Gulf of Mexico is particularly benign.

A similar wave atlas based on visual observations for the North Pacific, with particular emphasis on the seas around Japan, was published by Takaishi, Matsumoto and Ohmatsu (1980).

Wave statistics based on visual observations must always be considered less reliable than direct measurements of wave conditions even if the reliability has been enhanced as described above. However, a more serious criticism of visually observed wave data lies in the fact that ship's masters generally try to avoid bad weather and this is likely to introduce a fair weather bias into the results. So the published tables will tend to underestimate the probability of extremely severe

[4] The zero crossing periods have been translated into modal periods using Equation (2.41) although this is strictly valid only for the Bretschneider spectrum.

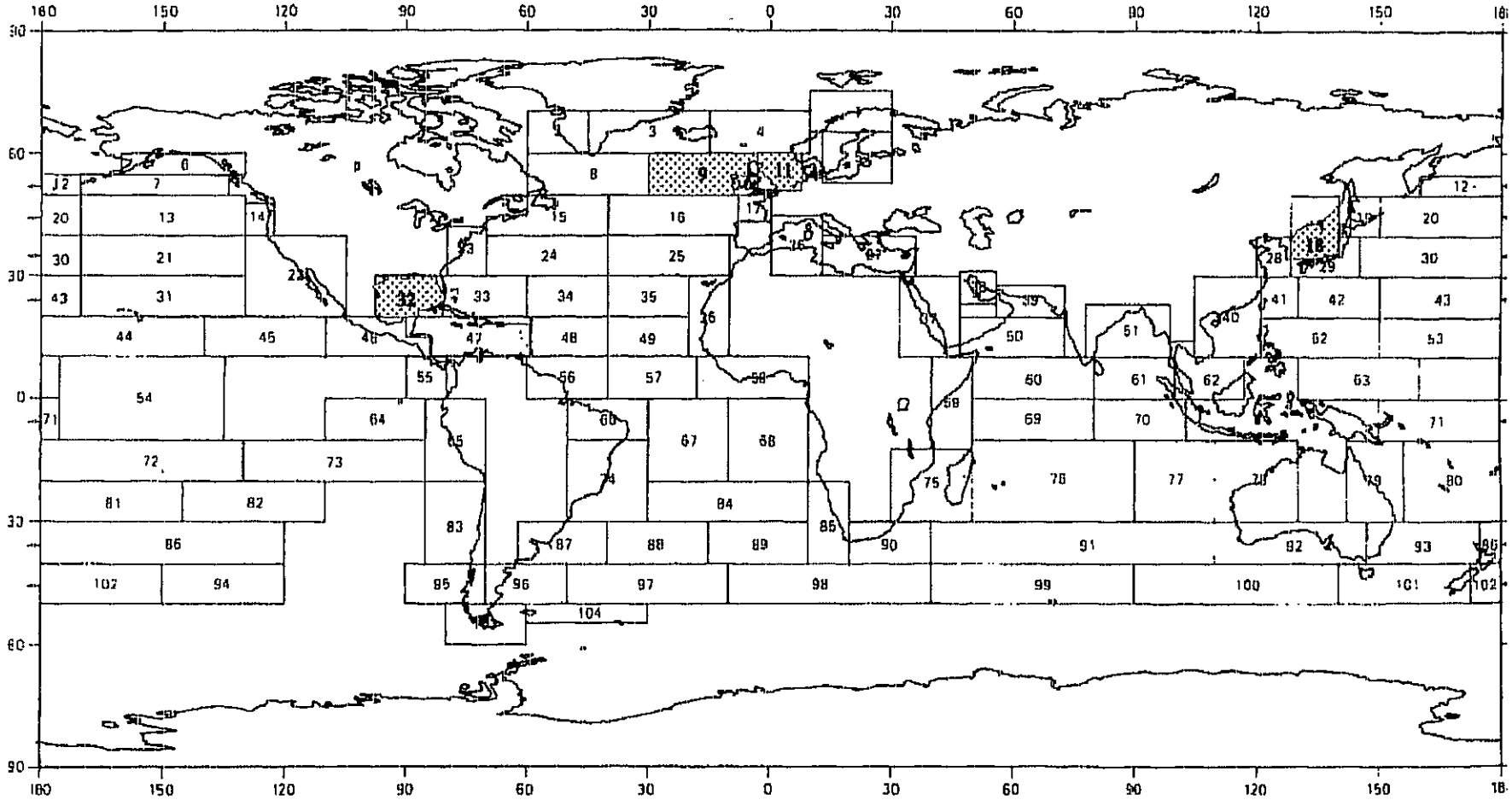

Fig 2.16 - Sea areas used by Hogben, Dacunha and Olliver (1986).
Data for shaded areas are given in Table 2.3 and Figures 2.17 and 2.18.
Reproduced by permission of British Maritime Technology Ltd.

TABLE 2.3
WAVE HEIGHT AND PERIOD STATISTICS;
Probabilities in parts per thousand.
December - February ; Sea Area 9
(After Hogben, Dacunha and Olliver (1986)

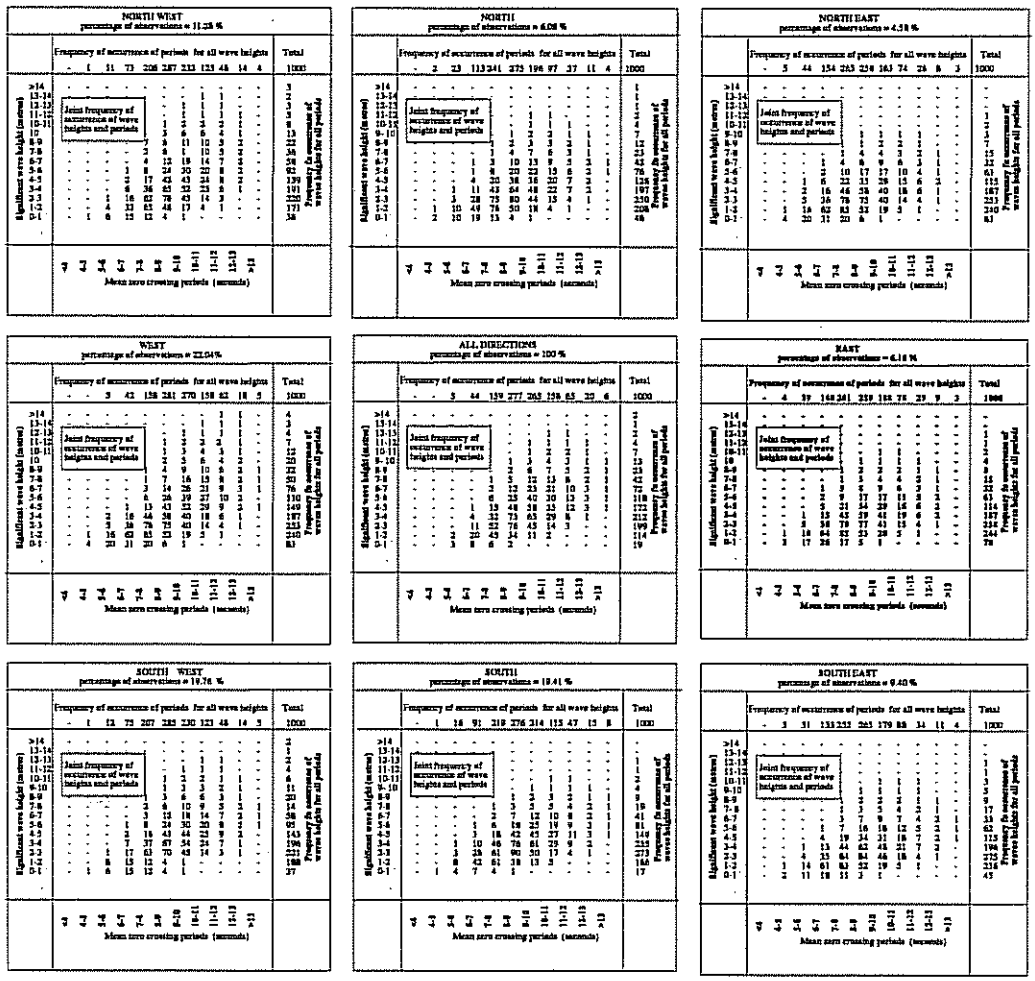

weather conditions. It may be argued that this bias makes the statistics applicable to ships which have freedom to avoid bad weather.Vessels which must remain on station such as warships, weather ships and offshore platforms may well experience bad weather more frequently than these statistics would imply.

Bales, Lee and Voelker (1981) published a wave atlas for the North Atlantic, North, Mediterranean, Black and Baltic Seas. They used measured wind data obtained over a period of twenty years for the sea areas in question to "hindcast" the waves which would have occurred as

a result of the measured winds. The prediction technique used was devised by Pierson, Tick and Baer (1966) and calculations of wave spectra were made at six hourly intervals for the period 1959 - 1969 for the sea areas shown in Figure 2.19. A total of over 133,000 wave spectra were calculated and compiled to produce statistics in much the same way as shown in Table 2.3.

In addition to data on wave heights and periods Bales' atlas gives information on wind speed and wind and wave direction. The atlas also contains limited data on visibility, cloud cover, precipitation, relative humidity, air and water temperatures, sea level pressure and ice. Table 2.4 shows an example of a scatter diagram for wind speed and significant wave height for the entire North Atlantic.

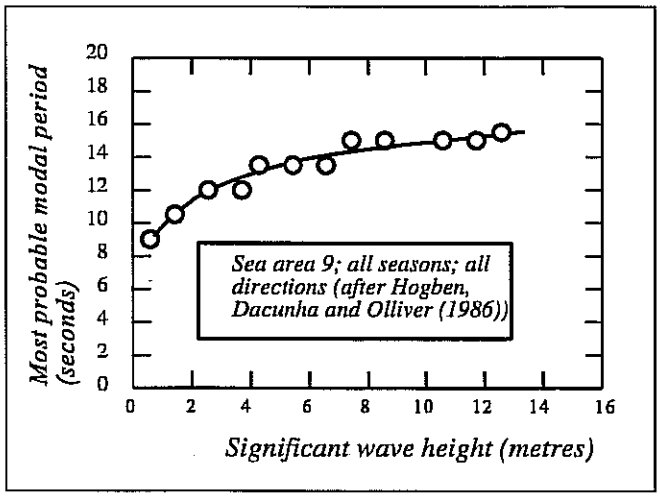

Fig 2.17 - Most probable modal periods

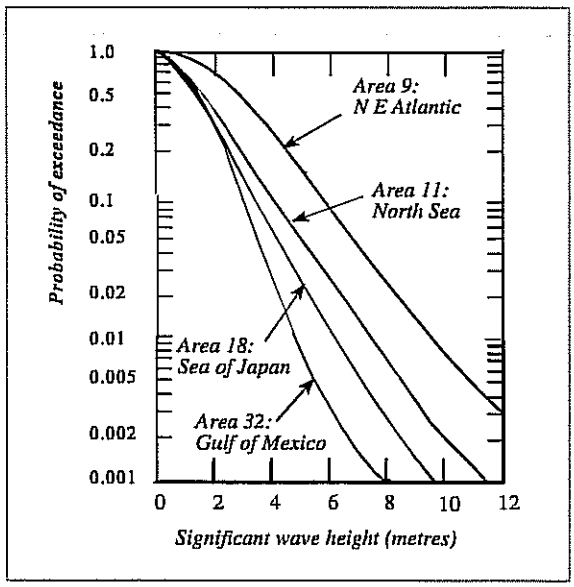

Fig 2.18 - Probability of exceeding specified significant wave heights in four sea areas. (After Hogben, Dacunha and Olliver (1986))

TABLE 2.4

ANNUAL WIND SPEED AND WAVE HEIGHT STATISTICS
FOR THE NORTH ATLANTIC

(Probabilities in parts per thousand)
(After Bales, Lee and Voelker (1981))

$\bar{H}_{1/3}$ *metres*	WIND SPEED (Knots) 0-4	4-7	7- 11	11-17	17-22	22-28	28-34	34-41	41-48	48-55	>55	Total
>24												
20-24												
16-20										+	+	+
14-16							+	+		+	+	+
12-14					+	+	+	+	+	1	+	1
10-12	+	+		+	+	+	+	1	2	1	+	4
9-10		+	+	+	+	+	1	2	2	+	+	6
8-9	+	+	+	+	+	1	2	5	2	+	+	11
7-8	+	+	+	1	1	2	5	8	1	+		18
6-7	+	+	1	2	3	7	11	8	+	+		32
5-6	+	1	1	5	7	14	21	3	+	+		52
4-5	1	12	4	12	16	30	15	1	+			80
3-4	2	4	10	28	37	43	2	+				125
2-3	5	12	26	66	67	10	+	+	+			187
1-2	17	34	69	23	16	+	+					259
0-1	41	68	92	24	+	+						225

+ indicates less than one part per thousand.

Lee, Bales and Sowby (1985) have published a similar atlas for the Pacific Ocean.

The hindcast technique avoids the problems of accuracy and fair weather bias associated with visually observed wave data but depends, of course, on the reliability of the mathematical model used to predict the wave conditions.

If both visually estimated and hindcast wave data are subject to uncertainties, direct measurements of wave spectra must provide the most reliable data of all. However, measuring wave data over a protracted period (years) is an expensive and complicated undertaking and few attempts at systematic data collection have been made. Probably the most comprehensive is that organised by the US National Oceanographic and Atmospheric Administration (NOAA) and published by Gilhousen et al (1983). The measurement buoys were deployed for at least three years and some were in continuous operation for as long as nine years at various locations around the United States. They recorded information on air and sea temperature and atmospheric pressure as well as wind and waves. The waves were sampled every three hours and a wave spectrum derived from the recorded time history. The significant wave height and mean zero crossing period were derived using Equations 2.31 and 2.28 and scatter diagrams similar to those shown in Table 2.3 prepared.

Many other measurements of wave conditions have been made for specific purposes at various locations throughout the world. Typically these are short term studies intended to provide data on the local environment for use in research or specific projects such as ship seakeeping trials or the design of offshore or harbour installations. Much of the data have been acquired by commercial organisations who regard them as proprietary information not available to the general public. However, in 1982 the United Kingdom Marine Information and Advisory Service (MIAS) published a catalogue listing the data sources open to general use. Over 1350 entries were catalogued. The majority of the measurements were made in the coastal waters around the British Isles and in the North Sea, but a significant quantity of data are also available for North American and Australian waters.

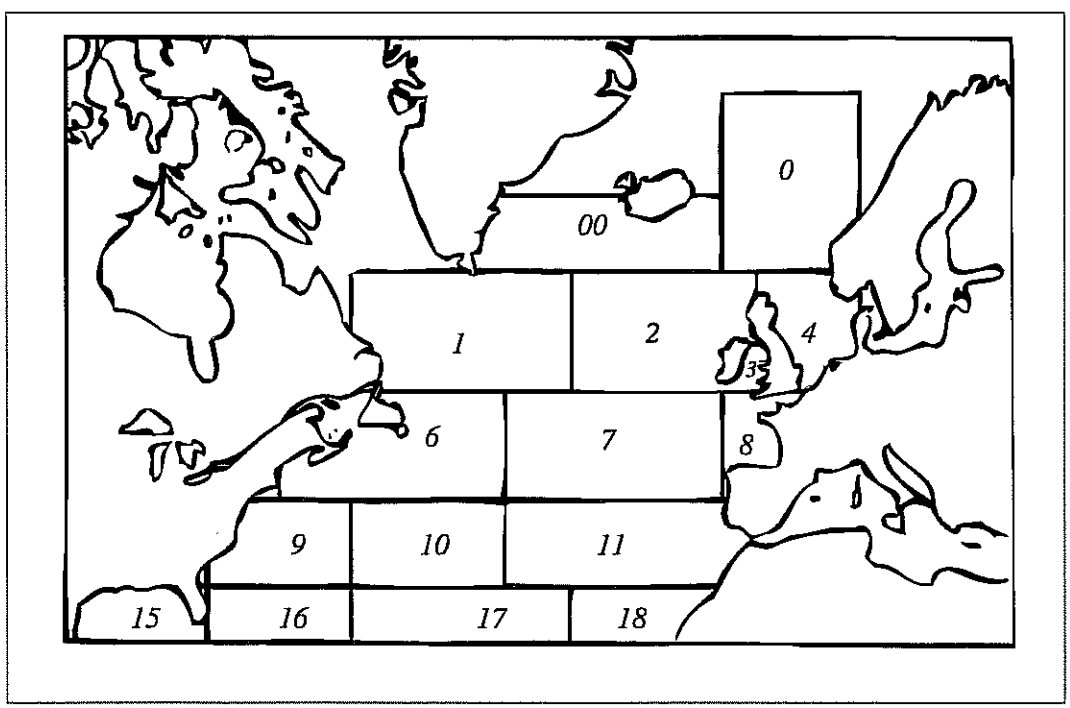

Fig 2.19 - Sea areas used by Bales, Lee and Voelker (1981)

2.12.4 Annual growth of wave heights

Bacon and Carter (1991) and Barrat (1991) showed that the wave heights measured and observed on ocean weather ships in the North Atlantic have been increasing for at least the last thirty years. Hogben (1994) summarised the data and showed that the mean significant wave height appears to be growing at a rate of about 1.5% per year, as shown in Figure 2.20. This implies that the wave heights derived from wave atlas data should be increased by a factor F to take account of the time lapse between data collection and the time when the ship is expected to be in service:

$$F = \frac{\left[\bar{H}_{1/3}\right]_{service}}{\left[\bar{H}_{1/3}\right]_{data}} = 1.015^{\Delta} \qquad (2.58)$$

where Δ is the elapsed time in years between the time the wave data were collected and the time the ship is to enter service.

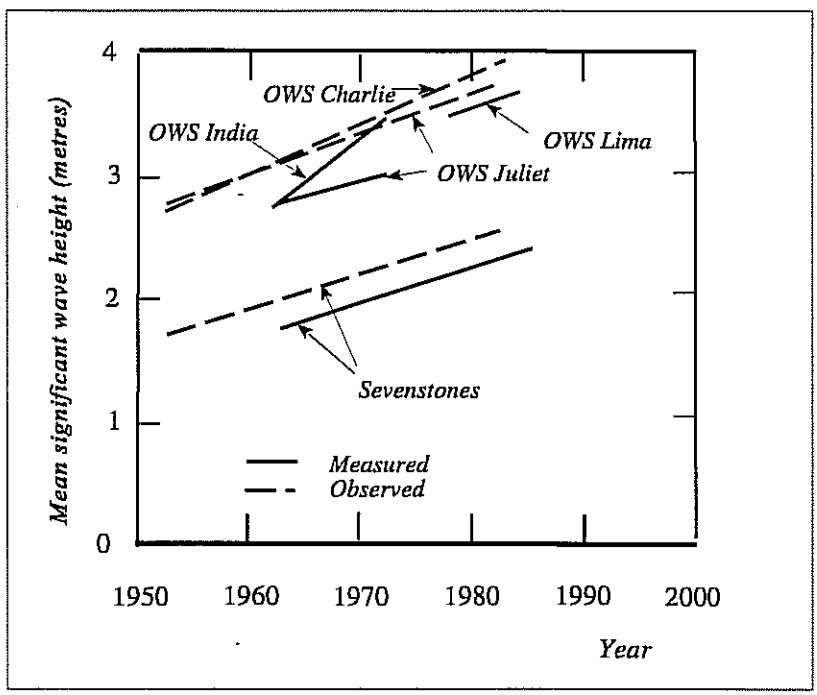

Fig 2.20 - Increase of mean significant wave heights in the North Atlantic (After Bacon and Carter (1991) and Barrat (1991))

3

LINEARISED EQUATIONS FOR SMALL AMPLITUDE SHIP MOTIONS IN REGULAR WAVES

3.1 INTRODUCTION

Ships do not, in the normal course of events, experience regular waves at sea. So the study of ship motions in regular waves appears at first sight to be an academic exercise of no practical significance. Yet it is an essential first step in the calculation of ship motions in a realistic irregular seaway; moreover, an appreciation of regular wave motions will give the reader an insight which will prove invaluable in understanding the general nature of the motions of ships in rough weather.

3.2 AXES AND SHIP MOTION DEFINITIONS

A ship in rough weather experiences a complex sequence of motions as it twists and turns its way across the ocean surface. The motions seem to defy any rational analysis, particularly by those who suffer from their effects on board the ship. Nevertheless, it is possible to make some observations on the characteristics of ship motions which will help to clarify their nature and will form a basis for the modern theory of seakeeping.

Let us suppose that the ship is attempting to maintain a straight course at a constant speed U metres/second. Waves continually cause the ship to deviate from its course and track and the helmsman may find it necessary to take corrective action. In addition the ship will rise and fall in response to the changing water level and the deck will seldom be truly horizontal. The ship will generally follow some kind of spiral path which is more or less aligned with the intended course. Finally the ship's speed will be continually varying around the nominal speed U as the ship surges along its track in response to the waves.[1]

Any particular ship's track and motion time history can be represented by a combination of the time histories of three linear[2] and three angular displacements. These six displacements are defined using the right handed axis system shown in Figure 3.1.

---

[1] The ship speed will generally be about the same as it would be at the same engine power setting in calm water: in head waves it will be reduced and in following waves it will be increased.

[2] "Linear" here means a displacement along an axis as opposed to a rotation about an axis. For the time being there is no necessary implication that the motions are linear in the sense that they are directly proportional to a force or moment.

The axis system Exy has its origin fixed at E at the mean water level and regular waves propagate along the Ex axis. A second axis system $E\ x_{E1}\ x_{E2}\ x_{E3}$ also has its origin at E but is rotated through the heading angle μ so that Ex_{E1} coincides with the mean track of the ship.[3]

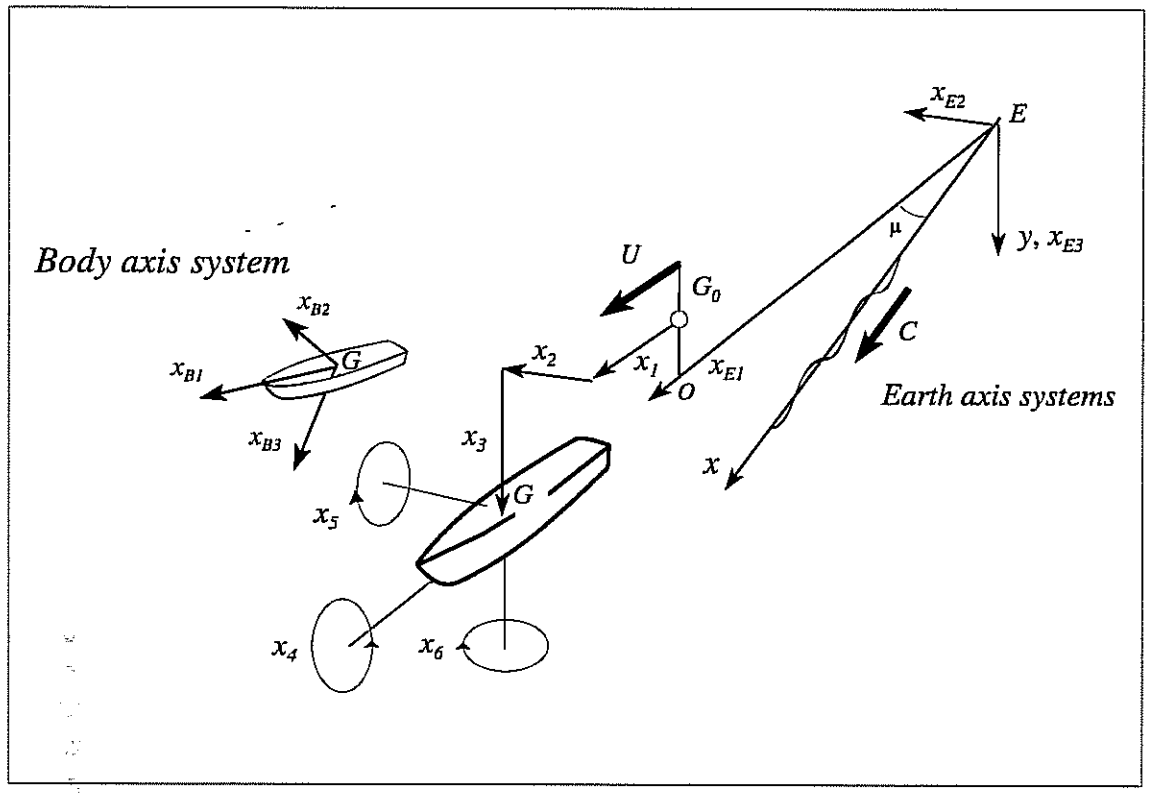

Fig 3.1 - Axes and ship motion definitions

A point O, lying at the mean water level, moves along Ex_{E1} at the mean speed of the ship, U metres/second. The mean position of the ship's centre of gravity G_0 lies vertically above O and is taken as the origin of a third axis system $G_0\ x_1\ x_2\ x_3$. At any instant of time the position of the ship's centre of gravity G relative to the moving origin G_0 is defined by three linear displacements:

Motion	Notation	Units	Positive
surge	x_1	metres	forward
sway	x_2	metres	to starboard
heave	x_3	metres	down

The attitude of the ship is defined by three angular rotations about the axes $G_0\ x_1$, $G_0\ x_2$ and $G_0\ x_3$:

[3] See Chapter 1 for the definition of heading angle.

Motion	Notation	Units	Positive
roll	x_4	radians	starboard side down
pitch	x_5	radians	bow up
yaw	x_6	radians	bow to starboard

Most ships have port/starboard symmetry and so surge, heave and pitch, which lie in the plane of symmetry, are called ***vertical plane*** or ***symmetric*** motions. Sway, roll and yaw are termed ***lateral plane*** or ***antisymmetric*** motions. The motions are often referred to as "***degrees of freedom***".

Another right handed set of axes $G\ x_{B1}\ x_{B2}\ x_{B3}$ is fixed in the ship and is used to define locations on (or in) the ship's structure. The origin of this ***body axis system*** is at the (moving) centre of gravity G and the axes rotate as the ship rolls, pitches and yaws. Locations are defined as:

Location	Notation	Units	Positive
Longitudinal	x_{B1}	metres	forward
Lateral	x_{B2}	metres	to starboard
Vertical	x_{B3}	metres	down

The wave depression at any point x is, according to Equation (1.9),

$$\zeta = \zeta_0 \sin (k x - \omega t) \quad m$$

where the time t is measured from an arbitrary datum. Transforming to the axis system aligned with the ship's track we find that the wave depression at any point $(x_{E1}\ ,\ x_{E2})$ is

$$\zeta = \zeta_0 \sin (k x_{E1} \cos \mu - k x_{E2} \sin \mu - \omega t) \quad m$$

If we choose a datum time such that the moving origin O is at E at time

$$t = \frac{\pi}{k\ U\ \cos \mu} \quad sec$$

the moving and Earth fixed frames of reference are related by

$$x_{E1} = x_1 + U \left(t - \frac{\pi}{k\ U\ \cos \mu} \right) \quad m$$

$$x_{E2} = x_2 \quad m$$

$$x_{E3} = x_3 - \overline{OG_0} \quad m$$

Then the wave depression at (x_1 , x_2) in the moving frame of reference is

$$\zeta = \zeta_0 \sin (\omega_e t - k x_1 \cos \mu + k x_2 \sin \mu) \quad m \qquad (3.1)$$

3.3 GENERAL EQUATIONS FOR SHIP MOTIONS IN REGULAR WAVES

3.3.1 Mass and moments of inertia

The ship may be regarded as being composed of a large number of very small masses δm tonnes. Figure 3.2 shows one of these masses located at (x_{B1} , x_{B2} , x_{B3}) (relative to the centre of gravity of the ship). If the ship has linear accelerations $\ddot{x}_1$, $\ddot{x}_2$ and $\ddot{x}_3$ m/sec^2 and angular accelerations $\ddot{x}_4$, $\ddot{x}_5$ and $\ddot{x}_6$ rad/sec^2 the mass δm will have linear accelerations

$$\ddot{x}_1' = \ddot{x}_1 + x_{B3} \ddot{x}_5 - x_{B2} \ddot{x}_6 \quad m/sec^2 \quad \text{forwards}$$

$$\ddot{x}_2' = \ddot{x}_2 - x_{B3} \ddot{x}_4 + x_{B1} \ddot{x}_6 \quad m/sec^2 \quad \text{to starboard}$$

$$\ddot{x}_3' = \ddot{x}_3 + x_{B2} \ddot{x}_4 - x_{B1} \ddot{x}_5 \quad m/sec^2 \quad \text{downwards}$$

From Newton's second law of motion, the forces and moments necessary to sustain these accelerations are

$$\delta F_1 = \delta m \ddot{x}_1' \quad kN \quad \text{surge force forwards}$$

$$\delta F_2 = \delta m \ddot{x}_2' \quad kN \quad \text{sway force to starboard}$$

$$\delta F_3 = \delta m \ddot{x}_3' \quad kN \quad \text{heave force downwards}$$

$$\delta F_4 = \delta m x_{B2} \ddot{x}_3' - \delta m x_{B3} \ddot{x}_2' \quad kN\ m \quad \text{roll moment to starboard}$$

$$\delta F_5 = \delta m x_{B3} \ddot{x}_1' - \delta m x_{B1} \ddot{x}_3' \quad kN\ m \quad \text{pitch moment bow up}$$

$$\delta F_6 = \delta m x_{B1} \ddot{x}_2' - \delta m x_{B2} \ddot{x}_1' \quad kN\ m \quad \text{yaw moment to starboard}$$

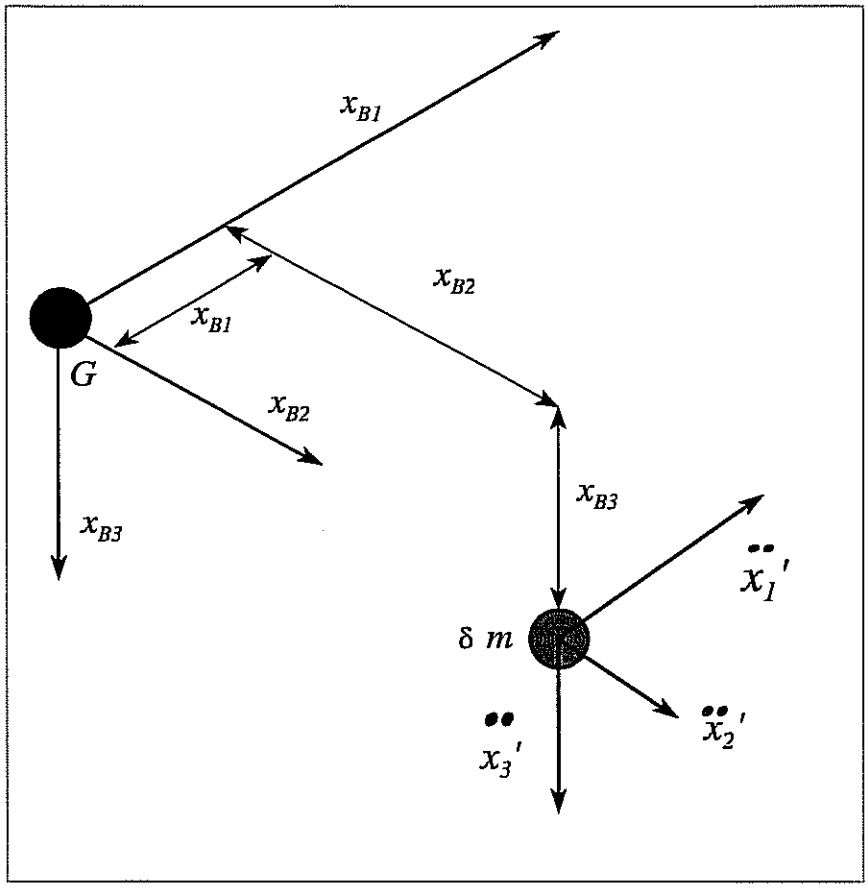

Fig 3.2 - Accelerations experienced by the mass δm

The forces and moments required to sustain the linear and angular accelerations of the whole ship are obtained by allowing δm to approach zero and integrating over the volume of the ship. Bearing in mind that by definition of the centre of gravity

$$\int x_{B1}\, dm = \int x_{B2}\, dm = \int x_{B3}\, dm = 0$$

we obtain

$$m\, \ddot{x}_1 = F_1 \quad kN$$

$$m\, \ddot{x}_2 = F_2 \quad kN$$

$$m\, \ddot{x}_3 = F_3 \quad kN$$

$$I_{44}\, \ddot{x}_4 - I_{45}\, \ddot{x}_5 - I_{46}\, \ddot{x}_6 = F_4 \quad kN\ m$$

$$-I_{54}\,\ddot{x}_4 + I_{55}\,\ddot{x}_5 - I_{56}\,\ddot{x}_6 = F_5 \quad kN\ m$$

$$-I_{64}\,\ddot{x}_4 - I_{65}\,\ddot{x}_5 + I_{66}\,\ddot{x}_6 = F_6 \quad kN\ m$$

where F_1, F_2 and F_3 are the surge, sway and heave forces and F_4 , F_5 and F_6 are the roll, pitch and yaw moments required to sustain the accelerations of the ship. m is the total mass in tonnes and I_{44} , I_{55} and I_{66} are the moments of inertia of the ship defined by

$$I_{44} = \int (x_{B2}^2 + x_{B3}^2)\, dm \quad t\ m^2 \quad \text{about the } x_{B1} \text{ axis}$$

$$I_{55} = \int (x_{B1}^2 + x_{B3}^2)\, dm \quad t\ m^2 \quad \text{about the } x_{B2} \text{ axis}$$

$$I_{66} = \int (x_{B1}^2 + x_{B2}^2)\, dm \quad t\ m^2 \quad \text{about the } x_{B3} \text{ axis}$$

In passing we note that it is often more convenient for practical engineering purposes to calculate the moments of inertia using the equations

$$I_{44} = m\ k_4^2 \quad t\ m^2 \qquad (3.2a)$$

$$I_{55} = m\ k_5^2 \quad t\ m^2 \qquad (3.2b)$$

$$I_{66} = m\ k_6^2 \quad t\ m^2 \qquad (3.2c)$$

where the radii of gyration for conventional ships may be estimated using the approximate equations:

$$k_4 \approx 0.3\ B \quad m$$

$$k_5 \approx 0.225\ L \quad m$$

$$k_6 \approx 0.225\ L \quad m$$

where B is the maximum waterline beam and L is the waterline length.

The product moments of inertia are defined by

$$I_{45} = I_{54} = \int x_{B1}\, x_{B2}\, dm \quad t\, m^2$$

$$I_{46} = I_{64} = \int x_{B1}\, x_{B3}\, dm \quad t\, m^2$$

$$I_{56} = I_{65} = \int x_{B2}\, x_{B3}\, dm \quad t\, m^2$$

For conventional ships the product moments of inertia are usually small and are invariably neglected. The equations of motion then reduce to

$$m\, \ddot{x}_i = F_i \quad kN; \qquad (\, i = 1\, ,\, 3\,) \tag{3.3a}$$

$$I_{ii}\, \ddot{x}_i = F_i \quad kN\, m\, ; \quad (\, i = 4\, ,\, 6\,) \tag{3.3b}$$

3.3.2 Motions in regular waves

The forces and moments in Equations (3.3) may be applied by any external means, but we are here concerned with the forces and moments applied to the ship by a train of regular waves.

For a given hull shape at a particular speed and heading in waves of a particular length the forces and moments F_i are assumed to be functions of the displacement, velocity and acceleration of the surface depression and the six possible motions. So we may write

$$F_i = F_i\left[\, \zeta,\, \dot{\zeta},\, \ddot{\zeta},\, (\, x_i\, ,\, \dot{x}_i\, ,\, \ddot{x}_i\, ;\quad (\, i = 1,\, 3\,)\,\right] \quad kN \tag{3.4a}$$

$$F_i = F_i\left[\, \zeta,\, \dot{\zeta},\, \ddot{\zeta},\, (\, x_i\, ,\, \dot{x}_i\, ,\, \ddot{x}_i\, ;\quad (\, i = 4,\, 6\,)\,\right] \quad kN\, m \tag{3.4b}$$

If the wave amplitude is small compared with the wave and ship lengths the motions will also be small and we may use a Taylor series expansion to obtain linear approximations to Equations (3.4):

$$F_i = a_i\, \ddot{\zeta} + b_i\, \dot{\zeta} + c_i\, \zeta + \sum_{j=1}^{6} (-a_{ij}\, \ddot{x}_j - b_{ij}\, \dot{x}_j - c_{ij}\, x_j) \quad kN\, ; \quad (\, i = 1,\, 3\,) \tag{3.5a}$$

$$F_i = a_i\, \ddot{\zeta} + b_i\, \dot{\zeta} + c_i\, \zeta + \sum_{j=1}^{6} (-a_{ij}\, \ddot{x}_j - b_{ij}\, \dot{x}_j - c_{ij}\, x_j) \quad kN\, m; \quad (\, i = 4,\, 6\,) \tag{3.5b}$$

The coefficients a_i, b_i and c_i are functions of the wave length and amplitude, heading angle, ship speed and hull form, and quantify the effect of the waves on the forces and moments. The other coefficients a_{ij} , b_{ij} and c_{ij} quantify the forces and moments required to sustain the motions of

the ship: these will be considered in detail in Section 3.4.

Substituting Equations (3.5) into the six Equations (3.3) we obtain six general linearised equations for small amplitude motions in regular waves:

$$\sum_{j=1}^{6} (A_{ij} \ddot{x}_j + b_{ij} \dot{x}_j + c_{ij} x_j) = F_{w\,i} \quad kN \; ; \; (i = 1 \, , \, 3) \qquad (3.6a)$$

$$\sum_{j=1}^{6} (A_{ij} \ddot{x}_j + b_{ij} \dot{x}_j + c_{ij} x_j) = F_{w\,i} \quad kN\,m; \; (i = 4 \, , \, 6) \qquad (3.6b)$$

where

$$A_{ij} = a_{ij} \quad (j = 1, 6 \; ; \quad i = 1, 6 \; ; j \neq i)$$

and the ***virtual masses and moments of inertia*** for each degree of freedom are

$$A_{ij} = m + a_{ij} \; (j = \; 1, 3 \; ; \quad i = 1, 3 \; ; \quad j = i) \qquad (3.7a)$$

$$A_{ij} = I_{ij} + a_{ij} \; (j = 4, 6 \; ; \quad i = 4, 6 \; ; \quad j = i) \qquad (3.7b)$$

The exciting forces and moments due to the waves are

$$F_{wi} = a_i \ddot{\zeta} + b_i \dot{\zeta} + c_i \zeta \quad kN \; ; \; (i = 1, 3) \qquad (3.8a)$$

$$F_{wi} = a_i \ddot{\zeta} + b_i \dot{\zeta} + c_i \zeta \quad kN\,m \; ; \; (i = 4, 6) \qquad (3.8b)$$

The regular wave ship motions are related to the nominal wave depression which would have been experienced at the moving origin O in the absence of the hull (in practice O will usually be within the hull so that the actual surface depression with the hull present cannot be defined).

Setting $x_1 = x_2 = 0$ in Equation (3.1) gives for this nominal surface depression at O

$$\zeta = \zeta_0 \, sin \, (\omega_e \, t) \quad m \qquad (3.9)$$

and the nominal vertical velocity and acceleration of the sea surface perceived by an observer on the ship at O are

$$\dot{\zeta} = \omega_e \, \zeta_0 \, cos \, (\omega_e \, t) \quad m/sec \qquad (3.10)$$

$$\ddot{\zeta} = -\omega_e^2 \, \zeta_0 \, sin \, (\omega_e \, t) \quad m/sec^2 \tag{3.11}$$

Substituting Equations (3.9)-(3.11) in Equations (3.8) we obtain

$$F_{wi} = F_{wi0} \, sin \, (\, \omega_e \, t + \gamma_i \,) \quad kN \; ; \; (\, i = 1, 3 \,) \tag{3.12a}$$

$$F_{wi} = F_{wi0} \, sin \, (\, \omega_e \, t + \gamma_i \,) \quad kN \, m \; ; \; (\, i = 4, 6 \,) \tag{3.12b}$$

where the excitation amplitudes are

$$F_{wi0} = \zeta_0 \sqrt{ (\, c_i - a_i \, \omega_e^2 \,)^2 + (\, b_i \, \omega_e \,)^2 } \quad kN \; ; \; (\, i = 1, 3 \,) \tag{3.13a}$$

$$F_{wi0} = \zeta_0 \sqrt{ (\, c_i - a_i \, \omega_e^2 \,)^2 + (\, b_i \, \omega_e \,)^2 } \quad kN \, m \; ; \; (\, i = 4, 6 \,) \tag{3.13b}$$

and the phases are given by

$$tan \, \gamma_i = \frac{b_i \, \omega_e}{c_i - a_i \, \omega_e^2} \; ; \quad (\, i = 1 \, , \, 6 \,) \tag{3.14}$$

The generalised equations of motion (3.6) may now be written as

$$\sum_{j=1}^{6} (\, A_{ij} \, \ddot{x}_j + b_{ij} \, \dot{x}_j + c_{ij} \, x_j \,) = F_{wi0} \, sin \, (\, \omega_e \, t + \gamma_i \,) \, kN \; ; \quad (\, i = 1, 3 \,) \tag{3.15a}$$

$$\sum_{j=1}^{6} (\, A_{ij} \, \ddot{x}_j + b_{ij} \, \dot{x}_j + c_{ij} \, x_j \,) = F_{wi0} \, sin \, (\, \omega_e \, t + \gamma_i \,) \, kN \, m \; ; \quad (\, i = 4, 6 \,) \tag{3.15b}$$

Solutions to these equations have the form

$$x_i = x_{i0} \, sin \, (\, \omega_e \, t + \delta_i \,) \quad m \; ; \quad (\, i = 1, 3 \,) \tag{3.16a}$$

$$x_i = x_{i0} \, sin \, (\, \omega_e \, t + \delta_i \,) \quad rad \; ; \quad (\, i = 4, 6 \,) \tag{3.16b}$$

So small amplitude regular sine waves impose sinusoidal exciting forces and moments on the ship and these result in sinusoidal motion time histories.

The motion amplitudes are directly proportional to the excitation amplitudes, which are in turn proportional to the wave amplitude. The phase angles γ_i and δ_i relate the excitation and motion time histories to the time history of the wave depression at O as shown in Figure 3.3. The peak excitation occurs γ_i / ω_e seconds before the maximum wave depression. Similarly the peak (positive) motion occurs δ_i / ω_e seconds before the maximum wave depression.

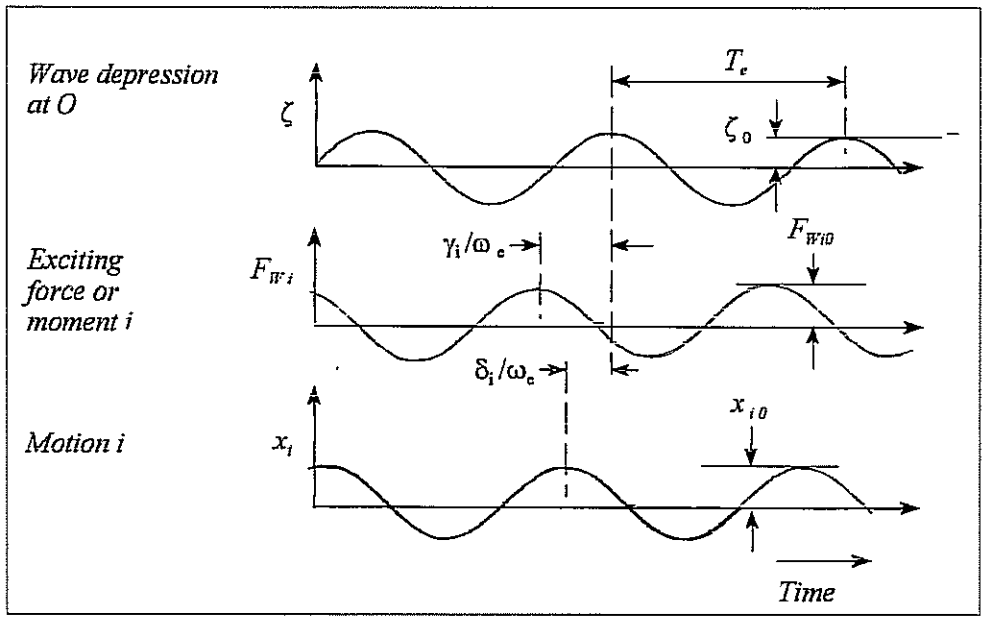

Fig 3.3 - Time histories of wave depression, exciting force and motion in regular waves

3.4 COEFFICIENTS IN THE EQUATIONS OF MOTION

3.4.1 Introduction

An understanding of the physical significance of the coefficients in the equations of motion can be gained by considering an experiment in which a model of the ship is forced to oscillate in a single degree of freedom (say heave) while being towed at constant speed in calm water. The model is constrained so that all other motions (pitch, roll, yaw etc) are suppressed. The forces and moments normally applied by the waves are replaced by externally applied forces and moments which are just sufficient to sustain the sinusoidal motion of the model in the chosen degree of freedom. We need not concern ourselves with how these forces and moments are generated, measured or applied, only with their magnitudes and effects.

In general (for an arbitrary hull shape) it will be necessary to apply forces and moments in all six degrees of freedom i to sustain the single motion x_j. The required forces and moments can be found from six equations analogous to the equations of motion (3.15):

$$\sum_{j=1}^{6} (A_{ij} \ddot{x}_j + b_{ij} \dot{x}_j + c_{ij} x_j) = F_{i0} \sin (\omega_e t) \; kN \; ; \; (i=1, 3) \qquad (3.17a)$$

$$\sum_{j=1}^{6} (A_{ij} \ddot{x}_j + b_{ij} \dot{x}_j + c_{ij} x_j) = F_{i0} \sin (\omega_e t) \; kN \; m \; ; \; (i=4, 6) \quad (3.17b)$$

where F_{i0} are the amplitudes of the applied forces and moments. All the motions except for x_j are set to zero and the single motion x_j leads the forces and moments by ε_j radians:

$$x_j = x_{j0} \sin (\omega_e t + \varepsilon_j) \qquad m \text{ or } rad \quad (3.18)$$

Equations (3.17) then reduce to six much simpler equations:

$$A_{ij} \ddot{x}_j + b_{ij} \dot{x}_j + c_{ij} x_j = F_{i0} \sin (\omega_e t) \; kN \; ; \quad (i=1, 3) \quad (3.19a)$$

$$A_{ij} \ddot{x}_j + b_{ij} \dot{x}_j + c_{ij} x_j = F_{i0} \sin (\omega_e t) \; kN \; m \; ; \quad (i=4, 6) \quad (3.19b)$$

and these may be recognised as the equations of motion of six second order linear damped spring mass systems with sinusoidal excitation (see Appendix 1). The equations express the six forces and moments required to sustain the single motion oscillation x_j. The in phase and quadrature components of each force and moment are given by Equations (A1.12) and (A1.13):

$$c_{ij} - A_{ij} \omega_e^2 = \frac{F_{i0}}{x_{j0}} \cos \epsilon_j \quad kN/m \; ; \qquad (i = 1, 3) \quad (3.20a)$$

$$c_{ij} - A_{ij} \omega_e^2 = \frac{F_{i0}}{x_{j0}} \cos \epsilon_j \quad kN \; m/rad \; ; \qquad (i = 4, 6) \quad (3.20b)$$

$$b_{ij} \omega_e = - \frac{F_{i0}}{x_{j0}} \sin \epsilon_j \quad kN/m \; ; \qquad (i = 1, 3) \quad (3.21a)$$

$$b_{ij} \omega_e = - \frac{F_{i0}}{x_{j0}} \sin \epsilon_j \quad kN \; m/m \; ; \quad (i = 4, 6) \quad (3.21b)$$

The components of the six applied forces and moments which are in phase with the motion are therefore associated with the stiffness and inertia coefficients, while the quadrature components are associated with damping.

3.4.2 Heave coefficients

If we set $j = 3$ in Equations (3.20) and (3.21) and use Equations (3.7) we may find expressions for the heave coefficients a_{33} , b_{33} , c_{33} , a_{53} , b_{53} and c_{53}. The most important coefficients are a_{33} , b_{33} and c_{33} which relate the heave motion ($j = 3$) to the applied heave force ($i = 3$). Figure 3.4 shows the physical mechanisms responsible for these coefficients.

At zero frequency the vessel has no heave velocity or acceleration and the heave force is related to the heave displacement through the single coefficient c_{33}. This arises because a steady downward heave force produces a steady downward heave displacement and an additional displaced volume of water. The heave force is required to oppose the resulting additional buoyancy force and sustain the heave displacement (see Figure 3.4(c)).

A typical relationship between the heave displacement and the heave force required to sustain it is shown in Figure 3.5(a). Provided that the heave displacement is small, this may be approximated by a straight line whose slope is c_{33}. c_{33} is specifically defined as the gradient of the curve at the origin.

At higher frequencies the in phase component of the applied heave force includes a contribution from the heave inertia or virtual mass A_{33} (see Equation (3.7a)).This is made up of contributions from the so called added mass a_{33} as well as the real mass m of the vessel.

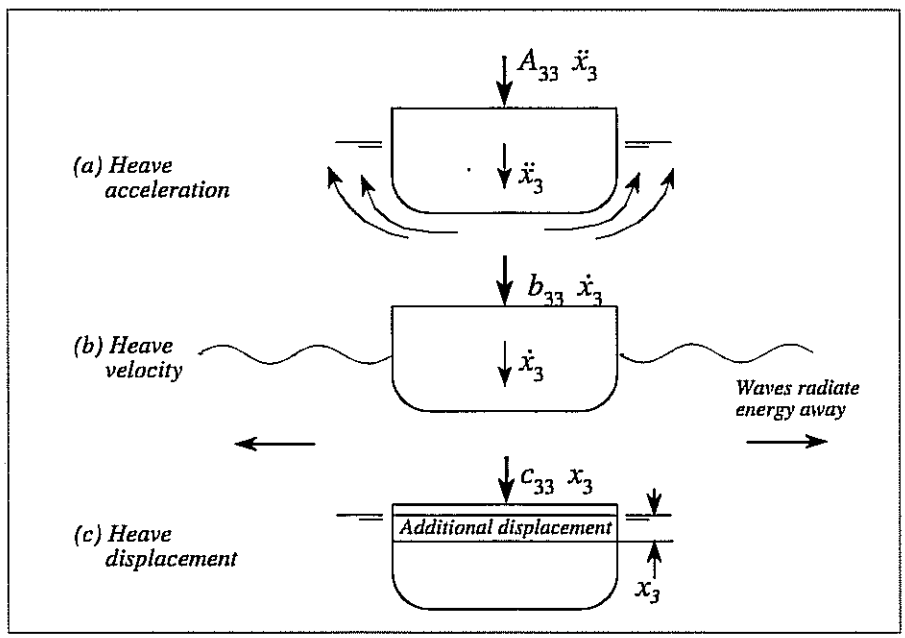

Fig 3.4 - Effects of heave motion

The former arises because the accelerating hull causes changes in the fluid velocities adjacent to its surface as shown in Figure 3.4(a). The additional force required to accelerate this water as well as the hull is included in the inertia coefficient and the ship behaves as though it has an increased mass. The heave damping coefficient b_{33} arises because the oscillating ship generates waves which radiate outward and dissipate energy as shown in Figure 3.4(b). A small amount of energy is also dissipated by friction.

The pitch moment required to sustain the heave oscillation yields estimates of the coefficients a_{53} , b_{53} and c_{53} (set i = 5 and j = 3 in Equation (3.19b)). These coefficients quantify the influence of heave on pitch in the equations of motion (3.15) and they occur because local inertia, damping and stiffness forces everywhere along the hull exert pitching moments about the centre of gravity.

TABLE 3.1

ADDED MASS AND DAMPING COEFFICIENTS IN THE EQUATIONS OF MOTION FOR A SHIP WITH PORT/STARBOARD SYMMETRY

Velocity and acceleration	surge force i=1	sway force i=2	heave force i=3	roll moment i=4	pitch moment i=5	yaw moment i=6
surge j=1	✓	$zero_2$	*small*	$zero_2$	*small*	$zero_2$
sway j=2	$zero_3$	✓	$zero_3$	✓	$zero_3$	✓
heave j=3	*small*	$zero_2$	✓	$zero_2$	✓	$zero_2$
roll j=4	$zero_3$	✓	$zero_3$	✓	$zero_3$	✓
pitch j=5	*small*	$zero_2$	✓	$zero_2$	✓	$zero_2$
yaw j=6	$zero_3$	✓	$zero_3$	✓	$zero_3$	✓

TABLE 3.2

STIFFNESS COEFFICIENTS IN THE EQUATIONS OF MOTION FOR A SHIP WITH PORT/STARBOARD SYMMETRY

Displacement	surge force i=1	sway force i=2	heave force i =3	roll moment i=4	pitch moment i=5	yaw moment i=6
surge j=1	$zero_1$	$zero_1$	$zero_1$	$zero_1$	$zero_1$	$zero_1$
sway j=2	$zero_1$	$zero_1$	$zero_1$	$zero_1$	$zero_1$	$zero_1$
heave j=3	*small*	$zero_2$	✓	$zero_2$	✓	$zero_2$
roll j=4	$zero_3$	*small*	$zero_3$	✓	$zero_3$	*small*
pitch j=5	*small*	$zero_2$	✓	$zero_2$	✓	
yaw j=6	$zero_3$	✓	$zero_3$	✓	$zero_3$	✓

Key: ✓: significant value
small: small: invariably neglected
$zero_1$: zero by geography
$zero_2$: zero by symmetry
$zero_3$: zero for small motions

If the ship has fore and aft symmetry like a canoe, the moments arising from the forces on the forward half of the ship will almost exactly balance those arising from the after half of the ship, and these ***"coupling"*** coefficients will be very small. For more orthodox forms residual moments, which may not be negligible, will remain.

For arbitrary shaped hull forms forces and moments in the other four degrees of freedom (surge, sway, roll and yaw) will also be required to sustain a pure heave oscillation and the relevant coefficients can be identified in a similar way. However, most practical ship forms have port/starboard symmetry so that the forces and moments generated by the pressure changes on the starboard side of the hull are exactly balanced by those on the port side. So all lateral plane excitations associated with motions in the vertical plane are zero. In other words the relationships between the lateral plane forces and moments and vertical plane motions have the form shown in Figure 3.5(b) and all the associated coefficients are zero.

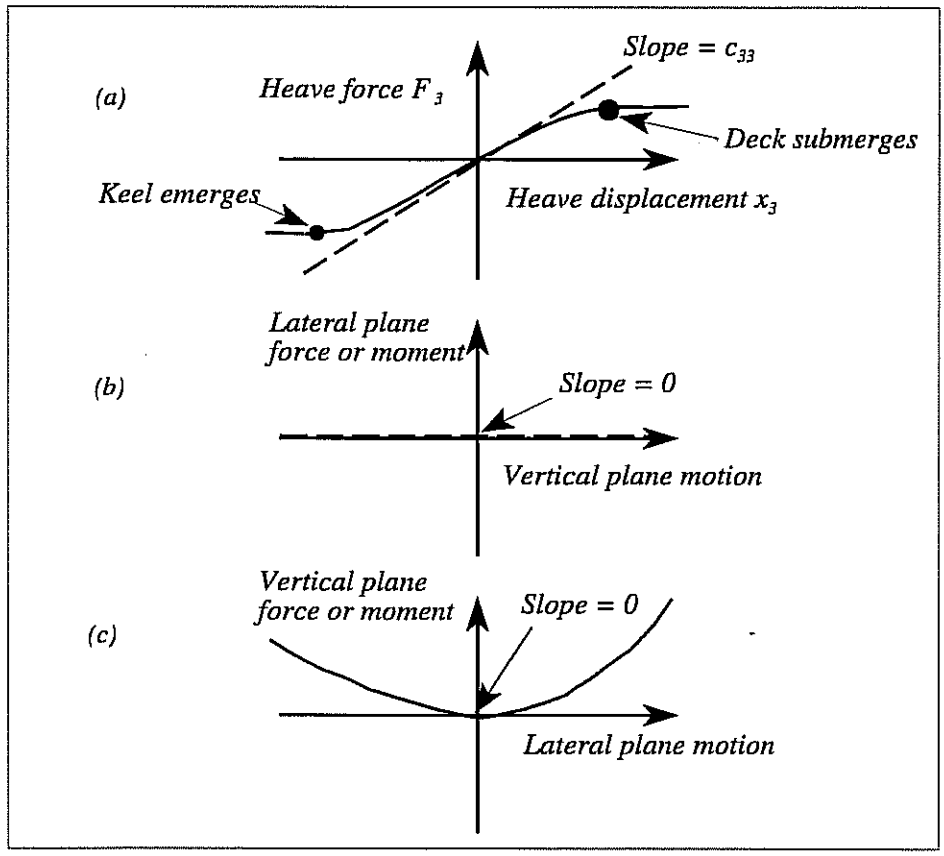

Fig 3.5 - Typical heave motion relationships

3.4.2 Pitch coefficients

We now consider an experiment in which the model is forced to undergo a pitch oscillation by setting $j = 5$ in Equations (3.20). The analysis proceeds along lines exactly similar to those used in the heave oscillation experiment and yields the terms a_{55} , b_{55} , c_{55} , a_{53} , b_{53} and c_{53}. Again all the lateral plane forces and moments and associated coefficients are zero if the hull has port/starboard symmetry.

The pitch oscillations cause local vertical motions everywhere along the hull so that each section of the hull experiences local inertia, damping and stiffness forces analogous to those experienced by the whole model in the heave oscillation experiment. These forces exert moments about the centre of gravity and are responsible for the coefficients a_{55} , b_{55} and c_{55}. The local forces distributed over the forward part of the hull oppose those on the after part of the hull so that the residual heave forces associated with the coefficients a_{53} , b_{53} and c_{53} are usually small. Indeed they would be zero on a hull with fore and aft symmetry at zero speed.

The pitch virtual inertia coefficient A_{55} includes contributions from the so called "added moment of inertia" as well as the true moment of inertia of the ship's structure. This is analogous to the heave added mass already discussed. The true mass moment of inertia may be calculated from Equation (3.2b).

3.4.3 Lateral plane coefficients

Expressions for the lateral plane coefficients may be determined in a similar way by setting $j = 2$, 4 and 6 in Equations (3.20).

In general, vertical plane forces and moments will always be required to sustain motions in the lateral plane even for ships with port/starboard symmetry. However, the relationship between the vertical plane excitation and the lateral plane motion for ships with lateral symmetry will have the symmetrical U shaped form shown in Figure 3.5 (c). In other words the vertical plane excitation will have the same magnitude and direction regardless of the direction of the lateral plane motion. Since we are concerned only with small motions and our linearisation requires the coefficients to be determined from the slope at the origin, all such coefficients are zero.

3.4.4 'Geographical' coefficients

We have seen that some coefficients are zero or small if the ship has port and starboard symmetry. Another class of coefficients are always zero regardless of the hull form. These are all stiffness coefficients associated with the ship's geographical location with respect to the origin G_O. No forces or moments are required to sustain surge and sway displacements x_1 and x_2 so that

$$c_{i1} = c_{i2} = 0 \; ; \quad (i = 1 , 6)$$

3.4.5 Summary of zero value coefficients

Tables 3.1 and 3.2 list 60 coefficients (out of a total of 108) which are zero for a ship with port/starboard symmetry. A further 12 coefficients are usually negligible and are invariably neglected. This results in six much simpler equations for small amplitude motions of a ship with lateral symmetry. These are listed in Section 3.5.

3.5 SIMPLIFIED EQUATIONS OF MOTION FOR A SHIP WITH PORT/STARBOARD SYMMETRY.

Surge: $$(m + a_{11})\,\ddot{x}_1 + b_{11}\,\dot{x}_1 = F_{w10}\,\sin(\omega_e\,t + \gamma_1) \quad kN \tag{3.22a}$$

Sway: $$(m + a_{22})\,\ddot{x}_2 + b_{22}\dot{x}_2 + a_{24}\,\ddot{x}_4 + b_{24}\,\dot{x}_4 + a_{26}\,\ddot{x}_6 + b_{26}\,\dot{x}_6 + c_{26}\,x_6 = F_{w20}\,\sin(\omega_e\,t + \gamma_2) \quad kN \tag{3.22b}$$

Heave: $$(m + a_{33})\,\ddot{x}_3 + b_{33}\,\dot{x}_3 + c_{33}\,x_3 + a_{35}\,\ddot{x}_5 + b_{35}\,\dot{x}_5 + c_{35}\,x_5 = F_{w30}\,\sin(\omega_e\,t + \gamma_3) \quad kN \tag{3.22c}$$

Roll: $$a_{42}\,\ddot{x}_2 + b_{42}\,\dot{x}_2 + (I_{44} + a_{44})\,\ddot{x}_4 + b_{44}\,\dot{x}_4 + c_{44}\,x_4 + a_{46}\,\ddot{x}_6 + b_{46}\,\dot{x}_6 + c_{46}\,x_6 = F_{w40}\,\sin(\omega_e\,t + \gamma_4) \quad kN\,m \tag{3.22d}$$

Pitch: $$a_{53}\,\ddot{x}_3 + b_{53}\,\dot{x}_3 + c_{53}\,x_3 + (I_{55} + a_{55})\,\ddot{x}_5 + b_{55}\,\dot{x}_5 + c_{55}\,x_5 = F_{w50}\,\sin(\omega_e\,t + \gamma_5) \quad kN\,m \tag{3.22e}$$

Yaw: $$a_{62}\,\ddot{x}_2 + b_{62}\,\dot{x}_2 + a_{64}\,\ddot{x}_4 + b_{64}\,\dot{x}_4 + (I_{66} + a_{66})\,\ddot{x}_6 + b_{66}\,\dot{x}_6 + c_{66}\,x_6 = F_{w60}\,\sin(\omega_e\,t + \gamma_6) \quad kN\,m \tag{3.22f}$$

3.6 COUPLING

As we have already seen, the vertical plane equations (heave and pitch) are coupled. In other words the heave equation includes terms dependent on pitch so that heave is influenced by pitch and vice versa. However, the surge equation is uncoupled and independent of the other motions. The lateral plane equations are also coupled so that these motions are affected by each other. There is, however, no coupling between the vertical plane motions and the lateral plane motions. This allows the vertical and lateral plane motions to be considered independently.[4]

[4] This is not necessarily true if the motions are large.

4

STRIP THEORY

4.1 INTRODUCTION

Solving the equations of motion (3.22) requires the evaluation of the coefficients and the excitation amplitudes and phases. These may be determined by experiment but this method is laborious and hardly practical for routine calculations. In any case, if experimental methods are to be used, it is more appropriate to measure ship motions directly as described in Chapters 9 and 10.

Considerable effort has therefore been devoted to developing theoretical methods of determining the coefficients and excitations to allow ship motions to be calculated without recourse to experiment. Various authors, including Tasai (1959), Gerritsma and Beukelman (1967), Salvesen, Tuck and Faltinsen (1970) and Schmitke (1978), have made significant contributions. Their theories are generally similar, differing only in detail and mathematical rigour. They are complicated and a complete description is beyond the scope of this book. This chapter is therefore intended to give an abbreviated presentation of the main features of strip theory in general and is largely based on the methods proposed by Gerritsma and Beukelman.

All the theories assume that

(a) The ship is slender (ie the length is much greater than the beam or the draught and the beam is much less than the wave length).

(b) The hull is rigid so that no flexure of the structure occurs.

(c) The speed is moderate so there is no appreciable planing lift.

(d) The motions are small.

(e) The ship hull sections are wall sided.

(f) The water depth is much greater than the wave length so that deep water wave approximations may be applied.

(g) The presence of the hull has no effect on the waves (the so called ***Froude-Kriloff hypothesis).***

The theories are grouped under the general heading of ***strip theory*** since they all represent the three dimensional underwater hull form by a series of two dimensional slices or strips as shown in Figure 4.1. Each strip is of length δx_{BI} metres (assumed to be small).

Each strip has associated local hydrodynamic properties (added mass, damping and stiffness) which contribute to the coefficients for the complete hull in the equations of motion. Similarly the wave excitations experienced by the hull are composed of contributions from all the strips.

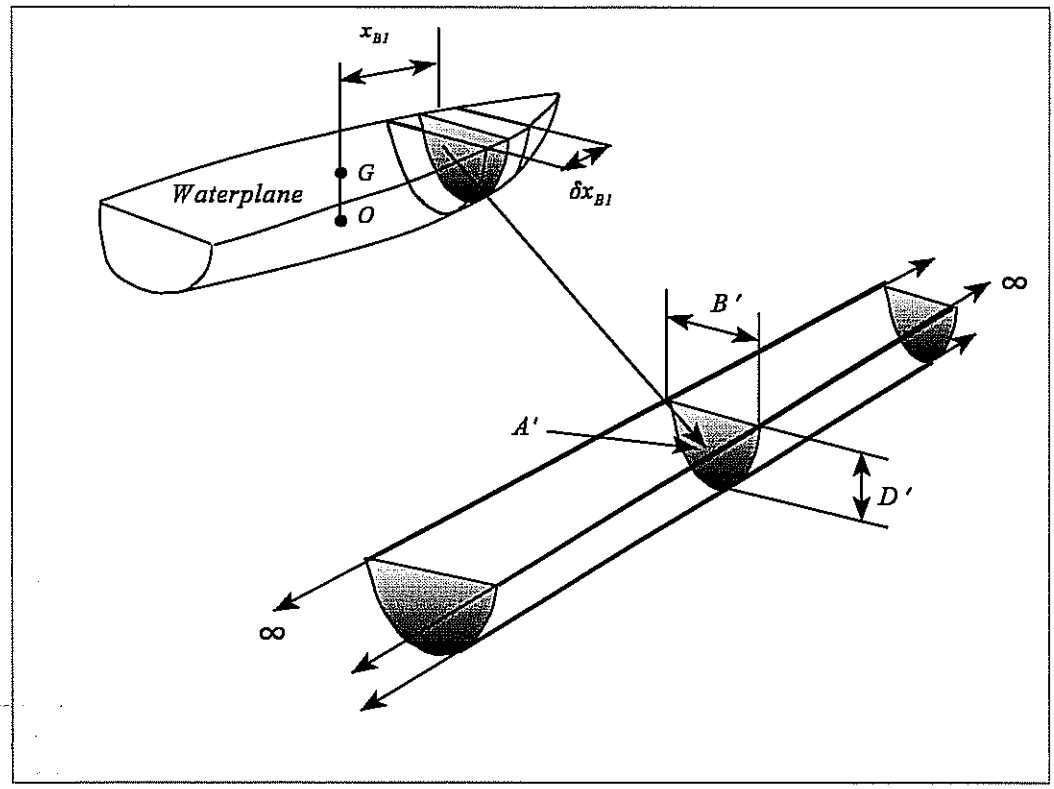

Fig 4.1 - Representation of underwater hull section shapes by an infinite cylinder

Strip theory assumes that these local hydrodynamic properties are the same as would be experienced if the strip were part of an infinitely long cylinder of the same cross sectional shape, as shown in Figure 4.1. In other words three dimensional effects, such as mutual interference between the strips, flow leakage around the ends of the ship and effects due to changes in the shape of the strip over the length δx_{BI}, are ignored.

4.2 STRIP MOTIONS

Let us first suppose that the ship is undergoing a generalised forced oscillation in all degrees of freedom except surge. If the pitch and yaw oscillations are small the motions of each strip will be essentially confined to the plane of the strip. If the strip is located x_{BI} metres forward of the centre of gravity the motions of a point on the Gx_{BI} axis will be

$$x'_{2G} = x_2 + x_{BI} \sin x_6 \approx x_2 + x_{BI}\, x_6 \quad m \text{ to starboard} \qquad (4.1)$$

$$x'_{3G} = x_3 - x_{B1} \sin x_5 \approx x_3 - x_{B1}\, x_5 \quad m \quad \text{downwards} \tag{4.2}$$

$$x'_{4G} = x_4 \quad rad \quad \text{starboard side down} \tag{4.3}$$

Consider an observer stationed at some fixed point alongside the Ex_{EI} axis in Figure 3.1. The oscillating ship passes him at a steady velocity U metres/second. At some instant of time a certain strip is adjacent to the observer and his perception of its lateral velocity is given by the total differential of Equation (4.1):

$$\dot{x}'_{2G} = \frac{D}{Dt}(x'_{2G}) = \dot{x}_2 + x_{B1}\,\dot{x}_6 + \dot{x}_{B1}\,x_6 \quad m/sec$$

Now the distance x_{B1} from the strip to the approaching centre of gravity is diminishing at the rate

$$\dot{x}_{B1} = -U \quad m/sec \tag{4.4}$$

Hence the lateral velocity perceived by the observer is

$$\dot{x}'_{2G} = \dot{x}_2 + x_{B1}\,\dot{x}_6 - U\,x_6 \quad m/sec \tag{4.5a}$$

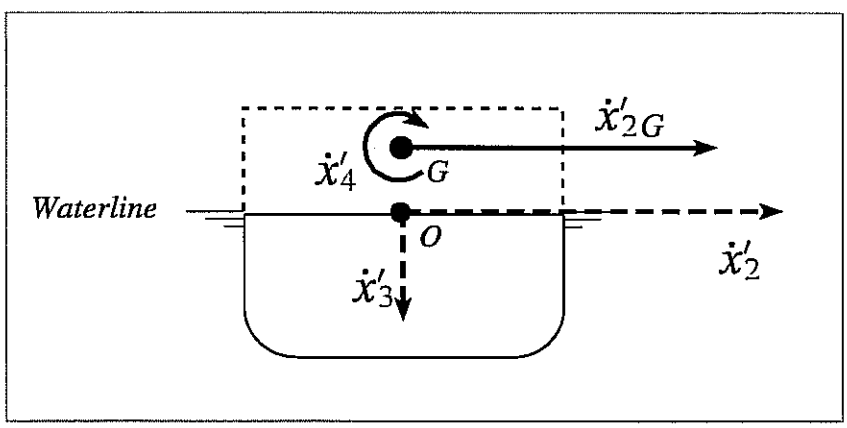

Fig 4.2 - Velocities of a strip

and by a similar argument the perceived lateral acceleration is

$$\ddot{x}'_{2G} = \ddot{x}_2 + x_{B1}\,\ddot{x}_6 - 2U\,\dot{x}_6 \quad m/sec^2 \tag{4.5b}$$

Similarly the perceived vertical velocity and acceleration are

$$\dot{x}'_{3G} = \dot{x}_3 - x_{B1}\,\dot{x}_5 + U\,x_5 \quad m/sec \tag{4.6a}$$

$$\ddot{x}'_{3G} = \ddot{x}_3 - x_{B1}\,\ddot{x}_5 + 2U\,\dot{x}_5 \quad m/sec^2 \tag{4.6b}$$

and the roll velocity and acceleration are simply

$$\dot{x}'_{4G} = \dot{x}_4 \quad rad/sec \tag{4.7a}$$

$$\ddot{x}'_{4G} = \ddot{x}_4 \quad rad/sec^2 \tag{4.7b}$$

An origin O in the waterplane, shown in Figure 4.2, is chosen for calculations of the local hydrodynamic properties of each strip. The velocities and accelerations of this point are

$$\dot{x}'_2 = \dot{x}'_{2G} - \overline{OG}\,\dot{x}'_4 \quad m/sec \tag{4.8a}$$

$$\ddot{x}'_2 = \ddot{x}'_{2G} - \overline{OG}\,\ddot{x}'_4 \quad m/sec^2 \tag{4.8b}$$

Vertical motions and roll motions are unaffected by this change of origin.

4.3 COEFFICIENTS IN THE EQUATIONS OF MOTION

4.3.1 General considerations

Consider a strip embedded in the infinitely long cylinder lying in calm water as shown in Figure 4.1. The excitations required to sustain the motions in the three possible degrees of freedom may be obtained from equations analogous to the sway, heave and roll equations for the complete ship (Equations (3.22)). Note that we are only concerned with that part of the excitation necessary to oppose the hydrodynamic and hydrostatic reactions to the motions. In other words the effects of the real mass and inertia of the strip are excluded from the calculation. For a strip with port/starboard symmetry we have

$$a'_{22}\,\ddot{x}'_2 + b'_{22}\,\dot{x}'_2 + a_{24}\,\ddot{x}'_4 + b'_{24}\,\dot{x}'_4 = \frac{\delta F_2}{\delta x_{B1}} \quad kN/m \tag{4.9a}$$

$$a'_{33}\,\ddot{x}'_3 + b'_{33}\,\dot{x}'_3 + c'_{33}\,x'_3 = \frac{\delta F_3}{\delta x_{B1}} \quad kN/m \tag{4.9b}$$

$$a'_{42}\,\ddot{x}'_2 + b'_{42}\,\dot{x}'_2 + a'_{44}\,\ddot{x}'_4 + b'_{44}\,\dot{x}'_4 + c'_{44}\,x'_4 = \frac{\delta F_4}{\delta x_{B1}} \quad kN\ m/m \tag{4.9c}$$

where all the motions and excitations are referred to an origin O in the waterplane. The primed coefficients a'_{22} , b'_{22} etc. are all local values (per metre length of strip) analogous to

the corresponding coefficients for the complete hull (with due allowance for the change of origin). These local coefficients are functions of the size and shape of the section and may be determined using the equations given in Chapter 5.

4.3.2 Coefficients in the heave and pitch equations

Consider a ship undergoing simultaneous forced heave and pitch motions in calm water. The momentum of the surrounding water in the plane of the strip is

$$M_3' = a_{33}' \dot{x}_3' \quad t\ m/sec$$

per metre length of the strip. The force required to oppose the hydrodynamic reactions and sustain the motions of the strip is composed of the rate of change of this momentum together with contributions from the damping and stiffness:

$$\delta F_3 = \left(\frac{D}{Dt} (M_3') + b_{33}' \dot{x}_3' + c_{33}' x_3' \right) \delta x_{BI} \quad kN$$

As successive strips pass the observer stationed alongside the Ex_{EI} axis he will perceive a changing local added mass a_{33}'. So the rate of change of momentum is

$$\frac{D}{Dt} (M_3') = \dot{a}_{33}' \dot{x}_3' + a_{33}' \ddot{x}_3' \quad kN$$

per metre length of strip.

Now we may write for the rate of change of added mass

$$\dot{a}_{33}' = \frac{d}{dx_{BI}} (a_{33}') \dot{x}_{BI} = - U \frac{d}{dx_{BI}} (a_{33}')$$

per metre length of strip (see Equation (4.4)). Using Equations (4.5) and (4.6) the downward vertical force on the strip becomes

$$\delta F_3 = \left[a_{33}' (\ddot{x}_3 - x_{BI} \ddot{x}_5 + 2U \dot{x}_5) \right.$$

$$+ \left(b_{33}' - U \frac{da_{33}'}{dx_{BI}} \right) (\dot{x}_3 - x_{BI} \dot{x}_5 + U x_5) \qquad (4.10)$$

$$\left. + c_{33}' (x_3 - x_{BI} x_5) \right] \delta x_{BI} \quad kN$$

The total heave force and pitch moment required to balance the hydrodynamic reactions and

sustain the heave and pitch motions of the ship are obtained by allowing δx_{Bl} to approach zero and integrating over the length of the hull:

$$F_3 = \int dF_3 \quad kN \tag{4.11}$$

$$F_5 = - \int x_{Bl}\, dF_3 \quad kN\ m \tag{4.12}$$

We note the following identities

$$\int \frac{da'_{33}}{dx_{Bl}}\, dx_{Bl} = a'_{33\,a} \quad t/m$$

$$\int x_{Bl}\, \frac{da'_{33}}{dx_{Bl}}\, dx_{Bl} = x_{Bl\,a}\, a'_{33\,a} \quad t$$

$$\int x^2_{Bl}\, \frac{da'_{33}}{dx_{Bl}}\, dx_{Bl} = x^2_{Bl\,a}\, a'_{33\,a} \quad t\ m$$

where $a'_{33\,a}$ is the local added mass at the stern in tonnes per metre and $x_{Bl\,a}$ is the distance of the stern (negative) from the centre of gravity[1]. Note that $a'_{33\,a}$ will be zero if the ship has no transom.[2]

We also note that the local heave force required to sustain a steady downward heave displacement x'_3 metres is

$$c'_{33}\, x'_3 = \rho\, g\, B'\, \delta x_{Bl}\, x'_3 \quad kN$$

and it follows that

$$\int c'_{33}\, dx_{Bl} = \rho\, g\, A_W \quad kN/m$$

$$\int c'_{33}\, x_{Bl}\, dx_{Bl} = \rho\, g\, M_L \quad kN\ m/m$$

$$\int c'_{33}\, x^2_{Bl}\, dx_{Bl} = \rho\, g\, I_L \quad kN\ m^2/m$$

where the waterplane area and its first and second moments about a transverse axis under the

---

[1] It is assumed that the cross sectional area at the stem is zero and $a'_{33\,f} = 0$.

[2] It is sometimes argued that the local added mass (and damping) at the stern must be nearly zero because of flow leakage effects whatever the shape of the stern.

centre of gravity are given by

$$A_W = \int B' \, dx_{Bl} \quad m^2$$

$$M_L = \int B' \, x_{Bl} \, dx_{Bl} \quad m^3$$

$$I_L = \int B' \, x_{Bl}^2 \, dx_{Bl} \quad m^4$$

Substituting Equation (4.10) in Equations (4.11) and (4.12) and comparing term by term with Equations (3.22c) and (3.22e) enables us to obtain expressions for each coefficient in the equations of motion for pitch and heave. The coefficients for the complete hull are then obtained in terms of the local two dimensional coefficients (a'_{33} , b'_{33}) and are listed in Tables 4.1 and 4.2.

4.3.3 Coefficients in the lateral plane equations

A similar approach is used to determine the coefficients in the lateral plane equations of motion ((3.22b, 3.22d and 3.22f). We now consider a ship undergoing simultaneous sway, roll and yaw motions in calm water and the lateral motions of a strip are given by Equations (4.7) and (4.8).in terms of the local two dimensional coefficients (a'_{33} , b'_{33}) and are listed in Tables 4.1 and 4.2.

The horizontal momentum of the surrounding water in the plane of the strip is

$$M'_2 = (a'_{22} \dot{x}'_2 + a'_{24} \dot{x}'_4) \quad t \; m/sec$$

per metre length of strip.

The lateral force required to balance the hydrodynamic reactions and sustain the motions of the strip includes contributions from the rate of change of momentum, the lateral motion damping and the lateral force required to sustain the roll velocity:

$$\delta F_2 = \left(\frac{D}{Dt} (M'_2) + b'_{22} \dot{x}'_2 + b'_{24} \dot{x}'_4 \right) \delta x_{Bl} \quad kN$$

The rate of change of momentum perceived by our stationary observer is

$$\frac{D}{Dt} (M'_2) = \left(a'_{22} \ddot{x}'_2 - U \frac{da'_{22}}{dx_{Bl}} \dot{x}'_2 + a'_{24} \ddot{x}'_4 - U \frac{da'_{24}}{dx_{Bl}} \dot{x}'_4 \right) \delta x_{Bl} \quad kN$$

and the lateral force is

$$\delta F_2 = \Bigg[a'_{22} \left(\ddot{x}_2 + x_{B1} \ddot{x}_6 - 2U \dot{x}_6 - \overline{OG} \ddot{x}_4 \right)$$

$$+ \left(b'_{22} - U \frac{da'_{22}}{dx_{B1}} \right) \left(\dot{x}_2 + x_{B1} \dot{x}_6 - U x_6 - \overline{OG} \dot{x}_4 \right) +$$

$$+ a'_{24} \ddot{x}_4 + \left(b'_{24} - U \frac{da'_{24}}{dx_{B1}} \right) \dot{x}_4 \Bigg] \delta x_{B1} \quad kN$$

The angular momentum of the water in the plane of the strip includes a contribution due to the lateral velocity $\dot{x}'_2$:

$$M'_4 = a'_{44} \dot{x}'_4 + a'_{42} \dot{x}'_2 \quad t\ m^2/sec$$

per metre length of strip.

The roll moment about the axis through G required to balance the hydrodynamic reactions and sustain the motions includes contributions from the rate of change of this angular momentum as well as contributions associated with the roll damping and the moment required to sustain the lateral velocity. In addition there are contributions associated with the roll stiffness c'_{44} and the moment due to the lateral force δF_2 acting through O:

$$\delta F_4 = \left(\frac{D}{Dt} \left(M'_4 \right) + b'_{44} \dot{x}'_4 + b'_{42} \dot{x}'_2 + c'_{44} x'_4 \right) \delta x_{B1} - \overline{OG}\ \delta F_2 \quad kN\ m$$

Expanding as before, we obtain

$$\delta F_4 = \Bigg[a'_{44} \ddot{x}_4 + \left(b'_{44} - U \frac{da'_{44}}{dx_{B1}} \right) \dot{x}_4 + c'_{44} x_4$$

$$+ a'_{42} \left(\ddot{x}_2 + x_{B1} \ddot{x}_6 - 2U \dot{x}_6 - \overline{OG} \ddot{x}_4 \right)$$

$$+ \left(b'_{42} - U \frac{da'_{42}}{dx_{B1}} \right) \left(\dot{x}_2 + x_{B1} \dot{x}_6 - U x_6 - \overline{OG} \dot{x}_4 \right) \Bigg] \delta x_{B1}$$

$$- \overline{OG}\ \delta F_2 \quad kN\ m$$

The total sway force, roll and yaw moments are obtained by allowing δx_{B1} to approach zero and

integrating over the length of the ship:

$$F_2 = \int dF_2 \quad kN \tag{4.13}$$

$$F_4 = \int dF_4 \quad kN\ m \tag{4.14}$$

$$F_6 = \int x_{BI}\ dF_2 \quad kN\ m \tag{4.15}$$

Comparing these equations with Equations (3.22b), (3.22d) and (3.22f) allows us to obtain expressions for the lateral plane hydrodynamic coefficients for the complete hull in terms of the local values (a'_{22}, b'_{22} etc). Again we note that for conventional ships with zero cross section area at the forward perpendicular

$$\int \frac{da'_{22}}{dx_{BI}}\, dx_{BI} = a'_{22\,a} \quad t/m$$

$$\int x_{BI}\, \frac{da'_{22}}{dx_{BI}}\, dx_{BI} = x_{BI\,a}\, a'_{22\,a} \quad t$$

$$\int x^2_{BI}\, \frac{da'_{22}}{dx_{BI}}\, dx_{BI} = x^2_{BI\,a}\, a'_{22\,a} \quad t\ m$$

where $a'_{22\,a}$ is the local added mass for horizontal motions in tonnes/metre at the stern. Again, $a'_{22\,a}$ will be zero for ships with no transom.[3] Similar expressions are valid for the coefficients a'_{24} and a'_{42}.

We also note that the roll moment required to sustain a steady roll angle x_4 radians to starboard is

$$c_{44}\, x_4 = m\, g\, \overline{GM}_F\, x_4 \quad kN\ m$$

so that

$$c_{44} = m\, g\, \overline{GM}_F \quad kN\ m/rad \tag{4.16}$$

where $\overline{GM}_F$ is the ***fluid*** metacentric height (ie the metacentric height corrected for free surface effects: see any text book on basic naval architecture.) Equating terms in equations (4.13) - (4.15) and (3.22b,), (3.22d) and (3.22f) we obtain the expressions listed in Tables 4.3 - 4.5.

---

[3] Again it is sometimes argued that the added mass and damping coefficients at the stern must be negligible because of three dimensional effects even when the ship has a transom.

4.4 EXCITATIONS IN REGULAR WAVES

4.4.1. General considerations

The linearisation of the equations of motion in Chapter 3 allows the wave excitations to be considered independent of any ship motions and to be expressed as functions of the wave amplitude alone. In other words the wave excitations are assumed to be the same as the ship would experience if it were rigidly restrained and allowed no motions at all.

According to Equation (3.1) the wave depression at any point (x_1 , x_2) related to the moving origin O is

$$\zeta = \zeta_0 \sin (\omega_e t - k x_1 \cos \mu + k x_2 \sin \mu) \quad m$$

Since the ship is allowed no motions, the centre of gravity remains above O and we may write

$$x_1 = x_{BI} \quad m$$

The wave depression varies across each strip but we assume the ship to be slender (that is, the waterline beam of all strips is much less than the wavelength) and this allows us to calculate the wave depression with sufficient accuracy by setting

$$x_2 = 0 \quad m$$

The wave depression experienced at each strip is then

$$\zeta = \zeta_0 \sin (\omega_e t - Q) \quad m \tag{4.17a}$$

where

$$Q = k x_{BI} \cos \mu \tag{4.17b}$$

The excitation experienced by each strip is related to the pressures, velocities and accelerations in the water beneath the wave surface. These quantities vary with depth (see Equations (1.17) - (1.23)) and it is usual to simplify the calculations by taking their values at a mean local draught defined by

$$\bar{D} = \frac{A'}{B'} \quad m \tag{4.18}$$

where A' is the cross sectional area of the strip in square metres and B' is the waterline beam of the strip in metres.[4]

---

[4] Note that $\bar{D}$ is a function of x_{BI}.

Referring to Equation (1.23) we find that the pressure fluctuation at the mean draught $\bar{D}$ is

$$\tilde{P} = - \rho g \zeta_0 \, exp \, (- k \bar{D}) \, sin \, (k x - \omega t) \quad kN/m^2 \tag{4.19}$$

relative to the local hydrostatic pressure $\rho g \bar{D}$ and, with the assumptions described above, this can be written as

$$\tilde{P} = - \rho g \zeta_0 \, exp \, (-k \bar{D}) \, sin \, (\omega_e t - Q) \quad kN/m^2 \tag{4.20}$$

Similarly the vertical velocity of the water at the mean draught is, from Equation (1.18),

$$v = \omega \zeta_0 \, exp \, (- k \bar{D}) \, cos \, (\omega_e t - Q) \quad m/sec \tag{4.21}$$

and the corresponding vertical acceleration is

$$\dot{v} = - \omega^2 \zeta_0 \, exp \, (- k \bar{D}) \, sin \, (\omega_e t - Q) \quad m/sec^2 \tag{4.22}$$

The horizontal velocity at the mean draught is, from Equation (1.17) ,

$$u = - \omega \zeta_0 \, exp \, (- k \bar{D}) \, sin \, (\omega_e t - Q)$$

$$= - \omega \zeta \, exp \, (- k \bar{D}) \quad m/sec$$

along the Ex_1 axis. The athwartships component of this horizontal velocity is

$$u_2 = \omega \zeta \, exp \, (- k \bar{D}) \, sin \, \mu \quad m/sec \tag{4.23}$$

and the corresponding athwartships component of the horizontal acceleration is

$$\dot{u}_2 = \omega v \, sin \, \mu \quad m/sec^2 \tag{4.24}$$

The slope of the pressure contour at depth $\bar{D}$ is, from Equation (1.15),

$$\alpha_{\bar{D}} = -k \zeta_0 \, exp \, (- k \bar{D}) \, cos \, (\omega_e t - Q) = - \frac{\omega v}{g} \quad rad$$

and this has an athwartships component given by

$$\alpha_{\overline{D2}} = \frac{\omega v}{g} \, sin \, \mu \quad rad \tag{4.25}$$

The angular velocity of the water in the plane normal to the ship's axis is equivalent to the rate of change of this component of the pressure contour slope:

$$\dot{\alpha}_{\bar{D}2} = -k\ \omega\ exp\ (\ -\ k\ \bar{D}\ )\ \zeta\ sin\ \mu \quad rad/sec \tag{4.26}$$

and the corresponding angular acceleration is

$$\ddot{\alpha}_{\bar{D}2} = -k\ \omega\ v\ sin\ \mu \quad rad/sec^2 \tag{4.27}$$

4.4.2 Vertical excitation

If we assume that the beam of the strip at the mean draught $\bar{D}$ is approximately the same as the local waterline beam, the vertical force due to the pressure fluctuation is

$$-\ B\ \tilde{P}\ \delta x_{Bl} \quad kN$$

In addition there are contributions arising from the rate of change of the vertical momentum of the water surrounding the strip and a force associated with the vertical velocity of the water. The total vertical force on the strip is then

$$\delta F_{w3} = \left(\frac{D}{Dt}\ (\ M'_{w3}\ ) + b'_{33}\ v\ -\ B\ \tilde{P} \right)\ \delta x_{Bl} \quad kN$$

where the vertical momentum is

$$M'_{w3} = a'_{33}\ v \quad t\ m/sec$$

per metre length of strip.

Our stationary observer perceives the rate of change of momentum as

$$\frac{D}{Dt}\ (\ M'_{w3}) = \dot{a}'_{33}\ v\ +\ a'_{33}\ \dot{v}$$

$$= -U\ \frac{da'_{33}}{dx_{Bl}}\ v\ +\ a'_{33}\ \dot{v} \quad kN/m$$

Obtaining P, v and $\dot{v}$ from Equations (4.20) - (4.22) we find that the vertical force on each strip and the associated pitch moment about the centre of gravity are

$$\delta F_{w3} = \zeta_0 \left[\ P_{3S}\ sin(\omega_e t - Q)\ +\ P_{3C}\ cos(\omega_e t - Q)\ \right] \delta x_{Bl} \quad kN \tag{4.28}$$

$$\delta F_{w5} = \zeta_0 \left[\ P_{5S}\ sin(\omega_e t - Q) + P_{5C}\ cos(\omega_e t - Q)\ \right] \delta x_{Bl} \quad kN\ m \tag{4.29}$$

where

$$P_{3S} = \left(\rho\ g\ B' - \omega^2\ a'_{33} \right)\ exp\ (\ -k\ \bar{D}\ )\quad t\ /\ (m/sec^2\ )$$

$$P_{3C} = \omega \left(b'_{33} - U\ \frac{da'_{33}}{dx_{B1}} \right)\ exp\ (\ -k\ \bar{D}\ )\quad t\ /\ (m/sec^2\ )$$

and

$$P_{5S} = x_{B1}\ P_{3S}\quad kN\ /\ m$$

$$P_{5C} = x_{B1}\ P_{3C}\quad kN\ /\ m$$

The total heave force and pitch moment amplitudes F_{w30} and F_{w50} and phases (relative to the maximum wave depression at O) are then obtained using the equations given in Appendix 2.

4.4.3 Sway and yaw excitation

Figure 4.3 shows the hydrostatic force experienced by a restrained strip in waves. The inclined water surface causes a lateral shift of the centre of buoyancy from B to B_1 and the buoyancy force vector is assumed to act normal to the pressure contour at the mean draught $\bar{D}$. The buoyancy force is

$$\rho\ g\ A'\ \delta x_{B1}\quad kN$$

and it has a horizontal component

$$\rho\ g\ A'\ \delta x_{B1}\ \alpha_{\bar{D}2}\quad kN\quad \text{to starboard}$$

In addition there are contributions due to the rate of change of horizontal momentum of the water surrounding the strip and forces associated with the lateral and rotational velocities of the water.

$$\delta F_{w2} = \left(\frac{D}{Dt}\ (\ M'_{w2}\ )\ +\ b'_{22}\ u_2\ +\ b'_{24}\ \dot{\alpha}_{\bar{D}2}\ +\ \rho\ g\ A'\ \alpha_{\bar{D}2} \right)\ \delta x_{B1}\quad kN$$

The horizontal momentum is

$$M'_{w2} = a'_{22}\ u_2\ +\ a'_{24}\ \dot{\alpha}_{\bar{D}2}\quad t\ m/sec$$

per metre length of strip.

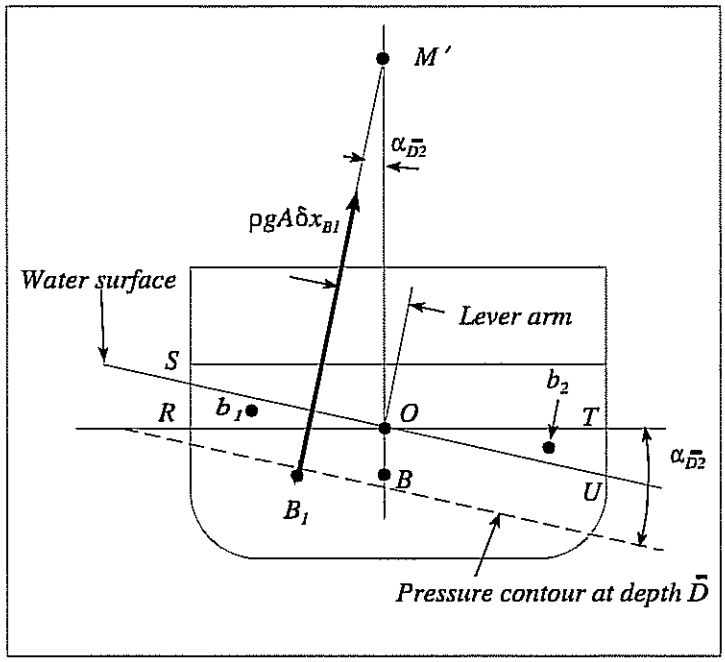

Fig 4.3 - Lateral plane hydrostatic force and moment on a restrained strip

The total horizontal force on the strip is then

$$\frac{D}{Dt}\left(M'_{w2} \right) = a'_{22}\,\dot{u}_2 - U\,\frac{da'_{22}}{dx_{B1}}\,u_2 + a'_{24}\,\dot{\alpha}_{\bar{D}2} - U\,\frac{da'_{24}}{dx_{B1}}\,\dot{\alpha}_{\bar{D}2} \quad kN$$

per metre length of strip.

Obtaining u_2, $\dot{u}_2$, etc, from Equations (4.23) - (4.27) we find that the total sway force on the strip and the yaw moment it exerts about the centre of gravity are

$$\delta F_{w2} = \zeta_0 \left[P_{2S}\,\sin\,(\omega_e\,t - Q) + P_{2C}\,\cos\,(\omega_e\,t - Q) \right] \delta x_{B1} \quad kN \qquad (4.30)$$

$$\delta F_{w6} = \zeta_0 \left[P_{6S}\,\sin\,(\omega_e\,t - Q) + P_{6C}\,\cos\,(\omega_e\,t - Q) \right] \delta x_{B1} \quad kN\ m \qquad (4.31)$$

where

$$P_{2S} = \omega \; exp\; (-k\bar{D})\; sin\; \mu \left[b'_{22} - U \frac{da'_{22}}{dx_{B1}} - k \left(b'_{24} - U \frac{da'_{24}}{dx_{B1}} \right) \right] \quad kN / m$$

$$P_{2C} = \omega^2 \; exp(-k\bar{D})\; sin\; \mu \left(a'_{22} + \rho A' - k\, a'_{24} \right) \quad kN / m$$

$$P_{6S} = x_{B1}\, P_{2S} \quad kN / m$$

$$P_{6C} = x_{B1}\, P_{2C} \quad kN / m$$

The amplitudes F_{w20} and F_{w60} and phases γ_2 and γ_6 of the sway force and yaw moment are found using the Equations given in Appendix 2.

4.4.4 Roll excitation

If the strip shown in Figure 4.3 is wall sided the two triangular wedges *ORS* and *OTU* will have equal volumes and identical shapes. Their centres of buoyancy will be at b_1 and b_2 and the strip's centre of buoyancy will move from B to B_1 such that the line BB_1 is parallel to the line b_1b_2 and

$$\overline{BB_1} = \frac{\delta A}{A'} \overline{b_1 b_2} \quad m$$

where δA is the area of each wedge in square metres. For small values of the slope of the pressure contour $\alpha_{\bar{D}2}$

$$\overline{BM'} \approx \frac{\overline{BB_1}}{\alpha_{\bar{D}2}} = \frac{\delta A\; \overline{b_1 b_2}}{A'\; \alpha_{\bar{D}2}} \quad m$$

The area of each wedge is

$$\delta A = \frac{B'^2}{8}\; \alpha\; sin\; \mu \approx \frac{B'^2 \alpha_{\bar{D}2}}{8} \quad m^2$$

and the centre of buoyancy of each wedge is $\frac{B'}{3}$ metres from the centreline.

Hence

$$\delta A\; \overline{b_1 b_2} = \frac{B'^3\; \alpha_{\bar{D}2}}{12} \quad m^3$$

and

$$\overline{BM'} = \frac{B'^3}{12A'} \quad m \tag{4.32}$$

The buoyancy force exerts a roll moment about O:

$$\rho\, g \left(\frac{B'^3}{12} - \overline{OB}\, A' \right) \alpha_{\bar{D}2} \quad kN\ m$$

per metre length of strip.

The total roll moment exerted on the strip about O also includes contributions from the rate of change of the angular momentum of the water surrounding a strip as well as contributions associated with the rate of rotation and the horizontal velocity of water. The equations of motion (3.22) require the roll moment to be related to an axis through the centre of gravity. The lateral force F_{W2} acting through O exerts a moment about G and this is included to give

$$\delta F_{w4} = \left[\frac{D}{Dt} (M'_{w4}) + b'_{44}\, \dot{a}_{\bar{D}2} + \rho g \left(\frac{B'^3}{12} - A'\, \overline{OB} \right) \alpha_{\bar{D}2} + b'_{42}\, u_2 \right] \delta x$$

$$- \overline{OG}\, \delta F_{w2} \quad kN\ m$$

The roll momentum is

$$M'_{w4} = a'_{44}\, \dot{\alpha}_{\bar{D}2} + a'_{42}\, u_2$$

The rate of change of momentum perceived by the fixed observer is

$$\frac{D}{Dt} \left(M'_{w4} \right) = a'_{44}\, \ddot{\alpha}_{\bar{D}2} - U \frac{da'_{44}}{dx_{B1}} \dot{\alpha}_{\bar{D}2} + a'_{42}\, \dot{u}_2 - U \frac{da'_{42}}{dx_{B1}} u_2 \quad kN\ m$$

per metre length of strip and the roll moment becomes

$$\delta F_{w4} = \zeta_0 \left[P_{4S}\, sin(\omega_e t - Q) + P_{4C}\, cos(\omega_e t - Q) \right] \delta x_{B1} \quad kN\ m \tag{4.33}$$

where

$$P_{4S} = \omega \; exp\; (-k\bar{D}) \; sin\; \mu \left(- k \left[b'_{44} - U \frac{da'_{44}}{dx_{B1}} \right] + b'_{42} - U \frac{da'_{42}}{dx_{B1}} \right.$$

$$\left. - \overline{OG} \left[b'_{22} - U \frac{da'_{22}}{dx_{B1}} - k \left[b'_{24} - U \frac{da'_{24}}{dx_{B1}} \right] \right] \right) \quad kN/m$$

$$P_{4C} = \omega^2 \; sin\; \mu \; exp\; (-k\bar{D}) \left(- k \; a'_{44} + \rho \left[\frac{B^3}{12} - A' \; \overline{OB} \right] + a'_{42} \right.$$

$$\left. - \overline{OG} \left[a'_{22} + \rho A' - k \; a'_{24} \right] \right) \quad kN \; / \; m$$

The roll moment amplitude F_{w40} and phase γ_4 are obtained using the equations given in Appendix 2.

TABLE 4.1
COEFFICIENTS IN THE HEAVE EQUATION OF MOTION

$$a_{33} = \int a'_{33} \; dx_{B1} \quad t \tag{4.34a}$$

$$b_{33} = \int b'_{33} \; dx_{B1} - U \; a'_{33\,a} \quad kN/(m/sec) \tag{4.34b}$$

$$c_{33} = \int c'_{33} \; dx_{B1} = \rho \; g \; A_W \quad kN/m \tag{4.34c}$$

$$a_{35} = - \int x_{B1} \; a'_{33} \; dx_{B1} \quad kN/(rad/sec^2) \tag{4.34d}$$

$$b_{35} = 2U \int a'_{33} \; dx_{B1} - \int x_{B1} \, b'_{33} \; dx_{B1} + U \; x_{B1\,a} \; a'_{33\,a} \quad kN/(rad/sec) \tag{4.34e}$$

$$c_{35} = U \int b'_{33} \; dx_{B1} - U^2 \; a'_{33\,a} - \rho \; g \; M_L \quad kN/rad \tag{4.34f}$$

TABLE 4.2
COEFFICIENTS IN THE PITCH EQUATION OF MOTION

$$a_{53} = -\int x_{B1}\, a'_{33}\, dx_{B1} \quad kN\ m/(m/sec^2) \tag{4.35a}$$

$$b_{53} = -\int x_{B1}\, b'_{33}\, dx_{B1} + U\, x_{B1}\, a'_{33\,a} \quad kNm/(m/sec) \tag{4.35b}$$

$$c_{53} = \int x_{B1}\, c'_{33}\, dx_{B1} = \rho\, g\, M_L \quad kN\ m/m \tag{4.35c}$$

$$a_{55} = \int x_{B1}^2\, a'_{33}\, dx_{B1} \quad kN\ m/(rad/sec^2) \tag{4.35d}$$

$$b_{55} = -2U \int x_{B1}\, a'_{33}\, dx_{B1} + \int x_{B1}^2\, b'_{33}\, dx_{B1} - U\, x_{B1\,a}^2\, a'_{33\,a} \quad kN\ m/(rad/sec) \tag{4.35e}$$

$$c_{55} = -U \int x_{B1}\, b'_{33}\, dx_{B1} + \rho\, g\, I_L + U^2\, x_{B1a}\, a'_{33\,a} \quad kN\ m/rad \tag{4.35f}$$

TABLE 4.3

COEFFICIENTS IN THE SWAY EQUATION OF MOTION

$$a_{22} = \int a'_{22}\, dx_{B1} \quad t \tag{4.36a}$$

$$b_{22} = \int b'_{22}\, dx_{B1} - U\, a'_{22\,a} \quad kN/(m/sec) \tag{4.36b}$$

$$a_{24} = \int a'_{24}\, dx_{B1} - \overline{OG} \int a'_{22}\, dx_{B1} \quad kN/(rad/sec^2) \tag{4.36c}$$

$$b_{24} = \int b'_{24}\, dx_{B1} - \overline{OG} \int b'_{22}\, dx_{B1} + \overline{OG}\, U\, a'_{22\,a} - U\, a'_{24\,a} \quad kN/(rad/sec) \tag{4.36d}$$

$$a_{26} = \int x_{B1}\, a'_{22}\, dx_{B1} \quad kN/(rad/sec^2) \tag{4.36e}$$

$$b_{26} = \int x_{B1}\, b'_{22}\, dx_{B1} - U\, x_{B1a}\, a'_{22\,a} - 2U \int a'_{22}\, dx_{B1} \quad kN/(rad/sec) \tag{4.36f}$$

$$c_{26} = -U \int b'_{22}\, dx_{B1} + U^2\, a'_{22\,a} \quad kN/rad \tag{4.36g}$$

TABLE 4.4
COEFFICIENTS IN THE ROLL EQUATION OF MOTION

$$a_{42} = \int a'_{42}\, dx_{B1} - \overline{OG} \int a'_{22}\, dx_{B1} \quad kN\ m/(m/sec^2) \tag{4.37a}$$

$$b_{42} = \int b'_{42}\, dx_{B1} - U\, a'_{42a} - \overline{OG} \int b'_{22}\, dx_{B1} + \overline{OG}\, U\, a'_{22\,a} \quad kN\ m/(m/sec) \tag{4.37b}$$

$$a_{44} = \int a'_{44}\, dx_{B1} - \overline{OG} \int a'_{42}\, dx_{B1} - \overline{OG} \int a'_{24}\, dx_{B1} + \overline{OG}^2 \int a'_{22}\, dx_{B1} \quad kN\ m/(rad/sec^2) \tag{4.37c}$$

$$b_{44} = \int b'_{44}\, dx_{B1} - U\, a'_{44\,a} + \overline{OG}\, U\, a'_{42\,a} - \overline{OG} \int b'_{42}\, dx_{1} - \overline{OG} \int b'_{24}\, dx_{B1} + \overline{OG}^2 \int b'_{22}\, dx_{B1} - \overline{OG}^2\, U\, a'_{22\,a} + \overline{OG}\, U\, a'_{24\,a} \quad kN\ m/(rad/sec) \tag{4.37d}$$

$$c_{44} = m\, g\, \overline{GM_F} \quad kN\ m/rad \tag{4.37e}$$

$$a_{46} = \int x_{B1}\, a'_{42}\, dx_{B1} - \overline{OG} \int x_{B1}\, a'_{22}\, dx_{B1} \quad kN\ m/(rad/sec^2) \tag{4.37f}$$

$$b_{46} = -2U \int a'_{42}\, dx_{B1} - U\, x_{B1\,a}\, a'_{42\,a} + \int x_{B1}\, b'_{42}\, dx_{B1} - \overline{OG} \int x_{B1}\, b'_{22}\, dx_{B1} + \overline{OG}\, x_{B1\,a}\, U\, a'_{22\,a} + 2\overline{OG}\, U \int a'_{22}\, dx_{B1} \quad kN\ m/(rad/sec) \tag{4.37g}$$

$$c_{46} = U^2\, a'_{42\,a} - U \int b'_{42}\, dx_{B1} + \overline{OG}\, U \int b'_{22}\, dx_{B1} - \overline{OG}\, U^2\, a'_{22\,a} \quad kN\ m/rad \tag{4.37h}$$

TABLE 4.5
COEFFICIENTS IN THE YAW EQUATION OF MOTION

$$a_{62} = \int x_{B1}\, a'_{22}\, dx_{B1} \quad kN\ m/(m/sec)^2 \tag{4.38a}$$

$$b_{62} = \int x_{B1}\, b'_{22}\, dx_{B1} - U\, x_{B1\,a}\, a'_{22\,a} \quad kN\ m/(m/sec) \tag{4.38b}$$

$$a_{64} = \int x_{B1}\, a'_{24}\, dx_{B1} - \overline{OG}\, x_{B1}\, a'_{22}\, dx_{B1} \quad kN\ m/(rad/sec^2) \tag{4.38c}$$

$$b_{64} = \int x_{B1}\, b'_{24}\, dx_{B1} - \overline{OG} \int x_{B1}\, b'_{22}\, dx_{B1} + \overline{OG}\, U\, x_{B1\,a}\, a'_{22\,a} - U\, x_{B1\,a}\, a'_{24\,a} \quad kN\ m/(rad/sec) \tag{4.38d}$$

$$a_{66} = \int x_{B1}^2\, a'_{22}\, dx_{B1} \quad kN\ m/(rad/sec^2) \tag{4.38e}$$

$$b_{66} = \int x_{B1}^2\, b'_{22}\, dx_{B1} - U\, x_{B1\,a}^2\, a'_{22\,a} - 2U \int x_{B1}\, a'_{22}\, dx_{B1} \quad kN\ m/(rad/sec) \tag{4.38f}$$

$$c_{66} = -U \int x_{B1}\, b'_{22}\, dx_{B1} + U^2\, x_{B1\,a}\, a'_{22a} \quad kN\ m/rad \tag{4.38g}$$

5

LEWIS FORMS AND THEIR HYDRODYNAMIC PROPERTIES

5.1 INTRODUCTION

Progress with strip theory requires the evaluation of the local (two dimensional) added mass and damping coefficients a_{ij}' and b_{ij}' in Equations (4.34) - (4.38). Methods of solution have been developed by Ursell (1949a, 1949b), Tasai (1959, 1960), Grim (1959), Porter (1960) and others. The techniques used are involved and laborious, requiring devious and intricate methods of solution for even the simplest cases. Their application is quite impractical without the aid of a computer.

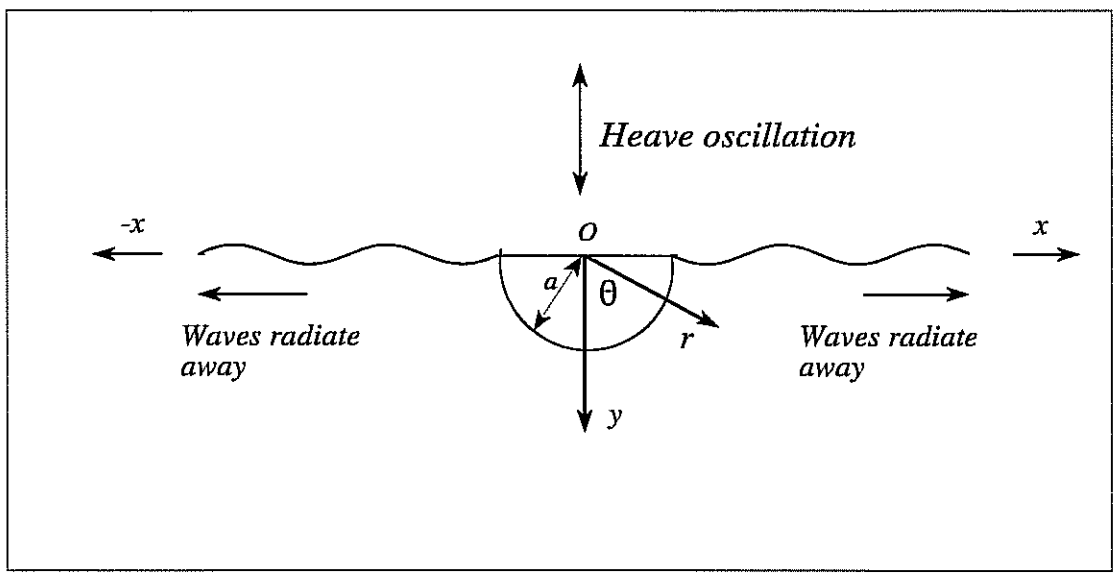

Fig 5.1 - Circular cylinder oscillating in the free surface

Fortunately computer routines for the calculation of these properties are widely available and naval architects need not usually concern themselves with the details of the complex mathematics involved. It is, however, important to understand the broad nature of the calculations and to appreciate their limitations. This chapter therefore discusses the properties of the commonly used Lewis form approximations for conventional hull cross- sections and gives the expressions for the added mass and damping coefficients, without proof, taken from a comprehensive paper by de Jong (1973).

The methods mentioned above generally begin by examining the properties of an infinitely long

semicircular cylinder[1] of radius a metres floating in the free surface of the water as shown in Figure 5.1. The heaving cylinder is shown in the figure, but sway and roll motions (about the longitudinal axis through the origin O) are also considered. Small motion amplitudes are assumed. The oscillating cylinder generates surface waves which radiate away in the $\pm x$ directions . The coefficients are calculated with the usual potential flow assumptions of negligible viscosity and compressibility, no flow separation and no skin friction.

Ship's hulls do not, as a general rule, have semicircular cross-sections and conformal transformation techniques[2] are used to extend the results for the circle into solutions for more realistic hull shapes. In this technique the circle and the flow around it (stream and potential functions) are calculated in the complex z plane where

$$z = x + i\,y = i\,r\,e^{-i\,\theta} \quad m \tag{5.1}$$

These results are mapped into the flow around a hull section in the complex ζ plane (the hull cross section plane) as shown in Figure 5.2.[3]

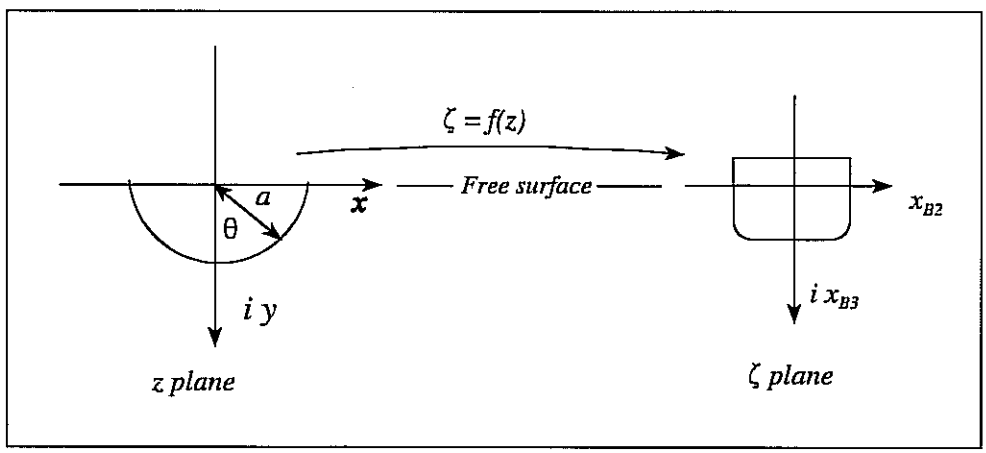

Fig 5.2 - Conformal transformation from the z (circle) plane to the ζ (ship) plane

ζ is defined as

$$\zeta = x_{B2} + i x_{B3} \quad m \tag{5.2}$$

and the two complex planes are related by the transformation

---

[1]The calculation relates only to the half cylinder below the free surface. The shape above the surface has no effect on the results.

[2] See any advanced text book on fluid dynamics.

[3] The mapping relates only to the underwater shape of the hull cross section.

$$\zeta = f(z)$$

The functional form of the transformation equations must be determined for every individual case, depending on the size and shape of the section in the ζ plane.

5.2 LEWIS FORMS

The transformation

$$\zeta = f(z) = a_0\, a \left(\frac{z}{a} + \frac{a\, a_1}{z} + \frac{a^3\, a_3}{z^3} + \frac{a^5\, a_5}{z^5} + \frac{a^7\, a_7}{z^7} + \ldots \right) \quad m$$

will map any point on a semicircle of radius a metres in the z plane into a corresponding point on a given shape in the ζ plane if appropriate values of the coefficients a_0, a_1, a_3, a_5 etc are chosen. The absence of even terms like a_2, a_4 etc. ensures that the transformed shapes have port/starboard symmetry like conventional ship sections.

It is usual to truncate the transformation series to only three terms:

$$\zeta = a_0\, a \left(\frac{z}{a} + \frac{a\, a_1}{z} + \frac{a^3\, a_3}{z^3} \right) \quad m \qquad (5.3)$$

We shall see that this allows a wide variety of ship like cross sections to be generated from the semicircle. These forms will not be exact replicas of any given hull cross section, but the match can usually be made sufficiently close to allow adequate estimates of the hydrodynamic coefficients for ship motion calculation. The resulting family of forms are known as ***Lewis forms,*** after F M Lewis who first proposed their use (for ship vibration studies) in 1929.

Lewis forms are defined by the values of the section area coefficient

$$\sigma = \frac{A'}{B'\, D'}$$

and the beam/draft ratio

$$H = \frac{B'}{D'}$$

and we now derive expressions for the transformation coefficients a_0 , a_1 and a_3 in terms of these two quantities.

Since we are here concerned with points on the semicircle of radius a metres we may set

$$r = a \quad m$$

Substituting Equations (5.1) and (5.2) into Equation (5.3) and separating real and imaginary parts we obtain a pair of parametric equations in θ describing the shape of the Lewis form in the ζ plane:

$$x_{B2} = a_0\, a \left[\left(1 + a_1 \right) sin\ \theta - a_3\, sin\ (3\theta) \right] \quad m \qquad (5.4a)$$

$$x_{B3} = a_0\, a \left[\left(1 - a_1 \right) cos\ \theta + a_3\, cos\ (3\theta) \right] \quad m \qquad (5.4b)$$

Substituting $\theta = 0$ in Equations (5.4) we obtain the bottom of the semicircle and the keel of the Lewis form:

$$x_{B2} = 0 \quad m$$

$$x_{B3} = D' = a_0\, a \left(1 - a_1 + a_3 \right) \quad m$$

Substituting $\theta = \pi/2$ in Equations (5.4), we obtain the intersections of the semicircle and the Lewis form with the water surface:

$$x_{B2} = \frac{B'}{2} = a_0\, a\, (1 + a_1 + a_3) \quad m$$

$$x_{B3} = 0 \quad m$$

The beam/draught ratio of the Lewis form is

$$H = \frac{B'}{D'} = \frac{2\, (1 + a_1 + a_3)}{1 - a_1 + a_3} \qquad (5.5)$$

The cross sectional area of the Lewis form is

$$A' = 2 \int_0^{\frac{B'}{2}} x_{B3}\, dx_{B2} \quad m^2$$

Substituting Equations (5.4) we obtain

$$A' = \frac{\pi\, a_0^2\, a^2}{2} (1 - a_1^2 - 3a_3^2) \quad m^2$$

and the section area coefficient is

$$\sigma = \frac{A'}{B'D'} = \frac{\pi}{4}\left(\frac{1 - a_1^2 - 3a_3^2}{1 - a_1^2 + 2a_3 + a_3^2}\right) \qquad (5.6)$$

Explicit equations for the coefficients a_1 and a_3 may be obtained by rearranging Equations (5.5) and (5.6) to give

$$a_1 = (1 + a_3)\left(\frac{H - 2}{H + 2}\right) \qquad (5.7a)$$

$$a_3 = \frac{3 - C + \sqrt{9 - 2C}}{C} \qquad (5.7b)$$

where

$$C = 3 + \frac{4\sigma}{\pi} + \left(1 - \frac{4\sigma}{\pi}\right)\left(\frac{H - 2}{H + 2}\right)^2$$

a_0 is simply a scale factor governing the overall size of the Lewis form.

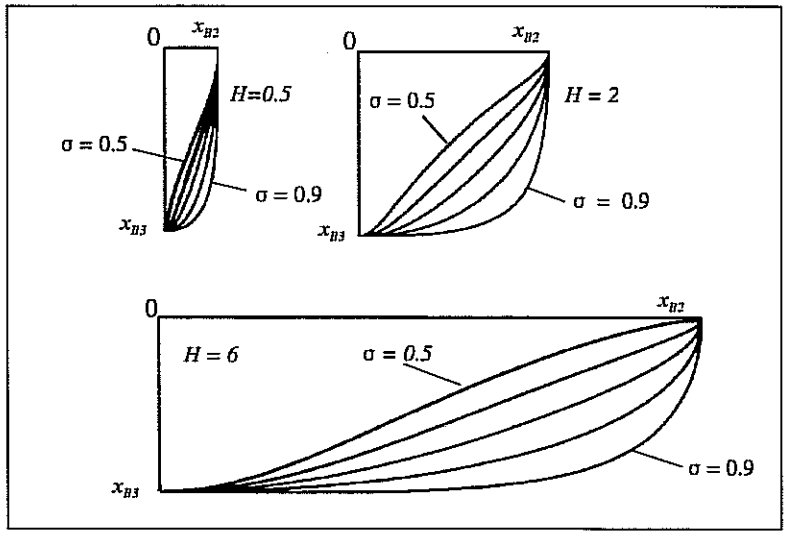

Fig 5.3 - Examples of Lewis forms

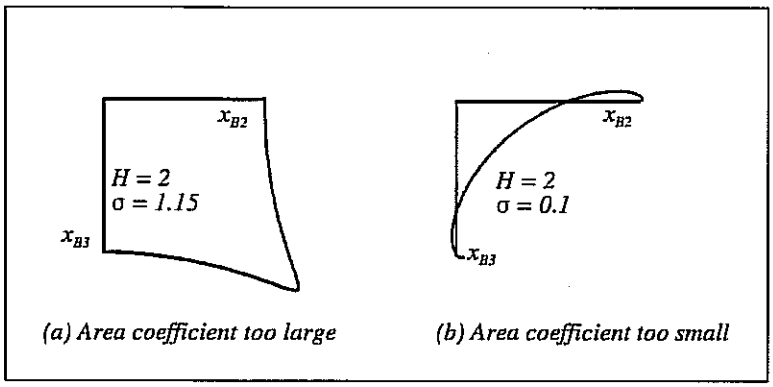

Fig 5.4 - Examples of invalid Lewis forms

The Lewis form corresponding to a real hull cross-section may therefore be defined in terms of its beam/draught ratio H and section area coefficient σ. Figure 5.3 shows a range of Lewis forms for various values of H and σ[4].

There is no limit to the permissible beam/draught ratio but only a limited range of section area coefficients are possible. Clearly the formula for a_3 (Equation (5.7b)) becomes invalid when $C > 9/2$ and this will happen if

$$\sigma > \frac{\pi}{64H}(H^2 + 20H + 4) \tag{5.8}$$

Lewis forms having section area coefficients greater than this cannot exist. In practice section area coefficients approaching this limit have rather angular shapes of the type shown in Figure 5.4(a). They are not representative of conventional hull forms: more to the point is the fact that such section shapes would probably experience flow separation around the sharp bilges, and the potential flow techniques employed for predicting the hydrodynamic coefficients would not be expected to give very reliable results. To avoid forms of this nature it is usual to suggest that the Lewis forms should lie completely within the circumscribing rectangle so that

$$x_{B2} \le \frac{B'}{2}; \qquad x_{B3} \le D'$$

If the section area coefficient is too small the Lewis form will adopt physically impossible shapes with negative values of x_{B2} and x_{B3} as shown in Figure 5.4(b). We therefore also insist that

$$x_{B2} \ge 0, \quad x_{B3} \ge 0$$

Applying these limits to Equations (5.4) with

[4] Only the right hand side of each section is shown.

$$0 \leq \theta \leq \frac{\pi}{2}$$

allows permissible ranges for the section area coefficient σ to be determined:

$$\frac{3\pi}{64}(4 - H) \leq \sigma \leq \frac{3\pi}{256}(24 + H) \quad \text{for } H \leq 2$$

$$\frac{3\pi}{16}\left(\frac{H - 1}{H}\right) \leq \sigma \leq \frac{3\pi}{64}\left(\frac{1 + 6H}{H}\right) \quad \text{for } H \geq 2 \qquad (5.9)$$

These limits are shown, together with the ideal upper limit given by the inequality (5.8), in Figure 5.5.

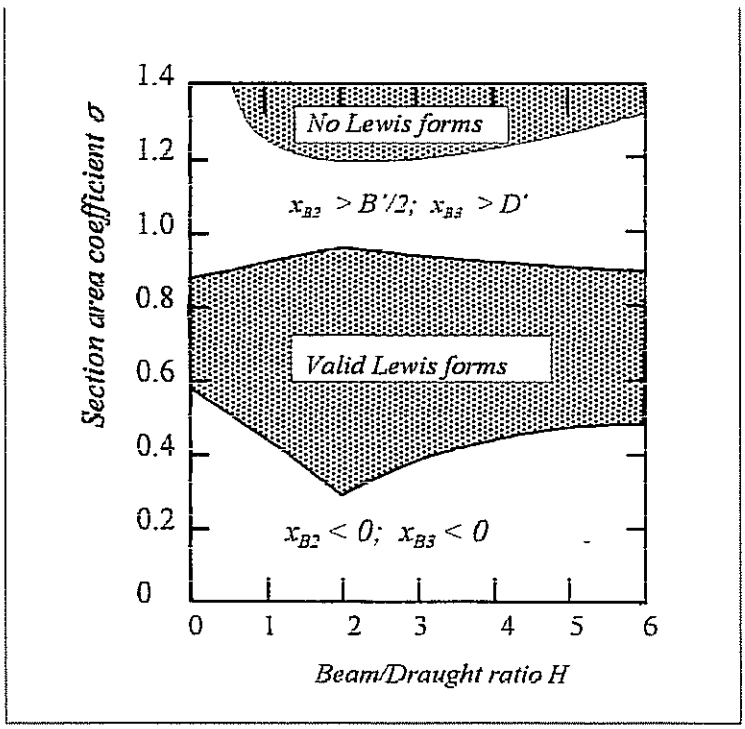

Fig 5.5 - Permissible ranges of Lewis forms

5.3 ADDED MASS AND DAMPING COEFFICIENTS FOR A HEAVING LEWIS FORM

According to de Jong (1973) the added mass and damping coefficients for the heaving Lewis form are given by [5]

$$a'_{33} = \frac{\rho B'^2 (A_* N_0 + B_* M_0)}{2 (A_*^2 + B_*^2)} \quad t \tag{5.10}$$

$$b'_{33} = \frac{\rho B'^2 \omega \pi^2}{4 (A_*^2 + B_*^2)} \quad kN/(m/sec) \tag{5.11}$$

where

$$A_* = \psi_C (0, \frac{\pi}{2}) + \sum_{m=1}^{\infty} \left[p_{2m} (-1)^{m-1} \frac{k B' Q_1}{2 Q_2} \right] \quad m^2/sec$$

$$B_* = \psi_S (0, \frac{\pi}{2}) + \sum_{m=1}^{\infty} \left[q_{2m} (-1)^{m-1} \frac{k B' Q_1}{2 Q_2} \right] \quad m^2/sec$$

$$M_0 = \int_0^{\frac{\pi}{2}} \phi_S (0, \theta) \frac{Q_3}{Q_2} d\theta + \frac{1}{Q_2} \left(\sum_{m=1}^{\infty} \left[q_{2m} (-1)^{m-1} Q_4 \right] + \frac{\pi k B' Q_5}{8 Q_2} \right) \quad m^2/sec$$

[5] All expressions given for the hydrodynamic coefficients of two dimensional sections in this chapter are per metre length of cylinder.

$$N_0 = \int_0^{\frac{\pi}{2}} \phi_C (0 , \theta) \frac{Q_3}{Q_2} d\theta$$

$$+ \frac{1}{Q_2} \left(\sum_{m=1}^{\infty} \left[p_{2m} (-1)^{m-1} Q_4 \right] + \frac{\pi k B' Q_5}{8 Q_2} \right) \quad m^2/sec$$

The stream and potential functions are given by

$$\psi_C = \pi \, exp (- k x_{B3}) \, sin (k |x_{B2}|) \quad m^2/sec$$

$$\phi_C = \pi \, exp (- k x_{B3}) \, cos (k x_{B2}) \quad m^2/sec$$

$$\psi_S = -\pi \, exp (- k x_{B3}) \, cos (k x_{B2})$$

$$+ \int_0^{\infty} \frac{exp (- \nu |x_{B2}|)}{\nu^2 + k^2} \left[\nu \, sin (\nu x_{B3}) + k \, cos (\nu x_{B3}) \right] d\nu$$

$$m^2/sec$$

$$\phi_S = \pi \, exp (-k x_{B3}) \, sin (k |x_{B2}|)$$

$$- \int_0^{\infty} \frac{exp (- \nu |x_{B2}|)}{\nu^2 + k^2} \left[\nu \, cos (\nu x_{B3}) + k \, sin (\nu x_{B3}) \right] d\nu$$

$$m^2/sec$$

The weighting coefficients p_{2m} and q_{2m} are obtained by approximate solution for a finite number of unknowns of the simultaneous equations

$$\psi_C (1 , \theta) - \frac{Q_6}{Q_2} \psi_C (1 , \pi/2) = \sum_{m=1}^{N} p_{2m} f_{2m} \quad m^2/sec$$

$$\psi_S (1 , \theta) - \frac{Q_6}{Q_2} \psi_S (1 , \pi/2) = \sum_{m=1}^{N} q_{2m} f_{2m} \quad m^2/sec$$

where

$$f_{2m} = -\left(\sin(2m\theta) + \frac{k B'}{2Q_2} Q_7 + \frac{k B'}{2Q_2^2} (-1)^m Q_8 Q_6 \right)$$

$$Q_1 = \frac{1}{2m-1} - \frac{a_1}{2m+1} - \frac{3a_3}{2m+3}$$

$$Q_2 = 1 + a_1 + a_3$$

$$Q_3 = (1 + a_1) \cos\theta - 3a_3 \cos(3\theta)$$

$$Q_4 = \frac{1 + a_1}{4m^2 - 1} + \frac{9a_3}{4m^2 - 9}$$

$$Q_5 = (1 + a_1 - a_1 a_3) q_2 - a_3 q_4$$

$$Q_6 = (1 + a_1) \sin\theta - a_3 \sin(3\theta)$$

$$Q_7 = \frac{\sin(2m-1)\theta}{2m-1} + \frac{a_1 \sin(2m+1)\theta}{2m+1} - \frac{3a_3 \sin(2m+3)\theta}{2m+3}$$

$$Q_8 = \frac{1}{2m-1} - \frac{a_1}{2m+1} - \frac{3a_3}{2m+3}$$

$\phi_C(r, \theta)$, $\phi_S(r, \theta)$, etc in these formulae imply values calculated at (r, θ) in the circle plane.

5.4 ADDED MASS AND DAMPING COEFFICIENTS FOR A SWAYING LEWIS FORM

The added mass and damping coefficients for a swaying Lewis form are

$$a'_{22} = \frac{\rho B'^2}{2} \left[\frac{p_0 N_0 + q_0 M_0}{p_0^2 + q_0^2} \right] t \qquad (5.12)$$

$$b'_{22} = \frac{\rho\ \omega\ B'^{2}}{2} \left[\frac{p_0\ M_0 - q_0\ N_0}{p_0^2 + q_0^2} \right] \quad kN/(m/sec) \tag{5.13}$$

$$a'_{42} = \frac{\rho\ B'^{3}}{2} \left[\frac{p_0\ X_R + q_0\ Y_R}{p_0^2 + q_0^2} \right] \quad kN\ m/(m/sec^2) \tag{5.14}$$

$$b'_{42} = \frac{\rho\ B'^{3}}{2} \left[\frac{p_0\ Y_R - q_0\ X_R}{p_0^2 + q_0^2} \right] \quad kN\ m/(m/sec) \tag{5.15}$$

where

$$M_0 = -\int_0^{\frac{\pi}{2}} \phi_S\ (0\ ,\ \theta\ )\ \frac{Q_9}{Q_2}\ d\theta\ -\ \frac{3\pi\ a_3\ p_2}{4Q_2} - \sum_{m\ =\ 1}^{\infty} \frac{q_{2m}\ Q_{10}\ k\ B'\ (-1)^{m-1}}{2Q_2^2} \tag{5.16}$$

$$N_0 = -\int_0^{\frac{\pi}{2}} \phi_C\ (0\ ,\ \theta\ )\ \frac{Q_9}{Q_2}\ d\theta\ -\ \frac{3\pi\ a_3\ p_2}{4Q_2} - \sum_{m\ =\ 1}^{\infty} \frac{p_{2m}\ Q_{10}\ k\ B'\ (-1)^{m-1}}{2Q_2^2} \tag{5.17}$$

$$X_R = \int_0^{\frac{\pi}{2}} \phi_C\ (0\ ,\ \theta\ )\ \frac{Q_{11}}{Q_2}\ d\theta\ +\ \frac{\pi\ k\ B'\ (\ a_1\ p_2\ -\ a_3\ p_4\ )}{16\ Q_2^2} + \sum_{m\ =\ 1}^{\infty} \frac{p_{2m}\ Q_{12}\ (-1)^{m+1}}{Q_2^2} \tag{5.18}$$

$$Y_R = \int_0^{\frac{\pi}{2}} \phi_S (0 , \theta) \frac{Q_{11}}{Q_2} d\theta + \frac{\pi k B' (a_1 p_2 - a_3 p_4)}{16 Q_2^2} + \sum_{m=1}^{\infty} \frac{q_{2m} Q_{12} (-1)^{m+1}}{Q_2^2} \qquad (5.19)$$

$\phi_C (r , \theta)$, $\phi_S (r , \theta)$, etc, in these formulae imply values calculated at (r , θ) in the circle plane.

The stream and potential functions are

$$\phi_C = -\pi \, exp (- k x_{B3}) \, sin (k x_{B2}) \quad m^2/sec$$

$$\psi_C = \pi \, exp (- k x_{B3}) \, cos (k x_{B3}) \quad m^2/sec$$

$$\psi_S = \pi \, exp (- k x_{B3}) \, sin (- k |x_{B3}|) - \int_0^{\infty} \frac{exp (- \nu |x_{B2}|)}{k^2 + \nu^2} \left[\nu \, cos (\nu x_{B3}) - k \, sin (\nu x_{B3}) \right] d\nu - \frac{x_{B2}}{k (x_{B2}^2 + x_{B3}^2)} \quad m^2/sec$$

$$\phi_S = \pm \pi \, exp (- k x_{B3}) \, cos (k |x_{B2}|) \pm \int_0^{\infty} \frac{exp (\mp \nu |x_{B2}|)}{k^2 + \nu^2} \left[k \, cos (\nu x_{B3}) + \nu \, sin (\nu x_{B3}) \right] d\nu + \frac{x_{B2}}{k (x_{B2}^2 + x_{B3}^2)} \quad m^2/sec$$

The weighting coefficients p_{2m} and q_{2m} are found by approximate solution for a finite number of unknowns of the simultaneous equations

$$\psi_C (0 , \theta) - \psi_C (0 , \pi/2) = \sum_{m=1}^{N} p_{2m} f_{2m} \quad m^2/sec$$

$$\psi_S (0 , \theta) - \psi_S (0 , \pi/2) = \sum_{m=1}^{N} q_{2m} f_{2m} \quad m^2/sec$$

where

$$f_0 = \frac{Q_{13}}{Q_2}$$

$$f_{2m} = cos [(2m + 1) \theta] + \frac{k B' Q_{14}}{2Q_2} + \frac{k B' (-1)^{(m+1)} Q_{15}}{2Q_2}$$

and the stream function for the multipoles is given by

$$\psi_{2m} (r , \theta) = \frac{cos [(2m + 1) \theta]}{r^{2m+1}} - \frac{k B cos (2m \theta)}{4Q_2 m r^{2m}} + \frac{a_1 cos [(2m + 2) \theta]}{(2m + 2) r^{2m+2}} - \frac{3a_3 cos [(2m + 4) \theta]}{(2m + 4) r^{2m+4}} \quad m^2/sec \qquad (5.20)$$

The following definitions are used in these formulae:

$$Q_9 = (1 - a_1) sin \theta + 3a_3 sin (3\theta)$$

$$Q_{10} = \frac{1}{4m^2 - 1} - \frac{a_1}{(2m + 2)^2 - 1} - \frac{3a_3}{(2m + 4)^2 - 1} + 3a_3 \left[\frac{1}{4m^2 - 9} - \frac{a_1}{(2m + 2)^2 - 9} - \frac{3a_3}{(2m + 4)^2 - 9} \right]$$

$$Q_{12} = \frac{2a_1 (1 + a_3)}{(2m + 1)^2 - 4} + \frac{8a_3}{(2m + 1)^2 - 16}$$

$$Q_{13} = (1 - a_1) cos \theta + a_3 cos (3\theta)$$

$$Q_{14} = \frac{\cos(2m\,\theta)}{2m} + \frac{a_1 \cos[(2m+1)\,\theta]}{2m+2} - \frac{3a_3 \cos[(2m+4)\,\theta]}{2m+4}$$

$$Q_{15} = \frac{1}{2m} - \frac{a_1}{2m+2} - \frac{3a_3}{2m+4}$$

5.5 ADDED MASS AND DAMPING COEFFICIENTS FOR A ROLLING LEWIS FORM

The added mass and damping coefficients for a rolling Lewis form are

$$a'_{44} = \frac{\rho B'^4}{16} \frac{p_0 X_R + q_0 Y_R}{p_0^2 + q_0^2} \quad t\,m^2 \tag{5.21}$$

$$b'_{44} = \frac{\rho \omega B'^4}{16} \frac{p_0 Y_R + q_0 X_R}{p_0^2 + q_0^2} \quad kN\,m/(rad/sec) \tag{5.22}$$

$$a'_{24} = \frac{\rho B'^3}{8} \frac{M_0 q_0 + N_0 p_0}{p_0^2 + q_0^2} \quad kN/(rad/sec^2) \tag{5.23}$$

$$b'_{24} = \frac{\rho \omega B'^3}{16} \frac{M_0 p_0 - N_0 q_0}{p_0^2 + q_0^2} \quad kN/(rad/sec) \tag{5.24}$$

X_R , Y_R , M_0 and N_0 are defined in Equations (5.16) - (5.19). However p_{2m} and q_{2m} are now obtained by approximate solution for a finite number of unknowns N of the simultaneous equations

$$\psi_C(1, \theta) - \psi_C(1, \pi/2) = \sum_{m=0}^{N} p_{2m} f_{2m} \quad m^2/sec$$

$$\psi_S\ (\ 1\ ,\ \theta\ ) - \psi_S\ (\ 1\ ,\ \pi/2\ ) = \sum_{m=0}^{N} q_{2m}\, f_{2m} \qquad m^2/sec$$

where

$$f_0 = 4\left[\ \frac{x_{B2}^2\ (\ 1\ ,\ \theta\ ) + x_{B3}^2\ (\ 1\ ,\ \theta\ )}{B'^2}\right] - 1$$

$$f_{2m} = \psi_{2m}\ (\ 1\ ,\ \pi/2\ ) - \psi_{2m}\ (\ 1\ ,\ \theta\ );\quad m \neq 0$$

ψ_{2m} in these formulae is given by Equation (5.20).

5.6 MEASUREMENTS OF LOCAL HYDRODYNAMIC PROPERTIES

Accurate calculation of the hydrodynamic properties of cylinders of ship-like cross-section is clearly of paramount importance in the prediction of ship motions in waves. It is therefore somewhat surprising to find that relatively few experiments to verify these calculations have been carried out.

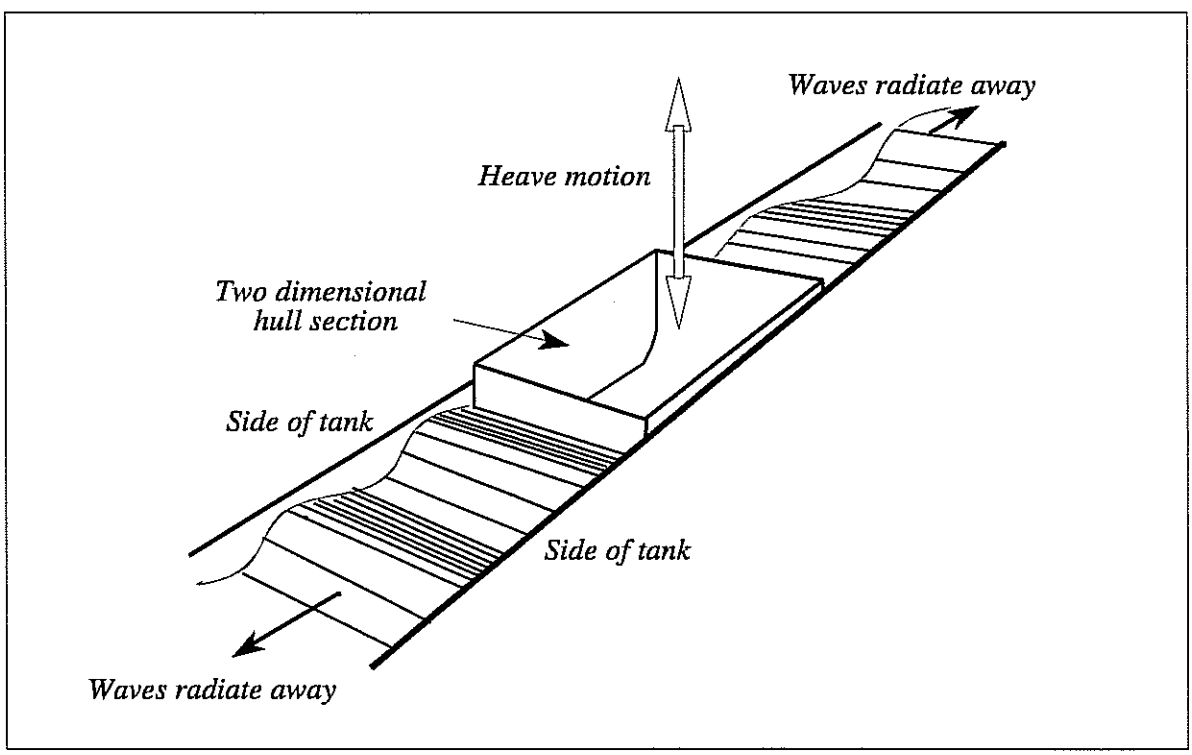

Fig 5.6 - Experiment to measure hydrodynamic coefficients for heave motion

Vugts published the results of the classic experiments in this field in 1968. He tested a number of cylinders in a towing tank at the Delft Shipbuilding Laboratory. Figure 5.6 shows, in simplified form, the arrangement he used. The cylinders were mounted across the tank and an oscillation mechanism was used to impose sinusoidal heave, sway and roll motions in turn. The waves generated by the cylinder motions radiated away and were absorbed by beaches at each end of the tank, some 70 metres from the cylinder. The forces and moments necessary to sustain the cylinder motions were measured and used to determine the added mass, damping and cross coupling coefficients for each motion. Some of his results are shown in Figures 5.7 - 5.10.

Cylinder A was circular with (by definition) $H = 2$ and $\sigma = \pi/4$ while cylinders B and C had ship like cross-sections but the same values of H and σ. Figure 5.7 shows that their heave added mass and damping coefficients were virtually identical, confirming that these are essentially functions only of beam/draught ratio and section area coefficient. Small local differences in the shape have little influence on the results. The heave added mass is generally of the same order as the displaced mass ρA and rises towards infinity at zero frequency. The coefficients are predicted quite well by the theory.

Cylinders D, E and F were all rectangular (except for a small radius at the bilge corners) with $\sigma \approx 1$ and beam/draught ratios $H = 2$, 4 and 8. Figure 5.8 shows how the heave added mass and damping increase with beam/draught ratio. The triangular cylinder H generally had the lowest coefficients. The opposite trend is shown for the sway coefficients in Figure 5.9.

Finally, Figure 5.10 shows some results for the rolling motion of rectangular cylinder D ($\sigma \approx 1$; $H = 2$). These experiments were conducted using two roll amplitudes of 0.05 and 0.15 radians respectively. The results show that roll motion coefficients depend on the amplitude of the motion: in other words the roll response is non linear, contrary to the assumptions made in the theory described in Chapter 3.

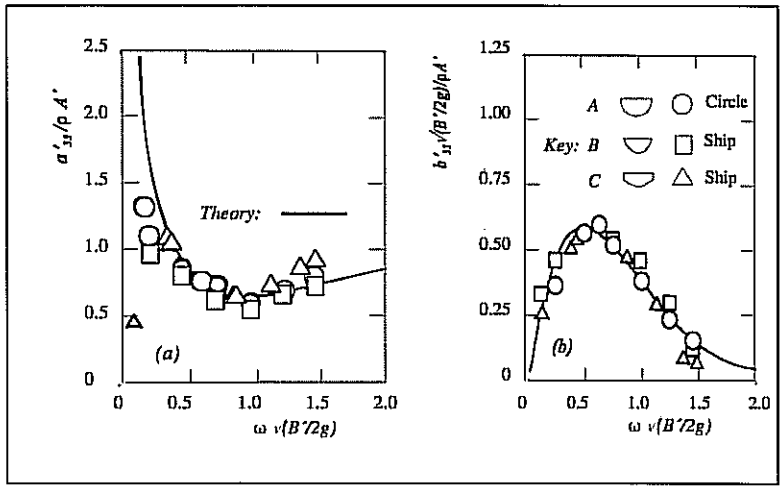

Fig 5.7 - Hydrodynamic coefficients (a) added mass and (b) damping for three heaving cylinders. All cylinders have H=2; σ=π/4. (After Vugts (1968)).

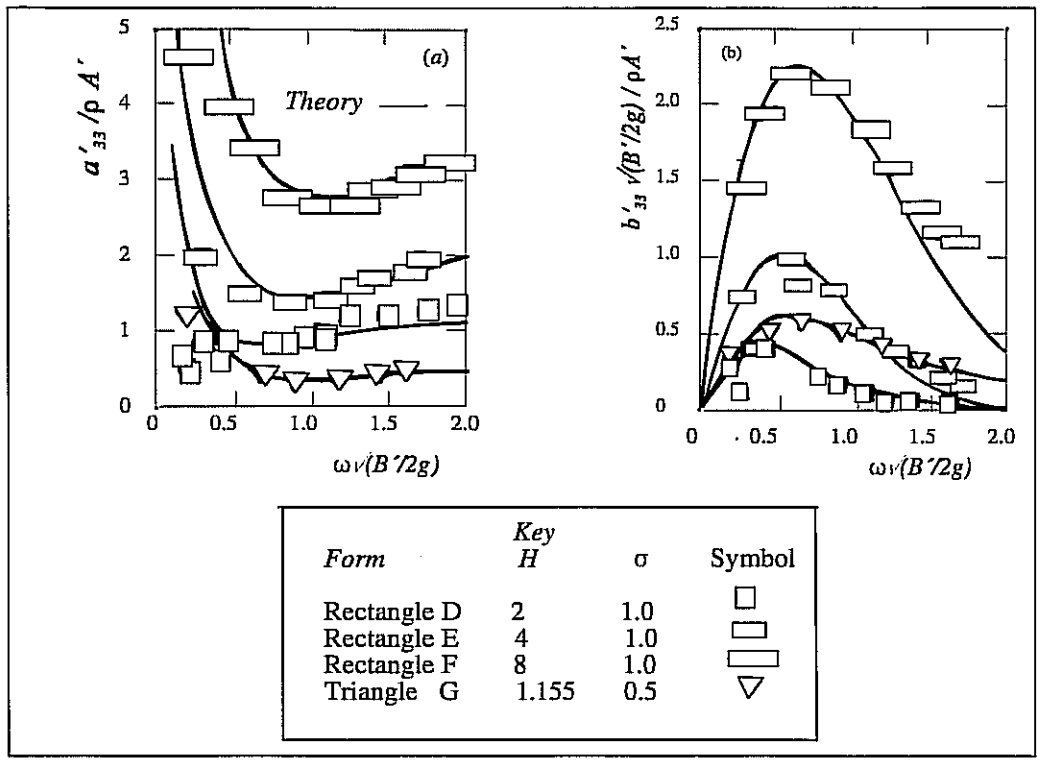

Fig 5.8 - Hydrodynamic coefficients (a) added mass and (b) damping for four heaving cylinders. (After Vugts (1968)).

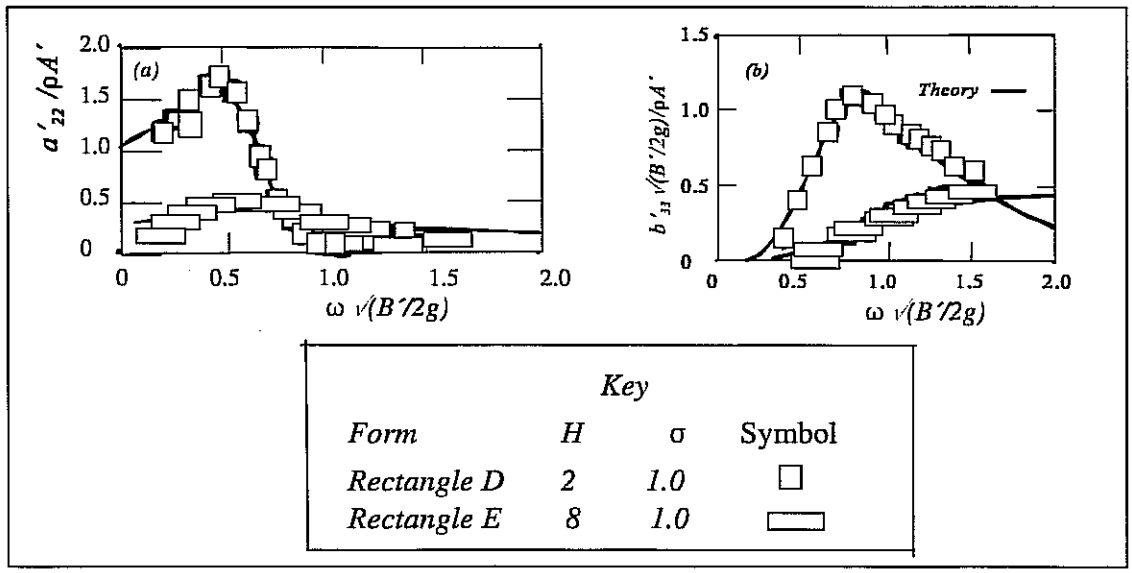

Fig 5.9 - Hydrodynamic coefficients (a) added mass and (b) damping for two swaying cylinders. (After Vugts (1968)).

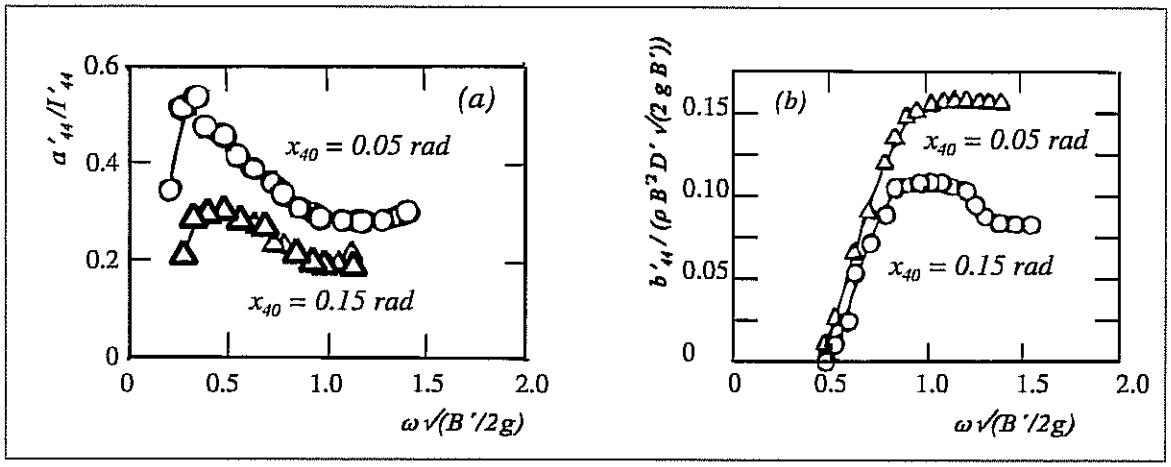

Fig 5.10 - (a) Added moment of inertia and (b) damping for a rolling rectangular cylinder showing the effect of roll amplitude (H=2; σ=1). (After Vugts (1968))

6

ROLL DAMPING

Signal from one corvette to another in full Atlantic gale:

Have just seen down your funnel. Fire is burning brightly.

From "Make a Signal" by Jack Broome. Douglas-Boyd Books 1994

6.1 SOURCES OF ROLL DAMPING

According to strip theory the motion damping arises because the oscillating hull radiates energy in the form of waves away from the ship. For most motions this constitutes the major mechanism for the dissipation of energy. So strip theory estimates of motion damping are generally adequate and reasonable motion predictions are usually obtained.

Rolling is unfortunately an exception to this general rule. The wave making damping b_{44W} predicted for the potential flow around most hull forms is only a small fraction of the total roll damping which is experienced in reality. Additional important contributions are illustrated in Figure 6.1.

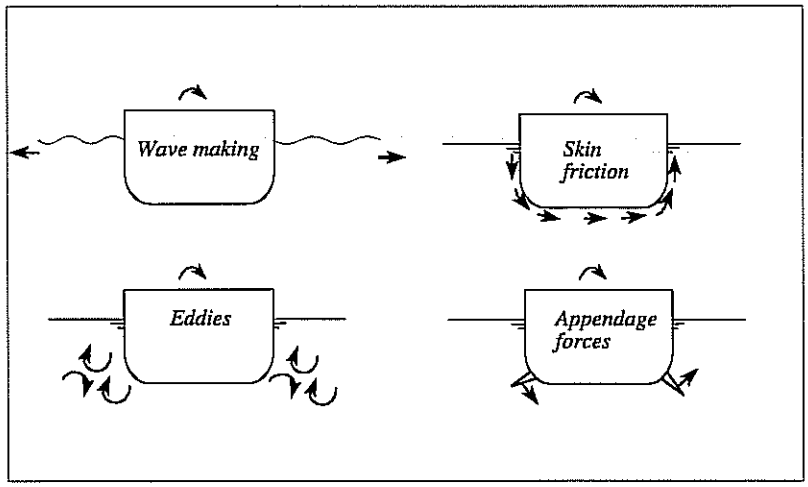

Fig 6.1 - Sources of roll damping

Hull forms with relatively sharp corners at the bilges and/or at the keel will shed eddies as the ship rolls. This absorbs a good deal of energy and is a significant source of additional roll damping. Skin friction forces on the surface of the rolling hull may also be significant and any appendages will generate forces which oppose the rolling motion.

Eddy shedding, skin friction and the appendage forces experienced at low forward speed arise because of the influence of viscosity which is neglected in strip theory.

6.2 NON LINEAR ROLL DAMPING: EQUIVALENT LINEARISATION

Wave making roll damping and the damping due to the appendage forces at high forward speed are linear (that is, the roll damping moment is directly proportional to the roll velocity). Viscous roll damping is, however, non linear and generally proportional to the square of the roll velocity. This means that the pure sinusoidal roll response to a sinusoidal wave input (Equation (3.16b)) given by the linear theory is no longer valid. Moreover, the linear spectral calculation for motions in irregular waves, which will be described in Chapter 8, is not applicable.

In order to circumvent these unwelcome problems we may calculate an equivalent linear damping coefficient which allows for the effects of the non linearities but is used in a linear way. This allows us to continue using the linear equations of motion and the spectral techniques for irregular wave calculations. The equivalent linear damping coefficient is chosen so that the calculated energy dissipated by this term in the equation of motion is the same as that which is actually dissipated by the non linear damping. In general this means that the equivalent linear damping coefficient depends on the roll motion being experienced and a new value of the damping must be calculated for every situation.

Since the predominant rolling motions experienced at sea occur at the natural roll frequency ω_{*4}, we may simplify the treatment of roll damping non linearities by considering only motions at that frequency. Suppose then that the rolling motion is given by

$$x_4 = x_{40} \sin(\omega_{*4} t) \quad rad \tag{6.1}$$

Then the roll moment exerted about the centre of gravity by the equivalent linear damping term will be $b_{44} \dot{x}_4$ kN m. In one roll period the work done and energy E dissipated by this linearised damping term will be the integral of the moment times the angular distance moved:

$$E = 4 \int_0^{x_{40}} b_{44} \dot{x}_4 \, dx_4 = 4 \omega_{*4}^2 b_{44} x_{40}^2 \int_0^{\pi/2\omega_{*4}} \cos^2(\omega_{*4} t) \, dt$$

$$= \pi \omega_{*4} b_{44} x_{40}^2 \quad kN\ m$$

and the equivalent linearised roll damping coefficient is therefore related to the dissipated energy by

$$b_{44} = \frac{E}{\pi \omega_{*4} x_{40}^2} \quad kN\ m/(rad/sec) \tag{6.2}$$

6.3 EDDY ROLL DAMPING

Tanaka (1960) conducted a series of model experiments to determine the eddy shedding roll damping characteristics of a number of different hull section shapes as shown in Figure 6.2. Schmitke (1978) used these results to develop expressions for the eddy making damping coefficients for each type of hull section. He postulated that the force due to the eddy shedding acts at the relevant sharp corner at a radius r_b metres from the centre of gravity. The local force resisting the roll motion is expressed in the form

$$F = \frac{1}{2} \rho \, (r_b \, \dot{x}_4)^2 \, s \, C_E \, \delta x_{BI} \quad kN$$

where s and δx_{BI} are the girth and length of the hull section and C_E is an eddy drag coefficient depending on the hull form. Now for sinusoidal rolling motion (Equation (6.1)) the force F exerts a moment about G given by

$$F_4 = F \, r_b = \frac{1}{2} \rho \, r_b^3 \, s \, C_E \, x_{40}^2 \, \omega_{*4}^2 \, cos^2 \, (\omega_{*4} \, t) \, \delta x_{BI} \quad kN \, m$$

and the energy dissipated by this moment in one roll period is

$$E = 4 \int_0^{x_{40}} F_4 \, dx_4 = \frac{4}{3} \rho \, r_b^3 \, x_{40}^3 \, \omega_{*4}^2 \, s \, C_E \, \delta x_{BI} \quad kN \, m$$

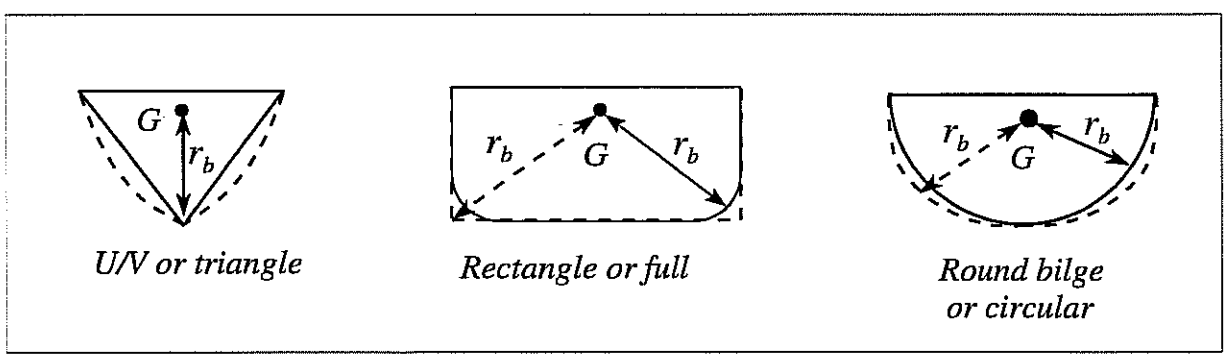

Fig 6.2 - Classification of section shapes and definitions of radius r_b for eddy roll damping calculations

Using Equation (6.2) we see that the equivalent linearised local damping coefficient attributed to eddy making is

$$b'_{44E} = \frac{4\rho \, \omega_{*4}}{3\pi} \, x_{40} \, r_b^3 \, s \, C_E \, \delta x_{BI} \quad kN \, m/(rad/sec)$$

The total equivalent linearised roll damping coefficient for the complete hull is obtained by integrating along the length of the hull:

$$b_{44E} = \int b'_{44E} = \frac{4\rho\ \omega_{*4}\ x_{40}^2}{3\pi} \int r_b^3\ s\ C_E\ dx_{BI} \quad kN\ m/(rad/sec) \tag{6.3}$$

It remains to determine the drag coefficient C_E which varies along the hull. Schmitke (1978) gave the following empirical formula:

$$C_E = Z_1\ Z_2\ exp\ (-u\ r_e\ /D')\ \tag{6.4}$$

where Z_1 and Z_2 are given as functions of $B/\overline{KG}$, γ (the inclination of the hull section at the waterline) and $r_e\ /D'$ in Figure 6.3; D' is the local draght and r_e is the effective radius at the keel given by

$$r_e = \frac{B}{2}\left[4.12 - 2.69\ \frac{\overline{KG}}{B} + 0.823\left(\frac{\overline{KG}}{B}\right)^2\right] \quad m \quad \text{for } \frac{\overline{KG}}{B} < 2.1$$

$$r_e = 0 \quad for\ \frac{\overline{KG}}{B} > 2.1$$

and

$$u = 14.1 - 46.7\ x_{40} + 61.7\ x_{40}^2 \tag{6.5}$$

with x_{40} in radians.

Tanaka (1960) found that Equations (6.4) and (6.5) also applied to very full almost rectangular sections (typical of the midship sections of merchant vessels) with r_e now equal to the radius of curvature of the bilge and $Z_2 = 1$.

For triangular sections at the aft end of cruiser stern ships Schmitke fitted the following quadratic to Tanaka's data:

$$C_E = 0.438 - 0.449\ \frac{B}{\overline{KG}} + 0.236\left[\frac{B}{\overline{KG}}\right]^2$$

Round bilge sections have negligible eddy shedding roll damping and

$$C_E = O$$

for these forms. Figure 6.2 shows the definition of r_b for each of the classes of section shape considered.

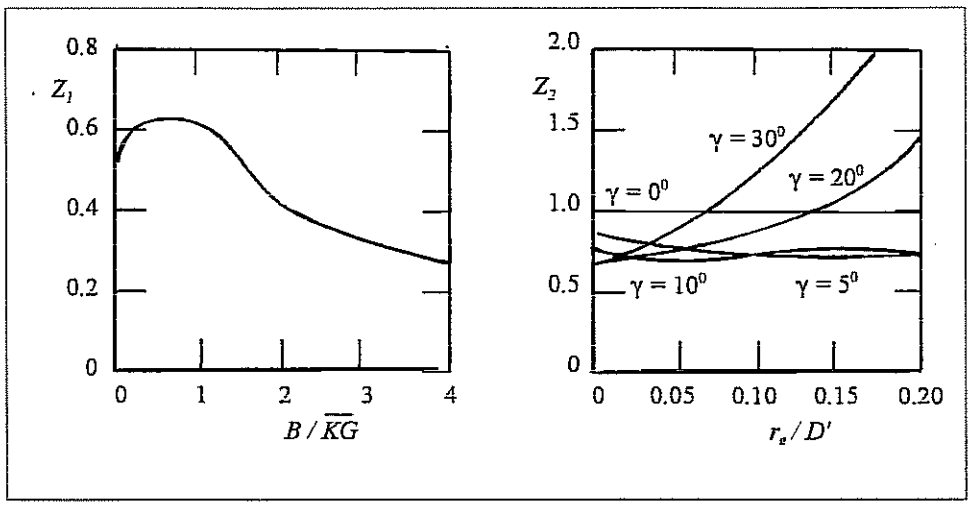

Fig 6.3 - Z_1 and Z_2 for U/V sections (After Tanaka (1960) and Schmitke (1978))

6.4 SKIN FRICTION ROLL DAMPING

The water flowing past the ship's hull exerts frictional forces on the hull surface. It is usual to express the force acting on a small element of the hull surface in terms of a non dimensional local skin friction drag coefficient defined as

$$C_F = \frac{\textit{frictional force on element}}{\frac{1}{2}\rho \times (\textit{local velocity})^2 \times \textit{area of element}}$$

Consider a girthwise element δs of length δx_{B1} metres as shown in Figure 6.4. Let the element be positioned at (x_{B2}, x_{B3}), a distance r metres from the centre of gravity. If the roll velocity is $\dot{x}_4$ radians/second the velocity at the element will be $r\,\dot{x}_4$ metres/second and the component velocity tangential to the surface of the hull will be

$$r\,\dot{x}_4\ sin\ (\theta_1 + \theta_2) \quad m/sec$$

θ_1 and θ_2 are the polar location of the element and the slope of the hull surface so that:

$$sin\ \theta_1 = \frac{x_{B3}}{r}, \quad cos\ \theta_1 = \frac{x_{B2}}{r}$$

$$\sin\ \theta_2 = -\frac{\delta x_{B3}}{\delta s}, \quad cos\ \theta_2 = \frac{\delta x_{B2}}{\delta s}$$

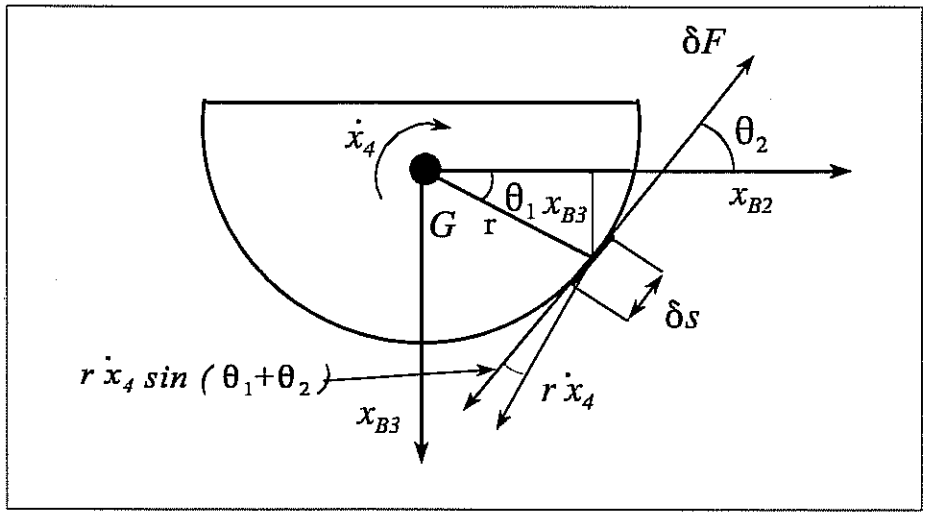

Fig 6.4 - Roll damping due to skin friction.

Then the frictional force acting on the element δs will be

$$\delta F = C_F \frac{1}{2} \rho [r \dot{x}_4 \sin (\theta_1 + \dot{\theta}_2)]^2 \delta s \, \delta x_{B1} \quad kN \tag{6.6}$$

and the moment about the centre of gravity is

$$\delta F_4 = C_F \frac{1}{2} \rho r^3 \dot{x}_4^2 \sin^2 (\theta_1 + \theta_2) \delta s \, \delta x_{B1} \quad kN\ m \tag{6.7}$$

The work done by the moment in a complete roll cycle is

$$E = 4 \int_0^{x_{40}} \delta F_4 \, \delta x_4 \quad kN\ m$$

and using Equations (6.1), (6.6) and (6.7) this becomes

$$E = \frac{4C_F}{3} \rho r \omega_{*4}^2 x_{40}^3 \left(x_{B3} \frac{\delta x_{B2}}{\delta s} - x_{B2} \frac{\delta x_{B3}}{\delta s} \right)^2 \delta s \, \delta x_{B1} \quad kN\ m$$

Then the equivalent linearised roll damping coefficient for skin friction is obtained from Equation (6.2) by allowing δx_{B1} and δs to approach zero and integrating along the hull and around the girth:

$$b_{44F} = \frac{4C_F}{3\pi} \rho\omega_{*4} x_{40} \int_0^L \int_0^s r \left(x_{B3} \frac{dx_{B2}}{ds} - x_{B2} \frac{dx_{B3}}{ds} \right)^2 ds \, dx_{B1} \qquad (6.8)$$

$kN\ m/(rad/sec)$

It remains to determine the local skin friction coefficient C_F. Schmitke (1978) suggested that the Schoenherr formula for the average skin friction coefficient for `smooth turbulent' flow used in calculations of ship resistance is appropriate:

$$C_F = 0.0004 + [3.36\ log_{10}R_N - 5.6]^{-2}$$

where the Reynolds number is based on the forward speed and length of the ship:

$$R_N = \frac{\rho\ U\ L}{\mu_w}$$

This is clearly inappropriate if the forward speed is zero, and Kato's (1958) formula may then be used:

$$C_F = 1.328\ R_N^{-0.5} + 0.014\ R_N^{-0.114}$$

where R_N is now a Reynolds number based on the average rolling velocity and the average distance from the centre of gravity:

$$R_N = \frac{0.512\ \rho\ (\bar{r}\ x_{40})^2\ \omega_{*4}}{\mu_w}$$

$$\bar{r} = \frac{1}{\pi} [(\ 0.887 + 0.145\ C_B\ )(\ 1.7D + B\ C_B\ )$$

$$+ 2\ (\ \overline{KG} - D\ )] \quad m$$

C_B is the block coefficient of the hull defined as

$$C_B = \frac{\Delta}{Length \times Beam \times Draught}$$

where Δ is the hull displacement in cubic metres.

6.5 APPENDAGE ROLL DAMPING

6.5.1 Drag forces on appendages

At zero forward speed the incidence induced on the appendages by the roll motion is 90° and the resulting drag force provides a contribution to the roll damping as illustrated in Figure 6.5(a).

If the roll velocity is $\dot{x}_4$ radians/second and the appendage is located at a radius r_A metres (measured from the centre of gravity to the mid span of the appendage) the roll motion will impart a transverse velocity $r_A\ \dot{x}_4$ metres/second to the appendage. The resulting drag force on the appendage will be

$$F_D = C_D \frac{1}{2} \rho\ (r_A\ \dot{x}_4)^2 A_A \quad kN \tag{6.9}$$

where C_D is the non dimensional drag coefficient.

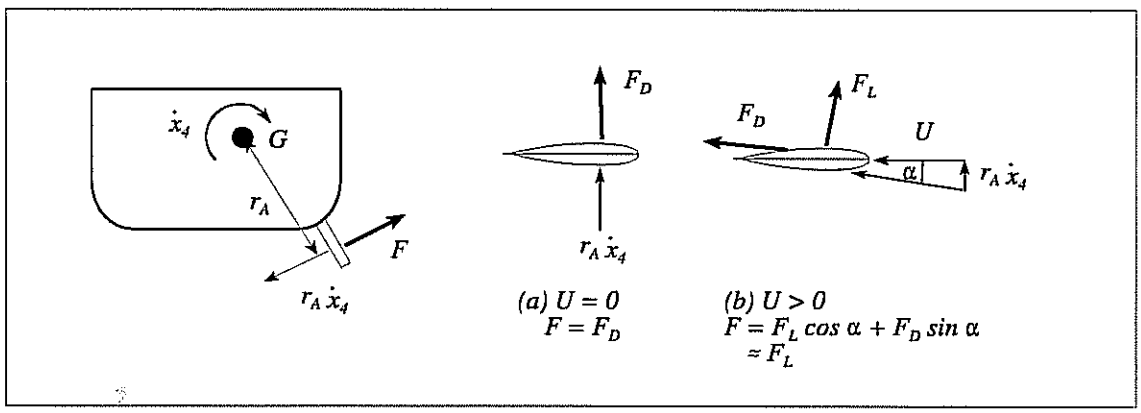

Fig 6.5 - Roll damping due to a lifting surface

The drag force yields a roll damping moment

$$F_4 = C_D \frac{1}{2} \rho\ r_A^3\ \dot{x}_4^2\ A_A \quad kN\ m$$

and the energy dissipated in one roll cycle is

$$E = 4 \int_0^{x_{40}} F_4\ dx_4 \quad kN\ m$$

Using Equation (6.9) this becomes

$$E = \frac{4}{3} C_D\ \rho\ A_A\ r_A^3\ x_{40}^3\ \omega_{*4}^2 \quad kN\ m$$

and Equation (6.2) then gives the equivalent linearised damping coefficient due to appendage drag forces at zero speed as

$$b_{44AD} = \frac{4}{3\pi} C_D\ \rho\ x_{40}\ \omega_{*4} \sum A_A\ r_A^3 \quad kN\ m/(rad/sec) \tag{6.10}$$

where the summation is over all appendages. According to Hoerner (1965) a suitable value for the drag coefficient for appendages like rudders or stabiliser fins is

$$C_D \approx 1.17$$

6.5.2 Lift forces on appendages

If the forward speed is not zero the rolling motion induces an angle of incidence on each appendage as shown in Figure 6.5(b). The angle of incidence is

$$\alpha = tan^{-1}\left(\frac{r_A\,\dot{x}_4}{U}\right) \quad rad$$

$$\approx \frac{r_A\,\dot{x}_4}{U} \quad rad \quad \text{if } r_A\,\dot{x}_4 \ll U$$

and the total velocity experienced by each appendage is

$$q = \sqrt{U^2 + r_A^2\,\dot{x}_4^2} \quad m/sec$$

$$\approx U \quad m/sec \quad \text{if } r_A\,\dot{x}_4 \ll U$$

The appendage develops lift and drag forces which are respectively normal and parallel to the local velocity vector as shown in Figure 6.5(b). The total force normal to the ship's longitudinal axis is

$$F = F_L\,cos\,\alpha + F_D\,sin\,\alpha \quad kN$$

$$\approx F_L \quad kN \quad \text{if } \alpha \text{ is small}$$

Hence if the induced angle of incidence α is small the total roll moment applied to the ship by the appendage is

$$F_4 = F\,r_A \approx \frac{dC_L}{d\alpha}\,\frac{1}{2}\,\rho\,U\,A_A\,r_A^2\,\dot{x}_4 \quad kN\,m$$

and the roll damping coefficient attributable to the lift force developed by the appendages is

$$b_{44AL} \approx \frac{1}{2}\,\rho\,U \sum \frac{dC_L}{d\alpha}\,A_A\,r_A^2 \quad kN\,m/(rad/sec) \qquad (6.11)$$

where the summation is for all appendages. It should be noted that this damping coefficient is independent of roll angle and no special linearisation techniques are necessary.

The lift curve slope $dC_L/d\alpha$ may be obtained from Whicker and Fehlner's (1958) formula

$$\frac{dC_L}{d\alpha} = \frac{1.8\pi\ a}{1.8 + \sqrt{a^2 + 4}} \quad rad^{-1} \tag{6.12}$$

where the equivalent aspect ratio of the appendage is

$$a = \frac{2b}{\bar{c}} = \frac{4b}{c_r + c_t}$$

and b is the outreach, $\bar{c}$ is the mean chord, c_r is the root chord and c_t is the tip chord.

6.6 TOTAL ROLL DAMPING

The total roll damping is obtained by adding the contributions from the individual roll damping sources discussed above:

$$b_{44} = b_{44W} + b_{44E} + b_{44F} + b_{44AD} \quad kN\ m/(rad/sec) \quad \text{for } U = 0 \tag{6.13a}$$

$$b_{44} = b_{44W} + b_{44E} + b_{44F} + b_{44AL} \quad kN\ m/(rad/sec) \quad \text{for } U > 0 \tag{6.13b}$$

7

SHIP MOTIONS IN REGULAR WAVES

7.1 INTRODUCTION

The strip theory outlined in previous chapters may be used to estimate the motions a ship would experience in regular sinusoidal waves of small amplitude. For conventional ships at moderate speeds these estimates are usually found to be of adequate accuracy for everyday engineering purposes. As an example, this chapter gives the results of a specimen set of calculations of the motions of a frigate of length 125 metres and explains the physical reasons for their nature. Ship motions are of course functions of hull shape and size, and the results given here should not be used to give numerical estimates of the motions of other hull forms. Nevertheless, the same general characteristics will be found to apply to the motions of all conventional monohull ships.

7.2 TRANSFER FUNCTIONS

We define the wave depression at the moving origin O (Equation (3.9)) as

$$\zeta = \zeta_0 \, sin \, (\, \omega_e \, t \,) \qquad m \tag{7.1}$$

and the resulting ship motions (Equations (3.16)) are taken to be

$$x_i = x_{i0} \, sin \, (\, \omega_e \, t + \delta_i \,) \qquad m; \qquad (i = 1, 3) \tag{7.2a}$$

$$x_i = x_{i0} \, sin \, (\, \omega_e \, t + \delta_i \,) \qquad rad; \qquad (i = 4, 6) \tag{7.2b}$$

The motion amplitudes x_{i0} and the phases δ_i are functions of the speed U, heading μ and encounter frequency ω_e. The amplitudes are assumed to be proportional to the wave amplitude ζ_0 and it is usual to express them in non dimensional form: linear motion amplitudes x_{10}, x_{20} and x_{30} are non dimensionalised by dividing by the wave amplitude ζ_0 ; angular motion amplitudes x_{40}, x_{50} and x_{60} (in radians) are divided by the wave slope amplitude $k\zeta_0$.

Graphs of the resulting non dimensional amplitudes plotted as a function of encounter frequency are called transfer functions[1]; they give the proportion of wave amplitude or wave slope amplitude "transferred" by the ship "system" into the ship motions.[2]

---

[1] Transfer functions are often wrongly called ***response amplitude operators*** (RAOs). Actually the RAO is the square of the transfer function.

[2] Transfer functions may also be plotted as a function of wave frequency or wave length. Each form of presentation has its merits, as discussed in section 7.6.

The phase angles δ_i give the phase relationship between the motion and the wave. A positive value means that the maximum positive motion occurs δ_i / ω_e seconds before the maximum wave depression is experienced at O. Negative values imply that the motion lags the wave depression at O.

7.3 VERTICAL PLANE MOTIONS IN REGULAR HEAD WAVES

We begin by considering the simplest case of ship motions in regular head waves ($\mu = 180°$). Symmetry ensures that roll, sway and yaw are absent and the motions are confined to surge, heave and pitch.

The heave and pitch Equations (3.22c) and (3.22e) are coupled so that heave motions are influenced by pitch and vice versa. However, the coupling is usually fairly weak and to a first approximation we may regard the equations as independent. The heave and pitch motions then approximate to the motions of two independent second order spring mass systems as described in Appendix 1. The analogy is not rigorous because the coefficients in the equations are frequency dependent, in contrast to the constant coefficients assumed in the classical equations. Nevertheless, we may define approximate natural frequencies for heave and pitch using Equation (A1.6):

$$\omega_{*3} = \sqrt{\frac{c_{33}}{m + a_{33}}} \quad rad/sec \tag{7.3a}$$

$$\omega_{*5} = \sqrt{\frac{c_{55}}{I_{55} + a_{55}}} \quad rad/sec \tag{7.3b}$$

where the heave added mass a_{33} and the pitch added inertia a_{55} are to be evaluated at the respective natural frequencies (see Equation (3.2b) for the definition of I_{55}). Since the natural frequencies are unknown and a_{33} and a_{55} are functions of frequency it is necessary to guess an initial value, estimate a_{33} and a_{55}, and compute second estimates of the natural frequencies. These second estimates are then used to compute third estimates of a_{33} and a_{55} and the natural frequencies and so on until the results of the iteration converge. Alternatively an approximate estimate of the natural frequencies may be obtained by assuming

$$a_{33} \approx m \quad t \; ; \qquad a_{55} \approx I_{55} \quad t\, m^2$$

The surge equation (3.22a) is independent of all the other equations and has no stiffness term $c_{11}\, x_1$. Surge motions would therefore be expected to be approximately analogous to those of a damped system with no stiffness and there is no natural surge frequency (see Appendix 1).

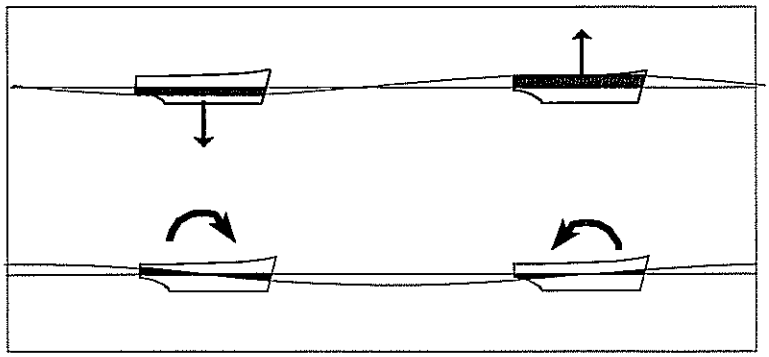

Fig 7.1 - Maximum heave and pitch excitations in very long head waves

In very long waves the encounter frequency ω_e is very low and dynamic effects associated with added mass and damping are virtually negligible. So the excitations and motion responses experienced by the ship are almost wholly attributable to the buoyancy changes as the waves pass the hull. Maximum pitch moment occurs at the wave nodes and maximum heave force occurs at the wave crests and troughs as shown in Figure. 7.1.

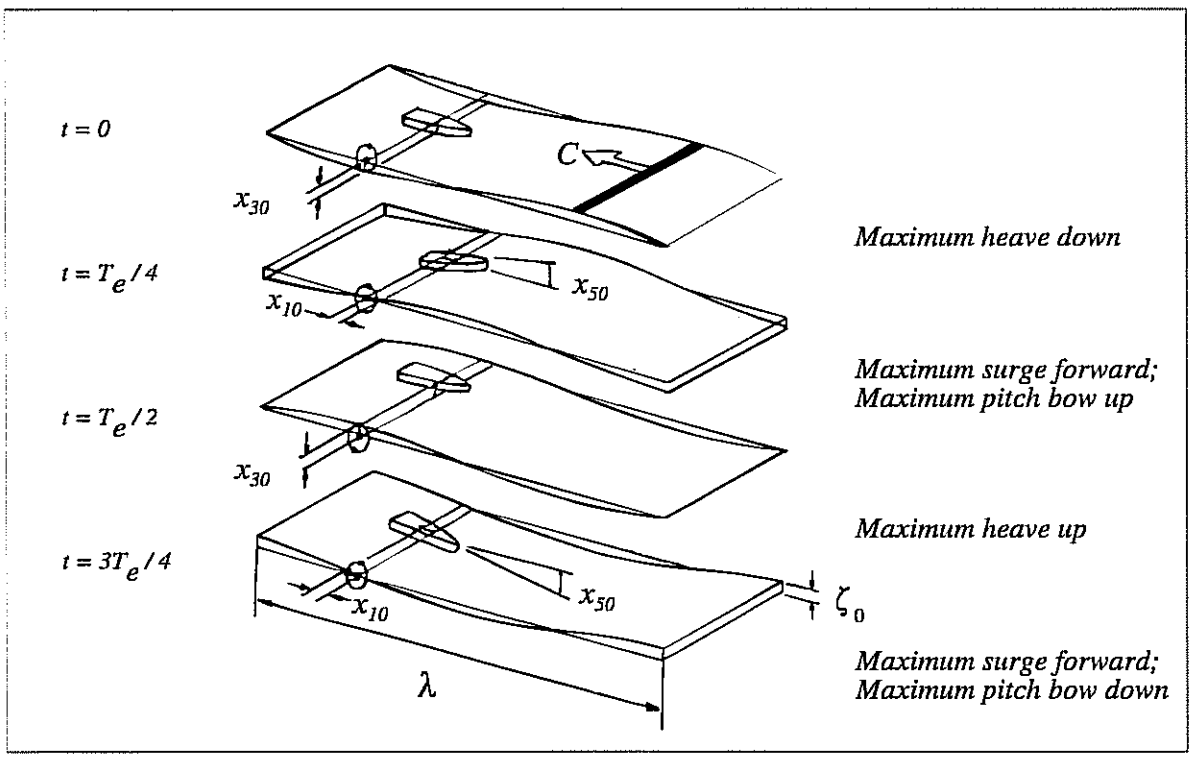

Fig 7.2 - Motions in very long head waves.

These large excitations in very long waves result in the large motion amplitudes illustrated in Figure 7.2. For moderate ship speeds the wave celerity is very much greater than the ship speed and the vessel may be regarded as virtually stationary as the wave passes by. The ship will behave more or less like a particle of water at the surface, following a circular orbit of radius ζ_0 given

by Equation (1.22). So maximum heave (equal to $\pm \zeta_0$) will occur at the wave crests and troughs and maximum surge (also equal to $\pm \zeta_0$) will be experienced at the wave nodes. The ship surges towards the approaching crests and recedes after the crest has passed by.

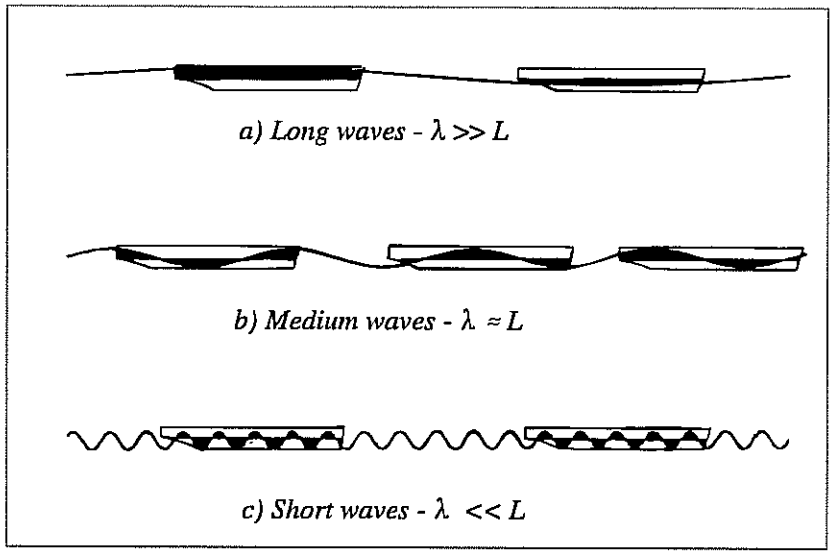

Fig 7.3 - Buoyancy forces on a restrained ship in regular head waves

An observer will see the ship appearing to crawl like a tiny ant over a succession of very long shallow hills. The ship will always be aligned with the wave surface so that maximum pitch (equal to the wave slope amplitude $\pm\ k\ \zeta_0$) will occur at the wave nodes.

Smith measured the total excitations experienced by a restrained model of the *Friesland* Class destroyer in regular head waves in 1966. Some of his results are shown in Figure 7.4. These show that the ship only experiences significant excitations in head waves when they are longer than about three quarters of the ship length. In shorter waves the buoyancy forces alternate along the ship's hull as shown in Figure 7.3. This, together with the growing importance of dynamic effects at the higher encounter frequencies, results in a general reduction in excitation in shorter waves.

Typical calculated heave and pitch transfer functions are shown for the frigate (see Introduction: Section 7.1) at various speeds in head waves in Figures 7.5 and 7.6. As expected, all responses approach unity at zero encounter frequency, corresponding to the long wave case discussed above.

At a given speed the responses are generally reduced at very high encounter frequencies because, as we have seen, short (high frequency) waves do not excite the ship very much. However, as the speed is increased, the wave lengths which do excite the ship are encountered over an ever widening range of frequencies (see the wave length scales in Figures 7.5 and 7.6). At very high speeds this range of frequencies may be wide enough to include the natural frequencies of heave and pitch given by Equations (7.3). The responses may then exhibit resonant peaks as shown at 30 knots in Figure 7.5. Pitch and heave motions are, however, invariably heavily damped and the resonant peaks are never very pronounced.

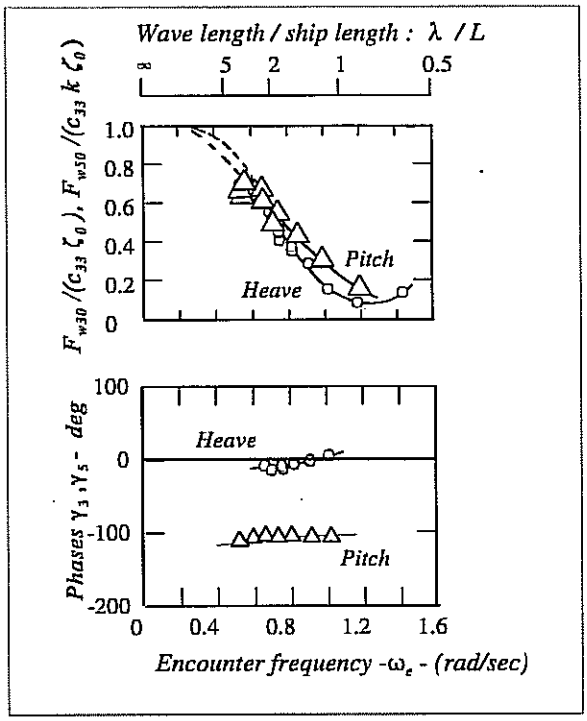

Fig 7.4 - Heave and pitch excitations in regular head waves: Friesland class destroyer. (After Smith (1966))

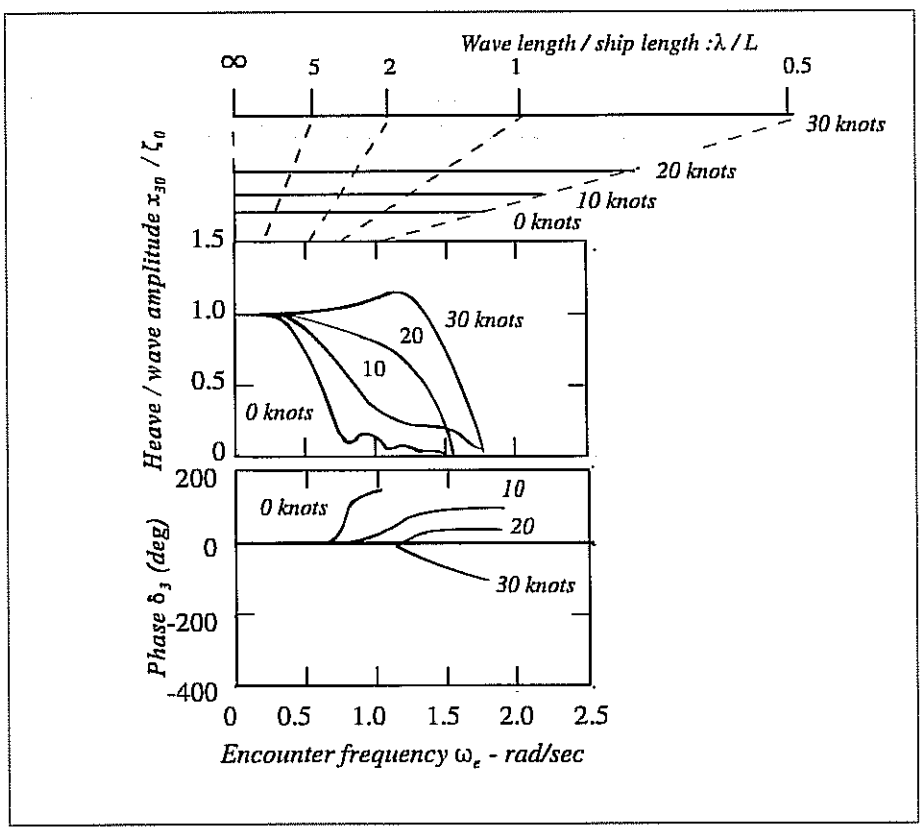

Fig 7.5 - Heave transfer functions for the frigate in regular head waves.

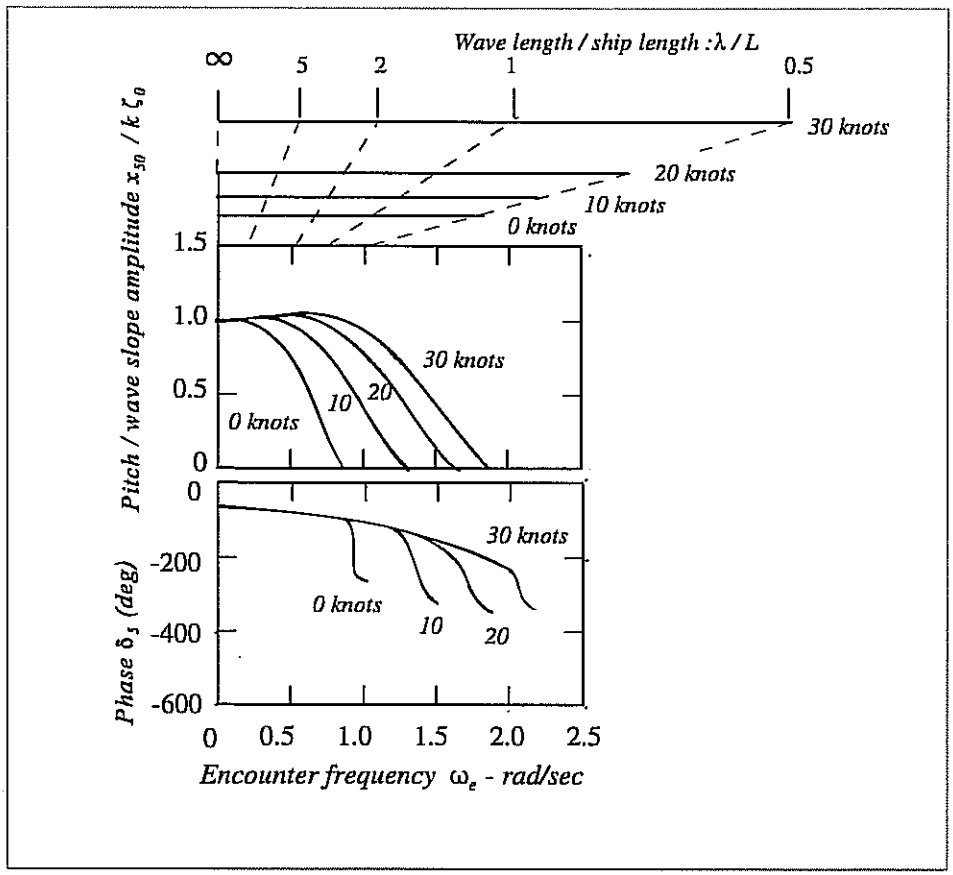

Fig 7.6 - Pitch transfer functions for the frigate in regular head waves

Figs 7.5 and 7.6 also show the heave and pitch phases. In very long waves the heave phase $\delta_3 = 0^0$ and this indicates that the heave motion is synchronised with the wave motion and that maximum heave (down) occurs in the wave troughs.

The pitch phase $\delta_5 = -90^0$ at zero encounter frequency. This indicates that maximum positive (bow up) pitch motion occurs at the wave node (one quarter of an encounter period after the wave trough has passed the ship's centre of gravity (see Figure 7.2)).

At higher frequencies these simple phase relationships are somewhat modified by dynamic effects and coupling with the other motions. Nevertheless, they remain largely true over much of the range of frequencies at which appreciable motions are experienced.

7.4 VERTICAL PLANE MOTIONS IN REGULAR FOLLOWING WAVES

In following waves the motions are again confined to surge, heave and pitch. Figures 7.7 and 7.8 show calculated heave and pitch transfer functions in regular following waves. These again approach unity when the waves are very long and the encounter frequency approaches zero. Only a limited range of (positive) frequencies can be encountered at any given speed for the reasons discussed in Chapter 1. The transfer functions consequently adopt the shapes shown with two

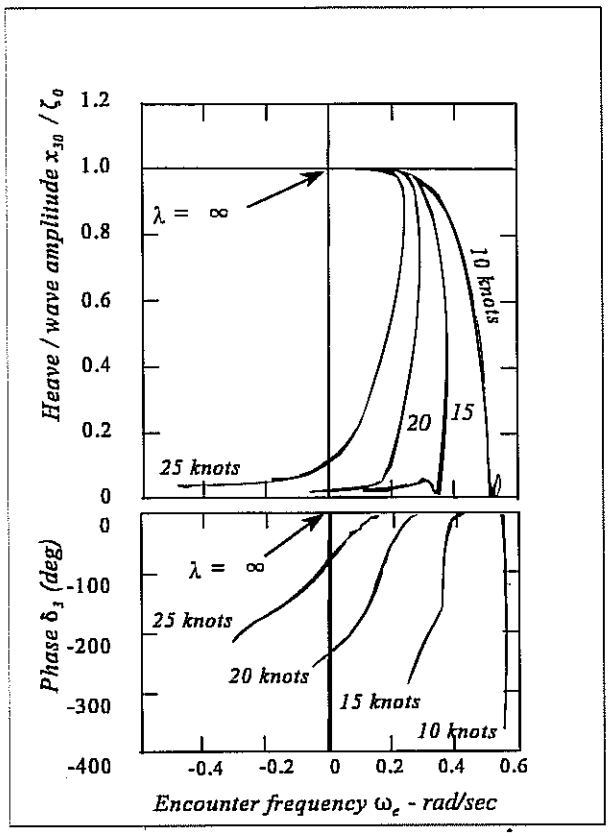

Fig 7.7 - Heave transfer functions for the frigate in regular following waves.

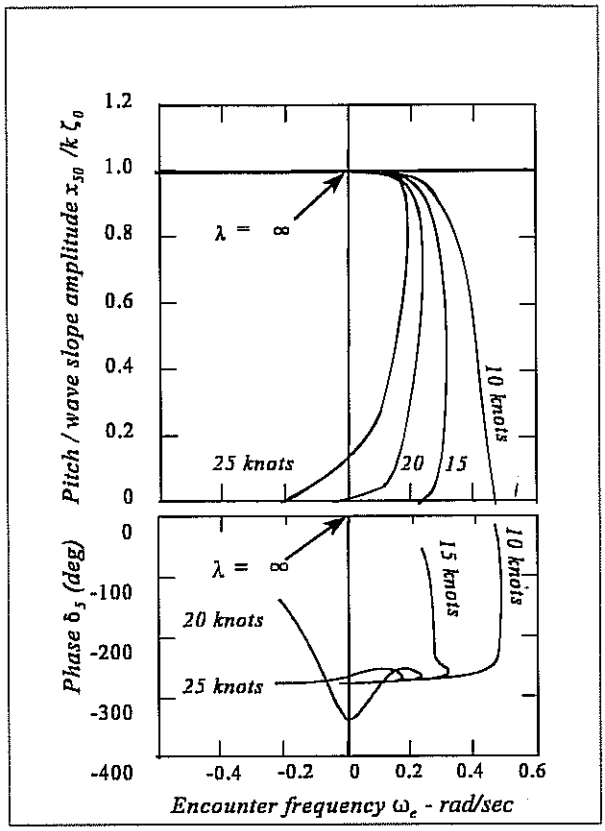

Fig 7.8 - Pitch transfer functions for the frigate in regular following waves.

possible motion responses (corresponding to different wave lengths) at any one positive encounter frequency.

A third motion response occurs at the corresponding negative encounter frequency (when the ship overtakes the waves). For moderate ship speeds this will only occur in very short waves and the excitations and resulting responses are usually very small.

The heave phase δ_3 is close to zero over most of the range of encounter frequencies for which the response is significant, indicating that the heave motion is again nearly synchronised with the wave motion. The pitch phase δ_5 is now approximately - 270^0 (or + 90^0) over most of the significant range of encounter frequencies. Maximum positive (bow up) pitch motion now leads the maximum wave depression at the centre of gravity by approximately one quarter of the encounter period.

7.5 VERTICAL PLANE MOTIONS IN REGULAR OBLIQUE WAVES

In oblique waves the ship motions are no longer confined to the vertical plane. Roll, sway and yaw motions also occur. However, the vertical plane equations of motion (3.22a), (3.22c) and (3.22e) for a symmetrical ship are independent of those for the lateral plane ((3.22b), (3.22d) and (3.22f). So the lateral plane motions in oblique waves of small amplitude will have no effect on the vertical plane motions and these may therefore be considered in isolation.

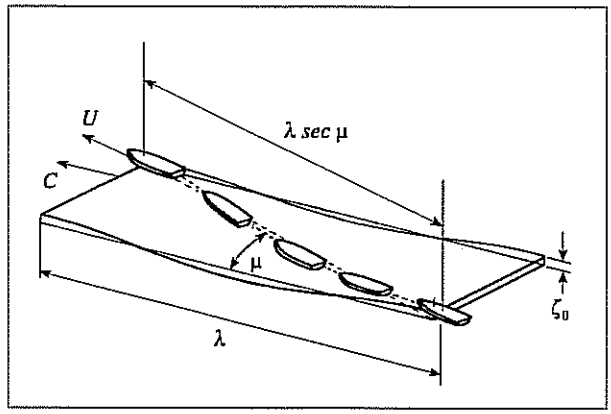

Fig 7.9 - Heave and pitch motions in very long oblique waves.

In very long oblique waves the ship again appears to be crawling over a succession of long shallow hills as shown in Figure 7.9. At the crests and troughs the heave motion will again equal the wave amplitude, exactly as in head and following waves.

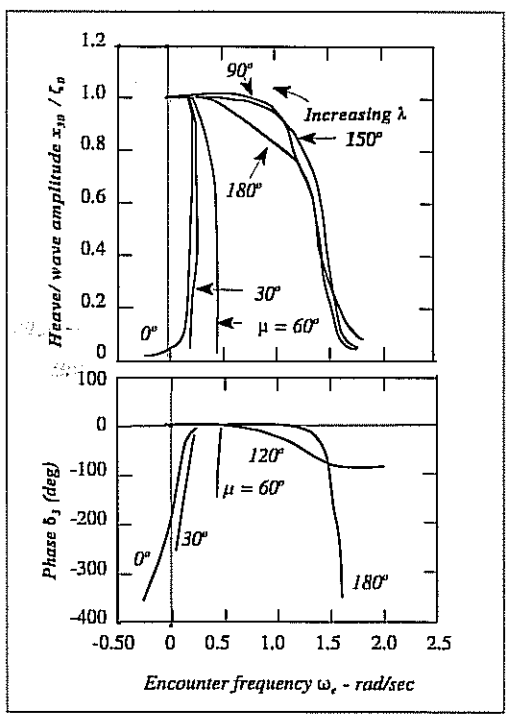

Fig 7.10 - Heave transfer functions for the frigate at 20 knots in regular oblique waves

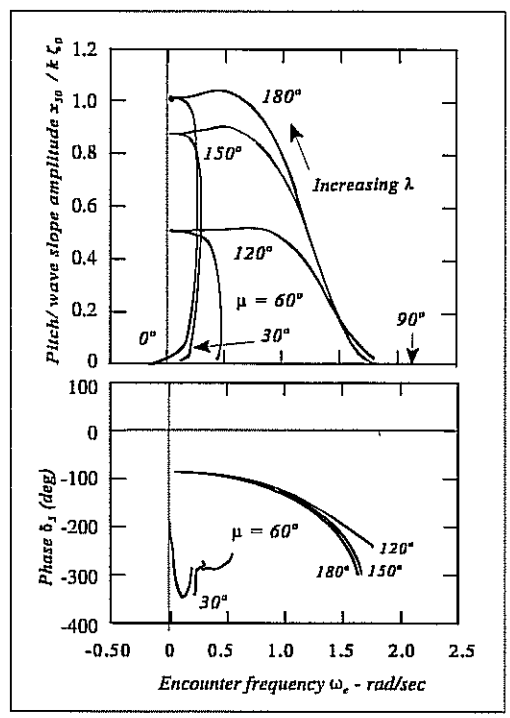

Fig 7.11 - Pitch transfer functions for the frigate at 20 knots in regular oblique waves

The "effective wave length" measured along the ship's track is $\lambda \; sec \; \mu$ metres and the corresponding effective wave slope amplitude in the pitch plane is therefore reduced to

$$\alpha_{10} = \frac{2\pi \; \zeta_0}{\lambda \; sec \; \mu} = k \; \zeta_0 \; cos \; \mu \quad rad \tag{7.4}$$

(see Equation (1.16)). In these long oblique waves the ship will again align itself with the wave surface, and the maximum pitch, equal to $\pm\ k\ \zeta_0\ cos\ \mu$, will occur at the wave nodes.

Figures 7.10 and 7.11 show typical oblique wave transfer functions for the frigate at 20 knots. On headings forward of the beam ($90° < \mu < 180°$) the responses are broadly similar to the head wave responses already discussed, but the pitch responses at zero encounter frequency (very long waves) now approach $cos\ \mu$ (see Equation (7.4)). Only one response is possible at any given encounter frequency and the motions generally decrease with increasing encounter frequency. The heave responses increase as the heading approaches 90° and the wave excitation becomes synchronised along the entire length of the hull.

The pitch response decreases as the heading approaches 90° and is usually negligible in beam waves.

On headings abaft the beam ($0° < \mu < 90°$) the responses adopt the general form of those already described for following waves. The range of possible encounter frequencies is reduced, depending on the heading, and more than one response is possible at any given encounter frequency.

Heave phase δ_3 is always zero in very long waves, indicating that heave is synchronised with wave depression at all headings. Pitch phase δ_5 is -90^0 on headings forward of the beam and -270^0 (or $+90^0$) on headings abaft the beam.

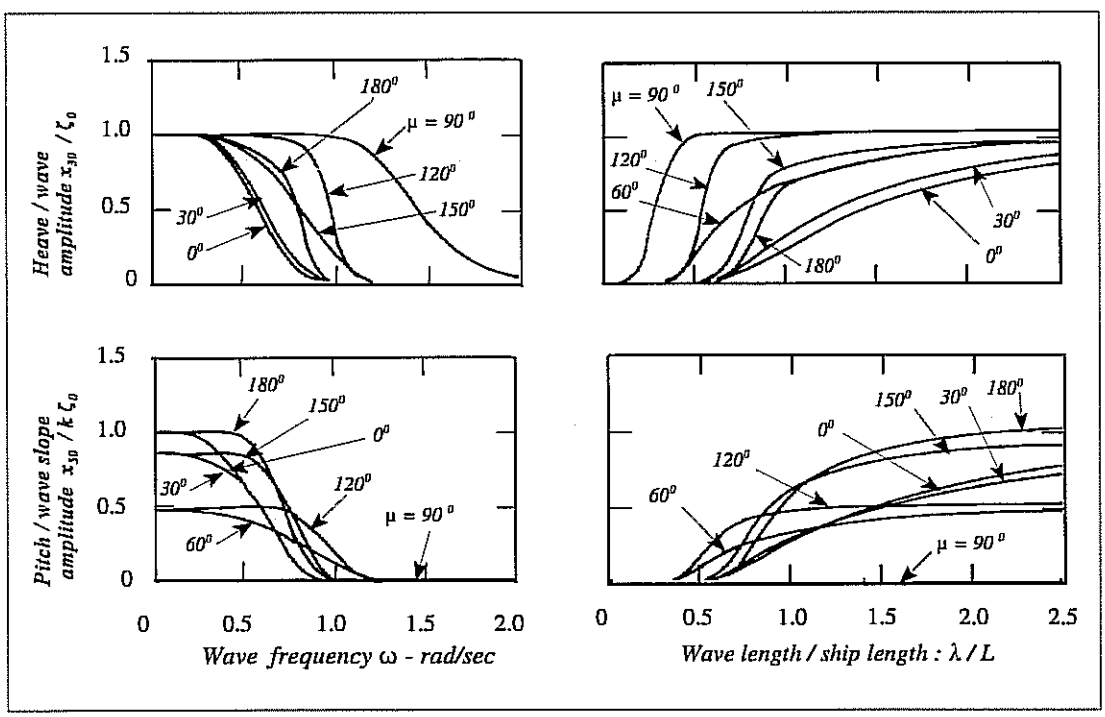

Fig 7.12 - Alternative presentations of transfer functions for the frigate at 20 knots in oblique waves.

7.6 ALTERNATIVE TRANSFER FUNCTION PRESENTATIONS

It is sometimes more convenient to present the motion responses as functions of wave frequency[1] or non dimensional wave length. Figure 7.12 shows the frigate's oblique wave transfer functions plotted in these forms. They have the singular advantage that the responses are now all single valued and the complications of multi valued responses at a given encounter frequency are avoided.

Each form of presentation has its own advantages: Plotting responses as a function of λ/L allows a physical picture of the ship and wave to be easily visualised: plotting responses as a function of ω_e allows an appreciation of the importance of natural frequencies (particularly for roll motions) and gives a true indication of the frequency of the motions experienced by the occupants of the ship; plotting responses as a function of ω is often more convenient for calculations of motions in irregular waves (see Chapter 8).

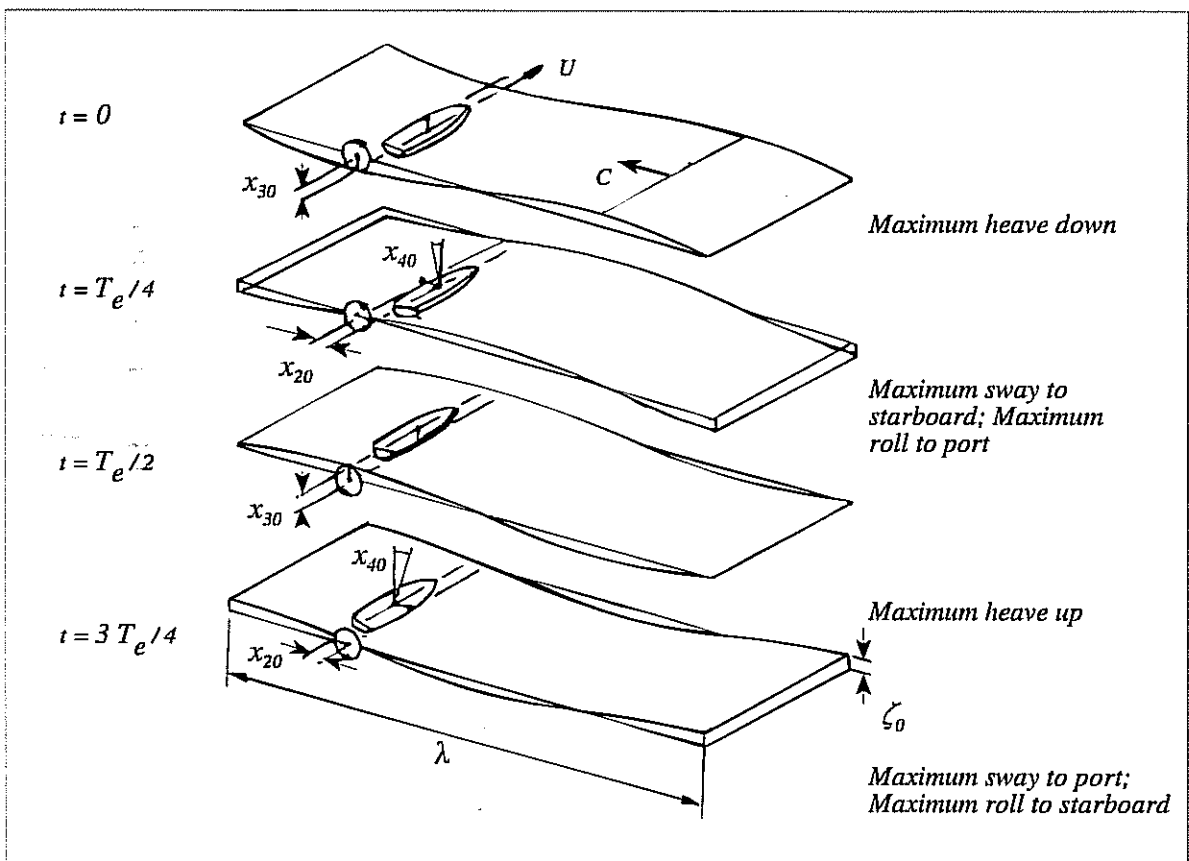

Fig 7.13 - Motions in very long beam waves

[1] Sometimes the wave frequency is made non dimensional as $\omega\sqrt{\frac{L}{g}}$

7.7 LATERAL PLANE MOTIONS IN REGULAR BEAM WAVES

In beam waves pitch motions are, as we have already seen, usually very small. Yaw is usually also negligible and the ship motions are essentially confined to heave, sway and roll. Figure 7.13 illustrates these motions in very long waves. The ship again follows the circular orbit of a particle of water at the surface. The heave and sway motions are therefore equal to the wave amplitude $\pm\ \zeta_0$: maximum heave motion occurs at the wave crests and troughs and maximum sway occurs at the wave nodes. The ship sways towards the approaching wave crest and recedes after the crest has passed by.

If there are no internal free surface effects to reduce the effective metacentric height[2] the ship's deck will always be aligned with the wave surface. Maximum roll, equal to the wave slope amplitude $\pm\ k\ \zeta_0$, will occur at the wave nodes.

Figure 7.14 shows the sway transfer function in beam waves. The sway equation (3.22b) has no stiffness term $c_{22}\ x_2$ so there is no sway resonance (see Appendix 1). Sway amplitudes decrease with increasing encounter frequency but the phase δ_2 remains essentially constant at about - 90^0 indicating that maximum positive sway (to starboard) occurs one quarter of an encounter period after the wave trough has passed by (see Figure 7.13).

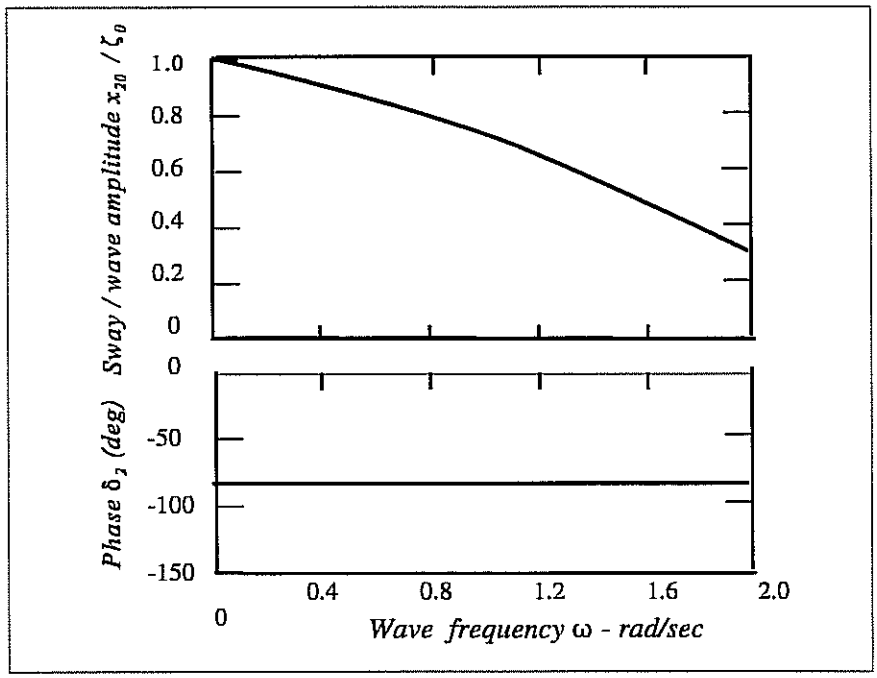

Fig 7.14 - Sway transfer function for the frigate at 20 knots in regular beam waves

[2] See any text book on naval architecture

Figure 7.15 shows roll transfer functions for the frigate in beam waves. Roll motion is affected by the sway and yaw motions (see Equation (3.22d)) but in beam waves the yaw coupling is negligible because there are practically no yaw motions. The sway coupling, though of significant proportions, does not alter the basic second order spring mass system characteristics of the roll motion. The roll motion is usually lightly damped so that there is a pronounced resonance close to the natural roll frequency, given by

$$\omega_{*4} = \sqrt{\frac{c_{44}}{I_{44} + a_{44}}} \quad rad/sec \tag{7.5a}$$

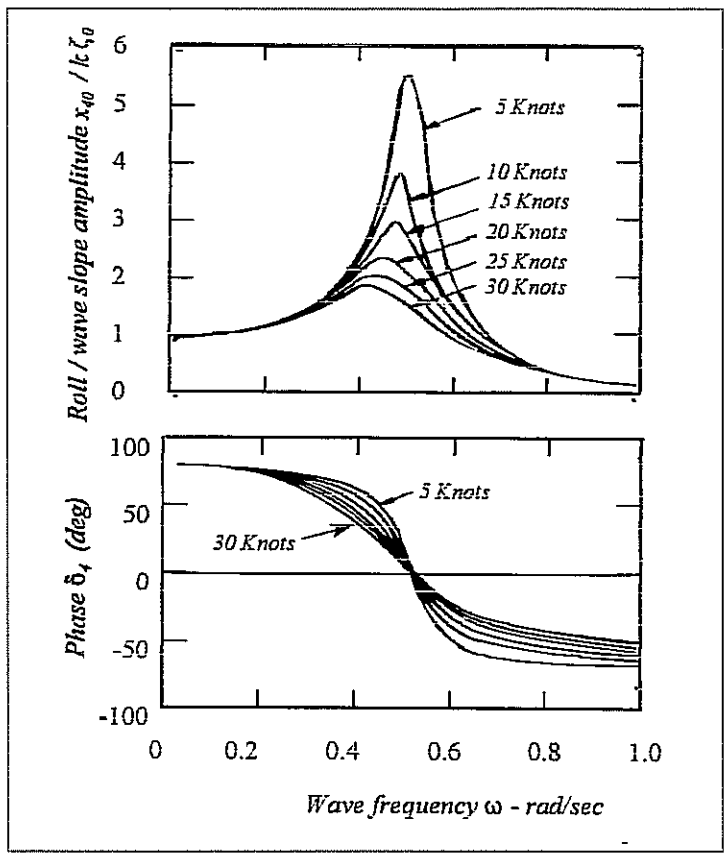

Fig 7.15 - Roll transfer functions for the frigate in beam waves: no free surface effects on metacentric height.

(See Equation (A1.6)). The natural roll frequency may then be determined using Equations (3.2a), (4.37c), and (4.37e). Alternatively an approximate estimate of the natural roll frequency may be obtained as follows.

The well known formula[3]

[3] See any text book on basic naval architecture

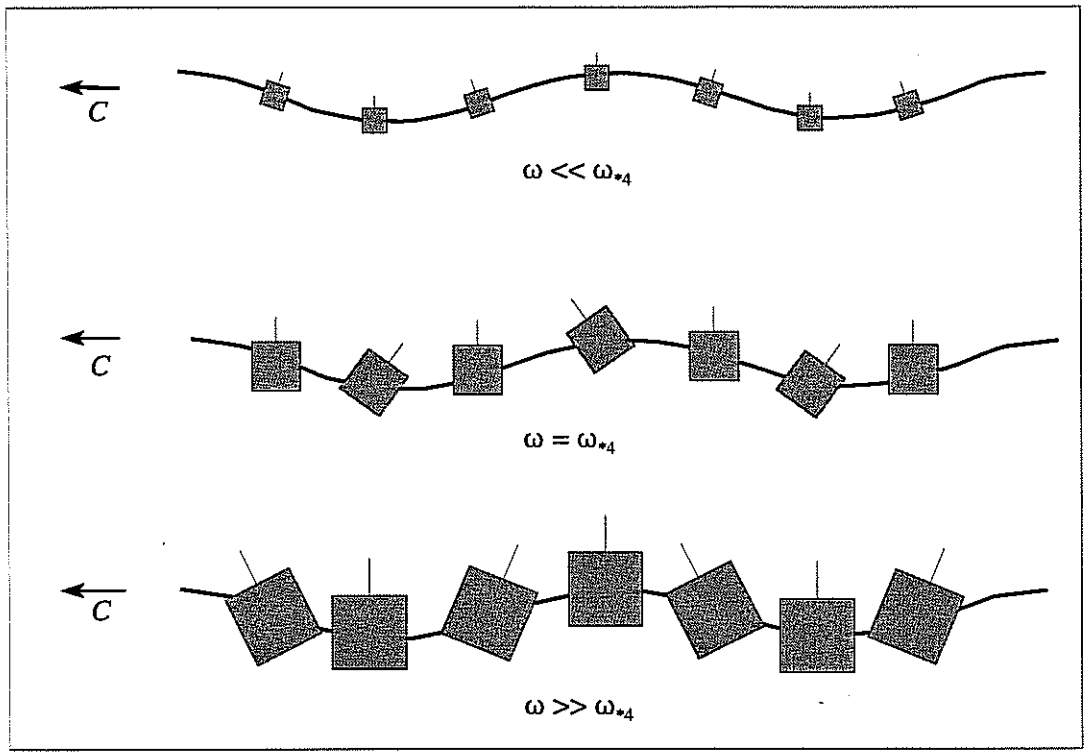

Fig 7.16 - Rolling motion in regular beam waves

$$\overline{BM} = \frac{I_T}{\Delta} \quad m$$

may be used to calculate the location of the metacentre M relative to the centre of buoyancy B. In this formula the transverse second moment of the waterplane area is

$$I_T = \frac{1}{12} \int B^{/3} \, dx_{Bl} \quad m^4$$

and Δ is the displaced volume in cubic metres. If the location of the centre of gravity has been determined the solid metacentric height $\overline{GM_S}$ may be calculated from

$$\overline{GM_S} = \overline{BM} - \overline{BG} \quad m$$

and the fluid metacentric height $\overline{GM_F}$, allowing for any free surface effects, may then be estimated. For preliminary design purposes we may also assume that the added roll inertia is given approximately by

$$a_{44} \approx 0.25 \, I_{44} \quad t \, m^2$$

and the natural roll frequency is then given approximately by

$$\omega_{*4} \approx \sqrt{\frac{m\ g\ \overline{GM_F}}{1.25\ I_{44}}} \quad rad/sec \qquad (7.5b)$$

The roll damping increases with forward speed. This gives a general reduction in the peak roll response and a slight reduction in the frequency at which the peak roll response occurs. At zero frequency the roll phase δ_4 is $+90^0$ indicating that positive roll (to starboard) leads the maximum wave depression by one quarter of a period as shown in Figures 7.13 and 7.16. At the natural roll frequency the roll phase is zero and the maximum roll is then synchronised with wave crests and troughs as shown in Figure 7.16. At very high frequencies δ_4 approaches -90^0 and the ship then rolls in opposition to the wave slope. Roll motions are then, however, quite small.

The responses shown in Figure 7.15 were calculated with no allowance for free surface effects on the metacentric height. If these effects are significant the reduction in the roll stiffness reduces the natural roll frequency and increases the roll response at low frequencies as shown in Figure 7.17.

7.8 LATERAL PLANE MOTIONS IN REGULAR OBLIQUE WAVES

Figure 7.18 shows roll transfer functions for the frigate in regular oblique waves. These are plotted in the alternative wave frequency form and the fluid and solid metacentric heights are assumed to be equal. In bow waves the forward speed of the ship increases the frequency of encounter and the roll resonance is excited at lower wave frequencies. In quartering waves the range of encounter frequencies is limited. At $\mu = 30°$ in the case shown the waves are never encountered at the roll natural frequency and the roll resonance is never excited. However, at $\mu = 60°$ a very wide range of wave lengths (and wave frequencies) is encountered at frequencies close to the natural roll frequency (see Figure 1.16) and the roll response is significantly increased. For this reason roll motion is often a maximum in quartering seas, particularly at high speed.

In very long waves ($\omega \approx 0$) the roll motion amplitude approaches the effective wave slope amplitude α_{10} given by Equation (7.4).

Figures 7.19 and 7.20 show the sway and yaw transfer functions in oblique waves. In very long waves ($\omega = 0$) the sway amplitude approaches the athwartships component of the wave orbit radius $\zeta_0\ sin\ \mu$. On headings forward of the beam both sway and yaw amplitudes decrease rapidly with increasing wave frequency. Maximum responses occur in quartering seas and rise to very high values when the encounter frequency approaches zero. Strip theory predictions are likely to be inaccurate in these circumstances. In practice the ship would be steered by a helmsman or an autopilot and this would effectively limit these large motion amplitudes.

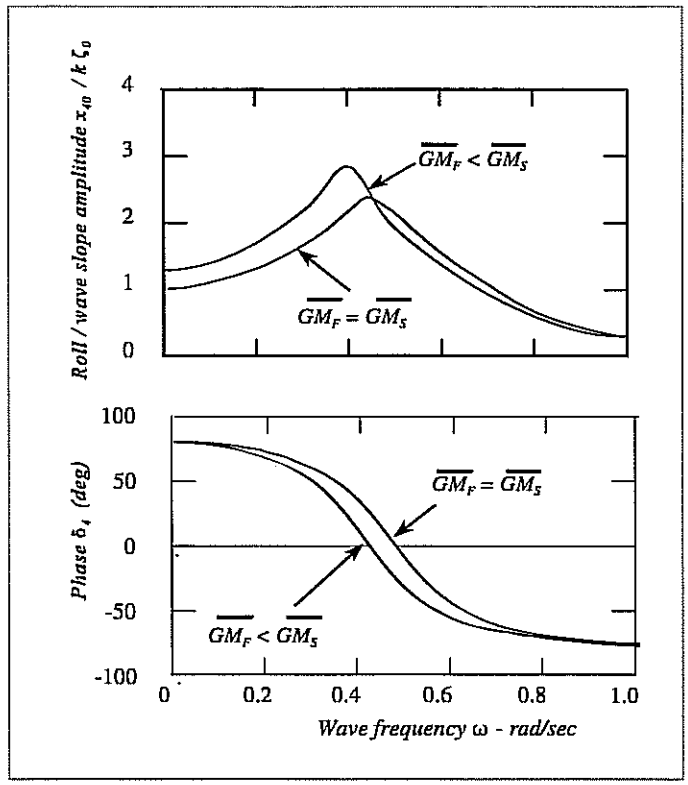

Fig 7.17 - Roll transfer functions for the frigate at 20 knots in regular beam waves: effect of fluid metacentric height.

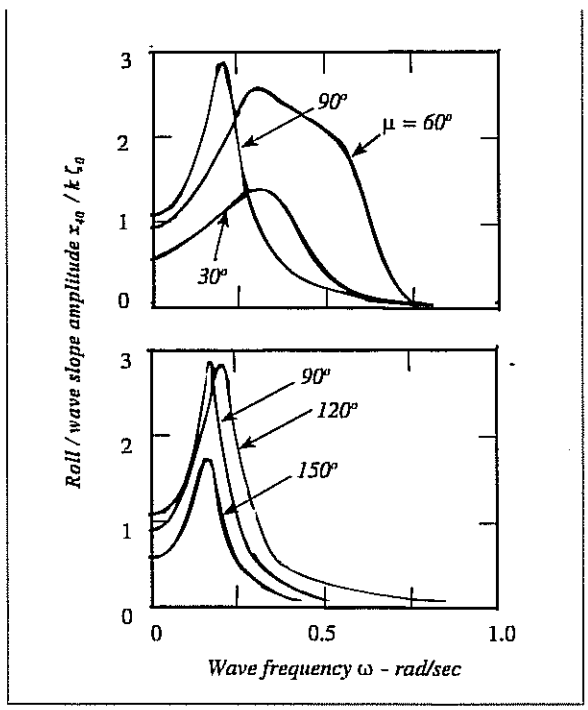

Fig 7.18 - Roll transfer functions for the frigate at 20 knots in regular oblique waves.

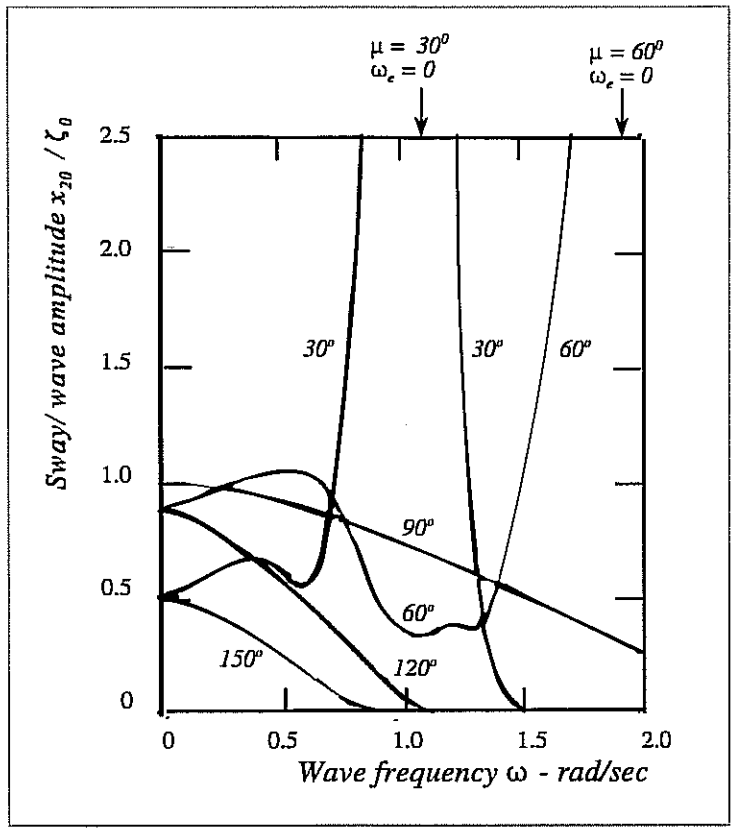

Fig 7.19 - Sway transfer functions for the frigate at 20 knots in regular oblique waves

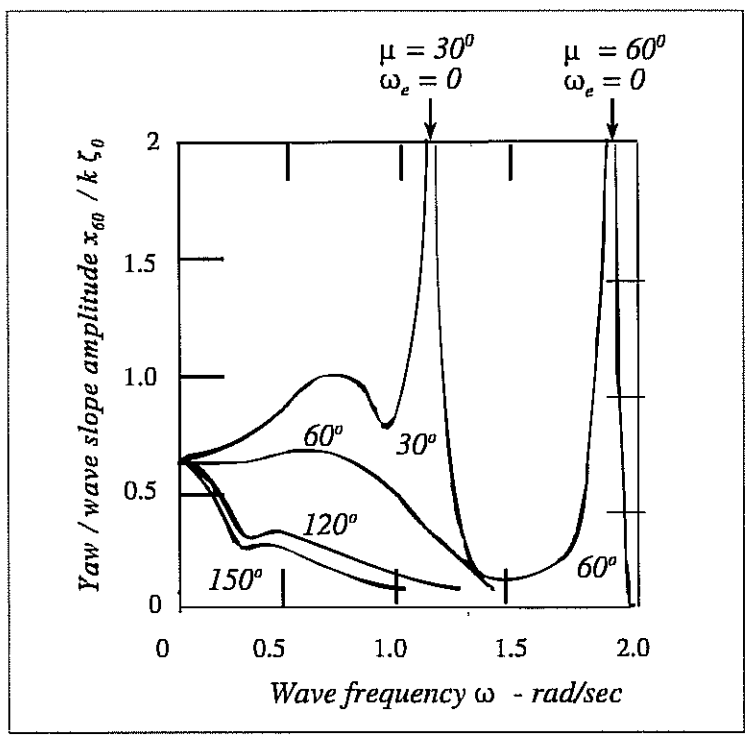

Fig 7.20 - Yaw transfer functions for the frigate at 20 knots in regular oblique waves.

7.9 ABSOLUTE MOTIONS

The six motions considered so far completely define the possible movements of a ship in a seaway. However, seakeeping studies often call for assessments of the motions experienced at some particular point on the ship, such as the bridge or the flight deck of a warship or the dining room in a passenger ferry. These can be calculated from a knowledge of the six motions we have already defined with respect to the centre of gravity.

The angular motions are the same everywhere in the ship but the local linear motions depend on the location within the ship. Let us consider a location defined by the coordinates (x_{B1} , x_{B2} , x_{B3}) with respect to the centre of gravity. The longitudinal displacement of this point includes contributions from the surge of the whole ship as well as the products of the lever arms and the pitch and yaw motions. If the angular motions are small the linear displacements relative to the moving origin O are

$$s_1 = x_1 - x_{B2}\, x_6 + x_{B3}\, x_5 \quad m \quad \text{(positive forward)} \tag{7.6}$$

$$s_2 = x_2 - x_{B3}\, x_4 + x_{B1}\, x_6 \quad m \quad \text{(positive to starboard)} \tag{7.7}$$

$$s_3 = x_3 + x_{B2}\, x_4 - x_{B1}\, x_5 \quad m \quad \text{(positive d} \tag{7.8}$$

Substituting Equations (7.2) we find that each motion is sinusoidal with

$$s_i = s_{i0}\, sin\, (\, \omega_e\, t + \delta_{si}\,) \quad m; \quad (i = 1, 3) \tag{7.9}$$

where the amplitudes are

$$s_{10} = \sqrt{P_7^2 + P_8^2} \quad m \tag{7.10a}$$

$$s_{20} = \sqrt{P_9^2 + P_{10}^2} \quad m \tag{7.10b}$$

$$s_{30} = \sqrt{P_{11}^2 + P_{12}^2} \quad m \tag{7.10c}$$

where

$$P_7 = x_{10}\, cos\, \delta_1 - x_{B2}\, x_{60}\, cos\, \delta_6 + x_{B3}\, x_{50}\, cos\, \delta_5 \quad m \tag{7.12a}$$

$$P_8 = x_{10}\, sin\, \delta_1 - x_{B2}\, x_{60}\, sin\, \delta_6 + x_{B3}\, x_{50}\, sin\, \delta_5 \quad m \tag{7.12b}$$

$$P_9 = x_{20}\, cos\, \delta_2 - x_{B3}\, x_{40}\, cos\, \delta_4 + x_{B1}\, x_{60}\, cos\, \delta_6 \quad m \tag{7.12c}$$

$$P_{10} = x_{20}\, sin\, \delta_2 - x_{B3}\, x_{40}\, sin\, \delta_4 + x_{B2}\, x_{60}\, sin\, \delta_6 \quad m \tag{7.12d}$$

$$P_{11} = x_{30} \cos \delta_3 + x_{B2}\, x_{40} \cos \delta_4 - x_{B1}\, x_{50} \cos \delta_5 \quad m \tag{7.12e}$$

$$P_{12} = x_{30} \sin \delta_3 + x_{B2}\, x_{40} \sin \delta_4 - x_{B1}\, x_{50} \sin \delta_5 \quad m \tag{7.12f}$$

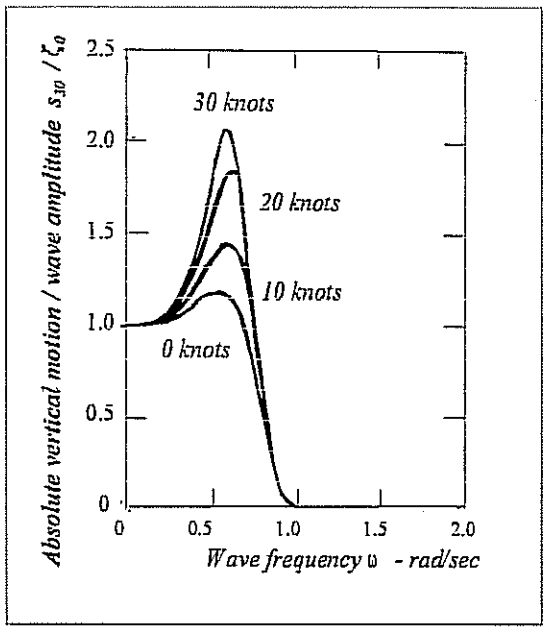

Fig 7.21 - Absolute vertical motion transfer functions at the bridge of the frigate in regular head waves

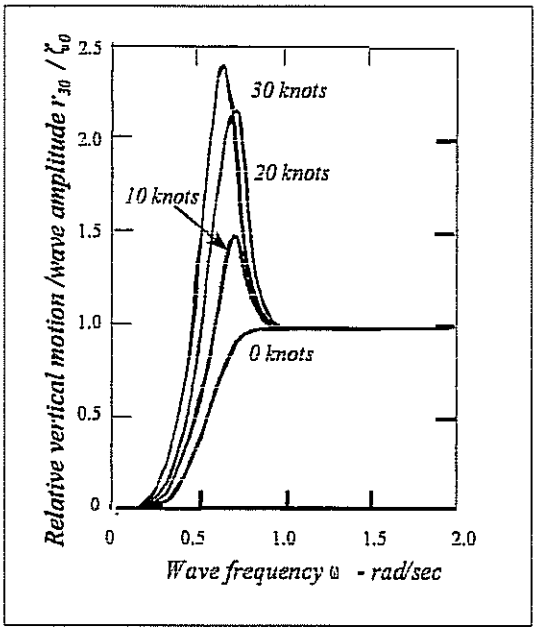

Fig 7.22 - Relative vertical motion transfer functions at the bow of the frigate in regular head waves

The form of the absolute motion transfer function depends on the position in the ship. Figure 7.21 shows some typical head wave absolute vertical motion transfer functions for a point on the bridge of the frigate. In very long waves ($\omega \approx 0$) the transfer functions approach unity as the ship contours the waves. At very high frequencies the motions become negligible; but at intermediate frequencies the motion phases are such that the contributions from pitch and heave are synchronised and large absolute motions, considerably greater than the wave amplitude, are the result.

7.10 RELATIVE MOTIONS

Slamming and deck wetness (see Chapter 14) are of considerable importance in assessing the seakeeping performance of a ship. They are largely determined by the magnitude of the relative motion between the hull and the adjacent sea surface.

The relative vertical motion at a point (x_{B1} , x_{B2} , x_{B3}) is given by

$$r_3 = s_3 - \zeta \quad m \quad \text{(positive for increasing immersion)} \tag{7.13}$$

where s_3 is the absolute vertical motion given by Equation (7.8) and ζ is the local wave depression given by Equation (4.17a). Substituting these equations we find that the relative

motion is

$$r_3 = r_{30} \sin(\omega_e t + \delta_{r3}) \quad m \tag{7.14}$$

where the relative motion amplitude is

$$r_{30} = \sqrt{s_{30}^2 - 2 s_{30} \zeta_0 \cos(\delta_{S3} + Q) + \zeta_0^2} \quad m \tag{7.15}$$

and the phase is given by

$$\tan \delta_{r3} = \frac{s_{30} \sin \delta_{S3} + \zeta_0 \sin Q}{s_{30} \cos \delta_{S3} - \zeta_0 \cos Q} \tag{7.16}$$

Q in these equations is given by Equation (4.17b).

In practice the presence of the hull causes a considerable distortion of the waves close to the ship and Equation (7.13) is only likely to be reliable at the forward perpendicular. Further aft the equation may underestimate the relative motion by as much as 50%. Techniques for estimating this distortion or `***swell up***' are still the subject of research and no method has yet won universal agreement. Nevertheless, Equation (7.13) is still used to estimate relative motion, sometimes with empirical corrections for the swell up as described in Chapter 14. Figure 7.22 shows some typical calculations (with no correction for swell up) for a point on the forefoot of the frigate in head waves.

In very long waves the relative motions are zero because the ship contours the waves. In short waves the ship is essentially stationary so that the wave motion is the only sizeable contribution to the relative motion and the transfer function approaches unity.

At some intermediate frequency the motion phases are such that the upward absolute motion is synchronised with the wave depression at the particular location chosen for the calculation. The relative motion is then a maximum and sharply peaked resonances can occur at high speed.

7.11 VELOCITIES AND ACCELERATIONS

Since all the motion displacements are of the form

$$x = x_0 \sin(\omega_e t + \delta) \quad m \text{ or } rad$$

the motion velocities and acceleration are given by

$$\dot{x} = x_0 \omega_e \cos(\omega_e t + \delta) \quad m/sec \text{ or } rad/sec$$

$$\ddot{x} = -x_0 \omega_e^2 \sin(\omega_e t + \delta) \quad m/sec^2 \text{ or } rad/sec^2$$

which may be written

$$\dot{x} = \dot{x}_0 \sin (\omega_e t + \delta + \pi/2) \quad m/sec \text{ or } rad/sec$$

$$\ddot{x} = \ddot{x}_0 \sin (\omega_e t + \delta + \pi) \quad m/sec^2 \text{ or } rad/sec^2$$

where the velocity and acceleration amplitudes are

$$\dot{x}_0 = x_0 \omega_e \quad m/sec \text{ or } rad/sec$$

$$\ddot{x}_0 = x_0 \omega_e^2 \quad m/sec^2 \text{ or } rad/sec^2$$

So the velocity and acceleration transfer functions for any motion can be obtained by multiplying the displacement amplitude responses by the encounter frequency and the square of the encounter frequency respectively.

8

SHIP MOTIONS IN IRREGULAR WAVES

8.1 THE ELECTRONIC FILTER ANALOGY

For many years the assessment of seakeeping performance at the design stage progressed no further than comparisons of ship motions in regular waves. The shortcomings of this approach were widely recognised but further progress had to await the development of new techniques first proposed by St Denis and Pierson (1953). These methods were based on ideas developed in the electronics and communications fields and it is no exaggeration to suggest that their introduction, together with the development of strip theory, form the two main foundations of the modern theory of seakeeping.

St Denis and Pierson suggested that the ship could be treated in much the same way as the "black box" electronic filter shown in Figure 8.1. The input signal received by the filter contains a number of different frequency components and these are amplified or attenuated to produce a modified output signal according to the characteristics of the filter.

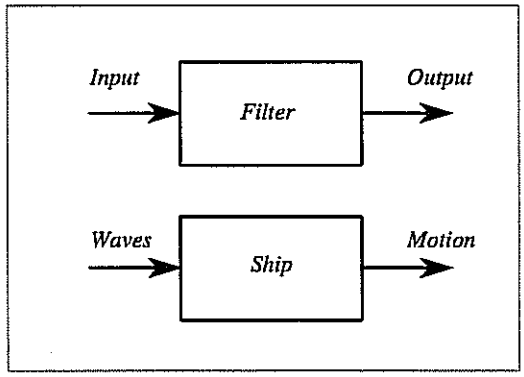

Fig 8.1 - The electronic filter analogy

The analogy suggests that the ship can also be regarded as a filter, not of electrical signals, but of the waves. In other words we can think of the ship as a "black box" which receives the waves as input and generates ship motions as output. Of course there are a number of different ship motion outputs so we should really regard the ship as a collection of filters, each with its own individual characteristics.

It is also assumed that the filter is 'linear' in the sense that the output signal amplitude (the ship motion) at any given frequency is linearly proportional to the input signal amplitude (the wave).

Let us consider the case of heave motion in head waves. Figure 7.5 shows typical heave transfer functions for various speeds at $\mu = 180°$ and we may regard these as defining the characteristics of the 'heave filter' of the black box ship. We can see that this is essentially a low pass filter; at low encounter frequencies the wave motions are translated into corresponding heave motions with little attenuation or phase shift. As the encounter frequency rises, the heave

motions are reduced and at very high frequencies the input is completely attenuated so that there are no resulting heave motions.

These ideas can be formalised and quantified by means of the so called "***spectral calculation***". This is mathematically valid and rigorous provided that the ship motion responses are linearly proportional to the wave amplitude at any given speed, heading and frequency. This is nearly always true, provided that the motions and waves are of small amplitude, and the spectral calculation is widely used in seakeeping calculations.

8.2 THE ENCOUNTERED WAVE SPECTRUM

The first step is to determine the wave energy spectrum as described in Chapter 2. For the time being we shall assume that the waves are long crested. The spectrum may be measured but it is more usual to employ one of the idealised wave energy spectrum formulae (Equations (2.32) or (2.44)). These formulae give the wave energy spectrum for a fixed point in the ocean: we require to transform this to the reference frame of an observer on the moving ship.

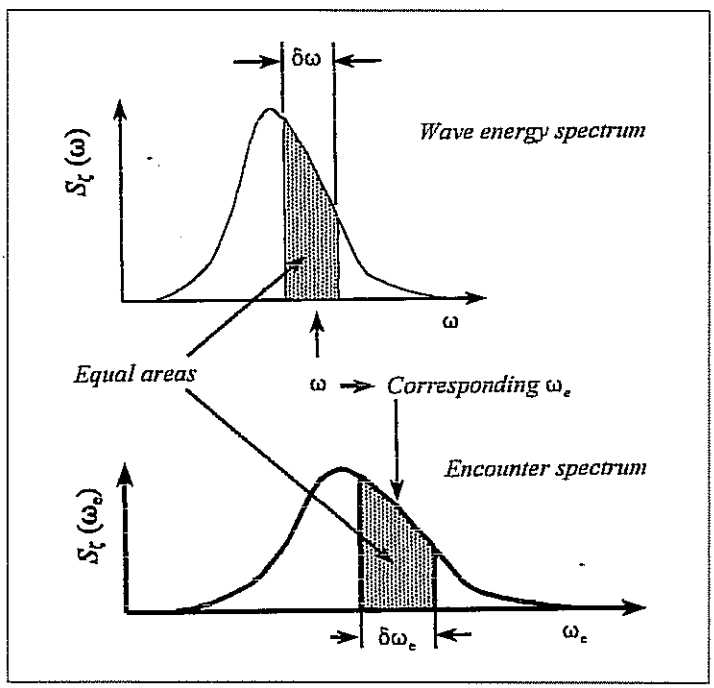

Fig 8.2 - Transforming the wave energy spectrum into the encounter spectrum.

We have already seen that waves are encountered by the ship at the encounter frequency defined in Equation (1.35). So the frequencies with which the waves are encountered are increased in head waves and decreased in following waves. It follows that the wave energy spectrum must be shifted along the frequency axis to cover a different range of frequencies when observed from a moving ship.

Figure 8.2 illustrates the result obtained in head waves: every wave frequency is transformed into a corresponding encounter frequency according to Equation (1.35). The frequency interval $\delta\omega$ centred on the wave frequency ω transforms into a corresponding encounter frequency interval $\delta\omega_e$. The relationship between the two intervals is obtained by differentiating Equation (1.35):

$$\delta\omega_e = \left(1 - \frac{2\omega\ U}{g} \cos\ \mu \right) \delta\omega \quad rad/sec \tag{8.1}$$

Now we have seen in Chapter 2 that the area under the wave energy spectrum within the small frequency interval $\delta\omega$ is proportional to the energy contained within that band of frequencies. Transforming the spectrum to the moving frame of reference of the ship does not change this energy and it follows that the area within the wave frequency range $\delta\omega$ must be exactly reproduced as an equal area within the corresponding encounter frequency range $\delta\omega_e$. Hence the ordinates of the wave spectrum perceived by a stationary observer and its counterpart in the encounter frequency domain must be related by

$$S_\zeta\ (\ \omega\ )\ \delta\omega\ =\ S_\zeta\ (\omega_e\ )\ \delta\omega_e \quad m^2 \tag{8.2}$$

or, if $\delta\omega$ and $\delta\omega_e$ are allowed to become infinitesimal

$$\begin{aligned} S_\zeta\ (\ \omega_e\ ) &= S_\zeta\ (\ \omega\ )\ \frac{d\omega}{d\omega_e} \\ &= S_\zeta\ (\ \omega\ )\ \frac{g}{g\ -\ 2\omega\ U\ \cos\ \mu} \quad m^2/(rad/sec) \end{aligned} \tag{8.3}$$

In head waves the effect is to increase the frequencies, widen their range and reduce the spectral ordinate heights as shown in Figure 8.2. The areas under the two spectra are of course, identical since the total wave energy and the significant wave height are unchanged by the transformation.

8.3 THE MOTION ENERGY SPECTRUM

8.3.1 Linear motion spectra

The spectrum for a linear (as opposed to angular) motion is calculated by filtering the encountered wave energy spectrum with the appropriate motion transfer function. This is achieved by multiplying each ordinate of the encountered wave spectrum by the ***square*** of the motion transfer function at the corresponding encounter frequency. This approach is valid and appropriate for any ship motion when the transfer function is normalised by dividing by the wave amplitude[1].

[1] It is usual to normalise the transfer functions for the linear motions like surge, sway, heave, absolute motion and relative motion by dividing by the wave amplitude.

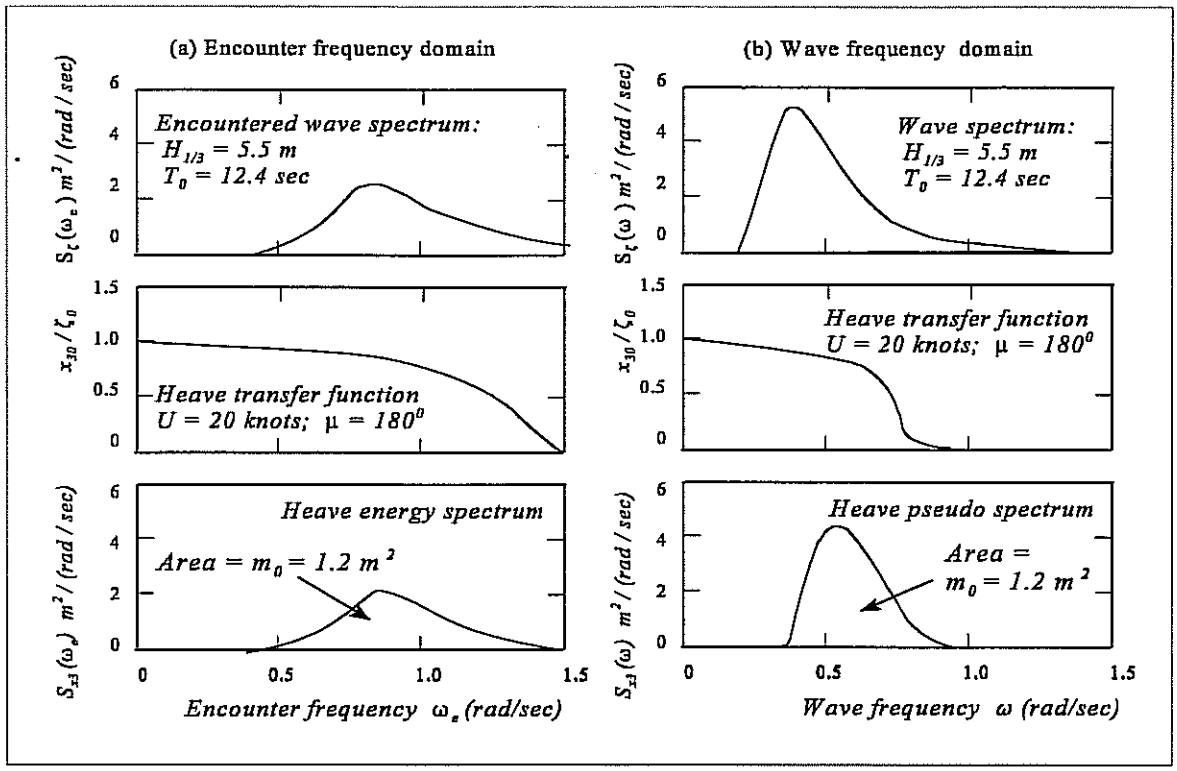

Fig 8.3 - Calculation of (a) heave energy spectrum in the encounter frequency domain and (b) heave pseudo spectrum in the wave frequency domain. The areas under the two spectra are the same.

The calculation for heave is illustrated in Figure 8.3(a). The motion energy spectrum ordinate at each encounter frequency ω_e is given by

$$S_{x3}(\omega_e) = S_\zeta(\omega_e) \left(\frac{x_{30}}{\zeta_0} \right)^2 \quad m^2/(rad/sec) \tag{8.4}$$

The variance of the heave motion is obtained by integrating the heave motion energy spectrum:

$$m_0 = \int_{-\infty}^{\infty} S_{x3}(\omega_e)\, d\omega_e \quad m^2 \tag{8.5}$$

and the rms heave motion is

$$\sigma_0 = \sqrt{m_0} \quad m$$

The heave energy spectrum obtained in the encounter frequency domain in this way can be transformed into a heave motion spectrum in the wave frequency domain by using the inverse of the transformation procedure defined in Equation (8.3):[2]

$$S_{z3}(\omega) = S_{z3}(\omega_e)\frac{d\omega_e}{d\omega}$$

$$= S_{z3}(\omega_e)\frac{g - 2\omega U\cos\mu}{g} \quad m^2/(rad/sec)$$

The resulting spectrum has no physical significance and we shall call it the ***pseudo spectrum.*** Nevertheless the variance and rms value of the motion may be still obtained by integrating the pseudo spectrum because the area under the pseudo spectrum in the wave frequency domain is the same as the area under the true spectrum in the encounter frequency domain. Now the same variance and rms heave motion could have been obtained by conducting the entire calculation in the wave frequency domain as shown in Figure 8.3(b). Here the heave motion pseudo spectral ordinate is given by

$$S_{z3}(\omega) = S_{\zeta}(\omega)\left(\frac{x_{30}}{\zeta_0}\right)^2 \quad m^2/(rad/sec) \qquad (8.6)$$

and the heave motion variance and rms heave are given by

$$m_0 = \int_0^{\infty} S_{z3}(\omega)\, d\omega \quad m^2 \qquad (8.7)$$

$$\sigma_0 = \sqrt{m_0} \quad m$$

The wave frequency domain procedure is generally preferred because no transformations are required and it avoids the complications of negative encounter frequencies and multiple responses in quartering and following waves. ***However it must be emphasised that the pseudo spectrum is not an indication of the motion spectrum experienced by the occupants of the ship*** . This can only be obtained by tranforming the psuedo spectral ordinates for the motion into the encounter frequency domain or by working entirely in the encounter frequency domain.

8.3.2 Angular motion spectra

Angular ship motion transfer functions[3] are usually normalised by dividing by the wave slope amplitude and this calls for a slightly different procedure, illustrated for pitch motion in Figure

---

[2] Noting that the transformation is valid for ship motions as well as for waves

[3]Roll, pitch, yaw, autopilot controlled rudder motions, active fin stabiliser motions etc.

8.4. The wave frequency domain is again preferred for the calculation and it is first necessary to calculate the wave slope spectrum S_α (ω) (see Equation (2.46)) . The rest of the calculation follows the procedure described for linear motions above. The pitch energy pseudo spectrum is given by

$$S_{x5} (\omega) = S_\alpha (\omega) \left(\frac{x_{50}}{k \zeta_0} \right)^2 \quad rad^2/(rad/sec) \tag{8.8}$$

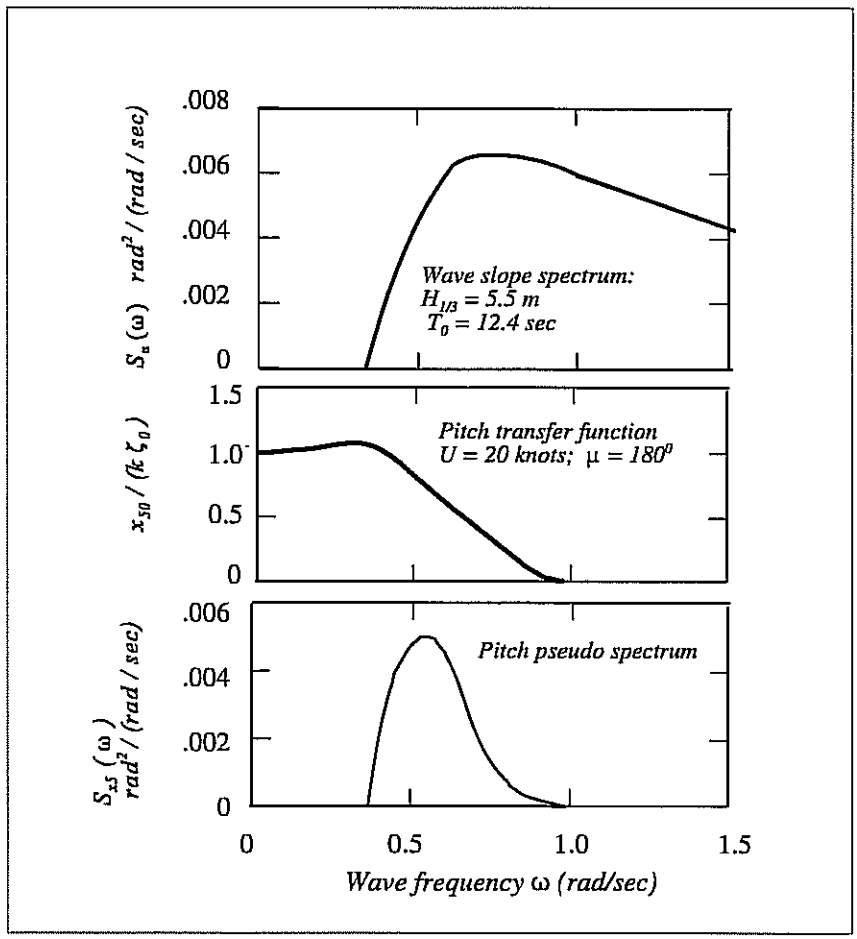

Fig 8.4 - Calculation of pitch pseudo spectrum for the frigate at 20 knots in irregular head waves.

The variance and rms motion are given by

$$m_0 = \int_0^\infty S_{x5} (\omega) \, d\omega \quad rad^2 \tag{8.9}$$

$$\sigma_0 = \sqrt{m_0} \quad rad$$

8.4 RMS VELOCITIES AND ACCELERATIONS

The rms velocity and acceleration and the motion periods may also be calculated in the wave frequency domain. Using Equations (1.35) and (2.24) the spectral moments for heave are

$$m_n = \int_0^\infty \omega_e^n \, S_{x3} (\omega_e) \, d\omega_e$$

$$= \int_0^\infty \left(\omega - \frac{\omega^2 \, U}{g} \cos \mu \right)^n S_{x3} (\omega) \, d\omega \quad m^2/sec^n \qquad (8.10)$$

$$(n = 0, 2, 4)$$

and for pitch

$$m_n = \int_0^\infty \omega_e^n \, S_{x5} (\omega_e) \, d\omega_e$$

$$= \int_0^\infty \left(\omega - \frac{\omega^2 \, U}{g} \cos \mu \right)^n S_{x5} (\omega) \, d\omega \quad rad^2/sec^n \qquad (8.11)$$

$$(n = 0, 2, 4)$$

and the rms velocity and acceleration are given by

$$\sigma_2 = \sqrt{m_2} \quad m/sec \text{ or } rad/sec \qquad (8.12)$$

$$\sigma_4 = \sqrt{m_4} \quad m/sec^2 \text{ or } rad/sec^2 \qquad (8.13)$$

Analogous equations apply for other linear and angular motions. Equations (2.26) - (2.28) may then be used to calculate the various mean periods of the motions.

8.5 EFFECT OF MATCHING THE WAVE SPECTRUM AND THE TRANSFER FUNCTION

High transfer function ordinates occurring at frequencies with a good deal of wave energy will give large contributions to the motion energy spectrum. It follows that the rms motion depends on the extent to which the motion transfer function "matches" the wave spectrum. Figure 8.5 shows as an example the effect of varying the modal period of the wave energy spectrum on the rms relative motion for the forefoot of the frigate in irregular head waves.

Figure 8.6 shows these and other motions plotted as a function of modal period. The motions which are most sensitive to modal period are those, like relative motion and roll, which have distinct transfer function peaks.

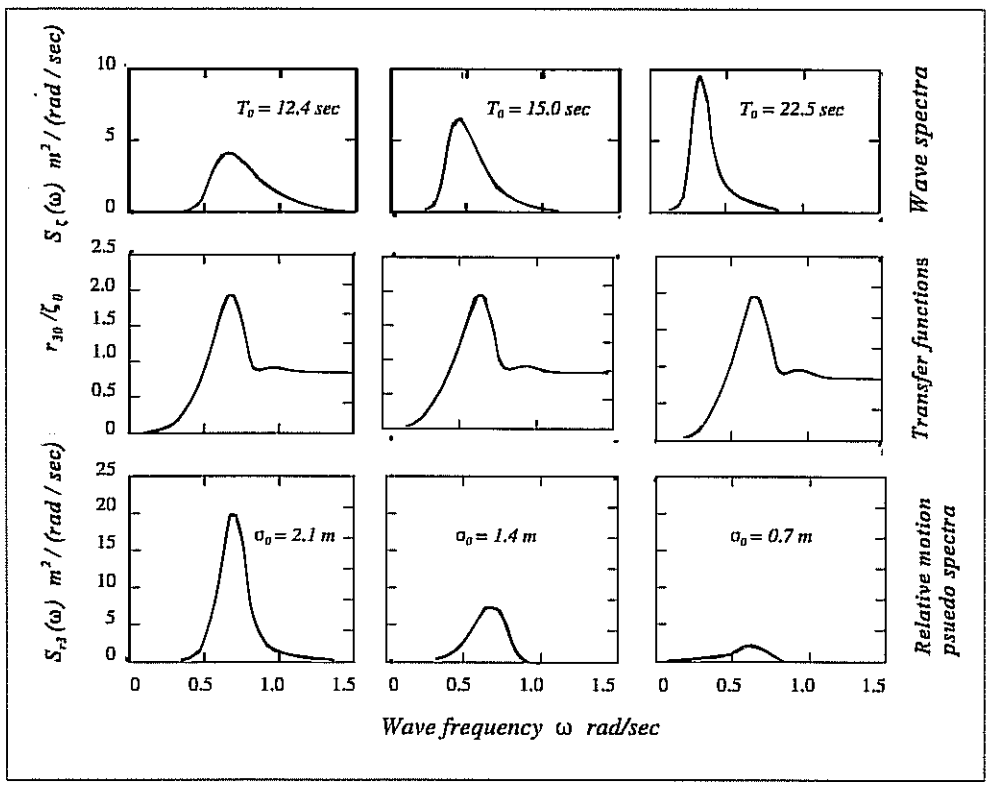

Fig 8.5 - Effect of matching the wave energy spectrum with the transfer function. Relative motions at the bow of the frigate at 20 knots in irregular head waves: Significant wave height 5.5 metres.

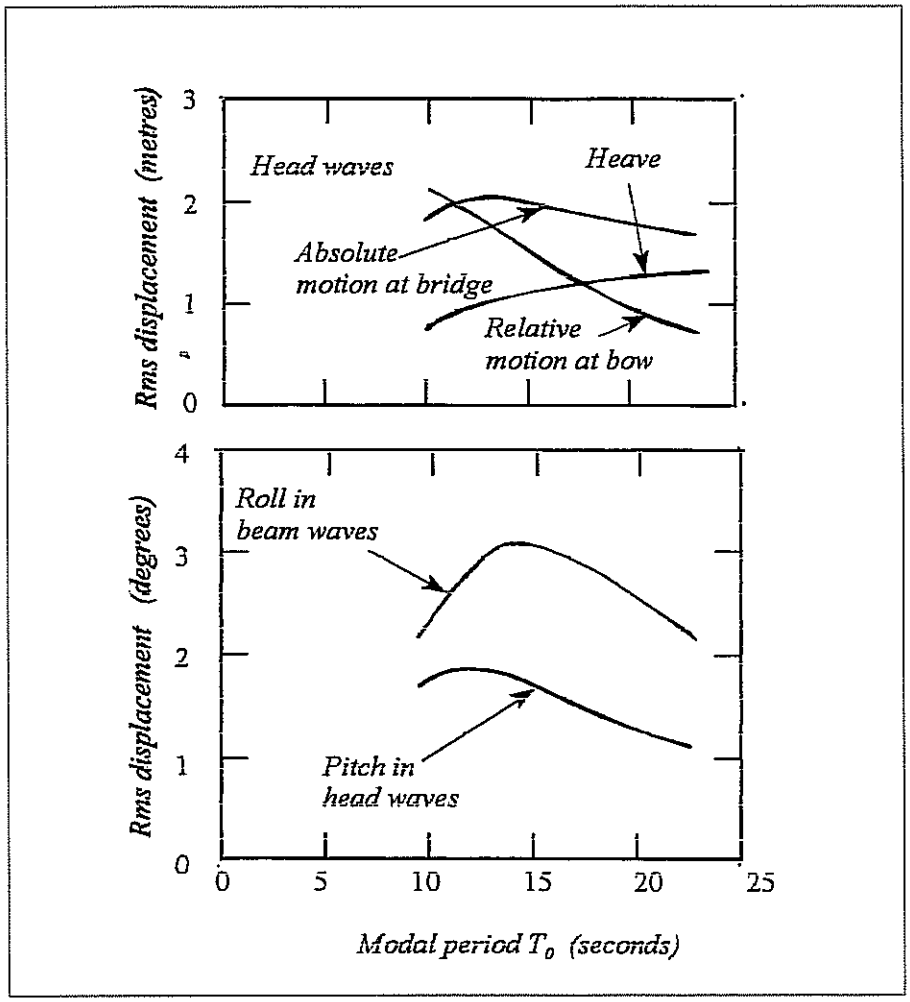

Fig 8.6 - Effect of modal period on the motions of the frigate at 20 knots. Significant wave height 5.5 metres

8.6 MOTIONS IN SHORT CRESTED WAVES

The procedures outlined above may be used to calculate motions in irregular long crested waves. These are rare, as we have seen, and it is often necessary to extend these techniques to cope with more realistic short crested waves. Now it was shown in Chapter 2 that the continuous short crested wave spectrum S_ζ (ω, ν) could be represented by a finite number of attenuated long crested spectra distributed around the predominant wave direction (see Figure 2.13). Each long crested spectrum is given by

$$S_\zeta (\omega , \nu) = W S_\zeta (\omega)$$

where W is a weighting factor depending on the secondary wave direction $\nu - \mu$ given in Table 2.1.

TABLE 8.1
SPECIMEN CALCULATION OF ROLL MOTION IN SHORT CRESTED WAVES

Cosine squared spreading over $\pm 90^0$.
Heading relative to predominant wave direction: $\mu = 45°$.
Significant wave height 5.5 metres. Modal wave period 12.4 seconds.
Bretschneider wave spectrum. Ship speed 20 knots.

Secondary wave direction relative to primary wave direction	Heading relative to secondary wave direction	Roll motion variance in long crested spectrum	Weighting factor (see Table 2.1)	Contribution to short crested variance
$\nu - \mu$	ν	m_0	W	δm_0
deg	deg	deg^2		deg^2
- 90	- 45	36.24*	0.000	0.00
- 75	- 30	12.11	0.011	0.13
- 60	- 15	2.92	0.042	0.12
- 45	0	0.00	0.083	0.00
- 30	15	2.92	0.125	0.37
- 15	30	12.11	0.156	1.89
0	45	36.24*	0.167	6.05
15	60	73.27	0.156	11.43
30	75	18.23	0.125	2.28
45	90	8.64	0.083	0.72
60	105	4.34	0.042	0.20
75	120	2.72	0.011	0.03
90	135	1.42	0.000	0.00

Total variance = $\sum \delta m_0 = 23.22\ deg^2$

Rms roll in short crested waves = $\sqrt{23.22} = 4.82\ deg$

* Rms roll in long crested waves = $\sqrt{36.24} = 6.03\ deg$

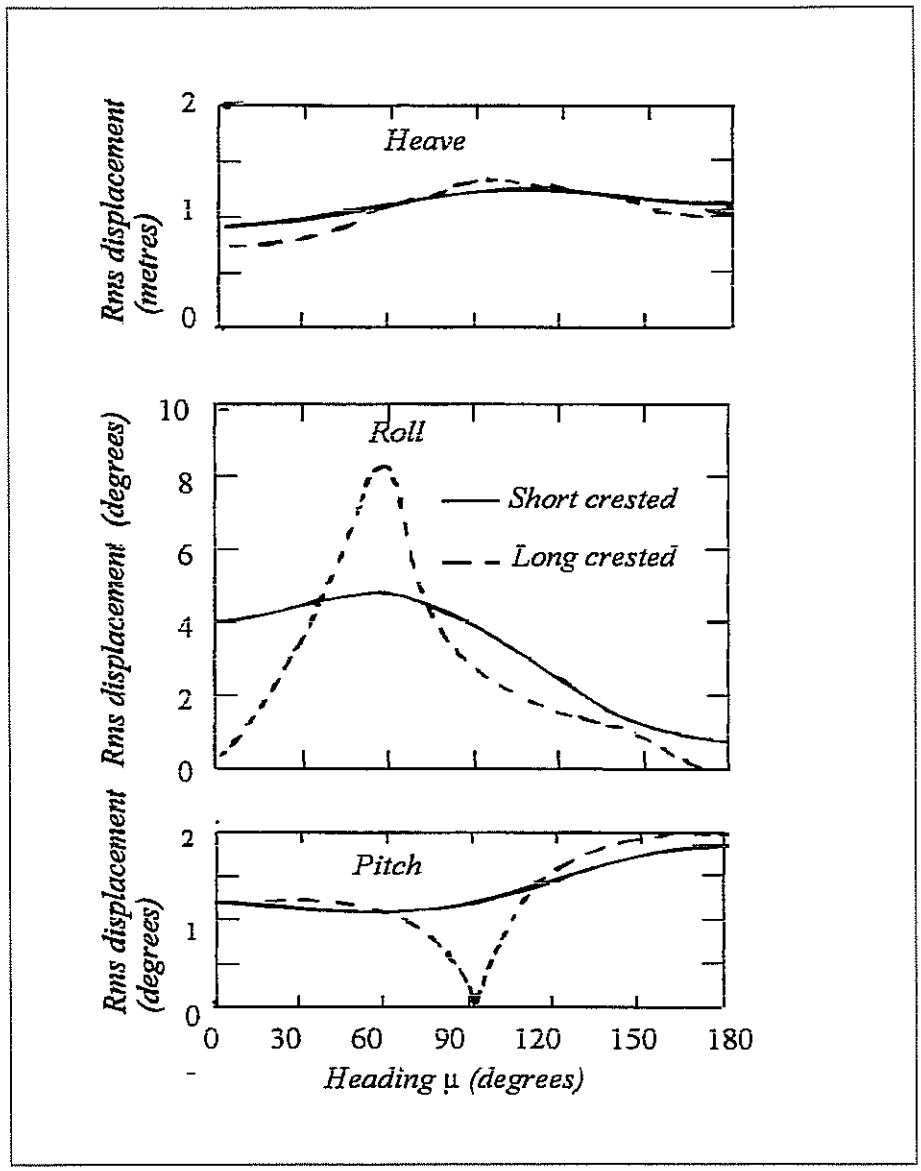

Fig 8.7 - Effect of wave spreading on the motions of the frigate at 20 knots in irregular waves.. Significant wave height 5.5 metres; modal period 12.4 seconds.

It follows that the contribution to the motion variance from each secondary wave direction is

$$\delta m_0 = W\, m_0 \quad m^2 \text{ or } deg^2$$

and the rms motion in short crested waves is

$$\sigma_{0S} = \sqrt{m_{0S}} \quad m \text{ or } deg$$

The total motion variance in short crested waves is obtained by summing the contributions from all the reduced long crested wave spectra:

$$m_{0S} = \sum_{\nu = -\pi/2}^{\nu = +\pi/2} \delta m_0 \quad m^2 \text{ or } deg^2$$

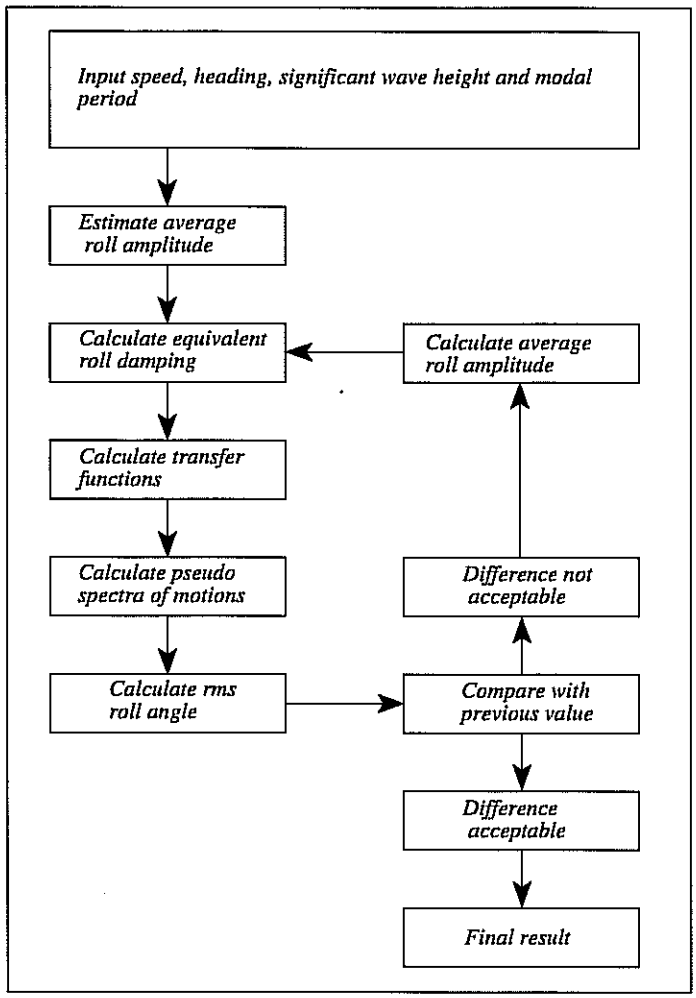

Fig 8.8 - Iterative calculation of non linear motions in irregular waves

Table 8.1 gives the results of a specimen calculation of the rolling motion of the frigate at 20 knots in quartering waves ($\mu = 45°$). In long crested waves the rms roll at this heading is 6.03° for the particular wave spectrum used in the calculation. Cosine squared wave spreading reduces this to only 4.82°.

Figure 8.7 shows the effect of wave spreading on heave and pitch as well as on roll. In general, wave spreading smooths out the more extreme variations of the motion. The effects are small for heave but quite dramatic for roll. Wave spreading results in significant roll motions in following waves and, to a lesser extent, in head waves. It also reduces the roll motions at the worst heading by a considerable amount. In the same way spreading increases the pitch motions in beam waves, but the effects at other headings are less pronounced.

8.7 SPECTRAL CALCULATIONS FOR NON LINEAR MOTION RESPONSES

The procedures outlined above rely on the assumptions that the motion responses are linearly proportional to the wave amplitude. We have seen that this is usually the case, but roll motions may be an exception to this general rule. In this case a slightly more involved procedure, illustrated in Figure 8.8, is required.

It is first necessary to estimate or guess the rms roll expected in the particular combination of speed, heading, significant wave height and modal period for which the calculation is being performed. The average roll amplitude may then be estimated using Equation (11.23). This done, the total equivalent linearised roll damping coefficient may be calculated for the chosen roll amplitude using the methods outlined in Chapter 6. The average frequency may be taken as the natural roll frequency of the ship. The calculation then proceeds through the usual stages of determining the motion transfer functions and combining these with the appropriate wave spectra to obtain rms values. Wave spreading should be taken into account.

The rms roll results are compared with the initial guess: if the differences are large (as will usually be the case) the calculation is repeated using the new rms value and an improved estimate of the roll damping. This procedure is repeated until the rms roll angle reaches an asymptotic value and the calculation is terminated. The whole calculation must then be repeated for every speed, heading, significant wave height and modal period specified.

9

SEAKEEPING TRIALS

"Believe me my young friends there is nothing - absolutely nothing - half so much worth doing as simply messing about in boats"[1]

From "Wind in the Willows" by Kenneth Graham 1908.

9.1 FULL SCALE TRIALS

Full scale seakeeping trials, in which the motions, deck wetness and other seakeeping phenomena of interest are monitored in a measured wave environment, seem to be an attractive method of assessing and comparing the performance of ships in rough weather. The waves are, of course, irregular and it is necessary to record them and the motions simultaneously and to analyse the results using the spectral analysis techniques discussed in Chapter 2. The rms motions (or other seakeeping responses such as deck wetness frequency) can then be plotted as a function of significant wave height and compared with those obtained from trials in other ships.

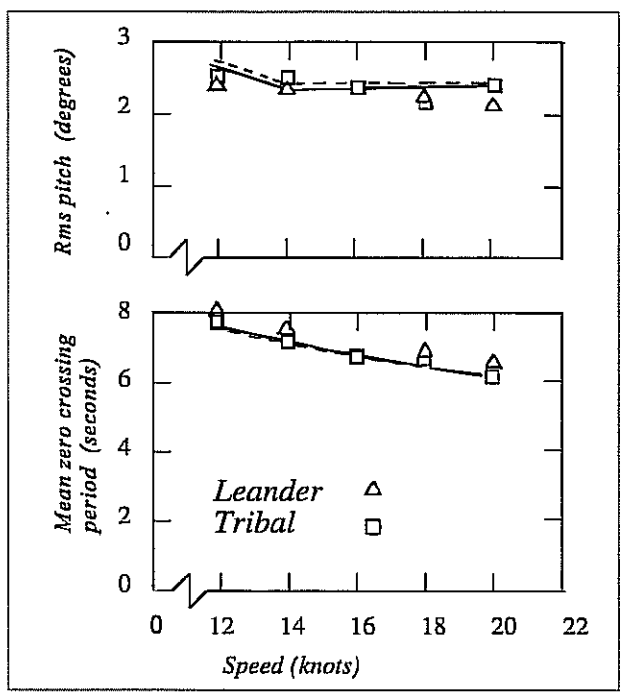

Fig 9.1 - Comparative seakeeping trial results: pitch motions in head waves (After Andrew and Lloyd (1981))

[1] There is no substitute for practical experience. Probably the most useful and rewarding times in the author's career were spent engaged in seakeeping trials with the Royal Navy.

However, we have seen that the rough weather behaviour of a ship is a function not only of the significant wave height, but also of the modal wave period, the shape of the wave spectrum and the degree of wave spreading. So results obtained and compared in this simple way are likely to be scattered and possibly misleading if the wave conditions at the time of the trials were in any way dissimilar. In short, seakeeping trials are difficult to conduct satisfactorily because the wave environment cannot be controlled in the experiment.

The only way that these problems can be overcome is by running two or more ships side by side in simultaneous trials in nominally identical wave conditions. Trials of this nature have been reported by Bledsoe, Bussemaker and Cummins (1960) and by Andrew and Lloyd (1981). Figure 9.1 shows the rms pitch motions and the mean zero crossing periods measured on two frigates in the latter trials in severe head waves (significant wave height 6-7 metres). These results form an objective comparison between the motions experienced by two particular ships in a particular rough weather environment: any peculiarities or changes in the wave conditions during the time of the trial must have been experienced in equal measure by both ships (since they were only about 400 metres apart) so any differences in the motions may be attributed to differences in the design of the two ships.

Trials with a single ship are infrequent because of the expense involved and comparative trials involving two ships are even more of a rarity. Such trials certainly cannot be regarded as a routine way of ascertaining the performance of a new design. In any case, seakeeping trials, by their very nature, cannot be used as part of the design process since they require the design to be finalised and the ship to be built before they can be conducted. Model experiments and theoretical studies provide the only practical method of estimating the seakeeping qualities of a new ship at the design stage.

Trials do, however, offer the definitive method of verifying theoretical calculations or predictions based on model experiments. If the wave spectrum is measured it may be used with estimated motion transfer functions to predict the rms motions and periods experienced during the trial as shown in Figure 9.1.

Alternatively the motion transfer functions may be estimated from the ratio of the measured motion energy spectrum to the measured wave energy spectrum. Equation (8.4) may be rearranged to give

$$\frac{x_{30}}{\zeta_0} = \sqrt{\frac{S_{x3}(\omega_e)}{S_\zeta(\omega_e)}} \qquad (9.1)$$

with similar expressions for other linear motion transfer functions. In the same way Equation (8.8) may be rearranged to give

$$\frac{x_{50}}{k\,\zeta_0} = \sqrt{\frac{S_{x5}(\omega_e)}{S_\alpha(\omega_e)}} \qquad (9.2)$$

with similar expressions for other angular motion transfer functions.

9.2 WAVE MEASUREMENTS.

The heart of any seakeeping trial is the measurement of the waves. Without a proper technique for recording and analysing the waves experienced by the ship the results obtained can only be related to potentially unreliable visual estimates of the sea state at the time of the trial. For this reason the use of relatively simple wave buoys such as the Waverider [2] (Figure 9.2) has become *de rigeur* in all serious seakeeping trials.

The Waverider consists of a stainless steel sphere of 700 mm diameter weighing 106 kg. An accelerometer to monitor vertical accelerations is mounted on a heavily damped pendulum within the sphere. The pendulum keeps the accelerometer aligned with the true vertical

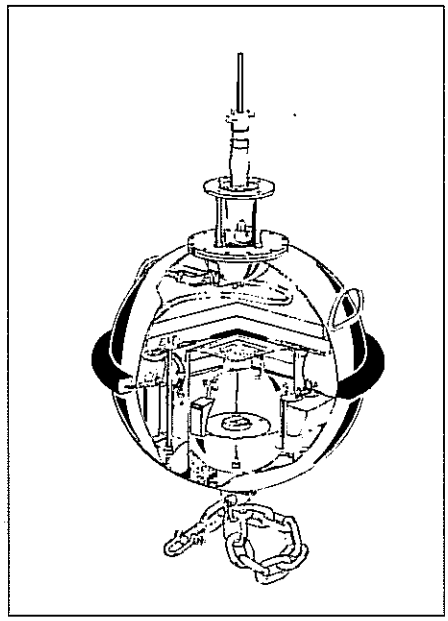

Fig 9.2 - Waverider buoy. (Reproduced by permission of Datawell bv.)

and the accelerometer's output is integrated twice by electronic circuits to provide an analogue record of the vertical displacement of the buoy. The resulting signal is transmitted to a receiver ashore or on board the trials ship. The buoy may be moored to the sea bottom or allowed to float freely. The system will give satisfactory measurements of waves covering a frequency range from 0.22 to 4.1 radians/second, corresponding to a wave length range from about 4 metres to 1300 metres. This is sufficient for most practical purposes except where measurements of very short waves are required (where, for example, trials are being conducted on a small boat).

---

[2] Registered trade mark. Manufactured by Datawell bv, Zomerlustraat 4, 2012 LM Haarlem, The Netherlands

Simple buoys of this kind can give no information about the directional spreading of the waves (or even the predominant wave direction). More sophisticated buoys which can give information on wave spreading are now becoming available and techniques of hindcasting the waves from measured wind data have also been used. These have not, however, yet become routine and most trials still use simple measurements of point wave spectra, relying on visual observations to determine the predominant wave direction.

9.3 SHIP MOTION MEASUREMENTS

Most seakeeping trials are concerned with the measurement of the ship's displacements in the six degrees of freedom. Angular motions are generally measured using gyros of the type used in aircraft navigation systems. In warships it is often possible to use the ship's own weapon system gyros but on other ships the trials team will usually have to supply its own transducers.

Direct measurements of the linear motion displacements are impossible because no suitable fixed datum levels are available. Instead, the usual practice is to measure the surge, sway and heave accelerations using accelerometers mounted on a small platform stabilised by gyros to remain in a horizontal plane (the gyros may also be used to measure the roll and pitch). Stabilisation is necessary because a "strapdown" accelerometer fixed to the ship's deck would measure the lateral force estimator or apparent acceleration in the plane of the deck (see Equation (15.12)) rather than the true horizontal acceleration. In the same way the apparent surge acceleration in the plane of the deck would be affected by pitch. Measurements of heave acceleration are reasonably immune from these effects providing the pitch and roll angles are not too large.

The stabilised accelerometers should ideally be located at the centre of gravity of the ship so that true measurements of the surge, sway and heave accelerations are obtained. In practice this is often impossible to achieve. Even if the location of the centre of gravity is known when the transducers are installed it may well turn out to be in some inaccessible or inconvenient location. It is, in any case, unlikely that the exact location of the centre of gravity will be known at the planning stage because it depends on the loading state of the ship and precise determination of its position will only be possible at the time of the trial.

So in practice it is likely that the transducers will be located at some arbitrary position relative to the centre of gravity and it will be necessary to correct their measurements to allow for this error. If the transducers are located at (x_{B1}, x_{B2}, x_{B3}) they will measure local absolute accelerations $\ddot{s}_1$, $\ddot{s}_2$ and $\ddot{s}_3$ given by differentiating Equations (7.6) - (7.8). The true accelerations of the centre of gravity are then given by

$$\ddot{x}_1 = \ddot{s}_1 + x_{B2}\,\ddot{x}_6 - x_{B3}\,\ddot{x}_5 \quad m/sec^2 \tag{9.3}$$

$$\ddot{x}_2 = \ddot{s}_2 + x_{B3}\,\ddot{x}_4 - x_{B1}\,\ddot{x}_6 \quad m/sec^2 \tag{9.4}$$

$$\ddot{x}_3 = \ddot{s}_3 - x_{B2}\,\ddot{x}_4 + x_{B1}\,\ddot{x}_5 \quad m/sec^2 \tag{9.5}$$

9.4 MEASUREMENTS OF OTHER SEAKEEPING RESPONSES

Seakeeping trials are often concerned with the measurement of responses other than motions in waves. Typical examples are deck wetness and slamming. Very simple instrumentation will often suffice for measurements of the frequency of occurrence of these events. Indeed a seasoned observer with a watch, a pencil and a log book is really all that is required. More permanent records of deck wetness, which can be analysed at leisure in the less distracting environment of the shore based laboratory, can be obtained by a video recording of the forecastle. This technique was used successfully in the comparative seakeeping trials reported by Andrew and LLoyd (1981) and their average deck wetness interval results are shown in Figure 9.3.

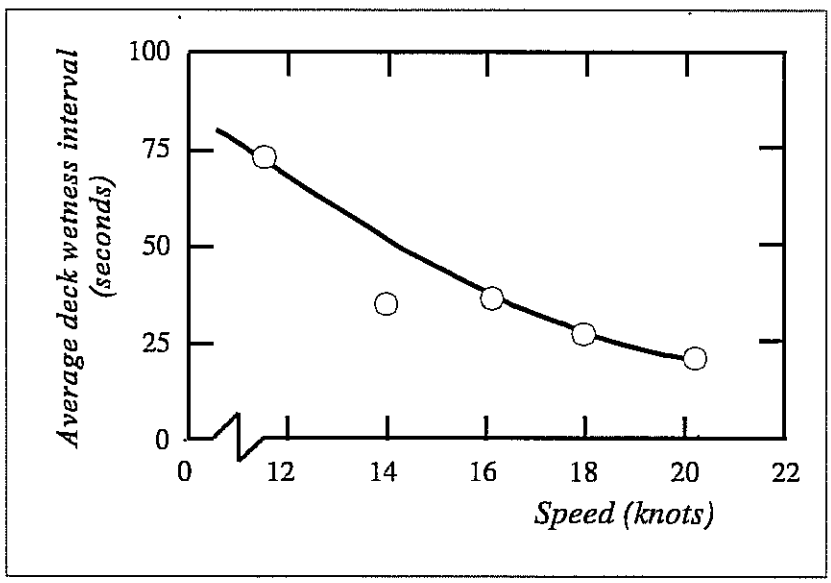

Fig 9.3 - Deck wetness measurements on a frigate in head waves. (After Andrew and Lloyd (1981))

Measurements of deck wetness severity can be obtained by mounting pressure transducers at suitable locations on the ship's upper works.

Slamming frequency measurements may be obtained by using strain gauges to monitor the bending moment experienced by the main hull girder. Slams will then be readily detected as short periods of high frequency (typically 1.0 - 2.0 Hz) oscillation in these records. These oscillations are caused by the hull whipping after each slam and are quite distinct from the longer period oscillations in the bending moment experienced at the wave encounter frequencies. Alternatively the high frequency vibrations may be detected using an accelerometer fixed to the ship's structure. Slamming severity may also be monitored by analysing these records.

Pressure transducers are sometimes let into the hull surface to measure local slamming impact pressures. It will, of course, be necessary to dock the ship if the transducers are to be fitted below the waterline. This technique requires transducers and a recording system capable of responding

to the very short rise times (of the order of milliseconds) typical of hydrodynamic impact phenomena. This will often be incompatible with the requirements for the recording system for ship motions and a separate system may be necessary.

9.5 RUN LENGTHS AND SHIP COURSES.

We have seen in Chapter 2 that at least 100 pairs of peaks and troughs are required in an irregular time history to ensure a reasonably reliable estimate of the rms motion. Each trial run must be of sufficient duration to achieve this minimum standard. The actual length required may be estimated from strip theory calculations of the motions in the wave spectrum expected during the trial. The mean period of the peaks for each motion may then be calculated from Equation (2.27). Figure 9.4 shows the results obtained for a trial planned in a frigate.

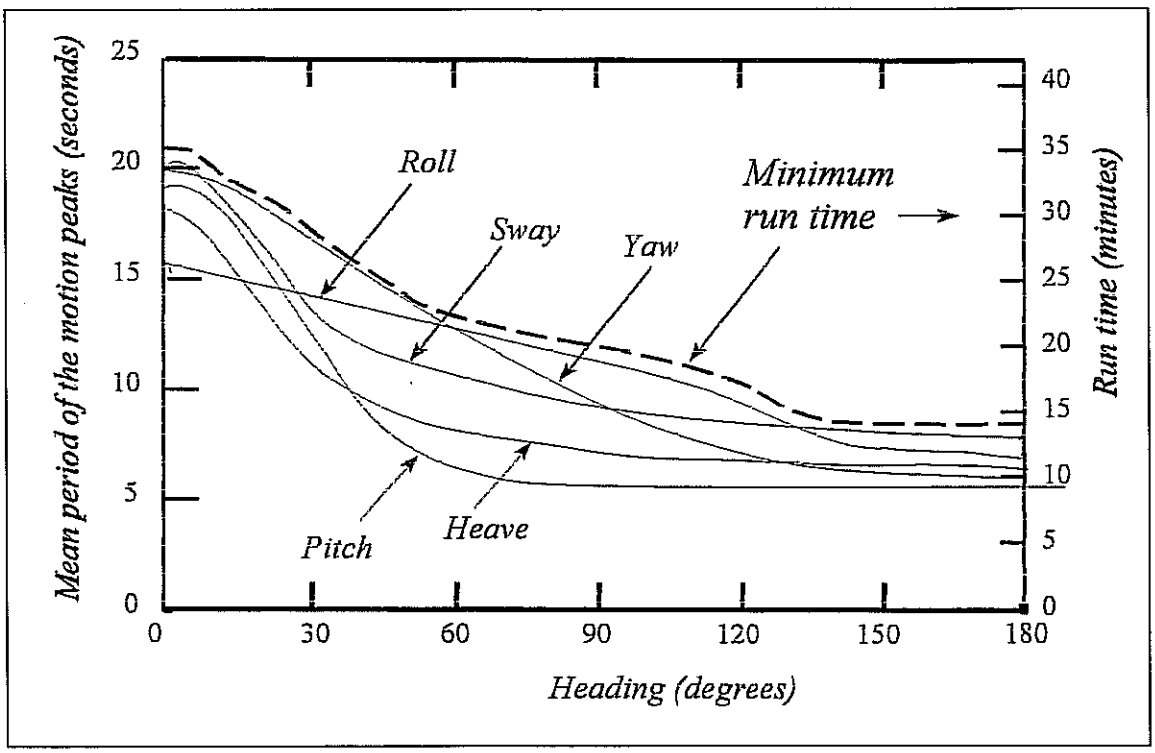

Fig 9.4 - Minimum run times for 100 motion peaks. Frigate at 20 knots: modal period 12.4 seconds

As expected, the mean periods are longest in following waves where the encounter frequencies are low. The run time required to achieve 100 motion cycles is given by

$$T_H = \frac{100\bar{T}_p}{60} \quad minutes \tag{9.6}$$

where $\bar{T}_p$ is the mean period of the peaks (in seconds) for the chosen motion. The required run time is given by the maximum envelope value of T_H for all the motions and this is also shown in Figure 9.4.

In practice longer runs than this absolute minimum are advisable. A certain amount of additional time should be allowed for the ship to settle onto its new course and speed at the beginning of each run: more importantly it should be realised that every precaution should be taken to ensure that data of adequate quality are collected. The opportunity of conducting a seakeeping trial occurs so rarely that it would be false economy to shorten the runs because of economic or operational pressures. If time is short it is better to reduce the number of runs rather than their lengths.

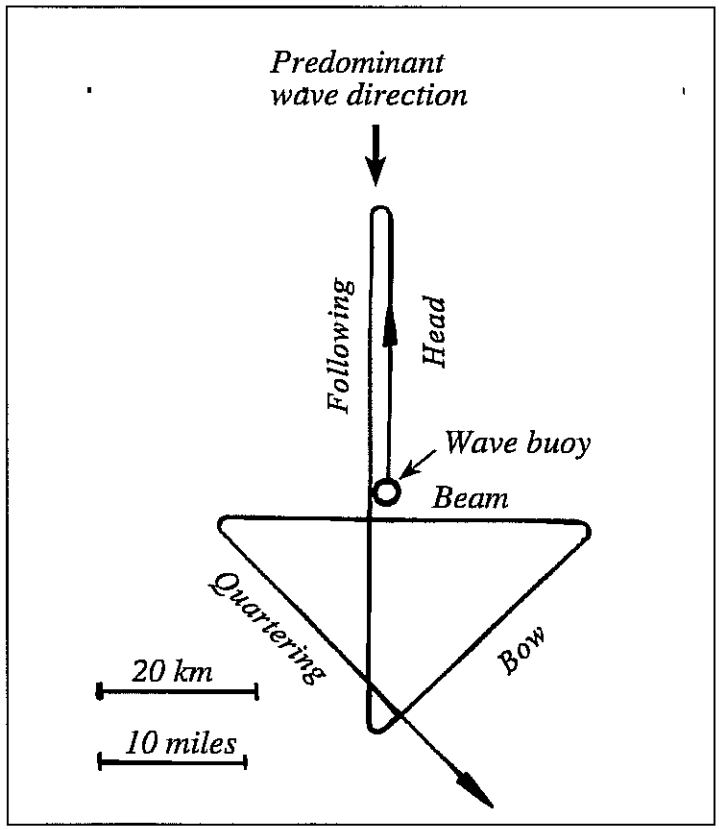

Fig 9.5 - Typical sequence of runs for a seakeeping trial at 20 knots

Very long runs are undesirable because they may take the ship too far away from the wave buoy. The wave measurements will then be unrepresentative of the conditions experienced by the ship during at least part of the run. Long runs also increase the risk of the wave conditions changing during the run.

A good rule of thumb is to add a contingency of 10 minutes to the minimum calculated run time for each course. Figure 9.5 shows a sequence of courses for a trial planned on this basis in the frigate at 20 knots. The wave buoy is launched at the beginning of the head sea run and the course sequence is chosen to minimise the distance from the ship to the buoy.

10

MODEL TESTING

"The only difference between men and boys is the size and cost of their toys"

Source unknown: seen by the author in a vintage car dealer's showroom in Monterey, California, USA in 1986.

10.1 MODEL SEAKEEPING EXPERIMENTS

Preparing a ship for a seakeeping trial is an expensive and time consuming business. It is usually necessary to select the trials period some time in advance and there can be no guarantee that suitable weather conditions will occur. Many a trial has been postponed or cancelled because there were no appreciable waves on the days allocated for it!

Even if waves of suitable severity are experienced, uncertainties about the degree of wave spreading may still limit the utility and general applicability of the results obtained. However, the main disadvantage of full scale trials is that they require the ship to be built before they can be run. As such they are virtually useless as a method of assessing the seakeeping qualities of a ship at the design stage.

Model testing provides an attractive alternative. Models are much less expensive than ships and can often be entirely dedicated to the required experiments. Moreover the model can be built before the prototype ship and a number of alternative designs can be tested. Indeed, before the advent of strip theory, model testing provided the only method of assessing the seakeeping qualities of the ship at the design stage.

If the model is to be tested in a towing tank or a seakeeping basin the waves can be produced (and reproduced) to order. Suitable measurements are generally easier to accomplish than at full scale. However, scaling problems can never be completely overcome and it must be admitted that model tests in the controlled artificial environment of the laboratory always lack something of the uncertain harsh reality of the real world experienced by the ship.

10.2 MODEL EXPERIMENT SCALING

10.2.1 Dimensional analysis

Consider a model ship in a system of regular long crested waves. How should the test conditions be scaled to ensure that the model's motions are an accurate reproduction of the motions which would have been experienced by the ship at full scale? To answer this question we employ the techniques of dimensional analysis. These are discussed in detail by Massey (1986) and in many other text books and we shall not give a general treatment here. Suffice it to say that the technique allows the proper identification of the correct model test conditions in terms of ***non dimensional*** groups of the quantities which are relevant.

TABLE 10.1

DIMENSIONS OF QUANTITIES APPEARING IN EQUATION (10.1)

Quantity	Mass (tonnes)	Length (metres)	Time (seconds)
x_{30}	0	1	0
ζ_0	0	1	0
λ	0	1	0
U	0	1	-1
μ	0	0	0
L	0	1	0
$[\ x_B\ ]$	0	1	0
$[\ I\ ]$	1	2	0
ρ	1	-3	0
μ_w	1	-1	-1
g	0	1	-2

Let us consider as an example the heave motion of a ship and its model in regular waves. For the time being we may assume that we have no detailed knowledge of the physical processes involved: even so we might surmise that the heave amplitude x_{30} will be a function of the wave amplitude ζ_0 and wave length λ, the speed U and heading μ and the size, shape and inertias of the hull. In addition, the heave amplitude would be expected to depend on the physical properties of the water (density ρ and viscosity μ_W) and the acceleration due to gravity. We might therefore write a general mathematical expression relating these eleven quantities as:

$$x_{30} = f_1 \left\{ \zeta_0,\ \lambda,\ U,\ \mu,\ L,\ [\ x_B\ ],\ [\ I\ ],\ \rho,\ \mu_w,\ g \right\} \quad m \qquad (10.1)$$

where f_1 is some as yet undetermined function which will be the same for both model and ship. $[\ x_B\ ]$ represents a sufficient number of coordinates to define the shape of the hull and $[\ I\ ]$ represents the moments of inertia of the hull. The dimensions of these quantities are listed in Table 10.1.

Massey (1986) shows how an expression of this form can be rearranged and written in terms of a smaller number of non dimensional parameters. The theory of dimensional analysis allows the required number of non dimensional parameters to be determined and for the case considered here the non dimensional heave amplitude can be expressed as a function of seven such groups. Many different formulations are possible and equally valid but it is convenient to consider the form

$$\frac{x_{30}}{\zeta_0} = f_2 \left\{ \frac{\zeta_0}{L} , \frac{\lambda}{L}, \frac{U}{\sqrt{g\,L}} , \mu, \frac{[\,x_B\,]}{L}, \frac{[\,I\,]}{\rho\,L^5}, \frac{\rho\,U\,L}{\mu_W} \right\} \qquad (10.2)$$

where f_2 is some unknown function which is the same for both model and ship.[1]

Equation (10.2) tells us that the non dimensional heave amplitude $\frac{x_{30}}{\zeta_0}$ will be the same at both model and full scale provided that all the parameter groups on the right hand side of the equation have the same numerical values at model and full scale. This requirement dictates the conditions required for the model experiment.

We define the model scale or dimension ratio as

$$R = \frac{L_S}{L_M} \qquad (10.3)$$

where L_M and L_S are the lengths of the model and the ship. The dimension ratio generally lies in the range from 10 to 100.

---

[1]These particular non dimensional parameters are chosen with the benefit of hindsight and a knowledge of the characteristics of ship motions in regular waves. Other selections are, in principle, equally valid providing that the total number of non dimensional groups is seven and that they are all independent. Any one of the groups may be multiplied or divided by any other non dimensional group (including ones that do not appear in Equation (10.2)). For example the non dimensional wave amplitude $\frac{\zeta_0}{L}$ may be divided by the non dimensional wave length $\frac{\lambda}{L}$ to express the non dimensional wave amplitude as $\frac{\zeta_0}{\lambda}$ and this is sometimes more convenient. Similarly the non dimensional wave length may be multiplied by $\sqrt{2\pi \left[\frac{L}{\lambda}\right]^3}$ to give an alternative non dimensional wave frequency parameter $\omega\sqrt{\frac{L}{g}}$ (see Table 1.1 for relevant formulae).

10.2.2 Model and wave dimensions

If the dimensionless coordinates $\frac{[\ x_B\ ]}{L}$ are to be identical for model and ship we require each corresponding dimension[2] to be related by

$$\frac{x_{BM}}{L_M} = \frac{x_{BS}}{L_S}$$

so that

$$x_{BM} = \frac{x_{BS}}{R} \quad m \tag{10.4}$$

In other words the model must be geometrically similar to the ship in all respects. The underwater hull shape should be accurately reproduced and it is convenient to model the hull up to the weather deck. It is not usually necessary to represent the superstructure as this has little effect on ship motions except possibly in very severe conditions.

In the same way the requirement that the non dimensional wave amplitude and wave length must be the same leads to

$$\zeta_{0M} = \frac{\zeta_{0S}}{R} \quad m \tag{10.5}$$

and

$$\lambda_M = \frac{\lambda_S}{R} \quad m \tag{10.6}$$

10.2.3 Mass and inertia

The requirement to represent the underwater hull form accurately demands that the model's waterline be correctly located. This requires that the model's mass be correctly scaled. The model's mass is

$$m_M = \rho_M \int B_M\, D_M\, \sigma\, dx_{BIM} \quad t \tag{10.7}$$

where the integration is performed over the length of the hull. Now all the model's dimensions must be scaled according to Equation (10.4). So the model mass may be written as

$$m_M = \frac{\rho_M}{R^3} \int B_S\, D_S\, \sigma\, dx_{BIS} = \frac{\rho_M\, m_S}{\rho_S\, R^3} \quad t \tag{10.8a}$$

---

[2] Dimensions' may be taken to include quantities such as the radii of gyration, metacentric height, centre of floatation and the coordinates of the centre of gravity.

If $\rho_M = \rho_S$ this becomes

$$m_M = \frac{m_S}{R^3} \quad t \tag{10.8b}$$

So if the water densities are identical ***the model mass is reduced in proportion to the cube of the dimension ratio.*** In practice it is usual to test models of ocean going ships in fresh water so that the water densities are not identical and this should be taken into account by using Equation (10.8a). In this case it is generally assumed that $\rho_S \approx 1.025$ tonnes/metre^3 for salt water and

$$\frac{\rho_M}{\rho_S} \approx 0.976$$

The model's moments of inertia are scaled by ensuring that

$$\frac{I_M}{\rho_M L_M^5} = \frac{I_S}{\rho_S L_S^5}$$

and the model's moments of inertia are then given by

$$I_M = \frac{\rho_M I_S}{\rho_S R^5} \quad t\ m^2 \tag{10.9a}$$

If $\rho_M = \rho_S$ this becomes

$$I_M = \frac{I_S}{R^5} \quad t\ m^2 \tag{10.9b}$$

So ***the model's moments of inertia must be reduced in proportion to the fifth power of the dimension ratio*** if the water densities are the same at model and full scale. Again it is necessary to allow for differing water densities by using Equation (10.9a.)

10.2.4 Frequencies and periods
The wave frequency is given by

$$\omega = \sqrt{\frac{2\pi g}{\lambda}} \quad rad/sec$$

(see Table 1.1). Using Equation (10.6) it follows that

$$\omega_M = \omega_S \sqrt{R} \quad rad/sec \qquad (10.10)$$

Model wave frequencies must therefore be increased in proportion to the square root of the dimension ratio and are higher than the corresponding frequencies in ship scale.

Since

$$T = \frac{2\pi}{\omega} \quad sec \qquad (10.11)$$

(see Table 1.1) it follows that the model and full scale wave periods are related by

$$T_M = \frac{T_S}{\sqrt{R}} \quad sec \qquad (10.12)$$

Model wave periods must therefore be reduced in proportion to the square root of the dimension ratio.

10.2.5 Heading
The heading μ, is of course, a non dimensional group in its own right and it is self evident that the model and full scale headings must be the same.

10.2.6 Speed: the experiment conundrum
Consider a small particle of water somewhere near the ship. Suppose that there is a corresponding model scale particle at the corresponding location (defined by Equation (10.4)) near to the model and that each particle has dimensions which are some small fraction of the ship's or model's length. Then the mass of the particle in each case will be proportional to ρL^3. The particle's velocity v will be proportional to the velocity of the ship or model and the distance ds it moves in a given time dt will be proportional to the ship's length. The particle's acceleration can be written

$$\frac{dv}{dt} = \frac{dv}{ds}\frac{ds}{dt} = v\frac{dv}{ds} \quad m/sec^2$$

which is proportional to U^2/L. So the inertia force (*mass x acceleration*) experienced by the particle will be proportional to $\rho\ L^2\ U^2$. The gravity force on the particle is (*mass* $\times$ *g*) which is proportional to $\rho\ g\ L^3$. So we find that the Froude number[3], which is one of the non dimensional parameters in Equation (10.2) , is the square root of the ratio of the inertia and gravity forces on the particle:

$$F_N = \sqrt{\frac{inertia\ force}{gravity\ force}} = \sqrt{\frac{\rho\ L^2\ U^2}{\rho\ g\ L^3}} = \frac{U}{\sqrt{g\ L}} \qquad (10.13)$$

The surface area of the fluid particle is proportional to L^2 and the viscous shear stress is proportional to μ_W times the velocity gradient.[4] The velocity gradient is proportional to U/L and the viscous force on the particle is therefore proportional to $\mu_W\ U\ L$. So we find that the Reynolds number [5], another non dimensional parameter in Equation (10.2), is the ratio of the inertia and viscous forces on the particle :

$$R_N = \frac{inertia\ force}{viscous\ force} = \frac{\rho\ U^2\ L^2}{\mu_W\ U\ L} = \frac{\rho\ U\ L}{\mu_W} \qquad (10.14)$$

Referring to Equation (10.2) we see that we require the model and full scale Froude numbers to be identical:

$$\frac{U_M}{\sqrt{g_M\ L_M}} = \frac{U_S}{\sqrt{g_S\ L_S}}$$

which leads to the speed scaling law

$$U_M = \frac{U_S}{\sqrt{R}} \quad m/sec \qquad (10.15)$$

so that ***the model speed must be reduced in proportion to the square root of the dimension ratio.***

---

[3] In honour of William Froude who realised its importance as a parameter for determining the required speed for model experiments in the nineteenth century. The French mathematician Reech also recognised its significance and it is sometimes known as the ***"Nombre de Reech"*** in France.

[4] See any text book on fluid mechanics.

[5] In honour of the nineteenth century mathematician Osborn Reynolds.

However, Equation (10.2) also demands that the Reynolds numbers for the model and ship are the same:

$$\frac{\rho_M U_M L_M}{\mu_{WM}} = \frac{\rho_S U_S L_S}{\mu_{WS}}$$

Then the model speed must be

$$U_M = \frac{\rho_S \mu_{WM} R}{\rho_M \mu_{WS}} U_S \quad m/sec$$

If the model and ship water densities and viscosities are the same this leads to

$$U_M = U_S R \quad m/sec \qquad (10.16)$$

So for identical water properties ***the model speed must be increased in proportion to the dimension ratio.*** Likely differences in density and viscosity do not substantially change this result.

Evidently Equations (10.15) and (10.16) cannot simultaneously be satisfied (except by testing at full scale so that $R = 1$). In other words it is impossible to satisfy the requirement for Froude and Reynolds number identities at the same time.

Model tests in which the proper relationship between inertia, gravity and viscous forces is maintained are therefore impossible.[6]

Fortunately viscous forces do not play a very important role in ship motion dynamics (except perhaps in roll motions). If this is the case, the requirement to scale viscous forces in the correct proportion to inertia forces may be waived and it is no longer essential to match model and full scale Reynolds numbers. In any case this matching is not usually a practical proposition since it would demand impossibly high model test speeds: for example, a ship speed of 30 knots at a model dimension ratio of 30 would demand a model test speed (Equation (10.16)) of 900 knots! In contrast, Froude number identity requires reduced model test speeds and this example would yield a much more practical model speed of about 5.5 knots (Equation (10.15).

Neglect of Reynolds number can yield misleading results in certain specific circumstances. If the Reynolds number is too low (as is usual in ship model experiments) the transition point will be too far aft and too much of the boundary layer will be laminar. Flow separation is then more likely and the skin friction forces will be too low. This may have some effect on the behaviour of the model. It is usual practice to stimulate turbulence by roughening the model surface at the

[6] In principle it would be possible to achieve proper Reynolds number scaling if the model could be tested in a fluid with decreased viscosity and/or increased density. No suitable fluid has yet been proposed.

estimated transition point near the bow to compensate for the neglect of Reynolds number scaling. This precaution can, however, only be regarded as a palliative measure and it always advisable to adopt the largest practical model scale to reduce Reynolds number scaling problems to a minimum.[7]

10.2.7 Functional form of motion responses in regular waves
For a correctly scaled model, Equation (10.2) reduces to

$$\frac{x_{30}}{\zeta_0} = f_3 \left\{ \frac{\zeta_0}{L} , \frac{\lambda}{L} , F_N , \mu \right\} \tag{10.17}$$

where f_3 is an unknown function of the four listed non dimensional quantities.

In practice the non dimensional motion amplitude is often found to be essentially independent of the non dimensional wave amplitude ζ_0 / L provided that it is relatively small (say $\zeta_0 / L < 0.02$). In this case the motion amplitude is linearly dependent on the wave amplitude, as assumed in strip theory. If this is the case we may write Equation (10.17) in the simpler form:

$$\frac{x_{30}}{\zeta_0} = f_4 \left\{ \frac{\lambda}{L} , F_N , \mu \right\} \tag{10.18}$$

In passing, it should be noted that the non dimensional wave length could be replaced by a non dimensional wave period or frequency or a non dimensional encounter period or frequency (see footnote 1 and Equation (1.35)).

10.2.8 Application of dimensional analysis to other seakeeping responses
The approach described above can be applied to all ship motions (linear and angular displacements, velocities and accelerations), and equations of the same general form as Equation (10.18) will always be obtained. These seakeeping responses must be non dimensionalised by dividing by appropriate combinations of the relevant variables. Since the response amplitudes are generally proportional to the wave amplitude it is convenient to include the wave amplitude in the denominator. For linear displacements like surge, sway, heave, relative and absolute motions this is sufficient to give a non dimensional quantity:

$$\frac{x_{10}}{\zeta_0} , \frac{x_{20}}{\zeta_0} , \frac{x_{30}}{\zeta_0} , \frac{r_{30}}{\zeta_0} , \frac{s_{30}}{\zeta_0} , \text{ etc}$$

For other seakeeping responses it will generally be necessary to include additional quantities to give the denominator the same dimensions as the numerator. For example, angular displacement amplitudes are usually non dimensionalised by dividing by the wave slope amplitude to give quantities like

---

[7] Model size is usually limited by considerations of run length and tank wall interference: see Sections 10.10 and 10.11.

$$\frac{x_{40}}{k\ \zeta_0}\ ,\ \frac{x_{50}}{k\ \zeta_0}\ ,\ \frac{x_{60}}{k\ \zeta_0}\ ,\ \text{etc}$$

Linear acceleration amplitudes may be non dimensionalised in the form

$$\frac{\ddot{x}_{20}\ L}{g\ \zeta_0}\ ,\ \frac{\ddot{x}_{30}\ L}{g\ \zeta_0}\ ,\ \frac{\ddot{s}_{20}\ L}{g\ \zeta_0}\ ,\ \text{etc}$$

10.2.9 Scaling laws for seakeeping responses

Scaling laws for seakeeping responses may easily be derived from these relationships. For example, if the non dimensional heave velocity is expressed as $\frac{\dot{x}_{30}}{\omega\ \zeta_0}$ we may infer that in a properly scaled model experiment

$$\frac{\dot{x}_{30M}}{\omega_M\ \zeta_{0M}} = \frac{\dot{x}_{30S}}{\omega_S\ \zeta_{0S}}$$

Using Equations (10.4) and (10.10) we find that

$$\dot{x}_{30M} = \frac{\dot{x}_{30S}}{\sqrt{R}} \quad m/sec$$

showing that the heave velocity, like the forward speed, is reduced in proportion to the square root of the dimension ratio. Similarly we may show that ***accelerations at model and ship scale are identical:***

$$\ddot{x}_{30M} = \ddot{x}_{30S} \quad m/sec^2$$

and that ***model encounter frequencies are, like wave frequencies, increased in proportion to the square root of the dimension ratio.*** One important consequence of this result is that the model's response to the waves appears, to the untutored eye, to be too hurried. A more realistic appearance can be obtained by recording the model's motions on film or video tape and playing back at a reduced speed. The playback speed should be reduced in proportion to the square root of the dimension ratio.

Table 10.2 gives a comprehensive list of scaling laws for model test conditions and responses.

10.2.10 Tests in irregular waves

All of the foregoing analysis applies to seakeeping experiments in regular waves. An analogous approach can be adopted for irregular waves but we must now deal in statistical rather than in deterministic quantities.

TABLE 10.2

MODEL SCALING LAWS

Quantity	Examples	Multiply ship scale value by
Mass	Ship mass	$\frac{\rho_M}{\rho_S R^3}$
Length	Ship length; all dimensions; surge, sway, heave, absolute and relative displacements; wave amplitudes and lengths, significant wave height	$\frac{1}{R}$
Time	Wave and motion periods, run time; intervals between events, modal wave period, mean zero crossing period etc.	$\frac{1}{\sqrt{R}}$
Velocity	Ship speed; surge, sway, heave, absolute and relative motion velocities; wave celerity and group velocity.	$\frac{1}{\sqrt{R}}$
Acceleration	Surge, sway, heave, absolute and relative accelerations; acceleration due to gravity	1
Angle	Roll, pitch and yaw angles; heading, stabiliser and rudder angles; phases	1
Angular velocity	Roll, pitch and yaw velocities; stabiliser and rudder rates.	$\sqrt{R}$
Angular acceleration	Roll, pitch and yaw accelerations; stabiliser and rudder angle accelerations	R
Pressure and stress	Slamming and wetness impact pressures; hydrostatic pressure; dynamic pressure; stress	$\frac{\rho_M}{\rho_S R}$
Frequency	Wave and encounter frequencies; frequency of intermittent events; propeller rpm.	$\sqrt{R}$
Force	Exciting force; shear force, tension; weight; thrust	$\frac{\rho_M}{\rho_S R^3}$
Moment	Exciting moment; bending moment; torsional moment; torque	$\frac{\rho_M}{\rho_S R^4}$
Linear spectral density ordinate	Spectral density ordinates for waves, surge, sway, heave, absolute and relative motion	$\frac{1}{R\sqrt{R}}$
Angular spectral density ordinate	Spectral density ordinates for wave slope, roll, pitch, yaw, rudder and stabiliser angles	$\frac{1}{\sqrt{R}}$

Let us consider again the heave motion of a model and its full scale prototype. Drawing a parallel with the regular wave Equation (10.1) we might suppose that the rms heave motion for a given spectrum formulation would have some functional relationship with a number of relevant quantities as follows:

$$\sigma_{0x3} = f_5 \left\{ \bar{H}_{1/3} \, , \, T_0 \, , \, U, \, \mu, \, L, \, [\, x_B \,], \, [\, I \,], \, \rho, \, \mu_W \, , \, g \right\} m \qquad (10.19)$$

Applying the same general approach we find that the non dimensional rms heave for a geometrically scaled model is conveniently expressed as

$$\frac{\sigma_{0x3}}{\bar{H}_{1/3}} = f_6 \left\{ \frac{\bar{H}_{1/3}}{L} \, , \, T_0 \sqrt{\frac{g}{L}} \, , \, F_N \, , \, \mu \right\} \qquad (10.20)$$

In other words the non dimensional rms heave is a function of the non dimensional significant wave height and modal period, the Froude number and the heading. It is easily seen that ***the significant wave height must therefore be scaled in proportion to the dimension ratio, and the modal period must be reduced in proportion to the square root of the dimension ratio.*** For moderate significant wave heights the functional dependence on the non dimensional significant wave height is often weak and the ***rms heave motion for a given modal period, Froude number and heading is then directly proportional to the significant wave height.***

10.3 OPEN WATER MODEL EXPERIMENTS

The simplest kind of model experiment involves testing an instrumented remote controlled model in the open sea in what amounts to a miniature seakeeping trial. A dimension ratio of the order of 10 is typical and the model may be powered by a small marine diesel engine or an electric motor. Ship motion instrumentation similar to that employed in full scale trials is used and motor speed setting and steering are achieved by radio control.

A wave buoy is required to measure the waves. This must be designed to respond to the short waves which will be of significance to the model and a standard full scale wave buoy will not usually be adequate in this respect. Wave and motion spectra and statistics are obtained in exactly the same way as at full scale.

Open water experiments have an intrinsic appeal for their apparent realism and they are certainly much cheaper than full scale trials. However they are fraught with difficulties and cannot generally be regarded as a serious option for the assessment of ship behaviour in rough weather.

The required full scale wave spectrum must be reproduced at model scale according to the appropriate scaling laws. This generally dictates a test area in sheltered water with a limited fetch. Unfortunately this often results in multiple wave reflections from the nearby coast and a high degree of directional spreading is usually present during these experiments. This makes the results difficult to interpret and misleading conclusions can easily be drawn.

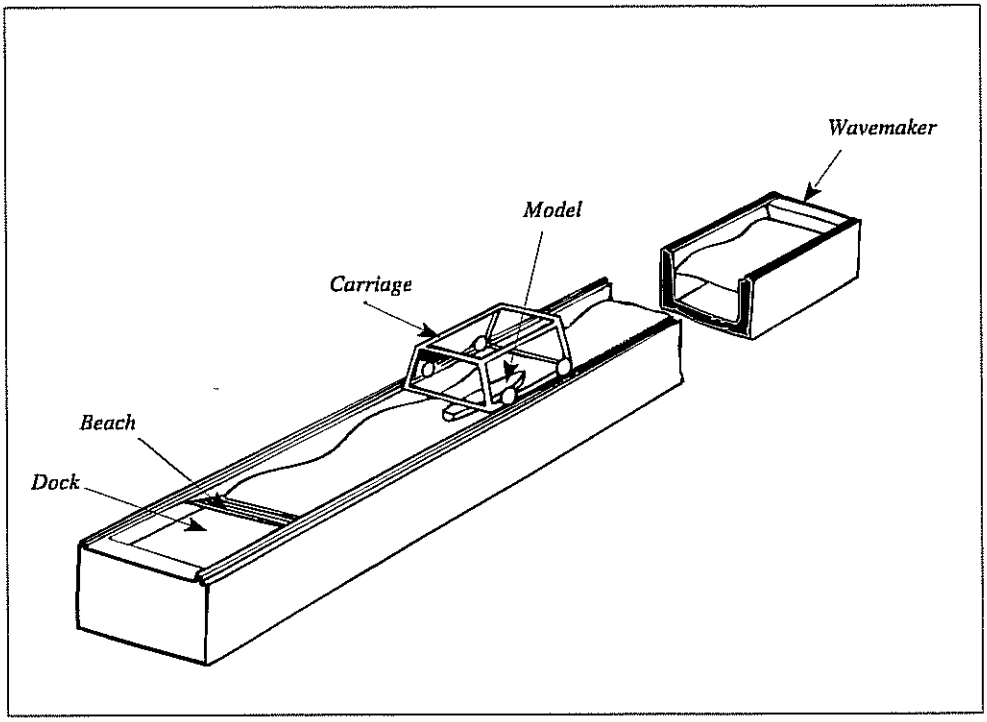

Fig 10.1 - Typical towing tank

10.4 LABORATORY TEST FACILITIES

Tests in the controlled environment of the indoor laboratory are much preferred to open water experiments. The traditional[8] type of long narrow towing tank is illustrated in Figure 10.1. Such tanks are usually of the order of 100 metres long and 5-10 metres wide. The depth should be at least half the longest wave length envisaged to avoid unwanted shallow water effects on the waves. A towing carriage runs on rails and is powered either by onboard electric motors or hauled by a winch at the end of the tank. Waves are generated at one end of the tank by a wave maker and absorbed by a beach at the other. A section of the beach can usually be lowered to allow the end of the tank to be used as a docking area for ballasting and trimming models.

---

[8] In 1865 William Froude conducted model experiments on the River Dart in Devon. He was concerned with developing scaling laws for ship resistance in calm water but often found that the uncontrolled environment (wind and waves) of the river estuary spoiled his results. Accordingly he approached the Admiralty with a proposal to build the World's first purpose built indoor towing tank at his home in Chelston Cross near Torquay. The tank was to be used for experiments on rolling as well as ship resistance. It was completed in 1872 and was known as the Admiralty Experiment Works. Froude died in South Africa in 1879 and was succeeded by his son R E Froude who moved the establishment to Haslar, near Gosport in 1886. A new tank was built and gave sterling service for over 100 years until it was closed and converted into offices by an unsympathetic management more interested in accountancy than historical significance or hydrodynamics. The author led the team which conducted the last experiment (on deck wetness) on 5th November 1993.

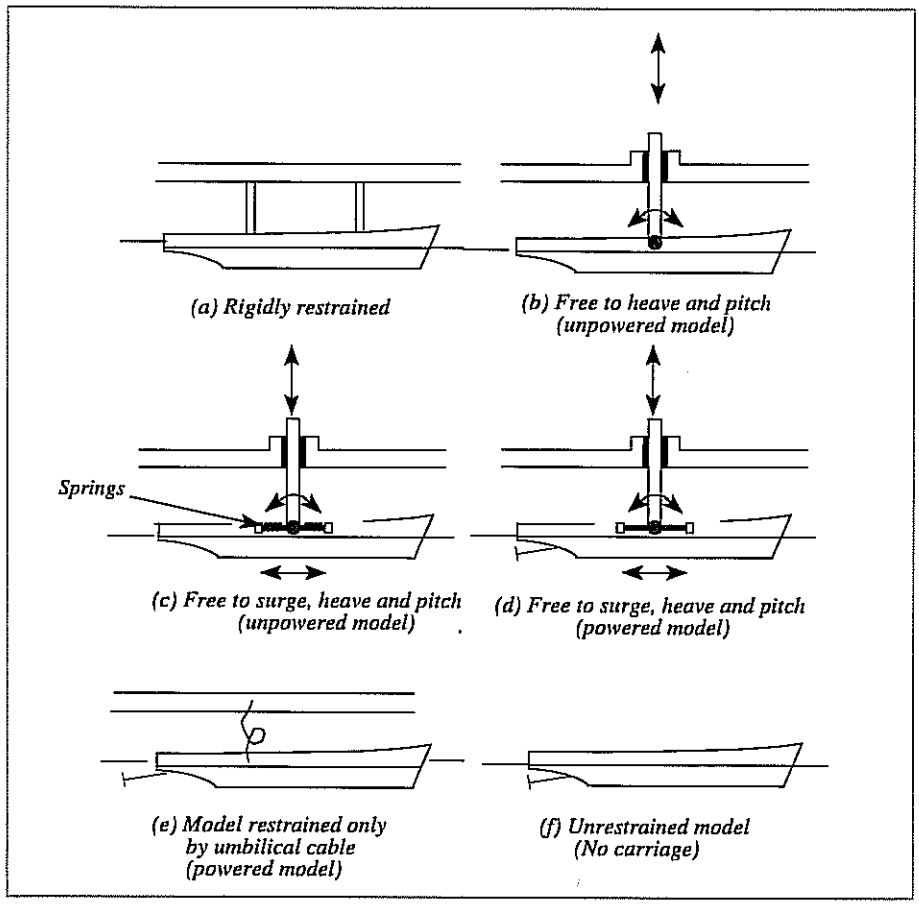

Fig 10.2 - Model restraint systems

Models may be tested at forward speed in head or following waves. In addition, tests at zero speed in beam waves (with the model aligned across the tank) are possible.

The model to be tested is mounted under the carriage using one of the arrangements shown in Figure 10.2. The rigidly restrained arrangement shown in Figure 10.2(a) is used only in specialised experiments to measure wave loads. Figure 10.2(b) shows the rig commonly used with an unpowered model in head or following waves. The model is free to pitch around a hinge pin at its centre of gravity. The pitch pivot is mounted at the end of a vertical rod which slides in linear bearings, allowing the model freedom to heave. No surge motion is allowed.

A limited freedom to surge can be obtained using the sprung arrangement shown in Figure 10.2(c). True surge motions can only be obtained if the model is self propelled and the arrangements shown in Figures 10.2(d), 10.2(e) and 10.2(f) are possible.

It is, of course, necessary to use very high quality bearings in these rigs to reduce frictional effects on the measured motions to an absolute minimum. Some of the weight of the rig will be supported by the model and due allowance for this must be made when ballasting and trimming. In any case the moving parts of the rig should be made as light as possible to minimise the added inertias which will contaminate the results. Frictional effects may be virtually eliminated by dispensing with any guidance arrangements as shown in Figure 10.2(e).

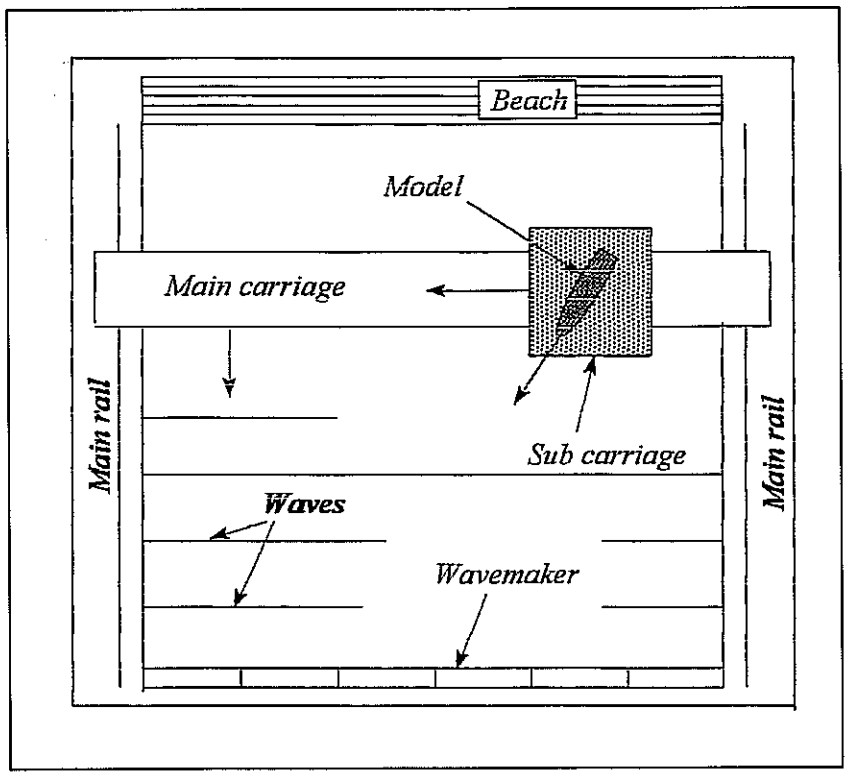

Fig 10.3 - Typical seakeeping basin

In recent years the seakeeping basin, specifically designed for seakeeping model tests, has been introduced. These tanks are usually of the order of 50 metres square and are fitted with wave makers and a beach at opposite ends. An ideal arrangement is shown in Figure 10.3. A main carriage spans the tank and runs on rails in much the same way as in the traditional towing tank. A subcarriage is mounted on the main carriage so that it may be positioned at any point over the water surface. During a self propelled experiment the subcarriage's position may be maintained over the model by an automatic control system. Alternatively for towed experiments the subcarriage may be driven across the tank at some predetermined heading to the waves.

For self propelled experiments the model is connected to the subcarriage by an umbilical cable as shown in Figure 10.2(e). This cable supplies the model with electric power for its propulsion and instrumentation and also serves to feed the model's response signals back to the carriage for recording and analysis. The cable is supposed to be sufficiently light and flexible to preclude any interference with the model's motions.

This ideal arrangement is of course very expensive and many tanks have no carriage, relying instead on free running self contained models as shown in Figure 10.2(f). This means that the model must carry its own batteries for power supply and that its responses must be recorded on board or telemetered ashore. In either case the additional weight makes the achievement of proper mass and inertia scaling more difficult and large models may be necessary to allow adequate freedom of ballast adjustment.

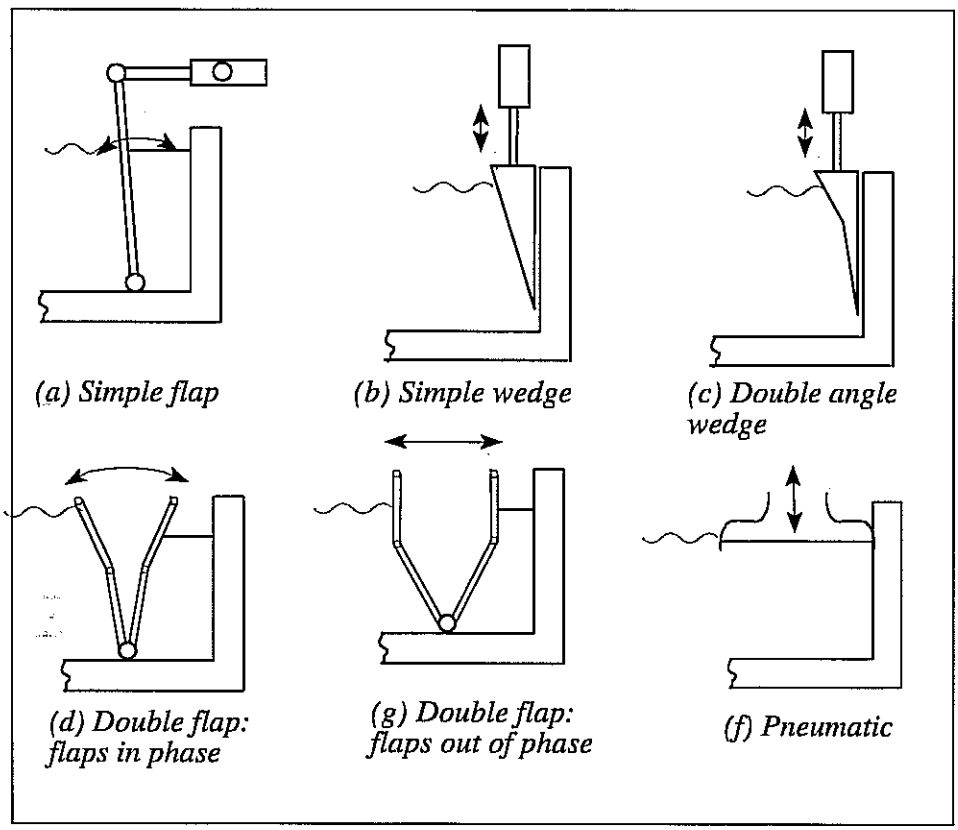

Fig 10.4 - Wave makers

10.5 WAVE MAKERS AND BEACHES

10.5.1 Wave makers

Figure 10.4 shows several different designs for laboratory wave makers in current use. In modern installations the wave maker is usually driven by a servo controlled hydraulic ram which will follow an electrical input drive signal as shown in Figure 10.5. Both regular and irregular waves can be reproduced provided that appropriate drive signals are available.

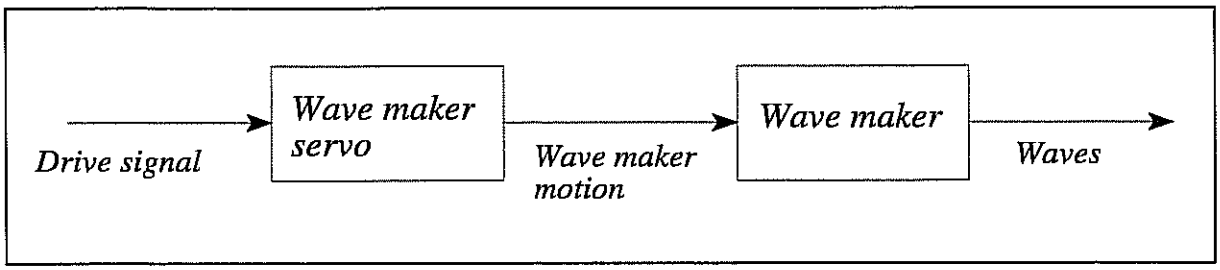

Fig 10.5 - Wave maker block diagram

The wave maker transfer function relating the wave and servo motions may in principle be calculated and Crapper (1984) gives a theory for a simple piston wave machine. However, most laboratory test tanks rely on an experimentally determined transfer function for the wave maker and its servo. Figure 10.6 shows a typical calibration for a wedge type wave maker. The diagram allows the voltage amplitude required to achieve any desired regular wave amplitude to be determined.

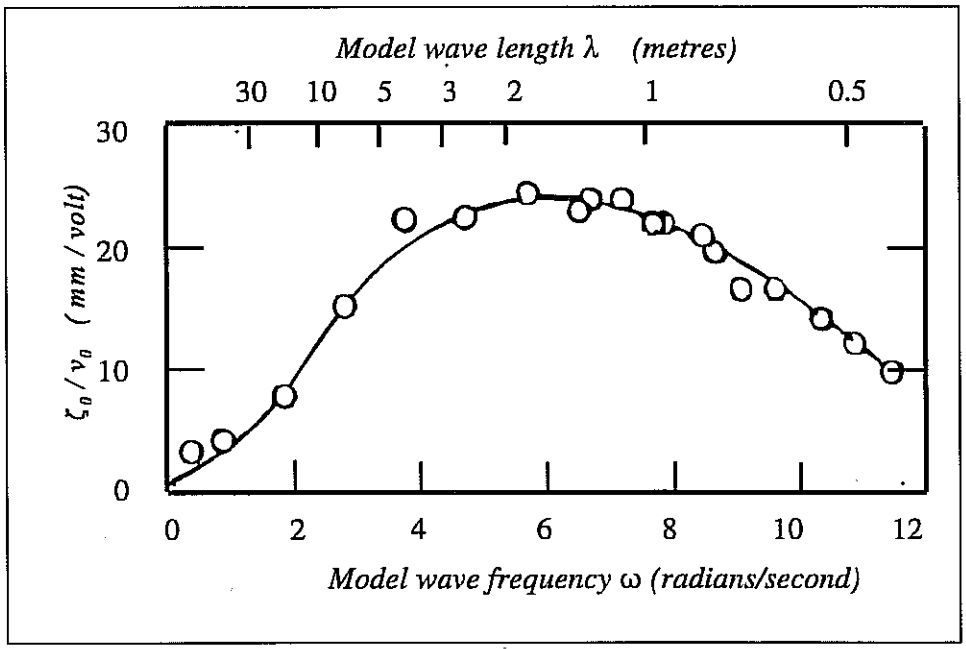

Fig 10.6 - Wave maker transfer function

10.5.2 Beaches

Most tanks are fitted with a beach to absorb the waves after they have travelled the length of the tank. All beaches allow a certain amount of wave energy to be reflected and tank superintendents are often strangely reluctant to reveal definitive data on beach performance. In a rare display of candour Hsuing et al (1983) measured the performance of the beach in a new tank at the Memorial University of Newfoundland and their results are shown in Figure 10.7. The reflection coefficient, defined as

$$C_R = \frac{amplitude\ of\ reflected\ wave}{amplitude\ of\ incident\ wave}$$

is plotted as a function of the non dimensional wave frequency $\omega\sqrt{\frac{d}{g}}$ (where d is the depth of the tank). The results show that the beach is most effective at high frequencies (ie in short waves) and the best results are obtained when the beach slope is very small. Such a shallow beach may well occupy a significant proportion of the length of the tank and practical considerations may place a limit on the beach slope which can actually be used.

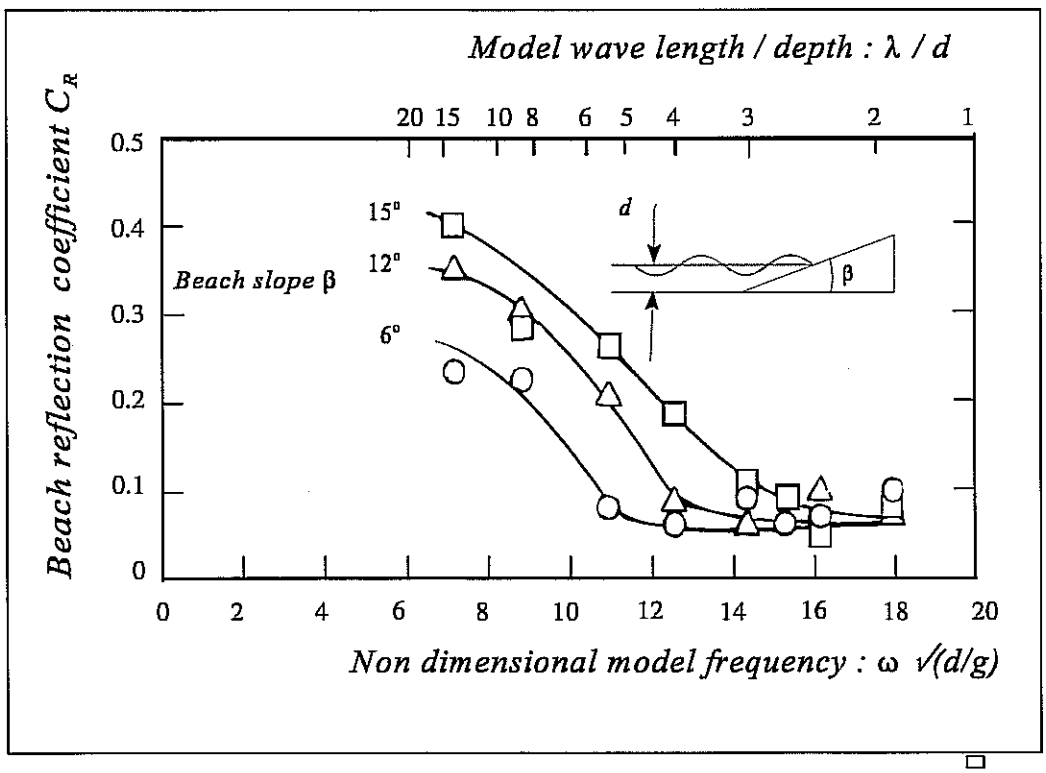

Fig 10.7 - Beach reflection coefficients (After Hsuing et al (1983))

Over the range of wave lengths of interest to most model experiments the reflection coefficient is usually of the order of 0.05 - 0.10. These reflections will mix with the incident waves and spoil their characteristics. It is therefore important to ensure that measurements are taken before these unwanted reflections reach the model. This is discussed in more detail in Section 10.9.

10.6 INSTRUMENTATION

Where a carriage is available this provides a convenient datum for the measurement of ship motions. Some examples of commonly used techniques for pitch and heave are shown in Figure 10.8 and adaptations of these systems are used for the other motions. A simple arrangement with strings and potentiometers is shown in Figure 10.8(a). The potentiometers give signals which

are proportional to the absolute motions at the attachment points and these may be combined to give estimates of the pitch and heave:

$$x_3 = \frac{s_F + s_A}{2} \quad m \tag{10.21}$$

$$x_5 = \frac{s_A - s_F}{2\,x_R} \quad rad \tag{10.22}$$

where s_F and s_A are the absolute motions measured forward and aft and $2x_R$ is the longitudinal separation of the two measurement locations.

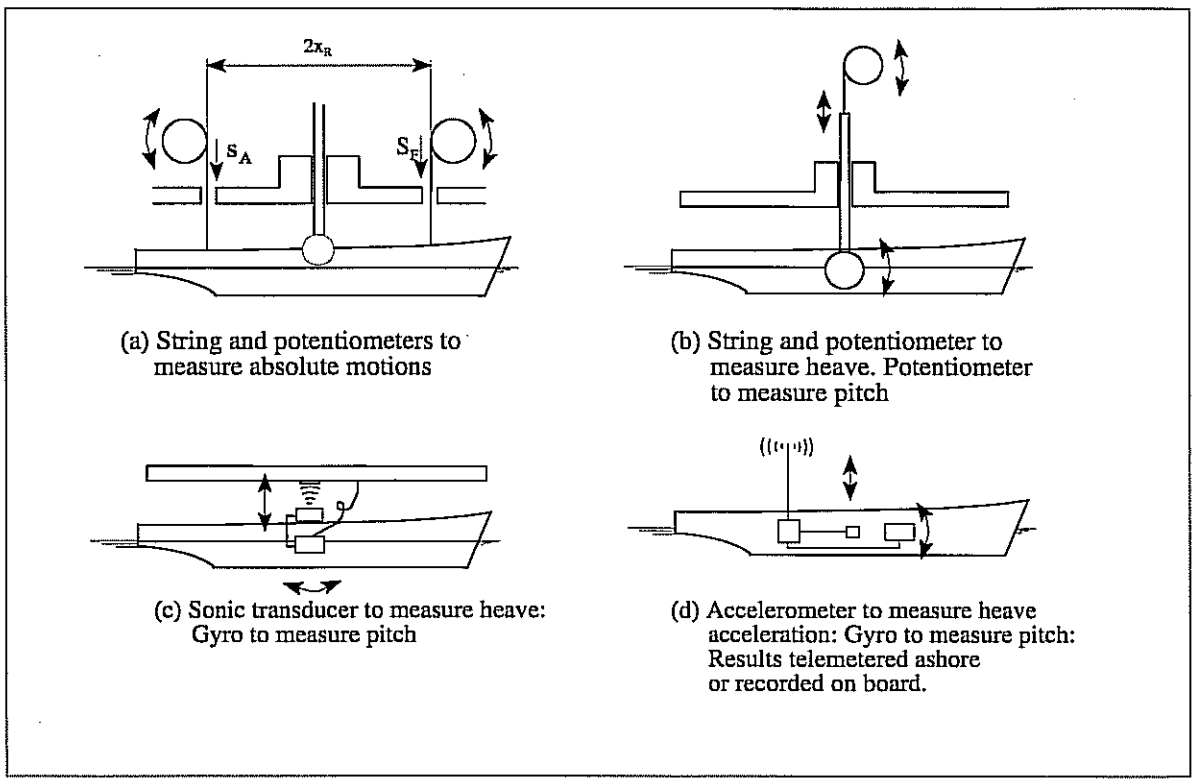

Fig 10.8 - Instrumentation for pitch and heave

Another technique is illustrated in Figure 10.8(b). Here the heave is measured directly by monitoring the motion of the heave post and the pitch is obtained by coupling a potentiometer to the pitch pivot pin in the model.

Where there is no physical connection (apart from the umbilical cable) between the model and the carriage, systems like that shown in Figure 10.8(c) have found favour. Here the pitch is measured by a gyro of the type used in aircraft navigation systems and the heave is monitored using a sonic transducer. The transducer emits a short duration pulse of high frequency sound (above the limit of human perception) and this is reflected from a horizontal board mounted under the carriage. The time required for the sound to travel from the transducer to the board and back again is monitored and is proportional to the distance from the transducer to the board.

Where there is no carriage, heave and other linear ship motions cannot be measured directly because no convenient datum level is available for use as a reference. It is then necessary to resort to gyros and accelerometers as in full scale ship trials and this is illustrated in Figure 10.8(d).

Two kinds of wave transducers are shown in Figure 10.9. Both involve a pair of metallic surface piercing elements. Electronic circuits are used to monitor the resistance of the water between the two elements and this is a function of the depth of immersion. Alternatively the elements may be regarded as the plates of a capacitor using the water as the dielectric medium. The capacitance is then monitored to provide an analogue of the depth of immersion.

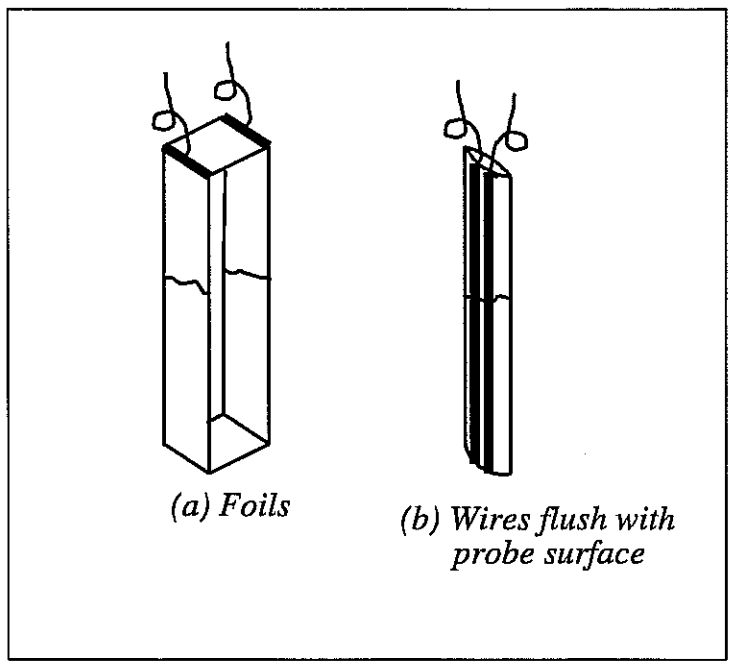

Fig 10.9 - Wave probes

These wave probes have some disadvantages. Surface tension effects may cause the water level experienced on the probe surface to be slightly different to the true level away from the immediate vicinity of the probe. The errors due to this effect are not, however, very serious unless the probes are used to measure very small waves. Much more significant effects are experienced if these surface piercing probes are used on a moving carriage to measure the wave encountered by the model. The probe inevitably causes some surface disturbance and this is likely to introduce errors in the measured wave profile due to the probe's own `bow' wave. Speeds in excess of 1-2 metres/second may introduce noticeable errors.

More sophisticated wave probes which avoid contact with the water surface have been developed. One type uses transducers to detect an ultrasonic pulse reflected from the water surface. Optical systems using lasers are also being considered and the `servo needle' is being developed in Japan. This uses a servo controlled probe which is continually adjusted so that it is just in contact with the water surface.

It is advisable to position the wave probe perhaps one metre ahead and one metre to one side of the model to avoid measuring any surface disturbance caused by the model. Care should be taken to ensure that any surface disturbance due to the probe does not interfere with the model.

Figure 10.10 shows some of the types of instrumentation used to measure relative bow motion. Most of the transducers are developments of those used to monitor waves. The simplest form, using a pair of foils ahead of the model, is shown in Figure 10.10(a). This gives a general indication of the relative motion ahead of the bow but is positioned so that the disturbance due to the proximity of the hull may not be measured.

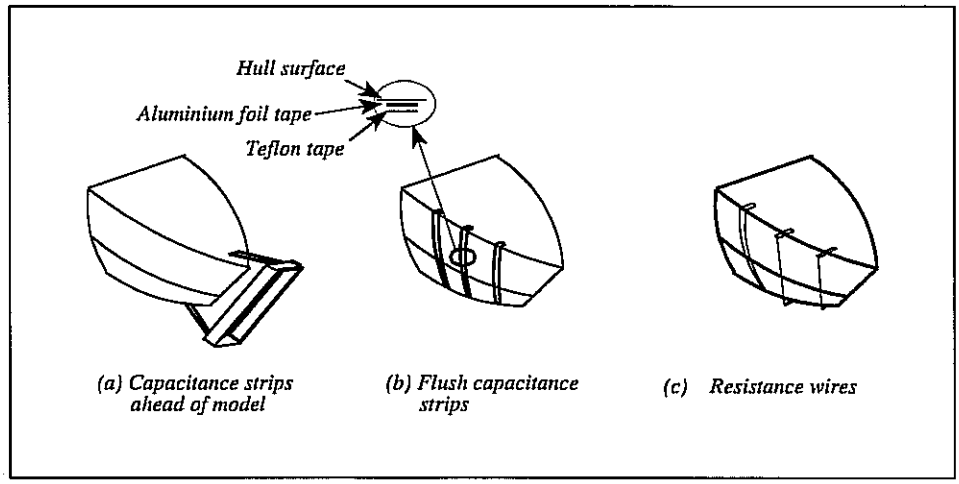

Fig 10.10 - Relative motion instrumentation

This problem is overcome with the arrangement of flush mounted tapes shown in Figure 10.10(b). Here an aluminium foil tape is fixed directly to the surface of the model using double sided adhesive tape. The aluminium is insulated from the water by a layer of 'Teflon' tape. The aluminium and the water form the plates of a capacitor, the Teflon tape being the dielectric. The electrical circuit of the capacitor is completed through an uninsulated aluminium tape on the surface of the hull, and this allows the capacitance, and hence the relative motion, to be monitored by suitable circuits. Insulated tapes may be located at a number of stations, allowing the measurement of the longitudinal variation of relative motion. A single return tape will suffice for several measurement locations.

Measurements with this arrangement will certainly include the effects of the disturbance due to the hull but may suffer from the surface tension effects experienced by wave probes. The rig shown in Figure 10.10(c) has been proposed as an alternative. Here resistance wires are stretched taut from keel to deck. The wires do not touch the hull surface so they should not be subject to the unwelcome effects of surface tension: at the same time they should be sufficiently close to the hull to give measurements which include the local wave disturbance effects due to the hull.

Experiments to investigate deck wetness and slamming are also of some importance and suitable transducers to monitor deck wetness are shown in Figure 10.11. In Figure 10.11(a) a vertical plate incorporating pressure sensitive cells is mounted on the forecastle and may be used to

measure both the impact pressures and the frequency of deck wetness. The cells are covered with a thin flexible diaphragm and are connected to pressure transducers mounted on the carriage by lengths of flexible tubing. An alternative technique using resistance wire probes is shown in Figure 10.11(b). Here the probes measure the depth of water on the deck but can again be used to monitor the frequency of deck wetness.

In slamming experiments pressure transducers are usually mounted flush with the model keel and under the bow flare to measure impact pressures directly.

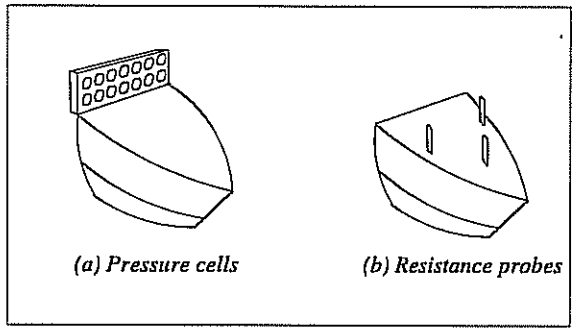

Fig 10.11 - Deck wetness instrumentation

10.7 MODEL MATERIALS

William Froude developed the technique of building models from paraffin wax and this is used in some establishments to this day. An oversize casting of the hull is first made using a simple mould of wood and fabric. Accurate waterlines are then cut in a special double cutter milling machine. The model is then finished by hand using templates taken from the body plan of the hull.

Paraffin wax has many advantages. It is easily worked and models can be modified at any time using simple hand tools. After a model's useful life has expired it can be melted down and the wax reused. However, wax models are not very robust: indeed they will gradually distort if left unsupported over a prolonged period. This can be avoided by keeping them submerged in water if they are required for future experiments. This is, however, hardly convenient since all the internal equipment must be removed. A harder wearing material is usually chosen for seakeeping model experiments.

Wood is a favourite material, being easily worked and durable. The usual technique is to cut out a series of boards to the shapes of the hull waterlines and to assemble these in the so called 'bread and butter' construction. The excess material is removed by hand using scrapers and templates for guidance in the final stages. The inside of the model is carved away to allow room for the required equipment and to reduce weight.

It is always necessary to allow a considerable wall thickness to ensure adequate strength in a wooden model and the usable internal space is often restricted. So wooden models are often quite heavy and only a small amount of additional ballast is needed to bring them up to the required mass. There is therefore little freedom to position the ballast to obtain the proper inertias and centre of gravity. Wood also has the disadvantage that it always seems to absorb moisture from

the water, no matter how well it is waterproofed. So dimensional stability is difficult to maintain as the wood swells and subsequently contracts as it dries out.

For this reason alternative modern materials are often used, particularly for free running models which must carry their own batteries for power supply. A favourite material is glass reinforced plastic (GRP). The shell of the hull need then be only a few millimetres thick and a very light yet strong and stiff model can be produced. It is first necessary to build a plug (male) mould to the exact finished shape of the hull and this is conveniently done in paraffin wax. The plug is coated with a release agent and a female mould is built up on the plug with layers of glass cloth impregnated with resin. When the resin has cured, the two moulds are separated and the plug is discarded and recycled. The inside of the female mould is then coated with the release agent and layers of resin impregnated cloth are built up to form the finished GRP hull. After curing, the hull and the mould are separated and the hull is ready for fitting out. If required the female mould can be used again to reproduce any number of identical models.

Expanded polystyrene foam has also been used in some laboratories. This is very light and stiff and has many of the advantages of glass reinforced plastic.

10.8 TRIMMING AND BALLASTING

The first step in trimming and ballasting a model is to weigh the hull, completed with all internal fittings such as instrumentation, batteries, propulsion motors etc. A temporary extra weight to represent the weight of any towing or restraint apparatus to be supported by the model should be included[9]. The additional ballast required to bring the model's mass up to the required value is then calculated and the necessary ballast weights stowed in the hull. The model is placed in the water and the positions of the ballast weights adjusted until the required trim is obtained. The model is usually required to have no heel angle and this can be checked by a spirit level sited on some suitable datum surface. The longitudinal trim is best determined by simple adjustable wire trim gauges of the type illustrated in Figure 10.12. These allow the freeboard F to be determined at specified locations forward and aft. If the model's trim is correct it follows that the longitudinal position of the centre of gravity must be correctly located.

It remains to determine the vertical location of the centre of gravity and to adjust it if necessary. This is done using an inclining experiment. A small measured heeling moment is applied to the model and the resulting heel angle is measured. The moment is most easily applied by moving a known weight a measured lateral distance.[10] This enables the solid metacentric height $\overline{GM}_S$ to be determined (see any text book on naval architecture). The position of the metacentre M will be known from the ship's hydrostatic diagrams and this allows an estimate of the vertical location of the centre of gravity. The VCG can be adjusted by appropriate vertical movement of ballast weights.

---

[9] This weight must be removed for the experiments.

[10] The weight should be part of the ballast already installed since adding a weight at this stage will change the model's displacement and underwater hull form.

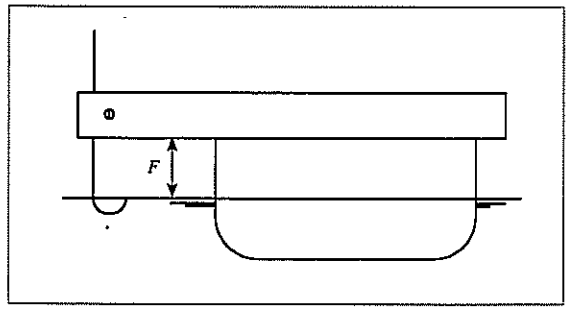

Fig 10.12 - Trim gauge

The moments of inertia are measured using the compound pendulum rigs illustrated in Figures 10.13 and 10.14. Figure 10.13(a) shows a simple technique for measuring the pitch moment of inertia I_{55}. The model is suspended in a light frame so that the centre of gravity is h metres below a pivot point. The entire rig is then oscillated by hand and the natural period of oscillation T_* determined by measuring the time required for, say, ten complete oscillations. The total moment of inertia of the complete rig is, by the parallel axis theorem

$$I = m\ k_5^2 + m\ h^2 + I_F \quad t\ m^2 \tag{10.23}$$

and the stiffness of the compound pendulum is

$$c = (\ m\ h + m_F\ h_F\ )\ g \quad kN\ m/rad \tag{10.24}$$

where m_F is the mass of the supporting frame in tonnes, I_F is its moment of inertia in tonne metres^2 and h_F is the distance from its centre of gravity to the pivot point in metres.

Now, from Equation (A1.6) the oscillation frequency is

$$\omega_* = \frac{2\pi}{T_*} = \sqrt{\frac{c}{I}} \quad rad/sec \tag{10.25}$$

and the model's radius of gyration is given by

$$k_5 = \sqrt{\frac{(\ m\ h + m_F\ h_F\ )\ g\ T_*^2}{4\ \pi^2\ m} - h^2 - \frac{I_F}{m}} \tag{10.26}$$

An exactly similar procedure is used for finding the roll radius of gyration as shown in Figure 10.13(b). In both cases it is desirable to keep the mass and inertia of the supporting frame as small as possible to minimise errors in the estimation of the hull's characteristics. The inertias of the frame may be found by measuring its natural period of oscillation without the hull attached.

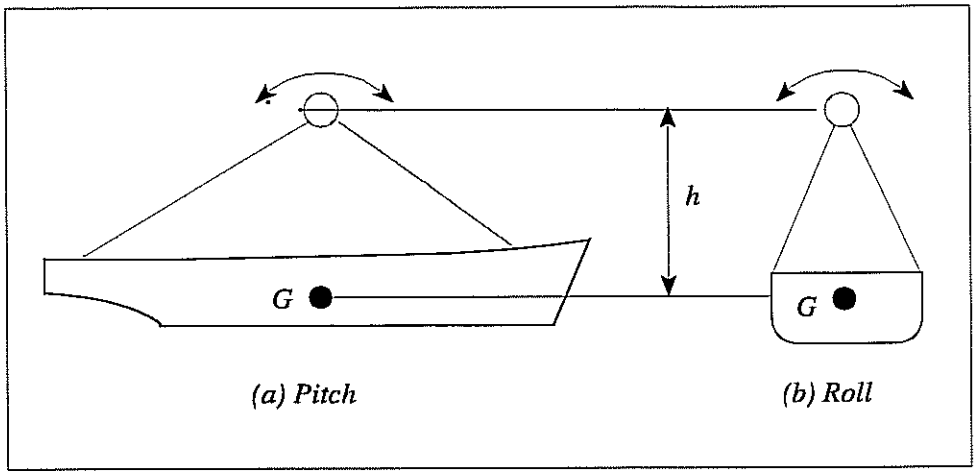

Fig 10.13 - Compound pendulum rigs for measuring pitch and roll radii of gyration

A somewhat simpler procedure for finding the yaw radius of gyration without using a supporting frame is shown in Figure 10.14. The model is suspended on two wires from a suitable overhead beam. Typically the wires will be five or six metres in length. The model is oscillated in yaw, taking care to avoid roll or sway motions. The natural period of oscillation is recorded as before. The stiffness of the system is calculated as follows.

Suppose that the model is yawed through a small angle x_6 radians as shown. Then the wires will swing through a small angle

$$\frac{x_6\, x_R}{h} \quad rad$$

Now the tension in each of the two wires must be half the model weight:

$$\frac{m\, g}{2} \quad kN$$

and the horizontal component of these forces tending to swing the model back to its equilibrium position is approximately

$$\frac{m\, g\, x_6\, x_R}{2h} \quad kN$$

So the restoring moment on the model is

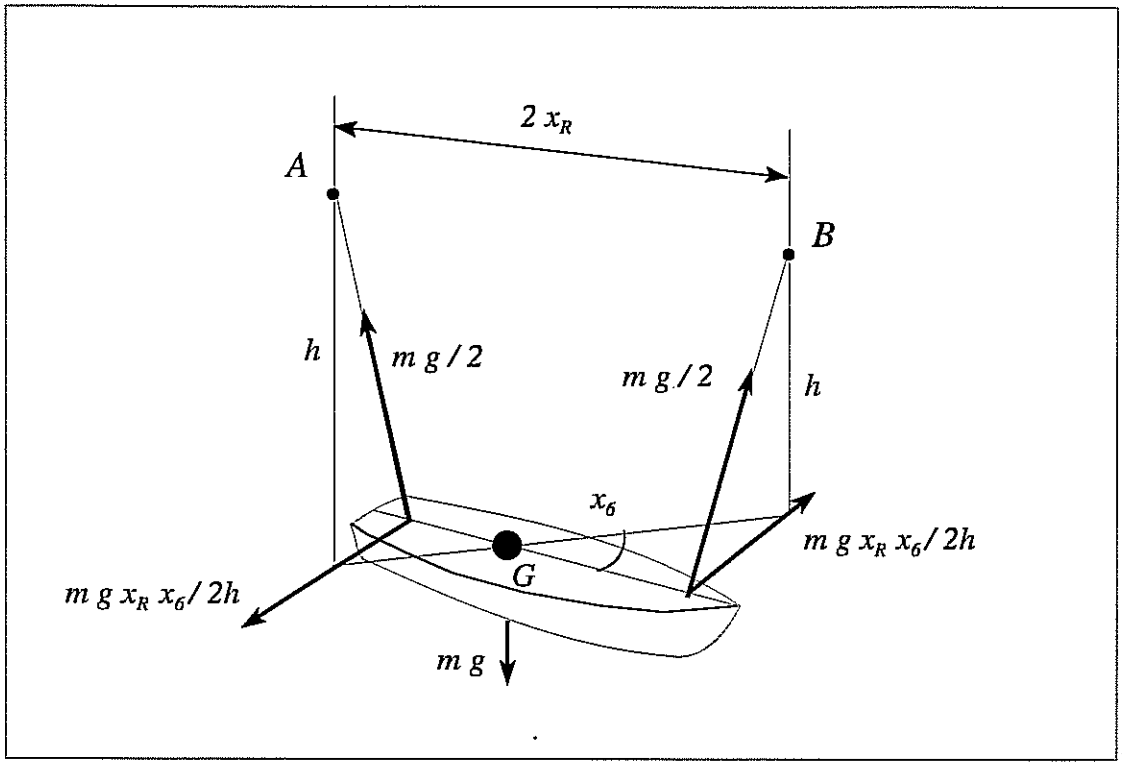

Fig 10.14 - Bifilar suspension rig for measuring yaw radius of gyration

$$\frac{m\ g\ x_6\ x_R^2}{h} \quad kN\ m$$

and the stiffness of the system is then

$$c = \frac{m\ g\ x_R^2}{h} \quad kN\ m/rad \tag{10.27}$$

The moment of inertia of the slender wires supporting the model is assumed to be negligible and the natural frequency of the system is, from Equation (A1.6),

$$\omega_* = \frac{2\pi}{T_*} = \sqrt{\frac{c}{m\ k_6^2}} = \frac{x_R}{k_6}\sqrt{\frac{g}{h}} \quad rad/sec \tag{10.28}$$

and the yaw radius of gyration is given by

$$k_6 = \frac{T_*\ x_R}{2\pi}\sqrt{\frac{g}{h}} \quad m \tag{10.29}$$

The bifilar suspension method is widely used to estimate the yaw radius of gyration because of its simplicity and convenience, requiring no more apparatus than a stopwatch and a pair of wires suspended from hooks in a suitable overhead beam. In principle the same method could also be used to estimate the pitch radius of gyration with the model turned on its side. This is, not usually practical, however, because much of the internal equipment may not be sufficiently well secured. Instead it is often assumed that the pitch radius of gyration is the same as the yaw radius of gyration.

The model's radii of gyration may be adjusted to the required values by moving the internal ballast weights. The radii of gyration may be reduced by moving ballast towards the middle of the model and vice versa. Care should be taken to ensure that any adjustment to ballast on one side (or end) of the model is exactly balanced by a corresponding adjustment as the other end. Otherwise the location of the model's centre of gravity will be changed. It is good practice to check the centre of gravity position after swinging the model to ensure that all is well in this respect.

10.9 TESTING IN REGULAR WAVES

10.9.1 Measurement of motion transfer functions

Most tests in regular waves are concerned with the experimental determination of the motion transfer functions. It is therefore necessary to record the sinusoidal motions of the model and to determine the motion amplitudes experienced for a variety of different wave lengths or frequencies. It is usual to keep the wave slope constant while varying the wave length, but experiments in waves of constant amplitude are also used. Care should be taken to ensure that the wave steepness is always small (unless the tests are specifically intended to investigate non linear effects) so that there is no risk of the wave breaking.

If phase information is required it is necessary to measure the incident waves using a wave probe mounted on the towing carriage. It is usual to position the probe ahead and to one side of the model, as shown in Figure 10.15. This avoids measuring the wave distortion caused by the presence of the model and prevents the bow wave generated by the probe interfering with the model. This introduces a phase shift in the recorded motions and this must be corrected in the analysis. Suppose that the wave probe is positioned x_{1P} metres forward of the mean position of the model's centre of gravity and x_{2P} metres to starboard. Then the probe will record the waves x_P metres after they have passed the centre of gravity. The distance x_P is given by

$$x_P = x_{1P} \cos \mu - x_{2P} \sin \mu \quad m$$

Now the waves are overtaking the model with a relative velocity

$$c - U \cos \mu \quad m/sec$$

and a wave trough recorded at the probe would have been alongside the model's centre of gravity at a time

$$t_P = \frac{x_P}{c - U \cos \mu} \quad sec$$

earlier. So the phase lead measured with reference to the waves recorded at the wave probe should be reduced by an amount

$$\delta_P = \omega_e \, t_P$$

$$= \frac{\omega_e \, (x_{1P} \cos \mu - x_{2P} \sin \mu)}{c - U \cos \mu} \quad rad \qquad (10.30)$$

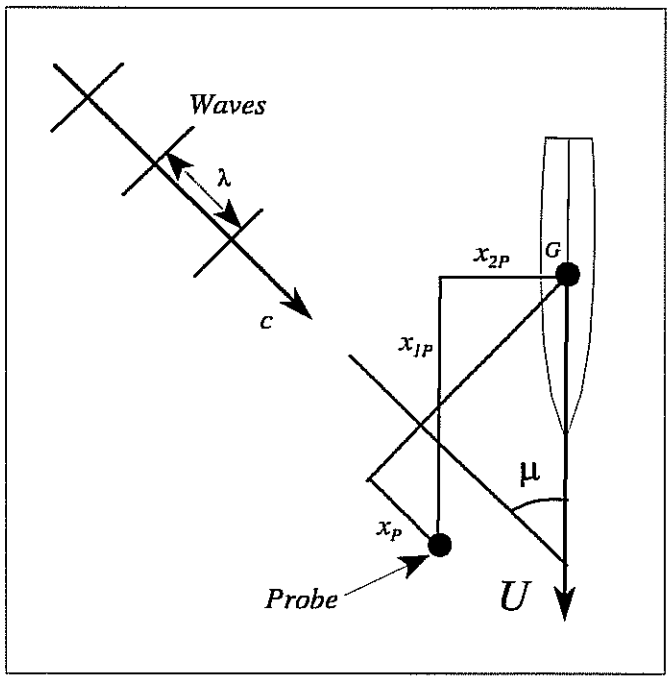

Fig 10.15 - Calculation of phase shift due to wave probe location

10.9.2 Effects of wave reflections

It was explained in Section 10.5 that all beaches reflect a certain amount of wave energy and that these reflections will eventually spoil the characteristics of the waves generated by the wave maker. Model experiments run in these contaminated waves will give misleading results. This problem can be avoided by careful attention to the timing of the experiment run in relation to the time at which the wave maker is started.

Consider the model in the experiment tank shown in Figure 10.16. It was shown in Chapter 1 that the main body of a group of waves having the proper wave amplitude propagates down the tank at the group velocity u_G. This is preceded by a secondary wave front of reduced amplitude travelling at the wave celerity c. The experiment run (ie that part of the model's run in which

measurements of its behaviour are recorded) must obviously be confined to the part of the tank which contains waves of the proper amplitude. In other words the model's responses should only be observed and recorded while the model is behind the advancing wave front WW. At the same time it is necessary to avoid taking measurements of the model's responses after it has encountered the initial wave disturbance RR reflected from the beach.

This may be analysed with the aid of the distance/time diagrams shown in Figure 10.17. In these diagrams x_T is the distance in metres from the wave maker and t is the time in seconds. The wave maker is started at $t = 0$ seconds and the model progresses 'down' the tank at a component velocity $U \cos \mu$ metres/second.

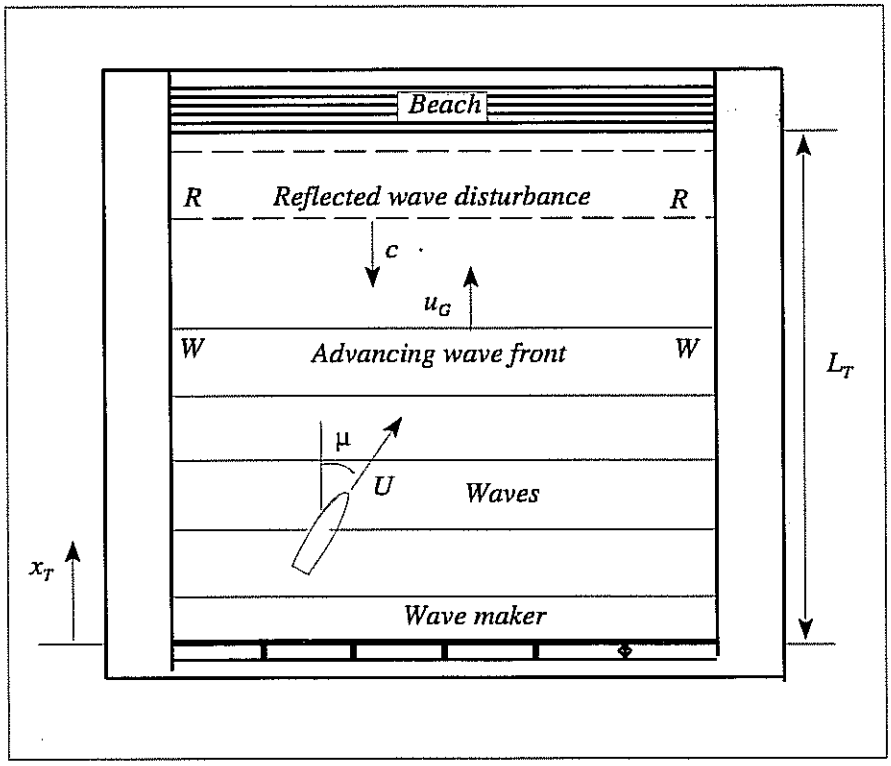

Fig 10.16 - Wave fronts and model location

The path of the initial wave disturbance is represented by the line OA with slope c metres/second. This initial disturbance will be reflected from the beach at time

$$t = t_L = \frac{L_T}{c} \quad sec \tag{10.31}$$

(where L_T is the effective length of the tank) and will arrive back at the wave maker at time

$$t = 2t_L \quad sec \tag{10.32}$$

The path of the "proper" wave front is represented by the line OB with slope u_G metres/second. Providing the tank depth is at least half the wave length the group velocity is half the celerity (see Equation 1.31) and the wave front reflects from the beach at time

$$t = 2t_L \quad sec \tag{10.33}$$

and arrives back at the wave maker at time

$$t = 4t_L \quad sec \tag{10.34}$$

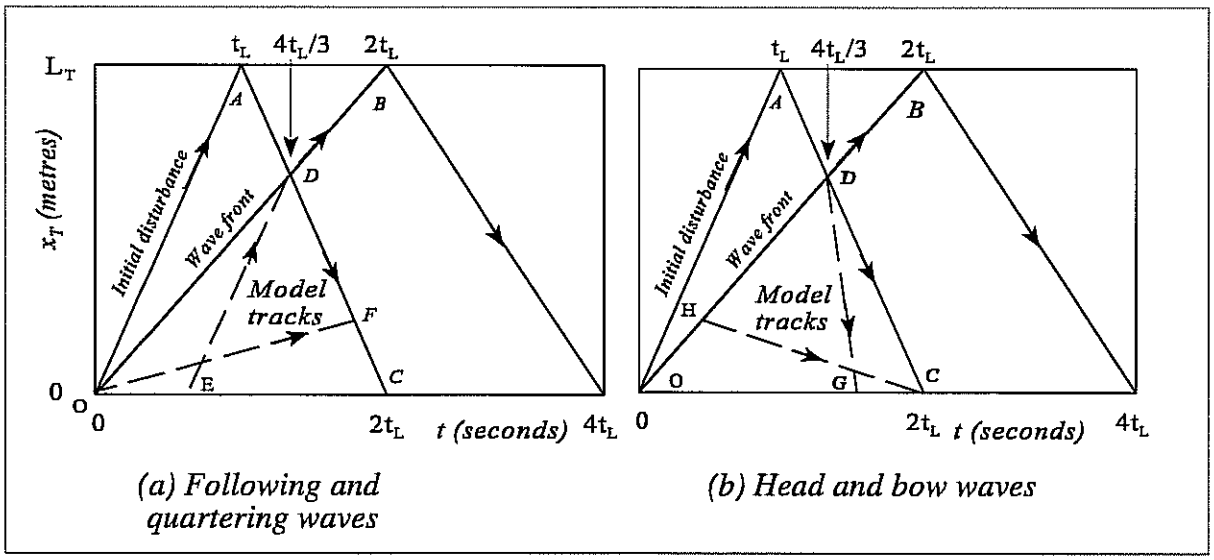

Fig 10.17 - Optimum experiment runs

When the model is at a location represented by a point above the line OB it will not be experiencing the proper wave amplitudes of the main body of waves. Similarly a model located at a position represented by a point above the line AC will be experiencing the unwanted reflected wave disturbance. It follows that the conditions outlined above for valid model test observations in regular waves are only experienced when the model's location is defined by points within the triangle ODC.

Let us first suppose that the model is to be tested in following or quartering waves and

$$U \cos \mu > u_G \quad m/sec$$

Ignoring the short distances needed to accelerate the model up to the required test speed and to bring it to rest at the end of the run, the model's progress down the tank can be represented as a line with a positive slope $U \cos \mu$ metres/second. The line may be positioned anywhere in the

diagram depending on the time chosen to start the experiment run, but the optimum location giving the longest run time is defined by the broken line ED in Figure 10.17(a). The run 'length' is given by

$$\frac{x_T}{L_T} = \frac{2}{3} \tag{10.35}$$

and this is achieved by starting the experiment observations at time

$$t = \frac{2L_T}{3}\left(\frac{2}{c} - \frac{1}{U\ cos\ \mu}\right) \quad sec \tag{10.36}$$

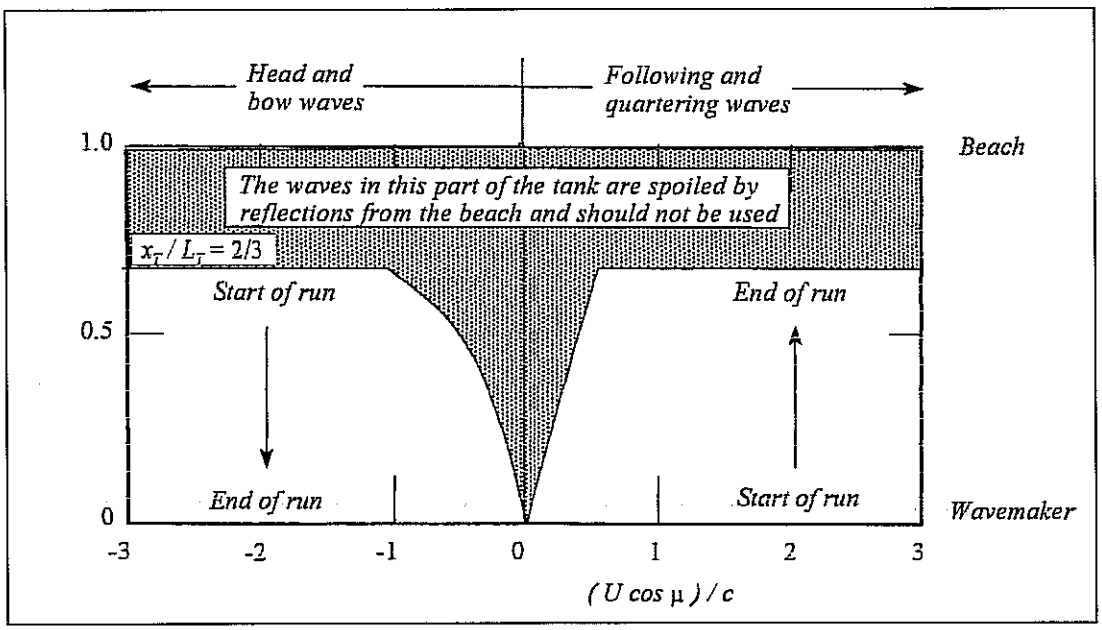

Fig 10.18 - Useful areas in a seakeeping basin

The run time is given by

$$T_H = \frac{x_T}{U\ cos\ \mu} = \frac{2L_T}{3U\ cos\ \mu} \quad sec \tag{10.37}$$

A similar analysis for the cases

$0 < U\ cos\ \mu < u_G$ (Following and quartering waves)

$0 > U\ cos\ \mu < -\ c$ (Head and bow waves)

$0 > U\ cos\ \mu > -\ c$ (Head and bow waves)

yields optimum tracks shown by the line OF in Figure 10.17(a) and the lines HC and DG in

Figure 10.17(b). Table 10.3 lists the run parameters and Figure 10.18 shows them in graphical form for all four cases. Even in the most favourable cases it can be seen that only two thirds of the tank length is available for testing.

TABLE 10.3
FORMULAE FOR EXPERIMENT PARAMETERS
TO AVOID WAVE REFLECTIONS

	Following and quartering waves $U\ cos\ \mu > 0$		Head and bow waves $U\ cos\ \mu < 0$	
	$U\ cos\ \mu > u_G$	$U\ cos\ \mu < u_G$	$U\ cos\ \mu > -c$	$U\ cos\ \mu < -c$
Model Track (see Figure 10.17)	ED	OF	HC	DG
Start position (metres from wave maker)	0	0	$\frac{2L_T\ U\ cos\ \mu}{2U\ cos\ \mu\ -\ c}$	$\frac{2L_T}{3}$
End position (metres from wave maker)	$\frac{2L_T}{3}$	$\frac{2UL_T\ cos\ \mu}{U\ cos\ \mu\ +\ c}$	0	0
Start time (seconds after wave maker)	$\frac{2L_T}{3}\left(\frac{2}{c}\ -\ \frac{1}{U\ cos\ \mu}\right)$	0	$\frac{4t_L\ U\ cos\ \mu}{2U\ cos\ \mu\ -c}$	$\frac{4t_L}{3}$
Run time T_H (seconds)	$\frac{2L_T}{3U\ cos\ \mu}$	$\frac{2L_T}{U\ cos\ \mu\ +\ c}$	$\frac{2L_T}{c\ -\ 2U\ cos\ \mu}$	$\frac{-\ 2L_T}{3U\ cos\ \mu}$

10.10 TESTING IN IRREGULAR WAVES

10.10.1 Wave spectrum

For experiments in irregular waves it is first necessary to scale the required wave energy spectral ordinates and frequencies using the scaling laws listed in Table 10.2:

$$S_{\zeta M}\ (\omega_M\ )\ =\ \frac{S_{\zeta S}\ (\omega_S)}{R\sqrt{R}} \qquad m^2/(rad/sec)$$

$$\omega_M = \omega_S\sqrt{R} \quad (rad/sec)$$

We require to drive the wave maker with an irregular electrical signal which will produce a train of irregular waves having this model wave spectrum. Treating the wave maker and its servo as a "black box" (see Figure 10.5) we may use the spectral calculation procedures described in Chapter 8 and write the wave energy spectrum as an equation analogous to Equation (8.4):

$$S_{\zeta M}(\omega_M) = S_V(\omega_M)\left(\frac{\zeta_0}{v_0}\right)^2 \quad m^2/(rad/sec) \tag{10.38}$$

where $\frac{\zeta_0}{v_0}$ is the wave maker transfer function in metres per volt. The drive signal spectrum is then given by

$$S_V(\omega_M) = S_{\zeta M}(\omega_M)\left(\frac{v_0}{\zeta_0}\right)^2 \quad volts^2/(rad/sec) \tag{10.39}$$

A suitable time history having the spectrum given by Equation (10.39) must then be constructed using the irregular wave synthesis techniques described in Chapter 2 (Equations (2.4) - (2.10)). Driving the wave maker with this signal would then be expected to produce a wave time history with the desired wave energy spectrum. In practice this simple technique may not give results of adequate accuracy. This is believed to be because the wave maker response suffers from poorly understood interactions between the many frequencies present in the irregular waves being generated. These interactions are absent when the wave maker is used to generate a single frequency regular wave. So the regular wave transfer function can only be regarded as a first approximation to that required to quantify the response in irregular waves. Moreover, the required transfer function apparently depends on the particular time history being generated and not just on the spectrum characteristics. So a different transfer function may be required for every new time history.

These difficulties can be overcome by empirical adjustments to the wave maker drive signal spectrum. Where the measured wave spectral ordinates are too low the drive signal spectral ordinates should be increased and vice versa. It is usually possible to achieve a good match to the desired wave spectrum with two or three adjustments of this kind.

10.10.2 Introducing the frequencies

Each component of the system of irregular waves will propagate down the tank at its own group velocity, preceded by an advance party of reduced amplitude waves of that frequency moving at the appropriate wave celerity. So the lowest frequency component, which has the highest group velocity and wave celerity, will overtake the rest of the waves and arrive at the end of the tank before the other frequency components. Clearly the 'complete' wave spectrum will not be experienced at a given location in the tank until the highest frequency component has arrived at that point. By this time the lowest frequency waves may well have been reflected from the beach and already be spoiling the waves propagating down the tank in the proper direction.

This can be avoided by introducing the frequency components to the wave maker drive signal (and hence to the generated waves) in descending order. The highest frequency is introduced first and subsequent components are included at times specified to ensure that all frequency components arrive simultaneously at some specified point in the tank.

Suppose that the required wave spectrum contains N frequency components

$$\omega_{1M} - \omega_{NM} \quad rad/sec$$

The wave component with the highest frequency ω_{NM} will propagate down the tank with the group velocity

$$u_{GN} = \frac{g}{2\omega_{NM}} \quad m/sec$$

and arrive at a point x_T metres from the wave maker at time

$$t = \frac{x_T}{u_{GN}} \quad sec \tag{10.40}$$

The nth wave component will take x_T / u_{Gn} seconds to arrive at this point and it is therefore necessary to delay its introduction into the wave time history until time

$$\begin{aligned} t_n &= x_T \left(\frac{1}{u_{GN}} - \frac{1}{u_{Gn}} \right) \\ &= \frac{2\,x_T}{g} \left(\omega_{NM} - \omega_{nM} \right) \quad sec \end{aligned} \tag{10.41}$$

The point x_T , at which the waves are required to coalesce, should be chosen to maximise the length of the tank available for the experiment. Reference to Figure 10.18 shows that for a given speed and heading the most critical conditions occur when the wave celerity is highest. In other words the available test length is small when the wave frequency is low.

So the lowest frequency in the wave spectrum will dictate the location of the coalescence point and this will also determine the permissible run time. This is illustrated in the following worked example.

Worked example

Consider a model to be tested in head waves (μ=180 °) in a ship tank with a usable length L_T = 100 metres. The model's dimension ratio is R = 36 and the model test speed is to represent a ship speed of 20 knots. The wave spectrum (at full scale) includes frequencies in the range 0.3-1.6 radians/second and this is to be represented by discrete frequency components at intervals of 0.1 radians/second at model scale.

It is required to find the optimum run time and start position for the test and the frequency component time lags for the wave maker drive signal.

The model component velocity is

$$U_M \cos \mu = \frac{U_S \cos \mu}{\sqrt{R}} = -3.3 \text{ knots} = -1.72 \text{ m/sec}$$

The lowest frequency component is

$$\omega_{M1} = \omega_1 \sqrt{R}$$

$$= 1.8 \quad \text{rad/sec}$$

and this will have the greatest celerity:

$$c_{M1} = \frac{g}{\omega_{M1}} = 5.45 \quad \text{m/sec}$$

TABLE 10.4

WAVE MAKER DRIVE SIGNAL LAGS FOR WORKED EXAMPLE

Frequency No n	Frequency ω_{Sn} (radians/second) (ship scale)	Frequency ω_{Mn} (radians/second) (model scale)	Lag t_n (seconds) (model scale)
1	0.3	1.8	10.3
2	0.4	2.4	9.5
3	0.5	3.0	8.7
4	0.6	3.6	7.9
5	0.7	4.2	7.1
6	0.8	4.8	6.3
7	0.9	5.4	5.5
8	1.0	6.0	4.7
9	1.1	6.6	3.9
10	1.2	7.2	3.2
11	1.3	7.8	2.4
12	1.4	8.4	1.6
13	1.5	9.0	0.8
N = 14	1.6	9.6	0.0

Now $0 > U_M \cos \mu > - c_{M1}$. Referring to Table 10.3 the start position is given by

$$x_T = \frac{2L_T \, U_M \cos \mu}{2U_M \cos \mu - c_{M1}} = 38.7 \quad m$$

(ie little more than one third of the tank is usable).

The run time is

$$T_{HM} = \frac{2L_T}{c_{M1} - 2U_M \cos \mu} = 22.5 \quad sec$$

corresponding to

$$T_{HS} = 22.5\sqrt{36} = 135 \; sec \quad \text{at ship scale}$$

The wave maker drive signal lags are derived using Equation (10.41) and are given in Table 10.4.

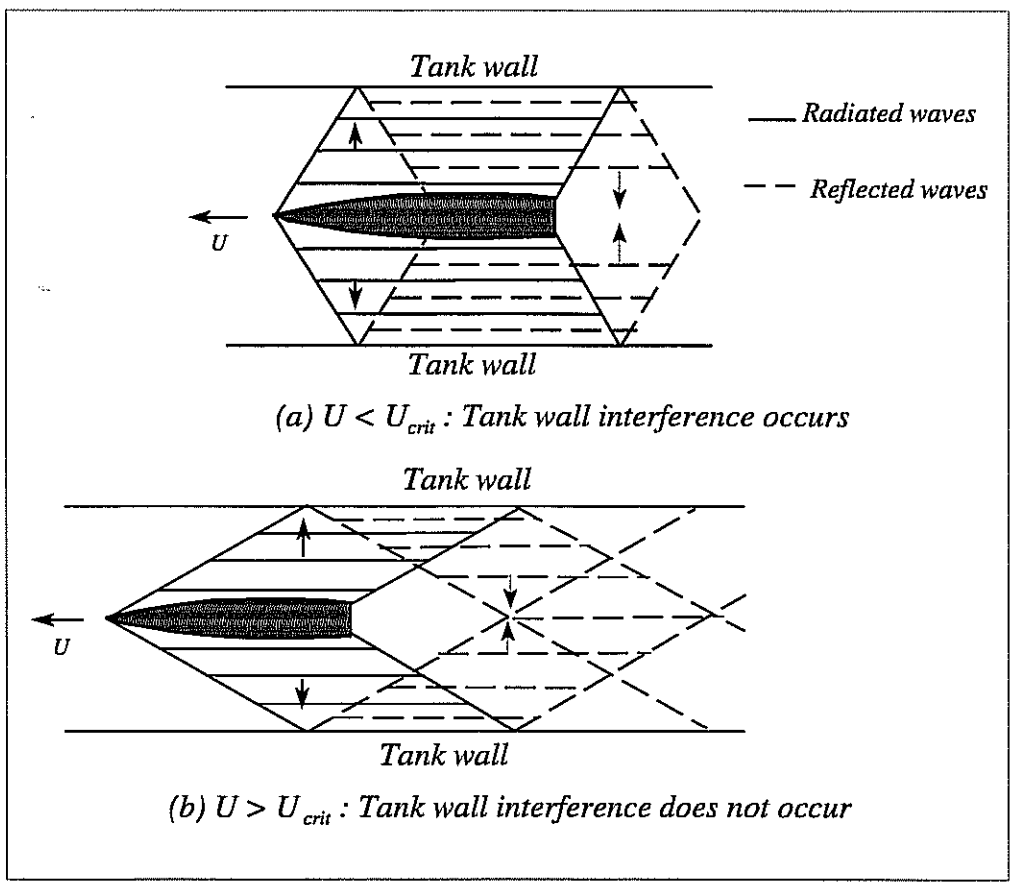

Fig 10.19 - Tank wall interference: radiated and reflected wave patterns.

10.11 TANK WALL INTERFERENCE

An oscillating model acts like a wave maker and radiates waves on either side. Indeed this is the mechanism responsible for dissipating energy and providing motion damping. The model will of course oscillate at the encounter frequency and the generated waves will radiate away from the model at the celerity appropriate to this frequency. The waves will eventually reach the tank walls and be reflected back towards the model, as shown in Figure 10.19. If the model speed is very low these reflected waves will return to the centre of the tank before the model has moved away, as shown in Figure 10.19(a). In this case the model's motions will be influenced by these reflected waves and misleading results will be obtained. If the model speed is high enough the reflections will reach the centre of the tank after the model has passed by and no interference occurs. The critical velocity at which tank wall interference occurs may be calculated as follows. Suppose that the model is running in head or following waves down the centre of a long narrow tank. The encounter frequency is then given by

$$\omega_e = \omega - \frac{\omega^2 U \cos \mu}{g} \quad rad/sec \tag{10.42}$$

where $\cos \mu$ is - 1 or + 1 depending on the model's heading. The celerity of the radiated waves is

$$c_e = \frac{g}{\omega_e} \quad m/sec \tag{10.43}$$

If we assume that the model beam is small compared with the tank width the time taken for the radiated wave to travel from the model to the tank wall and back again is approximately

$$t = \frac{B_T}{c_e} = \frac{B_T \omega_e}{g} \quad sec \tag{10.44}$$

where B_T is the width of the tank. Tank wall interference will occur if the model moves less than its own length in this time. In other words tank wall interference will occur if the model speed is less than a critical speed given by

$$U_{crit} = \frac{L}{t} \quad m/sec \tag{10.45}$$

Combining Equations (10.42) - (10.45) we find that the critical speed is

$$U_{crit} = \frac{g}{2 \omega \cos \mu} \left[1 \pm \sqrt{1 - 4 \cos \mu \frac{L}{B_T}} \right] \quad m/sec \tag{10.46}$$

In non dimensional form in head waves this becomes

$$F_{N\,crit} = -\frac{1}{2\omega}\sqrt{\frac{g}{L}}\left[1 - \sqrt{1 + \frac{4L}{B_T}}\right] \qquad (10.47a)$$

and in following waves

$$F_{N\,crit} = \frac{1}{2\omega}\sqrt{\frac{g}{L}}\left[1 \pm \sqrt{1 - \frac{4L}{B_T}}\right] \qquad (10.47b)$$

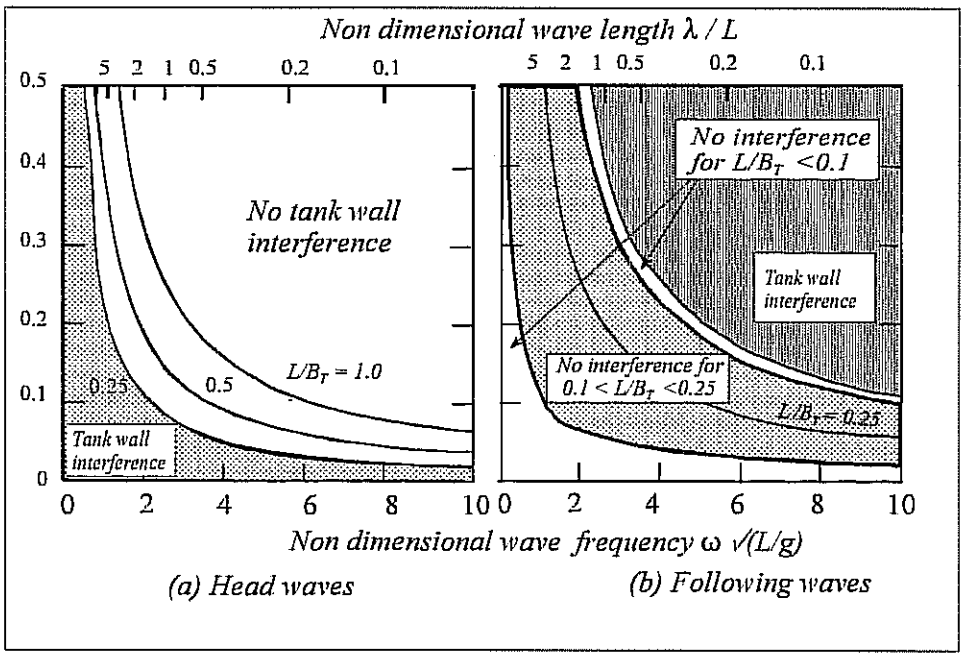

Fig. 10.20 - Tank wall interference diagrams showing permissible test speeds.

Figure 10.20(a) illustrates the relationship given by Equation (10.47a) for head waves. In this case the Froude number must be greater than $F_{N\,crit}$ to avoid tank wall interference: the critical Froude number increases with the length of the model and is very large for low frequencies (long waves).

Figure 10.20(b) shows the critical Froude number for model tests in following waves obtained from Equation (10.47b). In this case the Froude number must lie within a finite range to avoid interference and the range decreases as the model length increases. When the model length is one quarter of the width of the tank there is only one Froude number for each wave frequency that will give results which do not suffer from interference. Models of greater length will always experience tank wall interference whatever the Froude number or wave frequency. It follows that the maximum permissible model length for tests in following waves is one quarter of the width of the tank.

11

PROBABILITY FORMULAE

"There are three kinds of lies - lies, damned lies and statistics."

Quoted in Mark Twain's autobiography but also ascribed to others.

11.1 INTRODUCTION

In Chapters 2 and 8 it was shown that the irregular time histories of waves and ship motions could be characterised in terms of energy spectra and various statistical quantities like mean and rms values, zero crossing periods and so on. Seakeeping studies, however, often demand a more intimate knowledge of the characteristics of waves and motions. In particular the likelihood of a particular event occurring (such as a particular motion level being exceeded) is often of interest. Wave and ship motion time histories can be analysed to provide this sort of information.[1]

11.2 PROBABILITY ANALYSIS

Two methods of analysis of irregular time histories are commonly used. In the first the time history is analysed by reading discrete values of the record at set intervals of time (say every second) as shown in Figure 2.3.[2] This method can be used to find the probability or the ***proportion of time that the wave depression exceeds a particular level.***

Some of the measurements obtained in this way may, by chance, be peaks, troughs or zero crossings but they are not given any special significance. An alternative method of analysis is concerned only with these salient points in the record and is commonly used in many aspects of seakeeping work. Typically the analysis consists of measuring successive wave amplitudes and periods as defined in Figure 2.2. This technique is used to extract information on the ***probability of an individual peak or trough exceeding a given level.***

11.3 HISTOGRAMS

Whichever kind of analysis is used the results will consist of an apparently random sequence of measurements: these can be sorted according to their values into discrete ranges or histogram "***bins***".

---

[1] The analysis is presented in terms of the wave depression in metres, but applies equally well for ship motions with a change of units where appropriate. For example the probability density function f for pitch angle would have units radians $^{-1}$ or degrees^{-1}.

[2] Actually the discrete values may also be sampled at random time intervals.

TABLE 11.1

ANALYSIS OF A WAVE TIME HISTORY AT DISCRETE TIME INTERVALS

Histogram bin (metres)	Number of observations in each bin N_H	Probability of occurrence P	Probability density function ordinate f metres^{-1}
-3.5 to -3.0	0	0.000	0.000
-3.0 to -2.5	1	0.001	0.001
-2.5 to -2.0	3	0.002	0.003
-2.0 to -1.5	11	0.006	0.012
-1.5 to -1.0	23	0.013	0.026
-1.0 to -0.5	36	0.020	0.040
-0.5 to 0.0	71	0.039	0.079
0.0 to 0.5	122	0.068	0.136
0.5 to 1.0	180	0.100	0.200
1.0 to 1.5	210	0.117	0.233
1.5 to 2.0	240	0.133	0.267
2.0 to 2.5	250	0.139	0.278
2.5 to 3.0	210	0.117	0.233
3.0 to 3.5	172	0.096	0.191
3.5 to 4.0	120	0.067	0.133
4.0 to 4.5	75	0.042	0.083
4.5 to 5.0	37	0.021	0.041
5.0 to 5.5	20	0.011	0.022
5.5 to 6.0	9	0.005	0.010
6.0 to 6.5	5	0.003	0.006
6.5 to 7.0	4	0.002	0.004
7.0 to 7.5	1	0.001	0.001
7.5 to 8.0	0	0.000	0.000

Mean surface depression $\bar{\zeta} = 2.01$ m
Length of record: 1800 seconds
Time interval: 1 second

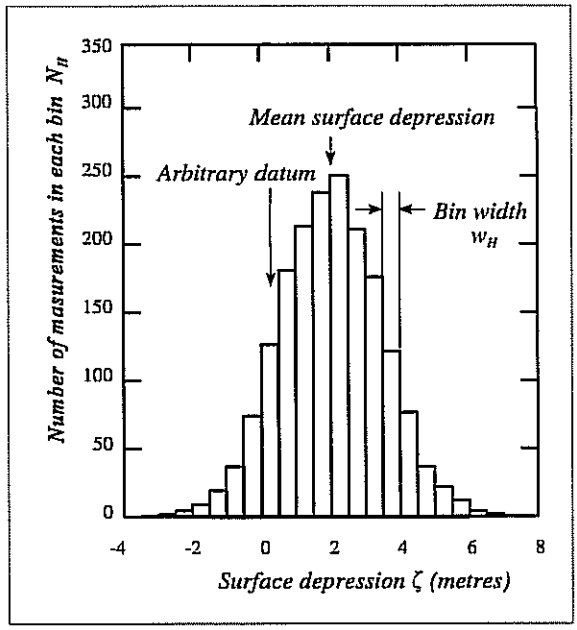

Fig 11.1 - Histogram of measurements of wave depression sampled at equal or random time intervals (Table 11.1).

TABLE 11.2

AMPLITUDE ANALYSIS OF WAVE TIME HISTORY

Histogram bin (metres)	Number of measurements of wave amplitude in each bin N_H	Probability of occurrence P	Probability density function f (metres $^{-1}$)
0.0 to 0.5	169	0.128	0.355
0.5 to 1.0	171	0.129	0.258
1.0 to 1.5	234	0.177	0.353
1.5 to 2.0	265	0.200	0.400
2.0 to 2.5	204	0.154	0.308
2.5 to 3.0	145	0.110	0.219
3.0 to 3.5	101	0.076	0.153
3.5 to 4.0	23	0.017	0.035
4.0 to 4.5	12	0.009	0.018
4.5 to 5.0	0	0.000	0.000
Mean wave amplitude $\bar{\zeta}_a$ = 1.7 metres			

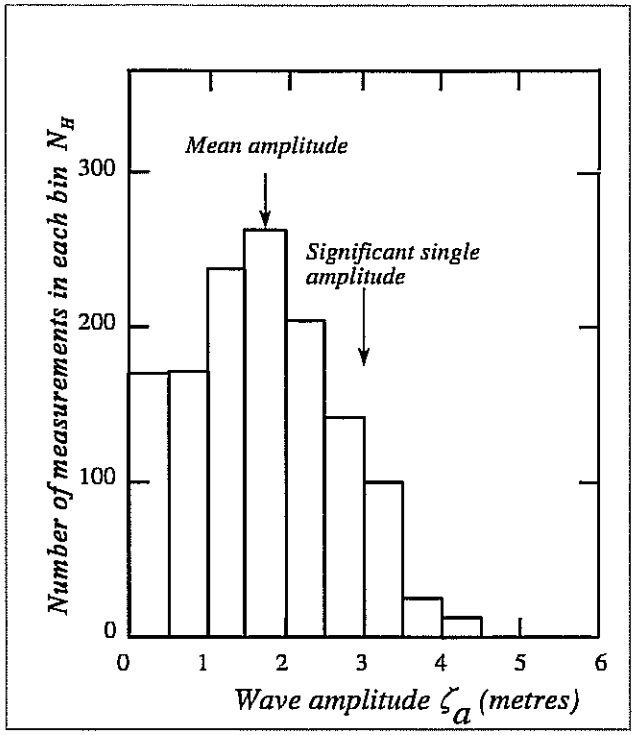

Fig 11.2 - Histogram of amplitudes (Table 11.2)

The total number of measurements (whether they be amplitudes or measurements obtained at fixed time intervals) is obtained by summing the observations in all the histogram bins:

$$N = \sum N_H \tag{11.1}$$

The probability of an individual measurement ζ lying in the range ζ_1 to ζ_2 is

$$P(\zeta_1 < \zeta < \zeta_2) = \frac{1}{N} \sum_{\zeta_1}^{\zeta_2} N_H \tag{11.2}$$

and the probability of an individual measurement ζ exceeding a given value ζ_1 is

$$P(\zeta > \zeta_1) = \frac{1}{N} \sum_{\zeta_1}^{\infty} N_H \tag{11.3}$$

TABLE 11.3

VALUES OF THE ERROR FUNCTION

$$erf(x) = \frac{1}{\sqrt{2\pi}} \int_0^x exp\left(-\frac{z^2}{2}\right) dz$$

x	$erf(x)$	x	$erf(x)$	x	$erf(x)$	x	$erf(x)$
0.00	0.000	1.00	0.341	2.00	0.477	3.00	0.499
0.05	0.020	1.05	0.353	2.05	0.480	3.05	0.499
0.10	0.040	1.10	0.364	2.10	0.482	3.10	0.499
0.15	0.060	1.15	0.375	2.15	0.484	3.15	0.499
0.20	0.079	1.20	0.385	2.20	0.486	3.20	0.499
0.25	0.099	1.25	0.394	2.25	0.488	3.25	0.499
0.30	0.118	1.30	0.403	2.30	0.489	3.30	0.500
0.35	0.137	1.35	0.412	2.35	0.491	3.35	0.500
0.40	0.155	1.40	0.419	2.40	0.492	3.40	0.500
0.45	0.174	1.45	0.427	2.45	0.493	3.45	0.500
0.50	0.192	1.50	0.433	2.50	0.494	3.50	0.500
0.55	0.209	1.55	0.439	2.55	0.495	3.55	0.500
0.60	0.226	1.60	0.445	2.60	0.495	3.60	0.500
0.65	0.242	1.65	0.451	2.65	0.496	3.65	0.500
0.70	0.258	1.70	0.455	2.70	0.497	3.70	0.500
0.75	0.273	1.75	0.460	2.75	0.497	3.75	0.500
0.80	0.288	1.80	0.464	2.80	0.497	3.80	0.500
0.85	0.302	1.85	0.468	2.85	0.498	3.85	0.500
0.90	0.316	1.90	0.471	2.90	0.498	3.90	0.500
0.95	0.329	1.95	0.474	2.95	0.498	3.95	0.500

The mean value of all the observations is given by

$$\bar{\zeta} = \frac{\sum \zeta}{N} \approx \frac{\sum_{-\infty}^{\infty} \zeta_H N_H}{N} \tag{11.4}$$

where ζ_H corresponds to the centre of each histogram bin of width w_H.

Tables 11.1 and 11.2 and Figures 11.1 and 11.2 show mean values of surface depression and wave amplitude obtained from Equation (11.4).

It is almost invariably found in seakeeping analysis that the histograms have peaks close to the calculated mean value. In other words observations close to the mean value are very common. The histogram of Figure 11.1 also shows the characteristic bell shaped symmetry about the mean value obtained from measurements at regular time intervals: large deviations from the mean are rare. The typical amplitude histogram (Figure 11.2) is not symmetrical about the mean: small amplitudes are more common than large ones.

11.4 THE PROBABILITY DENSITY FUNCTION.

The histogram has one major disadvantage: the ordinates (the numbers of observations in each bin) depend on the record length and the width of the histogram bins and this complicates comparisons between different results. The ***probability density function*** (PDF) is a form of histogram which eliminates this dependency on record length and bin width. The PDF is defined such that the area enclosed by the PDF curve over a bin is equivalent to the probability of the measurement falling within that bin.

If f is the probability density function ordinate and w_H is the width of the bin

$$f\, w_H = P = \frac{N_H}{N} \tag{11.5}$$

and the PDF ordinate is

$$f = \frac{P}{w_H} = \frac{N_H}{N\, w_H} \quad m^{-1} \tag{11.6}$$

The probabilities defined in Equations (11.2) and (11.3) can now be written as

$$P(\zeta_1 < \zeta < \zeta_2) = w_H \sum_{\zeta_1}^{\zeta_2} f \tag{11.7}$$

and

$$P(\zeta > \zeta_1) = w_H \sum_{\zeta_1}^{\infty} f \tag{11.8}$$

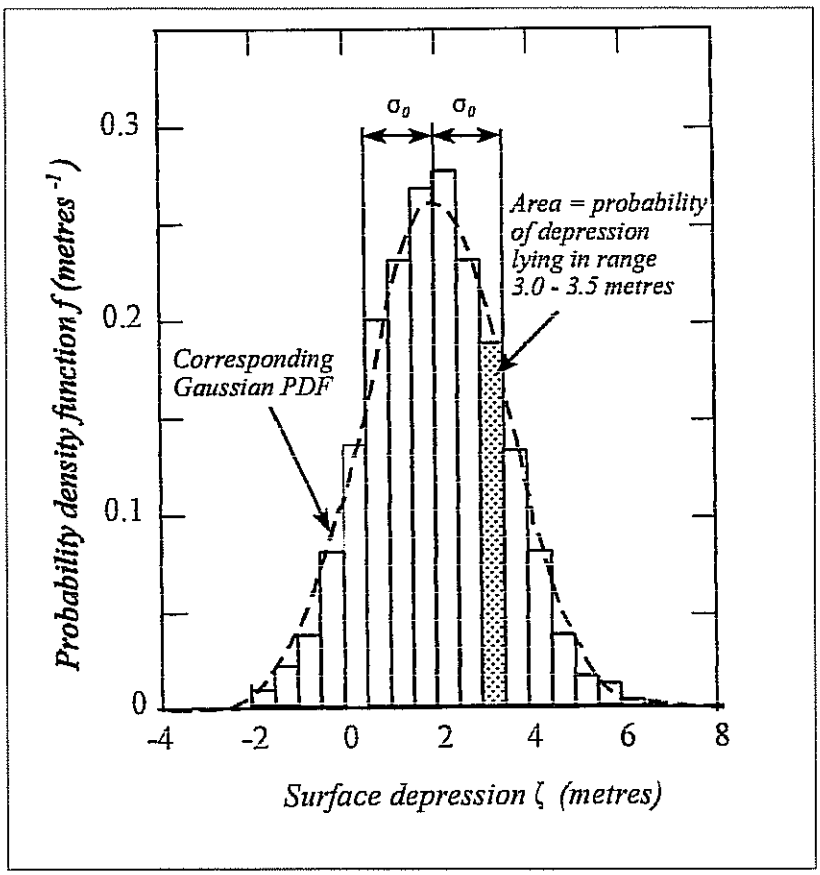

Fig 11.3 - Probability density function for measurements at regular or random time intervals (Table 11.1)

The total area under the PDF is equivalent to the probability that an individual measurement will lie within the range of all the measurements:

$$P(-\infty < \zeta < \infty) = w_H \sum_{-\infty}^{\infty} f = 1.0 \tag{11.9}$$

The mean surface depression is now given approximately by

$$\bar{\zeta} = w_H \sum_{-\infty}^{\infty} \zeta_H f \qquad (11.10)$$

Probability density function ordinates corresponding to the histograms already discussed are given in Tables 11.1 and 11.2. They are illustrated in Figures 11.3 and 11.4. The results are exactly the same shape as the histograms: all the ordinates have simply been reduced in the ratio $1/(Nw_H)$.

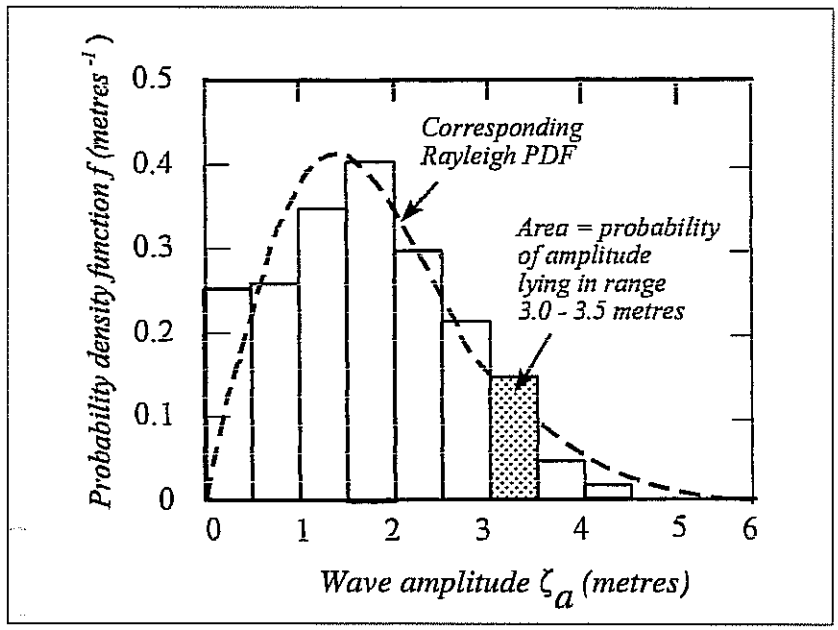

Fig 11.4 - Probability density function for amplitudes (Table 11.2).

The probability density function defined in this way is discontinuous with a finite number of bins and ordinates. If the bin width is reduced the number of ordinates is increased and if the record is of sufficient length the PDF will gradually tend towards a continuous smoothly varying curve. The probabilities defined earlier now become

$$P(\zeta_1 < \zeta < \zeta_2) = \int_{\zeta_1}^{\zeta_2} f \, d\zeta \qquad (11.11)$$

$$P(\zeta > \zeta_1) = \int_{\zeta_1}^{\infty} f \, d\zeta \qquad (11.12)$$

and the total area under the continuous PDF curve is unity:

$$P(-\infty < \zeta < \infty) = \int_{-\infty}^{\infty} f \, d\zeta = 1.0 \qquad (11.13)$$

11.5 THE GAUSSIAN OR NORMAL PROBABILITY DENSITY FUNCTION.

It is usually found that the probability density function for measurements of the wave depression ζ ***sampled at random or at regular time intervals*** is closely approximated by the Gaussian or Normal Distribution formula:

$$f = \frac{1}{\sqrt{2 \pi m_0}} \exp\left(\frac{-(\zeta - \bar{\zeta})^2}{2 m_0}\right) \quad m^{-1} \qquad (11.14)$$

where m_0 and $\bar{\zeta}$ are the variance and mean value of the time history as defined in Equations (2.1) and (2.2). This convenient result means that the PDF for a regularly sampled wave record can be estimated if the mean and variance are known.

As an example, Figure 11.3 shows the Gaussian PDF obtained for the wave time history analysed in Table 11.1.

In practice it is usual to arrange for the mean value $\bar{\zeta}$ to be zero by making the arbitrary datum for the measurements the same as the mean value and Equation (11.14) becomes

$$f = \frac{1}{\sqrt{2 \pi m_0}} \exp\left(\frac{-\zeta^2}{2 m_0}\right) \quad m^{-1} \qquad (11.15)$$

The probability that an individual measurement will lie within the range ζ_1 to ζ_2 is now given by

$$P(\zeta_1 < \zeta < \zeta_2) = \frac{1}{\sqrt{2 \pi m_0}} \int_{\zeta_1}^{\zeta_2} \exp\left(\frac{-\zeta^2}{2 m_0}\right) d\zeta \qquad (11.16)$$

$$= \frac{1}{\sqrt{2 \pi}} \int_{\zeta_1/\sigma_0}^{\zeta_2/\sigma_0} \exp\left[-\frac{1}{2}\left(\frac{\zeta}{\sigma_0}\right)^2\right] \frac{d\zeta}{d\sigma_0} = erf\left(\frac{\zeta_2}{\sigma_0}\right) - erf\left(\frac{\zeta_1}{\sigma_0}\right)$$

where the error function is defined as

$$erf\ (\ x\ ) = \frac{1}{\sqrt{2\ \pi}} \int_0^x exp\left(\frac{-z^2}{2}\right)\ dz \qquad (11.17)$$

and is tabulated in Table 11.3. The error function has the properties

$$erf\ (\ -\ x\ ) = -\ erf\ (\ x\ ) \qquad (11.18)$$

and

$$erf\ (\ -\ \infty\ ) = -\ erf\ (\ \infty\ ) = -\ 0.5 \qquad (11.19)$$

so that the probability of an individual measurement ζ exceeding a given positive level ζ_1 is

$$P\ (\ \zeta > \zeta_1\ ) = erf\ (\ \infty\ ) - erf\left(\frac{\zeta_1}{\sigma_0}\right) = 0.5 - erf\left(\frac{\zeta_1}{\sigma_0}\right) \qquad (11.20)$$

Note that Equation (11.20) refers to positive values and relates only to one side of the

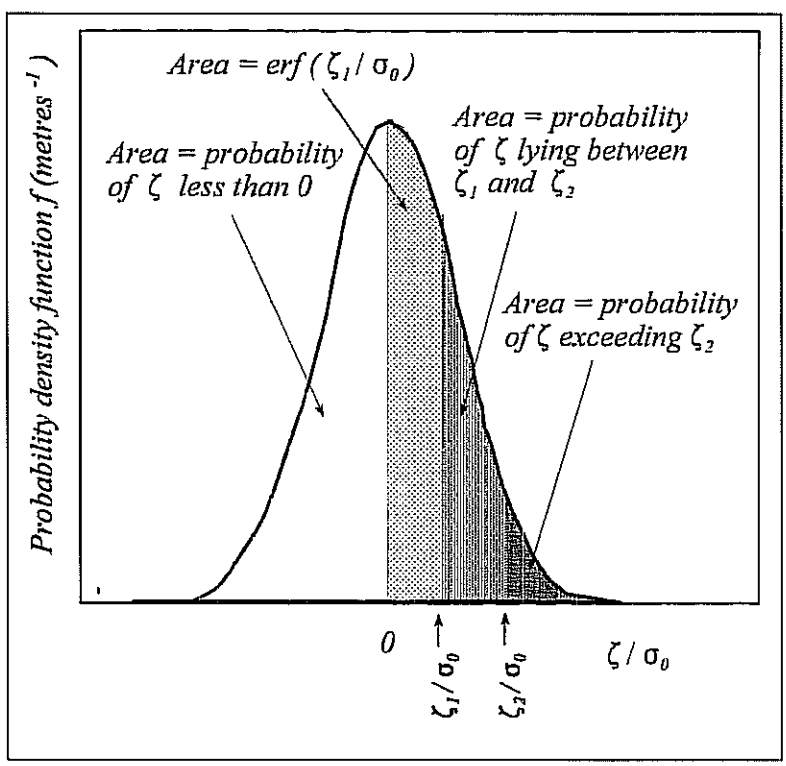

Fig 11.5 - Properties of the Gaussian probability density function

Gaussian probability density function. The probability of an individual measurement lying outside the range $\pm \zeta_1$ is given by

$$P\ (|\zeta| > \zeta_1\ ) = 1 - 2\ erf\left(\frac{\zeta_1}{\sigma_0}\right) \qquad (11.21)$$

The probability that an individual measurement will lie within the total range of all measurements is

$$P\ (\ -\infty < \zeta < \infty) = erf\ (\infty) - erf\ (-\infty) = 1.0 \qquad (11.22)$$

These properties are illustrated in Figure 11.5. Table 11.4 lists some of the salient properties of the Gaussian PDF based on Equations (11.20) and (11.21). From these results it can be seen that about 95% of all measurements obtained from a regularly sampled wave record will lie within twice the rms value.

TABLE 11.4

GAUSSIAN PROBABILITY FORMULA: PROBABILITIES OF AN INDIVIDUAL MEASUREMENT OF WAVE DEPRESSION ζ EXCEEDING A GIVEN VALUE ζ_1

$\frac{\zeta_1}{\sigma_0}$	Probability of exceeding ζ_1	Probability of exceeding $\pm\zeta_1$
0.0	0.500	1.00
0.5	0.308	0.616
1.0	0.159	0.318
1.5	0.067	0.134
2.0	0.023	0.046
2.5	0.006	0.012
3.0	0.001	0.002

The mean value of all the upward or downward observations in the record can be obtained from

$$|\bar{\zeta}| = \frac{\int_0^\infty \zeta\, f\, d\zeta}{\int_0^\infty f\, d\zeta} = 2\int_0^\infty \zeta\, f\, d\zeta = 0.798\sqrt{m_0} \quad m \qquad (11.23)$$

11.6 THE RAYLEIGH PROBABILITY DENSITY FUNCTION

It is usually found and invariably assumed that the probability density function for ***wave amplitudes*** is closely approximated by the ***Rayleigh*** distribution formula:

$$f = \frac{\zeta_a}{m_0}\, exp\left(\frac{-\zeta_a^2}{2\, m_0}\right) \quad m^{-1} \qquad (11.24)$$

where m_0 is the variance of the time history defined in Equation (2.2). This convenient result allows the amplitude PDF to be estimated if the variance of the wave depression is known. The Rayleigh PDF for the wave time history analysed in Table 11.2 is shown in Figure 11.4.

The probability that an individual measurement of amplitude ζ_a will lie within the range ζ_{a1} to ζ_{a2} is given by

$$P(\zeta_{a1} < \zeta_a < \zeta_{a2}) = \frac{1}{m_0}\int_{\zeta_{a1}}^{\zeta_{a2}} \zeta_a\, exp\left(-\frac{\zeta_a^2}{2\, m_0}\right) d\zeta_a$$
$$= exp\left(-\frac{\zeta_{a2}^2}{2\, m_0}\right) - exp\left(-\frac{\zeta_{a1}^2}{2\, m_0}\right) \qquad (11.25)$$

and the probability that the amplitude will exceed a given level ζ_{a1} is

$$P(\zeta_a > \zeta_{a1}) = \frac{1}{m_0}\int_{\zeta_{a1}}^{\infty} \zeta_a\, exp\left(-\frac{\zeta_a^2}{2\, m_0}\right) d\zeta_a$$
$$= exp\left(-\frac{\zeta_{a1}^2}{2\, m_0}\right) = exp\left[-\frac{1}{2}\left(\frac{\zeta_{a1}}{\sigma_0}\right]^2\right) \qquad (11.26)$$

and this function is plotted in Figure 11.6. Again, the probability that an individual amplitude will lie within the total range of all the measurements is unity:

$$P(-\infty < \zeta_a < \infty) = \frac{1}{m_0} \int_{-\infty}^{\infty} \zeta_a \, exp\left(-\frac{\zeta_a^2}{2\, m_0}\right) d\zeta_a \qquad (11.27)$$

$$= 1.0$$

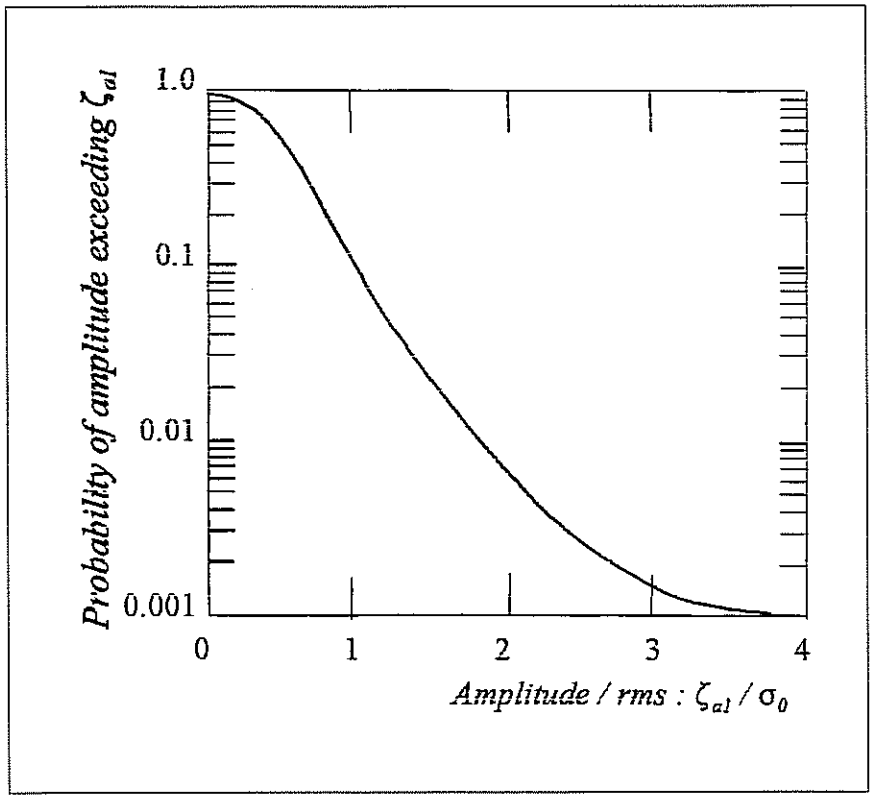

Fig 11.6 Probability of exceeding a given amplitude: (Rayleigh formula: Equation (11.26))

Equation (11.26) can be rewritten to give the amplitude which has a given probability of being exceeded:

$$\zeta_a = \sqrt{-2\, m_0\, log_e\, [P(\zeta_a > \zeta_{al})]} \quad m \qquad (11.28a)$$

or

$$\frac{\zeta_a}{\sigma_0} = \sqrt{-2\ log_e\ [P(\zeta_a > \zeta_{al})]}$$

$$= \sqrt{-4.605\ log_{10}\ [P(\zeta_a > \zeta_{al})]} \qquad (11.28b)$$

Table 11.5 gives some sample results from Equations (11.26) and (11.28). From these results it can be seen that the probability of an individual amplitude exceeding about three times the rms value is very small: only about one peak (or trough) in every hundred would be expected to exceed this level.

If the average zero crossing period is $\overline{T_z}$ seconds (see Equation (2.28)) it follows that the level ζ_{al} is exceeded M times per minute where:

$$M = \frac{60}{\overline{T_z}}\ exp\left(-\frac{\zeta_{al}^2}{2\ m_0}\right) \quad min^{-1} \qquad (11.29)$$

TABLE 11.5

RAYLEIGH PROBABILITY FORMULA:
PROBABILITY OF AN INDIVIDUAL AMPLITUDE ζ_a
EXCEEDING A GIVEN AMPLITUDE ζ_{al}

$\frac{\zeta_{al}}{\sigma_0}$	Probability of exceedance P		Probability of exceedance P	$\frac{\zeta_{al}}{\sigma_0}$
0.0	1.000		1.000	0.00
0.5	0.882		0.500	1.18
1.0	0.606		0.333	1.48
1.5	0.325		0.100	2.15
2.0	0.135		0.010	3.03
2.5	0.044		0.001	3.72
3.0	0.011		0.0001	4.29
3.5	0.002			
4.0	0.0003			

11.7 SIGNIFICANT WAVE HEIGHT AND RELATED STATISTICS.

It was shown in Chapter 2 that the significant wave height, defined as the mean of the highest third of the heights recorded in a wave time history, was closely related to the average wave height estimated visually by an experienced observer. In the same way it might be expected that the experienced sailor's estimates of "average" ship motions might be similar to their significant amplitudes. Interest is therefore often centred on these quantities.

In more general terms an expression is required for the mean value of the highest $1/n$ th of all observations of amplitudes (where $n = 3$ for significant values). If the probability density function is known the required amplitude $\bar{\zeta}_{1/n}$ is given by the moment of area of the shaded portion shown in Figure 11.7. The shaded area is, of course, equal to $1/n$.

If the PDF is given by the Rayleigh formula (Equation (11.24)) the amplitude $\bar{\zeta}_{1/n}$ (which is exceeded with a probability $1/n$ or once in n amplitudes) is given by Equation (11.28a):

$$\zeta_{1/n} = \sqrt{-2\, m_0\, log_e \left(\frac{1}{n}\right)} \quad m \tag{11.30}$$

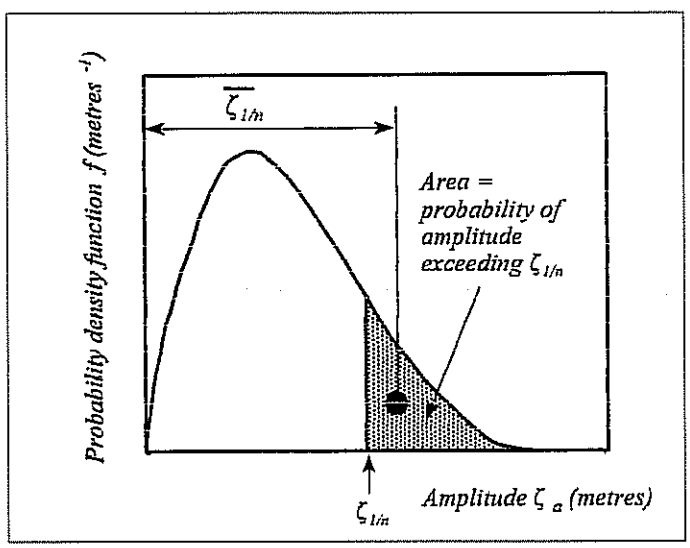

Fig 11.7 - Calculation of mean of the highest 1/n amplitudes.

If the PDF is given by the Rayleigh formula (Equation (11.24)), Equation (11.31) becomes

$$\bar{\zeta}_{1/n} = n \int_{1/n}^{\infty} \frac{\zeta_a^2}{m_0} \exp\left(-\frac{\zeta_a^2}{2\, m_0}\right) d\zeta_a \quad m$$

so

$$\frac{\bar{\zeta}_{1/n}}{\sigma_0} = n\sqrt{2}\left[\frac{\sqrt{\log_e n}}{n} + \sqrt{\pi}\left(\frac{1}{2} - erf\sqrt{2\log_e n}\right)\right] \qquad (11.32)$$

Selected results are given in Table 11.6. Of particular interest are the results for $n = 1$ and $n = 3$:

Putting $n = 1$ gives the mean value of all amplitudes:

$$\bar{\zeta}_a = 1.25\ \sigma_0 \quad m \qquad (11.33)$$

Putting $n = 3$ gives the significant single amplitude:

$$\bar{\zeta}_{1/3} = 2.00\ \sigma_0 \quad m \qquad (11.34)$$

and the significant height is

$$\bar{H}_{1/3} = 2.00\ \bar{\zeta}_{1/3} = 4.00\ \sigma_0 \quad m \qquad (11.35)$$

These results are widely assumed to apply to all wave records and ship motions. It should, however, be remembered that they are strictly only true if the Rayleigh formula (Equation 11.24) holds.

TABLE 11.6

MEAN OF THE HIGHEST 1/*n* AMPLITUDES
(RAYLEIGH FORMULA)

n	$\frac{\bar{\zeta}_{1/n}}{\sigma_0}$		n	$\frac{\bar{\zeta}_{1/n}}{\sigma_0}$
1	1.25		10	2.54
2	1.77		100	3.34
3	2.00*		1000	3.72
			10000	4.29

* Significant value

11.8 JOINT PROBABILITIES

In some seakeeping studies interest is centred on the probability of two events occurring simultaneously. If the two events are independent the probability of them both occurring is simply the product of the probabilities of each individual event occurring in isolation.

If the probabilities are given by the Rayleigh formula (Equation (11.26)) the probability of motion x_i exceeding some level x_{i1} at the same time as motion x_j exceeds some level x_{j1} is

$$P\ (\ x_i > x_{i1} \text{ and } x_j > x_{j1}\ ) = exp\left(-\frac{x_{i1}^2}{2\ m_{0\,i}}\right)\ exp\left(-\frac{x_{j1}^2}{2\ m_{0\,j}}\right)$$

$$= exp\left(-\frac{x_{i1}^2}{2\ m_{0\,i}} - \frac{x_{j1}^2}{2\ m_{0\,j}}\right) \qquad (11.36)$$

where m_{0i} and m_{0j} are the variances of the respective motions.

12

ROLL STABILISATION

12.1 MOTION REDUCTION.

If motions are an undesirable feature of the behaviour of a ship in rough weather it is natural to consider ways of reducing them. Methods of motion reduction are often known by the generic name of motion "stabilisation" although it should be understood that this is usually an incorrect use of the word. The oscillatory motions of all practical conventional ship designs are already "stable" in that they can generally be expected to return to an equilibrium datum level after some small disturbance: this is ensured by the stiffness terms in the equations of motion. The term "stabilisation" implies an increase in the stiffness coefficients like c_{44} but almost every practical motion stabilisation device achieves most of its motion reduction by increasing the motion damping (coefficients like b_{44} in Equation (3.22d)). They should therefore more correctly be called motion dampers. However, the term stabilisation is so widely used that the adoption of more pedantic terminology for this book would be confusing and will be avoided.

In principle, stabilisation is possible for any motion. It is simply necessary to provide some means (active or passive) of artificially increasing the damping terms in the appropriate equation of motion. We have already seen that certain ship motion responses can be approximately represented by the simple second order spring mass system. The possibility of motion reduction may be nicely illustrated by considering the response shown for such a system in Figure A1.3. If the damping is very small the system's amplitude response is very high at frequencies close to the natural frequency. With random excitation (as in the case of a ship at sea) most of the resulting motions will be experienced at frequencies close to this frequency.

Increasing the dampimg reduces these motions and Equation (A1.11) shows that doubling the decay coefficient η will halve the amplitude at the natural frequency. However this is only effective if the inherent damping is small. For very high initial values of the decay coefficient the maximum motion amplitudes occur at zero frequency rather than at the natural frequency and increasing the damping then has little effect. So motion stabilisation is only likely to be effective if the inherent damping of the unstabilised system is small. Practical considerations also demand that the damping force or moment required of the stabilisation system must be relatively small so that an effective degree of stabilisation can be achieved without the need for massive engineering.

Roll is the only motion which meets these two requirements of low inherent damping and relatively small stabilisation moment demands. Roll stabilisation has therefore received considerable attention and many successful systems have been installed in ships in service.

Pitch and heave stabilisation have received some attention and some success has been claimed for small craft. However the inherent damping is usually already so high and the required forces and moments so large that practical systems for ships remain an elusive goal.

12.2 BILGE KEELS

Bilge keels are the simplest form of roll stabilisation device. These are long narrow keels mounted at the turn of the bilge as shown in Figure 12.1 Gaps may be left in the bilge keels to accommodate active fin roll stabilisers if required.

Bilge keels are very effective and work well especially at low speeds. They have the significant advantage that they have no moving parts and require no maintenance beyond that normally given to the hull surface. Their only disadvantage is that they increase the resistance of the ship but the effects can be minimised by aligning the keels with the flow streamlines around the bilges. This is usually done using some kind of flow visualisation technique on a model during the design stage. Correct alignment can only be achieved at one speed (the cruising speed is usually chosen) but the resistance penalty at other speeds is usually small.

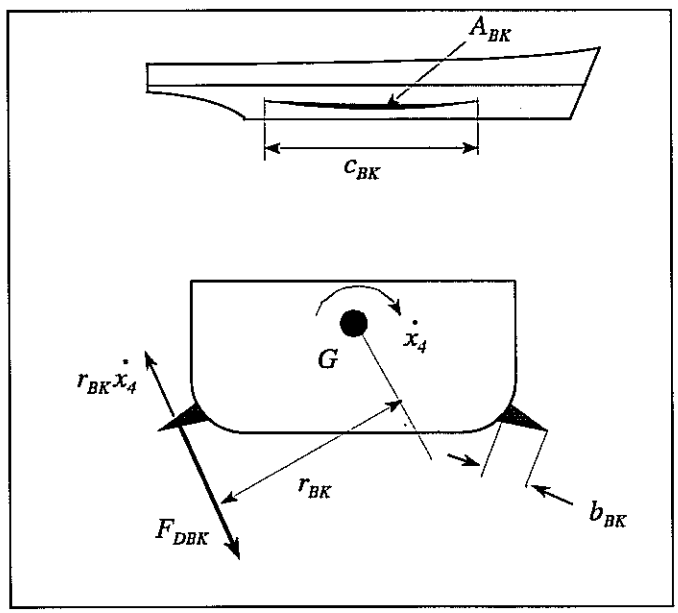

Fig 12.1 - Bilge keel notation

Bilge keels work by generating drag forces which oppose the rolling motion of the ship. The mechanism is similar to that shown for appendages at zero speed in Figure 6.5. The linearised roll damping coefficient is given by Equation (6.10). It remains to determine suitable values of the drag coefficient C_D for bilge keels. Cox and Lloyd (1977) cited experimental data published by Martin (1958) and Ridjanovic (1962).This is presented (in slightly different form) in Figure 12.2. The normal force coefficient is given as a function of the equivalent aspect ratio

$$a_{BK} = \frac{2b_{BK}}{c_{BK}} \tag{12.1}$$

and the non dimensional bilge keel radius parameter

$$r' = \frac{r_{BK}\,\bar{x}_{40}}{\sqrt{A_{BK}}} \tag{12.2}$$

where the radius r_{BK} is defined as the distance from the centre of gravity to the normal through the mid point of the bilge keel as shown in Figure 12.1. r_{BK} is usually evaluated at the mid length of the bilge keel.

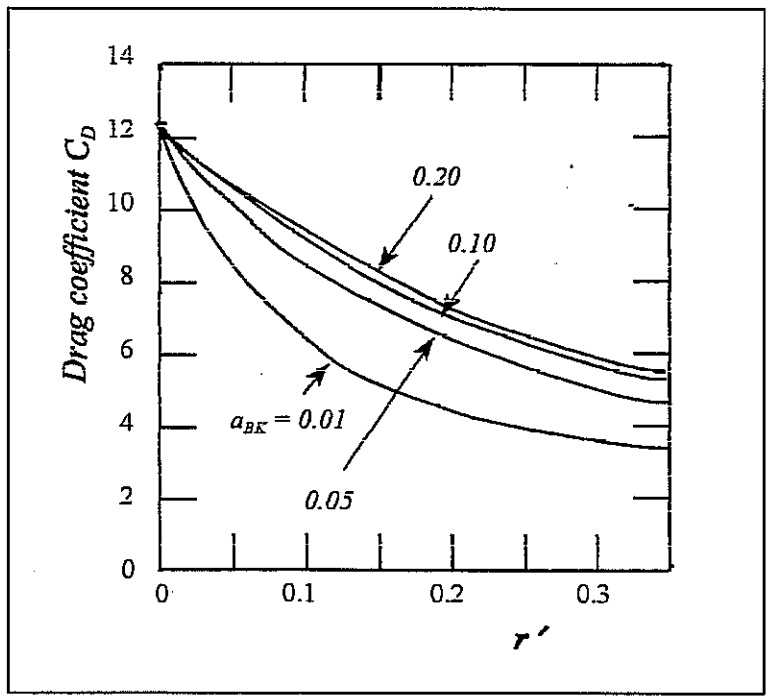

Fig 12.2 - Bilge keel drag coefficients (After Martin (1958) and Ridjanovic (1972))

The results may be expressed in the form

$$C_D = 0.849 \left(\frac{I}{r'} \left[1 - exp\,(- K\, r')\right] + J \right) \tag{12.3}$$

where

$$I = \frac{14.66 - J}{K} \tag{12.4}$$

$$J = 2.37 - 5.33\, a_{BK} + 10.35\, a_{BK}^2 \tag{12.5}$$

$$K = \frac{1}{\sqrt{a_{BK}}\,(\,14.66 - J\,)\,(\,0.0386 - 0.0735\, a_{BK}\,)} \tag{12.6}$$

Figure 12.3 shows the benefits of increasing the bilge keel aspect ratio. A short wide bilge keel is more effective than a long narrow bilge keel for the same bilge keel area.

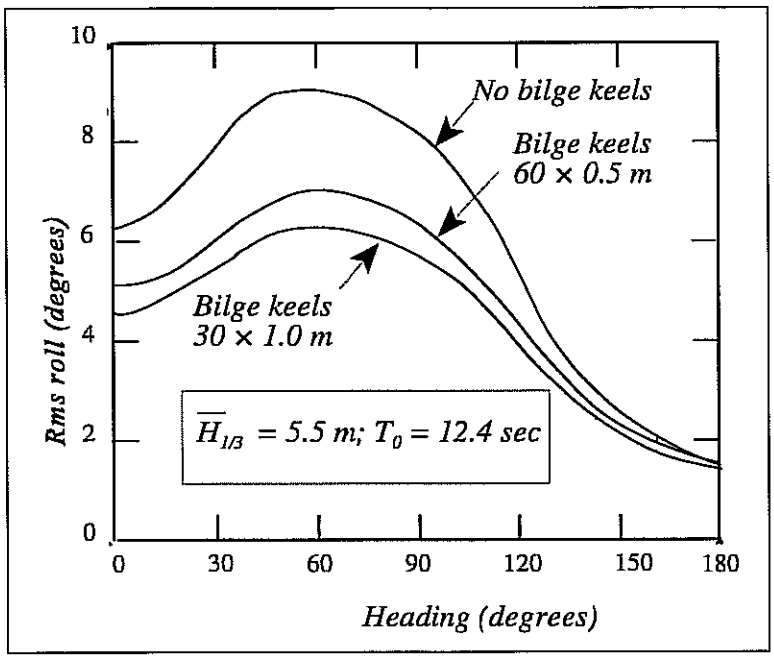

Fig 12.3 - Effect of bilge keel aspect ratio on the roll motions of the frigate at 20 knots.

12.3 ACTIVE ROLL STABILISER FINS.

Active roll stabiliser fins are usually mounted on rotatable stocks at the turn of the bilge near the middle of the ship as shown in Figure 12.4. The angle of incidence of the fins is continually adjusted by a control system which is sensitive to the rolling motion of the ship. The fins develop lift forces which exert roll moments about the centre of gravity of the ship. These roll moments are arranged to oppose the moment applied by the waves and the roll motion is reduced.

At speeds above 10 - 15 knots active fins are usually the most effective method of stabilising a ship. Reductions in rms roll motion of at least 50% are often possible in moderate waves with a well designed system. However the fins become progressively less effective as the speed is reduced and they are not usually specified for ships which habitually operate at low speed. It should also be understood that fins have a limited capacity and their ability to reduce roll motion decreases in very severe sea states. They are relatively sophisticated and expensive pieces of equipment and require considerable maintenance. Nevertheless, their ability to work well over a wide range of conditions has earned them almost universal acceptance and they are now fitted to many ships.

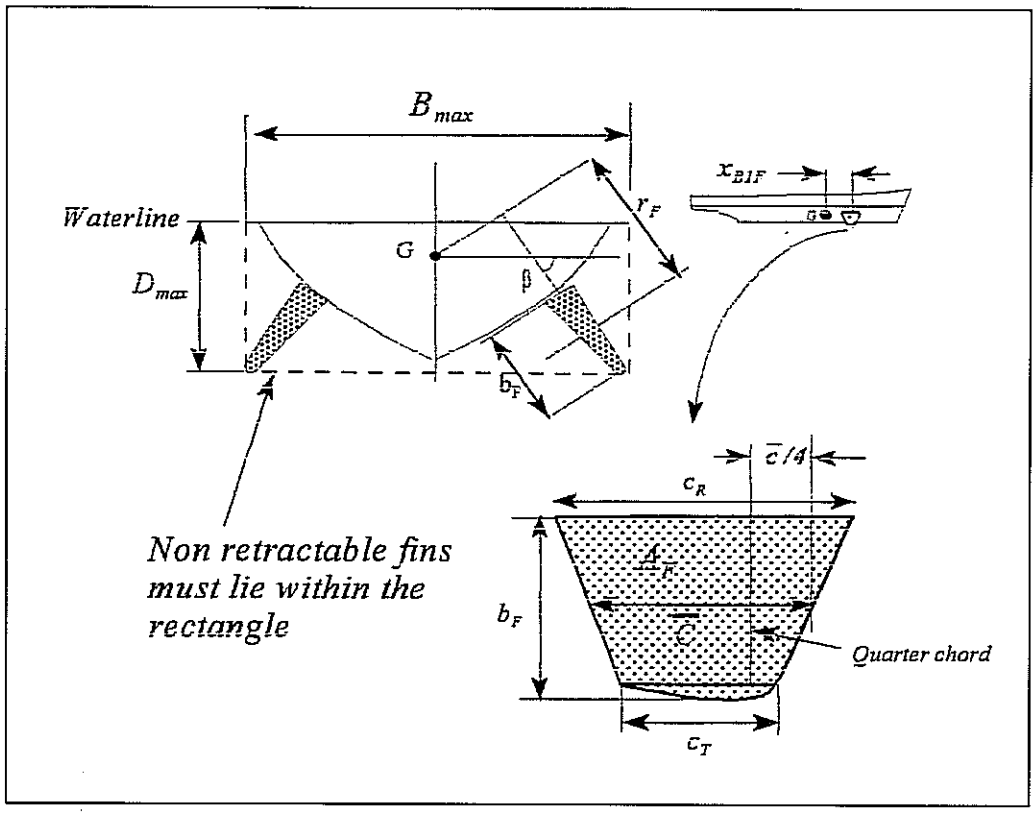

Fig 12.4 - Fin notation and constraints on outreach

Retractable fins are often specified for merchant ships. The fins can be withdrawn into the hull when the ship is operating in calm weather to eliminate their small resistance penalty. This feature is also used to eliminate the risk of grounding when the ship is operating in shallow water or coming alongside..

In warships it is usual to fit non retractable fins as these have a greater immunity to damage from shock and explosion. It is then necessary to confine the fins to the enclosing rectangle defined by the ship's midship section (see Figure 12.4). This places a practical limit on the area and aspect ratio and these fins are usually rather less effective than their retractable counterparts.

12.4 HYDRODYNAMIC CHARACTERISTICS OF STABILISER FINS

Roll stabiliser fins usually have a trapezoidal or rectangular planform as shown in Figure 12.4. The geometry of the surface is conveniently defined by the root and tip chords c_R and c_T and the outreach b_F. The mean chord is

$$\bar{c} = \frac{c_R + c_T}{2} \quad m \tag{12.7}$$

and the planform area is

$$A_F = b_F \, \bar{c} = \frac{b_F \, (c_R + c_T)}{2} \quad m^2 \tag{12.8}$$

The aspect ratio, defining the general shape of the fin, is

$$a_F = \frac{2 \, b_F}{\bar{c}} = \frac{4 \, b_F}{c_R + c_T} \tag{12.9}$$

When the fin is at an angle of incidence α radians to the incident flow it will generate a lift force F_L kN and a drag force F_D kN. These forces are respectively normal and parallel to the direction of the incident flow, as shown in Figure 12.5. The lift vector may be assumed to act through the intersection of the mid span and the quarter chord position (ie b_F / 2 metres from the root and $\bar{c}$ / 4 metres abaft the leading edge).

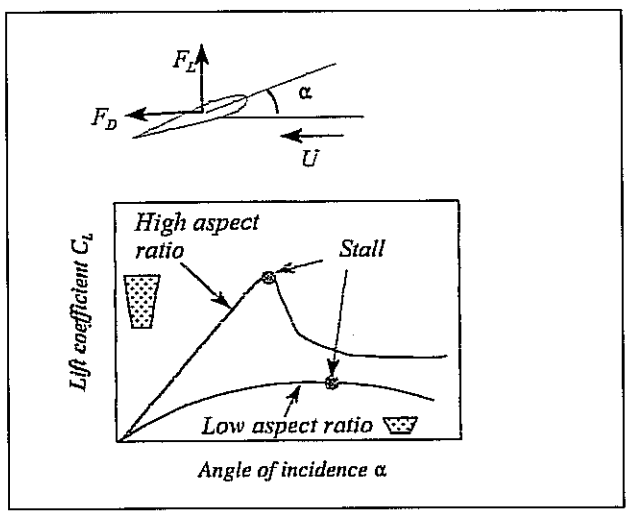

Fig 12.5 - Stabiliser fin lift characteristics: effect of fin aspect ratio

At a given angle of incidence and planform shape the lift and drag are proportional to the square of the forward speed and the planform area. So the lift and drag may be expressed in non dimensional terms as

$$C_L = \frac{F_L}{\frac{1}{2} \rho \, U^2 \, A_F} \tag{12.10}$$

and

$$C_D = \frac{F_D}{\frac{1}{2} \rho \, U^2 \, A_F} \tag{12.11}$$

Most stabiliser fins have a streamlined symmetrical section like that shown in Figure 12.5. For these sections there is no lift at zero incidence and the drag is a minimum. A fairly thick section (typically a thickness /chord ratio of 15%) is usually chosen to allow a substantial stock diameter to cope with the loads. The stock is usually located at the quarter chord to minimise the torque required to maintain the fin incidence.

For small angles of incidence the lift coefficient increases more or less linearly with incidence and we may write the lift coefficient as

$$C_L \approx \frac{dC_L}{d\alpha}\,\alpha \qquad (12.12)$$

where $\frac{dC_L}{d\alpha}$ is the lift curve slope at the origin (units rad^{-1}) and α is in radians.

The slope of the curve diminishes as the angle of incidence is increased and the maximum lift occurs at the stall angle α_{stall}. The lift curve slope increases with aspect ratio, but surfaces with a high aspect ratio stall earlier and more abruptly than those of low aspect ratio. The lift characteristics of symmetrical sections are only weakly dependent on the section shape.

Whicker and Fehlner (1958) tested a variety of.lifting surfaces of low aspect ratio and derived an empirical formula for the lift curve slope of rectangular planforms as a function of aspect ratio:[1]

$$\frac{dC_L}{d\alpha} = \frac{1.8\ \pi\ a_F}{1.8 + \sqrt{a_F^2 + 4}} \quad rad^{-1} \qquad (12.13)$$

Figure 12.6 shows this formula together with illustrations of the surface planforms associated with various aspect ratios. Clearly the lift curve slope increases dramatically with increasing aspect ratio: in other words long slender lifting surfaces (like the wings of a glider) are much more effective than short stubby surfaces.

Whicker and Fehlner also reported the stall angles found for their lifting surfaces. These are given approximately by

$$\begin{aligned} \alpha_{stall} &\approx 1.05 - 0.445\ a_F + 0.075\ a_F^2 \quad rad \quad \text{for } \alpha < 3.0 \\ \alpha_{stall} &\approx 0.39 \quad rad \quad \text{for } \alpha > 3.0 \end{aligned} \qquad (12.14)$$

If the angle of incidence approaches 90° the lift force (normal to the flow direction) becomes zero. The drag force is then very large and acts normal to the plane of the fin. For this case Hoerner (1965) gives

[1] The formula is also adequate for trapezoidal planforms.

$$C_D \approx 1.17 \qquad (12.15)$$

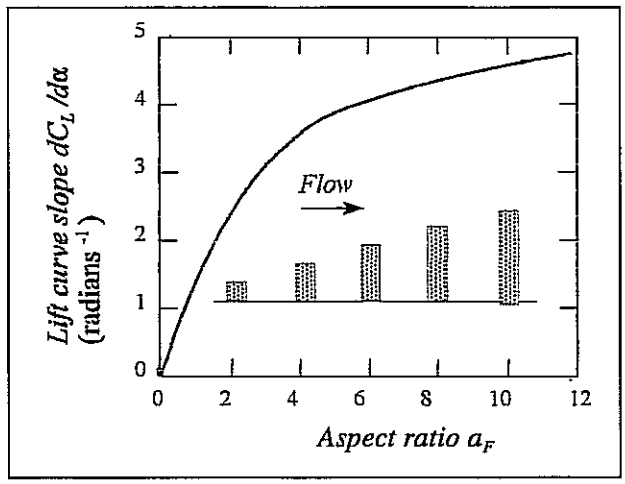

Fig12.6 - Lift curve slope and aspect ratio (After Whicker and Fehlner (1958))

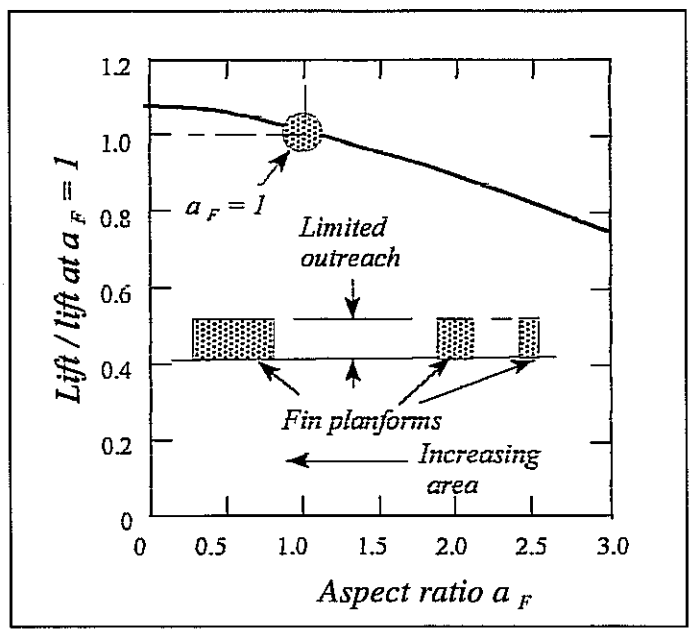

Fig 12.7 - Effect of aspect ratio for a fixed (limited) outreach

12.5 CONSTRAINTS ON STABILISER FIN OUTREACH.

To minimise the risk of grounding or damaging the stabiliser fins when berthing the ship it is usual to insist that the tips of non retractable fins are inside the enclosing rectangle defined by the maximum beam and draught of the ship. This limits the fin outreach as shown in Figure 12.4. It follows that the only way to increase the lift available from the fin is to increase the area by increasing the chord. Unfortunately this reduces the aspect ratio and the lift curve slope.

Consider a rectangular fin of unit aspect ratio and outreach limited by this constraint. Let the lift developed at some angle of incidence be F_{L1} kN. Let the lift developed by another fin of the same limited outreach but a different chord be F_L kN. Rearranging Equations (12.10), (12.12) and (12.13) it can be shown that the ratio of the lifts developed by the two fins is

$$\frac{F_L}{F_{LI}} = \frac{4.04}{1.8 + \sqrt{4 + a_F^2}} \qquad (12.16)$$

Equation (12.16) is plotted in Figure 12.7. The gains associated with increasing the chord if the outreach is limited are minimal if the aspect ratio is reduced below about 1.0. Thus practical non retractable fins are limited to an aspect ratio of about 1.0. More lift can be achieved only by installing more pairs of fins. Retractable fins do not suffer from this constraint and more efficient high aspect ratios can be used.

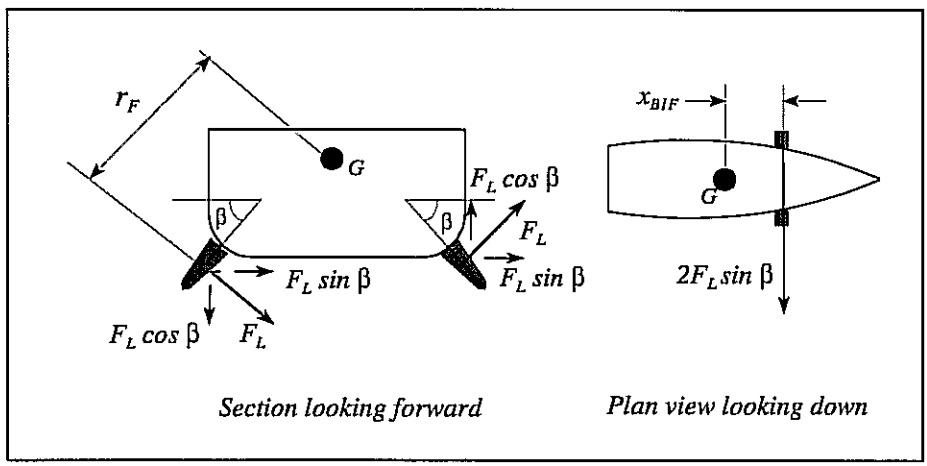

Fig 12.8 - Sway force and yaw moment caused by stabiliser fins.

12.6 EQUATIONS OF MOTION FOR A SHIP WITH STABILISER FINS

Figure 12.8 shows the forces and moments applied to the ship by a pair of fins at an angle of incidence to the flow. Each fin develops a lift force

$$F_L = C_L \frac{1}{2} \rho U^2 A_F = \frac{dC_L}{d\alpha} \frac{1}{2} \rho U^2 A_F \alpha \quad kN \qquad (12.17)$$

exerting a roll moment

$$2 F_L r_F \quad kN\ m \quad \text{port side down about the centre of gravity}$$

where r_F is measured from the axis through the centre of gravity to the lift vector (taken to be the mid point of the fin).

The vertical components of the two lift forces cancel so that there is no resultant vertical force on the ship. However, the horizontal components add and yield a sway force

$$2\ F_L\ sin\ \beta \quad kN \quad \text{to starboard}$$

If the fins are mounted x_{B1F} metres forward of the centre of gravity this horizontal force will exert a yaw moment

$$2\ F_L\ x_{B1F}\ sin\ \beta \quad kN\ m \quad \text{to starboard}$$

The effects of the stabiliser fins on the motions of the ship in waves may be computed by including these additional terms in the equations of motion (3.22). Only the lateral plane equations are affected and these become:

sway:

$$(m + a_{22})\ \ddot{x}_2 + b_{22}\ \dot{x}_2 + a_{24}\ \ddot{x}_4 + b_{24}\ \dot{x}_4 + a_{26}\ \ddot{x}_6 + b_{26}\ \dot{x}_6 + c_{26}\ x_6 + \sum E\ F_L\ sin\ \beta = F_{W20}\ sin\ (\omega_e\ t + \gamma_2)\ .\ kN \qquad (12.18a)$$

roll:

$$a_{42}\ \ddot{x}_2 + b_{42}\ \dot{x}_2 + (I_{44} + a_{44})\ \ddot{x}_4 + b_{44}\ \dot{x}_4 + c_{44}\ x_4 + a_{46}\ \ddot{x}_6 + b_{46}\ \dot{x}_6 + c_{46}\ x_6 - \sum E\ F_L\ r_F = F_{W40}\ \sin\ (\omega_e\ t + \gamma_4)\quad kN\ m \qquad (12.18b)$$

yaw:

$$a_{62}\ \ddot{x}_2 + b_{62}\ \dot{x}_2 + a_{64}\ \ddot{x}_4 + b_{64}\ \dot{x}_4 + (I_{66} + a_{66})\ \ddot{x}_6 + b_{66}\ \dot{x}_6 + c_{66}\ x_6 + \sum E\ F_L\ x_{B1F}\ sin\ \beta = F_{W60}\ sin\ (\omega_e\ t + \gamma_6)\quad kN\ m \qquad (12.18c)$$

In these equations the summations refer to the number of fins (not pairs of fins) fitted to the ship and E is an effectiveness factor defined as

$$E = \frac{Effective\ lift\ of\ fin}{Nominal\ lift\ of\ fin} \qquad (12.19)$$

E is generally less than 1.0 because of various hydrodynamic effects which are discussed in Section 12.7.

12.7 STABILISER FIN LOSSES

12.7.1 Location and alignment

For the maximum possible roll moment the fins should be mounted at the turn of the bilge to maximise the roll lever arm r_F (see Figure 12.4). It is also advantageous to mount the fin stock normal to the hull surface. This simplifies the mechanical arrangements and minimises the gap between the curved hull surface and the fin root when the fin is at an angle of incidence. Such gaps are a potential source of leakage between the high and low pressure sides of the fin and will result in a considerable loss of effectiveness. Fixed (non retractable) fins should also be aligned to maximise the fin outreach within the enclosing rectangle of the ship.

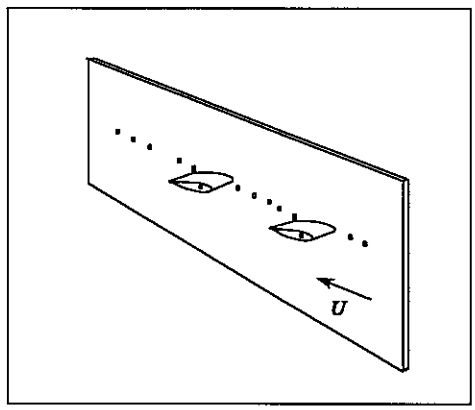

Fig 12.9 - Lloyd's fin experiments (1975,1977).

12.7.2 Hydrodynamic losses

Lloyd (1975,1977) investigated the effectiveness of roll stabiliser fins by measuring the lift developed by model stabiliser fins and bilge keels in a variety of configurations on a ground board. His experiments were conducted in the Circulating Water Channel at the Admiralty Experiment Works[1] at Haslar in the United Kingdom. His apparatus is sketched in Figure 12.9. He identified three major fin performance losses:

a) Hull boundary layer
b) Fin - fin interference
c) Fin - bilge keel interference

12.7.3 Losses due to hull boundary layer

The fins are partially immersed in the slow moving boundary layer on the hull surface. The flow velocity near the root of the fin and the lift developed in this region are reduced. Lloyd (1975) measured the boundary layer thickness (defined as the point at which the velocity is 99% of the free stream velocity) and the lift developed by an isolated fin at various locations on his ground board. Figure 12.10 shows the effectiveness of the fin as a function of the boundary layer thickness.

The results may be approximated by the empirical equation

---

[1] Now part of the Defence Evaluation and Research Agency

$$E_{BL} = \frac{\textit{Lift developed with boundary layer}}{\textit{Nominal lift (no boundary layer)}}$$

$$\approx 1.0 - 0.21 \frac{\delta}{b_F} \qquad (12.20)$$

The boundary layer thickness on the hull may be estimated using the equation

$$\delta \approx 0.377\, x_{FP}\, R_N^{-0.2} \quad m \qquad (12.21)$$

where R_N is the local Reynolds number defined as

$$R_N = \frac{\rho\, U\, x_{FP}}{\mu_W} \qquad (12.22)$$

and x_{FP} is the longitudinal distance from the Forward Perpendicular to the fin stock in metres.

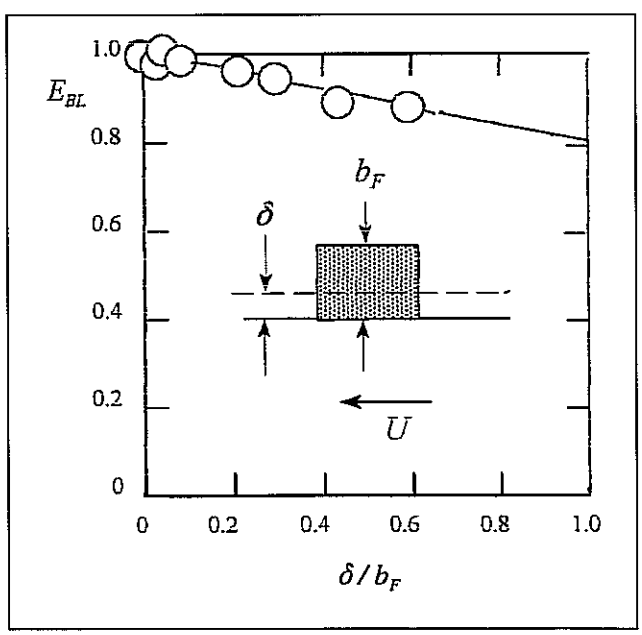

Fig 12.10 - Effect of hull boundary layer on fin lift (After Lloyd (1975))

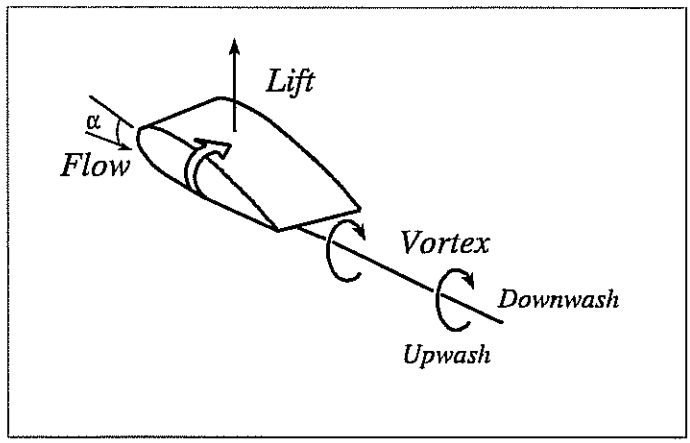

Fig 12.11 - Trailing vortex generated by a stabiliser fin.

12.7.4 Fin - fin interference

Roll stabiliser fins, like all lifting surfaces, work by developing a pressure difference between their upper and lower surfaces. The water is tempted to roll around the tip of the fin from the high pressure to the low pressure surface and a vortex is formed. Figure 12.11 shows the vortex generated by a fin at a fixed (nose up) angle of incidence α. This vortex is shed from close to the tip of the fin and trails away along the side of the hull imparting a swirling motion to the water close to the hull. This causes a ***downwash*** in the region between the vortex and the hull surface and an ***upwash*** in the region outboard of the vortex. If the fin incidence is negative (nose down) these flow directions are, of course, reversed.

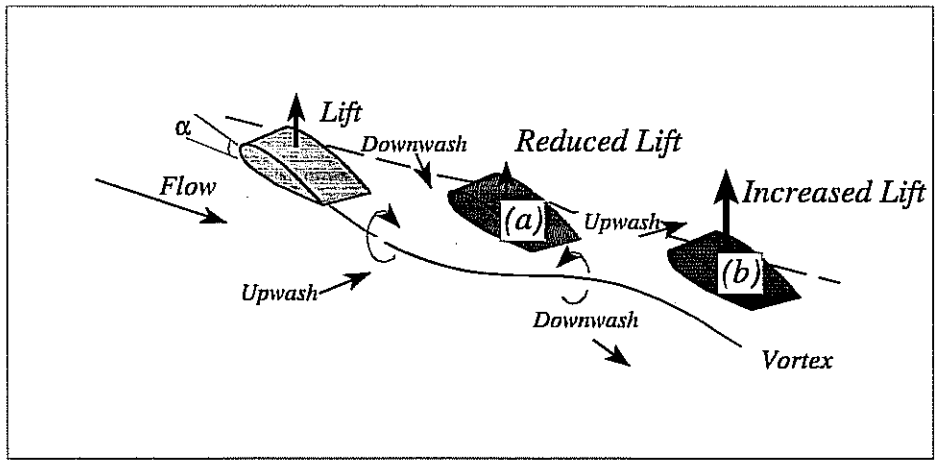

Fig 12.12 - Fin-fin interference.

An oscillating fin produces a vortex of continually varying strength and direction which is convected away along the side of the ship. In fact the vortex is a record or "memory" of the lift developed by the fin. Figure 12.12 illustrates the flow behind an oscillating fin and it can be seen that there are alternate regions of downwash and upwash in the wake of the fin, depending on the lift developed in the immediate past.

A second stabiliser fin mounted immediately downstream willl experience a downwash over most of its outreach. This will generally decrease its angle of incidence and reduce the lift developed. If the fin is moved further aft into a favourable region of upwash the lift will be increased.

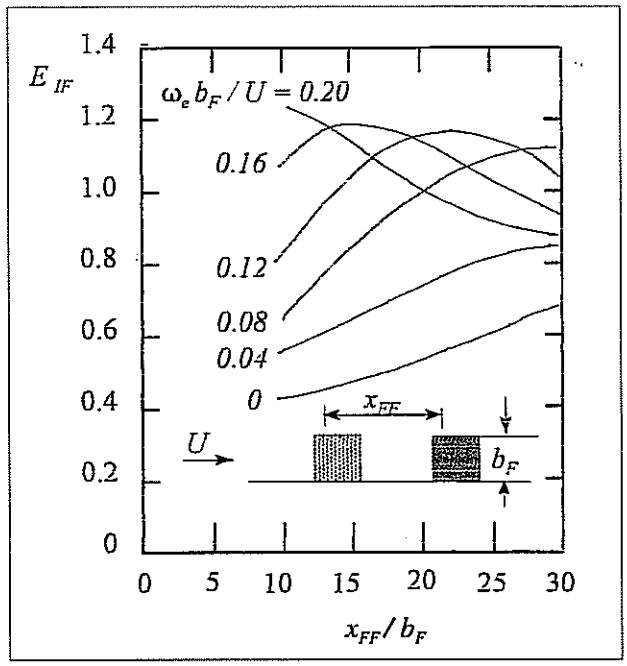

Fig 12.13 - Fin-fin interference factors.

Figure 12.13 shows the fin - fin interference factor

$$E_{IF} = \frac{Lift\ of\ second\ fin}{Nominal\ Lift}$$

measured by Lloyd (1977) for a pair of oscillating fins. The results are plotted as a function of a non dimensional frequency parameter and the longitudinal separation of the fins. At zero frequency the interference is quite dramatic even for well spaced fins. For example, a fin spaced 20 outreaches behind the first fin will develop only about 50% of the nominal lift. The interference effects become less important as the frequency and the separation are increased until, at very high frequencies and separations, the second fin is in a region of upwash and the interference becomes beneficial.

The fin separation may be optimised to achieve the best performance at the natural roll frequency (where most of the roll motion occurs) and at the ship's cruising speed. In principle we require the second fin to be at a distance x_{FF} metres abaft the first fin such that the time required for the vortex to convect from the upstream fin is equal to half a roll period:

$$\frac{x_{FF}}{U} = \frac{T_{*4}}{2} = \frac{\pi}{\omega_{*4}} \quad sec$$

so that

$$x_{FF} = \frac{\pi U}{\omega_{*4}} \quad m \tag{12.23}$$

Unfortunately this gives fin separations which are often impractical. For example, taking a cruising speed of 10.3 metres/second (20 knots) and a natural roll frequency of 0.5 radians/second (natural period 12.6 seconds) we find an optimum separation

$$x_{FF} = 63 \ m$$

which may be difficult to achieve on all but the largest ships.

12.7.5 Fin - Bilge Keel Interference

A bilge keel mounted abaft a stabiliser fin will also experience downwash and will develop a lift which opposes the fin lift. Lloyd (1975) measured this opposing lift for the case of zero frequency and his results are presented in the form of an effectiveness factor

$$E_{IBK} = 1.0 - \frac{Bilge\ keel\ lift}{Nominal\ fin\ lift} \approx 0.84 \tag{12.24}$$

in Figure 12.14.

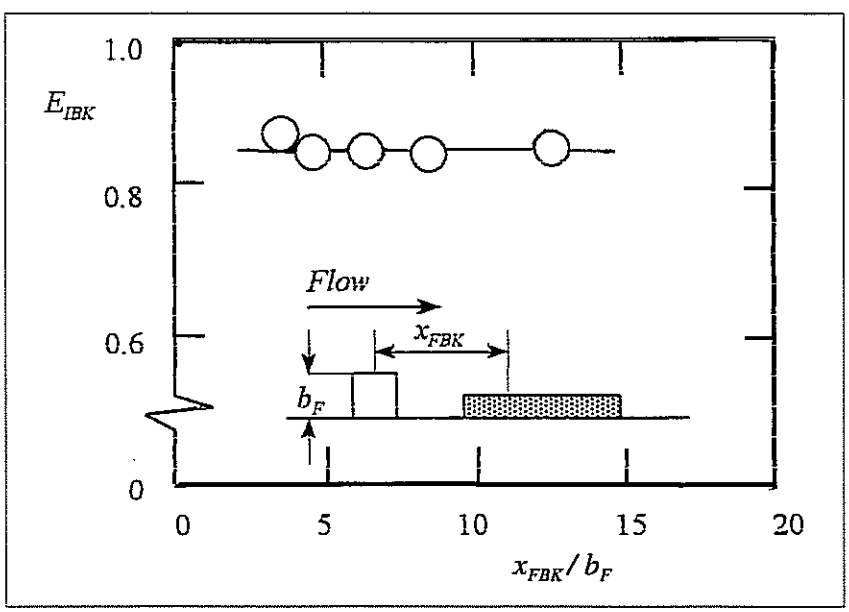

Fig 12.14 - Fin-bilge keel interference factors.

The detrimental effects of an aft mounted bilge keel are mitigated if the bilge keel is followed by a second stabiliser fin. The bilge keel has a straightening effect on the flow and removes some of the downwash due to the trailing vortex from the upstream fin. This enhances the lift generated by the second fin as shown in Figure 12.15. This effect can be approximated by setting

$$E_{IBK} \approx 1.0 \qquad (12.25)$$

for the case of a bilge keel between two fins.

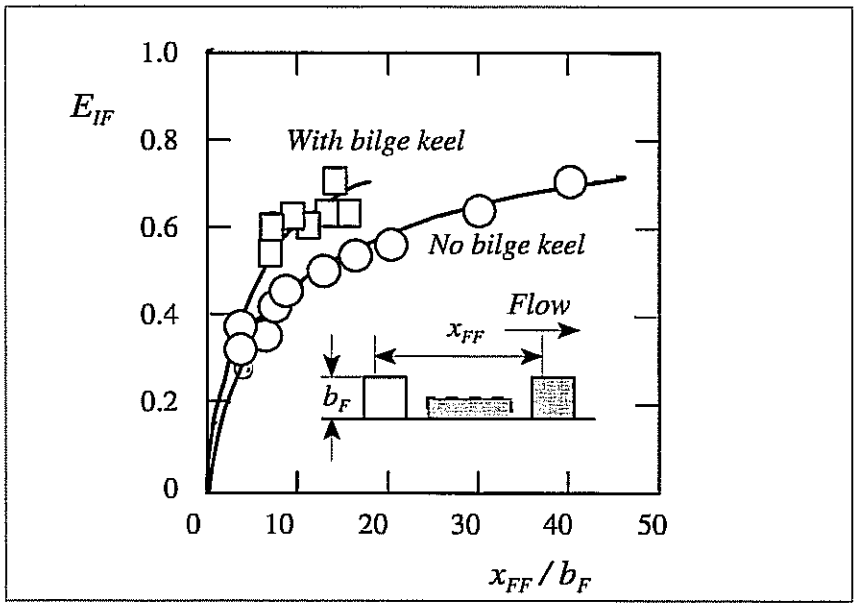

Fig 12.15 - Fin-fin interference factors: effect of bilge keel at zero frequency.

12.7.6 Overall hydrodynamic effectiveness

The hydrodynamic losses described above are cumulative and the overall effectiveness of each stabiliser fin - bilge keel combination is given by multiplying the individual affectiveness:

$$E = E_{BL}\, E_{IF}\, E_{IBK} \qquad (12.26)$$

12.7.7 Sway - yaw effects

Suppose that the fins are set to some fixed angle of incidence to give steady lift forces L kN to generate a stabilising roll moment to port as shown in Figure 12.16. We have already seen that this will result in a sway force and a yaw moment to starboard. The ship will respond in exactly the same way as it responds to motions of the rudders and will begin to turn to starboard. A centrifugal force to port then acts through the centre of gravity, opposed by inboard hydrodynamic forces acting to starboard below the waterline. These forces form a couple which tends to roll the ship to port, enhancing the port roll moment directly generated by the fins. The total roll moment generated by forward mounted fins is therefore increased by this sway - yaw effect.

If the fins are mounted abaft the centre of gravity x_{BIF} is negative. The ship then turns in the opposite direction in response to the fins (to port for the example given above). The roll moment caused by the turning motion of the ship then opposes the roll moment directly generated by the

fins and their effectiveness is reduced. In extreme cases with near vertical fins mounted well aft the roll moment due to the turning motion may actually exceed the roll moment directly generated by the fins and the total moment will then be in the "wrong" direction.

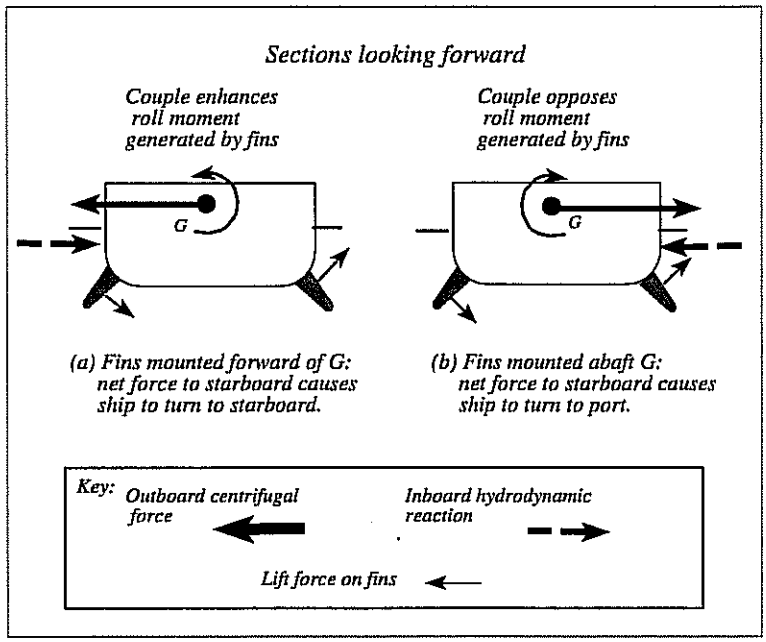

Fig 12.16 - Beneficial and detrimental effects of sway and yaw

These effects are reduced when the fins are oscillating at higher frequencies and they are not usually very significant at the natural roll frequency where most of the rolling motion occurs. However, we shall see in Section 12.10 that extreme aft fin locations with large angles of depression may result in motion ***amplification*** (as opposed to the required reduction in motion) at very low frequencies. For this reason these locations should be avoided if possible.[1]

Beneficial sway and yaw effects can be maximised by mounting the fins well forward with a large angle of depression. However, this makes it difficult to accommodate a bilge keel forward of the fins and is rarely attempted. Fin emergence and the risk of damage due to slamming in head waves could also be a problem.

In practice fins are usually mounted somewhere near the middle of the ship and the sway - yaw effects may then degrade their performance at low frequencies. The degradation can be minimised by keeping the depression angle β as small as possible but this will also tend to reduce the roll lever arm r_F and the outreach b_F if the fins are non retractable.

---

[1] The rudders may be regarded as stabiliser fins with extreme aft location and very large depression angles (of order 90^0) and systems using the rudders for roll stabilisation as well as for steering the ship have been developed. These overcome the low frequency amplification problem by switching the roll stabiliser functions off when the encounter frequency is low.

12.8 DESIGN RECOMMENDATIONS FOR STABILISER FINS AND BILGE KEELS

The discussion above may be summarised in the following design recommendations:

(a) Fin location
Maximise the roll lever arm by mounting the fins at the turn of the bilge near the middle of the ship. Do not fit bilge keels abaft the fins. The stock should be normal to the local hull surface. Avoid large depression angles especially for aft mounted fins.

(b) Fin size and shape
The fin area should be as large as possible. Fixed (non retractable) fins must lie within the enclosing rectangle defined by the maximum beam and draught. The aspect ratio of fixed fins should not be less than 1.0. Locate the fin stock at the quarter chord position of the fin to minimise torque requirements. Use a symmetrical section of sufficient thickness to allow an adequate stock diameter.

(c) Number of fins
Use a single pair of fins to avoid interference effects. If sufficient stabilisation cannot be obtained from a single pair of fins (bearing in mind the limitations which may be imposed on the fin outreach) it will be necessary to adopt a two fin configuration. If practical, the longitudinal separation should be chosen to take advantage of the favourable interference effects (see Equation (12.23)).

(d) Bilge keels
Bilge keels should be as large as possible with a high aspect ratio. If only a single pair of fins is fitted the bilge keel should be mounted forward of them. In multiple fin installations bilge keels may be mounted between the fins but there should be no bilge keel abaft the after fin.

12.9 ACTIVE FIN CONTROL SYSTEMS

12.9.1 Introduction

Figure 12.17 shows a block diagram representation of a ship stabilised with active fins. Each component or block in the diagram may be considered as a "black box" having an input and an output which are related by the block's transfer function. For example, the ship block accepts an input in the form of a roll moment F_{W4} from the waves and generates a roll motion output x_4. Similarly the stabiliser fin controller generates a demanded fin angle α_D in response to the roll motion of the ship. The fin servo mechanism responds and drives the fins to an achieved fin angle α and the fins convert this into a stabilising roll moment F_{F4}. This is subtracted from the roll moment generated by the waves, thus reducing the roll motion of the ship.

The transfer functions of the ship, the fin servo and the fin are essentially fixed for a given design. The fin controller transfer function is, however, adjustable and must be set up in such a way as to ensure that the fins develop roll moments which generally oppose the moments provided by the waves.

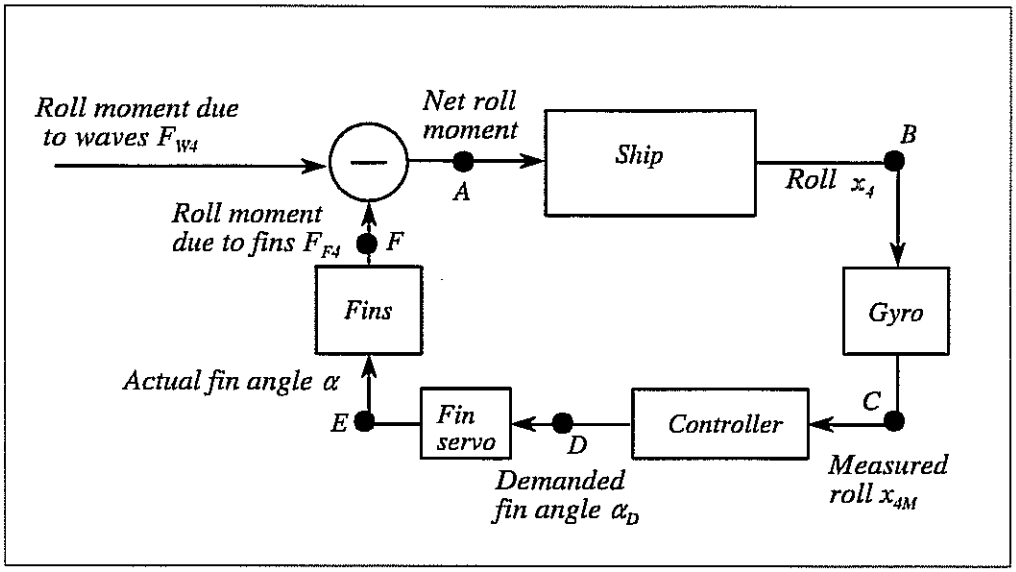

Fig 12.17 - Block diagram for a ship with roll stabiliser fins

12.9.2 The fin controller transfer function.
Fin controllers generally have transfer functions of the form

$$\frac{\alpha_D}{x_{4M}} = K_G\, K_U\, \frac{K_1 + K_2\, s + K_3\, s^2}{b_1 + b_2\, s + b_3\, s^2} \qquad (12.27)$$

where α_D is the demanded fin angle

x_{4M} is the measured roll angle

K_G is the overall gain setting

K_U is the speed dependent gain setting

K_1 is the (variable) roll angle sensitivity

K_2 is the (variable) roll velocity sensitivity

K_3 is the (variable) roll acceleration sensitivity

b_1, b_2 and b_3 are fixed controller coefficients

s is the Laplace transform operator (d/dt).

The coefficients K_G , K_U , K_1 , K_2 , and K_3 may be adjusted to achieve the desired roll stabiliser performance within the capacity of the stabiliser fins. Table 12.1 shows values which might be found on a typical controller. K_1 , K_2 , and K_3 should be adjusted to match the rolling characteristics of the ship and will remain fixed for a given loading condition, metacentric height and natural roll frequency. K_G and K_U govern the overall level of activity of the roll stabiliser system and are adjusted to achieve a given roll stabilisation performance. Note that the coefficients b_1 , b_2 and b_3 are fixed values inherent in the design of the controller.

The speed dependent gain K_U is introduced to compensate for the inherent reduction in stabiliser performance as the ship speed is reduced and to avoid overloading the fin stocks at very high speed. K_U is varied automatically with

$$K_U \text{ proportional to } \frac{1}{U^2}$$

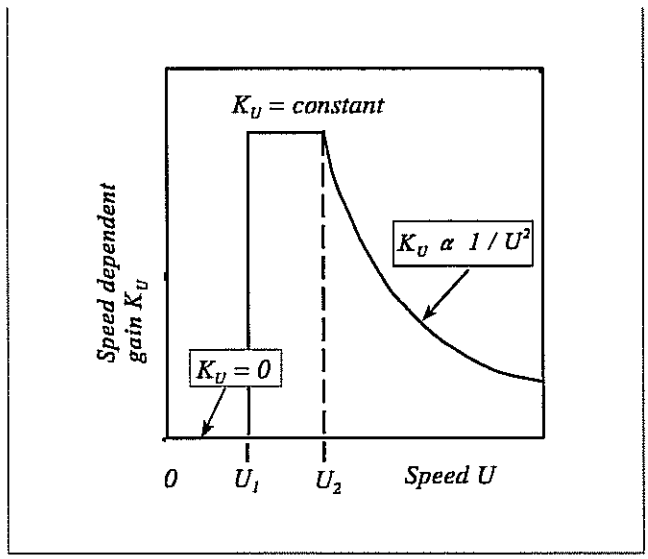

Fig 12.18 - Speed dependent gain

as shown in Figure 12.18. At very low speeds this would give very large gains resulting in excessive stabiliser fin activity and frequent demands for fin angles greater than the maximum available. The fin servo mechanisms would be continually driving the fins up against the mechanical stops which are usually set to limit their travel to 25 or 30 degrees, leading to rapid wear and possible damage to the mechanical components. So the speed dependent gain is usually limited to some finite value at speeds less than say, half the cruising speed. When the ship is hove to the fins are completely ineffective and the speed dependent gain is then set to zero to avoid needless wear on the system.

12.9.3 Choosing settings for the sensitivities K_1, K_2, and K_3

Consider the behaviour of the system illustrated in Figure 12.17. Let us suppose that the ship is in regular waves of small amplitude. Then the sinusoidal disturbance initiated by the waves will propagate around the system and each component block will generate a sinusoidal output depending on its individual sinusoidal input. In general each block will introduce a phase shift (positive or negative, depending on its individual characteristics).

TABLE 12.1

TYPICAL ACTIVE FIN ROLL STABILISER CONTROLLER COEFFICIENT VALUES

K_G	K_1	K_2	K_3
0.00	0	0	0
0.25	1	5	1
0.50	2	10	2
0.75	3	15	3
1.00	4	20	4
1.25	5	25	5
1.50	6	30	6
1.75	7	35	7
2.00	8	40	8
2.25	9	45	9
2.50	10	50	10

$b_1 = 1.00$
$b_2 = 0.50$
$b_3 = 0.05$

$K_U = 0.00$ for $U < 5$ knots
$= 1.0$ for $5 < U < 15$ knots
$= 225/U^2$ for $U > 15$ knots

Now the object of the stabiliser control system is to ensure that the roll moment generated by the fins exactly opposes the roll moment generated by the waves and this is achieved if the total phase around the loop from A to F is zero.

It is assumed that the only components which have significant phase responses are the ship, the controller and the fin servo. So the controller must provide a phase advance which exactly compensates, at the natural roll frequency, for the phase lags introduced by the other components. The controller phase is then given by

$$\sum \epsilon = \epsilon_S + \epsilon_C + \epsilon_{FS} = 0$$

$$\text{or } \epsilon_C = -\epsilon_S - \epsilon_{FS} \quad rad \tag{12.28}$$

This can only be achieved at one frequency and it is customary to choose the natural roll frequency since this is usually the dominant frequency in the roll motion.

By making the substitution $s = i\,\omega_e$ and setting $\omega_e = \omega_{*4}$ in Equation (12.27) it can be shown that the controller phase has two components:

$$\epsilon_C = \epsilon_{C1} + \epsilon_{C2} \quad rad \tag{12.29}$$

where the variable component is given by

$$tan\ \epsilon_{C1} = \left(\frac{K_2\ \omega_{*4}}{K_1 - K_3\ \omega_{*4}^2} \right) \tag{12.30}$$

and the fixed component is given by

$$tan\ \epsilon_{C2} = \left(\frac{-\ b_2\ \omega_{*4}}{b_1 - b_3\ \omega_{*4}^2} \right) \tag{12.31}$$

So the required variable phase ϵ_{C1} from the controller is

$$\epsilon_{C1} = -\epsilon_S - \epsilon_{FS} + tan^{-1} \left(\frac{b_2\ \omega_{*4}}{b_1 - b_3\ \omega_{*4}^2} \right) \quad rad \tag{12.32}$$

Equation (12.30) may be written

$$\frac{K_2}{K_3} = \frac{tan\ \epsilon_{C1}}{\omega_{*4}} \left(\frac{K_1}{K_3} - \omega_{*4}^2 \right) \quad sec^{-1} \tag{12.33}$$

from which it can be seen that the required phase must be achieved by choosing appropriate ratios between the sensitivities.

12.9.4 Forced rolling trials

Practical application of this technique requires the phases ϵ_S and ϵ_{FS} to be determined. These may be found in a forced rolling trial at sea. The ship is run in calm water so that the roll moment from the waves is negligible. If any waves are present their effects should be minimised by running in head or following seas. Rudder motions will influence the rolling motions of the ship so the helmsman should keep the wheel amidships and the autopilot, if the ship has one, should be switched off.

The stabiliser controller is isolated from the system by breaking the circuit at the point D in Figure 12.17. The fin servos are instead driven by a sinusoidal demand signal equivalent to, say, ± 15 degrees fin amplitude at some selected frequency. The ship will then roll at the same frequency and the roll response is measured at the point C. The actual fin angle is monitored at

point E. ϵ_S is the phase between the signals monitored at C and E.

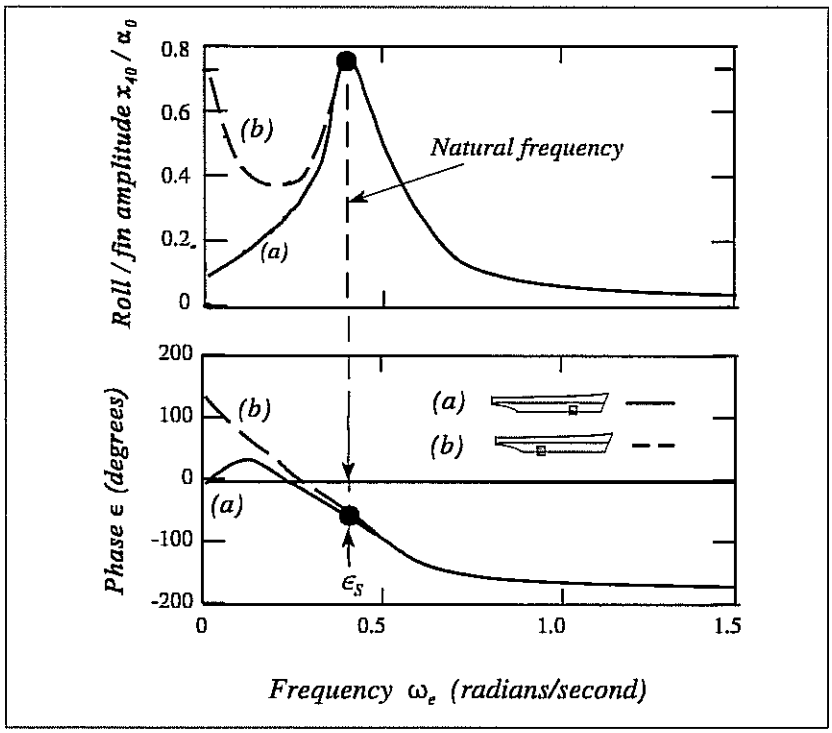

Fig 12.19 - Forced roll responses for (a) forward fins with small depression angle and (b) aft fins with large depression angle.

Figure 12.19 shows the form of the results. These depend on the location and depression of the fins. For fins mounted somewhere near the middle of the ship with a moderate angle of depression the phase at zero frequency is zero showing that the ship rolls in the expected sense: a fin incidence giving a steady roll moment to port results in a steady port heel.

If the fins are mounted well aft with a large depression angle the phase at zero frequency becomes 180° for the reasons already explained in Section 12.7.7. The roll response to the fins can be quite large but is then in the opposite sense to that expected.

In either case the ship phase ϵ_S can be measured at the natural roll frequency, as shown in Figure 12.19.

The fin servo phase ϵ_{FS} is measured between the signals monitored at points D and E in Figure 12.17. Typical results are given in Figure 12.20.

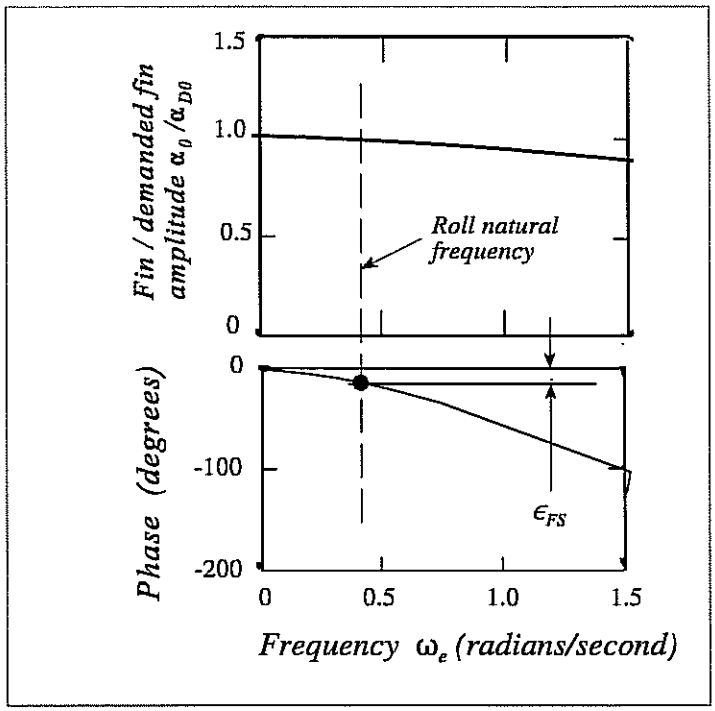

Fig 12.20 - Typical fin servo response

An alternative approach is to simulate a forced rolling trial using the equations of motion (12.18). The excitations from the waves on the right hand sides are set to zero and the lift force F_L is made to vary sinusoidally by putting

$$\alpha = \alpha_0 \sin \omega_e t \quad rad \tag{12.34}$$

The equations will then give sinusoidal motion responses (in sway and yaw as well as roll) and the phase ϵ_S may be determined.

12.9.5 Fin servo transfer function

The fin servo transfer function may be expressed in the form

$$\frac{\alpha}{\alpha_D} = \frac{a_1}{a_1 + a_2 s + a_3 s^2} \tag{12.35}$$

Putting $s = i \omega_e$ we obtain the amplitude response

$$\frac{\alpha_0}{\alpha_{D0}} = \frac{a_1}{\sqrt{(a_1 - a_3 \omega_e^2)^2 + a_2^2 \omega_e^2}} \tag{12.36}$$

and the phase response is given by

$$tan\ (phase) = \frac{-\ a_2\ \omega_e}{a_1\ -\ a_3\ \omega_e^2} \qquad (12.37)$$

The coefficients a_1, a_2, and a_3 are chosen to match these equations to the measured fin servo responses (Figure 12.20)

12.9.6 *Worked Example*:

Find appropriate controller coefficients to match the responses given for forward mounted fins in Figures 12.18 and 12.19 using the controller coefficients listed in Table 12.1.

Natural roll frequency: $\omega_{*4} = 0.45$ rad/sec

Phases at natural roll frequency:

Roll lags fin motion by 70° ; ie $\epsilon_S = -70°$;

Actual fin angle lags demanded fin angle by 10°; ie $\epsilon_{FS} = -10°$

From Equation (12.32) the required phase angle is

$$\epsilon_{CI} = 70 + 10 + tan^{-1}\left(\frac{0.5 \times 0.45}{1.0 - 0.05 \times 0.45^2}\right) = 93^o$$

Hence, from Equation (12.33)

$$\frac{K_2}{K_3} = \frac{tan\ (93^o)}{0.45}\left(\frac{K_1}{K_3} - 0.2\right)$$

$$= -\ 42.4\left(\frac{K_1}{K_3} - 0.2\right) \qquad (12.38)$$

This relationship can be achieved more or less exactly by many different combinations of the available control sensitivities in Table 12.1. For example, the following settings all satisfy Equation (12.38) and give the required phase advance within 1 degree:

K_1	0	0	0	0	0	0	1	1	1	1	1
K_2	10	15	25	35	40	50	40	30	25	15	10
K_3	1	2	3	4	5	6	10	9	8	7	6

All of these settings will give a satisfactory performance since they all ensure that the moment applied by the stabilisers exactly opposes the wave moment at the natural roll frequency. In practice it may be found that some of the settings are marginally preferable to others but the benefits to be gained are usually small. For example, setting K_1 to zero will ensure that the fins do not waste energy by attempting to correct a steady list or trying to hold the ship upright in a turn. The steady roll moment available at zero frequency is so small (see Figure 12.19) that efforts in this area are probably doomed to failure. The only appreciable effect will be an increase in the ship's fuel consumption due to the small increase in resistance. Similarly, high values of K_3 may lead to excessive stabiliser fin activity at high frequencies and increased wear, noise and vibration with no noticeable reduction in roll motion.

12.9.7 Choosing the overall gain K_G

Having chosen the sensitivities K_1, K_2, and K_3 to match the control system to the rolling characteristics of the ship the next step is to determine the overall gain setting K_G. This governs the magnitude of the roll reduction achieved by the stabilisers and should be chosen so that the ship meets some agreed roll specification in moderately severe weather conditions. An appropriate specification would be written in the form:

The rms roll motion at the worst heading at 20 knots in sea state 7 must not exceed 4°.
Fin motions in these conditions should not exceed ± 25° on more than one oscillation in ten.
Sea state 7 is to be interpreted using the WMO sea state code and the most probable modal wave period for annual conditions in the North Atlantic.
Cosine squared wave spreading is to be assumed.

The stabilised roll motion is computed using Equations (12.18) with the fin incidence α now given by Equations (12.27) and (12.35). Typical results of such a calculation, taking account of the speed dependent gain, are shown in Figure 12.21. As expected the roll motion decreases with increasing overall gain at the expense of increased fin motion.

Using the gains available in the control system specified in Table 12.1 we find that the roll target is achieved with

$$K_G = 1.25$$

The requirement to limit the fin activity is introduced to avoid excessive mechanical wear and possible damage to the fin mechanism which will occur if fin angles greater than the maximum available are continually demanded. Excessive fin demands will also lead to cavitation which, in extreme cases, may damage the fins and will certainly be noisy. The latter may be of particular importance in warships. It should also be noted that the assumptions of linearity inherent in Equation (12.17) describing the fin lift characteristics will lead to an overestimate of the stabiliser performance if the fin motion (and hence the lift) is actually limited by mechanical constraints. In any case the equation will overestimate the lift at large angles of incidence (see Figure 12.5).

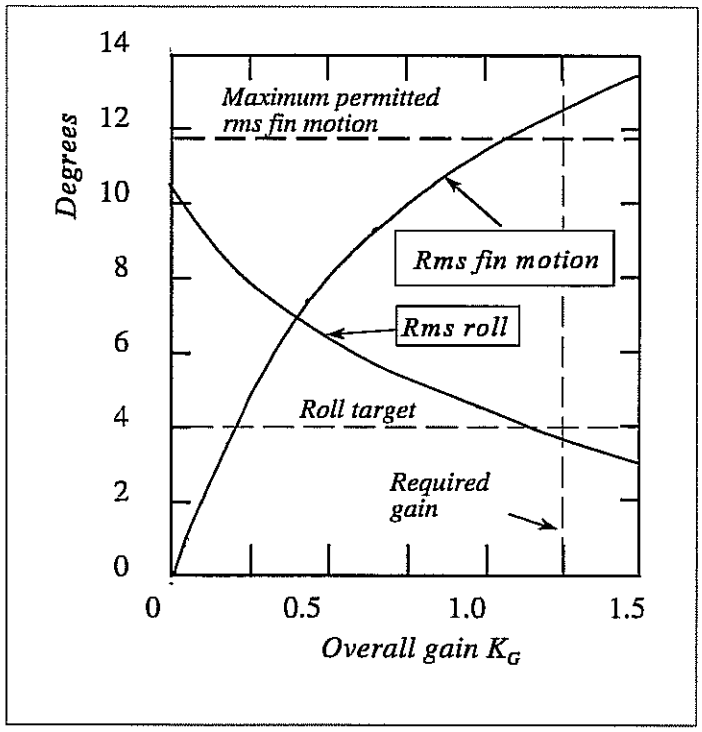

Fig 12.21 - Effect of gain on stabiliser performance

The specification given above requires the probability of the fin motion amplitude exceeding $\pm$ 25^o to be no more than 0.1. Equation (11.28) may be used to calculate the corresponding maximum allowable rms fin motion. Using Table 11.5 we find that

$$\frac{\alpha_{max}}{\sigma_0} = 2.15$$

and the maximum permissible rms fin motion is

$$\sigma_0 = \frac{25}{2.15} = 11.6^o$$

The rms fin motion required to meet the roll target in Figure 12.21 is 12.4° which is greater than 11.6°. So the stabiliser capacity will need to be enhanced by increasing the fin area, using a more effective aspect ratio, improving the fin/bilge keel layout to avoid interference or increasing the number of fins.

12.10 SYSTEM STABILITY

Roll stabiliser systems have the potential, like all automatic control systems, of becoming unstable at certain frequencies. Clearly this possibility must be considered at the design stage and steps must be taken to prevent it occurring.

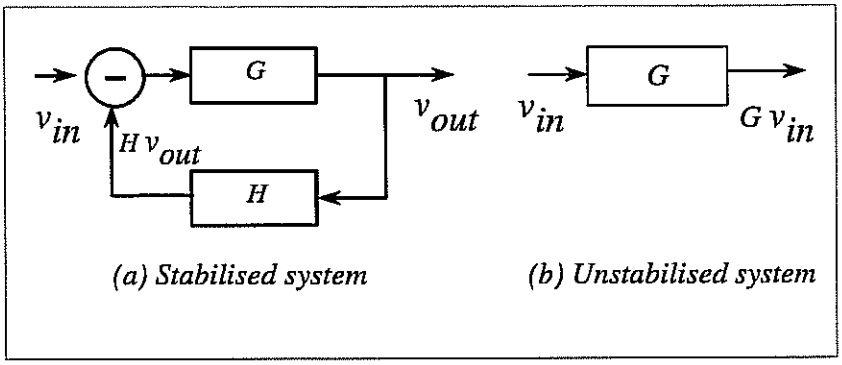

Fig 12.22 - Stabilised and unstabilised systems.

Figure 12.22 shows a simplified block diagram of the roll stabiliser system. The ship is represented by a block with a transfer function G (units rad / (kN m)) and the entire "feedback" network consisting of the gyro, the fin controller, the fin servo and the fins themselves is represented by the single block with a transfer function H (units kN m /rad). G and H are, of course, complex quantities of the form

$$G = |G| \; (\cos \epsilon_G + i \sin \epsilon_G) \tag{12.39}$$

where $|G|$ is the amplitude response or gain and ϵ_G is the phase response.

Suppose that the system is excited with an input v_{IN} (wave induced roll moment in kN m) and responds with an output v_{OUT} (roll angle in radians). Then the output of the feedback block will be $H\ v_{OUT}$ kN m and the total roll moment input to the ship will be $v_{IN} - H\ v_{OUT}$ kN m. So the input and output of the complete closed loop system are related by

$$v_{OUT} = G \; (v_{IN} - H\ v_{OUT}) \quad rad \tag{12.40}$$

and the transfer function or ***closed loop gain*** of the complete system is given by

$$\frac{v_{OUT}}{v_{IN}} = \frac{G}{1 + G\ H} \quad rad\ (kN\ m)^{-1} \tag{12.41}$$

$G\ H$ (no dimensions) is the transfer function the system would have if the feedback loop were left open and is termed the ***open loop gain***.

The stability of the closed loop system may be examined using the Nyquist diagram illustrated in Figure 12.23. In this diagram the dimensionless open loop gain is plotted as a vector of length $|G\ H|$ and argument ϵ_{GH} where

$$\epsilon_{GH} = \epsilon_G + \epsilon_H \quad rad$$

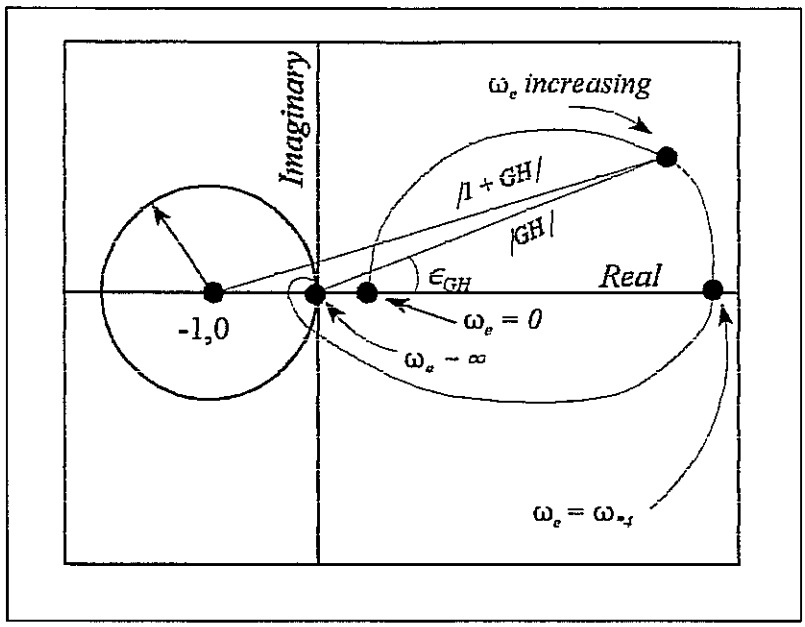

Fig 12.23 - Open loop gain Nyquist diagram

The locus of the end of the vector varies with frequency, moving around the diagram as the frequency increases. At zero frequency, in conventional systems with fins in the middle part of the ship, the phase is zero and the the open loop gain vector $G\ H$ lies along the positive real axis. As the frequency increases some phase advance is introduced by the ship (see Figure 12.19) and by the controller [2].

In a well designed system the phase is, as we have already seen, arranged to be zero at the natural roll frequency ω_{*4} and the gain vector once again lies along the positive real axis. The gain should be a maximum at this point so that maximum stabiliser activity occurs where it is needed at the natural roll frequency. At higher frequencies the phase becomes negative and, in a stable system, the gain steadily diminishes until it becomes zero at infinite frequency as the locus curve approaches the origin.

If the ship were unstabilised the response to the excitation v_{IN} kN m would be $G\ v_{IN}$ radians. So the roll stabilisers will only reduce the rolling motion at some particular frequency if

$$|v_{OUT}| < |G\ v_{IN}| \quad rad$$

This occurs if the quantity

$$|1 + G\ H| > 1$$

[2] i.e. ϵ_{GH} is positive

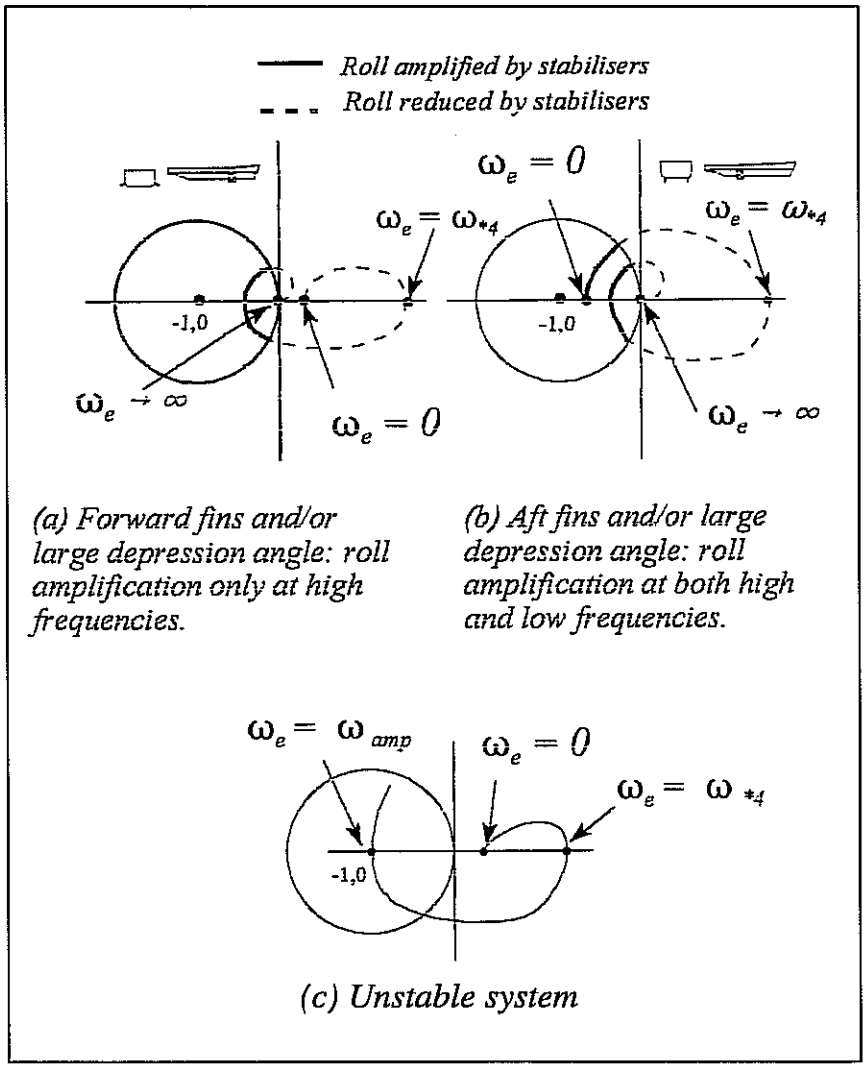

Fig 12.24 - Nyquist diagrams showing amplification and instability.

Now $|1 + G H|$ is the distance from the point (-1,0) to the appropriate point on the open loop gain locus (see Figure 12.23). So we can see that the stabilisers will only reduce the rolling motion at frequencies for which the open loop gain locus lies outside a circle of unit radius centred at the point (-1,0). The roll motion will be amplified for all frequencies lying within this unit circle. Figure 12.24(a) shows that this will always occur at high frequencies for conventional fin locations. For aft mounted fins with large angles of depression the phase reversal at zero frequency results in the locus of the open loop gain vector beginning somewhere on the negative real axis as shown in Figure 12.24(b). So these installations will always give motion amplification at low frequencies unless the gain is made zero by setting

$$K_1 = 0$$

Equation (12.41) shows that the system will become unstable (ie the amplitude response will become infinite) when the open loop gain

$$G\,H = -1 \tag{12.42}$$

and this occurs if the gain vector locus passes through the point (-1,0) on the negative real axis as shown in Figure 12.24(c). ie the phase is then - 180° and the roll moment due to the fins then enhances the roll moment due to the waves at some particular frequency. Any excitation at this frequency will then cause very large fin motions which will enhance the initial excitation and increase the fin motions still further. In practice, of course, the reponse will be limited by the mechanical stops, fin rate limits on the fin servos and fin stall but large undesirable fin oscillations may still occur.

Clearly we must ensure that open loop gain locus never passes through the point (-1,0) . It is also desirable to avoid approaching it too closely because this will result in motion amplification even though the motions will be stable. Two commonly used criteria for defining adequate safety margins are the gain and phase margins defined in Figure 12.25.

The ***gain margin*** is defined as

$$G_M = \frac{1}{\textit{open loop gain at } \epsilon_{GH} = -180^o} \tag{12.43}$$

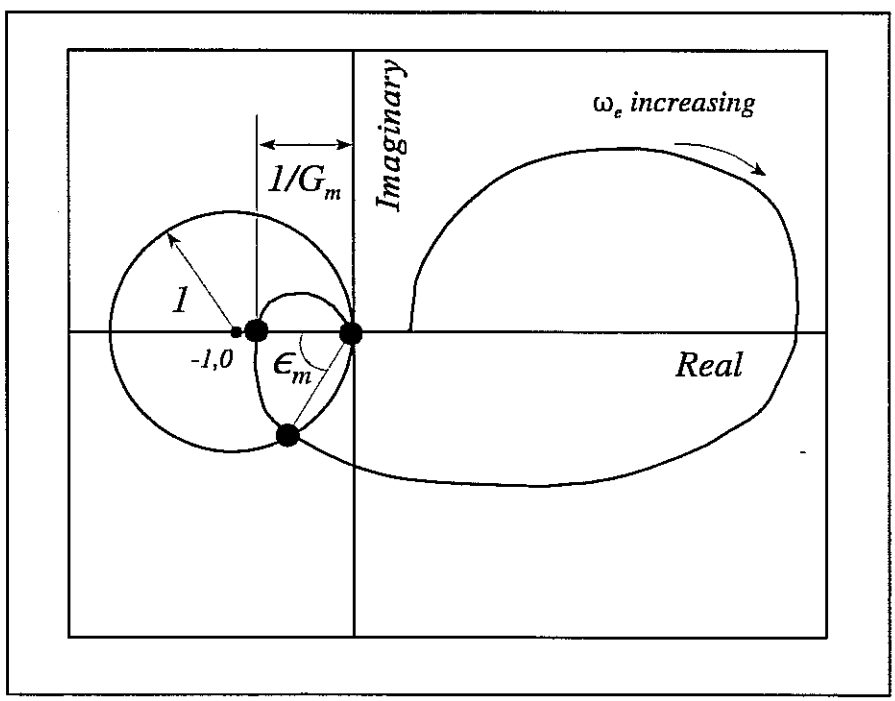

Fig 12.25 - Definition of phase and gain margins.

and the minimum acceptable value of G_M is generally taken to be 2 which implies that the open loop gain $G\,H$ must not exceed 0.5 when the phase is -180°.

The ***phase margin*** is defined as

$$\epsilon_M = 180^o + \text{open loop phase when } |1 + G\,H| = 1 \qquad (12.44)$$

and the minimum acceptable phase margin is 30°. 60° is regarded as very good practice.

If the system stability is unsatisfactory it can be improved by reducing the overall gain K_G or by choosing different values of the sensitivities K_1, K_2, and K_3 (but still satisfying Equation (12.33).

12.11 ACTIVE ROLL STABILISER FIN PERFORMANCE

Figure 12.26 shows the performance of a typical active fin roll stabiliser system with speed dependent gain installed in the frigate descibed in Section 7.1. At very low speeds the fins are completely ineffective because the overall gain is set to zero (see Figure 12.18). At speed U_1 the fins are switched on and a substantial roll reduction is achieved. As the speed is increased to U_2 the fins become progressively more effective and the stabilised roll motion decreases. At speeds above U_2 the gain is reduced and the stabilised roll motion becomes nearly independent of speed.

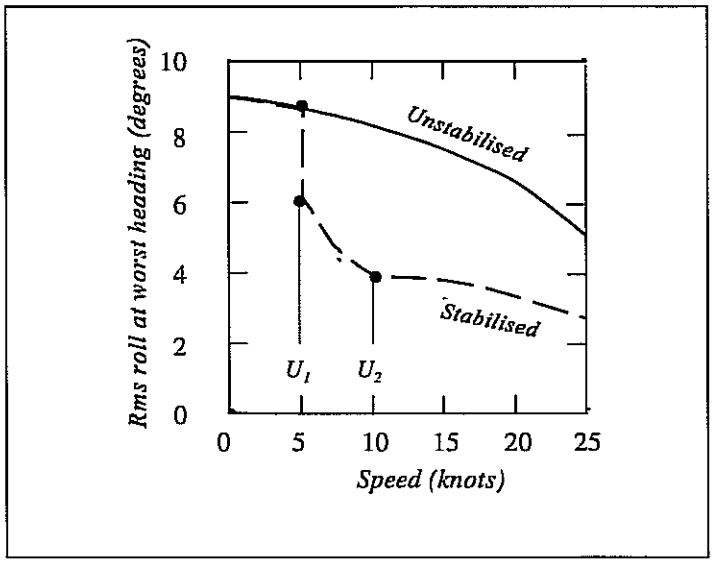

Fig 12.26 - Effect of speed on fin stabiliser performance for the frigate at the worst heading. Significant wave height 5.5 metres; modal period 12.4 seconds; cosine squared spreading.

12.12 PASSIVE TANKS

The fluid in a partially filled tank in a ship will slosh backwards and forwards across the tank as the ship rolls. The shifting weight of the fluid will exert a roll moment on the ship and, by suitable design, this can be arranged to damp the roll motion. Figure 12.27 shows the desired motion of the water in relation to the rolling motion of the ship and it can be seen that we require the motion of the fluid to lead the roll motion by 90° so that it is in phase with the roll velocity.

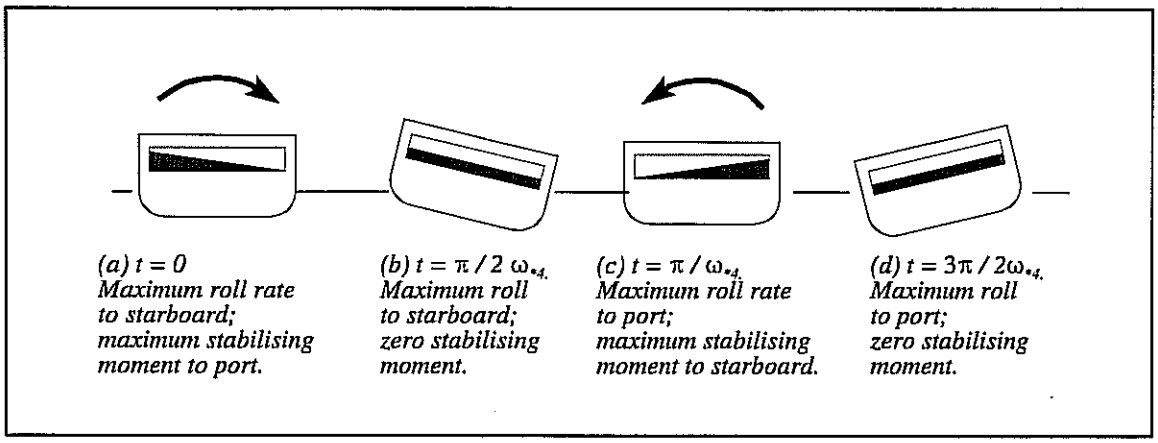

Fig 12.27 - Passive tank motions

Figure 12.28 shows some of the types of passive tanks which are in current use. The simplest is the flume or free surface tank which consists of a rectangular tank running athwartships. Sometimes a limited control is exerted over the motion of the fluid by installing a restriction or baffle in the centre of the tank.

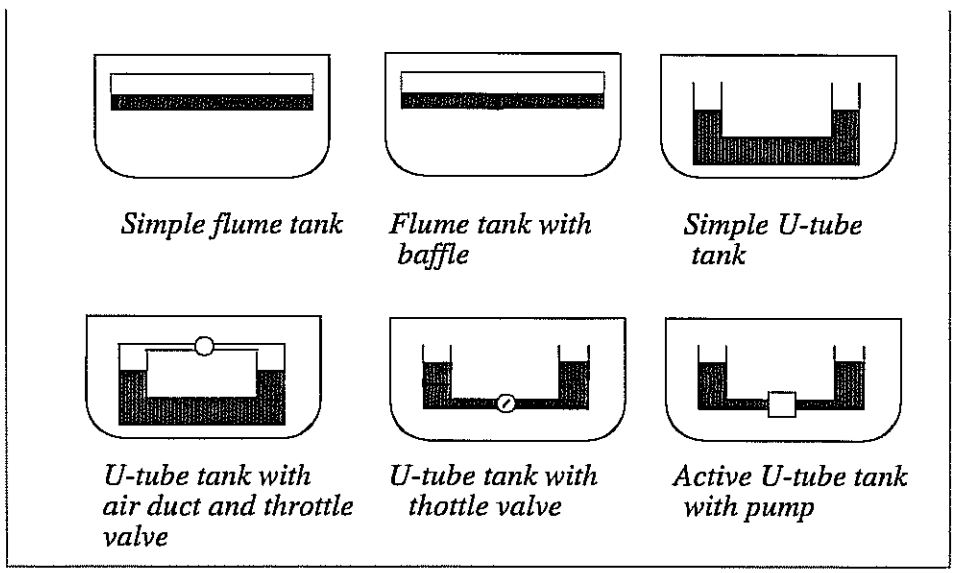

Fig 12.28 - Types of passive tank.

U tube tanks have also been fitted in a number of ships. In this case the free surface is confined to the two arms of the U tube which are connected by a horizontal duct. The tops of the vertical arms may be open to the atmosphere or they may be connected by a horizontal air duct. In this case a throttle valve may be included to exert some control over the motions of the fluid. Some designs incorporate a throttle valve or a pump in the bottom duct.

Passive tanks work well at low speeds but they are not usually as effective as a well designed active fin system at high speed. For this reason they are often specified for ships like survey

vessels or weather ships which must spend the majority of their time hove to.

Tanks have the advantage that they have no moving parts (except perhaps for a pump or controlled throttle valve) [1]and require little maintenance. They also avoid the small resistance penalty associated with fins and bilge keels. They take up a considerable volume of the ship's hull but it may be possible to use the fresh water supply or some of the fuel oil as the working fluid so this loss of volume may not be serious. The optimum tank position high in the ship often makes access along the ship difficult.

A major disadvantage is that the free surface always reduces the metacentric height so that roll stability will be reduced. As a consequence ***all passive tanks amplify roll motions at low encounter frequencies.*** In certain circumstances this amplification may become a serious problem and it may be necessary to immobilise the tank by draining it or filling it completely. This will invariably take a considerable time and passive tanks are therefore not suitable for ships which are required to change course frequently (eg warships).

In spite of the apparent simplicity of the flume tank no adequate theory for predicting its performance has been developed. However Stigter (1966) has developed a theory for U tube passive tanks and a simplified version of this is given below.

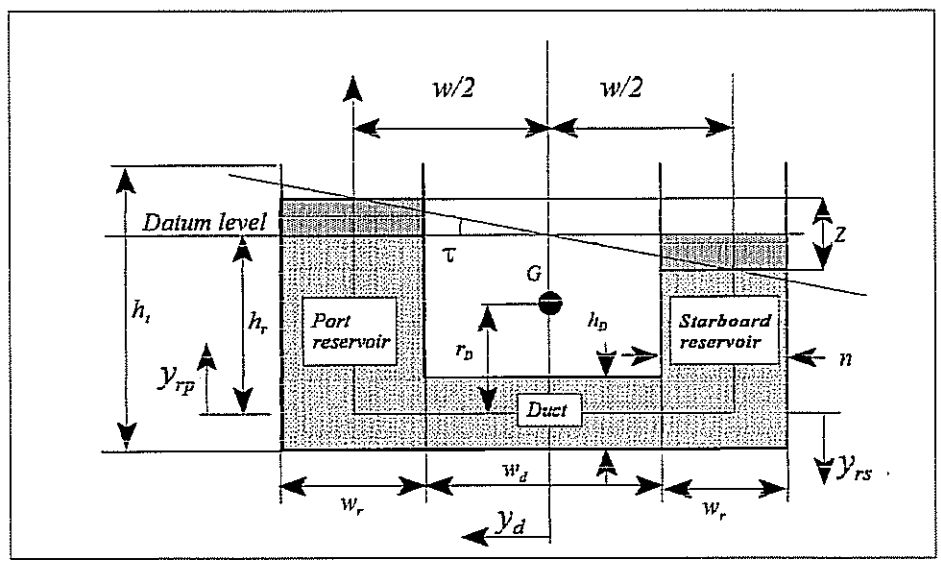

Fig 12.29 - Passive tank notation

12.13 THEORY FOR A U TUBE PASSIVE TANK

12.13.1 Equation of motion for the fluid in the tank

Figure 12.29 shows a simple U tube passive tank. The tank is assumed to consist of two reservoirs and a connecting duct of constant rectangular cross section.

[1] Strictly speaking such tanks are 'active.'

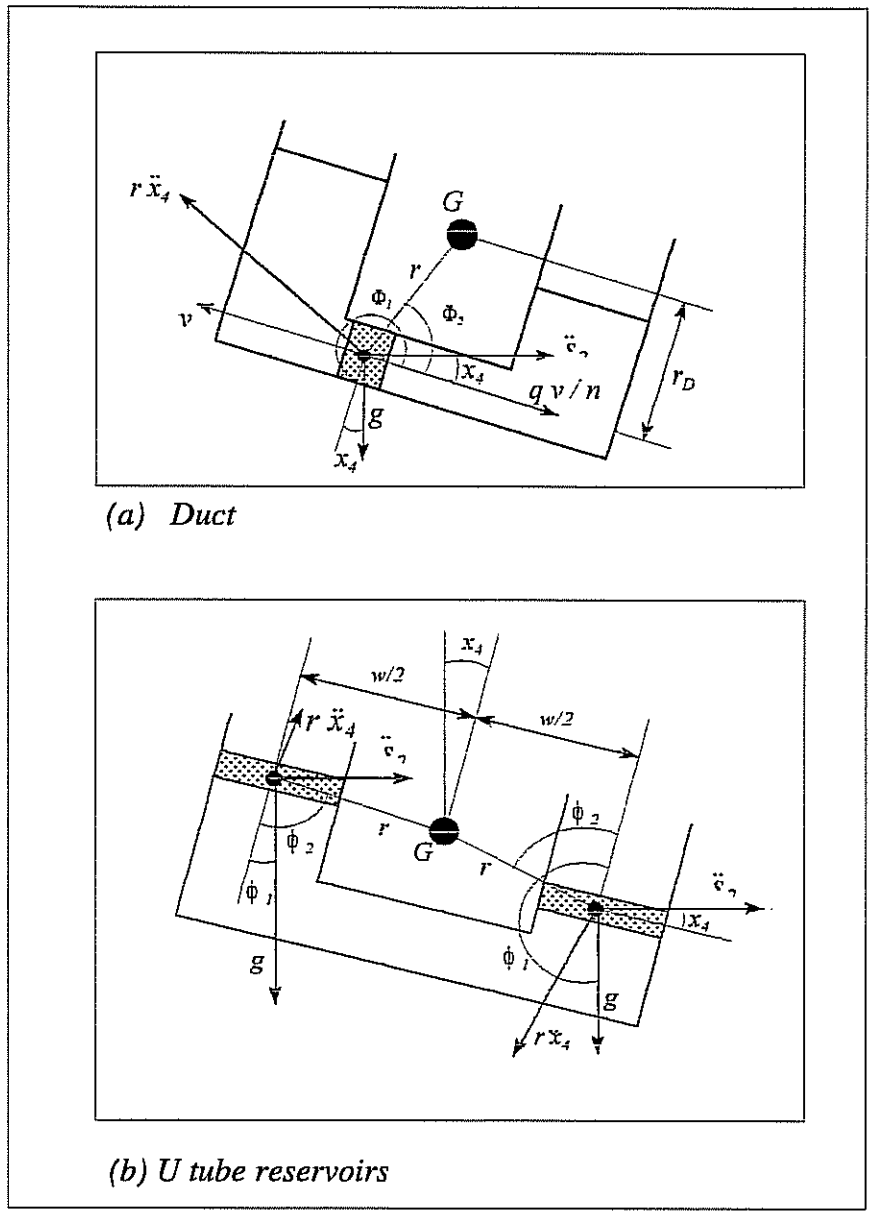

Fig 12.30 - External forces applied to a unit mass of fluid in the tank

The length of the tank (in the fore/aft direction) is x_t metres. We require to find the motions of the fluid within the tank under the influence of the motions applied to the tank by the ship. These may be analysed using the axis system shown. The origin O is at the midpoint of the connecting duct and an axis y runs along the duct and up the reservoirs of the U tube. The fluid velocity along the positive y direction (up the port reservoir) is v metres/second. Three additional axes are defined: y_d has its origin at O and runs parallel to the duct, positive to port; y_{rp} and y_{rs} have their origins on the duct centreline and run parallel to the port and starboard reservoir walls as shown.

n is the width of the tank perpendicular to the y axis. Note that n is a variable which has different (constant) values h_d on the duct and w_r on the two reservoirs. It is assumed that there is no flow in the "n" direction and the motions of a unit mass (1 tonne) of fluid in the tank will be governed by a simplified version of Euler's equation [2]

$$\frac{\partial v}{\partial t} + v\frac{\partial v}{\partial y} = Y - \frac{1}{\rho_t}\frac{\partial P}{\partial y} \quad m/sec^2$$

where Y is the external force per unit mass and ρ_t is the mass density of the fluid in the tank.

Now the duct and the reservoirs are assumed to be of constant cross section so we may write $\frac{\partial v}{\partial y} = 0$ everywhere except at the junctions between the duct and the reservoirs. Neglecting these corner effects Euler's equation reduces to

$$\frac{\partial v}{\partial t} = Y - \frac{1}{\rho_t}\frac{\partial P}{\partial y} \quad m/sec^2$$

or, since there are now only two variables,

$$\frac{dv}{dt} = Y - \frac{1}{\rho_t}\frac{dP}{dy} \quad m/sec^2 \qquad (12.45)$$

If the difference in the height of the fluid level in the two reservoirs is z metres the velocity in each reservoir will be

$$v_r = \frac{d}{dt}\left(\frac{z}{2}\right) = \frac{w\,\dot{\tau}}{2} \quad m/sec$$

where τ, which is assumed to be small, is the tank "angle" in radians, defined in Figure 12.29,

$$w = w_d + w_r \quad m \qquad (12.46)$$

and the velocity at any point in the tank is

$$v = \frac{w_r\, v_r}{n} = \frac{w_r\, w\,\dot{\tau}}{2\,n} \quad m/sec \qquad (12.47)$$

The external force per unit mass Y is made up of contributions due to the accelerations applied to the tank and the frictional forces arising from the losses in any throttle valve, wall friction etc. Figures 12.30(a) and 12.30(b) show these contributions. They are:

The component of the acceleration due to gravity along the y direction:

$$-\,g\,\cos\,\phi_1 \quad m/sec^2$$

The acceleration due to the roll acceleration:

---

[2] See any text book on fluid mechanics.

$$- r \ddot{x}_4 \cos\left(\phi_2 - \frac{\pi}{2}\right) = - r \ddot{x}_4 \sin \phi_2 \quad m/sec^2$$

c) The component of the local lateral acceleration in the y direction:

1) in the duct

$$Y_{LA} = \ddot{s}_2 \cos x_4 \approx \ddot{s}_2 \quad m/sec^2 \tag{12.48a}$$

2) in the reservoirs

$$Y_{LA} = \ddot{s}_2 \sin x_4 \approx 0 \quad m/sec^2 \tag{12.48b}$$

since both $\ddot{s}_2$ and x_4 are assumed to be small.

d) The frictional or damping forces. Although these would be expected to be proportional to the square of the local velocity it is convenient to assume that the damping can be linearised and is proportional to the velocity v. If the tank length x_t is much greater than the normal dimension n it can be shown that the frictional force per unit mass is approximately

$$- \frac{q\, v}{n} \quad kN/t$$

where q is a coefficient of resistance to be estimated or determined by experiment.

Equation (12.45) then becomes

$$\frac{w_r\, w\, \ddot{\tau}}{2\, n} + \frac{q\, w_r\, w\, \dot{\tau}}{2\, n^2} + g \cos \phi_1 + r \ddot{x}_4 \sin \phi_2 - Y_{LA} = - \frac{1}{\rho_t} \frac{dP}{dy} \quad m/sec^2 \tag{12.49}$$

We now integrate this equation with respect to y to obtain an equation giving the motion of the fluid in the tank (in terms of the angle τ) as a function of the pressure difference at the surface in the two reservoirs. Strictly the integration should proceed from the surface level in the starboard reservoir (negative y) to the surface level in the port reservoir (positive y). However the continually varying fluid levels introduce complications and we therefore obtain an approximate solution by integrating between the datum levels in each reservoir. We also assume that the lateral acceleration $\ddot{s}_2$ does not vary appreciably along y. We obtain

$$\frac{\rho_t\, w_r\, w\, I_1\, \ddot{\tau}}{2} + \frac{\rho_t\, q\, w_r\, w\, I_2\, \dot{\tau}}{2} + \rho_t\, g\, I_3 + \rho_t\, \ddot{x}_4\, I_4 + \rho_t\, \ddot{s}_2\, I_5 = P_s - P_p \quad kN/m^2 \tag{12.50}$$

where

$$I_1 = \int_{tank} \frac{dy}{n} = \int_{-w/2}^{w/2} \frac{dy_d}{h_d} + \int_{-h_r}^{0} \frac{dy_{rs}}{w_r} + \int_{0}^{h_r} \frac{dy_{rp}}{w_r} = \frac{w}{h_d} + \frac{2h_r}{w_r}$$

$$I_2 = \int_{tank} \frac{dy}{n^2} = \int_{-w/2}^{w/2} \frac{dy_d}{h_d^2} + \int_{-h_r}^{0} \frac{dy_{rs}}{w_r^2} + \int_{0}^{h_r} \frac{dy_{rp}}{w_r^2} = \frac{w}{h_d^2} + \frac{2h_r}{w_r^2} \quad m^{-1}$$

$$I_3 = \int_{tank} cos\ \phi_1\ dy = x_4 \int_{-w/2}^{w/2} dy_d - \int_{-h_r}^{0} dy_{rs} + \int_{0}^{h_r} dy_{rp} = w\ x_4 \quad m$$

$$I_4 = \int_{tank} r\ sin\ \phi_2\ dy = \int_{-w/2}^{w/2} r_d\ dy_d + \int_{-h_r}^{0} \frac{w}{2}\ dy_{rs} + \int_{0}^{h_r} \frac{w}{2}\ dy_{rp}$$

$$= w\ (\ r_d + h_r\ ) \quad m^2$$

$$I_5 = -\int_{duct} dy = -\int_{-w/2}^{w/2} dy_d = -\ w \quad m$$

where $\int_{tank}$ implies integration along the y axis from the datum level in the starboard reservoir to the datum level in the port reservoir and $\int_{duct}$ is confined to the duct. The angles ϕ_1 and ϕ_2 are defined for the duct and the reservoirs in Figures 12.30(a) and 12.30(b).

The hydrostatic pressures at the datum levels in the two reservoirs are

$$P_s = -\ P_p = -\ \rho_t\ g\ \frac{w}{2}\ \tau \quad kN/m^2 \qquad (12.51)$$

relative to atmospheric pressure.

Equation (12.50) may now be expressed as an equation giving the motion of the tank fluid as a function of the moment applied to the tank fluid by multiplying by the moment of the area of the reservoirs:

$$\frac{w\ w_r\ x_t}{2} \quad m^3$$

Using Equation (7.7) to calculate the lateral acceleration experienced by the tank located x_{BI} metres forward of the centre of gravity we obtain the equation of motion for the tank:

$$a_{\tau 2}\ \ddot{x}_2 + a_{\tau 4}\ \ddot{x}_4 + c_{\tau 4}\ x_4 + a_{\tau 6}\ \ddot{x}_6 + a_{\tau\tau}\ \ddot{\tau} + b_{\tau\tau}\ \dot{\tau} + c_{\tau\tau}\ \tau = 0 \quad kN\ m \tag{12.52}$$

where the coefficients are

$$a_{\tau 2} = -\ Q_t \quad kN\ m/(rad/sec)^2 \tag{12.53a}$$

$$a_{\tau 4} = Q_t\ (\ r_d + h_r\ ) \quad kN\ m/(rad/sec)^2 \tag{12.53b}$$

$$c_{\tau 4} = Q_t\ g \quad kN\ m/rad \tag{12.53c}$$

$$a_{\tau 6} = -\ Q_t\ x_{BI} \quad kN\ m/(rad/sec)^2 \tag{12.53d}$$

$$a_{\tau\tau} = Q_t\ w_r \left(\frac{w}{2\ h_d} + \frac{h_r}{w_r} \right) \quad kN\ m/(rad/sec)^2 \tag{12.53e}$$

$$b_{\tau\tau} = Q_t\ q\ w_r \left(\frac{w}{2\ h_d^2} + \frac{h_r}{w_r^2} \right) \quad kN\ m/(rad/sec) \tag{12.53f}$$

$$c_{\tau\tau} = Q_t\ g = c_{\tau 4} \quad kN\ m/rad \tag{12.53g}$$

where

$$Q_t = \frac{\rho_t\ w_r\ w^2\ x_t}{2} \quad t\ m$$

12.13.2 Equations of motion for a ship with a passive stabilising tank

The tank angle τ may be regarded as an additional degree of freedom in the equations of motion for the ship (3.23). Its effects are taken into account by including additional terms of the form

$$a_{i\tau}\ \ddot{\tau}, \quad b_{i\tau}\ \dot{\tau}, \quad c_{i\tau}\ \tau \quad (\ i = 1,\ 6)$$

in these equations. Many of these coefficients are zero. In particular, the tank has no effects on the surge, heave or pitch motions so that

$$a_{i\tau} = b_{i\tau} = c_{i\tau} = 0 \qquad (i = 1;\ i = 3;\ i = 5\ )$$

Simple physical arguments also demonstrate that no sway force or yaw moments can be caused by a steady tank angle and that the rate of change of tank angle can have little appreciable effect. So

$$b_{i\tau} = c_{i\tau} = 0 \qquad (i = 2;\ i = 6)$$

In addition it is assumed that the rate of change of tank angle has a negligible influence on the roll moment so that

$$b_{4\tau} = 0$$

The lateral plane equations of motion for a ship stabilised with a passive tank are then:

sway:
$$(m + a_{22})\, \ddot{x}_6 + b_{22}\, \dot{x}_2 + a_{24}\, \ddot{x}_4 + b_{24}\, \dot{x}_4 + a_{26}\, \ddot{x}_6 + b_{26}\, \dot{x}_6 + c_{26}\, x_6 + a_{2\tau}\, \ddot{\tau} = F_{w20} \sin (\omega_e\, t + \gamma_2) \quad kN \qquad (12.54a)$$

roll:
$$a_{42}\, \ddot{x}_2 + b_{42}\, \dot{x}_2 + (I_{44} + a_{44})\, \ddot{x}_4 + b_{44}\, \dot{x}_4 + c_{44}\, x_4 + a_{46}\, \ddot{x}_6 + b_{46}\, \dot{x}_6 + c_{46}\, x_6 - [a_{4\tau}\, \ddot{\tau} + c_{4\tau}\, \tau] = F_{w40} \sin (\omega_e\, t + \gamma_4) \quad kN\ m \qquad (12.54b)$$

yaw:
$$a_{62}\, \ddot{x}_2 + b_{62}\, \dot{x}_2 + a_{64}\, \ddot{x}_4 + b_{64}\dot{x}_4 + (I_{66} + a_{66})\, \ddot{x}_6 + b_{66}\, \dot{x}_6 + c_{66}\, x_6 + a_{6\tau}\, \ddot{\tau} = F_{w60} \sin (\omega_e\, t + \gamma_6) \quad kN\ m \qquad (12.54c)$$

(where the expression inside the square brackets in Equation (12.54b) is the tank stabilising moment).

The vertical plane equations remain as for the unstabilised ship (Equations (3.22a), (3.22c) and (3.22e)).

We now derive the tank acceleration coefficients $a_{2\tau}$, $a_{4\tau}$ and $a_{6\tau}$. These may be considered as the sway force, roll and yaw moments required to sustain a tank angle acceleration of $\ddot{\tau} = 1.0$ radian/second ^{2}.

Consider the tank shown in Figure 12.31. If the tank angle acceleration is $\ddot{\tau}$ radians/ second^2 the fluid acceleration in the reservoirs and the duct are, by Equation (12.47)

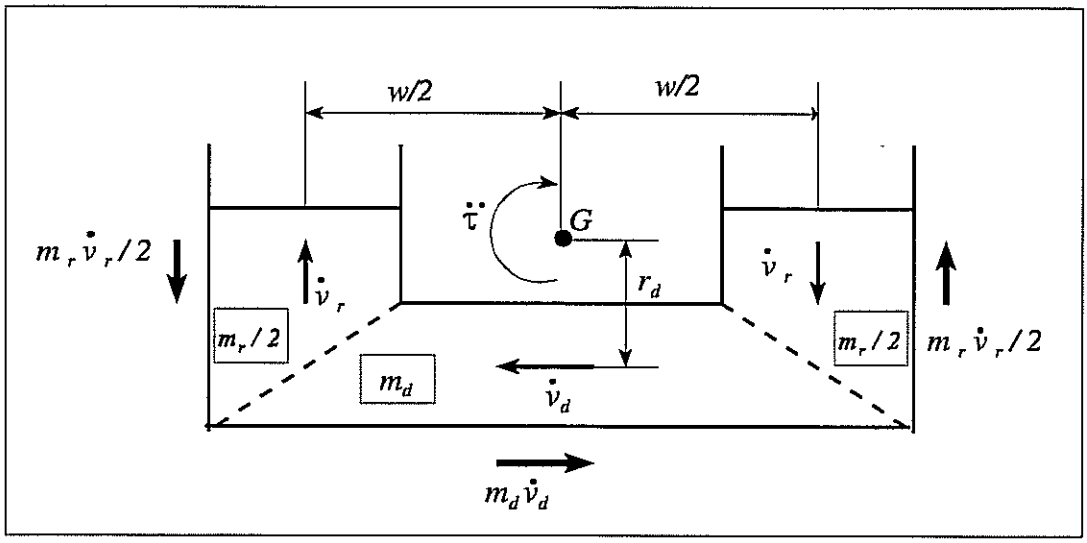

Fig 12.31 - Fluid accelerations and reaction forces in a passive tank

$$\dot{v}_r = \frac{w\ \ddot{\tau}}{2}\ ; \quad \dot{v}_d = \frac{w_r\ w\ \ddot{\tau}}{2\ h_d} \quad m/sec^2$$

and the masses of the fluid in the two reservoirs and the duct are

$$m_r = 2\ \rho_t\ h_r\ w_r\ x_t\ ; \quad m_d = \rho_t\ w\ h_d\ x_t \quad t$$

The lateral force which must be applied to the tank to sustain these clockwise (positive) accelerations is:

$$a_{2\tau}\ \ddot{\tau} = m_d\ \dot{v}_d = \frac{\rho_t\ w_r\ w^2\ x_t\ \ddot{\tau}}{2} \quad kN \quad \text{to starboard}$$

so that

$$a_{2\tau} = Q_t = -\ a_{\tau 2} \quad kN\ /\ (rad/sec^2) \qquad (12.55a)$$

Since the tank is located x_{BI} metres forward of the centre of gravity the yaw moment required to sustain the accelerations is

$$a_{6\tau}\ \ddot{\tau} = x_{BI}\ a_{2\tau}\ \ddot{\tau} \quad kN\ m \text{ to starboard}$$

so that

$$a_{6\tau} = Q_t\ x_{BI} = -\ a_{\tau 6} \quad kN\ m\ /\ (rad/sec^2) \qquad (12.55b)$$

The roll moment required to sustain the acceleration of the fluid in the reservoirs is

$$\frac{m_r \dot{v}_r w}{2} = \frac{\rho_t h_r w_r w^2 x_t \ddot{\tau}}{2} \quad kN\ m \quad \text{to port}$$

and the roll moment required to sustain the acceleration of the fluid in the duct is

$$m_d \dot{v}_d r_d = \frac{\rho_t r_d w_r w^2 x_t \ddot{\tau}}{2} \quad kN\ m \quad \text{to port}$$

so that the total roll moment is

$$a_{4\tau} \ddot{\tau} = \frac{\rho_t w_r w^2 x_t (h_r + r_d) \ddot{\tau}}{2} \quad kN\ m \quad \text{to port}$$

and we obtain

$$a_{4\tau} = Q_t (h_r + r_d) = a_{\tau 4} \quad kN\ m\ /\ (rad/sec^2) \qquad (12.55c)$$

Finally we obtain the coefficient $c_{4\tau}$ by considering the roll moment required to sustain a steady positive tank angle τ. The mass of fluid above the datum level in the port reservoir in Figure 12.32 is

$$\frac{\rho_t w_r w x_t \tau}{2} \quad t$$

and a similar mass is displaced from the starboard reservoir. So the applied moment is

$$c_{4\tau} \tau = \frac{\rho_t g w_r w^2 x_t \tau}{2} \quad kN\ m \quad \text{to port}$$

and

$$c_{4\tau} = Q_t g = c_{\tau\tau} = c_{\tau 4} \quad kN\ m\ /\ rad \qquad (12.55d)$$

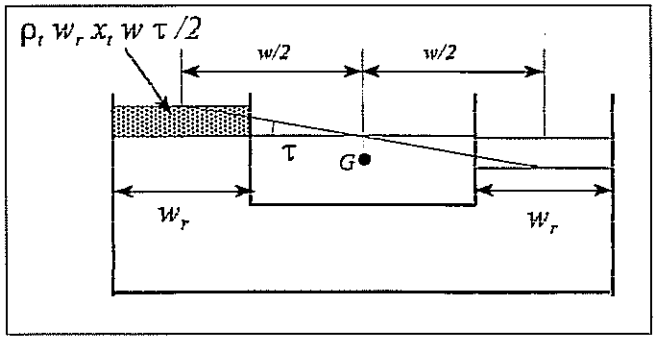

Fig 12.32 - Roll moment due to tank angle.

12.14 PASSIVE TANK NATURAL FREQUENCY AND DAMPING

The motion of the fluid in the tank is governed by Equation (12.52) which may be rewritten in the form

$$a_{\tau\tau}\,\ddot{\tau} + b_{\tau\tau}\,\dot{\tau} + c_{\tau\tau}\,\tau = -\,a_{\tau 4}\,\ddot{x}_4 - c_{\tau 4}\,x_4 - a_{\tau 2}\,\ddot{x}_2 - a_{\tau 6}\,\ddot{x}_6 \quad kN\ m \tag{12.56}$$

This has the same form as the equation for the motion of a second order linear damped spring mass system (Equation (A.1.1)) with the right hand side providing the excitation to the tank from the ship. Using Equations (A1.6) and (12.53) we find that the undamped natural frequency of the tank is:

$$\omega_{nt} = \sqrt{\frac{c_{\tau\tau}}{a_{\tau\tau}}} = \sqrt{\frac{2\,g\,h_d}{w_r\,w + 2\,h_r\,h_d}} \quad rad/sec \tag{12.57}$$

The non dimensional tank damping or decay coefficient is, from Equation (A1.10),

$$\eta_t = \frac{b_{\tau\tau}}{2\sqrt{c_{\tau\tau}\,a_{\tau\tau}}} \tag{12.58}$$

The tank decay coefficient may be determined with a simple free decay experiment on a fixed model of the tank. The model should be of fairly large scale and is conveniently made in acrylic sheet or some other transparent material so that the oscillations of the fluid may easily be observed. The tank fluid should be displaced towards one side of the tank and then released. The subsequent decay of the tank angle oscillations should be recorded and the decay coefficient estimated from Equation (A1.18). The dimensional tank damping coefficient is then given by

$$b_{\tau\tau} = 2\eta_t\,Q_t\sqrt{g\,w_r\left(\frac{w}{2h_d} + \frac{h_r}{w_r}\right)} = \frac{2\,\eta_t\,Q_t\,g}{\omega_{nt}} \quad kN\ m\ /(rad/sec) \tag{12.59}$$

12.15 DESIGN OF PASSIVE STABILISING TANKS

Figure 12.33 shows a block diagram representation of a ship stabilised with a passive tank. The basic requirement for optimum tank performance is exactly the same as for active fin roll stabilisers. We again require the open loop phase to be zero so that the stabilising moment applied by the tank is in exact opposition to the roll moment excitation applied by the waves. Once again it is impossible to achieve this desirable state at all frequencies simultaneously and we choose to optimise the performance at the natural roll frequency where most of the rolling motion occurs. The roll motion lags the wave excitation by 90° at the natural roll frequency and we therefore require the stabilising moment to lead the roll motion by 90° at this frequency. It will also be desirable to arrange for the stabilising moment to be a maximum at the natural roll frequency.

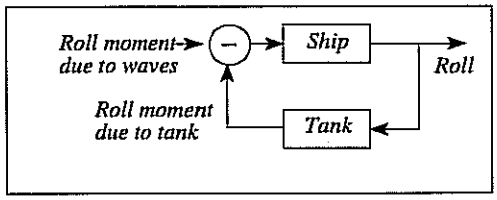

Fig 12.33 - Block diagram for a ship with a passive stabiliser tank.

The roll moment applied by the tank to the ship may be calculated using Equations (12.56) and (12.54b). The algebra is considerably simplified if we neglect the influence of sway and yaw accelerations. We suppose that the ship is rolling in regular waves and that the roll motion is given by

$$x_4 = x_{40} \sin (\omega_e t) \quad rad$$

and that the resulting tank motion is

$$\tau = \tau_0 \sin (\omega_e t + \epsilon_{t1}) \quad rad$$

Substituting these expressions and their derivatives in Equation (12.56) we obtain the tank angle amplitude for a given roll angle amplitude as

$$\frac{\tau_0}{x_{40}} = \frac{(c_{\tau 4} - a_{\tau 4} \omega_e^2)}{\sqrt{(c_{\tau\tau} - a_{\tau\tau} \omega_e^2)^2 + b_{\tau\tau}^2 \omega_e^2}} \quad kN\ m/rad \qquad (12.60)$$

The stabilising moment applied to the ship is

$$F_{\tau 4} = F_{\tau 40} \sin (\omega_e t + \epsilon_{t2}) = a_{4\tau} \ddot{\tau} + c_{4\tau} \tau \quad kN\ m$$

(See Equation (12.54b). Making the same substitutions we obtain the tank moment amplitude response to roll motion

$$\frac{F_{\tau 40}}{x_{40}} = c_{4\tau} - a_{4\tau} \omega_e^2$$

and using Equations (12.55c) and (12.55d) we find the tank stabilising moment amplitude

response to roll motion is

$$\frac{F_{\tau 40}}{x_{40}} = \frac{(c_{\tau 4} - a_{\tau 4}\,\omega_e^2)^2}{\sqrt{(c_{\tau\tau} - a_{\tau\tau}\,\omega_e^2)^2 + b_{\tau\tau}^2\,\omega_e^2}}$$

$$= \frac{Q_t\, g \left(1 - \frac{a_{\tau 4}}{a_{\tau\tau}} \Lambda^2 \right)^2}{\sqrt{(1 - \Lambda^2)^2 + 4\,\eta_t^2\,\Lambda^2}} \quad kN\ m/rad \qquad (12.61)$$

and the phase is given by

$$tan\ \epsilon_{t2} = tan\ \epsilon_{t1} = \frac{-\,b_{\tau\tau}\,\omega_e}{c_{\tau\tau} - a_{\tau\tau}\,\omega_e^2} = \frac{-\,2\,\eta_t\,\Lambda}{1 - \Lambda^2} \qquad (12.62)$$

showing that the tank moment is always in phase with the tank motion.

Figure 12.34 shows the tank stabilising moment amplitude and phase responses calculated from these equations for a tank with the following characteristics:

$w = 20\ m$; $w_r = 3\ m$; $h_r = 5\ m$; $h_d = 1\ m$; $h_t = 10\ m$; $\eta_t = 0.1$
$r_d = -\,1.5\ m$; $x_t = 1.0\ m$; $\rho_t = 1.0\ t/m^3$

giving a tank natural frequency (Equation (12.57))

$$\omega_{nt} = 0.529\ rad/sec$$

This shows that the stabilising moment is a near maximum at the tank natural frequency ω_{nt} and that the phase at this frequency is

$$\epsilon_{t1} = 90^o$$

Evidently the optimum tank performance will be assured if we arrange for the tank and ship roll natural frequencies to be the same. This ensures that the stabilising moment is a maximum and leads the roll motion by 90° at the natural roll frequency.

12.16 PASSIVE TANK CHARACTERISTICS AND DESIGN RECOMMENDATIONS

12.16.1 Natural frequency

Equation (12.57) gives the tank natural frequency as a function of the tank dimensions and the depth of the fluid. The equation may be used to show that the tank natural frequency decreases with the widths w and w_r and increases with the duct depth h_d . However the natural frequency is quite insensitive to the depth of fluid h_r in the tank. It follows that there is little scope for

adjusting the natural frequency after the tank has been designed and fitted to the ship.

12.16.2 Fluid depth and maximum tank angle

In practice h_r should be selected to give a datum fluid level halfway up each reservoir. This gives the greatest possible scope for fluid motion and maximises the available stabilising moment. The maximum possible tank angle is then given by

$$tan\ \tau_{max} = \frac{h_t - h_d}{w} \tag{12.63}$$

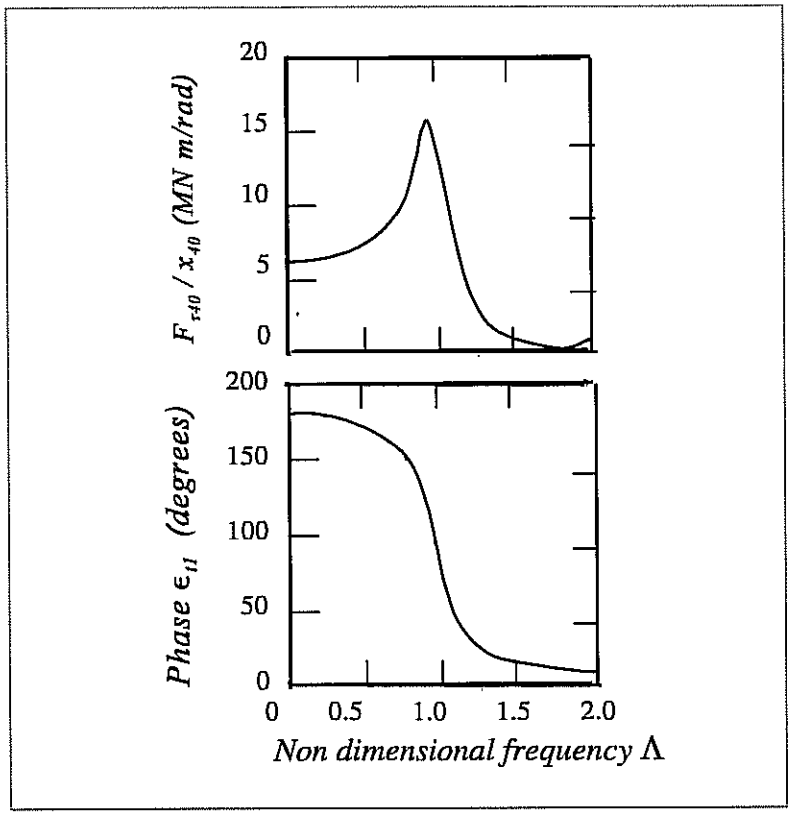

Fig 12.34 - Passive tank stabilising moment characteristics

12.16.3 Maximum stabilising moment

The stabilising moments developed at the natural roll frequency may be obtained by setting $\Lambda = 1.0$ in Equation (12.61) to give

$$\frac{F_{\tau 40}}{x_{40}} = \frac{Q_t\ g \left(1 - \frac{a_{\tau 4}}{a_{\tau\tau}} \right)^2}{2\ \eta_t} \quad kN\ m/rad \tag{12.64}$$

Now we have seen that the natural frequency is determined by the tank dimensions w, w_r and h_d

(see Equation (12.57)). The remaining parameters ρ_t , x_t , η_t and r_d have no effect on the natural frequency but may be chosen to achieve the required maximum stabilising moment . The stabilising moment clearly increases with the fluid density ρ_t and the tank length x_t and Equation (12.64) may be used to show that the peak stabilising moment increases if the tank is located high in the ship (ie r_d is small or negative).

12.16.4 Loss of metacentric height

As already mentioned one penalty of passive stabilising tanks is the inherent loss of roll stability because of the free surface effect[3] .This may be estimated using Equation (12.54b). If we consider the roll behaviour of the ship at zero frequency we may neglect all the velocity and acceleration terms and write

$$c_{44}\, x_4 - c_{4\tau}\, \tau = F_4 \quad kN\ m$$

where F_4 is some steady applied roll moment. Now the tank angle is, from Equations (12.52) and (12.53g),

$$\tau = - x_4 \quad rad$$

and using Equation (12.55d) we find

$$m\ g\ \overline{GM_S}\ (\ 1 - \mu_t\ )\ x_4 = F_4 \quad kN\ m$$

where μ_t is the fractional loss in metacentric height:

$$\mu_t = \frac{Q_t}{m\ \overline{GM_S}} \tag{12.65}$$

Clearly this loss of stability is undesirable and μ_t is usually limited to about 0.25.

12.16.5 Mass of working fluid

The mass of fluid in the tank is given by

$$m_t = \rho_t\, x_t\, (\ w\ h_d + 2\ h_r\ w_r\ ) \quad t \tag{12.66}$$

and it is usually found that a satisfactory degree of stabilisation can be achieved if m_t is of the order of 1% - 5% of the ship mass.

[3] See any text book on naval architecture or seamanship.

12.16.5 Tank damping

The tank damping may be adjusted by installing an obstruction or a throttle valve in the duct as shown in Figure 12.28. Figure 12.35 shows the effect of increasing the tank damping on the roll transfer function for a ship in beam waves at zero speed. With low tank damping the roll response peak at the natural roll frequency is effectively eliminated but this is at the expense of resonant peaks at higher and lower frequencies. These indicate that the tank will amplify the motions at these frequencies, possibly leading to an overall amplification of the roll motion, depending on the shape of the wave energy spectrum. They may be eliminated, or at least reduced, by increasing the tank damping. The motion at low frequencies is still amplified but this is a characteristic common to all passive tanks since the loss in stability ensures that the "stabilised" roll motion at zero frequency always exceeds the unstabilised roll motion.

12.17 PERFORMANCE OF PASSIVE STABILISING TANKS.

Figure 12.36 shows the performance of the tank described earlier fitted to a 4000 tonne ship. The calculations are for a loss in stability of $\mu = 0.2$ and a tank mass of 1.87% of the ship mass.

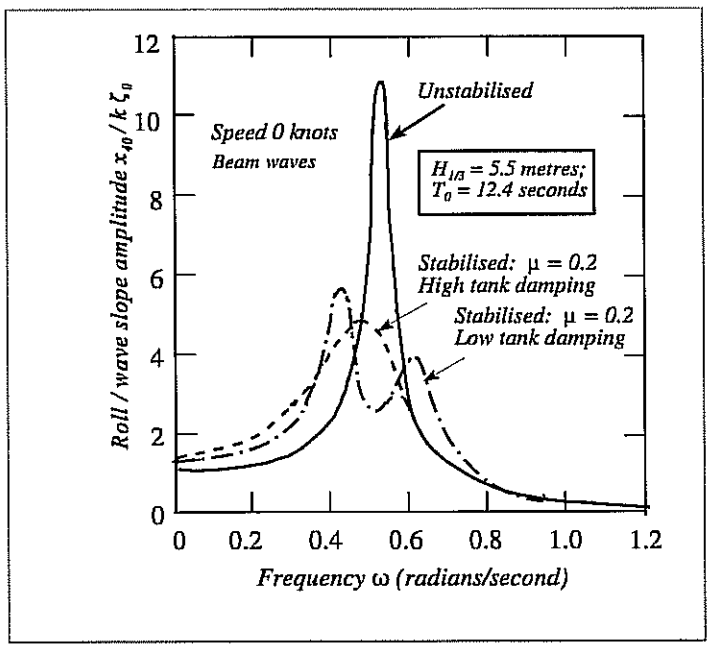

Fig 12.35 - Typical roll transfer functions showing the effect of tank damping

At zero speed the tank gives a useful reduction in roll motion at all headings. This is because the inherent roll damping due to the hull, bilge keels and other appendages at low speed is small and the damping provided by the tank makes a substantial additional contribution. At 20 knots the hydrodynamic damping is much higher and the contribution provided by the tank is relatively insignificant. So the tank is unable to achieve a worthwhile reduction in roll motion.

Figure 12.36 also shows the penalty of the loss of stability at high speed in following seas. The encounter frequencies are then very low and the tank amplifies the roll motion.

Also shown in Figure 12.36 is the rms tank motion for each speed. Equation (12.62) gives the maximum permissible tank angle as $\tau_{max} = 24.2^0$. The rms tank angles corresponding to various

probabilities of exceeding this level may be estimated from Table 11.5:

Probability of tank angle exceeding 24.2°	Rms tank angle (degrees)
0.1	11.3
0.01	7.4
0.001	6.0

These are plotted in Figure 12.36. Evidently the tank motion is sufficient to reach the tops of the reservoirs and the duct about once in every 100 oscillations on the worst heading in this particular sea condition. This would be regarded as satisfactory in practice. A more frequent rate of exceedance would invalidate the calculation which takes no account of any such limits in the tank's stabilising capacity. This could be rectified by increasing the height of the reservoirs and the depth h_r of the working fluid.

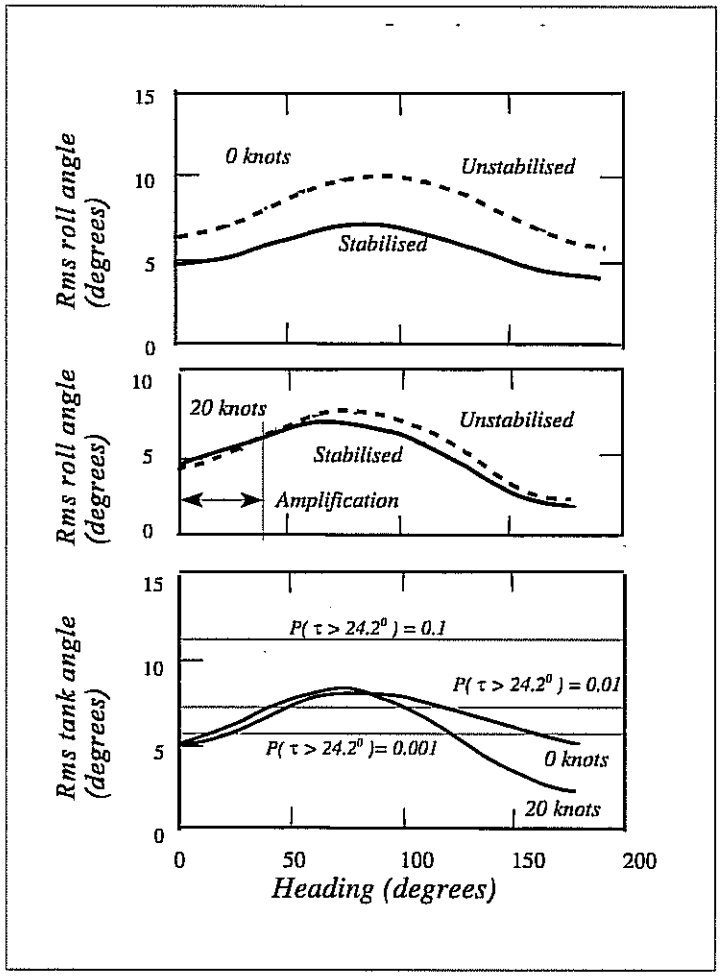

Fig 12.36 - Passive stabilising tank performance

13

ADDED RESISTANCE AND INVOLUNTARY SPEED LOSS IN WAVES

13.1 INTRODUCTION

The speed a ship can achieve in calm water is governed by its resistance, propeller efficiency and the power of its engines. In rough weather the resistance may be changed by the action of the waves and the wind and the resulting change in the load on the propeller usually reduces the propeller efficiency. The speed the ship can achieve for a given engine power is usually reduced by these effects. This 'involuntary' speed loss does not often amount to more than two or three knots but may still result in substantial financial losses for merchant ships.

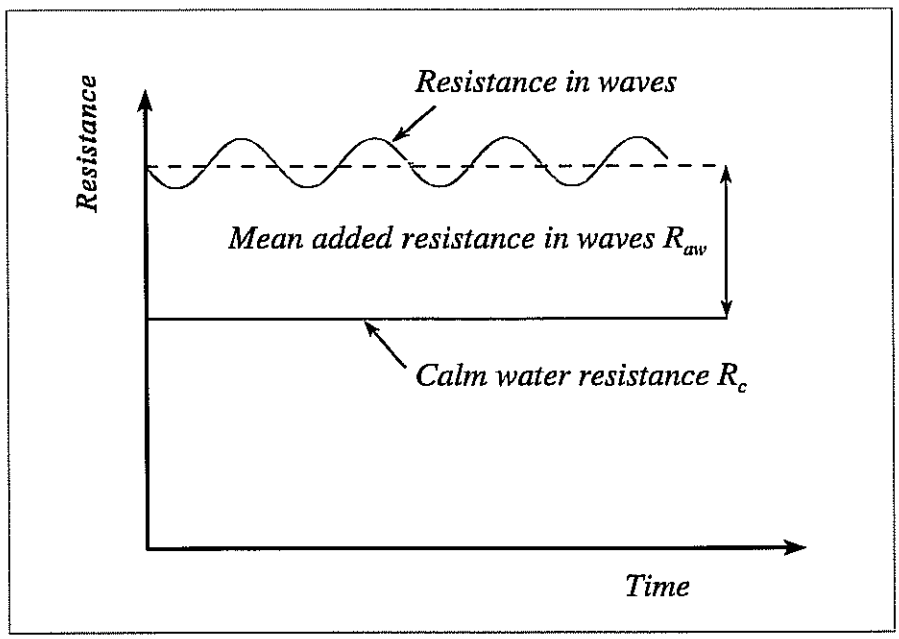

Fig 13.1 - Resistance in regular waves.

13.2 SIMPLE THEORY FOR ADDED RESISTANCE IN REGULAR HEAD WAVES

A ship towed in regular waves will have a fluctuating resistance as illustrated in Figure. 13.1. In head waves the mean value of the resistance will be greater than the calm water resistance and the difference may be attributed to the effects of the waves.

The simple theory for this added resistance presented here is based on that proposed by Gerritsma and Beukelman (1971) and has its origins in the strip theory described in Chapter 4. We shall confine our attention to long crested head waves which is generally accepted as the most severe case. Only vertical plane motions then occur.

Consider the relative motion of a strip located x_{BI} metres forward of the centre of gravity. At the water surface this is given by Equation (7.13) as:

$$r_3 = s_3 - \zeta \quad m$$

where s_3 is the absolute motion of the strip given by Equation (7.8):

$$s_3 = x_3 - x_{BI}\, x_5 \quad m$$

Since we are here concerned with the average relative vertical motion experienced over the draught of the ship, it is appropriate to take the wave elevation at the local mean draught $\bar{D}$:

$$\bar{D} = \frac{A'}{B'} \quad m$$

rather than at the surface. In this case the relative motion becomes

$$r_3 = s_3 - \zeta\, exp\, (-\, k\, \bar{D}\,) \quad m \tag{13.1}$$

The force required to sustain this motion is, by analogy with Equation (4.10),

$$\delta F_3 = \left[(m' + a'_{33})\, \ddot{r}_3 + \left(b'_{33} - U\frac{da'_{33}}{dx_{BI}} \right) \dot{r}_3 + c'_{33}\, r_3 \right] \quad kN \tag{13.2}$$

per metre length of strip. Now the relative motion may be written (Equation (7.14))

$$r_3 = r_{30}\, sin\, (\, \omega_e\, t + \delta_{r3}\,) \quad m$$

and the work done by the strip in one complete cycle is then

$$\delta E = \int_0^{T_e} \delta F_3\, \delta r_3 = \pi \left(b'_{33} - U\frac{da'_{33}}{dx_{BI}} \right) \omega_e\, r_{30}^2 \quad kN\, m \tag{13.3}$$

The total work done by the whole ship in one encounter period is obtained by allowing δx_{B1} to approach zero and integrating Equation (13.3) over the hull length:

$$E = \pi\, \omega_e \int_0^{L} \left(b'_{33} - U\, \frac{da'_{33}}{dx_{BI}} \right) r_{30}^2\, dx_{BI} \quad kN\, m \tag{13.4}$$

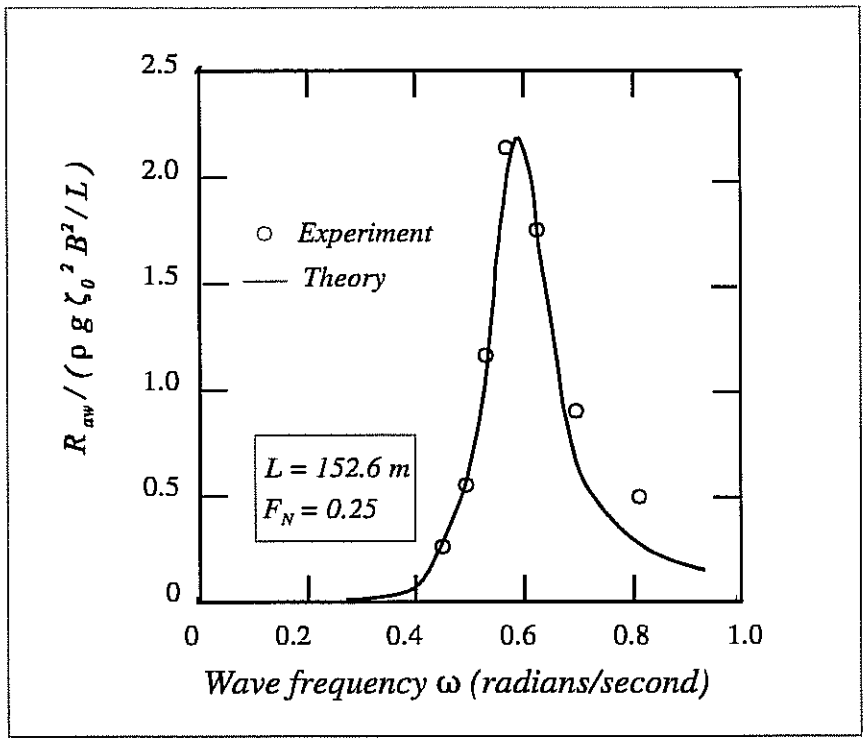

Fig 13.2 - Added resistance response curve for a fast cargo ship in regular head waves (After Gerritsma and Beukelman (1971))

This work must be supplied by the ship's engine as an additional quantity over that required to drive the ship in calm water. If the total resistance of the ship in waves is written as

$$R = R_c + R_{aw} \quad kN$$

where R_c is the calm water resistance and R_{aw} is the added resistance due to the waves, the additional work required to drive the ship through one wave length is

$$E = R_{aw}\ \lambda \quad kN\ m$$

and the added resistance is

$$R_{aw} = \frac{\pi\ \omega_e}{\lambda} \int_0^{L_p} \left(b_{33}' - U \frac{da_{33}'}{dx_{BI}} \right) r_{30}^2\ dx_{BI} \quad kN \qquad (13.5)$$

Now the relative motion amplitude r_{30} is proportional to the wave amplitude ζ_0 and it follows that the added resistance in regular waves must be proportional to the square of the wave amplitude. A suitable non dimensional added resistance 'transfer function' applicable to all wave amplitudes must therefore include the wave amplitude squared in the denominator. Figure. 13.2 shows a widely accepted non dimensional form for plotting the added resistance in regular waves. These results were obtained by Gerritsma and Beukelman (1971) and show

an encouraging comparison between their predictions and measurements on a model of a fast cargo ship in regular head waves. The added resistance response peak occurs when the relative motions are a maximum. In very long waves (low wave frequencies) the relative motions are very small (see Figure 7.22) and the added resistance tends to zero. In very short waves the relative motion approaches the wave amplitude as the absolute motions become negligible. The added resistance is then due to wave diffraction and reflection and approaches some small but finite value.

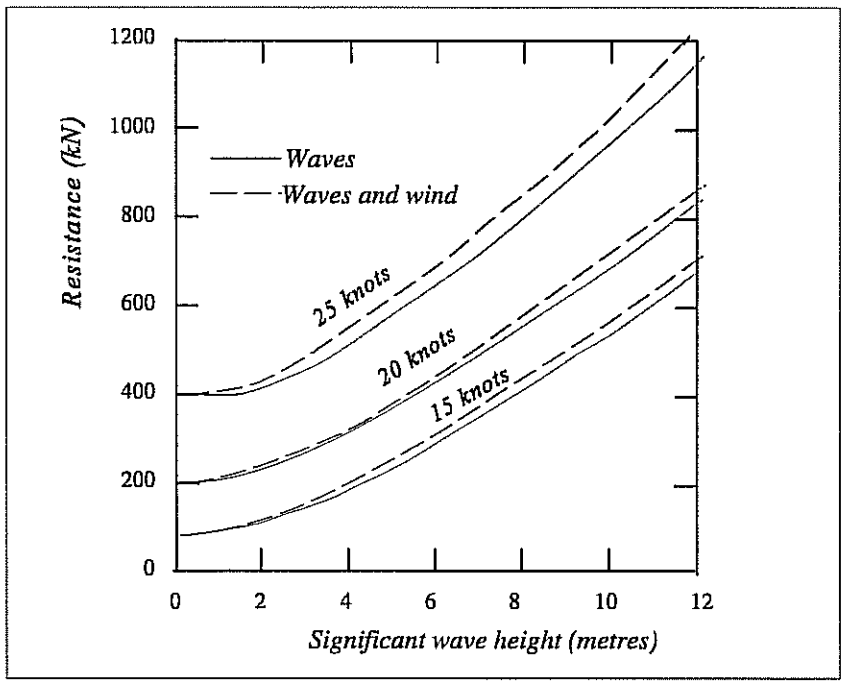

Fig 13.3 - Resistance of the frigate in head winds and irregular head waves

13.3 ADDED RESISTANCE IN IRREGULAR HEAD WAVES

Consider the narrow band of frequencies centred on some encounter frequency ω_e in the encountered wave energy spectrum shown in Figure 8.2.

If we replace the wave components in this small range of frequencies by a single sine wave, the amplitude of the sine wave must be, by analogy with Equation (2.13a)

$$\zeta_0 = \sqrt{2\, S_\zeta\, (\, \omega_e\,)\, \delta\omega_e} \quad m$$

and the added resistance due to this single sine wave is

$$2\, C_{aw}\, S_\zeta\, (\omega_e)\, \delta\omega_e \quad kN$$

where

$$C_{aw} = \frac{R_{aw}}{\zeta_0^2} \quad kN/m^2 \qquad (13.6)$$

is a dimensional added resistance response function. The total added resistance due to all the wave components in the encountered wave spectrum is obtained by allowing $\delta\omega_e$ to approach zero and integrating to give

$$\overline{R}_{aw} = 2 \int_0^\infty C_{aw} \, S_\zeta(\omega_e) \, d\omega_e \quad kN \tag{13.7}$$

Figure. 13.3 shows the results of some typical calculations of the resistance in irregular waves for a frigate. The resistance rises rapidly with significant wave height, and the greatest increase relative to the calm water resistance occurs at low speed.

13.4 ADDED RESISTANCE DUE TO WIND

Part of the resistance of the ship in calm water is accounted for by the aerodynamic drag of the superstructure and the above water part of the hull. It is customary to express this drag in the form

$$F_{Dc} = C_D \, \tfrac{1}{2} \, \rho_A \, U^2 \, A_s \quad kN \tag{13.8}$$

where

F_{Dc} is the drag force in kN
ρ_A is the density of air in tonnes/metres^3
U is the speed of the ship in metres/second
A_s is the maximum cross section area of the superstructure and above water part of the hull in metres^2.

The drag coefficient C_D may be determined from wind tunnel tests on a model of the above water hull form and superstructure of the ship.

Head waves are generally accompanied by head winds and this increases the aerodynamic drag to

$$F_{DA} = C_D \, \tfrac{1}{2} \, \rho_A \, (\, U + U_A \,)^2 \, A_s \quad kN$$

and the additional drag due to the ambient wind U_A is

$$F_{DAaw} = C_D \, \tfrac{1}{2} \, \rho_A \, (\, U_A^2 + 2 \, U \, U_A \,) \, A_s \quad kN \tag{13.9}$$

There is of course no direct relationship between the wind and the sea state, but estimates of the aerodynamic drag associated with a particular sea state may be obtained by calculating the drag for the most probable wind speeds given in Table 2.4. Figure. 13.3 shows the additional drag calculated in this way for the frigate. The contribution from the wind is quite small compared with the increase in resistance due to the waves.

13.5 PROPELLER CHARACTERISTICS

The speed attained by the ship for a given resistance depends on the hydrodynamic characteristics of the propeller. Figure 13.4 shows a typical set of these characteristics obtained from cavitation tunnel tests on a model propeller. The diagram shows, in non dimensional form, the thrust developed and the torque absorbed by the propeller as a function of the advance coefficient. The advance coefficient is a measure of the 'slip' of the propeller and is defined by

$$J = \frac{U_p}{N\ d} \tag{13.10}$$

where

U_p is the mean velocity of the flow through the propeller disc in metres/second
N is the number of propeller revolutions/second
d is the propeller diameter in metres.

The velocity through the propeller disc is somewhat less than the forward speed of the ship because of the effects of the boundary layer on the hull. The two velocities are related by the ***Taylor wake fraction*** which is defined as

$$w_T = \frac{U - U_p}{U} \tag{13.11}$$

from which we find that the mean velocity through the propeller disc is

$$U_p = U\ (\ 1 - w_T\ ) \quad m/sec \tag{13.12}$$

The Taylor wake fraction is usually of the order of 10% and may be measured in suitable model experiments.

Combining Equations (13.10) and (13.12) we see that the advance coefficient may also be written as

$$J = \frac{U\ (\ 1 - w_T\ )}{N\ d} \tag{13.13}$$

The thrust and torque coefficients in Figure 13.4 are defined as

$$K_T = \frac{T}{\rho\ N^2\ d^4} \tag{13.14}$$

$$K_Q = \frac{Q}{\rho\ N^2\ d^5} \tag{13.15}$$

where T is the thrust kN and Q is the torque in kN metres.

The efficiency of the propeller is defined as the ratio

$$\eta = \frac{power\ delivered}{power\ absorbed} = \frac{T\ U\ (\ 1\ -\ w_T\ )}{2\ \pi\ N\ Q} \qquad (13.16)$$

At high values of advance coefficient the propeller is turning very slowly in relation to the forward speed of the ship and the thrust developed and the torque absorbed are both small. The thrust will be less than the resistance and the ship will slow down. At low values of the advance coefficient the propeller revolutions are high in relation to the forward speed and the thrust and torque coefficients are both large. The thrust will then exceed the resistance and the ship will accelerate.

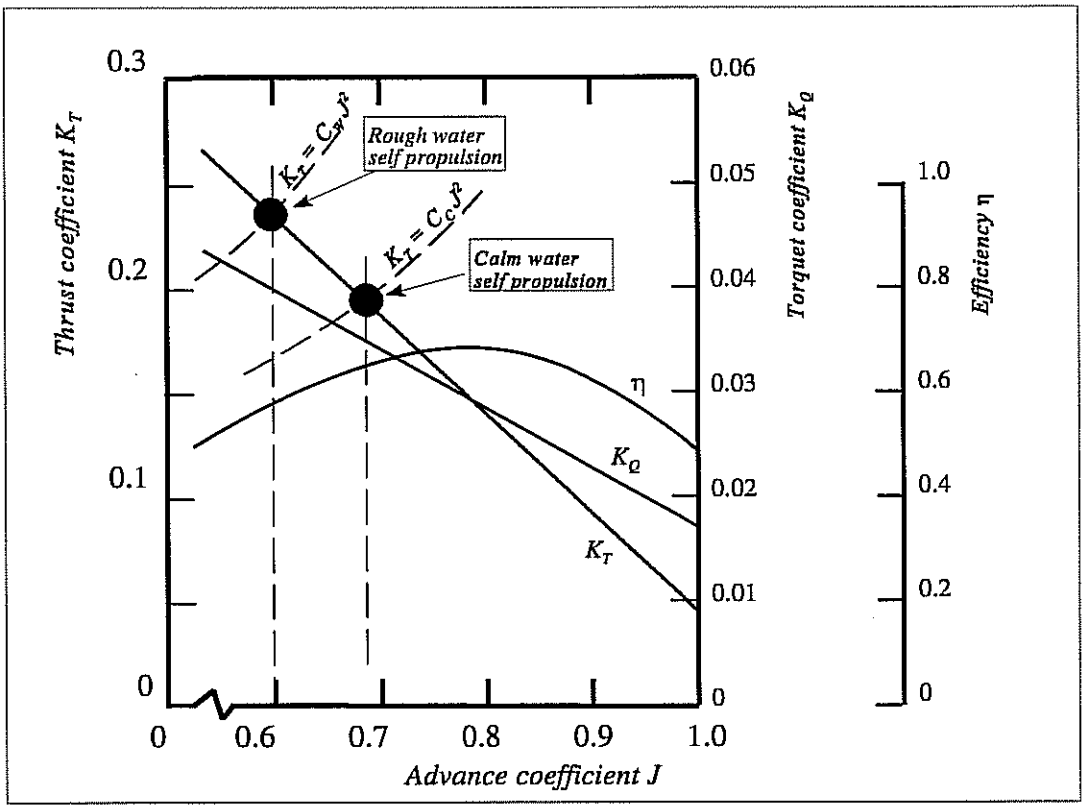

Fig 13.4 - Typical propeller characteristics

At some intermediate value of the advance coefficient the thrust will equal the ship resistance and the ship speed will be maintained. This condition determines the advance coefficient for 'self propulsion'.

The presence of the propeller augments the ship resistance by a small fraction a so that the effective resistance for the self propulsion calculation for calm water is

$$R_{ca} = R_c\ (1\ +\ a) \quad kN$$

The total thrust required at self propulsion in calm water is then

$$T = R_c \, (\, 1 + a \,) \quad kN \tag{13.17}$$

giving a thrust coefficient

$$K_T = C_c \, J^2 \tag{13.18}$$

where C_c is a constant for a given speed:

$$C_c = \frac{R_c \, (\, 1 + a \,)}{\rho \, U^2 \, d^2 \, (\, 1 - w_T \,)^2} \tag{13.19}$$

Equation (13.18) defines the relationship required between K_T and J to propel the ship at speed U metres/second in calm water. The values of K_T and J which define the operating conditions of the propeller are determined by the intersection of Equation (13.18) and the K_T versus J curve as shown in Figure 13.4. The resulting self propulsion advance coefficient J_c determines the propeller revolutions required to drive the ship at the chosen speed in calm water:

$$N_c = \frac{U \, (\, 1 - w_T \,)}{J_c \, d} \quad revs/sec \tag{13.20}$$

The power required to achieve these revolutions is given by

$$\begin{aligned} P_c &= 2 \, \pi \, Q_c \, N_c \\ &= 2 \, \pi \, K_{Qc} \, \rho \, N_c^3 \, d^5 \quad kW \end{aligned} \tag{13.21}$$

The characteristics of the propeller are determined for the steady flow conditions experienced in calm water. In rough weather the waves and the ship motions will cause the flow around the propeller to fluctuate but it is generally assumed that the operating characteristics of the propeller, the Taylor wake fraction and the resistance augment will remain unchanged from their calm water values. In this case the self propulsion advance coefficient and the power required to drive the ship at a given speed in waves may be determined in exactly the same way as for calm water. The resistance in now given by

$$R = (\, R_c + R_{aw} \,)(\, 1 + a \,) + D_{aw} \quad kN \tag{13.22}$$

and the required relationship between K_T and J is given by

$$K_T = C_w \, J^2 \tag{13.23}$$

where

$$C_w = \frac{(\, R_c + R_{aw} \,) \, (\, 1 + a \,) + D_{aw}}{\rho \, U^2 \, d^2 \, (\, 1 - w_T \,)^2} \tag{13.24}$$

The self propulsion advance coefficient J_w for rough water is determined by the intersection of Equation (13.23) with the K_T versus J curve as shown in Figure 13.4. The effect of the added resistance is to reduce the self propulsion advance coefficient so that the propeller revolutions required to maintain a given speed become

$$N_w = \frac{U\ (\ 1\ -\ w_T)}{J_w\ d} \quad revs/sec \tag{13.25}$$

The propeller efficiency is reduced and the power required to maintain this speed is

$$P_w = 2\ \pi\ K_{Qw}\ \rho\ N_w^3\ d^5 \quad kW \tag{13.26}$$

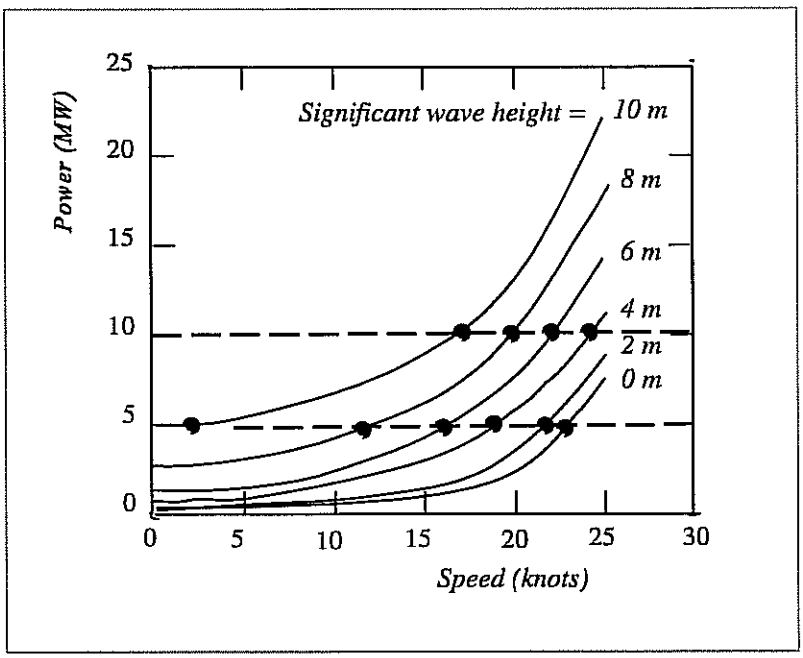

Fig 13.5 - Power for the frigate in irregular head waves

13.6 INVOLUNTARY SPEED LOSS

In the previous section it was shown that the advance coefficient is decreased and the propeller loading increased in rough weather. The consequent reduction in speed depends on how the engines respond to this change in load. In general we should expect the propeller revolutions to fall, although the actual decrease in propeller speed may be difficult to determine. For the sake of simplicity we shall assume here that the engine delivers constant power at a given throttle setting regardless of the load.

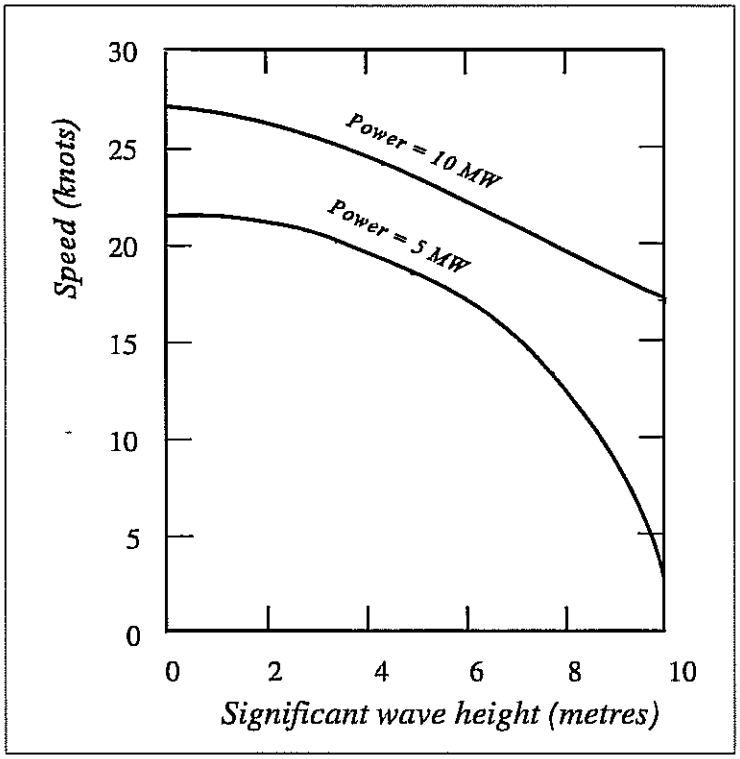

Fig 13.6 - Speed loss at constant power for the frigate in irregular head waves

The power required to drive the ship/propeller combination at a given speed in a specified wave system may be calculated using the methods described above. Figure 13.5 shows the results of such a calculation for the ship whose resistance characteristics are given in Figure 13.3, fitted with the propeller of Figure 13.4. As expected the power rises steeply with the forward speed and the significant wave height. The speed that can be achieved at a given power level may be determined for a number of significant wave heights and the results plotted as shown in Figure 13.6.

The loss of speed due to the increase of resistance in waves and wind is termed the ***involuntary speed loss*** since the captain has no control over it, in contrast to the voluntary speed loss discussed in Chapter 16.

The speed loss is quite small at high power. At lower power levels much more dramatic losses occur and in extreme cases the speed may even be reduced to zero.

14

SLAMMING, DECK WETNESS AND PROPELLER EMERGENCE

"When the cabin port-holes are dark and green
Because of the seas outside;
When the ship goes wop (with a wiggle between)
And the steward falls in the soup-tureen,
And the trunks begin to slide;
When Nursey lies on the floor in a heap,
And Mummy tells you to let her sleep,
And you aren't waked or washed or dressed,
Why then you will know (if you haven't guessed)
You're 'Fifty North and Forty West' ".

From "How the whale got his throat" by Rudyard Kipling.

14.1 INTRODUCTION

The relative motions between the ship and the water surface are generally largest at the ends of the ship. In high waves the motions may be so large that the forefoot and propeller are exposed and the deck submerged. This occurs most frequently at high speed in head waves although it is not unknown in other conditions.

The re-entry of the keel after emergence may result in a substantial impact or ***'slam'*** as the ship's bottom strikes the water surface. Ships with heavily flared bows may also experience similar, but less severe, impacts under the bow flare even when there is no keel emergence. These slam impacts may be severe enough to cause local structural damage to the ship's plating. In extreme cases the loading may be sufficient to distort the ship's hull permanently and some ships are believed to have broken up following slamming. Even moderate slamming will cause the hull to vibrate at its natural frequency (generally of the order of a few cycles per second) and the resulting fatigue loading will reduce the life of the hull. The vibration following a slam is called ***'whipping'*** and often provides the captain with his first indication that a slam has occurred.

Deck wetness may occur anywhere along the ship, particularly where the freeboard is low. However, the most severe deck wetness generally occurs, like slamming, at the bow at high speed in head waves. In these conditions the forward speed of the ship accentuates the effects of the water shipped onto the foredeck, and damage to deck fittings and cargo may occur. Any crew or passengers on deck may be injured or washed overboard. In extreme cases the ship might even capsize and sink due to the weight of water taken on board.

Propeller emergence and ***propeller racing*** will begin to occur when the upper tips of the blades emerge from the sea surface. The sudden reduction and subsequent increase of torque loading as the propeller becomes fully submerged again may damage the engine and propeller shaft or even the propeller itself.

Clearly these phenomena are undesirable and the prudent captain will try to avoid them if possible. Since they generally become more severe at high speed they impose an effective limit on the ship speed in rough weather, especially in head waves. This aspect is discussed in Chapter 16.

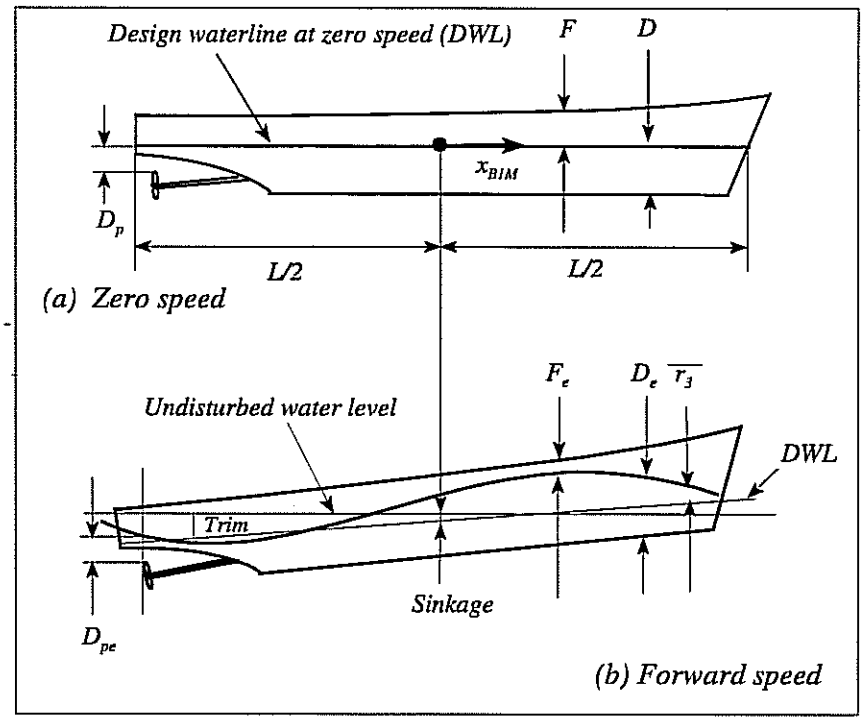

Fig 14.1 - Effective draught and freeboard

14.2 PROBABILITY OF OCCURRENCE

The probabilities of occurrence of slamming, deck wetness and propeller emergence are essentially dependent on the probability of the local relative motion exceeding the draught, freeboard and the depth of the upper tips of the propeller blades.

Figure 14.1 shows how the ship adopts a running trim and creates a wave system which depends on the speed. This gives a steady motion $\bar{r}_3$ even when the ship is running in calm water. If we assume that this datum relative motion is unchanged when the ship is in waves, we may regard it as a change to the draught, freeboard, etc. Thus the effective draught to the keel becomes

$$D_e = D + \bar{r}_3 \quad m \tag{14.1}$$

The effective freeboard is

$$F_e = F - \bar{r}_3 \quad m \tag{14.2}$$

and the effective depth of the tips of the upper propeller blades is

$$D_{pe} = D_p + \bar{r}_3 \quad m \tag{14.3}$$

where $\bar{r}_3$ is of course determined at the appropriate location on the ship.

The ***notional relative motion*** in waves is obtained by subtracting the wave depression from the absolute motion (see Equation (7.13)). As the hull dips into the water the increasing submerged volume causes a local `swell up' of the water surface. The effect disappears as the hull rises. This enhances the relative motion over and above the notional value. We define a ***swell up coefficient*** as

$$C_s = \frac{actual\ relative\ motion\ amplitude}{notional\ relative\ motion\ amplitude} \tag{14.4}$$

and it is found that C_s is a function of hull form, location on the hull, speed and wave length. At the time of writing no universally accepted method of calculating C_s has been developed, but it has been measured in model experiments by several authors. Probably the most comprehensive set of experiment data was published by Blok and Huisman (1984). A selection of their results for a small frigate in regular head waves of length equal to the ship is shown in Figure. 14.2.

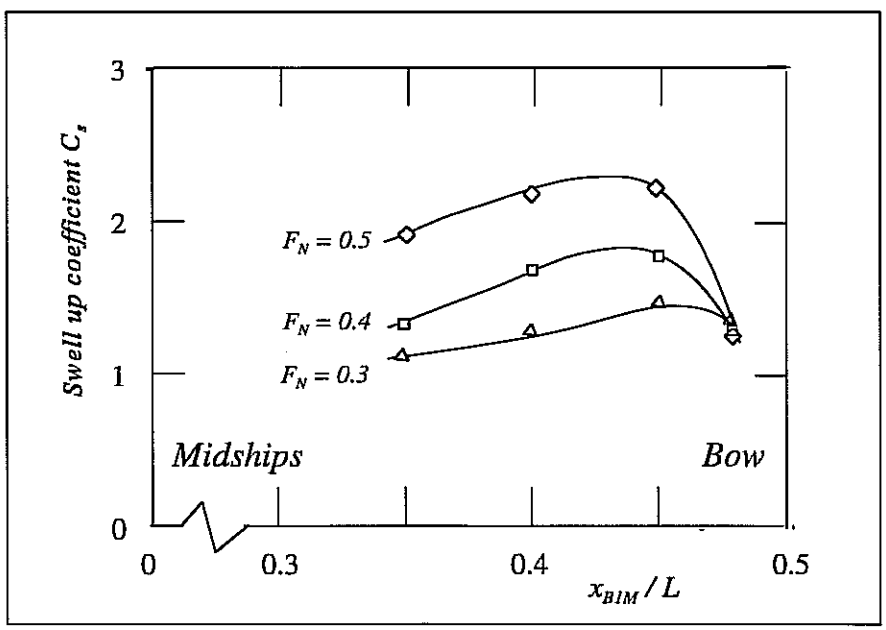

Fig 14.2 - Swell up coefficients for a small frigate. (After Blok and Huisman (1984))

Referring to Equation (11.26) the probability of the local relative motion exceeding the effective draught (i.e the probability of keel emergence) is

$$P_{ke} = exp\left(- \frac{1}{2} \frac{D_{ke}^2}{C_s^2\ m_0} \right) \tag{14.5}$$

where m_0 is the variance of the notional relative motion at the appropriate location on the ship.

A similar expression may be written for the probability of deck submergence:

$$P_{ds} = exp\left(- \frac{1}{2} \frac{F_e^2}{C_s^2 \, m_0} \right) \tag{14.6}$$

and the probability of propeller emergence is

$$P_{pe} = exp\left(- \frac{1}{2} \frac{D_{pe}^2}{C_s^2 \, m_0} \right) \tag{14.7}$$

.

The average period of the peaks may be calculated from Equation (2.27) as

$$\overline{T}_p = 2 \, \pi \sqrt{\frac{m_2}{m_4}} \quad sec \tag{14.8}$$

where m_2 and m_4 are the variance of the notional relative velocity and acceleration at the appropriate location on the ship. The average number of keel emergences, deck submergences and propeller emergences per hour are then

$$N_{ke} = \frac{3600 \, P_{ke}}{\overline{T}_p} \quad per \ hour \tag{14.9}$$

$$N_{ds} = \frac{3600 \, P_{ds}}{\overline{T}_p} \quad per \ hour \tag{14.10}$$

$$N_{pe} = \frac{3600 \, P_{pe}}{\overline{T}_P} \quad per \ hour \tag{14.11}$$

14.3 SLAMMING

14.3.1 Introduction

Figure. 14.3 shows a frigate at high speed in rough weather. The relative motion is sufficient to expose a considerable length of the keel and a slam is clearly imminent. The ship is shrouded in spray from a previous deck wetting and much of the water that was shipped is pouring down the sides to return to the sea beneath the keel. Some water may be drawn up under the keel as it emerges from the sea surface.

The subsequent slam will be into a mixture of air and water which probably helps to cushion the impact. Slamming impact loads are also affected by the local hull section shape, the relative velocity at impact, the relative angle between the keel and the water surface, the local flexibility of the ship's bottom plating and the overall flexibility of the ship's structure. A complete prediction of slamming phenomena is a complex task which is beyond the scope of any existing theory.

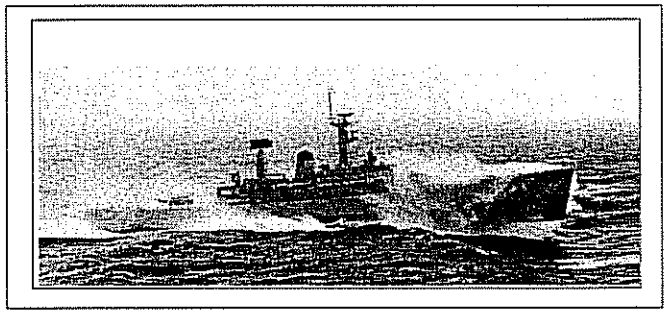

Fig 14.3 - A Leander class frigate struggles to maintain station with the aircraft carrier HMS Ark Royal (from which the picture was taken) in rough weather. A telling illustration of the reasons why seakeeping performance is so important in small warships which may be expected to escort larger vessels which are less susceptible to the weather. (MoD photo)

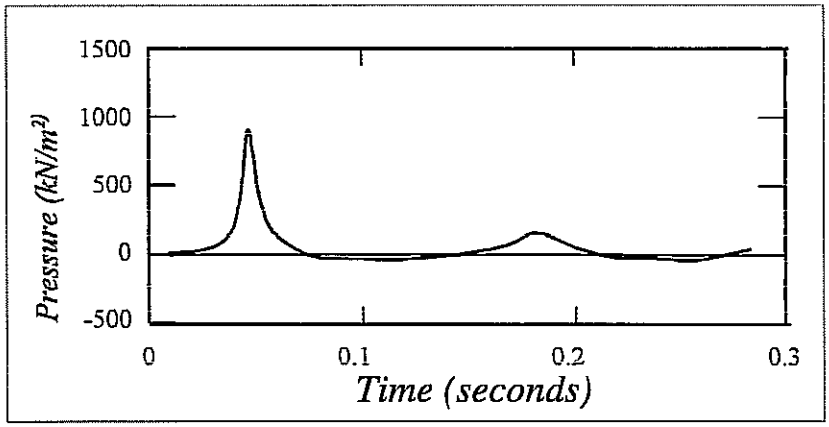

Fig 14.4 - Slamming impact pressure recorded on US Coastguard vessel Unimak (After Sellars (1972))

Full scale measurements of slamming pressures at sea are rare because of the practical difficulties involved, but Figure 14.4 shows a slamming pressure time history recorded by Sellars (1972) on the keel of the US Coast Guard vessel *Unimak* during a severe slam. The pressure rises very quickly after the initial impact: indeed it is suspected that the measured rise is probably limited by the relatively sluggish response of the pressure transducer in all experiments performed to date.

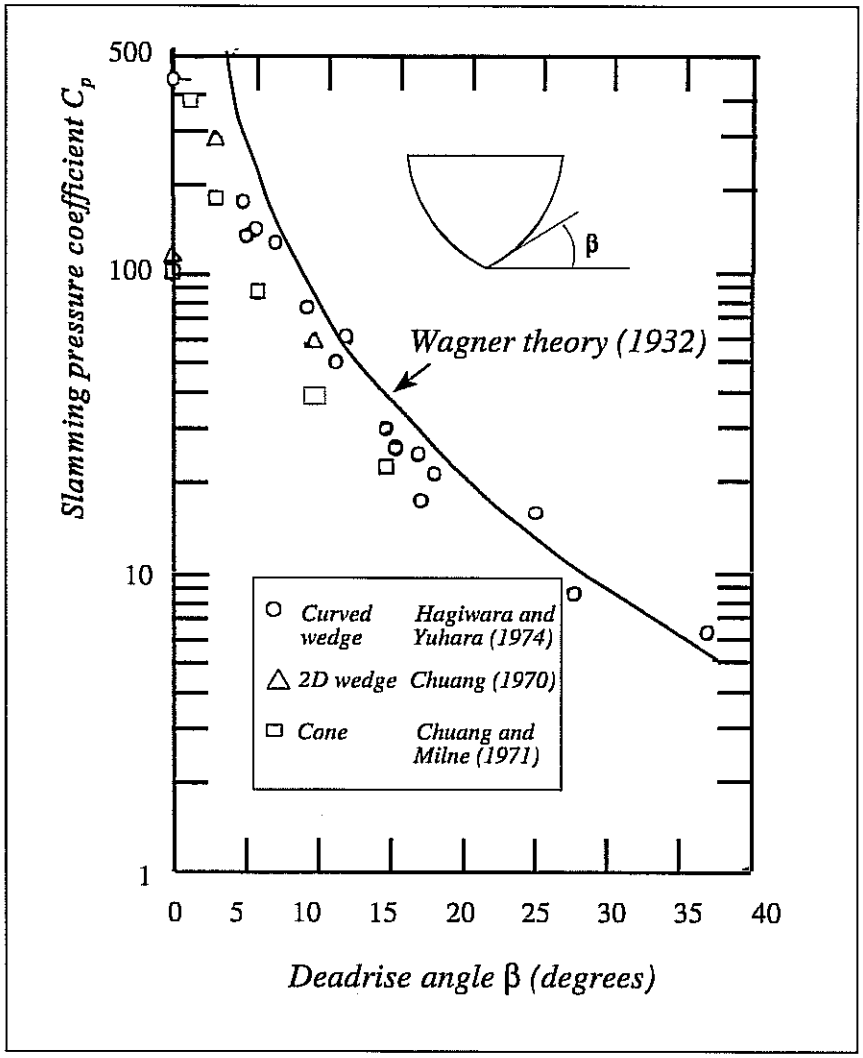

Fig 14.5 Slamming pressure coefficients from model experiments

14.3.2 Slamming drop tests

The section shapes of most ships in way of the keel may be approximated by simple wedge sections of the appropriate deadrise angle defined in Figure. 14.5. The slamming characteristics of these sections may therefore be examined by dropping two dimensional wedge sections into water.

Dimensional analysis (Chapter 10) suggests that the peak impact pressure developed on the

wedge during a slam will be given in the form

$$P = C_p \frac{1}{2} \rho \dot{r}_3^2 \quad kN/m^2 \tag{14.12}$$

where C_p is the slamming pressure coefficient which is a function of the deadrise angle β. This relationship has been confirmed in a number of experiments and Figure. 14.5 shows how C_p has been found to vary with β.

For deadrise angles above about 20° these results agree well with a theoretical result derived by Wagner (1932) in connection with impact loads on seaplane floats:

$$C_p = 1 + \left(\frac{\pi \cot \beta}{2} \right)^2 \tag{14.13}$$

Slamming pressures estimates using these results are likely to be too high because two dimensional drop tests take no account of the effect of the air/water mixture likely to be below the keel just before impact; nor do they allow for the effect of the relative 'pitch' angle between the keel and the water surface. These effects are likely to decrease the impact pressure. Nevertheless, the results do give a general indication of the effect of deadrise angle and confirm the basic physics of the phenomena involved.

14.3.3 Model experiments in waves

The alternative approach of measuring slamming pressures on scale models in waves has been pursued by a number of workers in the field. However, scale effects are likely to be important and it is always difficult to measure the relative velocity at impact.

Ochi (1964), in a classic paper, described measurements of slamming pressures on a model of a merchant ship in waves. Although he was unable to measure the impact velocities directly, he confirmed the relationship given in Equation (14.12) but found that no appreciable slamming impact occurred if the relative velocity was less than a certain value. According to Ochi this critical velocity was about 3.7 metres/second for a 161 metre ship. Assuming that the critical velocity obeys the Froude scaling law, it may be expressed as

$$\dot{r}_{3\ crit} = 0.093 \sqrt{g\ L} \quad m/sec \tag{14.14}$$

Ochi concluded that a slam will occur at a particular location if

(a)	the relative motion exceeds the local effective draught D_{ke}
(b)	the relative velocity at impact exceeds $\dot{r}_{3\ crit}$

Now if the relative motion is considered independent of the relative velocity, the probability of the relative motion exceeding the effective draught at the same time as the relative velocity exceeds $\dot{r}_{3\ crit}$ is given by

$$P_{slam} = exp\left(- \frac{D_{ke}^2}{2\ C_s^2\ m_0} - \frac{\dot{r}_{3\ crit}^2}{2\ C_s^2\ m_2} \right) \tag{14.15}$$

(see Equation (11.36)). m_0 and m_2 in this formula are the variances of the notional relative motion and velocity.

The slamming frequency is

$$N_{slam} = \frac{3600\ P_{slam}}{\overline{T}_p} \quad per\ hour \tag{14.16}$$

14.3.4 Estimation of slamming pressures during a typical severe slam

The time history of the relative motion during the short period encompassing an impact will vary from slam to slam. This makes determination of the severity of the event difficult, but some progress can be made if we choose to approximate the relative motion for this short period by

$$r_3 = r_{30}\ sin\ (\ \omega_{r3}\ t + \delta_{r3}\ ) \quad m \tag{14.17}$$

as shown in Figure 14.6. The relative motion at impact is then

$$-\ D_{ke} = r_{30}\ sin\ \delta_{r3} \quad m \tag{14.18}$$

so that

$$\delta_{r3} = sin^{-1}\left(\frac{-\ D_{ke}}{r_{30}} \right) \quad rad \tag{14.19}$$

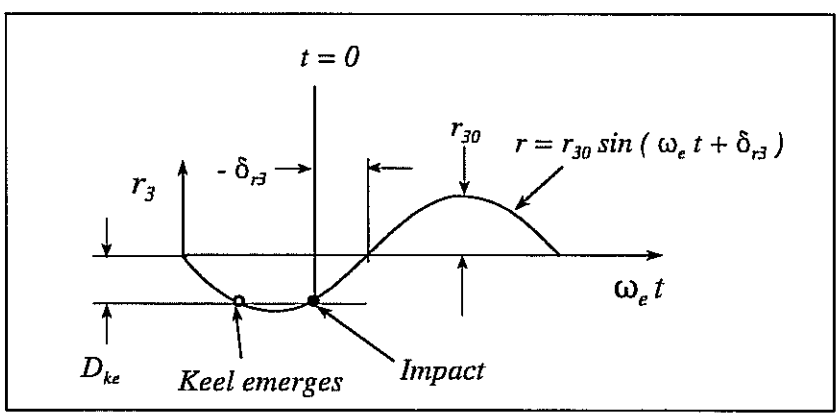

Fig 14.6 - Relative motion time history

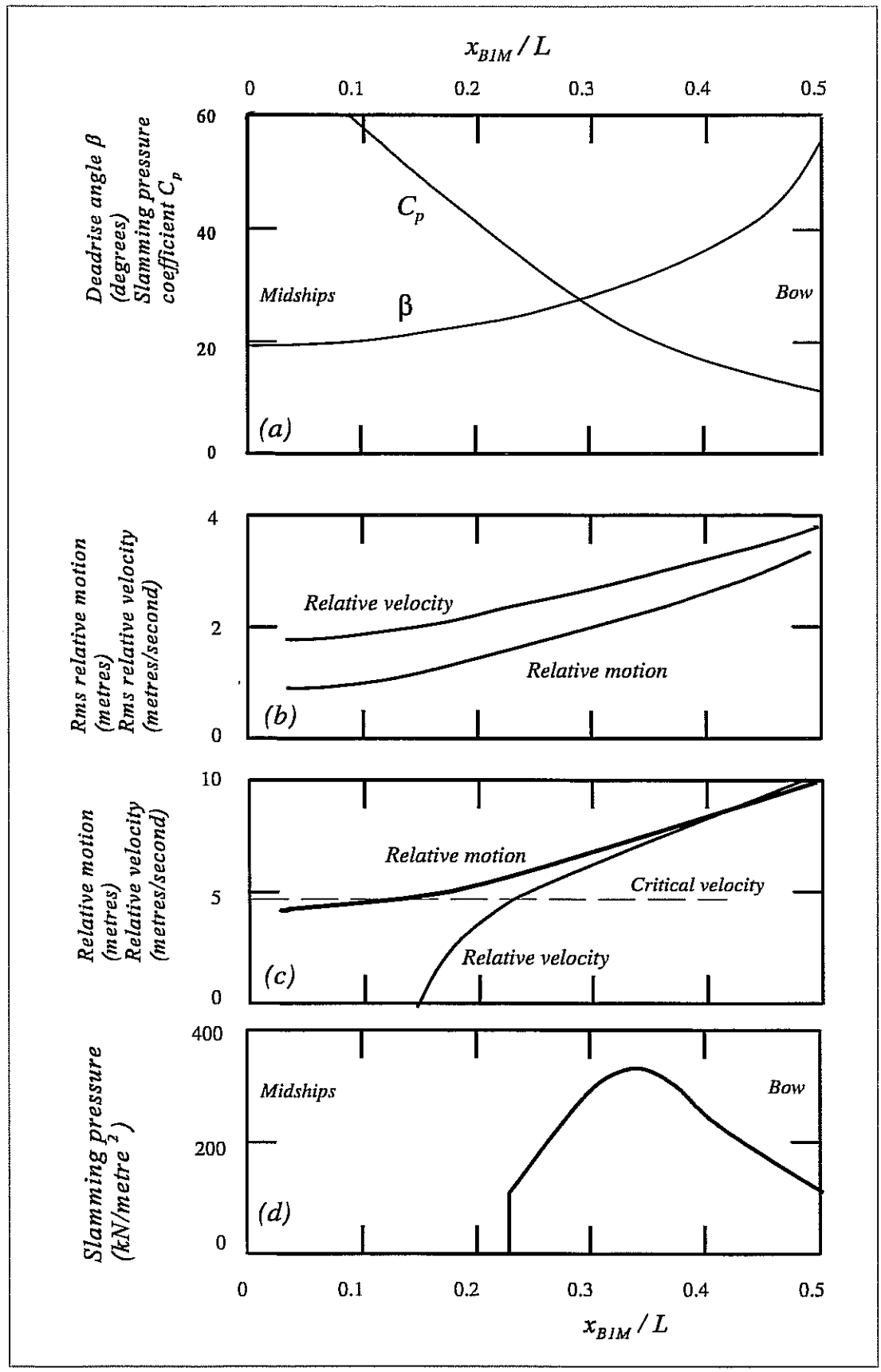

Fig 14.7 - Slamming pressure calculation for the frigate in irregular head waves

The relative velocity during the motion cycle is given by

$$\dot{r}_3 = \omega_{r3}\, r_{30}\, cos\, (\, \omega_{r3}\, t + \delta_{r3}\,) \quad m/sec \tag{14.20}$$

and the relative velocity at impact is obtained by setting $t = 0$:

$$\dot{r}_{3slam} = \omega_{r3}\, r_{30}\, cos\, \delta_{r3} = \omega_{r3} \sqrt{r_{30}^2 - D_{ke}^2} \tag{14.21}$$

It remains to determine a suitable value for the relative motion amplitude r_{30} and the motion frequency ω_{r3}. The probability of the relative motion exceeding a peak value r_{30} is, from equation (14.5),

$$P = exp\left(- \frac{1}{2} \frac{r_{30}^2}{C_s^2\, m_0} \right) \tag{14.22}$$

and this peak relative motion will occur once in N oscillations, where

$$P = \frac{1}{N} = \frac{2\,\pi}{T_H\, \omega_{r3}} \tag{14.23}$$

where T_H is an arbitrary sample period. Hence the relative motion amplitude which will be exceeded once in T_H seconds is

$$r_{30} = C_s\, \sigma_0 \sqrt{- 2\, log_e \left(\frac{2\,\pi}{T_H\, \omega_{r3}} \right)} \quad m \tag{14.24}$$

where σ_0 is the rms notional relative motion.

The frequency ω_{r3} is assumed to be the same as the average frequency of the relative motion peaks (see Equation (2.27)):

$$\omega_{r3} = \sqrt{\frac{m_4}{m_2}} \quad rad/sec \tag{14.25}$$

Using these equations we may now estimate the peak slamming pressures which are likely to be exceeded once in T_H seconds. Figure 14.7 shows the results of a specimen calculation for the frigate described in Section 7.1 in head seas with T_H set at 900 seconds. Figure 14.7(a) shows the deadrise angle at keel and the corresponding slamming pressure coefficient C_p given by Equation (14.13). The rms relative motion and velocity for the chosen speed and wave conditions calculated by strip theory are shown in Figure 14.7(b). Figure 14.7(c) shows the derived relative motion amplitude and impact velocity given by Equations (14.24) and (14.21).

These represent the worst conditions likely to occur in a period of 900 seconds. Note that the impact velocity is a maximum at the forward end of the ship and falls to zero at some location where keel emergence is unlikely. Some of the predicted impact velocities are less than the critical velocity calculated according to Equation (14.14). It is assumed that no slamming will occur at these stations.

Finally Figure 14.7(d) shows the slamming pressure calculated according to Equation (14.12). The pressure is set to zero where the impact velocity is less than the critical velocity.

14.4 DESIGN RECOMMENDATIONS TO AVOID SLAMMING

Slamming frequency may be minimised by adopting a deep draught forward to reduce the frequency of keel emergence. Slamming severity may be minimised by adopting fine lines forward with a high deadrise angles.

14.5 DECK WETNESS

Figure 14.8 shows a frigate experiencing deck wetness at high speed in rough seas. The bow is buried in the sea and has thrown a corona of solid water and spray high into the air. The forward speed of the ship will ensure that some of this water comes onto the deck although much of it will be cast aside by a well designed bow. The remnants of a previous wetting can be seen surrounding the ship along the entire length of the hull and as high as the top of the funnel.

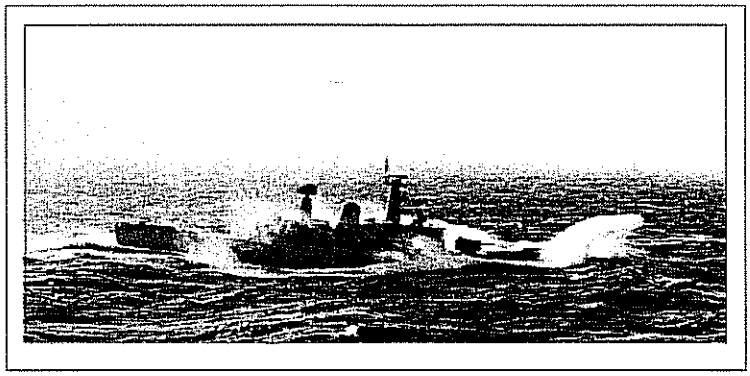

Fig 14.8 - A companion picture taken on the same occasion as Figure 14.3 showing deck wetness on a frigate.

Analytical prediction of deck wetness frequency and severity is impossible at the time of writing and seems likely to remain so in the near future. Model experiments can give useful information but even here the results should be treated with caution. Shipping 'solid' water ('green seas') is believed to be modelled correctly in a conventional Froude scaled experiment, but it is clear from visual observations that the formation of spray is not modelled properly. This is because the surface tension which governs the size of the spray droplets is incorrectly scaled. The model spray droplets are then much too large and would scale to the size of footballs on the ship.

14.6 FREEBOARD EXCEEDANCE

In considering the frequency of deck wetness it is necessary to distinguish between occasions when the water rises above the level of the deck but does not come on board, and true deck wetness where water is actually taken onto the weather deck of the ship. At low speed freeboard exceedance will almost always be accompanied by deck wetness, but at higher speeds a well designed bow can throw the water up and away from the ship as shown in Figure 14.9. Freeboard exceedance therefore does not necessarily result in deck wetness, but all deck wettings must be preceded by a freeboard exceedance.

It is at present impossible to calculate the frequency of deck wetness proper, but some idea of the characteristics of a design can be obtained by calculating the probability and frequency of freeboard exceedance using Equations (14.6) and (14.10).

Figure 14.10 shows the results of some calculations of freeboard exceedance in head waves using these equations. In Figure 14.10(a) the notional relative motion increases towards the bow. The swell up effect amplifies the relative motion but gives a maximum value some distance abaft the stem.

The effective freeboard is reduced by the bow wave and the running trim of the ship (see Figure 14.10(b)).

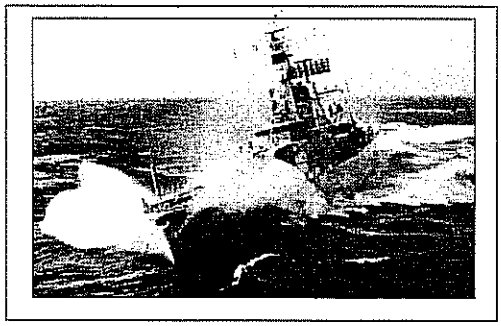

Fig 14.9 - Freeboard exceedance without deck wetness

Equation (14.6) then gives the probability of freeboard exceedance which is typically a maximum some way abaft the stem as seen in Figure 14.10(c).

While this result is typical it will generally overestimate the actual frequency of deck wetness since most of the freeboard exceedances which occur at this location will not result in water coming onto the foredeck. Figure 14.9 shows this phenomenon very well. Lloyd, Salsich and Zseleczky (1986) found that the observed frequency of deck wetness was most closely correlated with freeboard exceedances at the stem head. In other words a deck wetting is almost always the result of a freeboard exceedance at the stem head and freeboard exceedances elsewhere do not usually result in wetness unless they are also accompanied by exceedance at the stem head. It follows that the frequency of freeboard exceedance at the stem head will probably give a reasonably accurate estimate of the true deck wetness frequency at least at high speed in head waves.

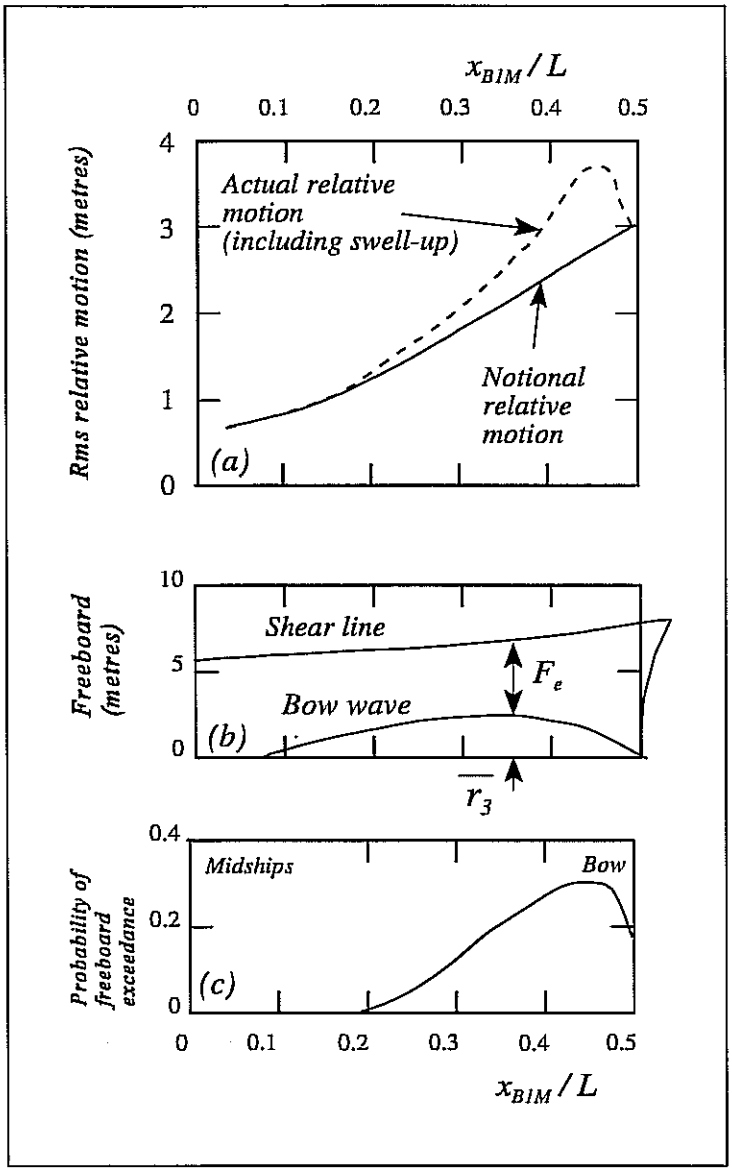

Fig 14.10 - Calculation of freeboard exceedance for the frigate at 20 knots: significant wave height 5.5 metres; modal period 12.4 seconds.

14.7 EFFECT OF BOW SHAPE

It seems obvious that deck wetness frequency and severity must be affected by the above water form of the bow. It is therefore surprising to find that freeboard is the only characteristic which is universally agreed to have any effect on deck wetness, high freeboard being, of course, desirable. There is no universal agreement on the effects of features like flare, stem rake or knuckles.

The reasons for this are not hard to find. A proper objective comparison of the performance of two different bows at sea requires two ships with identical underwater hull forms (to ensure the same motion responses) but different above water bow shapes to be run side by side in rough weather (to ensure the same wave conditions). No such trial has ever been conducted. Hearsay

reports of deck wetness at sea are inherently subjective and unreliable because they are drawn from observations made from different ships in different wave conditions.

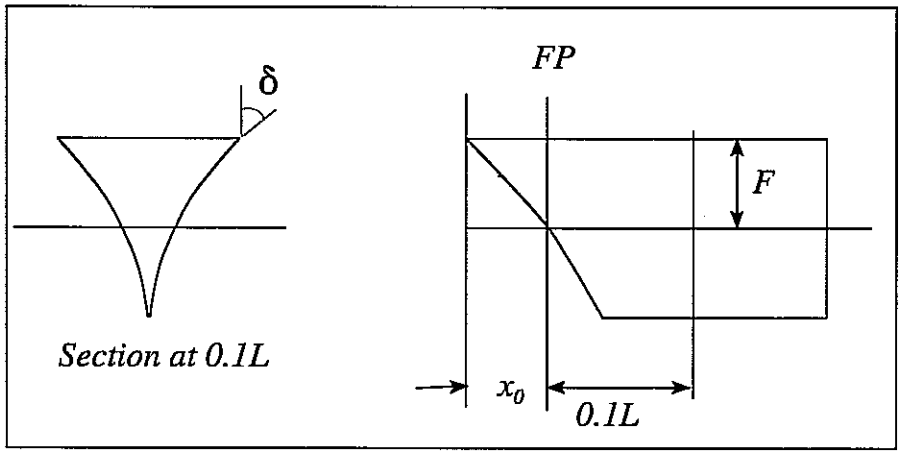

Fig 14.11 - Definition of flare and overhang

Model experiments provide a viable alternative but even here there are formidable practical difficulties. In very severe conditions almost every encountered wave will be shipped over the bow and all bow designs having the same freeboard will have virtually the same performance. It follows that model experiments to examine the effects of the more subtle design features must be run in moderate waves to allow differences in performance to be revealed. In these conditions deck wetness will be relatively infrequent (perhaps one or two wettings per run) and it will be necessary to conduct many runs to allow reliable wetness statistics to be established. Each run must be at the same speed in waves having the same energy spectrum but a different time history.

This was recognised by Lloyd, Salsich and Zseleczky (1986) who tested a total of nine different bow designs on a model frigate at the US Naval Academy. Each bow was tested for one hour (full scale equivalent) requiring no less than eighteen tank runs. The wave spectrum and model speed were chosen to give about fifty wettings in this time. Flare was quantified by the angle δ (measured at 0.1 L abaft the Forward Perpendicular: see Figure 14.11). Freeboard was the same for all the bows tested. The bow lines were developed using polynomial waterlines arranged to fair in to the lines of the hull at 0.25L abaft the FP. The stem overhang was related to the flare angle by the equation

$$\frac{x_0}{L} = 0.002\ \delta \quad (\delta \text{ in degrees}) \qquad (14.26)$$

so that heavily flared bows had a large overhang.

Visual observations during the experiments suggested that the heavily flared bows appeared to work well, throwing impressive quantities of water aside, apparently keeping most of the water off the deck. However, objective measurements of freeboard exceedance and deck wetness frequency showed the opposite trend (see Figure 14.12). A very fine bow with only 20° of flare

and $x_0 / L = 0.08$[1] had the best performance. Figure 14.13 shows a comparison of the body plan of this bow with that of the worst bow in the series.

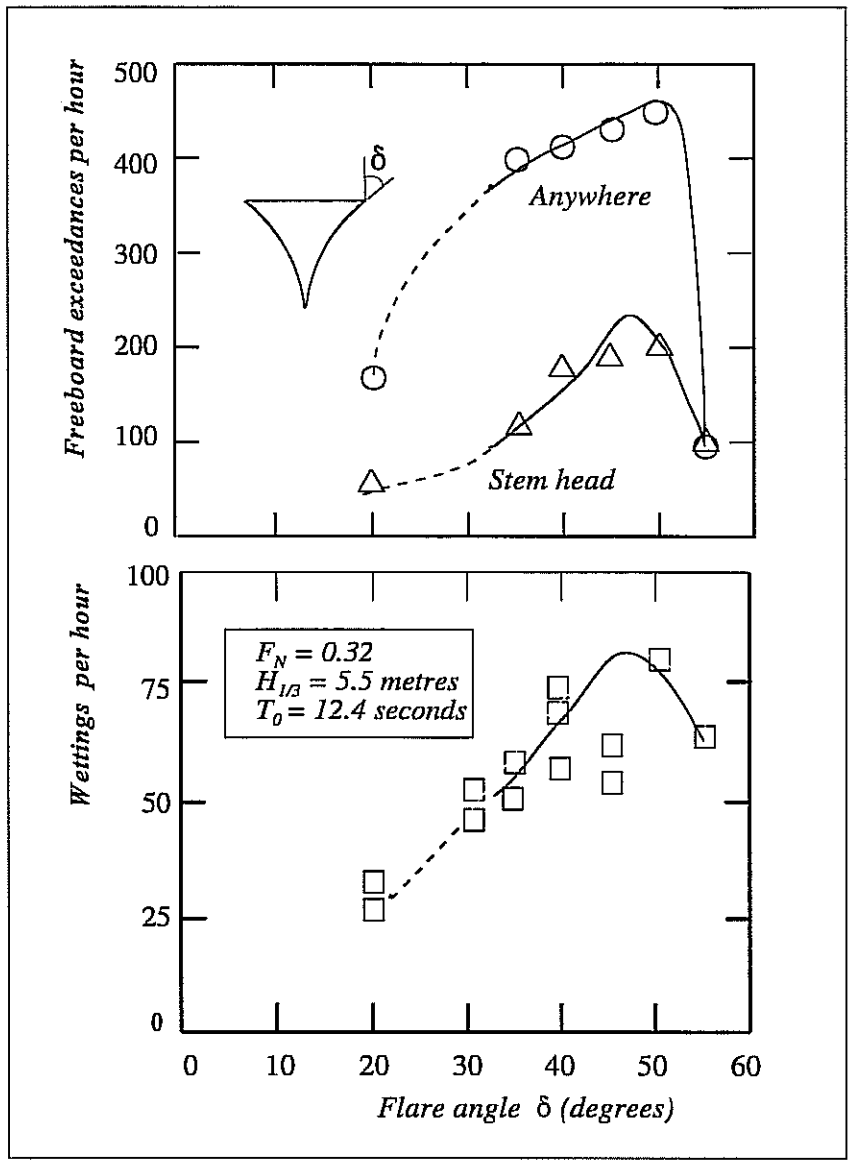

Fig 14.12 - Effect of bow flare on freeboard exceedance and deck wetness on a model of the US Navy FFG7 class frigate (After Lloyd, Salsich and Zseleczky (1986))

The good performance of the fine bow was explained by the observation that the swell up coefficient increased with flare as shown in Figures 14.14 and 14.15. In other words well flared bows appear to work well because they amplify the relative motions and then atone for this undesirable characteristic by successfully disposing of some of the wetness they generate. A slender bow with little flare slices easily through the waves with little disturbance. It will ship the occasional sea but not as often as a wave enhancing well flared bow.

---

[1] Not one of the family defined by Equation (14.26).

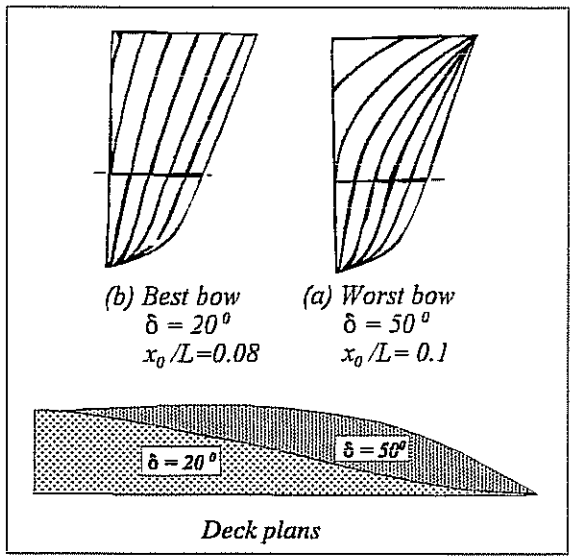

Fig 14.13 - Body and deck plans for the best and worst bows (After Lloyd, Salsich and Zseleczky (1986))

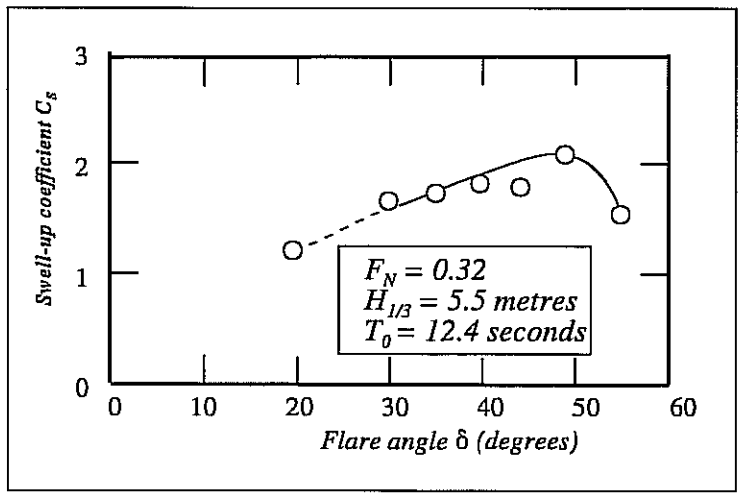

Fig 14.14 - Effect of flare on swell up coefficient

14.8 DESIGN RECOMMENDATIONS TO MINIMISE DECK WETNESS

Most deck wetness in head waves arises from freeboard exceedances at the stem head. Deck wetness may therefore be minimised by adopting a high freeboard forward. Excessive flare should be avoided since this appears to amplify the encountered waves and increase deck wetness frequency. Limited experimental evidence suggests that the best wetness performance will be achieved by adopting very fine lines with a sharp stem. Bluff bows should be avoided.

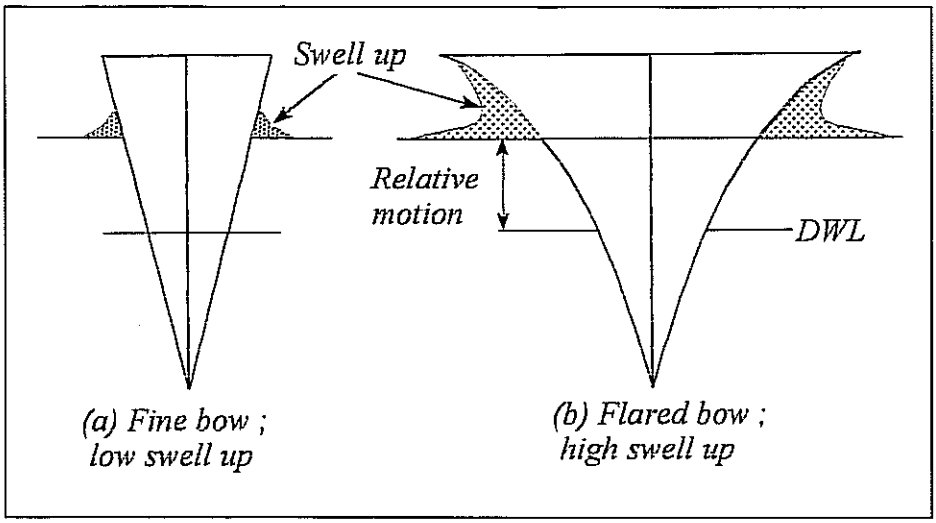

Fig 14.15 Flare and swell up

15

EFFECTS OF SHIP MOTIONS ON PASSENGERS AND CREW

"The wonder is always new that any sane man can be a sailor"

R W Emerson 1803 - 1882

15.1 INTRODUCTION

Ship motions have two undesirable effects on the people within the ship. They cause motion sickness and also make it more difficult to move in a controlled and coherent manner so that the performance of every day tasks is impaired.

The balance organs located in the inner ear can detect changes of both the magnitude and direction of the apparent gravitational acceleration as well as angular accelerations. Excessive stimulation of these organs will, in most individuals, result in motion sickness. The condition is, to some extent, alleviated if the accelerations are confirmed by visual cues from the eyes. Thus a ride on a fairground switchback railway can be enjoyable and exciting even if large accelerations are experienced. The same accelerations experienced by a blindfolded rider would almost certainly result in quite distressing motion sickness. In the same way it is possible to stimulate motion sickness without any motions being present at all. This can be done for, some individuals, by showing them a film of a violent fairground ride.

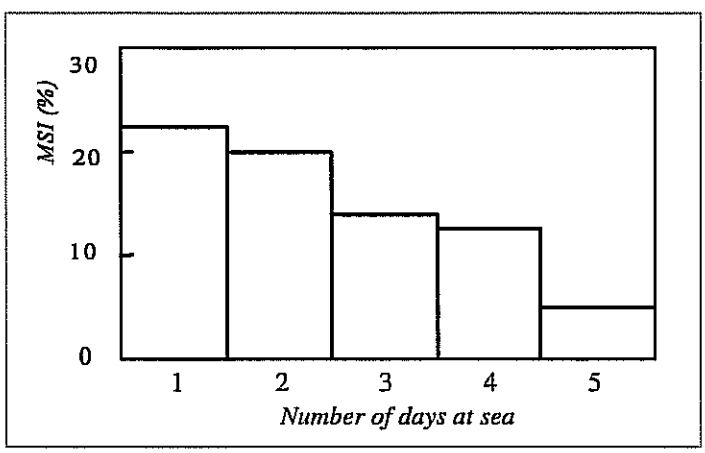

Fig 15.1 - Motion sickness incidence: effect of acclimatisation. (After Walters (1964))

On board ship it follows that motion sickness is most likely to occur if passengers or crew are confined below decks so that they cannot see the horizon. Bittner and Guignard (1985) also showed that motion sickness can be exacerbated by facing diagonally across the ship. Fore and aft or athwartships seating is to be preferred. Other factors which may promote seasickness are anxiety, fatigue, hunger, smells (particularly cooking and fuel oil), greasy food, reading and carbonated or alcoholic drinks. Nieuwenhuijsen (1958) found that women and young children

in the liner *SS Masdam* were more susceptible to sea sickness than men. Elderly people were generally less affected than people of middle age.

Fortunately the symptoms of seasickness usually disappear after a few days. Figure 15.1 shows this effect in graphical form, based on a study of seasickness in the Royal Navy. Nevertheless seasickness remains a deterrent to travel by sea for many people and an inconvenience to sailors. This has led to a considerable research effort in developing drugs to alleviate the symptoms. Rather less effort has been devoted to establishing the precise nature of the relationship between motions and seasickness.

Motions also impair the ability to work effectively even when there are no problems with seasickness. Moving around the ship becomes more difficult and the prudent sailor or passenger will always hang on to some suitable anchorage to minimise his chances of injury in severe conditions. The old adage "one hand for the ship and one for yourself" is sound advice. Even in more moderate conditions performance at tasks requiring good hand/eye coordinations such as tracking targets on a radar screen may be affected.

15.2 MOTION SICKNESS INCIDENCE

The principle cause of motion sickness in an individual is believed to be the vertical acceleration experienced at his locality in the ship. Other motions might, if sufficiently high, also cause motion sickness: but in conventional ships these are usually too small to offer any significant additional stimulation.

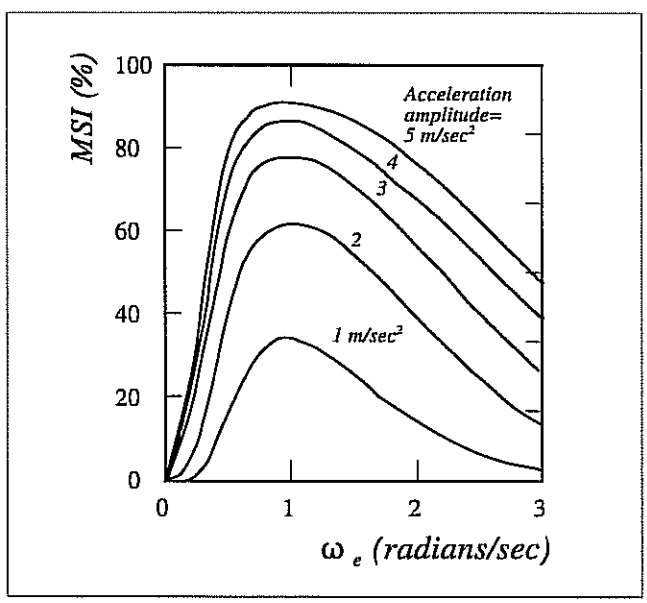

Fig 15.2 - Motion sickness incidence (After O'Hanlan and McCawley (1974))

Determining the motion sickness likely to be experienced by an individual subjected to some random motion response on board ship is a difficult problem. Individuals differ in their susceptibility to motions so it is immediately clear that a statistical approach is required with a

large number of subjects tested. An individual's response may also vary from day to day depending on the contributory factors listed above. In particular a person who has a job to do is much less likely to suffer badly from seasickness than one who has nothing better to do than to contemplate the agonies of life at sea.

In a classic experiment O'Hanlan and McCawley (1974) measured the motion sickness response of over 300 American male college student paid volunteers. None of the students had any recent acclimatisation to motions. They were tested in pairs in a ship motion simulator which was capable of driving the small enclosed test cabin through a vertical sinusoidal motion with amplitudes up to about ± 3.5 metres. The cabin had no windows so that the subjects could not receive any visual motion cues and their only task was to monitor their state of nausea by pressing buttons on a control panel. The experiments lasted for up to two hours, or until the subjects vomited.

O'Hanlan and McCawley found that the *Motion Sickness Incidence* (defined as the percentage of subjects who vomited within two hours) could be expressed in the form

$$MSI = 100 \left[0.5 + erf \left(\frac{log_{10} \left(\frac{|\ddot{s}_3|}{g} \right) - \mu_{MSI}}{0.4} \right) \right] \qquad (15.1)$$

where $|\ddot{s}_3|$ is the vertical acceleration averaged over a half motion cycle and

$$\mu_{MSI} = - 0.819 + 2.32 \, (log_{10} \, \omega_e)^2 \qquad (15.2)$$

(with ω_e in radians/second).

Equation 15.1 may be evaluated with the help of Table 11.3 and is plotted in Figure 15.2. This shows how MSI increases with acceleration and is most severe at a frequency of about 1.07 radians/second. This frequency is unfortunately close to the average frequencies of vertical motions for many ships and this explains why motion sickness is such a common problem at sea.

Application of these results to the real life environment of a ship in rough weather requires us to make assumptions about the equivalence of the random motions of the ship and the sinusoidal motions of the simulator. If we assume that the ship accelerations are distributed according to the Gaussian probability density function the average modulus of the acceleration is given by Equation (11.23):

$$|\ddot{s}_3| = 0.798 \sqrt{m_4} \quad m/sec^2 \qquad (15.3)$$

where m_4 is the variance of the vertical acceleration.

From Equation (2.27) the average frequency of the motion peaks is[1]

$$\bar{\omega}_e = \sqrt{\frac{m_4}{m_2}} \quad rad/sec \tag{15.4}$$

These approximations allow the MSI formula (Equation (15.1)) to be used to make an estimate of the proportion of people who will suffer from seasickness in a given set of conditions at sea. The estimate may not be very accurate because of the difficulty of allowing for the many secondary factors which are involved in motion sickness and the various assumptions made above. Nevertheless, the technique may be used to give some indication, at least in a comparative sense, of the ride comfort of ships in rough weather. As an example Figure 15.3 shows a calculation of MSI for a passenger ferry at 10 knots in head waves. The MSI is highest at the bow and falls to a minimum a little way abaft midships. Knowledgable passengers who suffer from seasickness would do well to make for this part of the ship. In practice the high MSI at the bow may be immaterial because there will probably be no passengers or crew at that location. A better impression of the MSI generally suffered by the occupants of the ship may be obtained by applying a weighting function to represent the distribution of the occupied spaces within the ship.

The weighted average MSI is then given by

$$\overline{MSI} = \frac{\int MSI \; W \; dx_{BIM}}{\int W \; dx_{BIM}} \tag{15.5}$$

where the integrals are evaluated over the length of the ship. Figure 15.3 shows a simple weighting function giving equal weight to all the occupants of the ship over the length of the passenger accommodation. For this example the weighted average MSI is 7.9%.

15.3 SUBJECTIVE MAGNITUDE

An experienced, well motivated and acclimatised crew will not suffer unduly from seasickness but they will may still find that ship motions will inhibit their ability to work effectively. One technique which has been used to roughly quantify this effect is based on some experiments by Shoenberger (1975).

---

[1] Logic requires the average frequency of the acceleration peaks $\sqrt{\frac{m_8}{m_6}}$ to be used here but this involves the calculation of the sixth and eighth moments of area of the motion spectrum. In practice it is found that the integrals m_6 and m_8 may not converge and it is better to use the average frequency of the motion peaks.

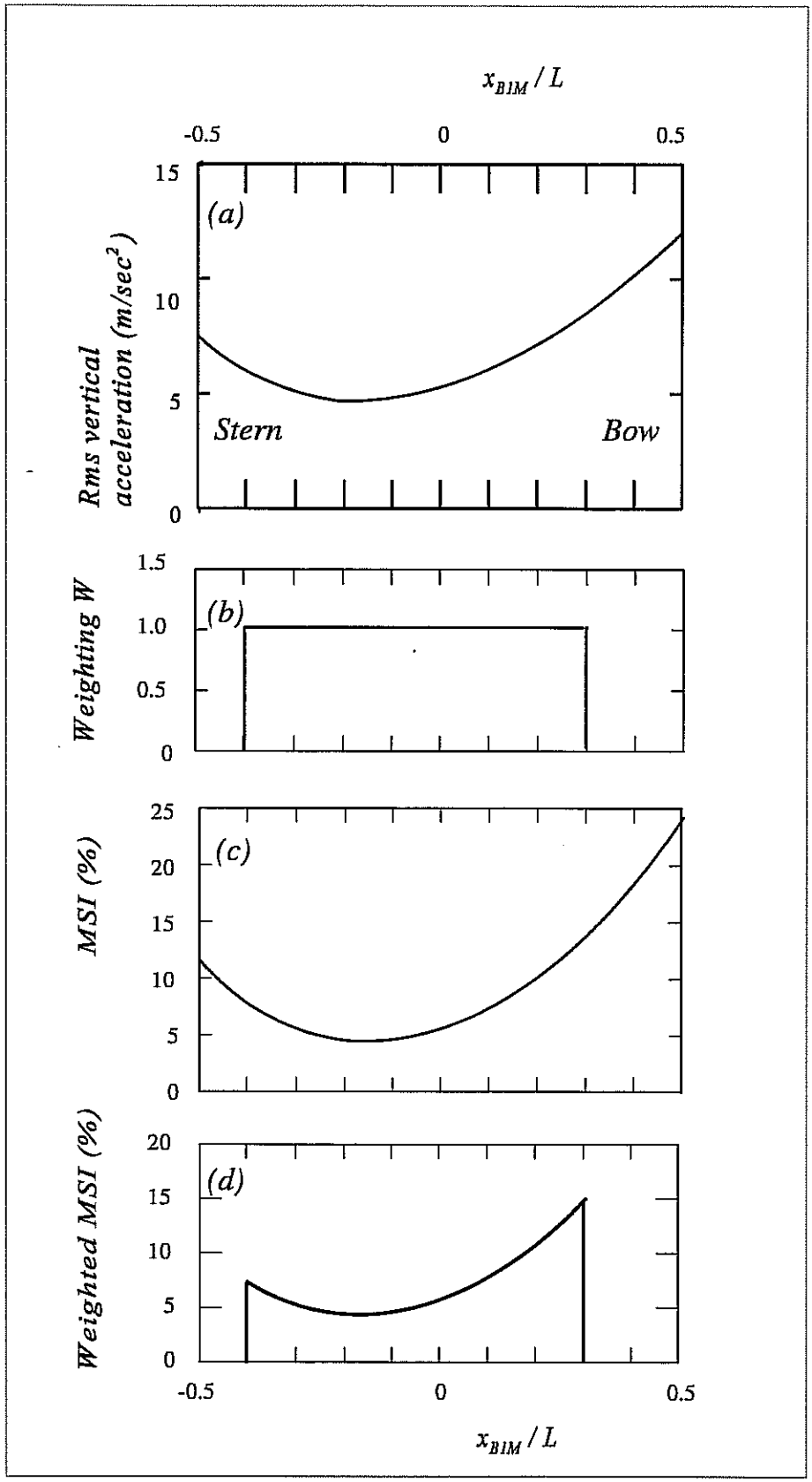

Fig 15.3 - MSI calculation for a passenger ferry at 10 knots. Significant wave height 5.5 metres; Modal period 12.4 seconds.

He subjected eight experienced US Air Force pilots to vertical sinusoidal motions in a simple oscillating chair capable of amplitudes up to ± 1.5 metres. The pilots were blindfolded to remove any visual motion cues.

After some preliminary experiments they were subjected to a "standard" reference motion of ± 0.6g at 1.0 Hz. This motion was assigned a value of 10 on an arbitrary "***Subjective Magnitude***" (SM) scale. The frequency and amplitude of the motions were then changed and each subject was asked to assess the severity of the new motion in relation to the standard. Thus a motion which felt twice as severe was assigned an SM of 20 and one which felt half as severe was assigned a value of 5.

The subjects were generally able to make their assessments within a minute and none suffered from motion sickness during the experiments. Shoenberger obtained remarkably consistent results which could be expressed in the form

$$SM = A \left(\frac{\ddot{s}_{30}}{g} \right)^{1.43} \tag{15.6}$$

where A is a parameter which is a function of frequency. Figure 15.4 shows the relationship obtained from Shoenberger's results. Apparently humans are least sensitive to motions at frequencies around 6 radians/second. Sensitivity is enhanced at both higher and lower frequencies.

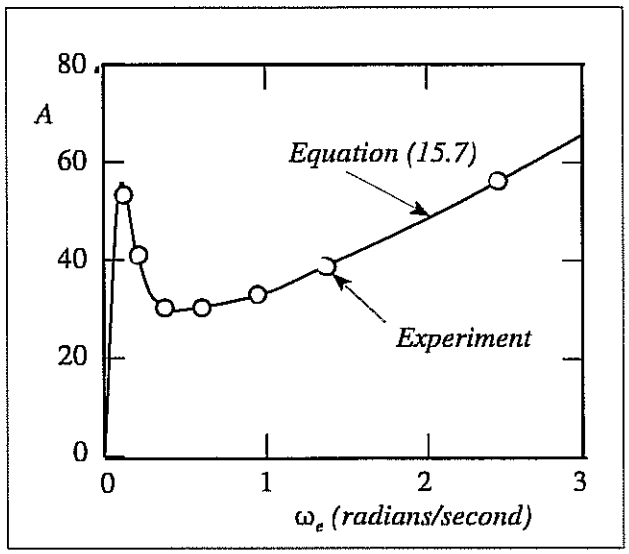

Fig 15.4 - Subjective magnitude parameter A (After Schoenberger (1975))

The equation

$$A = [\ 1 - exp\ (\ -\ 1.65\ \omega_e^2\ )] \times [\ 75.6 - 49.6\ log_e\ \omega_e + 13.5\ (\ log_e\ \omega_e\ )^2\ ] \tag{15.7}$$

fits the experiment data well and exhibits a maximum at $\omega_e = 1.07$ radians/second, corresponding to the most sensitive frequency for MSI.

These experiments were, like the MSI experiments, conducted using sinusoidal oscillations and it is again necessary to devise some suitable means of applying the results to the irregular motion environment found on board ship. Lloyd and Andrew (1977) suggested equating the sinusoidal acceleration amplitude to the significant single amplitude:

$$\ddot{s}_{30} = 2\sqrt{m_4} \quad m/sec^2 \tag{15.8}$$

and the appropriate frequency $\bar{\omega}_e$ may be obtained from Equation (15.4).

Figure 15.5 shows the relationship between SM and the rms vertical acceleration according to Equation (15.6) for the worst frequency $\bar{\omega}_e = 1.07$ radians/second. Also shown are semantic descriptions of the resulting motion environment based on the experience of rough weather trials in two frigates described by Andrew and Lloyd (1981).

SM may be calculated for any part of the ship and diagrams similar to that shown for MSI in Figure 15.3 produced. A weighted mean SM may then be calculated using an equation analogous to Equation (15.5):

$$\overline{SM} = \frac{\int SM\ W\ dx_{BIM}}{\int W\ dx_{BIM}} \tag{15.9}$$

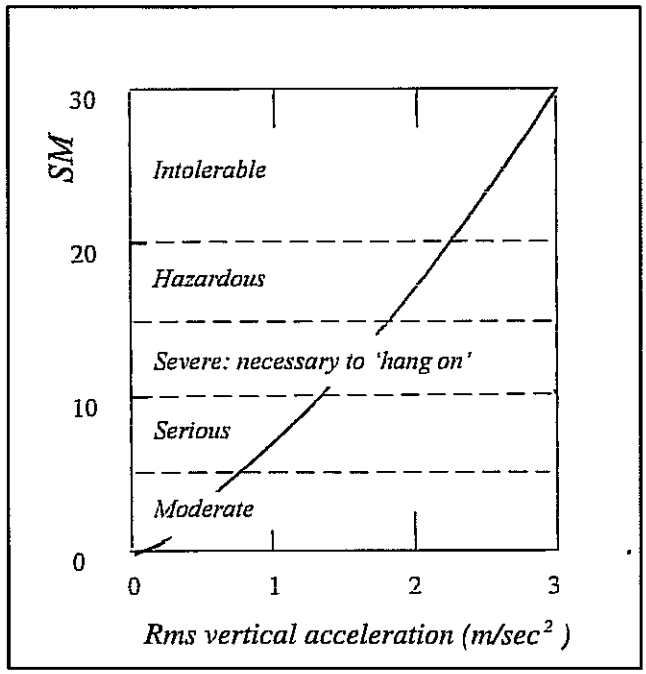

Fig 15.5 - Subjective magnitude and rms vertical acceleration at $\omega_e = 1.07$ radians /second.

15.4 MOTION INDUCED INTERRUPTIONS

15.4.1 Introduction

Although MSI is a reasonable parameter for judging the severity of ship motions from the passenger's point of view it is widely acknowledged that it has little relevance to the ability of professional sailors to function effectively even though they may suffer from seasickness. SM is a strictly limited measure of how severe a motion feels to the crew but is still not related to the tasks they are required to perform.

Batis, Woolaver and Beck (1983) defined a *Motion Induced Interruption* (MII) as an occasion when a member of the crew would have to stop working at the current task and hold on to some convenient anchorage to prevent loss of balance. The frequency of MIIs can therefore be taken as an indication of the severity of the ship motions which are relevant to the effectiveness of the ship and the crew.

The analysis which follows is based on that proposed by Graham, Batis and Meyers (1992) who suggested that MIIs could occur if the person slipped on the deck or toppled over (tipping). Graham *et al* included the effects of longitudinal accelerations and wind but we shall confine our attention to the effects of vertical and lateral accelerations which are usually the most important.

Consider, for example, a person of mass m tonnes on the deck of a ship as shown in Figure 15.6. The person's centre of gravity is at (x_{B1}, x_{B2}, x_{B3}) and the absolute lateral and vertical accelerations at a particular time are $\ddot{s}_2$ and $\ddot{s}_3$ relative to the Earth. Resolving these accelerations in directions parallel and normal to the deck we obtain

$$\ddot{s}_{B2} = \ddot{s}_2 \cos x_4 + \ddot{s}_3 \sin x_4 \quad m/sec^2 \quad \text{(positive to starboard)}$$

in the plane of the deck and

$$\ddot{s}_{B3} = \ddot{s}_3 \cos x_4 - \ddot{s}_2 \sin x_4 \quad m/sec^2 \quad \text{(positive downwards)}$$

normal to the deck.

For small roll angles these reduce to

$$\ddot{s}_{B2} \approx \ddot{s}_2 + \ddot{s}_3 x_4 \quad m/sec^2 \quad \text{(positive to starboard)} \qquad (15.10a)$$

$$\ddot{s}_{B3} \approx \ddot{s}_3 - \ddot{s}_2 x_4 \quad m/sec^2 \quad \text{(positive downwards)} \qquad (15.10b)$$

Positive values of these accelerations will tend to lift people off the deck and slide them towards the port side.

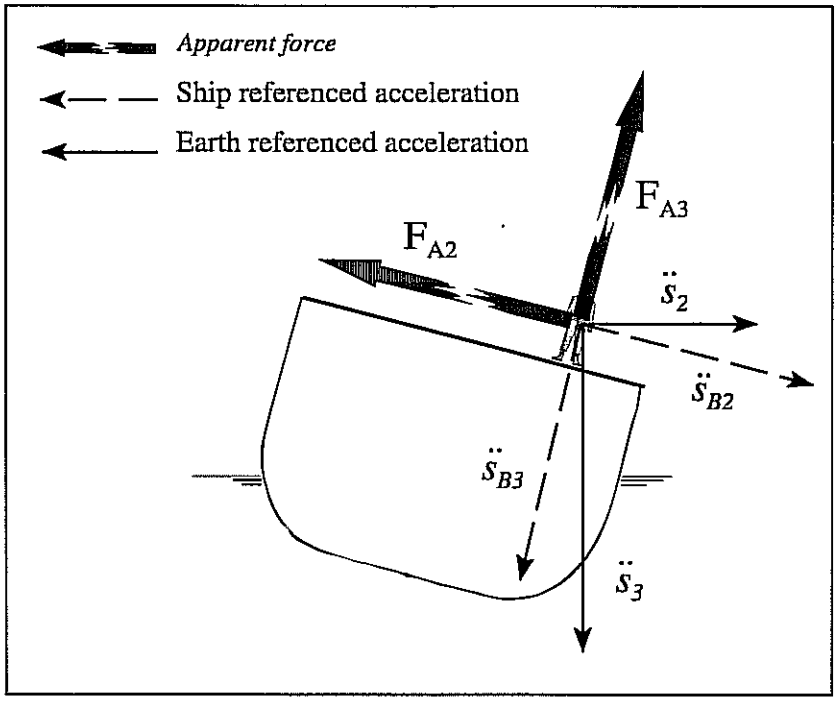

Fig 15.6 - Accelerations and apparent forces perceived by a sailor

The person is also subject to the components of gravity resolved in directions normal and parallel to the deck. For small roll angles the total apparent force parallel to the deck is

$$F_{A2} = m\ \ddot{s}_{B2} - m\ g\ x_4 \quad kN \quad \text{positive to port}$$

and using Equation (15.10a) this becomes

$$F_{A2} = m\ [\ \ddot{s}_2 + \ddot{s}_3\ x_4 - g\ x_4\ ] \quad kN \quad \text{positive to port} \qquad (15.11)$$

The apparent acceleration parallel to the deck has been called the ***Lateral Force Estimator*** (LFE) and is given by

$$\ddot{s}_{A2} = [\ \ddot{s}_2 + \ddot{s}_3\ x_4 - g\ x_4\ ] \quad m/sec^2 \quad \text{positive to port} \qquad (15.12)$$

When the ship is upright the gravity force on the person is $m\ g$ kN downwards, but this is reduced to $m\ g\ \cos x_4$ kN normal to the deck when the ship is rolled. For small roll angles $\cos x_4 \approx 1$ and the total apparent force normal to the deck is

$$F_{A3} \approx m\ \ddot{s}_{B3} - m\ g \quad kN \quad \text{positive upwards}$$

and using Equation (15.10b) this becomes

$$F_{A3} = m\ (\ \ddot{s}_3 - \ddot{s}_2\ x_4 - g\ ) \quad kN \quad \text{positive upwards}$$

and the apparent weight of the person is

$$W_A = - F_{A3} = m (\ddot{s}_2 x_4 - \ddot{s}_3 + g) \quad kN \tag{15.13}$$

15.4.2 Sliding

Consider a person on the deck of a ship as shown in Figure 15.7. The frictional force opposing sliding is μW_A kN where μ is the coefficient of friction between the deck and the person's shoes.[2] The person will slide to port if the apparent lateral force to port exceeds the frictional force to starboard:

$$F_{A2} > \mu W_A \quad kN$$

A slide to starboard will occur if the apparent lateral force to starboard exceeds the frictional force to port:

$$F_{A2} = < - \mu W_A \quad kN$$

Substituting Equations (15.11) and (15.13) we obtain the condition for sliding to port as

$$\ddot{s}_2 (1 - \mu x_4) + \ddot{s}_3 (x_4 + \mu) - g x_4 > \mu g \quad m/sec^2 \tag{15.14a}$$

and to starboard as

$$\ddot{s}_2 (1 + \mu x_4) + \ddot{s}_3 (x_4 - \mu) - g x_4 < - \mu g \quad m/sec^2 \tag{15.14b}$$

Using Equation (11.29) the number of MIIs per minute caused by slides to port is

$$MII_{sp} = \frac{60}{T_z} exp \left(- \frac{(\mu g)^2}{2 m_0} \right) \quad min^{-1} \tag{15.15}$$

where m_0 is the variance of the left hand side of inequality (15.14a). A similar equation gives the frequency of slides to starboard MII_{ss} with m_0 now obtained from inequality (15.14b). The total number of MIIs due to slides is given by

$$MII = MII_{sp} + MII_{ss} \quad min^{-1} \tag{15.16}$$

---

[2] Graham, Baitis and Meyers (1992) found $\mu \approx 0.19$ for a worn linoleum floor in some experiments to validate the procedure on board the USCGC *Morganthau* but suggested a value $\mu \approx 0.7$ for a dry weather deck.

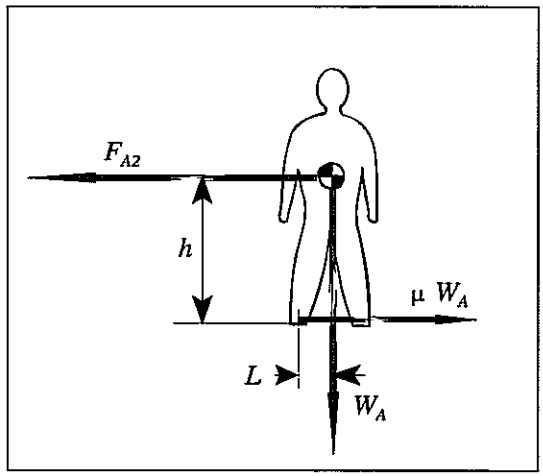

Fig 15.7 - Sliding forces and tipping moments on a sailor

15.4.3 Tipping

Consider a sailor standing facing forward as shown in Figure 15.7. The natural stance adopted in rough conditions is assumed with the feet spread to make tipping less likely. It is suggested that a suitable value for the ratio of half the stance width to the centre of gravity height is

$$\frac{L}{h} \approx 0.25$$

The apparent force to port and the apparent weight are again given by Equations (15.11) and (15.13). Taking moments about the left foot the sailor will tip to port if the moment due to the apparent lateral acceleration at the body's centre of gravity exceeds the righting moment due to his apparent weight:[3]

$$F_{A2}\ h > W_A\ L \quad kN\ m$$

Similarly, by taking moments about the right foot, the sailor will tip to starboard if

$$F_{A2}\ h < -\ W_A\ L \quad kN\ m$$

Substituting Equations (15.11) and (15.13) we obtain the condition for tipping to port as

$$\ddot{s}_2\ (\ 1\ -\ \frac{L}{h}\ x_4\ )\ +\ \ddot{s}_3\ (x_4\ +\ \frac{L}{h}\ )\ -\ g\ x_4 > \frac{L\ g}{h} \quad m/sec^2 \qquad (15.17a)$$

and to starboard as

[3] Graham *et al* also include a term representing the inertial moment due to the roll acceleration of the ship.

$$\ddot{s}_2 \left(1 + \frac{L}{h} x_4 \right) + \ddot{s}_3 \left(x_4 - \frac{L}{h} \right) - g\, x_4 < - \frac{L\, g}{h} \quad m/sec^2 \qquad (15.17b)$$

Equation (11.29) is again used to find the number of MIIs caused by tipping to port:

$$MII_{tp} = \frac{60}{T_z} \exp\left(- \frac{\left(\frac{L\, g}{h} \right)^2}{2\, m_0} \right) \quad min^{-1} \qquad (15.18)$$

where m_0 is the variance of the left hand side of inequality (15.17a). A similar equation yields the frequency of tipping to starboard MII_{ts} with m_0 now obtained from inequality (15.17b). The total number of MIIs due to tipping is given by

$$MII = MII_{tp} + MII_{ts} \quad min^{-1} \qquad (15.19)$$

15.4.4 General remarks

The analysis outlined above is quasi static in that the person is assumed to be a rigid body. In practice he may change his stance, crouch or sit down if he anticipates an imminent MII. So the actual frequency of MIIs will probably be over estimated by the equations given above. Nevertheless, the person must do something to avert the impending MII and it follows that his attention to the task in hand is distracted and the calculated MII frequency ought to be a good estimator of crew effectiveness. MIIs due to tipping are expected to be more frequent than MIIs due to sliding unless the deck is very slippery.

16

SEAKEEPING CRITERIA AND VOLUNTARY SPEED LOSS IN ROUGH WEATHER

Senior Officer Atlantic convoy escort to rejoining corvette in very bad weather:
"Why have you taken so long to rejoin convoy?"
Reply:
"It was uphill all the way."

From "Make a Signal" by Jack Broome. Douglas Boyd Books 1994.

16.1 INTRODUCTION

The methods described so far in this book have been aimed at predicting the responses experienced by a ship in rough weather. We now need to consider whether these responses will be acceptable in practice. This requires us to determine limiting values or ***criteria*** for each of the responses we predict.

Ships are required to carry out many different tasks and activities at sea and criteria for acceptable responses depend on the task in hand. For example, motions which are acceptable in a warship hunting a submarine would not be tolerated by the fare paying passengers on a cruise liner. Deck wetness which might be acceptable in a frigate closed down for a high speed dash in rough weather would not be condoned for operations which require men to work on the exposed upper deck.

It is first essential to identify the responses which actually limit performance of the task. Consider, for example, the task of retrieving an unmanned submersible from the sea on an oceanographic research vessel. This is undoubtedly inhibited in rough weather and we might expect the following problems to arise in severe conditions:

Problem	Associated ship response
It is difficult to attach a line to the submersible	*Local relative motion*
The handling party are sea sick.	*Local MSI*
The submersible strikes the side of the ship.	*Local LFE*
It is difficult for the handling party to keep their balance.	*Local LFE and MII*
The risk of slipping on the wet deck is unacceptable	*Local deck wetness*

Criteria should be expressed in terms of the responses which are directly responsible for the problems which have been identified and not in terms of motions which have no direct relevance

to the activity being considered. For example, although heave motion (at the centre of gravity) contributes to all the associated ship responses (at the retrieval station) but a heave motion criterion *per se* would be inappropriate because it has no direct correlation with the problems associated with the task.

Having determined the motions which are believed to influence performance the next step is to estimate numerical values of the criteria. The ideal method would be to conduct controlled trials in a variety of sea states to measure performance at the task as a function of measured ship motions and to determine the conditions in which the task becomes essentially impossible. Unfortunately this is generally impractical for the following reasons:

a) Sea state cannot be varied in a controlled manner and trials covering the required range of conditions would be very protracted and expensive.

b) Tasks involving human intervention (as most tasks do) would be heavily influenced by all the psychological and physiological factors to which humans are susceptible (motivation, morale, fatigue, acclimatisation etc) and it would be very difficult to obtain consistent results unless a very large number of experiments with different personnel was conducted. These experiments would inevitably be conducted in a variety of sea states making a proper analysis very difficult.

Trials in ship motion simulators have the advantage that the same sequence of ship motions may be reproduced over and over again so that controlled experiments on a large number of subjects can be undertaken. However, most simulators are incapable of reproducing the very large ship motions which are required to inhibit performance and they cannot usually reproduce all six degrees of freedom (and other more intangible aspects of life at sea) simultaneously. Furthermore, practical experiments in most simulators are limited to non strenuous tasks rather than tasks requiring great physical effort and manual dexterity.

In most cases the only practical method of determining criteria is to observe the apparent performance of actual ship's crews (and passengers) in the ordinary everyday ocean environment. This can be done in a number of different ways. One of the most successful is to collect performance data using questionnaires and this is discussed in Section 16.3 below. An alternative is to measure and monitor ship motions over a long period of time (months or years) and to correlate the measured motions with the activities of the ship recorded in a log book. This will eventually build up an envelope of motions which were actually tolerated while specific tasks were being performed in the ship.

We may summarise the requirements discussed above in terms of three "rules" for the determination of criteria:

1) Criteria must be related to a particular task.
2) The responses chosen for criteria assessment should be of actual concern to the task being considered.
3) Numerical values of criteria should be determined by monitoring the apparent performance of actual ships at sea.

16.2 EQUIPMENT CRITERIA

Although the criteria for many tasks are dependent on human performance some limitations arise from equipment design. In these cases a detailed analysis of the equipment used in the task can be a useful first step towards determining appropriate criterion levels. Consider for example a radar antenna. Most antennae are stabilised so that the radar beam is maintained in the horizontal plane regardless of the pitch and roll motions of the ship. However the stabilisation system has physical limits so that the beam will no longer be horizontal and the radar will cease to function properly if the angular motions exceed certain critical values.

The critical motion level will not, of course, be exceeded all the time even in the most severe conditions. So we still need to decide on some measure of the acceptable probability of exceedance. Generally the choice is between an estimate of the proportion of time or the frequency with which the critical value is exceeded.

The choice depends on the nature of the equipment and the way in which the performance is degraded. Consider, for example, a roll stabiliser fin which cavitates if the angle of incidence exceeds a certain value. Cavitation is undesirable because it erodes the fin surface. Let us suppose that we are interested in the rate of erosion and the proportion of time the motion exceeds the critical value. This is given by Equation (11.21), derived from the Gaussian probability density function. If the critical incidence is α_{crit} we have

$$P\ (\ |\alpha| > \alpha_{crit}\ ) = 1 - 2\ erf\left(\ \frac{\alpha_{crit}}{\sigma_0}\ \right) \tag{16.1}$$

where σ_0 is the rms fin motion and the modulus is required because cavitation occurs for both positive and negative incidence. The time the fin is being eroded is then given by

$$t = T_H\ P\ (\ |\alpha| > \alpha_{crit}\ )\quad sec \tag{16.2}$$

where T_H is the total time spent in the cavitation prone conditions of the calculation.

On the other hand we might be interested in the frequency with which the fin emits bursts of cavitation noise because this might be detected by a submarine hunting the ship. We are then concerned with the probability that the peak fin incidence in each motion cycle will exceed α_{crit}. This may be obtained from the Rayleigh probability density function by using Equation (11.26):

$$P\ (\ \alpha > \alpha_{crit}\ ) = exp\left[\ -\frac{1}{2}\left(\frac{\alpha_{crit}}{\sigma_0}\right)^2\ \right] \tag{16.3}$$

The mean period of the fin motion peaks is, from Equation (2.27),

$$\bar{T}_P = 2\ \pi \sqrt{\frac{m_2}{m_4}} \quad sec \tag{16.4}$$

where m_2 and m_4 are the variances of the fin angular velocity and acceleration. The critical incidence is then exceeded

$$N = \frac{3600\ P\ (\ \alpha > \alpha_{crit}\ )}{\bar{T}_P} \quad times\ per\ hour \tag{16.5}$$

t and N in these formulae may be regarded as criteria for acceptable fin motions. Numerical values of these criteria are best established by monitoring the actual performance of ships at sea as required by Rule 3.

16.3 QUESTIONNAIRES

Questionnaires provide one of the few practical methods of obtaining data on actual performance at specific tasks at sea. A typical questionnaire to obtain criteria relating to damage to deck cargo on container ships is shown in Table 16.1. The compiler of the questionnaire should always bear in mind that the recipient will probably not be very interested in the business of criteria determination and the questionnaire should therefore be made as concise and self explanatory as possible. Otherwise it is likely to be consigned to the waste paper basket rather than be properly completed. The questionnaire should therefore open with the minimum number of questions designed to establish the identity of the recipient and his ship and follow with a brief summary of the scenario postulated. A statement promising confidentiality should always be included since some recipients (and their employers) may consider any confession of rough weather damage as an admission of poor seamanship. Questions soliciting opinions on design changes often yield fruitful results and have the added advantage of boosting the ego of the recipient, thus encouraging a timely response.

Ship operators will rarely be able to provide reliable direct estimates of limiting ship motions or other criteria because they generally have no measurement systems available to monitor the rough weather behaviour of their ship. Sailors are, however, often reasonably well schooled in estimating wave conditions and much more fruitful results will be obtained by asking for estimates of the worst sea state in which a particular task can be completed. Subsequent calculations based on strip theory or model tests may then be used to estimate the corresponding motions (or other rough weather phenomena) in suitable idealised sea spectra. If this technique is used the speed and heading must, of course, be specified in the questionnaire.

TABLE 16.1

SEAKEEPING QUESTIONNAIRE ON CONTAINER DAMAGE IN ROUGH WEATHER

Questionnaire on Container Damage in Rough Weather

Name of Captain

Name of ship

How long have you served in this ship? years months

Container ships running at high speed in rough weather are liable to damage the forward row of containers due to green sea impacts. Containers have also been lost overboard in heavy rolling conditions. This questionnaire is designed to obtain data on the problem and to determine the conditions in which it is likely to happen.

YOUR REPLIES WILL BE TREATED IN STRICTEST CONFIDENCE.

1) Head seas.

Deck wetness and risk of container damage is increased at high speed in head seas. In the table below please indicate the maximum speed you believe you could maintain in each sea state in the North Atlantic with an acceptable risk of container damage:

Sea state	0	1	2	3	4	5	6	7	8	9
Max speed (knots)										

2) Beam seas

In beam seas rolling will increase in high sea states. In severe sea states it may be necessary to change course to avoid a beam sea heading and minimise the risk to the containers,. In the table below please indicate the maximum sea state you believe could be maintained in beam seas at your normal cruising speed.

Sea state	0	1	2	3	4	5	6	7	8	9

3) Design Improvements

Which of the following design improvements would you recommend to alleviate container damage? (Please tick)

1) Increased freeboard forward
2) Remove forward row of containers
3) Roll Stabilisers
4) Stronger lashings
5) Instrumentation to give warning of imminent problems
6) Other (please specify)

Thank you for your assistance. Please now return this questionnaire to:

16.4 ANALYSIS OF NUMERICAL DATA FROM QUESTIONNAIRES

16.4.1 Mean values and standard deviations

Numerical data such as sea state estimates may be analysed to determine mean values and standard deviations using the formulae given below. If the questionnaires yield N estimates of a numerical quantity x (say the limiting sea state for a particular activity) the mean value is

$$\bar{x} = \sum \frac{x}{N} \tag{16.6}$$

and the standard deviation is

$$\sigma_0 = \sqrt{\frac{\sum (x - \bar{x})^2}{N - 1}} \tag{16.7}$$

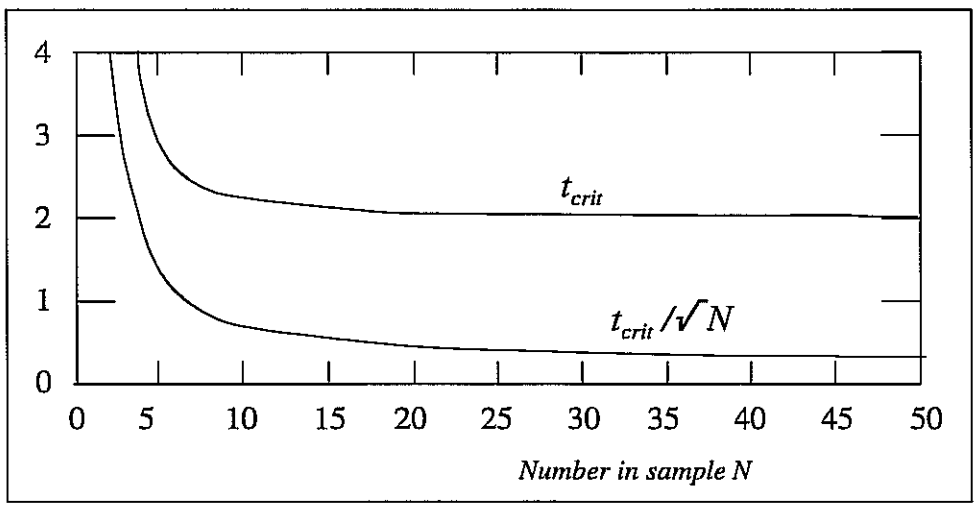

Fig 16.1 - Critical values for Student's t function for 95% confidence

16.4.2 Student's t test for confidence in the mean value

It is almost inevitable that the number of questionnaire returns will be small and there will probably be quite a wide divergence in the individual estimates giving large values of the standard deviation. We must then consider the possibility that the derived mean value $\bar{x}$ might be a freak result because the particular sample canvassed in the questionnaire was biased or untypical in some way. We need to establish whether $\bar{x}$ is a good estimate of the "true" mean value which would have been obtained if it had been possible to obtain estimates from many more ships. This may be done using Student's t test (see Mack (1966) and other text books on statistics). Briefly we may state that there is a 95% probability or ***confidence*** that the true mean value which would have been obtained from a much larger sample will lie within the range

$$\bar{x} \pm \frac{\sigma_0 \, t_{crit}}{\sqrt{N}}$$

where t_{crit} and $\frac{t_{crit}}{\sqrt{N}}$ are given as functions of N in Figure 16.1.

16.4.2 Tests for significant differences between ship classes

Questionnaires are often used to compare the performance of different ship classes. This will yield two mean values $\bar{x}_A$ and $\bar{x}_B$ and two standard deviations σ_A and σ_B from the two samples of N_A and N_B returns. We need to determine whether there is a significant difference between the two mean values. Two tests are used. We define a test function

$$\sqrt{F} = \frac{\sigma_A}{\sigma_B} \tag{16.8}$$

where $\sigma_A > \sigma_B$ so that $\sqrt{F} > 1$ and $F > 1$.

If $\sqrt{F}$ is greater than the critical value given in Figure 16.2 there will be a 95% probability that the two standard deviations are significantly different. If $\sqrt{F}$ is less than $\sqrt{F_{crit}}$ the two samples may be combined to give a single estimate of standard deviation for both samples:

$$\sigma_0 = \sqrt{\frac{(N_A - 1)\,\sigma_A^2 + (N_B - 1)\,\sigma_B^2}{N_A + N_B - 2}} \tag{16.9}$$

If the standard deviations are not significantly different and have been pooled in this way we may apply a further test to establish whether the two mean values are significantly different.

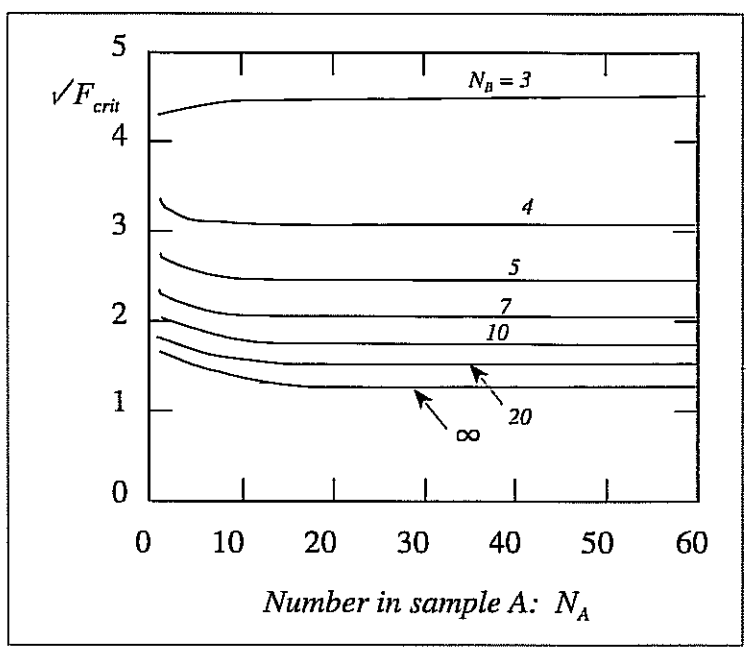

Fig 16.2 - Critical values of $\sqrt{F}$ for 95% confidence

If the test function

$$t = \frac{|\bar{x}_A - \bar{x}_B|}{S_{ed}} \qquad (16.10)$$

exceeds the critical value t_{crit} given in Figure 16.1 the two means are significantly different at 95% confidence level (ie there is a significant difference in the performance of the two ship classes). N is taken as the total number of returns from both classes for this test. In this formula S_{ed} is the standard error of the differences defined by

$$S_{ed} = \sigma_0 \sqrt{\frac{1}{N_A} + \frac{1}{N_B}} \qquad (16.11)$$

Worked Example:

A questionnaire issued to two ship classes yields the following data for limiting sea state for a particular activity:

Class	Mean value	Standard deviation σ_0	Number in sample N	$t_{crit} / \sqrt{N}$
A	5.7	1.2	7	0.9
B	4.9	1.4	10	0.7

What confidence levels can be attributed to each individual result? Are the results significantly different?

Using Student's t test and Figure 16.1 there is a 95% confidence that the true mean value for each sample lies within the following ranges:

Class A : $5.7 \pm 1.2 \times 0.9 = 5.7 \pm 1.08$: ie range is 4.62 - 6.78

Class B : $4.9 \pm 1.4 \times 0.7 = 4.9 \pm 0.98$: ie range is 3.92 - 5.88

Using the F test we find that the ratio of the standard deviations is

$$\sqrt{F} = \frac{\sigma_A}{\sigma_B} = 1.17$$

and the critical value of $\sqrt{F}$ is, from Figure 16.2,

$$\sqrt{F_{crit}} = 2.0$$

So $\sqrt{F} < \sqrt{F_{crit}}$ and the two standard deviations are not significantly different. Equation (16.9) then gives the combined standard deviation as

$$\sigma_0 = 1.32$$

and the standard error of the differences is, from Equation (16.11),

$$S_{ed} = 0.65$$

The test function t is, from Equation (16.10),

$$t = 1.23$$

and there is a total of 17 samples from the combined questionnaires. Figure 16.1 gives the critical value of t as

$$t_{crit} = 2.04$$

so that $t < t_{crit}$ and the results obtained from the two classes are seen to be not significantly different at 95% confidence level. The two samples may therefore be combined to yield a mean value

$$\bar{x} = \frac{5.7 \times 7 + 4.9 \times 10}{17} = 5.2$$

and Student's t test may again be applied to find the confidence limits for this combined result. We find a 95% confidence that the true mean value will lie within the range

$5.2 \pm 1.32 \times 0.53 = 5.2 \pm 0.7$: ie range is 4.5 - 5.9

It can be seen that combining the samples, where this can be justified, results in an improved estimate of the mean value.

16.4.3 Analysis of "Box Ticking" Questions

Box ticking questions yielding "yes/no" type answers require a different technique for determining the reliability of the results. The returns are usually analysed to give the proportion or "vote" for a particular opinion: for example, we might find that out of ten recipients of the questionnaire shown in Table 16.1, seven think that roll stabilisers would be a useful design

improvement. The question is whether this can be taken as a valid indication with, say, a 95% confidence level that roll stabilisers would be favoured by a majority of the masters of a (hypothetical) very much larger sample of ships of the same class. It is quite possible that the seven who favoured stabilisers might be ill informed and not typical of the population of masters at large so that the 70% majority vote is a freak result.

To examine this possibility we need to consider whether a majority vote might be achieved by chance. As an example consider the possible results of sending the questionnaire to four ships. If Y means "yes" and N means "no" the sixteen possible outcomes from a box ticking question are:

	Result No															
Ship No	1	2	3	4	5	6	7	8 *	9	10	11	12 *	13	14 *	15 *	16 *
1	N	Y	N	Y	N	Y	N	Y	N	Y	N	Y	N	Y	N	Y
2	N	N	Y	Y	N	N	Y	Y	N	N	Y	Y	N	N	Y	Y
3	N	N	N	N	Y	Y	Y	Y	N	N	N	N	Y	Y	Y	Y
4	N	N	N	N	N	N	N	N	Y	Y	Y	Y	Y	Y	Y	Y

Suppose now that three or more of the recipients voted "yes", to give a majority vote in favour of fitting stabilisers. This could be achieved in the five different ways marked with an asterisk. The probability that this result occurred by chance is therefore 5/16 = 0.3125 and the probability that it was not a chance result is 1 - 0.3125 = 0.6875. So the confidence level that the majority of a hypothetical much larger population of ship's masters would vote positively is only 68.75% in spite of the fact that 75% of the sample voted "yes".

Standard practice in statistical analysis is to demand a confidence level of at least 95% and we can see that this cannot be achieved with a sample of only four returns. Even if all four recipients respond with a 'yes' vote (outcome No 16) there is a 1/16 probability that the result is by chance and the confidence level that this would indicate a majority opinion in the world at large is only 1 - 1/16 = 93.75%.

We may extend this approach to an arbitrary number of questionnaire returns as follows. We require to find the minimum number of "yes" votes q for a sample size N which indicate a majority opinion with a 95% confidence level. Consider a questionnaire sample of N returns with r "yes" answers to a particular question. The proportion voting "yes" is

$$P_V = \frac{r}{N} \qquad (16.12)$$

TABLE 16.2

MINIMUM NUMBER OF "YES" RETURNS FOR A MAJORITY VOTE
AT 95% CONFIDENCE LEVEL

Sample size N	Number of "yes" returns q	Sample size N	Number of "yes" returns q	Sample size N	Number of "yes" returns q	Sample size N	Number of "yes" returns q
2	-	17	13	32	21	47	30
3	-	18	13	33	22	48	31
4	-	19	14	34	22	49	31
5	5	20	15	35	23	50	32
6	6	21	15	36	23	51	32
7	7	22	16	37	24	52	33
8	7	23	16	38	25	53	33
9	8	24	17	39	26	54	34
10	9	25	18	40	26	55	34
11	9	26	18	41	27	56	35
12	10	27	19	42	27	57	36
13	10	28	19	43	28	58	36
14	11	29	20	44	28	59	37
15	12	30	20	45	29	60	37
16	12	31	21	46	30	61	38

This vote could be achieved in

$$N_{C_r} = \frac{N!}{r!\ (N - r)!} \tag{16.13}$$

different ways.

The total number of possible combinations of answers is

$$\sum_{r=0}^{N} N_{C_r} = 2^N \tag{16.14}$$

If the answers to the questions were truly random all possible combinations of answers would be equally likely. Hence the probability of q or more "yes" answers is

$$P = \frac{\sum_{r=q}^{N} {}_{N}C_{r}}{2^{N}} \qquad (16.15)$$

and the probability or *confidence level* that this is not a chance result is

$$C = 1 - P \qquad (16.16)$$

Table 16.2 gives the minimum number of positive responses q required for a 95% confidence level as a function of the sample size N, calculated using the equations derived above. From this it can be seen that the absolute minimum number of returns required is five and they must all vote positively before this can be accepted as a valid indication of a majority opinion. The required proportion of positive votes falls as the sample size is increased.[1]

16.4.4 Increasing the Sample Size

Evidently there are considerable benefits to be obtained if the sample size is made as large as possible. Unfortunately it is usually only the largest navies which have more than, say, half a dozen ships in a class and we have seen that a sample of this size will generally yield results of only marginal reliability. For some aspects of seakeeping it may be possible to pool the results from more than one class of ship, as described above, but this, of course, precludes the possibility of distinguishing any effects of design differences between the classes.

It is sometimes tempting to increase the sample size by canvassing the opinions of former captains. This is not good practice as these individuals may suffer from the so called "fisherman's tales" effect by which experiences of long ago become distorted in the mind and generally exaggerated. One technique which is, however, acceptable is to repeat the investigation at intervals over a number of years so that the opinions of successive captains are canvassed in the same ships. Large sample sizes can be gradually built up in this way.

16.5 VOLUNTARY SPEED LOSS IN ROUGH WEATHER.

One "mission" which has received considerable attention is the ability to maintain speed in severe head seas. This is often regarded as a general indication of the seakeeping qualities of a ship since excessive motions, slamming, deck wetness, etc force the captain to reduce speed to avoid damaging his ship and its contents and injuring his crew and passengers.

A typical questionnaire designed to obtain data on speed loss in rough weather is shown in Table 16.3. Some results for two classes of frigates are shown in Figure 16.3. Estimates of mean speed and standard deviation have been calculated using Equations (16.6) and (16.7). As expected the ships suffer a dramatic speed loss as the sea state worsens. The standard deviation increases in

[1] Note that the same analysis applies with equal validity to negative opinions (ie not ticking a box).

TABLE 16.3

QUESTIONNAIRE ON SPEED IN ROUGH WEATHER

Name of Captain

Name of Ship

How long have you served in this ship? years months

Ship speed is limited in rough weather by two factors:
a) In moderate sea states the action of the wind and waves causes the ship to slow down even if full power is maintained.
b) In more severe sea states the captain may decide to reduce power or change course in order to alleviate slamming, deck wetness, propeller emergence, ship motions etc.

Imagine that you are required to make a high speed passage in rough weather. All ship equipment should be fully operational at the end of the passage. In the table below please indicate the maximum speed that you could maintain in your ship in the given sea states. Please also indicate with a tick the sea state in which you would first reduce power.

Sea state	0	1	2	3	4	5	6	7	8	9
Max speed (knots)										
Sea state for power reduction (tick one box)										

In the table below please indicate the reasons for your decision to reduce power in their order of importance. For example if you consider that slamming is the primary reason for speed reduction, closely followed by deck wetness, mark slamming "1" and deck wetness "2".

Slamming	
Deck wetness	
Ship motions	
Propeller emergence	
Other cause(s) (please state)	

high sea states, reflecting the difficulty of estimating speed loss and perhaps the lack of extreme rough weather experience of the commanding officers.

Application of Student's t test gives the confidence limits shown as shaded areas in Figure 16.3. The high standard deviation and the small number of ships in Class B widen the confidence limits considerably so that the estimates of mean speed for this class are much less reliable than those for Class A.

Application of the F test described above shows that the standard deviations are not significantly different and they may be pooled to give a common value using Equation (16.9). The test

function t is greater than the critical value (t_{crit} = 2.03 for N = 37 , see Figure 16.1) for all but the highest sea states. So the two results are significantly different at the 95% confidence level and we may be confident that the performance of Class A is better than that of Class B at least in moderate sea states.

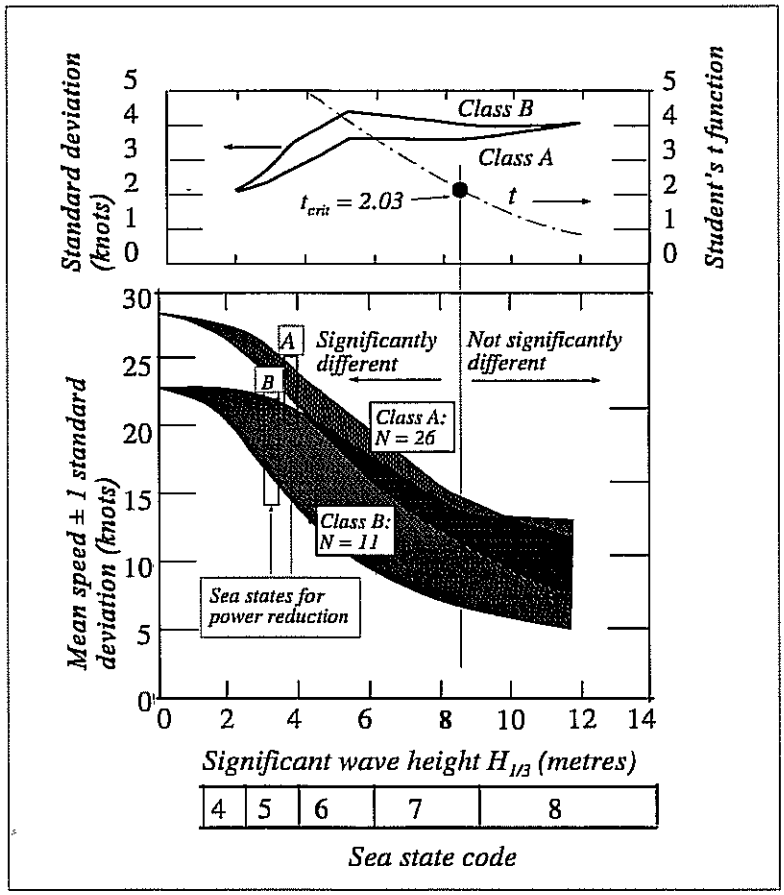

Fig 16.3 - Results of a questionnaire on speed in rough weather

16.6 CRITERIA FOR VOLUNTARY SPEED LOSS

The questionnaire shown in Table 16.3 asks for the captain's reasons for reducing speed. For most conventional ships it is usually found that slamming is the primary cause of speed reduction with either deck wetness or ship motions given as the secondary factor. Propeller emergence is usually only important for merchant ships in ballast. For the frigates described above the order of importance found from the questionnaire was

1. Slamming
2. Ship Motions
3. Deck Wetness

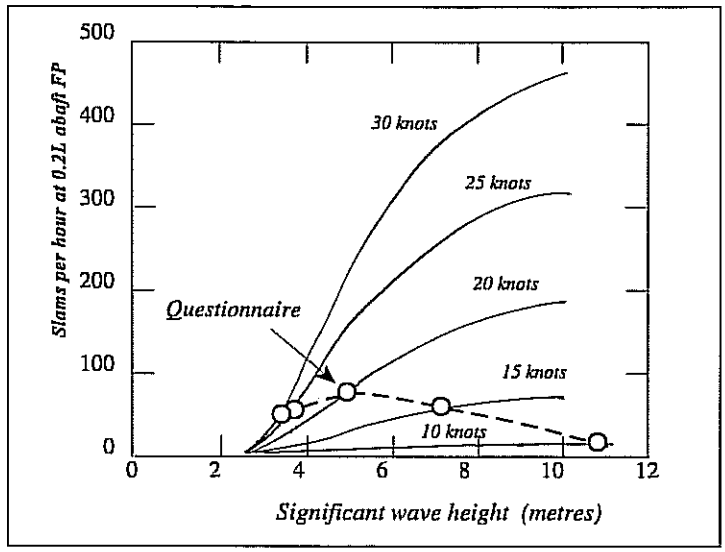

Fig 16.4 - Limiting slamming frequency for ship class A

Figure 16.4 shows predictions of slamming frequency for Ship A using the methods outlined earlier. The calculation is for head seas with the most probable modal periods for the North Atlantic. Now the questionnaire gives the maximum permissible speeds in given wave conditions and the results have been plotted in Figure 16.4 as a locus of acceptable combinations of speed and wave height. This allows us to estimate the maximum tolerable slamming frequency: in this case the captains of Ship Class A apparently tolerate about 60 - 80 slams per hour. and we may take this as a suitable criterion for slamming.

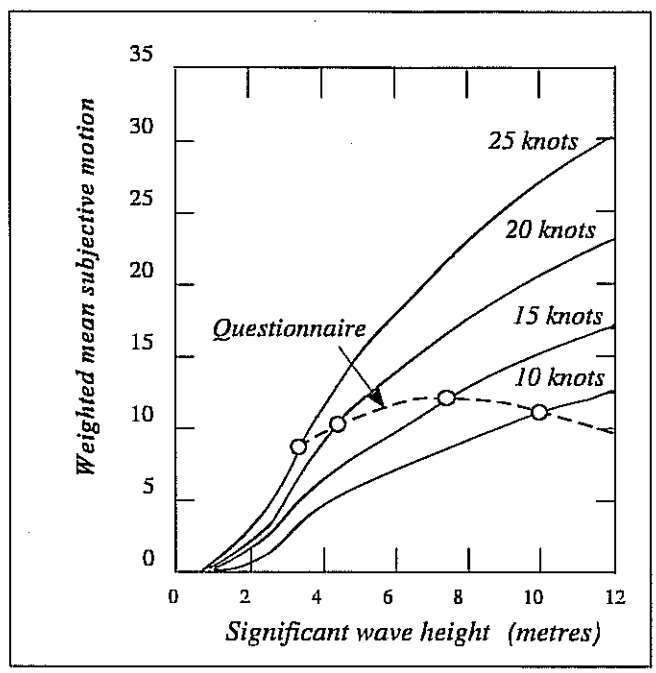

Fig 16.5 - Tolerated subjective motion in Ship class A

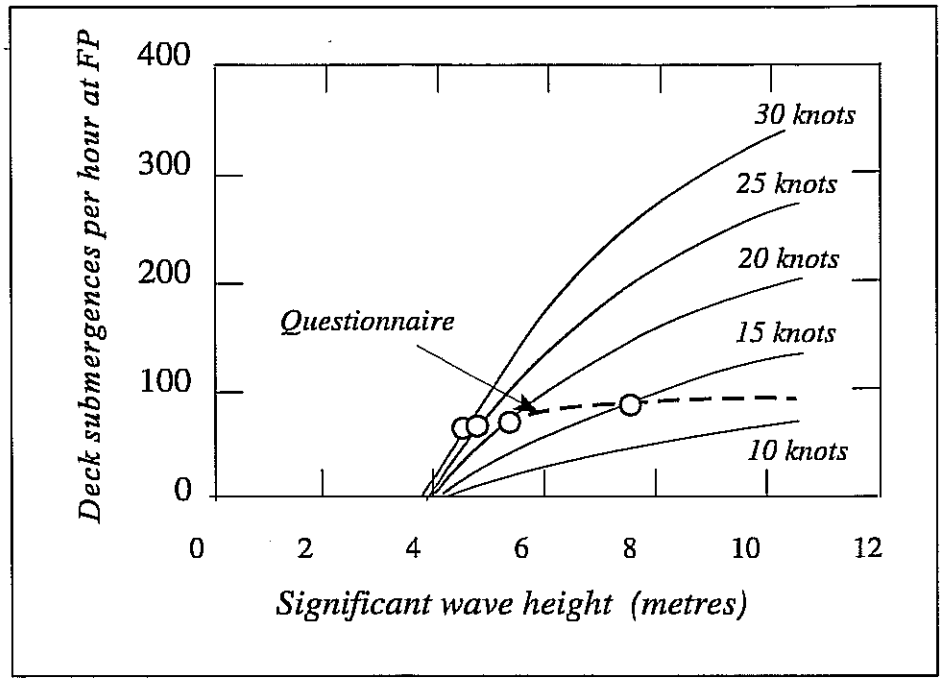

Fig 16.6 - Tolerated freeboard exceedance frequency for ship class A

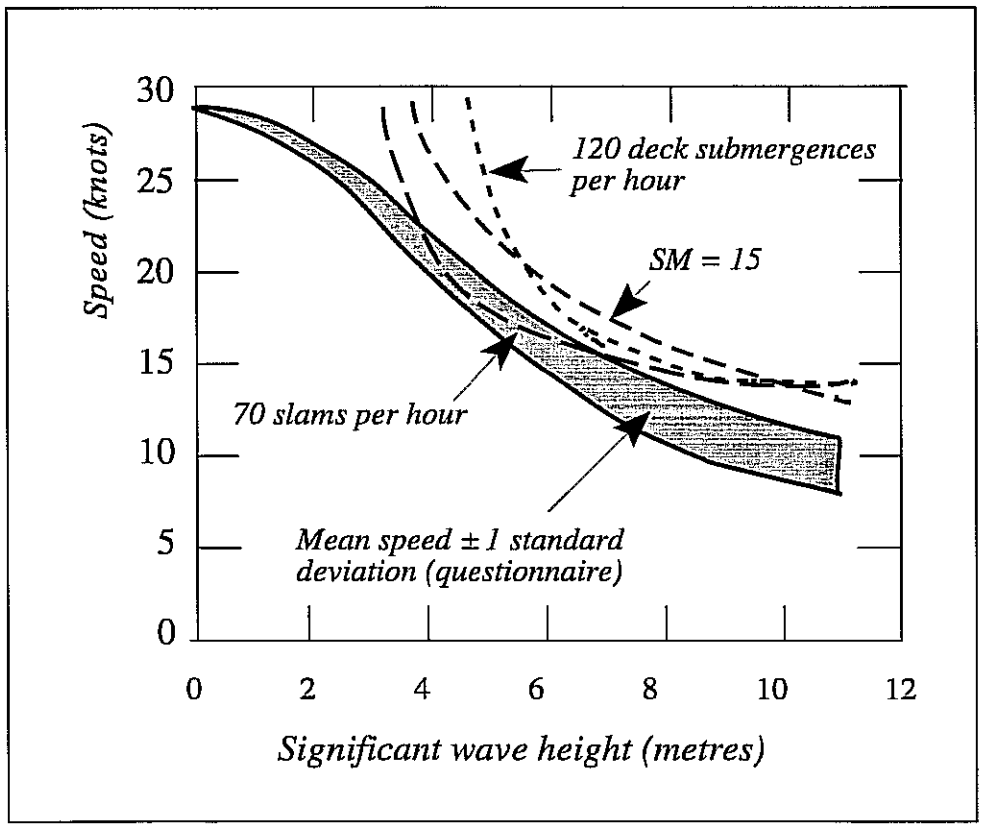

Fig 16.7 - Voluntary speed loss curves for ship class A

TABLE 16.4

SEAKEEPING CRITERIA FOR SPEED IN ROUGH WEATHER

Author	Ship type	Slamming	Deck wetness	Propeller emergence	Vertical acceleration
Kehoe (1973)	Warship	60 / hour at 0.15 L	60 / hour at FP		
Ochi and Motter (1974)	Merchant ship	Probability 0.03	Probability 0.07		
Shipbuilding Research Assoc. of Japan (1975)	Merchant ship	Probability 0.01	Probability 0.02	Probability 0.1	
Lloyd and Andrew (1977)	Warship		36 / hour		$\overline{SM} = 15$
Lloyd and Andrew (1977)	Merchant ship			120 / hour	
Aertssen (1963, 1966,1968,1972)	Merchant ship	Probability 0.03 or 0.04		Probability 0.25	
Andrew and Lloyd (1981)	Warship		90 / hour		$\overline{SM} = 12$
Comstock *et al* (1982)	Warship	20 / hour	30 / hour	Probability 0.02 at FP	0.2g rms at bridge
Yamamoto (1984)	Merchant ship	Probability 0.02	Probability 0.02 at FP		Probability of exceeding 0.4g at bridge = 0.05
Walden and Grundmann (1985)	Warship	Probability 0.03	Probability 0.07		

We may follow the same approach for ship motions and deck wetness and similar diagrams are shown for suitable measures of these phenomena in Figures 16.5 and 16.6. We see that the captains of these frigates apparently tolerate about 80 - 100 freeboard exceedances[2] per hour at the Forward Perpendicular (Equation (14.10)) and a weighted mean subjective magnitude of about 11 - 12 (Equation (15.5) with SM substituted for MSI).

However, deck wetness and ship motions are not, in this case, the limiting factors which force the captain to reduce speed. So these results cannot be taken as criteria for acceptable levels. All

[2] Strictly the captain is only concerned with deck submergences (ie occasions when the water actually comes on to the deck) rather than freeboard exceedances (when some of the water above the deck is thrown aside) but with the present state of prediction techniques it is not possible to distinguish between these two phenomena (see Section 14.6).

we can say is that the captain would tolerate more frequent deck submergence and higher levels of motions if slamming were not so frequent. These results may help in the determination of criteria but they cannot be used in the definitive way which was possible for slamming. We may therefore guess that the maximum tolerable deck submergence frequency in this ship is about 120/hour and that the maximum tolerable Subjective Magnitude is about 15.

Figure 16.7 shows the speed loss from the questionnaire compared with speed loss curves derived from Figures 16.4 - 16.6 for these estimated criteria. As expected, the slam limited speeds fit the questionnaire data tolerably well, at least in the middle range of sea states, while the other curves are higher. Note that all three limits are too high in high sea states. This may arise because the ship and its crew must then tolerate severe levels of all three phenomena simultaneously and this will be expected to reduce their tolerance to each individual factor. In other words severe motions and deck wetness will reduce the crew's tolerance of slamming and the and the maximum possible speed.

Table 16.4 lists a selection of seakeeping criteria for speed in rough weather derived by various authors from questionnaires, trials and intuition.

17

OPERATIONAL EFFECTIVENESS

"Their hulls whipped and shuddered in the huge Atlantic seas.... Solid green water swept destructively along their decks... For hour after hour this process repeated itself. Damage mounted, hull plates splitting, boats being smashed, men swept overboard and delicate anti submarine devices put out of order...."

Captain D MacIntyre DSO, DSC, RN: The Battle of the Atlantic.

17.1 INTRODUCTION

Operational effectiveness is defined in semantic terms as the ability of a ship to go to sea and accomplish its mission in whatever weather conditions it may find. In numerical terms we may express operational effectiveness as the ***proportion of time the ship can successfully accomplish its mission*** [1] ***in a given combination of sea areas and seasons***. Operational effectiveness can then be used as a yardstick for comparing the seakeeping performance of competing ship designs.

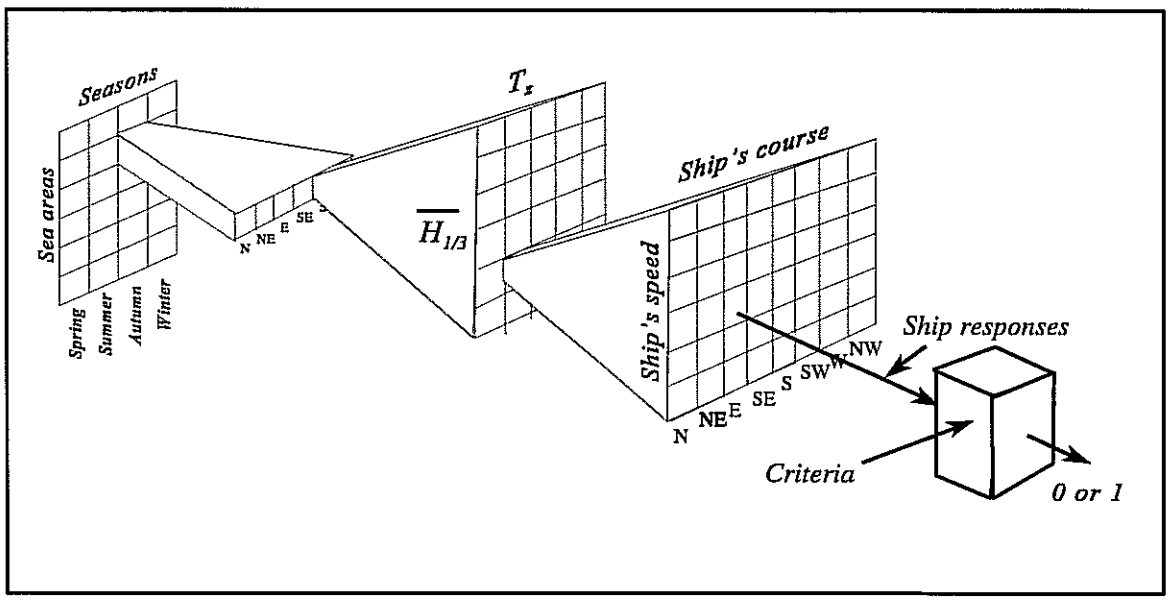

Fig 17.1 - Calculation of operational effectiveness

[1] "Mission" might be any activity undertaken by the ship; for example serving a meal in the passenger's dining room on a ferry, refuelling a helicopter on a warship, gutting fish on a trawler etc.

We have seen in previous chapters how we may calculate the rough weather responses of a ship for any combination of weather condition, ship speed and heading. If we know the limiting values of these responses (criteria) for a particular mission we may then determine whether it can be accomplished in that particular set of circumstances. Generalising the calculation to include all possible combinations of sea area, season, primary wave direction, significant wave height, modal period, ship speed and course allows us to calculate operational effectiveness as the proportion of time for which the mission is possible.

The method of calculating operational effectiveness given here is a simplified version of that proposed by Andrew, Loader and Penn (1984). The calculation is illustrated in graphical form in Figure 17.1.

TABLE 17.1

TYPICAL FREQUENCY DISTRIBUTIONS OF f_{season}

	Spring	Summer	Autumn	Winter
Tourist ferry	0.20	0.60	0.20	0.00
Warship	0.25	0.25	0.25	0.25

17.2 SEASON AND SEA AREA

The first essential in the calculation of operational effectiveness is to specify the seasons in which the ship is to operate. This is quantified by the frequency distribution f_{season} and examples are shown in Table 17.1. The tourist ferry is laid up in winter and spends most of its time at sea during the summer months. In contrast the warship is required to operate year round.

Having specified the frequency distribution for seasons the next step is to define the sea areas in which the ship will be required to operate in each season. This is conveniently done in terms of scatter diagrams like those shown in Table 17.2. Two examples of the ***conditional frequency distributions*** (CFD)[2] of sea area for a given season are shown for a merchant ship on a great circle transatlantic route and a warship operating in the North Atlantic. Sea areas are defined according to Hogben, Dacunha and Olliver (1986) (see Figure 2.16).

---

[2] "Conditional frequency distribution" is the proportion of time spent in a given condition when another condition is held constant. Thus, for example, f_{area} is the proportion of time spent in a particular sea area for a given season.

The merchant ship is required to operate between Europe and North America and the CFD of sea areas for each season reflects the time it is expected to spend in each area along the route. The warship is required to operate throughout the North Atlantic with most of its time spent in the northern areas 1, 3 and 4. In winter its operational area is moved south.

17.3 WAVE HEIGHT AND PERIOD

Scatter diagrams for wave height and period like those shown in Table 2.3 are required for each sea area, season and direction. Suitable data can be found in the wave atlases reviewed in Chapter 2. It may be necessary to convert the period into the preferred modal period parameter using Equation (2.41).

TABLE 17.2

TYPICAL CONDITIONAL FREQUENCY DISTRIBUTIONS FOR GIVEN SEASONS IN THE NORTH ATLANTIC.

	Merchant ship					Warship			
Sea area	Spring	Summer	Autumn	Winter		Spring	Summer	Autumn	Winter
1	0	0	0	0		0.10	0.10	0.10	0.05
2	0	0	0	0		0.03	0.03	0.03	0
3	0	0	0	0		0.20	0.20	0.20	0.10
4	0	0	0	0		0.20	0.20	0.20	0.10
8	0	0	0	0		0.04	0.04	0.04	0.07
9	0	0	0	0		0.04	0.04	0.04	0.07
10	0.11	0.11	0.11	0.11		0.07	0.07	0.07	0.10
11	0	0	0	0		0.07	0.07	0.07	0.10
15	0.25	0.25	0.25	0.25		0.04	0.04	0.04	0.07
16	0.44	0.44	0.25	0.25		0.04	0.04	0.04	0.07
17	0	0	0	0		0.07	0.07	0.07	0.10
23	0.07	0.07	0.07	0.07		0.04	0.04	0.04	0.07
24	0.13	0.13	0.13	0.13		0.03	0.03	0.03	0.05
25	0	0	0	0		0.03	0.03	0.03	0.05

TABLE 17.3

TYPICAL FREQUENCY DISTRIBUTIONS f_{course}

Course	N	NE	E	SE	S	SW	W	NW
Merchant ship	0.0	0.0	0.5	0.0	0.0	00	0.5	0.0
Warship	0.125	0.125	0.125	0.125	0.125	0.125	0.125	0.125

17.4 SHIP'S COURSE AND SPEED

The frequency distribution of ship's course is defined as f_{course} in Table 17.3 and the CFD for speed f_U for a given course is shown in Tables 17.4a and 17.4b. For the merchant ship the required course is easterly or westerly, depending on the direction of the voyage and half its time is spent on each heading. The ship is to be run at its maximum economical cruising speed in the range 15 - 20 knots. The warship is again required to be much more versatile. All courses are equally likely and a wide range of speeds is demanded. Nevertheless the economical cruising speed is frequently used. Very high and very low speeds are rare.

TABLE 17.4a

TYPICAL CONDITIONAL FREQUENCY DISTRIBUTION OF SPEED f_U FOR GIVEN SHIP COURSES (MERCHANT SHIP)

	SHIP COURSE							
Ship speed (knots)	N	NE	E	SE	S	SW	W	NW
25 - 30	0	0	0	0	0	0	0	0
20 - 25	0	0	0	0	0	0	0	0
15 - 20	0	0	1	0	0	0	1	0
10 - 15	0	0	0	0	0	0	0	0
5 - 10	0	0	0	0	0	0	0	0
0 - 5	0	0	0	0	0	0	0	0

TABLE 17.4b

TYPICAL CONDITIONAL FREQUENCY DISTRIBUTION OF SPEED f_U FOR GIVEN SHIP COURSES (WARSHIP)

	SHIP COURSE							
Ship speed (knots)	N	NE	E	SE	S	SW	W	NW
25 - 30	0.01	0.01	0.01	0.01	0.01	0.01	0.01	0.01
20 - 25	0.10	0.10	0.10	0.10	0.10	0.10	0.10	0.10
15 - 20	0.50	0.50	0.50	0.50	0.50	0.50	0.50	0.50
10 - 15	0.30	0.30	0.30	0.30	0.30	0.30	0.30	0.30
5 - 10	0.07	0.07	0.07	0.07	0.07	0.07	0.07	0.07
0 - 5	0.02	0.02	0.02	0.02	0.02	0.02	0.02	0.02

17.5 CALCULATION OF OPERATIONAL EFFECTIVENESS

The proportion of time the ship spends in a given season, sea area, primary wave direction, zero crossing period, significant wave height, course and speed is given by the product

$$P = f_{season}\, f_{area}\, f_{\chi}\, f_{TH}\, f_{course}\, f_U \qquad (17.1)$$

where

f_{season} is the frequency distribution of ship's time spent at sea

f_{area} is the conditional frequency distribution of sea areas for a given season

f_{χ} is the conditional frequency distribution of primary wave directions relative to North for a given season and sea area

f_{TH} is the conditional joint frequency distribution of mean zero crossing periods and significant wave heights for a given sea area, season and primary wave direction

f_{course} is the frequency distribution of ship courses relative to North

f_U is the conditional frequency distribution of ship speed for a given ship course.

For each combination of season, sea area, primary wave direction, significant wave height,

modal period, ship course and speed we may calculate the N ship responses[3] (r_n ; n = 1...N) of relevance to the mission. If the nth calculated response exceeds the corresponding criterion for the mission $r_{n\ crit}$ the mission cannot be accomplished and a counting functional Γ_n is set to 0:

$$\Gamma_n = 0 \quad \text{for } r_n > r_{n\ crit}$$

Otherwise the mission is not limited by the response r_n and the counting functional is set to 1.0:

$$\Gamma_n = 1 \quad \text{for } r_n < r_{n\ crit}$$

The proportion of time for which the mission can be accomplished is the operational effectiveness OE and this is obtained from the weighted sum of all the possible values of P. Mathematically this may be written as

$$OE = \sum P\ \Gamma_1\ \Gamma_2\ \Gamma_3\ \ldots\ \Gamma_N \qquad (17.2)$$

where $\sum$ implies summation over all seasons, areas, primary wave directions, zero crossing periods, significant wave heights, ship courses and speeds respectively.

TABLE 17.5

OPERATIONAL EFFECTIVENESS OF A FRIGATE IN THE NORTH ATLANTIC. (AFTER ANDREW, LOADER AND PENN (1984))

Criterion	Unstabilised	Stabilised
Rms pitch < 2 ^{0} no roll limit	0.976	0.976
Rms roll < 3 ^{0} no pitch limit	0.650	0.851
Rms pitch < 2 ^{0} Rms roll < 3 ^{0}	0.649	0.851

Table 17.5 shows an example of a calculation of operational effectiveness taken from Andrew, Loader and Penn (1984). This shows the operational effectiveness of a frigate with and without roll stabilisers in the North Atlantic. For this example it is assumed that the

[3] The responses are often rms motions but may include factors like Subjective Magnitude and the probability of slamming or deck wetness.

frigate's mission will be impossible if the rms pitch exceeds 2.0 degrees and the rms roll exceeds 3.0 degrees.

Considering first the pitch motions in isolation we see that the ship is able to achieve its mission almost all the time. Roll stabilisers, of course, have no influence on this result. Roll motions have a much greater effect on the ship's ability to achieve its mission and the unstabilised ship is effective for little more than half the time. These effects are considerably alleviated by the stabilisers.

18

THE EFFECT OF HULL SIZE AND FORM ON SEAKEEPING

" ...Then I'll pray for fine weather for all you Big Steamers,
For little blue billows and breezes so soft
Oh billows and breezes don't bother Big Steamers,
For we're iron below and steel-rigging aloft..."

From "Big Steamers: 1914-1918" by Rudyard Kipling.

18.1 INTRODUCTION

The methods outlined in this book allow the designer to quantify and assess the seakeeping qualities of a new design before the ship is built. If the predicted performance is inadequate the designer will need to change the size and/or shape of the hull to effect the necessary improvements. The designer therefore requires some guidance on the performance improvements which are likely to result from changes to hull form and size. The methods described earlier may be used to provide information on these trends and this Chapter gives the results of some specimen calculations. The trends described will be found to be generally applicable and the results may be used to suggest suitable changes in size and shape to a wide range of hulls. However, the results shown are necessarily specific to particular hull forms and should not be used to give definitive numerical estimates of the changes in performance of other hull forms. The actual performance of a particular design should always be estimated from strip theory calculations or model tests.

18.2 VERTICAL PLANE MOTIONS

18.2.1 Introduction and rationale

We will first consider the effect of hull size and form on motions in the vertical plane and confine our attention to head waves. This heading generally gives the worst vertical plane motions and it is found that a form which has low motions in head waves nearly always has a satisfactory performance at other headings. The most important motions to be considered in this context are the absolute vertical accelerations in the occupied spaces in the ship and the relative motions at the bow. The former are an indication of the severity of the motions experienced by the crew and passengers and we choose to calculate the acceleration at $x_{BIM} = 0.15L$, a typical location for the bridge of a warship or the passenger accommodation on a ferry. In general it is found that a ship which has satisfactory motions at this location will also have acceptable motions at other locations occupied by passengers or crew.

We shall calculate the relative motion at $x_{BIM} = 0.3L$, a typical location for a severe slam, and use this result to estimate the probability of keel emergence at this station.

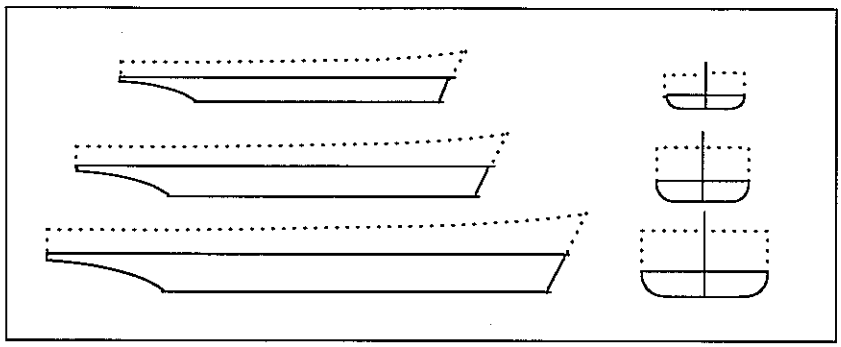

Fig 18.1 - Geometrically similar ships

18.2.2 Effect of hull size

The effect of hull size may be determined by calculating the responses of a series of geometrically similar ships all having the same hull shape but differing lengths as shown in Figure 18.1. Changing the length of the hull while keeping the shape constant results in proportional changes to all the linear dimensions (beam, draught, freeboard etc) and the displacement varies as the cube of the length. So these hulls may be regarded as scale models or *geosims*[1] of each other.

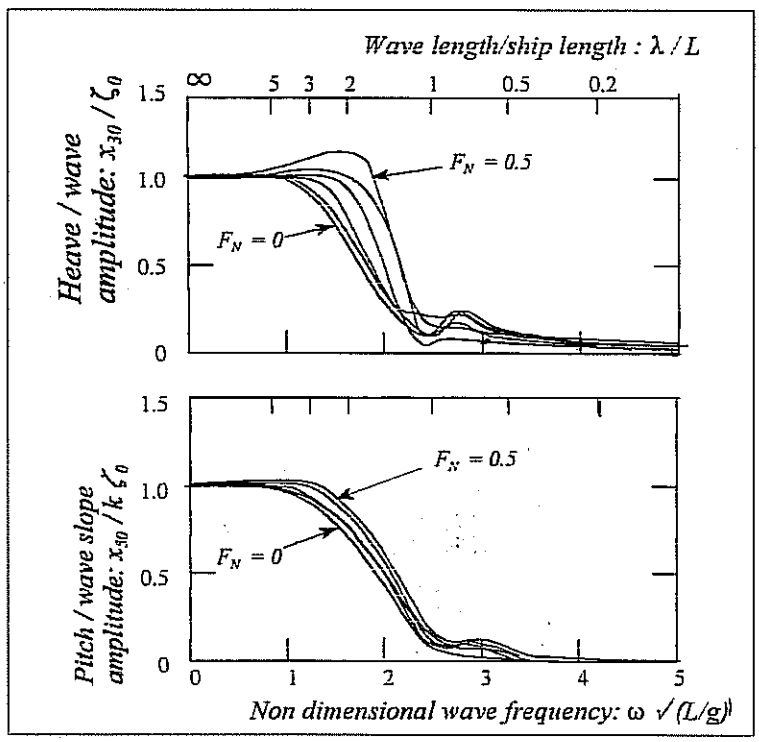

Fig 18.2- Heave and pitch transfer functions for the geosims in regular head waves

[1]Acronym for *geometrically similar*

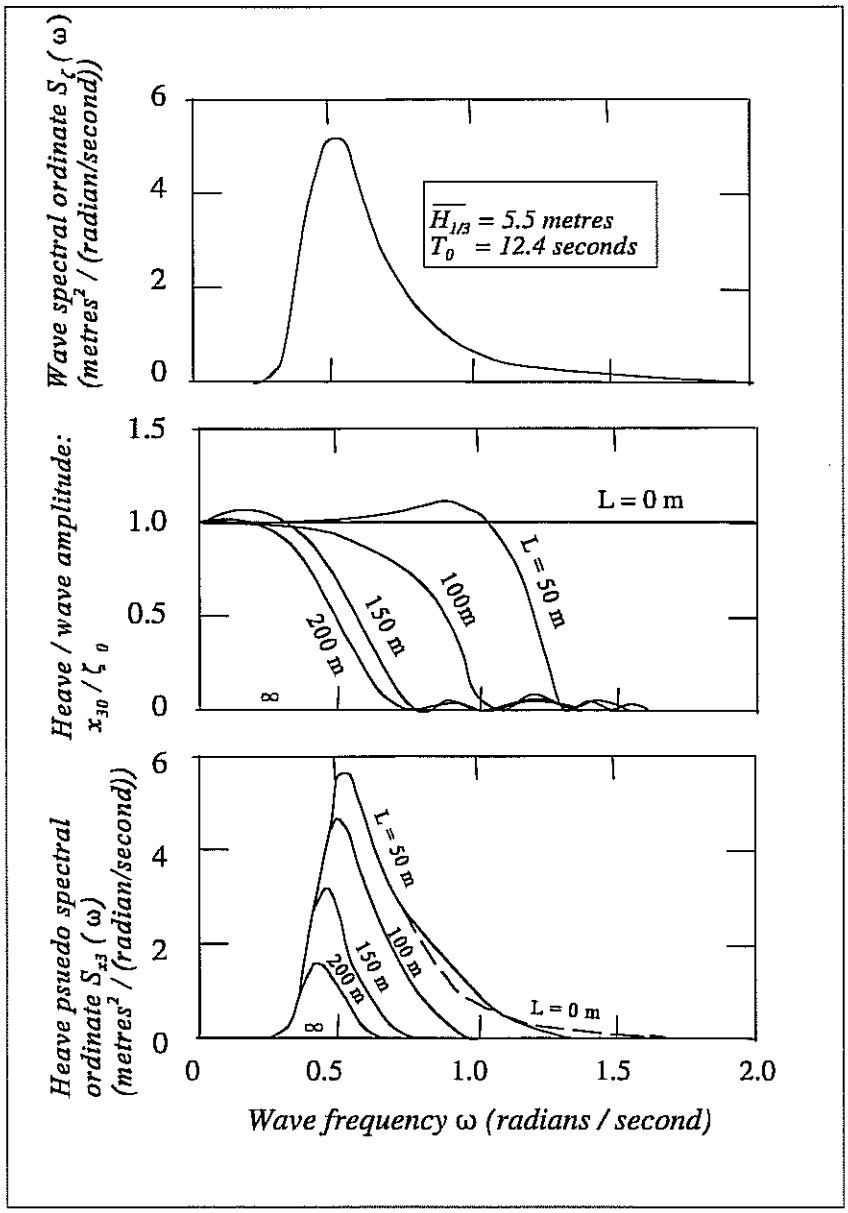

Fig 18.3 - Effect of hull size on heave pseudo spectrum at 20 knots in irregular head waves

For the purpose of this study we choose a frigate form with the following proportions:

$$\frac{D}{L} = 0.034; \qquad \frac{B}{L} = 0.12$$

Non dimensional transfer functions for heave and pitch of this hull shape in head waves at various Froude numbers are shown in Figure 18.2. In this form these transfer functions apply to all the geosim hull forms because they all have the same shape. All the motion responses are essentially unity in waves which are much longer than the ship and more or less negligible in waves shorter than a critical length which is about three quarters of the ship length. In

other words ships tend to contour very long waves but do not respond to very short waves, as already discussed in Chapter 7.

Transfer functions for a given ship length and speed may be derived from these results and examples for 20 knots are shown in Figures 18.3 and 18.4.

These figures show the calculation of the rms motions in a typical long crested Bretschneider wave energy spectrum using the wave frequency domain method described in Chapter 8.

Consider first an infinitely long ship. All the waves in the seaway are shorter than the critical wave length, the heave and pitch transfer functions are zero over the entire range of frequencies and the ship does not respond to the wave input at all.

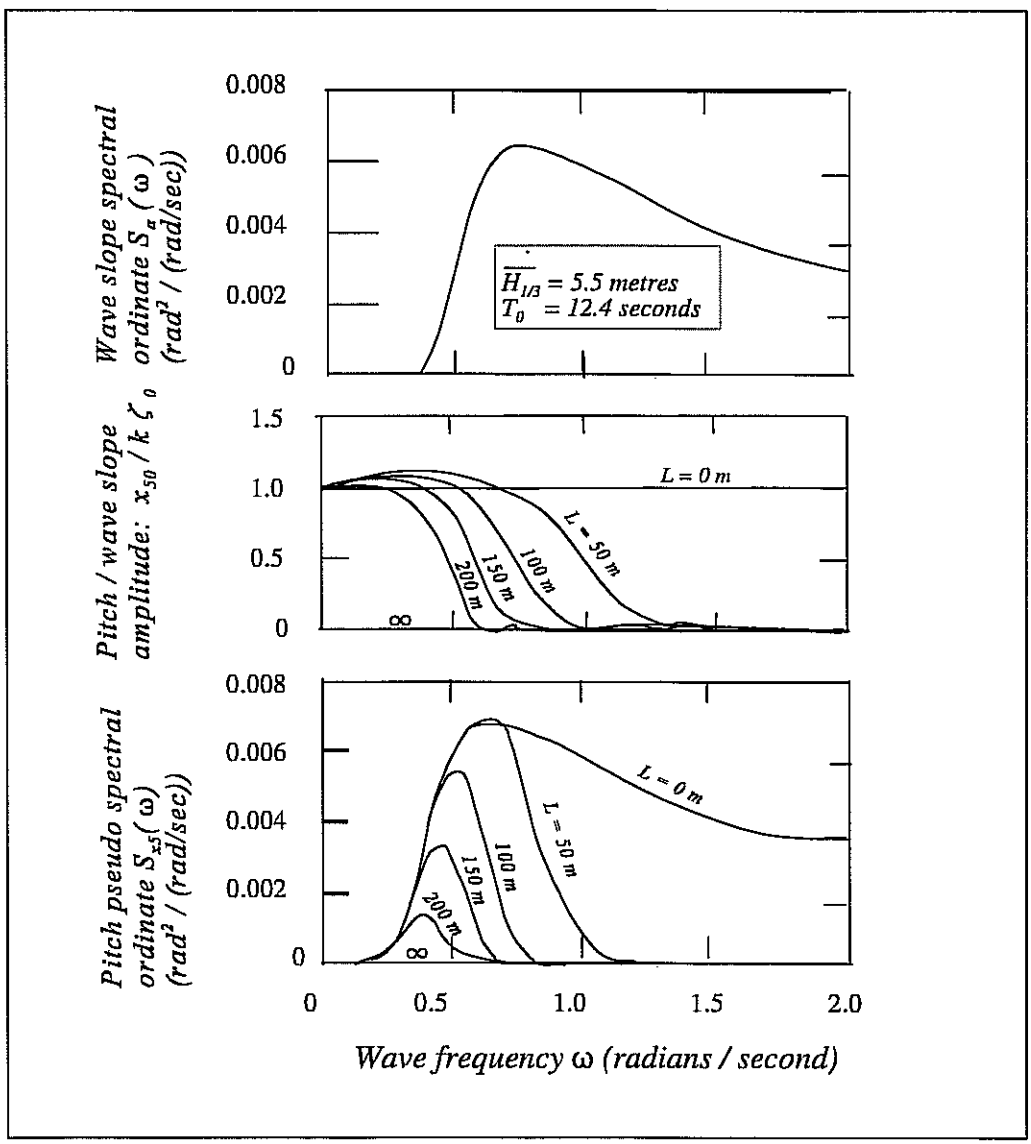

Fig 18.4 - Effect of hull size on pitch pseudo spectrum at 20 knots in irregular head waves

As the ship length is reduced some of the waves in the seaway begin to exceed the critical length and the transfer functions adopt appreciable values in the range of important wave frequencies. So the heave and pitch pseudo spectral ordinates are increased, as shown in Figures 18.3 and 18.4.

For a very small ship (for example a toy boat) with $L \approx 0$ metres all the waves in the seaway are longer than the ship and the transfer functions are unity over the entire range of frequencies. The ship contours the waves aligning itself to the wave slope: the heave is the same as the wave depression and the pitch is the same as the wave slope.

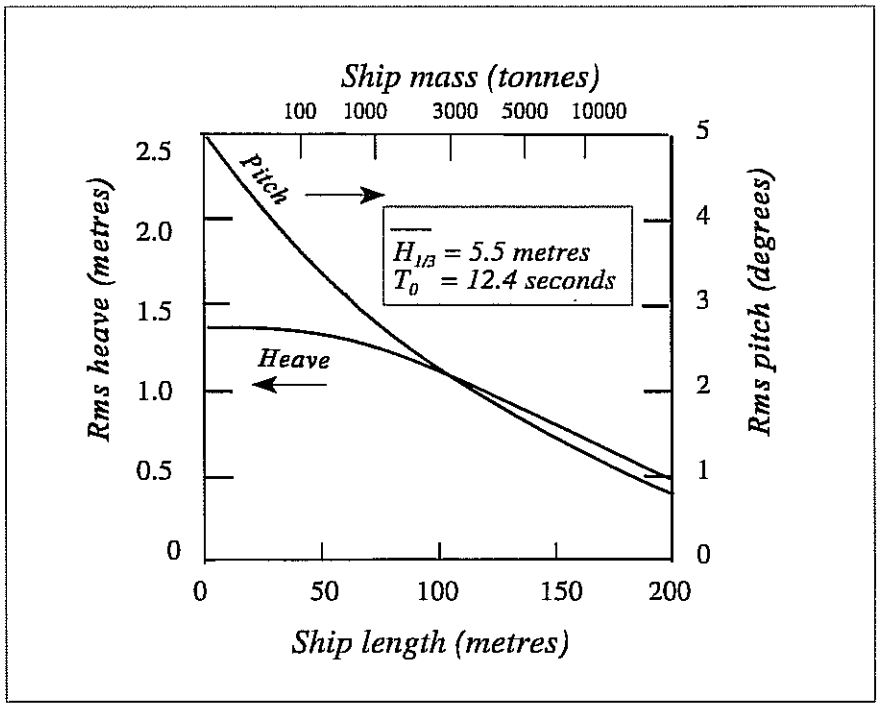

Fig 18.5 - Effect of hull size on rms heave and pitch motions at 20 knots in irregular head waves

Figure 18.5 shows the rms heave and pitch motions obtained from the area under the motion pseudo spectra shown in Figures 18.3 and 18.4. These clearly demonstrate that small ships suffer from increased absolute motions in a given seaway.

Figure 18.6 shows a similar calculation for the vertical acceleration at $x_{BIM} = 0.15\ L$. The acceleration pseudo spectral ordinates are given by

$$S_{\ddot{z}_3}(\omega) = \left(\frac{\omega_e^2\ s_{30}}{\zeta_0} \right)^2 S_\zeta(\omega) \quad (\ m/sec^2\ )^2\ /\ (rad/sec)$$

(see Equations (2.21) and (8.10)).

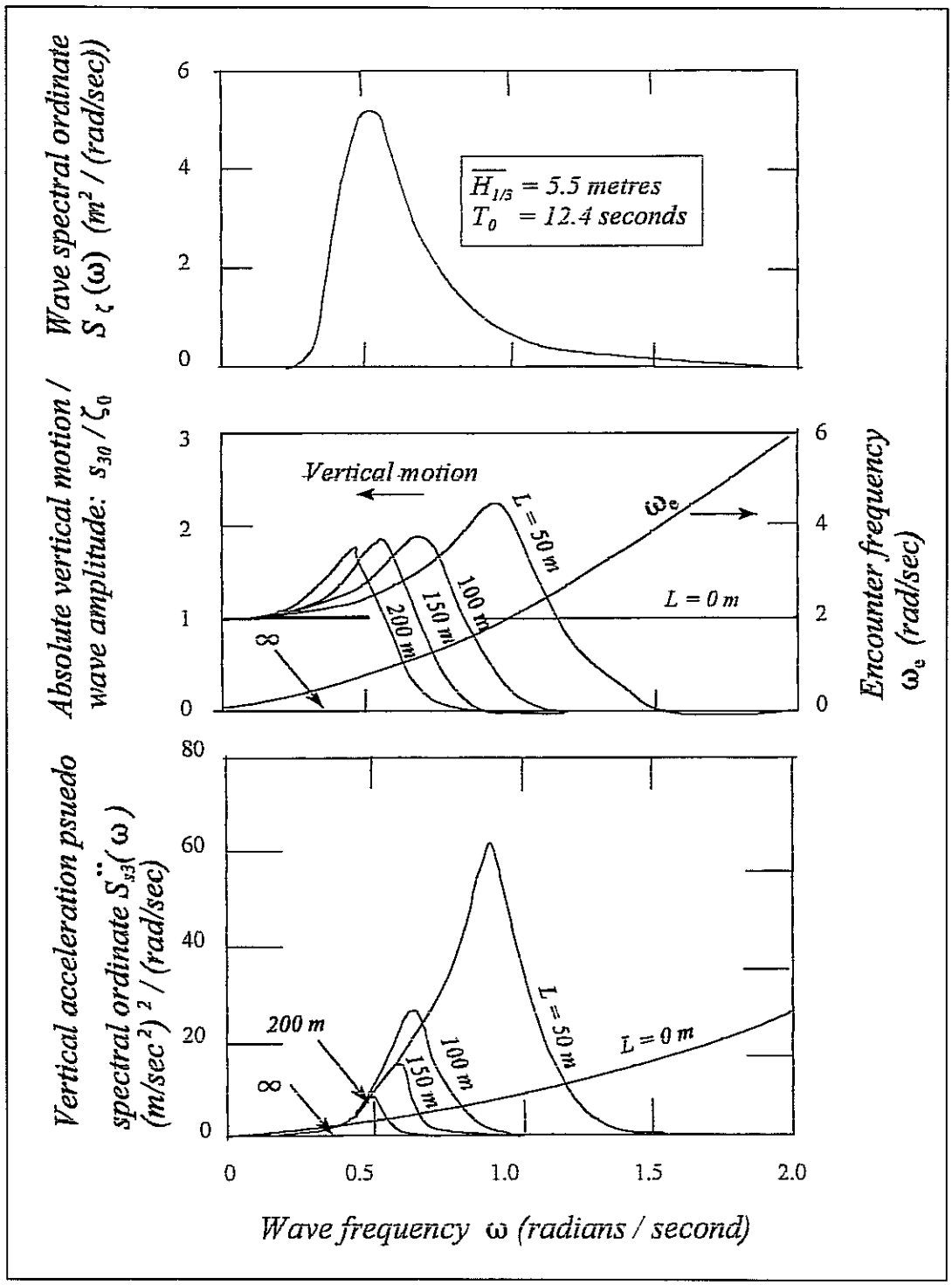

Fig 18.6 - Effect of hull size on vertical acceleration pseudo spectrum at 20 knots in irregular head waves: x_{B1M}= 0.15L.

The effects of encounter frequency become progressively more important as the ship length is reduced (in other words small ships respond more vigorously to the shorter waves). In the limit, a very small ship of length $L \approx 0$ metres will contour all the waves and suffer very large accelerations.

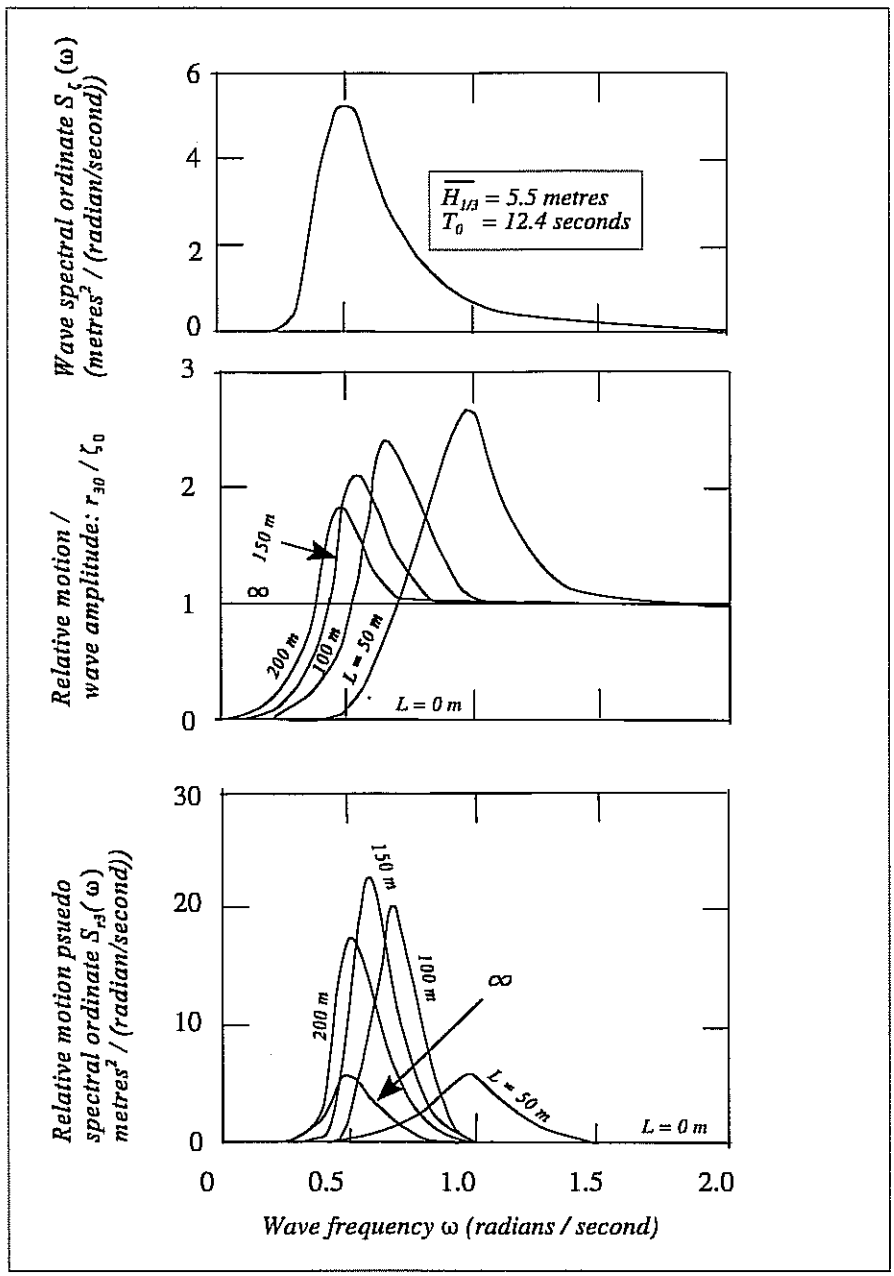

Fig 18.7 - Effect of hull size on relative motion pseudo spectrum at 20 knots in irregular head waves: $x_{B1M} = 0.3L$

Figure 18.7 shows a similar calculation for relative motion at $x_{B1M} = 0.3\ L$. We have seen that the infinitely long ship does not respond to the waves and it follows that the relative motion must then be the same as the wave depression (apart from any swell up effects (see Equation (7.13)).

This is confirmed in Figure 18.7 where we see that the infinitely long ship has a relative motion transfer function which is unity over the entire range of frequencies. So the response is the same as the wave energy spectrum and the rms relative motion is

$$\sigma_0 = \sqrt{m_0} = 0.25\ \overline{H}_{1/3} \quad m$$

Again, the displacement transfer function s_{30} / ζ_0 for an infinitely long ship is zero at all frequencies and the ship does not respond to the seaway at all. As the ship length is reduced the transfer functions increase and the response output becomes appreciable.

As the length is reduced the ship begins to contour the longer waves and the transfer function encompasses a smaller range of frequencies. However peaks appear in the transfer function and the response is amplified if these peaks coincide with the peak of the wave energy spectrum. For very small ships ($L \approx 0$) contouring all the waves the transfer function r_{30} / ζ_0 is everywhere zero and there are no relative motions.

These trends are summarised in Figure 18.8.

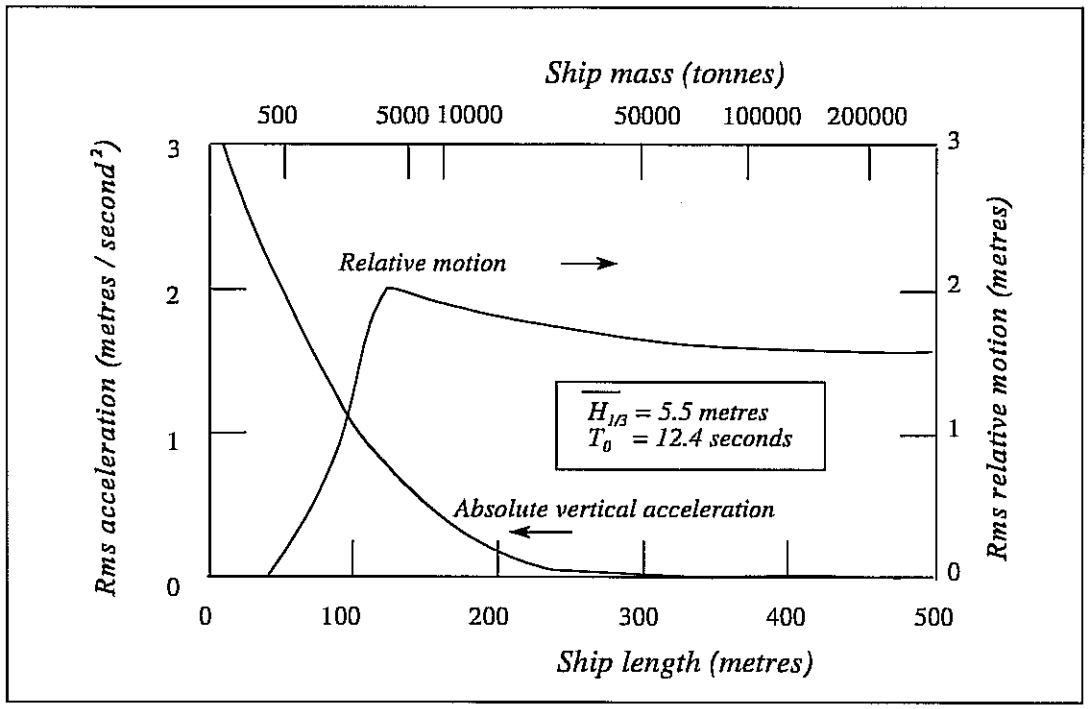

Fig 18.8 - Effect of hull size on rms relative motions at $x_{BIM} = 0.3L$ and rms absolute acceleration at $x_{BIM} = 0.15L$

The probability of keel emergence calculated using Equation (14.5) is shown in Figure 18.9. For the wave spectrum considered here keel emergence is common for ships in the range 70 - 200 metres and is most common for ships about 120 metres in length[2]. Smaller ships are less susceptible because they tend to contour the waves so that their relative motions are small. These ships will, however, suffer from high vertical accelerations which would make life on board intolerable at the speed considered in this example.

[2] A typical frigate length!

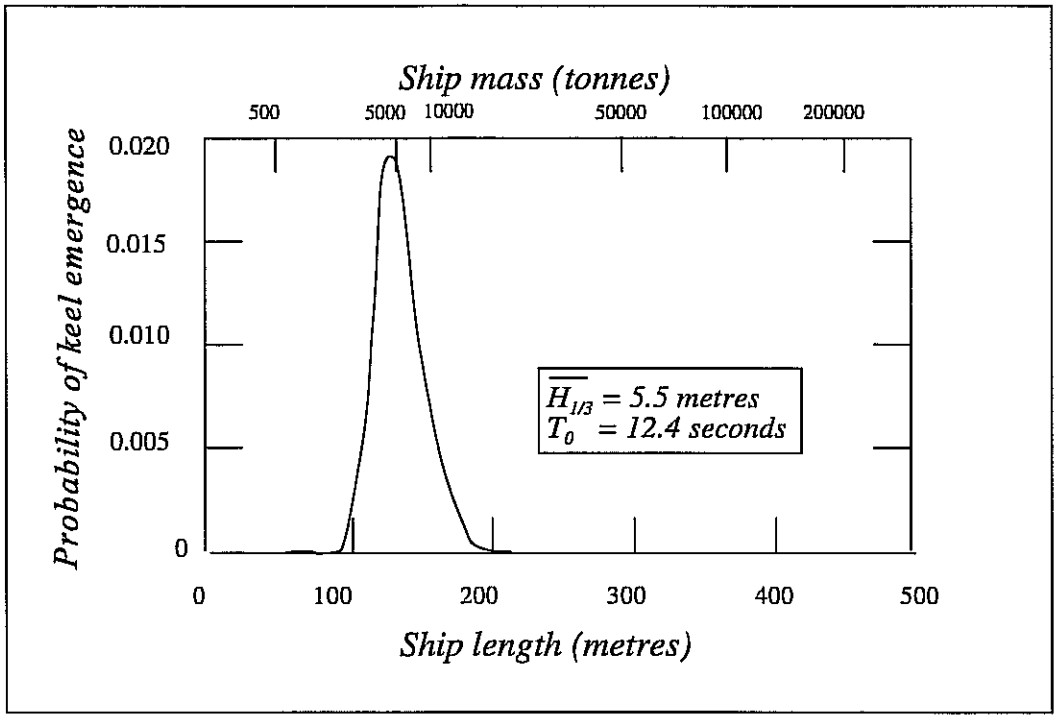

Fig 18.9 - Effect of hull size on keel emergence at 20 knots in irregular head waves

The greater draught of the larger ships ensures that keel emergence is unlikely for these vessels in spite of their appreciable relative motions. Increasing the size of the ship also gives a dramatic reduction in vertical acceleration. Large ships are generally more comfortable than small ones in rough weather.

18.2.3 Effect of hull form

Detail changes of hull form such as easing the radius of curvature of the bilges have little discernible effect on ship motions in the vertical plane. The designer seeking an improvement in seakeeping performance must think in terms of changes to the overall proportions of the ship rather than piecemeal modifications. Seakeeping performance assessment must therefore be considered at an early stage in the design process before the major proportions and dimensions of the hull have been settled.

A number of published works (for example Bales (1981), Schmitke and Murdey (1981), Lloyd (1988)) offer useful guidance but they do not provide a method of developing an actual design. All use different methods of quantifying 'good' seakeeping performance and changes in hull form. Defining the hull form parameters which are kept constant is all important: for example increasing the ship mass without corresponding changes to the overall dimensions of the ship (length, beam and draught) would change the block coefficient and lead to results which would be different from those obtained if the block coefficient had remained constant and the mass accommodated by increases in the length, beam and draught.

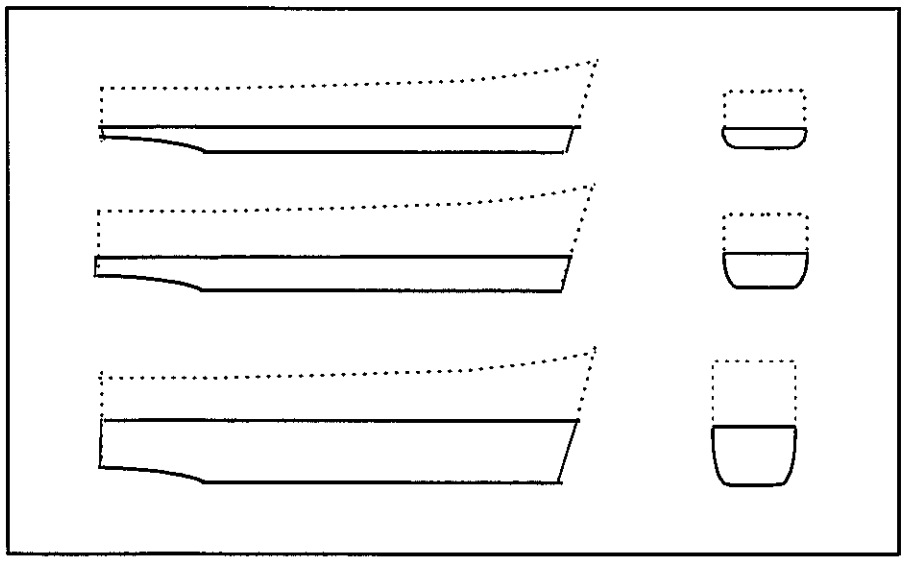

Fig 18.10 - Draught/length variations

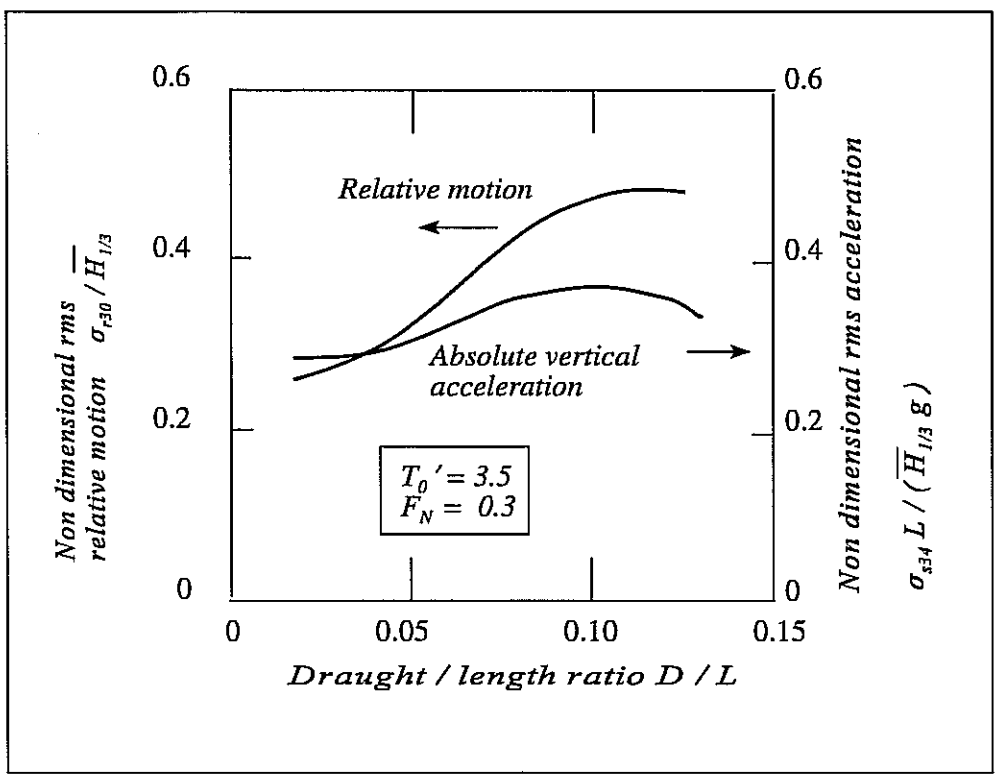

Fig 18.11 - Effect of draught/length ratio on rms absolute vertical acceleration at x_{BIM} = 0.15L and rms relative motions at x_{BIM} = 0.3L in irregular head waves

We shall here examine the effects of changing the draught/length and beam/length ratios and the forward waterplane area coefficient while keeping the block coefficient constant. In other words the ship mass is changed in proportion to the changes in beam and draught. These particular parameters have been selected because they have appreciable and well defined effects on seakeeping performance. Other parameters such as transom beam, midships section area coefficient etc have relatively minor effects and it would not normally be considered worthwhile changing them to improve seakeeping performance. Figure 18.10 illustrates changes to the draught/length ratio. The effects on the motions are shown in Figure 18.11. These are given in non dimensional form which makes them more easily applicable to ships of different length and waves of different significant wave height. They are presented for a Froude number of 0.3 and a non dimensional modal period defined as

$$T_0' = T_0 \sqrt{\frac{g}{L}} = 3.5$$

which corresponds approximately to a modal period of 12.4 seconds for a ship length of 125 metres. Similar trends are found for other modal periods and ship lengths.

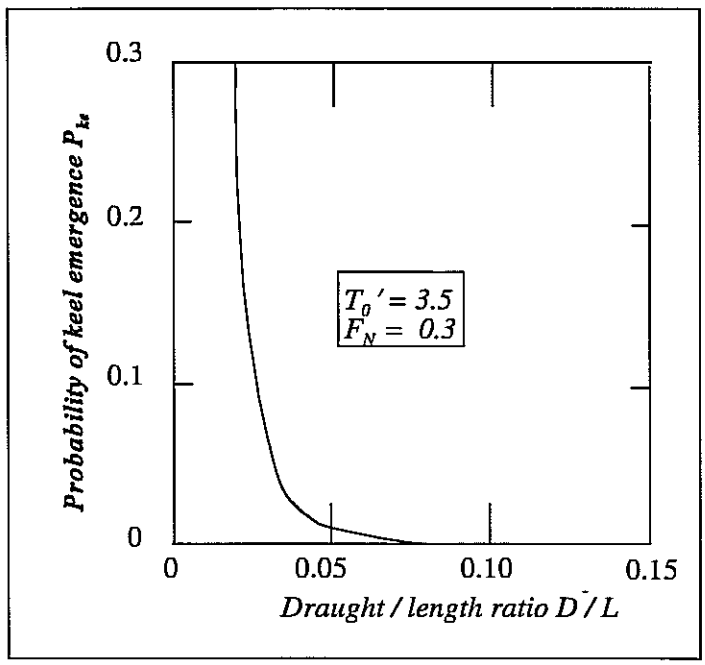

Fig 18.12 - Effect of draught/length ratio on probability of keel emergence in irregular head waves

Reducing the draught with a corresponding reduction in ship mass increases the added mass and damping coefficients, as shown in Figure 5.8, and this has the generally beneficial effect of reducing both the absolute and relative motions.

Figure 18.12 shows the corresponding effects on the probability of keel emergence. This rises dramatically as the draught is reduced, in spite of the associated reduction in relative motion.

Figures 18.13 - 18.15 show similar results for beam/length ratio. Again increases to the beam are associated with increased displacement and the larger added mass and damping coefficients would be expected to yield reduced motions. However the excitation from the waves is also increased because of the larger waterplane area and the resulting changes to the motions are not dramatic. The probability of keel emergence is greatest for ships with beam/length ratios in the range 0.1 - 0.2 (typical of many modern designs).

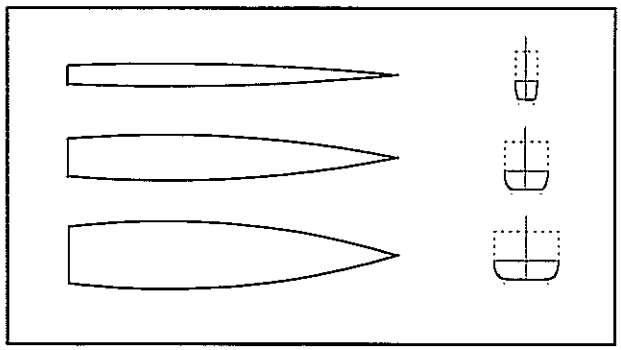

Fig 18.13 - Beam/length ratio variations

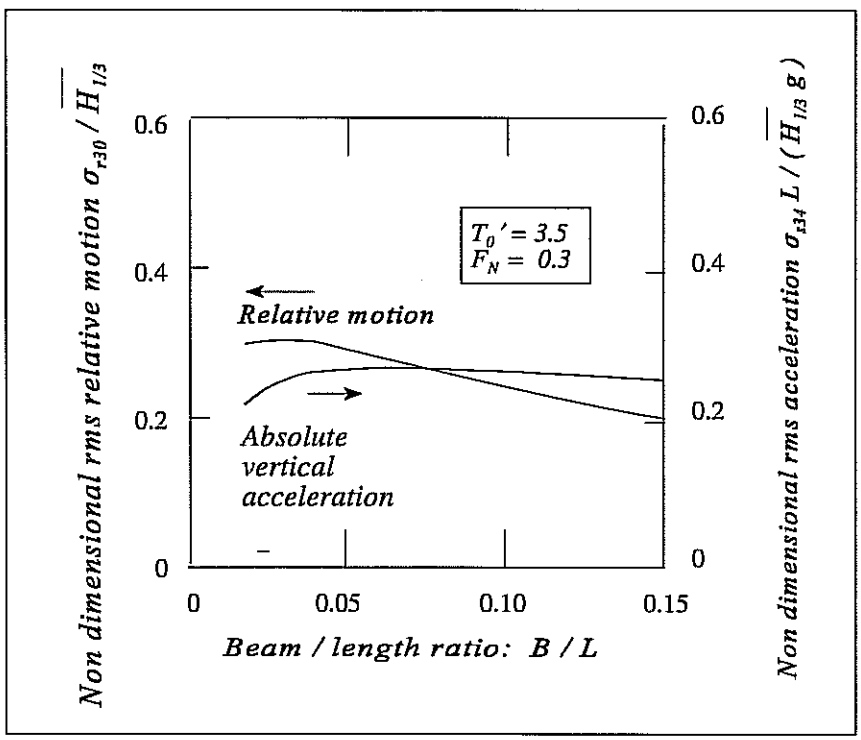

Fig 18.14 - Effect of beam/ length ratio on rms absolute vertical acceleration at $x_{BIM} = 0.15L$ *and rms relative motions at* $x_{BIM} = 0.3L$ *in irregular head waves*

The effects of changing the forward waterplane area coefficient are shown in Figures 18.16 - 18.18. A large forward waterplane area coefficient increases the local beam at the bow and gives favourable changes to the hydrodynamic coefficients in this region, again at the expense of increased wave excitation. It also leads to more favourable section shapes (for the reduction of slamming pressures) with higher deadrise angles, as shown in Figure 18.16.However, extremely large forward waterplane area coefficients imply heavily flared bows above the waterline and these may suffer from flare slamming and increased deck wetness (see Section 14.7)

Nevertheless, a large forward waterplane is clearly beneficial, reducing both absolute and relative motions and the probability of keel emergence. The more favourable deadrise angles will alleviate slamming when it does occur.

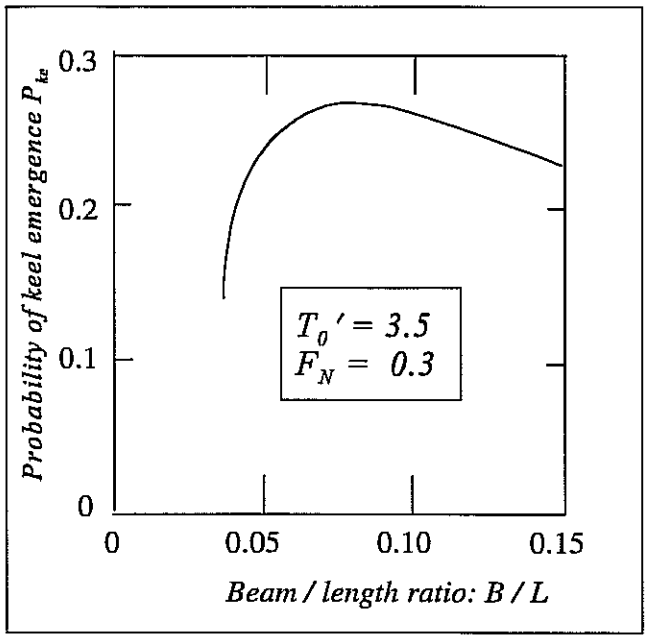

Fig 18.15 - Effect of beam/length ratio on keel emergence in irregular head waves

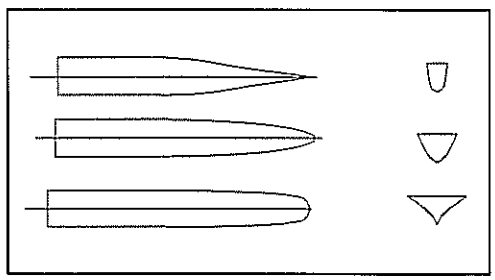

Fig 18.16 - Forward waterplane area coefficient variations

18.3 LATERAL PLANE MOTIONS

Lateral plane motions are also influenced by changes in hull form and size. However, it is generally considered better to reduce motions by installing suitable roll reduction devices such as bilge keels, active fins or passive tanks and, of course, the rudder. However the metacentric height can have a considerable influence on roll motions and it is worth ensuring that a suitable value is chosen.

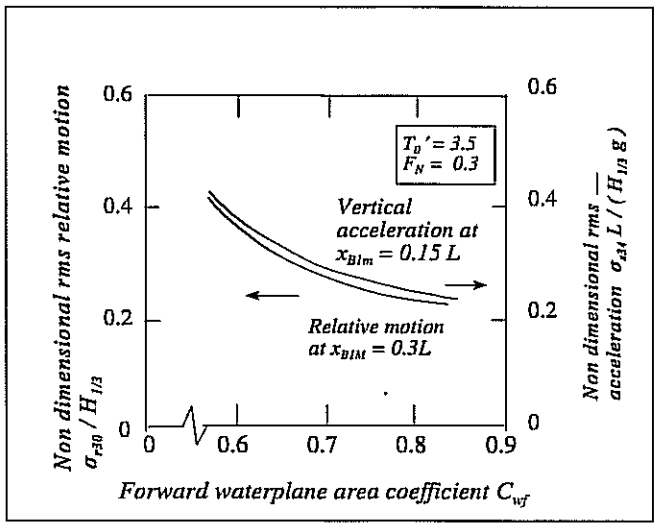

Fig 18.17 - Effect of forward waterplane area coefficient on rms absolute vertical acceleration at x_{B1M} = 0.15L and rms relative motions at x_{B1M} = 0.3L in irregular head waves

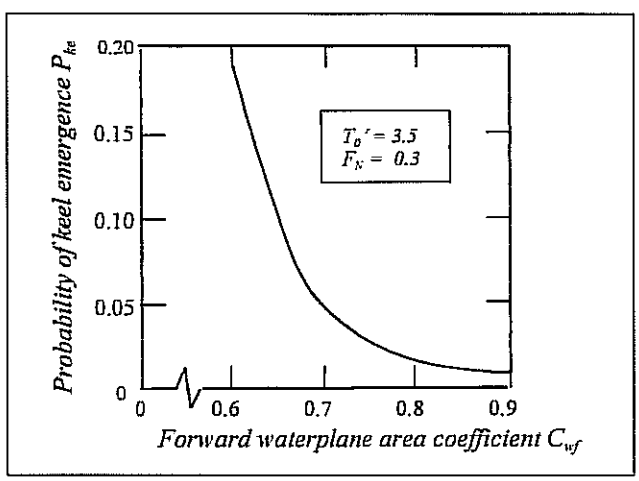

Fig 18.18 - Effect of forward waterplane area coefficient on the probability of keel emergence in irregular head waves

Equation (7.5b) gives an approximate relationship between the natural roll frequency and the fluid metacentric height:

$$\omega_{*4} \approx \sqrt{\frac{m\ g\ \overline{GM_F}}{1.25\ I_{44}}} \quad rad/sec$$

Assuming that the metacentric height is sufficient to meet the stability regulations the designer should ensure that it is chosen to yield a natural frequency which does not coincide with peaks in the encountered wave spectrum in which the ship is expected to operate (see Section 8.5). It is also desirable to arrange for the natural frequency to lie in the range

$$0.3 < \omega_{*4} < 0.6 \quad rad/sec$$

Lower natural frequencies with long natural periods lead to a "lazy" roll motion and the feeling, which may well be justified, that the ship is in danger of capsize. Higher frequencies lead to high roll and local lateral accelerations, especially in the upper parts of the ship. Motion induced interruptions may then become commonplace (see Chapter 15).

18.4 THE SEAKEEPING DESIGN PACKAGE

We have seen that the available methods of predicting seakeeping performance for a given design cannot, in themselves, be used to optimise a hull form. Lloyd (1992,1993) overcame this problem with the Seakeeping Design Package (SDP). This is a computer based design system which develops optimum hull forms within parameter ranges (length, beam, draught etc) specified in advance by the designer. The designer must specify seakeeping response targets for accelerations at two places, deck wetness and slamming in head waves. An error sum is defined as

$$\epsilon = \sum (log_e\ P_k - log_e\ P_{*k})^2 ; \quad (k = 1,4) \qquad (18.1)$$

where

P_1 is the probability of the vertical acceleration exceeding 3.0 m/sec^2 at $x_{BIM} = 0.15L$

P_2 is the probability of the vertical acceleration exceeding 3.0 m/sec^2 at $x_{BIM} = -0.425L$

P_3 is the probability of the relative motion exceeding the freeboard at the FP

P_4 is the probability of the highest slamming pressure exceeding a level specified in the coding

and

P_{*k} .....(k=1,4) are the target values set by the user.

The optimum design is the one which achieves the minimum value of the error sum ϵ (hopefully zero if all the targets are achieved).

The Package searches an extensive database of over 1750 previously assessed designs. Ships similar to the current design are selected and quadratic regression techniques (see Dom and

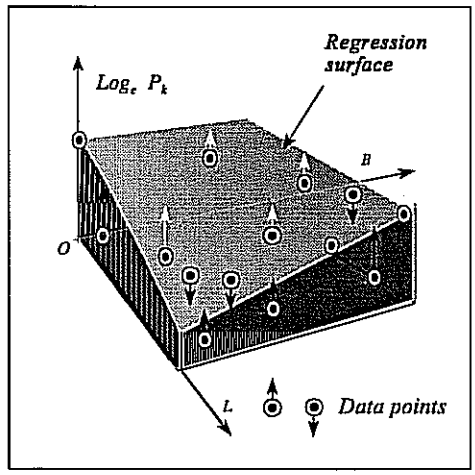

Fig 18.19 - Sketch of quadratic regression surface for two hull form parameters

McCracken (1972)) are used to derive empirical equations of the form

$$Y_k = log_e P_k$$

$$= \sum a_{ij} x_i x_j \quad (i = 0, n; \quad j = 0, n); \quad (k = 1, 4)$$

relating each of the four responses to the hull form parameters. Table 18.1 lists the n parameters and the number of ship designs N found to be necessary for each regression. The indicated parameters may be taken as having significant effects on the individual seakeeping responses.

With five or more parameters it is impossible to visualise this process but Figure 18.19 shows a sketch of a regression surface which would be appropriate if there were only two parameters L and B. The regression equation for this case is of the form

$$Y_k = a_{00} + a_{01}L + a_{02}B + a_{11}L^2 + a_{12}LB + a_{22}B^2$$

and the regression technique finds the values of the coefficients a_{ij} which give the minimum differences between the data points and the surface ordinates (ie it finds the surface which fits the data best). These regression equations are then combined to produce a single equation relating the error sum (Equation (18.1)) to the hull form variables. This is illustrated for the case of only two variables in Figure 18.20. The Package searches the surface for the minimum value of the error sum ϵ and interpolates to find the corresponding hull form parameters. These represent the optimum design having the closest possible match to the target responses within the range of parameters specified by the user. As a check the parameters and the actual responses of the new design are computed and added to the database. The search is repeated several times using the

progressively improving database. In this way the Package "learns by its own mistakes" and ships outside the range of the original database can be designed.

TABLE 18.1
SEAKEEPING DESIGN PACKAGE
HULL FORM PARAMETERS USED IN REGRESSION ANALYSIS
(After Lloyd (1993)

Regression	L	B	D	m	x_G/L	C_{wf}	C_m	F	θ **	N
Accelerations	*	*		*	*	*				60
Wetness	*	*		*		*		*		60
Slamming	*	*	*	*	*	*	*	*	*	150

* indicates that this parameter is used in the regression
** Keel trim angle; the angle beteween the keel (assumed straight) and the horizontal (positve bow up)

Lloyd (1993) demonstrated how the Seakeeping Design package could be used to improve the performance of existing designs by allowing some freedom to vary the hull form parameters (typically ±10%) and specifying stringent target responses.

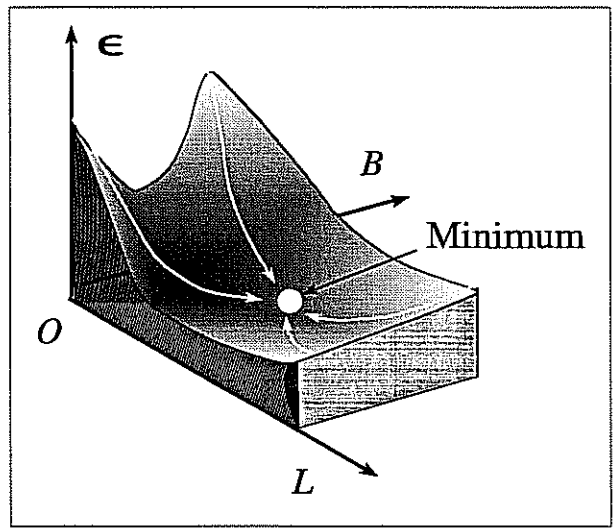

Fig 18.20 - Finding the minimum value of the error sum

Figure 18.21 shows the result obtained for a Ro-Ro ferry and the required changes in parameter values are listed in Table 18.2. For this case substantial improvements were achieved with relatively small changes to the hull form: the only significant changes are moving the centre of gravity forward (ie shifting volume forward from the after part of the ship; increasing the forward waterplane area coefficient and building in a 2 degrees bow down trim to the keel. These changes lead to much increased deadrise angles forward which are largely responsible for the dramatic reduction in slamming.

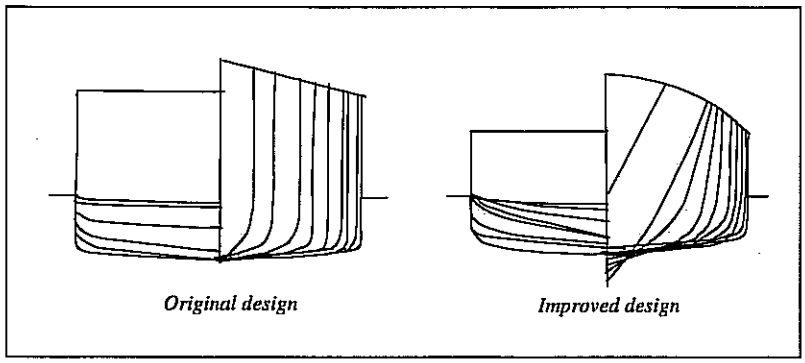

Fig 18.21 Original and improved designs for a Ro-Ro ferry (After Lloyd(1993))

TABLE 18.2
IMPROVING THE SEAKEEPING PERFORMANCE OF A RO-RO FERRY
After Lloyd (1993)

Parameter	Actual design		Improved design	
L (metres)	146		140	
B (metres)	23.3		24.5	
D (metres)	5.4		5.2	
m (tonnes)	12,000		11,060	
$2x_G$ / L	0		0.10	
C_{wf}	0.68		0.78	
C_m	0.95		0.90	
F (metres)	10.9		10.0	
θ (degrees)	0		-2.0	
Performance at 15 knots in sea state 7	rms acceleration at 0.15L	rms acceleration at -0.425 L	Wetness probability	Slamming probability
Original design	0.130g	0.194g	0.032	0.206
Target	0.100	0.100	0.010	0.010
Improved design	0.098	0.102	0.011	0.004

18.5 DESIGN RECOMMENDATIONS

In rough weather a large ship will generally be more comfortable than a small one. Increasing hull size will almost always result in improved seakeeping performance.[1] However small ships will tend to contour the waves and suffer less from slamming and deck wetness[2].

If the ship length is already determined low levels of vertical acceleration can be achieved with a shallow draught and/or a wide beam hull form (with consequent changes to the ship mass). Shallow draught forms may, however, suffer from frequent keel emergence and slamming.

Immunity from slamming can best be achieved by increasing the draught (especially forward by adopting a bow down rake to the keel with high deadrise angles) at the penalty of increased vertical accelerations. Larger rudders and/or a skeg may be required to compensate for the associated reduction in directional stability.

It is for the designer to decide on the best compromise for these conflicting requirements.

Immunity from wetness is best achieved by adopting a high freeboard forward with adequate freeboard elsewhere. Excessively flared above water bows should be avoided.

A large forward waterplane area coefficient reduces all motions in head waves.. However, large angles of entrance associated with a large forward waterplane area coefficient may increase bow swell up and increased wetness may be a problem.

A forward location for the centre of gravity is generally beneficial.

The metacentric height should be chosen to meet stability regulations and to give natural roll frequencies in the range 0.3 - 0.6 radians/second.

---

[1] M C Eames of the Canadian Defence Research Establishment (Atlantic) propounded the poison gas theory: the cheapest way to improve the seakeeping performance of a warship is to build a larger hull with lots of unused compartments. Unfortunately politicians and naval officers then see the ship as not fulfilling its potential as a weapons platform and these spaces will inevitably be filled with costly weapons and sensor systems, making the ship prohibitively expensive. Eames' tongue in cheek solution was to fill the unused spaces with poison gas to keep the money spenders out.

[2] The battleships of the past suffered from excessive deck wetness because they were too long to contour the waves; the problem was compounded by the universal adoption of low freeboard (see Brown (1997))

APPENDIX 1

THE SPRING MASS SYSTEM

"If you ask a sinusoidal question you will get a sinusoidal answer"

- Professor R E D Bishop in a lecture on ship dynamics at The Admiralty Experiment Works, Haslar. circa 1973.

A1.1 INTRODUCTION

The behaviour of a ship in rough weather is fundamentally similar to the oscillatory response of the classical damped spring mass system illustrated in Figure. A1.1. So an understanding of the characteristics of the spring mass system is a good basis for the study of ship motions. This Appendix presents the governing equations without proof, which can be found in many books on applied mathematics.

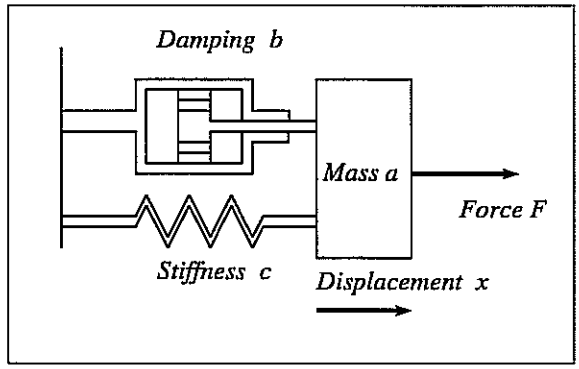

Fig A1.1 - Spring mass system

The classical spring mass system consists of a mass a (tonnes) which is connected to a fixed rigid base (say the Earth) through a dashpot and a spring. The dashpot exerts a damping force b kN in response to a velocity of 1 metre/second and the spring exerts a restoring force c kN if the displacement is 1 metre. If the system is not disturbed it will adopt an equilibrium position which we shall define as a datum displacement[1]

$$x = 0 \quad m$$

At any instant of time the total force F applied to the mass is related to the motion by the equation

$$a\ddot{x} + b\dot{x} + cx = F \quad kN \tag{A1.1}$$

[1] Although the system described has a linear displacement in response to a force the analysis is equally valid for angular displacements in radians (or degrees) in response to a moment in kN m.

A1.2 HARMONIC RESPONSE

Suppose that the force F varies in a sinusoidal manner with amplitude F_0 kN and frequency ω radians/second:

$$F = F_0 \sin (\omega t) \quad kN \tag{A1.2}$$

then the motion is given by

$$x = x_0 \sin (\omega t + \epsilon) \quad m \tag{A1.3}$$

where x_0 is the motion amplitude in metres and ϵ is a phase angle in radians. ϵ is negative so that the displacement sine wave lags the force sine wave as shown in Figure A1.2. The maximum (positive) displacement x_0 occurs ϵ/ω seconds after the maximum (positive) force F_0.

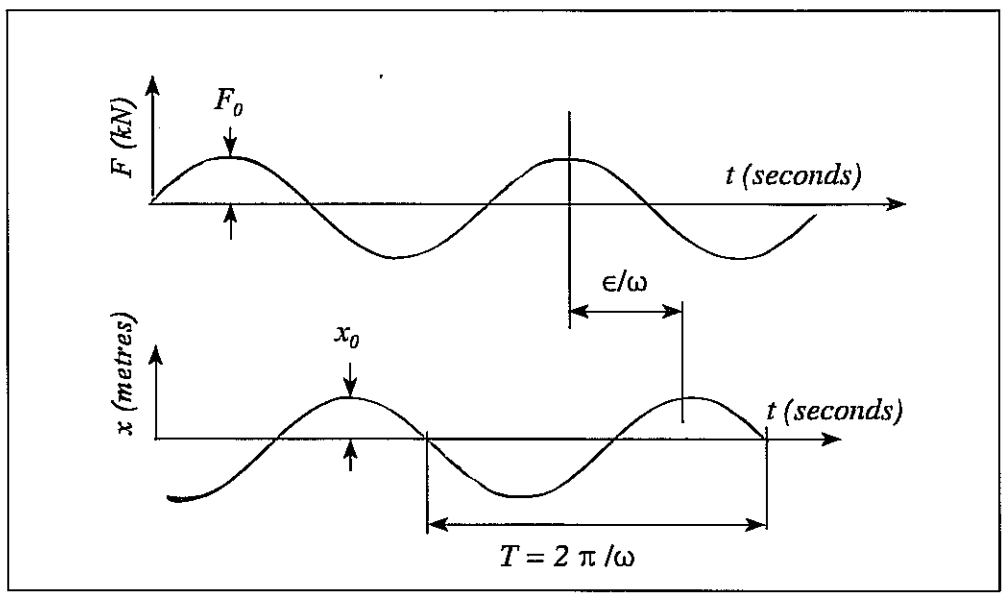

Fig. A1.2 - Sinusoidal motion response to a sinusoidal force acting on a linear spring mass system

The motion amplitude and the phase are given by

$$\frac{x_0}{F_0} = \frac{1}{\sqrt{(c - a \omega^2)^2 + b^2 \omega^2}} \quad m/kN \tag{A1.4}$$

$$\tan \varepsilon = \frac{- b \omega}{c - a \omega^2} \tag{A1.5}$$

If $b = 0$ there is no damping and the motion amplitude becomes infinite at the *undamped*

natural frequency ω_* given by

$$\omega_* = \sqrt{\frac{c}{a}} \quad rad/sec \qquad \text{(A1.6)}$$

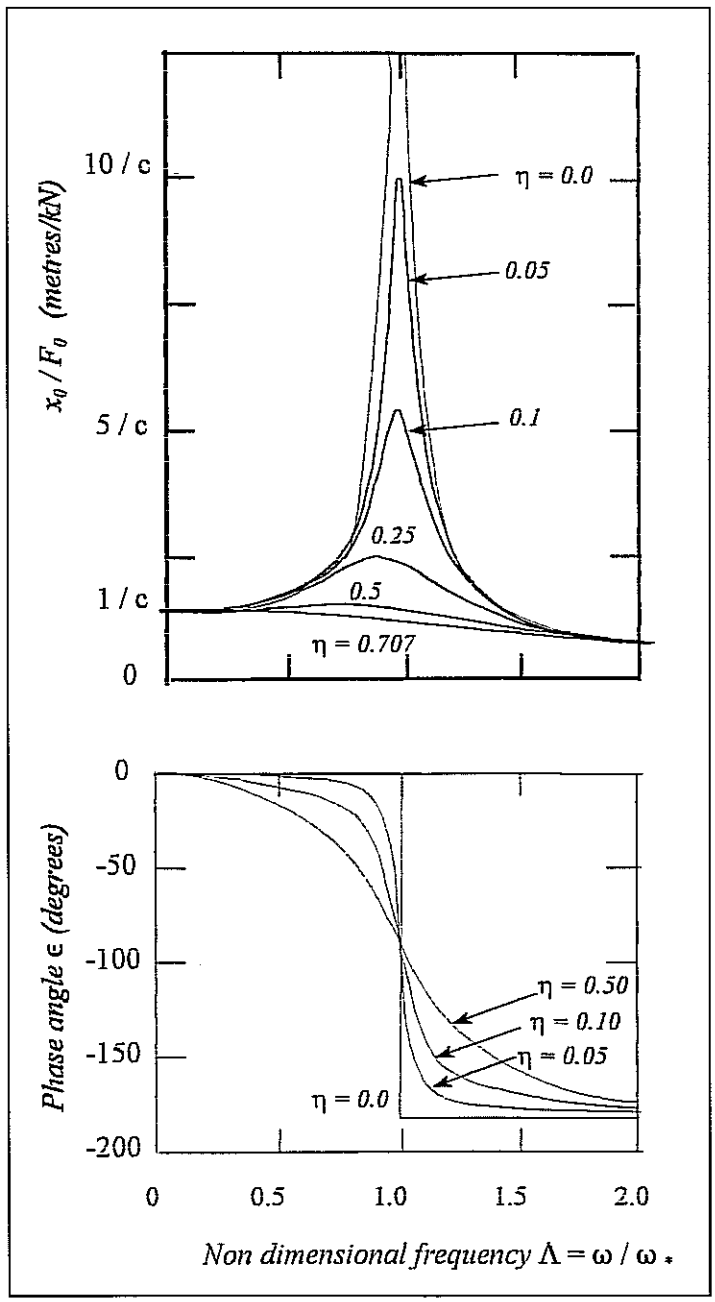

Fig A1.3 - Response of a linear spring mass system

The amplitude and phase responses may be written in non dimensional form as

$$\frac{x_0}{F_0} = \frac{1}{c\sqrt{(1 - \Lambda^2)^2 + (2\eta\Lambda)^2}} \quad m/kN \tag{A1.7}$$

and

$$\tan\varepsilon = \frac{-2\eta\Lambda}{1 - \Lambda^2} \tag{A1.8}$$

where the non dimensional frequency or ***tuning factor*** is

$$\Lambda = \frac{\omega}{\omega_*} \tag{A1.9}$$

and the non dimensional damping or ***decay coefficient*** is

$$\eta = \frac{b}{2\sqrt{c\,a}} \tag{A1.10}$$

Figure A1.3 shows the amplitude and phase response for the system for various values of the decay coefficient η. At zero frequency the applied force is steady and the damping and inertia have no effect because there is no velocity or acceleration. The displacement is governed only by the spring stiffness:

$$\frac{x_0}{F_0} = \frac{1}{c} \quad m/kN$$

At $\Lambda = 1.0$ (the non dimensional natural frequency) the force due to the spring stiffness exactly balances the force due to the inertia of the mass. The amplitude response is then

$$\left(\frac{x_0}{F_0}\right)_{\Lambda = 1.0} = \frac{1}{2\eta c} \quad m/kN \tag{A1.11}$$

When there is no damping the amplitude becomes infinite at the natural frequency, as we have already seen. However, for finite damping the maximum amplitude occurs at a lower frequency. When η is small the difference is very small, as shown in Figure A1.3. For larger values of η the peak amplitude and frequency are reduced until the maximum response occurs at zero frequency when η exceeds 0.707. The system is said to be *critically damped* when $\eta = 0.707$.

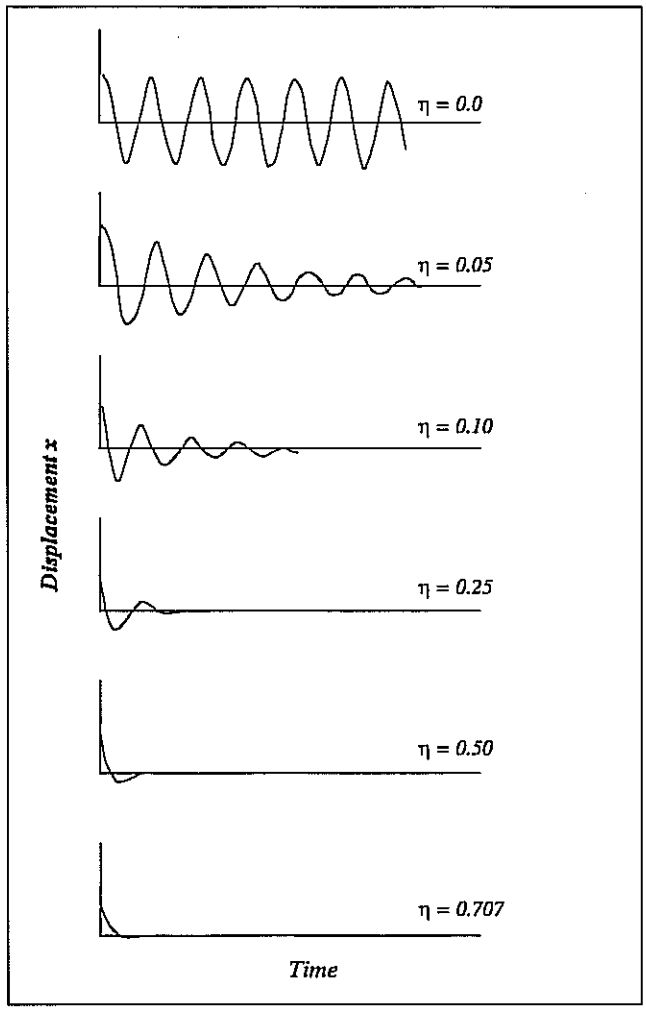

Fig. A1.4 - Decay of oscillations in a linear second order spring mass system

At higher frequencies the amplitude response falls towards zero regardless of the decay coefficient or the spring stiffness. Physically this corresponds to the situation where the oscillation is so rapid that the system has insufficient time to respond appreciably.

Figure A1.3 also shows the phase response of the system. At very low frequencies the phase is nearly zero and the displacement x is almost in phase with the applied force F. In other words the system responds nearly instantaneously to the slowly varying force. As the frequency is increased, the displacement begins to lag behind the force and the phase ε becomes negative. The lag increases with damping, showing that a well damped system responds sluggishly to the applied force. The phase is always - 90° at the undamped natural frequency regardless of the damping. At higher frequencies the phase decreases (ie the lag increases) still further and tends to -180° at infinite frequency.

Combining Equations (A1.4) and (A1.5) yields equations for the in phase and quadrature components of the applied force:

$$c - a\,\omega^2 = \frac{F_0}{x_0}\cos\epsilon \quad kN/m \;; \tag{A1.12}$$

$$b\,\omega = -\frac{F_0}{x_0}\sin\epsilon \quad kN/m \tag{A1.13}$$

The component of the applied force which is in phase with the motion is therefore associated with the stiffness and inertia coefficients, while the quadrature component is associated with damping.

A1.3 FREE DECAY

Let us now suppose that the mass is deflected to some initial displacement x_{00} and then released. We require to examine the subsequent motion. Since there is no applied force after the mass is released, $F = 0$ and Equation (A1.1) becomes

$$a\ddot{x} + b\dot{x} + cx = 0 \quad kN \tag{A1.14}$$

and the resulting oscillation resembles a `sine' wave with a continually decreasing amplitude:

$$x = x_{00}\exp\left(-\frac{t}{\tau}\right)\cos(\omega\,t) \quad m \tag{A1.15}$$

where the time constant is given by

$$\tau = \frac{2\,a}{b} = \frac{1}{\eta\,\omega_*} \quad sec \tag{A1.16}$$

Figure A1.4 shows the free decay of a linear damped spring mass system for various values of the decay coefficient η. When $\eta = 0$ there is no damping and the oscillation continues indefinitely with no loss of amplitude because there is no mechanism for energy dissipation. As η increases, the oscillations decay more rapidly until they effectively disappear after only a single cycle when η is greater than about 0.5. Free decays are often used to obtain an estimate of a system's natural frequency and damping. For low damping the oscillation will decay at a frequency which is approximately the same as the natural frequency. If the peaks occur at intervals (peak to peak) of T_P seconds the natural frequency is

$$\omega_* \approx \frac{T_P}{2\pi} \quad sec \tag{A1.17}$$

and the decay coefficient is given by

$$\eta = \frac{1}{\pi} \log_e \left(\frac{x_{0J}}{x_{0J+1}} \right) \qquad \text{(A1.18)}$$

where x_{0J} and $x_{0\,J+1}$ are the Jth and the $(J + 1)$th amplitudes. Note that if the damping is low several estimates can be made from one record.

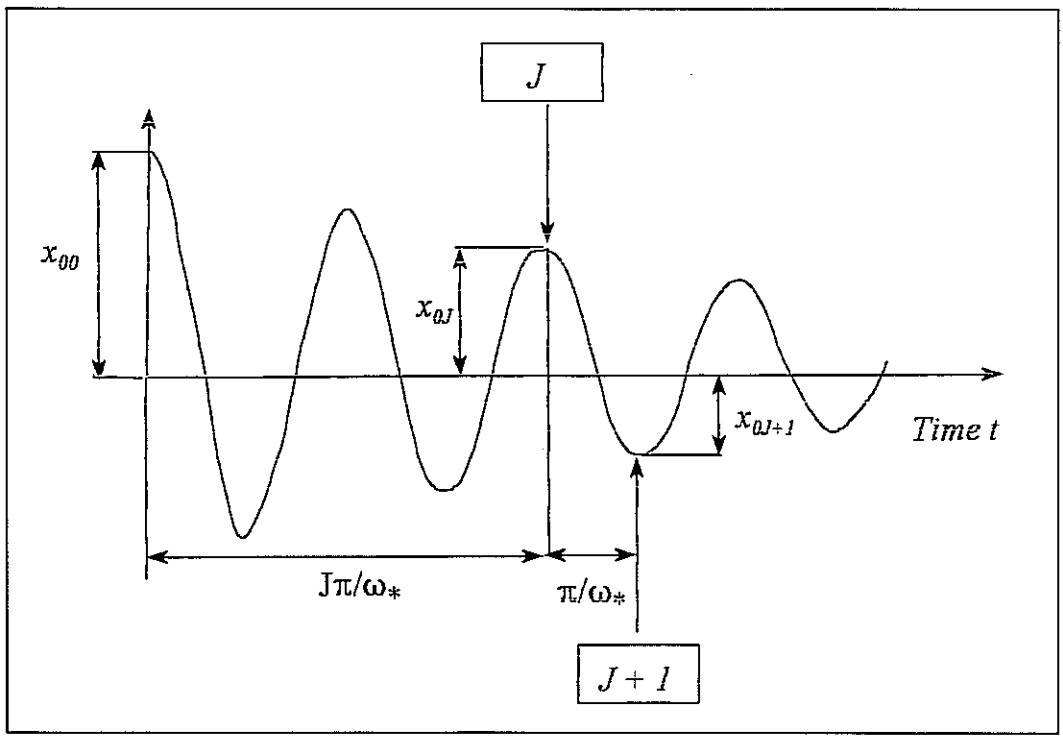

Fig A1.5 - Estimation of decay coefficient

A1.4 SYSTEM WITH NO STIFFNESS

Figure A1.6 shows a related system in which there is no spring stiffness so that it only has damping and inertia. The equation of motion is now

$$a\ddot{x} + b\dot{x} = F_0 \sin(\omega t) \quad kN \qquad \text{(A1.19)}$$

and the response is

$$x = x_0 \sin(\omega t + \varepsilon) \quad m \qquad \text{(A1.20)}$$

so that the application of a sinusoidally varying force again results in a sinusoidally varying displacement.

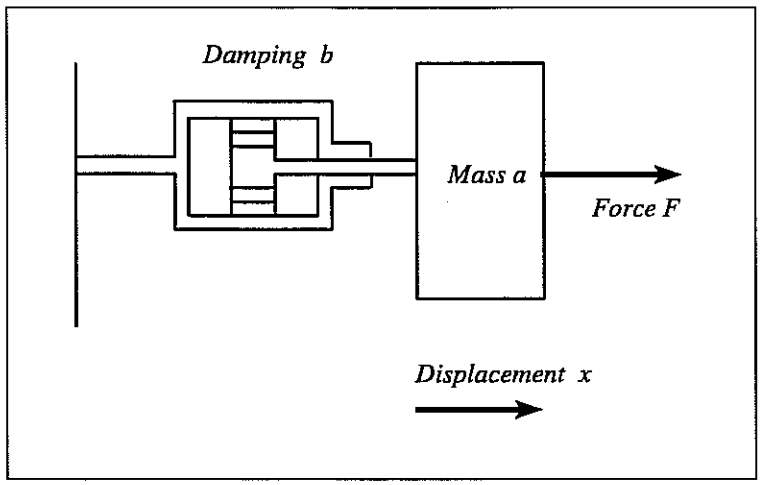

Fig A1.6 - System with no stiffness

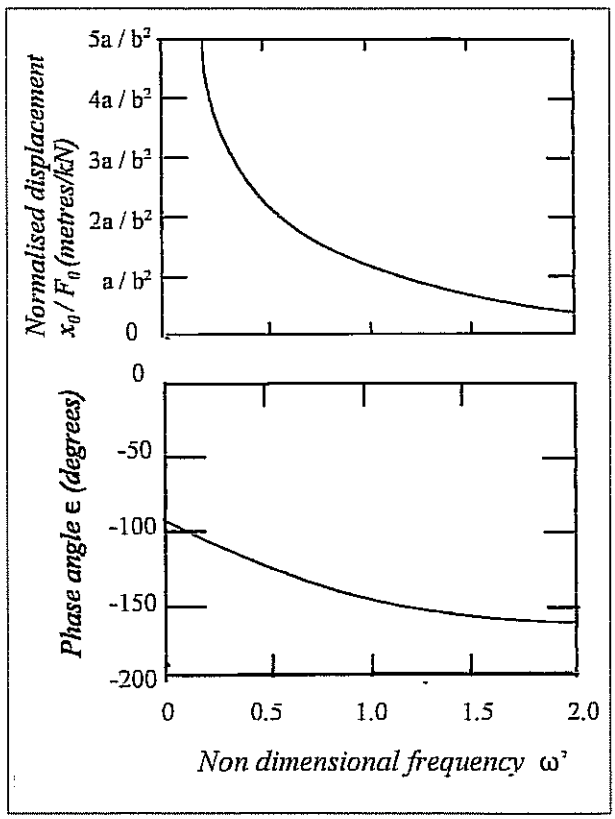

Fig A1.7 - Amplitude and phase responses for a second order systeem with no stiffness.

The amplitude and phase are given

$$\frac{x_0}{F_0} = \frac{a}{b^2} \frac{1}{\omega' \sqrt{1 + \omega'^2}} \quad m/kN \tag{A1.21}$$

$$tan\ \varepsilon = \frac{1}{\omega'} \tag{A1.22}$$

where the non dimensional frequency is

$$\omega' = \frac{a\ \omega}{b} \tag{A1.23}$$

Figure A1.7 shows the amplitude and phase response of the zero stiffness system The responses are quite different from those of the spring mass system. There is no natural frequency and the amplitude rises steadily as the frequency approaches zero. At zero frequency the steady force F_0 is resisted only by the damping force $b\dot{x}$ (since the acceleration, after an initial transient, is zero) and the mass moves at a steady velocity given by

$$\dot{x} = \frac{F_0}{b} \quad m/sec$$

Since this velocity continues indefinitely, the amplitude x_0 is infinite at zero frequency.

APPENDIX 2

EXCITATION AMPLITUDES AND PHASES

If the force on a strip or the moment applied by the force about the centre of gravity is

$$\delta F = \zeta_0 \left[P_S \sin (\omega_e t - Q) + P_C \cos (\omega_e t - Q) \right] \delta x_{BI}$$

then the total force or moment is obtained by integrating along the hull

$$F = \int dF = F_0 \sin (\omega_e t + \gamma)$$

where the excitation amplitude is

$$F_0 = \zeta_0 \sqrt{\left(\int R_1 \, dx_{BI} \right)^2 + \left(\int R_2 \, dx_{BI} \right)^2}$$

and the phase is given by

$$\tan \gamma = \frac{\int R_2 \, dx_{BI}}{\int R_1 \, dx_{BI}}$$

where

$$R_1 = (P_S \cos Q + P_C \sin Q)$$

$$R_2 = (- P_S \sin Q + P_C \cos Q)$$

APPENDIX 3

BIBLIOGRAPHY

Abbreviations

The following abbreviations are used in the bibliography:

AM	Aerospace Medicine (USA)
ASEM	Aviation, Space and Environmental Medicine (USA)
ATTC	American Towing Tank Conference
BMT	British Maritime Technology Limited (UK)
DMVW	First International Symposium on the Dynamics of Marine Vehicles in Waves, IMechE, London, (UK) 1974
DTMB	David Taylor Model Basin (USA)
HMSO	Her Majesty's Stationery Office, London (UK)
HSV	Hamburgische Schiffbau-Versuchsanstalt (West Germany)
IMechE	Institute of Mechanical Engineers, London (UK)
IOS	Institute of Oceanographic Sciences, Wormley (UK)
ISP	International Shipbuilding Progress (Netherlands)
JSNAJ	Journal of the Society of Naval Architects of Japan
MIAS	Marine Information and Advisory Service (UK)
NA	The Naval Architect (RINA) (UK)
NACA	National Advisory Council for Aeronautics (USA)
NEJ	Naval Engineer's Journal (USA)
NSRC	Netherlands Ship Research Centre TNO
NSRDC	Navy Ship Research and Development Center (USA) (formerly DTMB)
ONR	Office of Naval Research Hydrodynamics Symposium (USA)
PRS	Proceedings of the Royal Society (UK)
QJMAM	Quarterly Journal of Mechanics and Applied Mathematics (UK)
SRAJ	Shipbuilding Research Association of Japan
SRI	Ship Research Institute, Tokyo (Japan)
STAR	SNAME Ship Technology and Research Symposium (USA)
TAGU	Transactions of the American Geophysical Union (USA)
TRINA	Transactions of the Royal Institution of Naval Architects (UK)
TSNAME	Transactions of the Society of Naval Architects and Marine Engineers (USA)
USDC	US Department of Commerce National Weather Service
USNI	US Naval Institute
UCEP	University of California Engineering Publication (USA)

Aertssen, G. (1963) Service, performance and seakeeping trials on MV *Lukuga*. TRINA 105.
Aertssen, G. (1966) Service, performance and seakeeping trials on MV *Jordaens*. TRINA 105.
Aertssen, G. (1968) Labouring of ships in rough seas with special emphasis on the fast ship. SNAME Diamond Jubilee International Meeting.
Aertssen, G. ,van Sluys, M. F. (1972) Service, performance and seakeeping trials on a large container ship. TRINA 114.
Andrew, R. N. , Lloyd, A. R. J. M. (1981) Full scale comparative measurements of the behaviour of two frigates in severe head seas. TRINA 123.
Andrew, R. N., Loader, P. R. , Penn, V. E. (1984) The assessment of ship seakeeping performance in likely to be encountered wind and wave conditions. RINA International Symposium on Wave and Wind Climate Worldwide, London.
Bacon, S, Carter D. J. T. (1991) Wave climate changes in the North Atlantic and North Sea. International Journal of Climatology 11.
Baitis, E., Woolaver, D. A. , Beck, T. A. (1983) Rudder roll stabilization for Coast Guard cutters and frigates. NEJ 95 No. 3.
Bales, N. K. (1981) Optimising the performance of destroyer - type hulls 13th ONR, Tokyo.
Bales, S. L., Lee, W. T. , Voelker, J. M. (1981) Standardized wind and wave environments for NATO operational areas. DTNSRDC Report SPD-0919-01.
Barrat, M.J. (1991) Waves in the North East Atlantic. Account of an investigation by BMT Ltd. Department of Technology report OT190545: HMSO.
Bittner, A. C. , Guignard, J. C. (1985) Human factors engineering principles for minimizing adverse ship motion effects: Theory and practice. NEJ 97 No. 4.
Bledsoe, M. D., Bussemaker, O. , Cummins, W. E. (1960) Seakeeping trials on three Dutch destroyers.TSNAME 68.
Blok, J. J. , Huisman, J. (1984) Relative motions and swell up for a frigate bow. TRINA 126.
Bretschneider E.L. (1952) The generation and decay of wind waves in deep water TAGU (37)
Bretschneider E L. (1957) Review of practical methods of observing and forecasting ocean waves by means of wave spectra and statistics. TAGU April.
Brown, D K (1997) Warrior to Dreadnought. Chatham Publishing.
Cartwright, D. E. , Longuet-Higgins, M. S. (1956) The statistical distribution of the maxima of a random function. PRS (Series A) 237.
Chuang, S. L. (1970) Investigation of impact of rigid and elastic bodies with water. NSRDC Report 3248.
Chuang S. L. , Milne, D. T. (1971) Drop tests of cones to investigate the three dimensional effects of slamming. NSRDC Report 3453.
Comstock, E. N., Bales, S. L. , Gentile, D. M. (1982) Seakeeping performance comparison of air capable ships. NEJ.
Cox G. G, Lloyd A.R.J.M. (1977) Hydrodynamic design basis for navy ship roll motion stabilization. SNAME 85
Crapper, G. D. (1984) Introduction to Water Waves. Ellis Horwood, Chichester.
Cummins, W. E. , Bales, S. L. (1980) Extreme value and rare occurrence statistics for Northern Hemisphere shipping lanes. 5th STAR, Coronado, California.
de Jong, B. (1973) Computation of the hydrodynamic coefficients of oscillating cylinders. NSRC Report 145S.
Dom, W.S., McCracken D.D. (1972) Numerical methods with FORTRAN case studies. John Whiley and Sons.
Ewing J. (1975) Some results from the Joint North Sea Wave Project of interest to engineers DMVW
Gerritsma, J. , Beukelman, W. (1967) Analysis of modified strip theory for the calculation of ship motion and wave bending moments. NSRC Report 96S

Gerritsma, J. , Beukeln, W. (1971) Analysis of the resistance increase in waves of a fast cargo ship. Laboratorium voor Scheepsboukunde Report No. 334. Technische Hogeschool Delft, the Netherlands.
Gilhousen, D. B., Quayle, R. G., Baldwin, R. G., Karl, T. R. , Brines, R. O. (1983) Climatic summaries for NOAA Data Buoys. USDC.
Graham, R., Baitis, A. E., Meyers W. G.,(1992) On the development of seakeeping criteria, NEJ.
Grim, 0. (1959) Oscillation of buoyant two dimensional bodies and the calculation of the hydrodynamic forces. HIV Report 1171
Hagiwara, K. , Yulara, T. (1974) Study of wave impact load on ship bow. Japan Shipbuilding and Marine Engineering 8 No. 4.
Hoerner, S. F. (1965) Fluid Dynamic Drag. Published by the author, 148 Busted Drive, Midland Park, New Jersey 07432. USA
Hogben, N. (1994) Increases in wave heights over the North Atlantic: a review of the evidence and some implications for the naval architect. NA July/August (1994).
Hogben, N., Dacunha, N. M. C. , Olliver, G. F. (1986) Global Wave Statistics. BMT.
Hogben, N. , Lumb, F. E. (1967) Ocean Wave Statistics. HMSO.
Hsiung, C. C., Friis, D., Milne, W., Peters, G. R., Weber, H. W. (1983) New towing facilities at Memorial University of Newfoundland. 20th ATTC.
Kato, H. (1958) On the frictional resistance to the roll of ships. JSNAJ 102.
Kehoe, J. W. (1973) Destroyer Seakeeping -- Ours and Theirs. USNI.
Lamb, H. (1932) Hydrodynamics. Cambridge University Press.
Lee, W. T., Bales, S. L. Sowby, S. E. (1985) Standardized wind and wave environments for North Pacific Ocean areas. DTNSRDC Report SPD-0919-02.
Lewis, F. M. (1929) The inertia of the water surrounding a vibrating ship. TSNAME.
Lloyd, A. R. J. M. (1975) Roll stabiliser fins: a design procedure. TRINA 117.
Lloyd, A. R. J. M. (1977) Roll stabiliser fins: interference at non-zero frequencies. TRINA 119.
Lloyd, A. R. J. M., Salsich, J. 0. , Zseleczky. J. J. (1986) The effect of bow shape on deck wetness in head seas. TRINA 128.
Lloyd, A. R. J. M. (1988) The effect of hull form and length on seakeeping CADMO, Southhampton UK
Lloyd, A. R. J. M. (1992) The Seakeeping Design Package. TRINA
Lloyd, A. R. J. M. (1993) Latest developments with the Seakeeping Design Package. NA, May 1993
Lloyd, A. R. J. M., Andrew, R. N. (1977) Criteria for ship speed in rough weather. 18th ATTC.
Mack, C. (1966) Essentials of Statistics for Scientists and Technologists. Heinemann Educational Books, London.
Marine Information and Advisory Service (1982) Catalogue of wave data. MIAS, IOS.
Martin, M. (1958) Roll damping due to bilge keels. Iowa University Institute of hydraulic research report for ONR under contract number 161(01).
Massey, B. S. (1986) Measures in Science and Engineering, their expression, relation and interpretation. Ellis Horwood, Chichester.
Nieuwenhuijsen, J. H. (1958). Experimental Investigations on Seasickness. Drukkerij Schotanus and Jens, Utrecht.
Nordenström, N. (1969) Methods for predicting long term distributions of wave loads and probability of failure for ships, AP11. DNV Report No. 69-22-S.
Ochi, M. K. (1964) Extreme behaviour of ships in rough seas -- slamming and shipping of green water. TSNAME 72.
Ochi, M. K. , Bolton, W. E. (1973) Statistics for prediction of ship performance in a seaway.Parts 1-3. ISP Nos 222, 224, 229.
Ochi, M. K. , Motter, I,. E. (1974) Predictions of extreme ship responses in rough seas of the North Atlantic. DMVW.
O'Hanlon, J. F. , McCauley, M. E. (1974) Motion sickness incidence as a function of the frequency and acceleration of vertical sinusoidal motion. AM.

Pierson, W. J., Tick, L. J. , Baer, I. (1966) Computer based procedures for preparing global forecasts and wind field analyses capable of using wave data obtained by spacecraft. 6th ONR, Washington DC.

Porter, W. (1960) Pressure distribution, added mass and damping coefficients for cylinders oscillating in a free surface. UCEP Series 82-16.

Ridjanovic , M, (1962) Drag coefficients of flat plates oscillating normally to their planes.Schiffstechnik, 9, 45.

St Denis, M. Pierson, W. J. (1953) On the motions of ships in confused seas. TSNAME.

Salvesen, N., Tuck, E. O., Faltinsen, 0. (1970) Ship motions and sea loads. TSNAME.

Schmitke, R. T. (1978) Ship sway, roll, and y'aw motions in oblique seas, TSNAME 86.

Schmitke, R., T. Murdey, D. C. (1981) Seakeeping and resistance trade-offs in frigate hull form design. 13th ONR Tokyo.

Sellars, F. H. (1972) Comparison of model and full-scale slamming impact pressure data. Report MPR-351. MPR Associates Inc., Washington DC.

Shipbuilding Research Association of Japan (1975). Report on the seakeeping performance of a super high speed container ship. 125th Research Committee, SRAJ Report No. 211.

Shoenberger, R. W. (1975) Subjective response to very low frequency vibration. ASEM.

Smith, W. E. (1966) Equation of motion coefficients for a pitching and heaving destroyer model NSRC Report 98S.

Stigter, C. (1966) The performance of U-tanks as a passive anti-rolling device. ISP 13 No. 144.

Takaishi, Y., Matsumoto, T. , Ohmatsu, S. (1980) Winds and waves of the North Pacific Ocean 1964-1973.SRI.

Tanaka, N. (1960) A study on the bilge keels (Part 4 - On the eddy making resistance to the rolling of a ship hull). JNSAJ 109.

Tasai, F. (1959) On the damping force and added mass of ships heaving and pitching. JSNAJ 105.

Tasai, F. (1960) On the damping force and added mass of ships heaving and pitching. UCEP Series No. 82.

Ursell, F. (1949a) On the heaving motion of a circular cylinder in the surface of a fluid. QJMAM (2).

Ursell, F. (1949b) On the rolling motion of cylinders in the surface of a fluid. QJMAM (2).

Vugts, J. H. (1968) The hydrodynamic coefficients for swaying, heaving and rolling cylinders in a free surface. NSRC Report; 112S.

Wagner, H. (1932) Landing of seaplanes. NACA TN 622.

Walden, D. A, Grundmann, P (1985) Methods for designing hull forms with reduced motions and dry decks.. NEJ.

Walters, J. D. (1964) Motion Sickness, Medicine and Travel. Documenta Geigy. J. R. Geigy SA, Basle.

Whicker, L. F., Fehlner, L. F. (1958) Free stream characteristics of a family of low aspect ratio all moveable control surfaces for application to ship design. DTMB Report 933.

Yamamoto, O. (1984) Fuel saving obtained by a navigation under economical ship speeds. Nippon Kokan (Japan) Technical Report (overseas) No 41.

APPENDIX 4

NOTATION

A	(1) Coefficient in the ITTC two parameter wave spectrum (2) Area (3) Section area of hull below waterplane
A_{ij}	Virtual mass or inertia coefficient: ith total (hydrodynamic + inertial) force or moment required to sustain unit jth acceleration
A_n, B_n	Coefficients in Fourier series representation of an irregular wave
A_*, B_*	Parameters in Lewis form calculation
a	(1) Radius of circle (2) Aspect ratio (3) Resistance augment fraction (4) Mass or inertia
a_i	ith force or moment due to unit wave depression acceleration
a_{ij}	Added mass or inertia coefficient: ith hydrodynamic force or moment required to sustain jth unit acceleration
$a_{i\tau}$	Passive tank inertia coefficient: ith force or moment on ship caused by unit tank angle acceleration $\ddot{\tau}$
$a_{\tau i}$	Passive tank inertia coefficient: Tank moment required to sustain unit ith acceleration
$a_{\tau\tau}$	Passive tank inertia coefficient: tank moment required to sustain unit tank acceleration $\ddot{\tau}$
a_0, a_1 etc	(1) Parameters in Lewis form transformation (2) Fin servo parameters
B	(1) Coefficient in the ITTC two parameter wave spectrum; (2) Waterline beam (3) Width
$\overline{BG}$	Height of centre of gravity above centre of buoyancy
$\overline{BM}$	Height of metacentre above centre of buoyancy
b	(1) Appendage outreach (2) Damping coefficient
b_i	ith force or moment due to unit wave depression velocity

$b_{\tau i}$ Passive tank damping coefficient; ith force or moment on ship caused by unit tank angle velocity $\dot{\tau}$

$b_{\tau\tau}$ Passive tank damping coefficient: tank moment required to sustain unit tank angle velocity $\dot{\tau}$

b_1, b_2, b_3 Fixed roll stabiliser control coefficients

b_{ij} ith force or moment required to sustain jth unit velocity

C (1) Coefficient in JONSWAP wave spectrum
(2) Parameter in Lewis form calculation
(3) Confidence level

C_{aw} Added resistance in waves coefficient

C_B Block coefficient

C_D Drag coefficient

C_E Drag coefficient in eddy making calculations

C_F Skin friction coefficient

C_L Lift coefficient

C_m Midships section area coefficient $A_m /(B_m D_m)$

C_R Beach reflection coefficient

C_{WF} Forward waterplane area coefficient $2A_{WF} /(B_m L)$

c (1) Wave celerity: velocity of crest
(2) Stiffness coefficient
(3) Chord

c_e Celerity of radiated waves

c_i ith force or moment due to unit wave depression

c_{ij} ith force or moment required to sustain unit jth displacement

$c_{\tau i}$ Passive tank stiffness coefficient: tank moment required to sustain ith unit displacement

$c_{i\tau}$ Passive tank stiffness coefficient: ith force or moment on ship due to unit tank angle τ

$c_{\tau\tau}$ Passive tank stiffness coefficient: tank moment required to sustain unit tank angle τ displacement

c_n Celerity of nth wave component

D	Draught
$\overline{D}$	Mean local draught
d	(1) Depth of ocean or tank (2) Propeller diameter
$\frac{dC_L}{d\alpha}$	Appendage lift curve slope
E	(1) Energy (2) Fin effectiveness factor
F	(1) Factor for increase of significant wave height year by year (2) Force (3) Freeboard (4) Parameter in statistical F test
F_D	Drag force
F_L	Lift force
F_N	Froude number
f	(1) Probability density function (2) Frequency distribution
G	Gain of ship system
G_M	Gain margin
$\overline{GM_F}$	Fluid metacentric height allowing for internal free surface effects
$\overline{GM_S}$	Solid metacentric height
g	Acceleration due to gravity
H	(1) Height of regular wave (2) Local beam/draught ratio (3) Gain of feedback network
H_a	Height of irregular wave
$\bar{H}_{obs}$	Observed average wave height
$\bar{H}_{1/3}$	Significant wave height
h	(1) Height of pivot point above centre of gravity of model (2) Depth or height of fluid (3) Height of centre of gravity
h_F	Height of pivot point above centre of gravity of frame

h_t	Height of passive tank
I	Total moment of inertia of model and supporting frame
I_F	Pitch moment of inertia of supporting frame
I_L	Second moment of area of waterplane about transverse axis through centre of gravity
I_T	Transverse second moment of area of the waterplane
I_{44}	Roll moment of inertia
I_{55}	Pitch moment of inertia
I_{66}	Yaw moment of inertia
i	$\sqrt{-1}$
J	Propeller advance coefficient
$\overline{KG}$	Height of centre of gravity above keel
K_G	Overall gain setting
K_Q	Propeller torque coefficient
K_T	Propeller thrust coefficient
K_U	Speed dependent gain
K_1	Roll angle sensitivity
K_2	Roll velocity sensitivity
K_3	Roll acceleration sensitivity
k	Wave number
k_n	Wave number of *n*th sine wave component in Fourier series representation of an irregular wave record
k_4	Roll radius of gyration
k_5	Pitch radius of gyration
k_6	Yaw radius of gyration
L	(1) Waterline length (2) Half stance width
M	Number of times an event occurs per minute
MII	Motion induced interruption
M_i	Momentum in *i*th direction

M_L	First moment of area of waterplane about transverse axis through centre of gravity
M_{Wi}	Momentum in *i*th direction of water in a wave
MSI	Motion sickness incidence
M_0, N_0	Parameters in Lewis form calculation
m	Mass
m_F	Mass of supporting frame
m_{0S}	Variance of an irregular wave record in short crested waves
m_0	Variance of an irregular record displacement
m_2	Variance of velocity of an irregular record of displacement
m_4	Variance of acceleration of an irregular record
N	(1) Number of observations (2) Number of frequencies (3) Propeller revolutions per second (4) Number of events per hour (5) Number of questionnaire returns (6) Number of ships selected for regression analysis
N_H	Number of observations in histogram bin
n	Width of duct or reservoir
OE	Operational effectiveness
$\overline{OG}$	Height of centre of gravity above waterplane
p_0, q_0	Parameters in Lewis form calculation
P	(1) Pressure (2) Probability of occurrence (3) Proportion of time
P_V	Proportion voting "yes"
$\tilde{P}$	Fluctuating part of pressure under a regular wave
Q	(1) $k\ x_{B1}\ cos\ \mu$ (2) Propeller torque
q	(1) Total velocity (2) Passive tank resistance coefficient
R	(1) Model dimension ratio (2) Total resistance in waves

R_N	Reynolds number
r	(1) Radial polar coordinate (2) Number of "yes" returns from a questionnaire
r_b	Radial location of eddy shedding
r_e	Effective radius of bilge
r_n	*n*th ship response in calculation of *OE*
r_3	Relative motion
S_A	Aft vertical motion at measurement point
$S_{B\alpha}(\omega)$	Spectral ordinate for Bretschneider wave slope spectrum
$S_{B\zeta}(\omega)$	Spectral ordinate for Bretschneider or ITTC two parameter wave spectrum
S_F	Forward vertical motion at measurement point
$S_{J\alpha}(\omega)$	Spectral ordinate for JONSWAP wave slope spectrum
$S_{J\zeta}(\omega)$	Spectral ordinate for JONSWAP wave spectrum
SM	Subjective magnitude
$S_v\ (\omega_M)$	Wave maker drive signal spectral ordinate
$S_{xi}(\omega)$	Pseudo spectral ordinate for *i*th motion in wave frequency domain
$S_{xi}(\omega_e)$	Encounter spectral ordinate for *i*th motion
$S_\zeta(\omega)$	Wave spectral ordinate
$S_\zeta(\omega,\nu)$	Directional wave spectral ordinate
$S_\zeta(\omega_e)$	Encountered wave spectral ordinate
s	(1) Local girth of hull (2) Laplace transform operator
s_i	*i*th absolute motion
T	(1) Regular wave period: time interval between successive peaks or troughs (2) Propeller thrust
T_e	Encounter period
T_H	(1) Duration of an irregular wave time history (2) Duration of model experiment run

$\overline{T_{obs}}$	Observed average period
T_P	Period of the peaks of an irregular wave: time interval between successive peaks or troughs
T_Z	Zero crossing period: time interval between successive upward or downward zero crossings in an irregular wave record
T_0	Modal period corresponding to the peak of the wave spectrum
T_*	Natural period
t	(1) Time (2) Student's test function
t_L	Time for waves to travel length of the tank
t_n	Time delay for introduction of nth wave component
t_P	Time when wave trough is alongside model centre of gravity
U	Velocity of ship
U_{crit}	Tank wall interference occurs if $U < U_{crit}$
u	(1) Velocity of a water particle in the x direction (2) Parameter in eddy making calculation
u_G	Wave group velocity
u_{Gn}	Group velocity of nth wave component
u_2	Athwartships component of u
v	(1) Velocity of a water particle in the y direction (2) Voltage
v_0	Amplitude of v
W	(1) Weighting factor (2) Weight
w	Width of passive tank
w_T	Taylor wake fraction
w_H	Width of histogram bin
X	Force on particle of water in x direction
X_R , Y_R	Parameters in Lewis form calculation
x	(1) Distance from origin in direction of wave propagation (2) Real variable in z plane

x_{Bi}	Location of a point in the ship relative to centre of gravity
x_{B1a}	Longitudinal distance from centre of gravity to AP (negative)
x_{E1}	Distance from earth fixed origin E to moving origin G_0 in direction of ship's mean course
x_{FBK}	Distance from fin to bilge keel
x_{FF}	Distance between stabiliser fins
x_{FP}	Distance from FP
x_G	Longitudinal distance from midships to centre of gravity (positive forward)
x_i	ith ship motion displacement relative to moving origin G_0
x_P	Waves are recorded x_P metres after they pass the centre of gravity
x_R	Distance from centre of gravity to measurement or suspension point
x_{i0}	Amplitude of x_i
$\dot{x}_i'$	ith velocity of strip
$\ddot{x}_i'$	(1) ith acceleration of elemental mass (2) ith acceleration of strip
x_{iG}'	ith displacement of strip relative to centre of gravity
x_T	Distance from wave maker
x_t	Length of passive tank
x_0	(1) Bow stem overhang (2) amplitude of x
$\dot{x}_2'$	Sway velocity of strip relative to origin O in the waterline
x_{1P} , x_{2P}	Location of wave probe ahead and to starboard of model centre of gravity
Y	(1) Force on particle of water in y direction (2) External force per unit mass
Y_{LA}	Component of local lateral acceleration in y direction
y	(1) Depth below surface (2) Imaginary variable in z plane (3) Coordinate in passive tank analysis
y_P	Depth where pressure is P in calm water

y_{rp}, y_{rs} Vertical coordinates in port and starboard reservoirs

Z_1, Z_2 Parameters in eddy making roll damping calculation

z (1) Complex variable in circle plane for Lewis form calculations
(2) Difference in fluid height in tank reservoirs

(b) GREEK SYMBOLS

α (1) Instantaneous slope of wave surface
(2) Appendage incidence

α_{10} Component of wave slope amplitude in surge direction

α_{n0} Wave slope amplitude of *n*th sine wave component in Fourier representation of an irregular wave slope record

$\alpha_{\bar{D}}$ Slope of constant pressure contour at depth $\bar{D}$

$\alpha_{\bar{D}2}$ Athwartships component of $\alpha_{\bar{D}}$

β (1) Beach slope
(2) Fin depression angle
(3) Deadrise angle at keel

Γ_n Counting functional in calculation of OE

γ (1) Coefficient in JONSWAP wave spectrum
(2) Slope of hull section at the waterline

γ_i *i*th phase angle: *i*th wave force leads maximum wave depression by γ_i radians

Δ (1) Width of water particle
(2) Displacement volume of hull

Δx Deviation of water particle in x direction from datum position

Δy Deviation of water particle in y direction from datum position

δ (1) Thickness of boundary layer
(2) Bow flare angle

δ_i *i*th phase angle: *i*th motion leads maximum wave depression by δ_i radians

δ_P Correction to phase angle due to wave probe location

δ_{r3} Phase angle for relative motion: Relative motion leads maximum wave depression by δ_{r3}radians

δ_{Si} *i*th phase angle for absolute motion: *i*th motion leads maximum wave depression by δ_{Si} radians

δF_i	(1) *i*th Force or moment applied to elemental mass (2) *i*th force or moment applied to strip
δF_{Wi}	*i*th force or moment applied to strip by wave
δm	mass of element of ship
δm_0	Contribution to variance in short crested waves from a single secondary wave direction
δx_{BI}	Length of strip
$\delta\omega$	Frequency interval
ϵ	(1) Bandwidth parameter (2) Phase angle (3) Error sum in Seakeeping Design Package
ϵ_G	Phase of ship system
ϵ_{GH}	Phase of ship and feedback system
ϵ_H	Phase of feedback system
ϵ_M	Phase margin
ϵ_n	Phase angle of *n*th sine wave component in a Fourier series representation of an irregular wave record
ζ	(1) Instantaneous wave depression relative to mean level (2) Complex variable in ship section plane
ζ_a	Amplitude of an irregular wave
ζ_{n0}	Amplitude of sine wave component *n* in a Fourier series representation of an irregular wave or motion record
ζ_P	Depression of constant pressure contour below depth y_P
$\bar{\zeta}_{1/n}$	Mean value of highest $1/n$ observations of ζ_a
η	(1) Decay coefficient (2) Propeller efficiency
θ	(1) Angular coordinate in z plane (2) Keel trim angle
θ_1	Polar angular location of element on surface of hull
θ_2	Slope of hull surface
Λ	Tuning factor ω / ω_*
λ	Regular wave length

ρ	Mass density of water
ρ_t	mass density of tank fluid
σ	Section area coefficient
σ_{0xi}	Root mean square value of *i*th motion
σ_{0S}	Root mean square value of an irregular wave record in short crested waves
σ_0	Root mean square value of displacement of an irregular wave record
σ_2	Root mean square value of velocity of an irregular wave record
σ_4	Root mean square value of acceleration of an irregular wave record
τ	(1) Passive tank angle (2) Time constant $1 / (\eta \omega_*)$
ϕ_C , ϕ_S	Potential functions in Lewis form calculations
ϕ_1, ϕ_2	Angles in passive tank analysis
μ	(1) Ship heading relative to primary wave direction (2) Coefficient of friction
μ_W	Viscosity of water
μ_t	Fractional loss of metacentric height
ν	Ship heading relative to secondary wave direction
ϕ	Velocity potential
ψ_C , ψ_S	Stream functions in Lewis form calculations
Ω	Force potential
ω	(1) Frequency (2) Wave frequency
ω_e	Encounter frequency
ω_n	*n*th frequency in Fourier series representation of an irregular wave record
ω_*	Undamped natural frequency
ω_{*i}	Undamped natural frequency for *i*th motion

(3) SUFFIXES, SUBSCRIPTS ETC

Symbol	Examples	Meaning
bar	$\bar{\zeta}$	Mean value
1/3	$\bar{H}_{1/3}$	Significant value (mean of highest third)
prime /	$A^{/}$ $T_0^{/}$	(1) Local value (2) Non dimensional value
A	A_A ρ_A F_{A2}	(1) Appendage (stabiliser fin, rudder etc) (2) Air (3) Apparent value
AD	b_{44AD}	Appendage drag at zero speed
AL	b_{44AL}	Appendage lift
amp	ω_{amp}	amplification
aw	R_{aw}	Added value in waves and wind
BK	A_{BK}	Bilge keel
BL	E_{BL}	Boundary layer
C	ϵ_C P_C	(1) Roll stabiliser controller (2) In quadrature value
c	R_c	Calm water value
ca	R_{ca}	Augmented value in calm water
crit	$F_{N\ crit}$	Critical value
D	α_D	(1) Demanded value (2) Drag
d	w_d	Passive tank duct
ds	P_{ds}	Deck submergence
E	$b_{44E}^{/}$	Eddy shedding
e	F_e	Effective value
F	A_F	Stabiliser fin
IBK	E_{IBK}	Bilge keel interference
IF	E_{IF}	Fin Interference

i, j	x_i, F_j	Indicates motion, force or moment: 1: surge, positive forward 2: sway, positive to starboard 3: heave, positive downwards 4: roll, positive starboard side down 5: pitch, positive bow up 6: yaw, positive bow to starboard
in, out	v_{in} , v_{out}	Input and output
k	E_k	Kinetic
ke	P_{ke}	Keel emergence
L	F_L	Lift
M	L_M x_{4M} x_{BIM}	(1) Model value (2) Measured value (3) Measured from origin at midships
m	A_m	Value at midships
max	B_{max}	Maximum value
p	$\overline{T_p}$ P_p U_p C_p E_p	(1) Peaks (2) Port side (3) Propeller (4) Slamming pressure (5) Potential
pe	P_{pe}	Propeller emergence
r	v_r c_r	(1) Reservoir (2) Root
S	L_S P_S	(1) Ship value (2) In phase
s	P_s A_s C_s	(1) Starboard side (2) Superstructure (3) Swell up
slam	P_{slam}	Slamming
sp	MII_{sp}	Slides to port
ss	MII_{ss}	Slides to starboard
stall	α_{stall}	Value when appendage stalls
T	B_T	Towing tank

t	c_t	(1) Tip
	x_t	(2) Passive tank
tp	MII_{tp}	Tipping to port
ts	MII_{ts}	Tipping to starboard
w	A_w	(1) Waterplane
	F_{wi}	(2) Wave
wf	A_{wf}	Waterplane forward of midships
0	ζ_0	Amplitude

APPENDIX 5

A NOTE ON UNITS AND NUMERICAL VALUES

Système International (SI) units are used throughout this book. The tonne (t) is adopted as the unit of mass with the kilonewton (kN) as the corresponding unit of force which will accelerate a unit mass at 1 metre/second^2. The metre (m) and the second (sec) are adopted as the units of length and time, unless otherwise stated in the text. Angles are generally measured in radians (rad) and angular velocities and frequencies are given in rad/sec. Following common practice ship speeds are given in knots or nautical miles per hour. The mass density of fresh water is 1.0 t/m^3.

Appropriate units are quoted for all equations. Some readers of the first edition of this book criticised this decision on the grounds that it implies that the equations are not valid in other systems of units. This is, of course, not true and readers may substitute their own units providing that a rational system is used with a unit force imparting a unit acceleration to a unit mass.

Quoting the units of equations is retained since this helps to reinforce the reader's understanding of their physical meanings. For example Equation (4.22d) for b_{44} gives the units as kN m /(rad/sec) highlighting the fact that the roll damping coefficient is the roll moment (in kNm) required to sustain a unit roll velocity (in rad/sec).

Mass density of fresh water	1.0 t/m^3
Mass density of sea water	1.025 t/m^3
Mass density of air at 15^0 C	0.00122 t/m^3
Viscosity of fresh water at 15^0 C	1.14×10^{-6} kN sec/m^2
Viscosity of air at 20^0 C	1.81×10^{-8} kN sec/m^2
Acceleration due to gravity	9.81 m/sec^2
1 knot	0.515 m/sec

The following notation is used:

deg	degrees
kN	kilo Newtons
kJ	kilo Joules
m	metres
rad	radians
sec	seconds
t	tonnes

APPENDIX 6

GLOSSARY

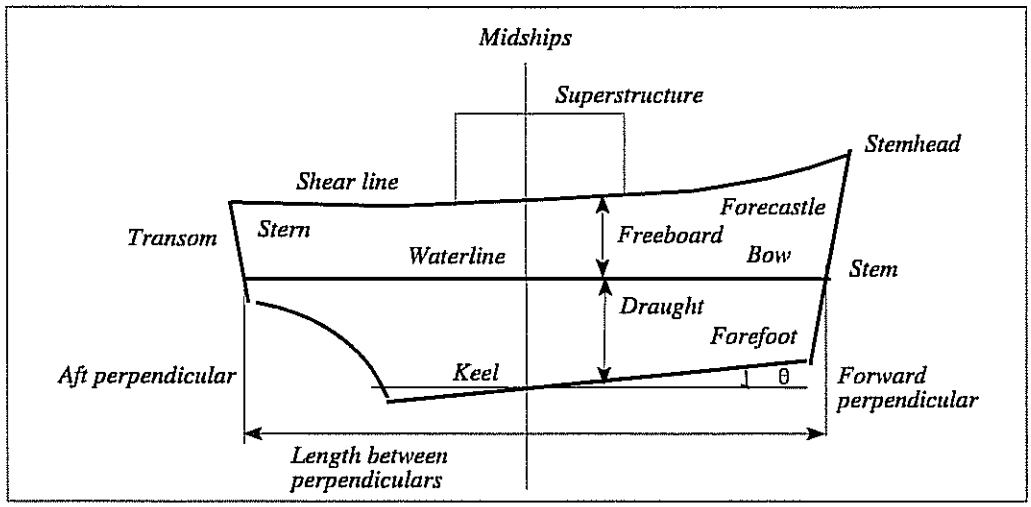

Aft perpendicular (AP)	Vertical line drawn through intersection of the stern profile and the waterplane
Beam	The width of the ship at the widest part of the waterplane
Bow	The foremost part of the ship
Draught	Local depth of the keel below the waterline at zero speed in calm water
Fetch	Length of ocean along wind vector exposed to the wind
Forecastle	The raised part of the hull at the bow
Forefoot	The keel close to the bow
Forward Perpendicular (FP)	Vertical line drawn through the intersection of the stem and the waterline
Freeboard	Vertical distance from the water surface to the edge of the weather deck
Length	Water line length of the ship in calm water
Shear line	Side view of the edge of the weather deck
Sinkage	Increase of draught at midships at forward speed in calm water
Stem	The line joining the keel and the deck at the bow
Stemhead	The top of the stem
Stern	The aftermost part of the ship
Superstructure	The part of the ship above the weather deck
Swell	Waves generated at some distance from the observation site
Transom	Stern truncated as a flat transverse section
Trim	Steady pitch at forward speed in calm water
Wall sided	The sides of the hull at the waterline are vertical
Waterline	Side view of waterplane
Waterplane	The plane of intersection of the hull and the calm water surface
Weather deck	The main deck exposed to the weather

A

B

C

D

E

F

G

H

I

Q

R

S

T

U

V

W

Y

Z

Transfer Functions and page numbers

Heading (deg)	Sway	Heave	Roll	Pitch	Yaw	Absolute motion	Relative motion
0		138 139 140		138 139 140			
30	147	139 140	146	139 140	147		
60	147	139 140	146	139 140	147		
90	142	139 140	143 146				
120	147	139 140	146	139 140	147		
150	147	139 140	146	139 140	147		
180		136 139 140 155 341 342		137 139 140 157 341 343		149 345	149 159 346

Adrian Lloyd

BIOGRAPHICAL NOTES

Adrian Lloyd gained an honours degree in Aeronautical Engineering at the University of Bristol in 1962. He then took a one year course in Experimental Aerodynamics at the Von Karman Institute at Rhode-st-Genèse in Belgium where he was awarded a diploma with distinction and had the honour of meeting Theodore von Karman himself. Returning to Bristol in 1963 he spent the next four years reading for a PhD in Industrial Aerodynamics. His work involved wind tunnel modelling of the diffusion of the effluent discharged by power station chimneys into the turbulent atmospheric boundary layer. His PhD was awarded in 1967, by which time he had joined the Admiralty Experiment Works at Haslar, Gosport as a Scientific Officer.

After a short period spent developing improved control systems for the Royal Navy's submarines he was promoted to Senior Scientific Officer to head the newly formed Seakeeping Research Group. He embarked on an extensive programme of work evaluating the performance of roll stabiliser fins, culminating in a new design method. His paper based on this work (with G G Cox) was awarded the Linnard Prize by the Society of Naval Architects and Marine Engineers in New York in 1977.

Meanwhile the scope of the Haslar research group was growing to cover all aspects of the behaviour of ships in rough weather including voluntary and involuntary speed loss, slamming, deck wetness, broaching and capsizing as well as more fundamental work on the prediction of ship motions. Promotion to Principal Scientific Officer followed in 1975.

In 1982 he was appointed NAVSEA Visiting Research Professor at the United States Naval Academy where he taught ship dynamics to the midshipmen and conducted a study on the effect of bow shape on deck wetness in rough seas. The work was described in a paper (with J O Salsich and J J Zseleczky) published by the Royal Institution of Naval Architects and was awarded their Bronze Medal in 1986.

Returning to Haslar in 1983 he was promoted to Individual Merit Senior Principal Scientific Officer and began developing the Seakeeping Design Package, a computer aided design system which allows, for the first time, a hull form to be optimised within given constraints to achieve preset seakeeping targets. A paper describing the technique was awarded the RINA's Silver Medal in 1992.

He acted as curator of the Froude museum and Admiralty Experiment Works archives before they were moved from the Haslar site to the Science museum.

He served as Secretary and later as Chairman of the International Towing Tank Conference Seakeeping Committee and was United Kingdom delegate on various NATO committees.

He was elected a Fellow of the Royal Academy of Engineering and awarded the William Froude Gold Medal by the Royal Institution of Naval Architects in 1992. He retired in 1994.

He is married to Sonya, a teacher, and has two grown up children who are currently embarking on careers in occupational therapy and information technology. He is a keen amateur cabinet maker and model maker and has exhibited several models at the annual International Model Show in London. He enjoys restoring and driving vintage Alvis motor cars.